Geochemistry and petrology of ~ 3.8 Ga mafic - ultramafic enclaves in the Itsaq Gneiss Complex, SW Greenland

Inaugural-Dissertation

zur

Erlangung des Doktorgrades

der Mathematisch-Naturwissenschaftlichen Fakultät

der Universität zu Köln

Köln, 2019

vorgelegt von

Julia van de Löcht

1. Gutachter	Prof. Dr. Carsten Münker
2. Gutachter	Prof. Dr. Reiner Kleinschrodt

Mündliche Prüfung	09.01.2019

ABSTRACT

Remnants of Earth´s Archaean mantle are scarce, thus, information about early mantle evolution was mainly gained by indirect evidence, e.g., from volcanic rocks, geophysical data, experiments, or much younger mantle rocks. Highly debated issues concerning early Earth´s history are for example the timing and mixing history of late accreted meteoritic material, mantle-crust differentiation, early crustal recycling processes, and the onset of modern style plate tectonics. Yet, direct measurements of Eoarchean mantle rocks can provide important information concerning those issues.

The 3.6-3.9 Ga Itsaq Gneiss Complex (IGC) of southern West Greenland hosts the most promising localities of potential well-preserved Eoarchean mantle remnants. In order to gain new insights into early Earth´s mantle evolution and mantle-crust interaction, a new, carefully collected sample set including mafic and ultramafic rocks from three of such localities were investigated in terms of their petrology and geochemistry. The sample set include variable altered ultramafic rocks from the region south of the Isua supracrustal belt (SOISB) located in the Isukasia terrane, and from the Narssaq ultramafic body (NUB) and Akilia Island located in the Færingehavn terrane. This study combines new petrological observations, comprehensive major and trace element data for mafic and ultramafic rocks as well as Lu-Hf, Sm-Nd and Rb-Sr isotope compositions for the ultramafic rocks. In addition, Os, Ir, Ru, Pt and Pd concentrations and Re-Os isotope signatures of some peridotites were obtained. Moreover, this study includes Lu, Hf, Sm, Nd, Rb and Sr concentrations and isotope data for olivine, orthopyroxene and amphibole separates of selected peridotites.

Combined petrological and geochemical investigations, including platinum group element and Re-Os isotope data, provide evidences that indeed remnants of > 3.8 Ga mantle peridotites occur in both Eoarchean terranes of the IGC. The well-preserved peridotites show whole rock, olivine and orthopyroxene major and minor element compositions either consistent with mantle or crustal cumulate origin. Moreover, several peridotites show fractionated primitive mantle normalized PGE pattern typical for depleted mantle rocks.

Modelled PGE abundances in Earth´s mantle after core segregation are in marked contrast to measured PGE abundances in Proterozoic and Phanerozoic mantle rocks. Therefore, late accretion of meteoritic material that supplied highly siderophile elements to Earth's mantle after core segregation have been advocated to explain the discrepancy. Importantly, the Os, Ir, and Ru abundance of the investigated Eoarchean mantle peridotites are similar to present-day mantle rocks. Hence, the abundances of Os, Ir, and Ru combined with Os isotope

compositions of the mantle peridotites indicate that primitive late accreted material appears to have been efficiently mixed into the sampled mantle domains by Eoarchean time.

The Lu–Hf system yields isochron relationships for most of the peridotites. Lutetium-Hf whole rock age regression lines mainly yield Eoarchean ages of ca. 3.9 to 3.8 Ga, in good agreement with minimum ages inferred from field relationships (≥ 3.8 Ga). Yet, the Sm-Nd and especially the Rb-Sr isotope patterns exhibit larger scatter, indicating subsequent disturbance of the Sm-Nd and Rb-Sr isotope systems by late post-emplacement tectono-metamorphic events. The major and minor element abundances combined with Hf-Nd-Sr isotope data for olivine, orthopyroxene and amphibole separates support the conclusions that the Lu-Hf isotope system was less disturbed than the Sm-Nd and Rb-Sr systems by late Archean to Paleoproterozoic tectonothermal metamorphic events.

The Major element compositions and the nearly flat primitive mantle-normalized REE patterns obtained for the mantle peridotites resemble geochemical characteristics of re-fertilized modern abyssal peridotites. Their Th-REE-HFSE characteristics also indicate re-enrichment of initially depleted peridotite by melt-like subduction components. Based on a simple evolution-model for the investigated mantle peridotites, we suggest depletion by hydrous partial melting in the spinel stability field, followed by subsequent addition of low quantities of melts, similar to melts derived from subducted slabs of oceanic crust.

Based on geochemical data and field observation a subduction zone related origin was postulated for some mafic rocks from the IGC. The Amphibolites investigated in this study also show such geochemical characteristics similar to modern subduction suite related mafic rocks. Thus, our findings, including geochemical data for mafic and ultramafic rocks, support that subduction-like processes were in operation since at least the Eoarchean.

ZUSAMMENFASSUNG

Gesteinsproben des Archaischen Erdmantels sind äußerst selten zu finden. Daher müssen Erkenntnisse über frühe Entwicklungen des Erdmantels hauptsächlich indirekt ermittelt werden. Zum Beispiel durch geochemische Untersuchungen an vulkanischen Gesteinen oder jüngeren Mantelgesteinen, sowie geophysikalischen Untersuchungen oder Experimenten. Wichtige und großteils noch ungeklärte Fragestellungen hinsichtlich der Frühgeschichte der Erde sind z. B. die zeitliche Einordnung sowie der Verlauf der Beimengung von meteoritischem Material in den Erdmantel nach Bildung des Erdkerns (late accretion), die Differenzierung der Erdkruste, frühe Recycling-Mechanismen der Erdkruste oder der Beginn der modernen Plattentektonik.

Direkte Messungen an eoarchaischen Mantelgesteinen können wichtige Informationen liefern zur Klärung dieser offenen Fragen. Potenzielle Aufschlüsse für eoarchaisches Mantelgestein befinden sich im 3.6 – 3.9 Milliarden Jahre alten Itsaq Gneiss Complex im Südwesten Grönlands. Im Rahmen dieser Arbeit wurden drei innerhalb dieses Komplexes liegende Aufschlüsse, sorgfältig beprobt, und die mineralogische und geochemische Zusammensetzung der Proben bestimmt. Der neue Probensatz umfasst unterschiedlich alterierte mafische und ultramafische Gesteine. Ein Teil der Proben stammt aus der Region südlich des Isua - Grünsteingürtels („south of the Isua supracrustal belt“: SOISB) und somit aus dem nördlichen eoarchaischen IGC Gesteinskomplex, dem Isukasia-Terrane. Weitere Proben stammen von der Narssaq Halbinsel, dem „Narssaq ultramafic body” (NUB) sowie vom südwestlichen Teil Akilia Islands. Die Narssaq Halbinsel und Akilia Island sind Teil des Færingehavn-Terranes, dem anderen eoarchaischen Gesteinskomplex des IGC.

Die vorliegende Arbeit umfasst mineralogische Beobachtungen und umfangreiche Haupt- und Spurenelementanalysen der mafischen und ultramafischen Proben, sowie Lu-Hf, Sm-Nd und Rb-Sr Isotopenzusammensetzungen der Peridotite. Des Weiteren wurden an ausgewählten Peridotitproben sowohl die Konzentrationen an Os, Ir, Ru, Pt und Pd, als auch die die Re-Os-Isotopenzusammensetzungen bestimmt. Von vier ausgewählten Peridotiten wurden zusätzlich Olivin-, Orthopyroxen- und Amphibol-Separate angefertigt, um deren Lu-Hf-Sm-Nd-Rb-Sr Gehalte und Isotopenzusammensetzungen zu ermitteln.

Die gut erhaltenen Peridotite zeigten Olivin- und Orthopyroxen-, sowie Gesamtgesteinszusammensetzungen, welche entweder Mantelperidotiten, oder ultramafischen Kumulaten der Erdkruste entsprechen. Zusätzlich zeigen einige Peridotite eine deutliche Fraktionierung der Platinmetalle, die charakteristisch für Mantelperidotite ist.

Modellierte Gehalte an Platinmetallen im Erdmantel nach der Kernbildung sind um ein vielfaches geringer als die gemessenen Gehalte in proterozoischen und phanerozoischen Mantelgesteinen. Um diese Diskrepanz zu erklären, wird daher zumeist eine späte Akkretion meteoritischen Materials nach der Kernbildung angenommen (late accretion). .

Ein wichtiges Ergebnis dieser Arbeit ist, dass die Gehalte an Os, Ir und Ru in den untersuchten eoarchaischen Mantelperidotiten in dem Bereich der heutigen Mantelperidotite liegen. In Kombination mit den Os-Isotopien der untersuchten Mantelperidotiten deuten die Daten darauf hin, dass das später hinzugekommene meteoritische Material eine überwiegend primitive Zusammensetzung hatte und bereits zur Zeit des Eoarchaikums schon im beprobten Bereich des Erdmantels weitgehend untergemischt war.

Die meisten Peridotite weisen miteinander korrelierende Lu-Hf Isotopen Daten auf und ergeben Altersabschätzung von 3.9 bis 3.8 Mrd. Jahren. Diese stimmen gut mit den Mindestaltern von ≥3.8 Mrd. Jahren überein, welche auf Grund der Geländebefunde angenommen werden. Die Sm-Nd und Rb-Sr Isotopen Daten zeigen hingegen, dass diese Isotopensysteme während späterer metamorphen Ereignisse gestört wurden. Die Lu, Hf, Sm, Nd, Rb und Sr Konzentrationen in Kombination mit den Hf-Nd-Sr Isotope Daten der Olivine-, Orthopyroxen- und Amphibol-Separate bekräftigen die Schlussfolgerung, dass die Überprägung durch tektono-metamorphe Ereignisse während des späten Archaikums und Proterozoikums bezüglich des Lu-Hf Isotopensystem weniger ausgeprägt ist als bezüglich der Sm-Nd und das Rb-Sr Isotopensysteme.

Die Hauptelementkonzentrationen der Mantelperidotite, sowie die Muster ihrer auf den primitiven Mantel normierten Seltenen Erdenelemente (SEE) sind vergleichbar mit denen von heutigen an SEE wiederangereicherten abyssalen Mantelperidotiten. Ebenso deutet ihre Th-SEE-HFSE (HFSE: *high field strength elements*) Signaturen darauf hin, dass die verarmten Mantelperidotite durch Schmelzen mit einer Subduktions-Signatur wieder angereichet wurden. Basierend auf einem vereinfachten petrogenetischen Modell der eoarchaischen Mantelperidotite wurde eine mögliche Entstehungsgeschichte der Gesteine wie folgt rekonstruiert: nach partiellem Aufschmelzen und Schmelzextraktion hauptsächlich im Spinell-Stabilisationsfeld folgte eine Wiederanreicherung der Mantelgesteine durch geringe Mengen an Schmelze mit einer Zusammensetzung vergleichbar mit Schmelzen einer subdukzierten ozeanischen Platte.

Auf Grund geochemischer Daten und Geländebeobachtungen wurde geschlussfolgert, dass einige mafische Gesteine des IGC vermutlich in einem Subduktionszonen-Milieu entstanden. Die in dieser Arbeit untersuchten Amphibolite weisen ebenfalls geochemische Merkmale auf die denen von mafischen Gesteinen heutiger Subduktionszonen ähneln. Daher unterstützen die Ergebnisse der geochemischen Untersuchungen an den mafischen und ultramafischen Gesteinsproben, die Hypothese, dass bereits im Eoarchaikum geodynamische Prozesse aktive waren, ähnlich derer in heutigen Subduktionszonen.

TABLE OF CONTENTS

Chapter 1

Introduction

1-1 INTRODUCTION AND AIM OF THIS STUDY

During the first two eons of Earth´s history (Hadean ~4.56-4.0 Ga and Archean 4.0-2.5 Ga), several processes changed the interior and surface of the Earth fundamentally. Such processes include core-mantle and mantle-crust differentiation, continental crust formation and initiation of modern style plate tectonics. Highly debated questions in early Earth research regard the composition and the evolution of early Earth´s atmosphere and her hydrosphere, as well as the emergence of life. However, the terrestrial geological record is very limited and key questions in early Earth´s history are therefore still not fully understood.

The only preserved remnants from the Hadean eon in present-day continental rocks are zircon grains. The oldest zircons (ca. 4.4 Ga) are found in the Jack Hills and Mt. Narryer in 3.3 Ga old metasediments from Western Australia, and are interpreted as remnants of differentiated crust (e.g., Froude et al. 1983; Compston and Pidgeon 1986; Wilde et al. 2001; Harrison et al. 2007; Menneken et al. 2007; Valley 2008, 2014; Kemp et al. 2010; Nebel-Jacobsen et al. 2010). The combined rare-earth-element (REE) and oxygen isotope signatures of silicate inclusions in 4.4 Ga old Jackson Hill zircons indicate the presence of differentiated magmas. These data also show, that the Earth´s surface was already cold enough to trigger condensation of water and the formation of the first oceans (e.g., Wilde et al., 2001; Harrison et al., 2007). The oldest uncontroversially dated rocks on Earth are the Acasta gneisses from Canada (ca. 4.03 Ga years, e.g., Stern and Bleeker 1998; Bowring and Williams 1999; Iizuka et al. 2007; Bowring et al. 2015), marking the transition between the Hadean and the Archean. Archean rocks are part of the “old cores” (cratons) of our present continents. However, only about 5% of the presently exposed continental crust on Earth is unambiguously Archean (4.0 – 2.5 Ga) in age (e.g., Nisbet, 1987) and much less than 1% of this Archean crust is older than 3.5 Ga (Nutman et al., 1996). Eoarchean (4.0 – 3.6 Ga) rocks were found at several localities worldwide (Fig. 1-1). Most of the prominent Eoarchean localities are part of the Northern Atlantic Craton (NAC). Those are (1) the up to 3.95 Ga old Saglek-Hebron Gneisses of Labrador (e.g., Komiya et al. 2017), (2) the > 3.7 Ga old Nuvvuagittuq Greenstone belt and associated gneisses (e.g., O’Neil et al. 2011, 2012; David et al. 2009), and (3) the 3.65 to 3.9 Ga old Itsaq Gneiss Complex (IGC) of southwest Greenland (e.g., Nutman et al., 1996).

The available outcrops of Eoarchean rocks are restricted to low- to high-grade metamorphic terranes, where in most cases deformation and metamorphism have modified the original compositions and the primary structures almost entirely. However, the IGC hosts extraordinarily well preserved exposures of Eoarchean continental and oceanic crust, sediments and ultramafic rocks of potential mantle origin (e.g., Nutman et al. 1984, 1996; Bennett et al. 2002; Friend et al. 2002; Nutman et al. 2009b; Hoffmann et al. 2011a, 2014). Hence, the IGC provides unique opportunities to study the evolution of the Eoarchean crust and mantle.

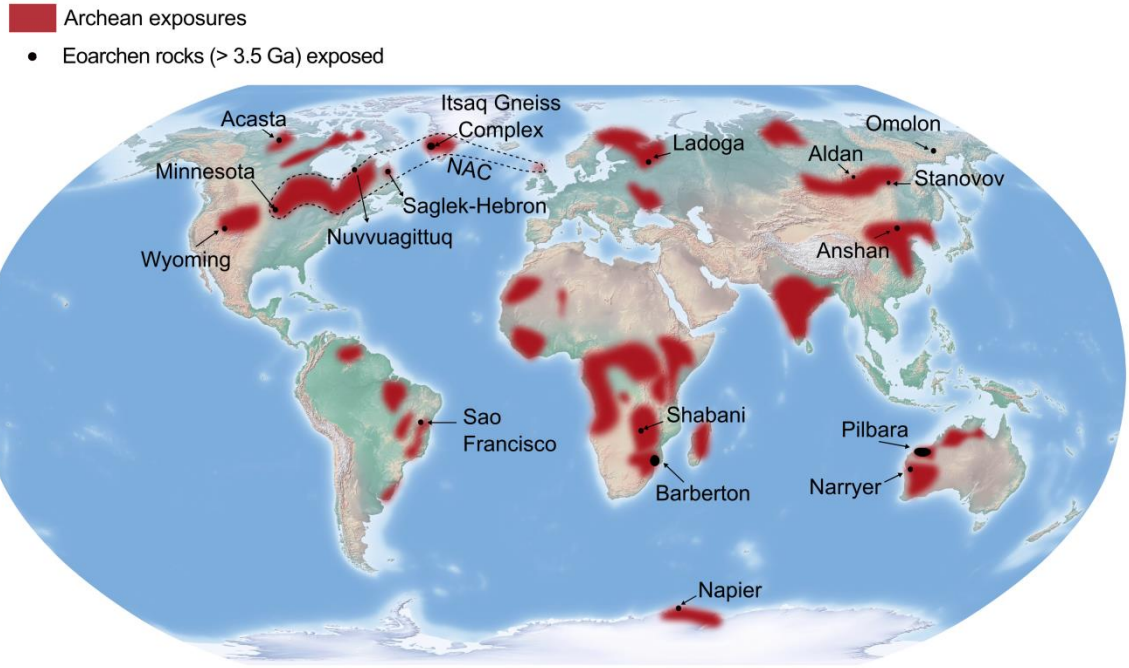

Figure 1-1: Overview of exposed Archean continental crust modified after Bleeker et al. (2003). The areas of exposed Archean continental crust are shown in red on top of a "map of the world" from Maplands.com (2018). Dashed line extended across oceanic areas show links between the NAC cratonic fragments that are thought to have once comprised single cratonic blocks (Bleeker, 2003). The black shaded areas mark exposed Eoarchean crust with ages older than 3.5 Ga.

Key issues concerning Eoarchean mantle evolution and mantle-crust interaction are, for example, the timing and mixing history of late accreted material, crustal recycling into the mantle, or as to whether present day geodynamic processes were also already active in the Eoarchean e.g., (e.g., Condie and Benn, 2006; Bennett et al. 2007; Maier et al. 2009; Van Kranendonk 2011; Moyen and van Hunen 2012; Johnson et al. 2014; O'Neill and Debaille 2014; Touboul et al. 2014; Willbold et al. 2015; Rizo et al. 2016; Creech et al. 2017; Dale et al. 2017).

Earth´s core-mantle differentiation triggered extensive depletion of the highly siderophile elements (HSE: Os, Ir, Ru, Rh, Pt, Pd, Re, Au) in the mantle, but the HSE concentrations in the Earth´s mantle today are orders of magnitude higher than inferred from core formation models (e.g., Chou, 1978). Therefore, late accretion of chondritic material after Earth´s core formation has been advocated to explain the excess of HSE and the broadly condritic osmium isotope ratios in Earth´s mantle. Yet, when and how the accreted material was stirred into the mantle is still a highly debated issue.

Short-lived radioactive nuclides are ideal tools to constrain early differentiation processes of the main terrestrial reservoirs (Caro et al., 2003; Bennett et al. 2007; Touloule et al. 2014, Wilbold et al., 2015; Puchtel, et al., 2016; Rizo et al., 2016). For example the short-lived ^{182}Hf-^{182}W (half-life 9 Myr) system is sensitive to core formation as well to the admixing of HSE-rich (including W) late accreted material after core formation. Earth´s core formation result in enrichment of Hf (lithophile) and depletion in W in Earth´s mantle and thus in the increase of ^{182}W/^{184}W during the decay of ^{182}Hf. In contrast, late accretion of HSE-rich meteoritic material would lower the ^{182}W/^{184}W ratio of the mantle. Thus, mantle with no or incomplete admixing of late accreted material would be enriched in ^{182}W and strongly depleted in HSE concentrations in comparison to mantle to which a full complement of late accreted material was added (e.g, Willbold et al., 2011). Therefore, sluggish mixing of late accreted material into the Hadean and Eoarchean mantle and a HSE poor Eoarchean mantle were proposed based on resolvable excesses in ^{182}W in 3.8 – 3.7 Ga old rocks from the IGC (Greenland) and 4.0-3.6 Ga rocks from Acasta (Canada) in combination with apparently low HSE contents in Archean komatiites (Maier et al. 2009; Willbold et al., 2015, Dale et al. 2017).

In contrast, HSE abundance data on ultramafic Eoarchean rocks from the IGC in Greenland and Nuvvuagittug (Canada) appear to be similar to modern analogues and thus modern mantle-like HSE compositions for the mantle sources of these rocks were suggested (Szilas et al., 2015; Rizo et al., 2016; Touboul et al., 2014). Alternative, metal-silicate, or silicate-silicate differentiation in an early magma ocean, during the first 50 Ma of Solar System history, can generate ^{182}W heterogeneities (e.g., Touboule et al. 2012; Puchtel et al., 2016). The short-lived ^{142}Nd system is a useful tool to track early silicate differentiation events (e.g., Caro et al., 2003; Bennett et al., 2007; Rizo et al., 2016). Highly variable ^{142}Nd signatures in Archean rocks from the IGC were interpreted as evidence for early silicate differentiation processes. With respect to ^{142}Nd, the apparent decoupling of the ^{182}W and HSE concentrations in Archean rocks from the IGC were explained by models that invoke

substantial addition of late accretion material as well as early silicate differentiation (e.g., Bennett et al., 2007; Rizo et al., 2016).

However, none of those sample sets unambiguously included Eoarchean mantle rocks. In fact, most of the HSE abundance data were obtained from mantle derived magmatic rocks. Thus, direct information from ancient mantle rocks would offer more accurate constraints on early Earth´s mantle composition.

Modelling of Earth´s thermal history indicates larger abundance of heat-producing radiogenic isotopes in the Hadean and Archean mantle and a less differentiated mantle-crust system, which likely resulted in about 150-200 °C higher mantle temperatures in the Archean compared to the present value (e.g., Herzberg et al. 2010; Brown 2014). These conditions likely caused geodynamic processes that were different from those prevailing at present day (e.g., Bédard 2006; Kamber 2015). Commonly proposed geodynamic regimes for the Eoarchean involve stagnant lid tectonics and crustal recycling driven by delamination (e.g., Goodwin and Smith 1980; Bédard 2006; Johnson et al., 2014) or by episodic subduction events (e.g., Stern et al., 2004; Van Kranendonk 2011; Moyen and van Hunen 2012; O'Neill and Debaille 2014) (Fig. 1-2).

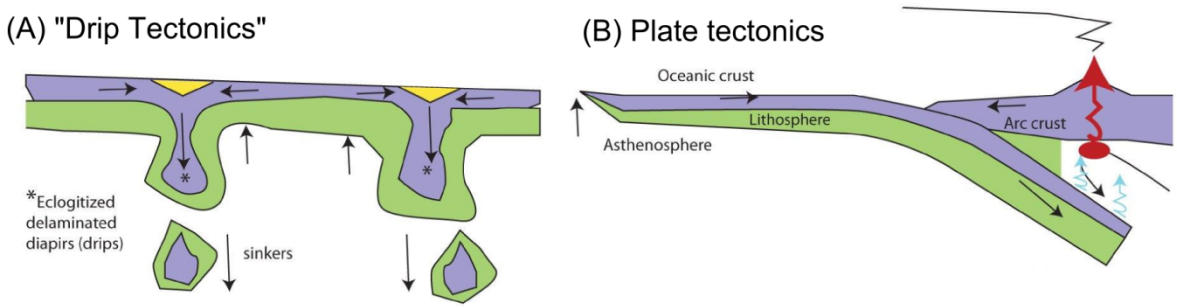

Figure 1-2: Cartoon illustrating the two main crustal recycling processes postulated for the Archean (after Stern 2013); (A) delamination of the lower part of a thickened mafic crust ("Drip Tectonics") and (B) subduction of an oceanic plate.

Many recent studies postulated the onset of modern style plate tectonics by the Meso- to Neoarchean (3.2 – 2.5 Ga; e.g., Dhuime et al., 2011; Shirey and Richardson, 2011; Van Kranendonk, 2011; Naeraa et al., 2012; Laurent et al., 2014). However, mafic and ultramafic rocks from Eoarchean terranes of the IGC (Polat et al. 2002, 2003, 2011; Polat and Hofmann 2003; Jenner et al. 2009; Hoffmann et al. 2011b) and Hadean/Eoarchean supracrustal enclaves of the Minto Block of the Superior Province, Canada (e.g., O'Neil et al., 2008; 2011; Turner et al., 2014; Caro et al., 2017) may resemble analogues of modern subduction zone assemblages (boninites, picrites, tholeiites, high-K basalts). Moreover, within the IGC

geochemical evidence for horizontal tectonics is supported by field observations (e.g., Nutman et al., 2007, 2013; Furnes et al., 2009).

Diagnostic signatures for a mantle overprint by a subduction-related re-enrichment agent are selective Nb-Ta depletion and enrichment of light-rare-earth-elements (LREE). Yet, similar trace element signatures can be caused by metasomatism. Therefore, careful sampling as well as chemical screening is necessary prior to interpreting such signatures obtained for ancient rocks. Trace element systematics of well-preserved boninite-like and island-arc tholeiite- and picrite-like rocks from the ISB of the IGC indicate the overprint of their mantle sources by fluid- and melt-like components that are subduction-related (Polat et al., 2002; Polat and Hofmann, 2003; Jenner et al., 2009; Hoffmann et al., 2011b).

For several of those well characterised mafic rocks from the ISB Hf-Nd isotope data and high-precision concentrations of high-field-strength-elements (HFSE) are now available (e.g., Polat et al. 2002; Hoffmann et al. 2010, 2011a, b). These combined investigations were done to improve constraints on their mantle sources, to check possible shallow level contaminations and to evaluate the possible disturbance of their Hf-Nd isotope systematics during metamorphism (Hoffman et al., 2010, 2011a, 2011b). Importantly, Lu-Hf isotope data as well as major and trace element systematics indicate extensive depletion of the mantle source of the boninite-like metabasalts and contamination of the basalts with an isotopically enriched crustal component during ascent (Hoffman et al., 2010, 2011a). Apparent decoupling of initial εHf and εNd values was found in TTGs and metabasalts from the IGC (e.g., Hoffmann et al. 2011a,b). Such a decoupling might be a source signature inherited by the metabasalts and the precursors of the TTGs and might therefore indicate a metasomatized depleted mantle source with a subduction-derived component (e.g., Jenner et al. 2009; Hoffmann et al. 2011b). Alternative models (e.g.,Rizo et al. 2011) suggests that the Hf-Nd decoupling is an ancient feature inherited from magma ocean cumulates.

Notably, most of the studies concerning Eoarchean mantle evolution mainly obtained indirect compositional information about Eoarchean mantle from metamorphosed basalts, magmatic crustal cumulates and komatiites that represent partial mantle melts and related crystallisation products. Any direct information from ancient mantle rocks would allow better constraints on key processes in the early mantle evolution. Such relicts of Eoarchean mantle were proposed to occur at several localities within the IGC (e.g., Nutman et al. 1996, 2002; Bennett et al. 2002; Friend et al. 2002; Friend and Nutman 2011; Ishikawa et al. 2017)as ultramafic enclaves. Minimum ages of up to > 3.8 Ga are constrained for these localities by U-Pb zircon geochronology of the surrounding TTGs and Ameralik dykes that locally intrude

the ultramafic bodies (e.g., Nutman et al., 1996; Friend et al., 2002; Amelin et al., 2010). Hence, these ultramafic enclaves potentially represent the oldest remnants of Earth´s mantle found so far. However, their mantle origin has been controversially discussed (e.g., Dymek et al., 1988; Nutman et al., 1996, 2002; Bennett et al., 2002; Friend et al., 2002; Rollinson, 2007; Szilas et al., 2015).

In order to directly address some of the important issues in Earth´s earliest history a new sample set was collected in southern west Greenland, covering different ultramafic-mafic assemblages. The samples also include ultramafic rocks of potential mantle origin and associated mafic rocks from three distinct locations within the IGC. The aim of this study is to contribute to still highly debated issues concerning the composition and evolution of the Eoarchean mantle.

The Lu-Hf isotope system behaves covariant to the Sm–Nd isotope system during mantle melting, where Hf and Nd (daughter isotopes: ^{143}Nd and ^{176}Hf) are more incompatible than Lu and Sm (mother isotopes: ^{176}Lu and ^{147}Sm). In contrast to the Lu-Hf and Sm-Nd isotope systems, Rb (mother isotope: ^{87}Rb) is highly incompatible during partial melting of the mantle and Sr is more compatible. Hence, mantle melting leading to lower Lu/Hf, Sm/Nd and higher Rb/Sr ratios in the melt than in the residual solid. Therefore, the radionuclide systems such as Lu–Hf, Sm–Nd and Rb–Sr isotope systems have been used to track the differentiation history of Earth's mantle–crust system (e.g., Moorbath et al., 1977; Patchett and Tatsumoto, 1981, 1983; Jacobsen, 1988; Collerson et al., 1991; Bennett et al., 1993; Bowring and Housh, 1995; Vervoort and Blichert-Toft 1999).

The platinum group elements (PGE) are HSEs and behave rather robustly during alteration and metamorphism (Barnes et al., 1985). Thus, PGE abundances in peridotites can provide constraints on mixing history of the late accreted material that supplied HSE to the Earth's mantle after core segregation. Furthermore, the PGE signatures in peridotites are useful indicators to distinguish between mantle rocks and crustal cumulates, as the PPGE (Pt and Pd) partition into the extracted melt due to their moderately incompatible behaviour at high degrees of melting (e.g., Mungall and Brenan, 2014; Becker and Dale, 2016). The residual mantle peridotites contain high contents of IPGE (Os, Ir, Ru), whereas magmas and their cumulates have fractionated patterns with low IPGE and high PPGE levels (Fig. 1-3).

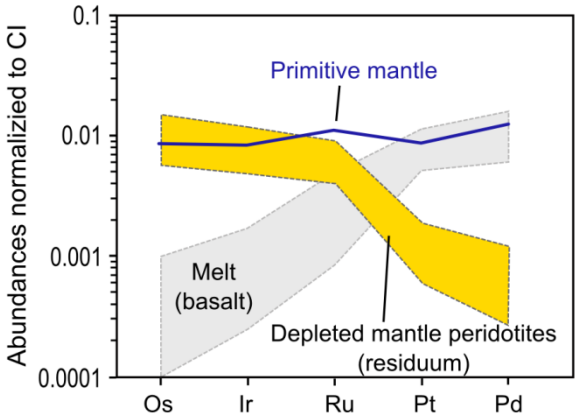

Figure 1-3: The schematic sketch illustrates the different fractionated chondritic (CI) normalized platinum group patterns of residual mantle peridotites and melt (basalt) (after Becher et al. 2006, Dale et al., 2008 and Walker, 2016). The unfractionated chondritic (CI) normalized platinum group pattern of primitive mantle is shown for comparison. Primitive mantle values are from Becker et al. (2006) and chondritic values from Fischer-Gödde (2010).

To get robust insights into the trace element and isotope composition of the studied samples, diverse geochemical methods have been applied. Major and trace element compositions were obtained for the mafic and ultramafic samples. Further measurements were done on radiogenic isotope systems (Lu-Hf, Sm-Nd and Rb-Sr), high–precision high–field–strength–elements (HFSE) and platinum group element (PGE) measurements by isotope dilution. Moreover, Lu-Hf, Sm-Nd and Rb-Sr concentration and isotope data were obtained for mineral separates of four selected peridotite sample.

The focus of this study is on the petrology as well as the geochemical and isotopic characteristics of the peridotites in order to address several important topics:

- Origin of the ultramafic rocks (mantle versus crustal cumulate origin)
- Trace element and isotope characteristics (Lu-Hf, Sm-Nd, Rb-Sr, Re-Os) of the Eoarchean mantle rocks
- Similarities and differences in the chemical composition of Eoarchean upper mantle in comparison to modern mantle rocks
- Timing and mixing history of late accreted material
- The effect of crustal recycling on the petrogenesis of the mantle rocks
- Elucidating, as to whether present day geodynamic processes were also active during the Eoarchean
- Potential petrogenetic relationship between the mantle rocks and the associated metabasalts
- The effects of subsequent metamorphism and metasomatism on the geochemical compositions of the ultramafic rocks

This study provides new petrological observations and for the first time combined comprehensive major and trace element data for Eoarchean ultramafic rocks from the SOISB and for the first time for the NUB and Akilia Island. Moreover, this study includes for the first time combined Lu-Hf, Sm-Nd and Rb-Sr abundances and isotope compositions of olivine, orthopyroxene and amphibole separates of selected peridotites from SOISB and NUB.

1-2 GEOLOGICAL OVERVIEW

1-2.1 The Itsaq Gneiss Complex (IGC)

With >3000 km^2 the 3.9 - 3.6 Ga old IGC of southern West Greenland comprises the largest preserved unit of Eoarchean continental crust, predominantly being of tonalitic-trondhjemitic-granodioritic (TTG) composition (Fig. 1-4; e.g., Nutman et al. 1996). Several supracrustal units, including the Isua Supracrustal Belt (ISB), and numerous smaller occurrences of peridotitic enclaves (e.g., Friend et al., 2002) and remnants of layered ultramafic-mafic complexes (e.g., Appel et al. 2001) are intruded by and tectonically intercalated with TTG grey gneisses. The supracrustal rocks include sequences of amphibolites, serpentinites, garnet-mica schists, chemical sediments and carbonates. At low strain zone localities, supracrustal rocks locally preserve primary magmatic and sedimentary textures (e.g., Nutman et al. 1984, 2009b). The IGC is made up of two terranes, the Færingehavn and the Isukasia terrane, each have distinct tectono-thermal histories and were juxtaposed together and with younger terranes during the Meso- to Neoarchean (e.g., Griffin et al. 1980; Nutman et al. 2000, 2002; Friend and Nutman 2005; Nutman and Friend 2007; Dziggel et al. 2014). Superimposed metamorphic events recognised throughout the IGC mainly occurred from 3.65 to 3.55 Ga and from 2.82 to 2.55 Ga (e.g., Frei and Rosing 2001; Frei et al. 2002; Nutman et al. 2002; Rollinson et al. 2002; Nutman and Friend 2007; Polat et al. 2015). For the Isukasia terrane, U–Pb geochronology records important tectono-thermal events at ca. 2960 Ma, whereas the Færingehavn terrane appears to be devoid of a ca. 2960 Ma metamorphic overprints (e.g., Nutman and Friend, 2005). The Eoarchaean Færingehavn terrane underwent polybaric high temperature metamorphism between 2.72 and 2.71 Ga, apparently followed by rapid exhumation (Nutman and Friend 2007; Dziggel et al. 2014).

Field observations, structural, geochronological and geochemical data obtained for the IGC over the last 20 years supported tectono-metamorphic interpretations where the Archean craton of West Greenland grew at convergent plate margins during Eoarchean to Neoarchean times (e.g., Friend et al. 2002; Hanmer et al. 2002; Hanmer and Greene 2002; Nutman et al. 2009a; Naeraa et al. 2012; Dziggel et al. 2014; Komiya et al. 2015; Polat et al. 2015; Dziggel

et al. 2017). The structural characteristics of the terrane boundaries are largely consistent with horizontal tectonics, similar to modern style tectonics (e.g., Nutman et al., 2013). This is in good agreement with geochemical data from Eoarchean mafic rocks throughout the IGC that show similarities to modern subduction suite related rocks (e.g., Polat et al., 2002; Polat et al., 2003; Polat and Hofmann, 2003; Jenner et al., 2009; Hoffmann et al., 2010; Hoffmann et al., 2011b; Szilas et al., 2015). For example, Eoarchean mafic rocks of the ISB that have been characterised as tholeiitic and boninitic metabasalts and metagabbros, show geochemical similarities to modern subduction-related rock suites. (e.g., Polat et al., 2002, 2003; Polat and Hofmann, 2003; Jenner et al., 2009; Hoffmann et al., 2010, 2011a). Moreover, field observations indicate similarities of some ultramafic units with obducted sequences of oceanic abyssal peridotites at convergent plate margins. Thus, according to recent studies, several ultramafic enclaves (including the studied locations) were likely formed at convergent plate boundaries, as do supra-subduction zone ophiolites in more recent times (e.g., Friend et al., 2002; Nutman et al. 2007, 2013; Polat et al. 2015).

Generally, in the ICG ultramafic rocks occur as part of supracrustal belts or separate enclaves tectonically intercalated in ca. 3.8 Ga tonalitic gneisses (Nutman et al., 1996; Friend et al., 2002). The ultramafic enclaves are often embedded together with amphibolites and smaller outcrops of cherts that may represent chemical sediments (e.g., Friend and Nutman, 2010). Most of the peridotites are strongly altered, except for low strain zones where extremely well preserved peridotites can be found in the central parts of enclaves that can be up to several hundred meters in diameter. Massive dunitic and harzburgitic rocks can be distinguished from layered, cumulate ultramafic to leuco-gabbroic rocks, chemical sediments and other supracrustal amphibolites (Friend et al., 2002).

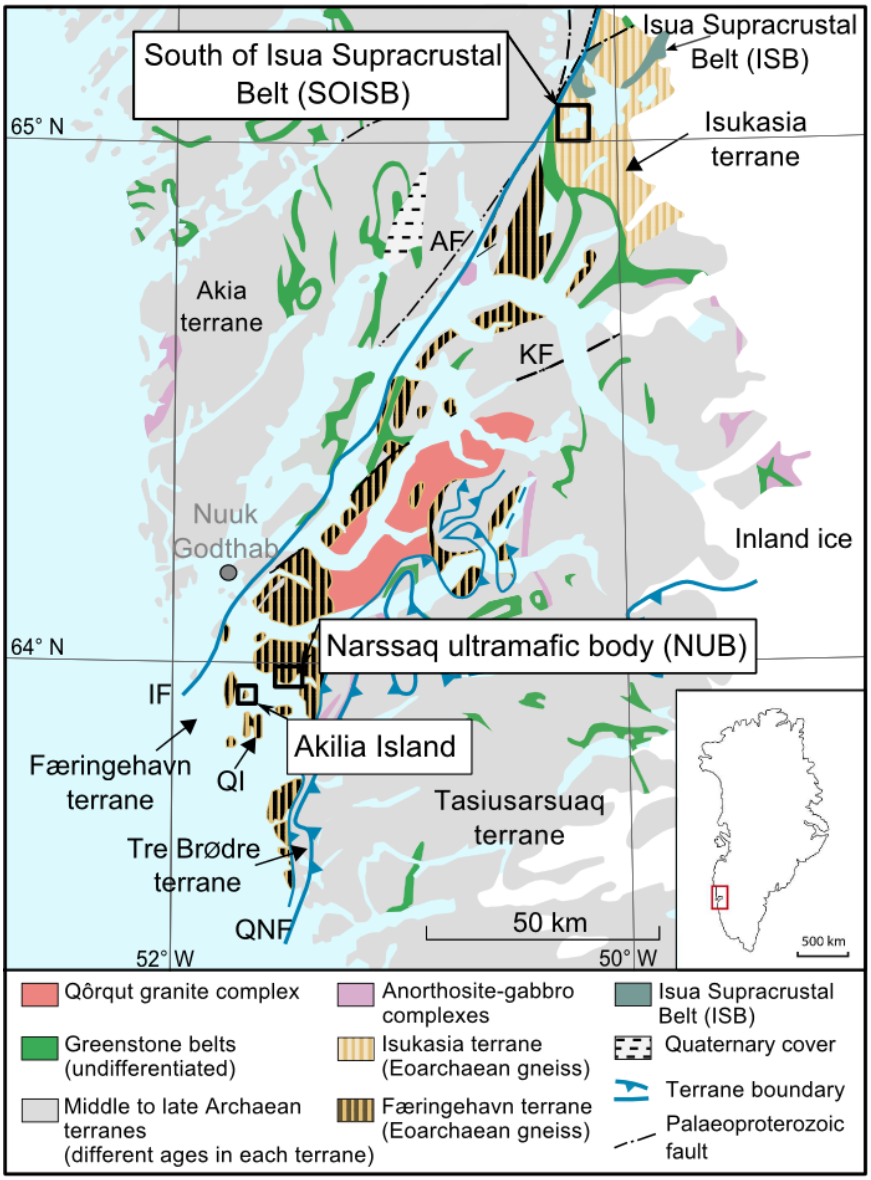

Figure 1-4: Map of southern West Greenland, showing the Itsaq Gneiss Complex. The sample localities SOISB, NUB and Akilia Island are marked. Map modified after Naeraa et al. (2012). AF, Ataneq fault; IF, Ivinnguit fault; KF, Kobbefjord fault; QI Qilanngaarsuit island; QNF, Qualiit Nunaat thrust.

1-2.2 Occurrences of potential mantle peridotites in the Itsaq Gneiss Complex

At two localities in low strain regions in the Isuakasia terrane, possible mantle rocks are exposed as ultramafic lenses in the 3.8–3.7 Ga Isua supracrustal belt (ISB) (e.g., Friend and Nutman, 2011) and in peridotite bodies older than 3.8 Ga from SOISB (Bennett et al., 2002; Friend et al., 2002). In the Færingehavn terrane, proposed Eoarchean mantle rocks are exposed in the Narssaq ultramafic body (Nutman et al., 2007; Fig. 1-4). Moreover, ultramafic lenses on islands south of Ameralik, including Akilia Island and Qilanngaarsuit Island, have been tentatively suggested to represent remnants of Eoarchaean mantle rocks (e.g., Nutman et al. 2002).

In the ISB, some peridotite bodies were considered to represent Eoarchean abyssal peridotites that were accreted and dismembered in an Eoarchean convergent plate margin setting (e.g., Friend et al., 2002; Friend and Nutman, 2011) or, alternatively, ultramafic cumulates (e.g., Dymek et al., 1988; Friend and Nutman, 2011). A study of PGE abundances in ultramafic bodies in the ISB (Szilas et al., 2015) argued that many of these rocks represent ultramafic cumulates of the ISB metabasalts and not mantle rocks, as evident from IPGE depleted chondritic normalized PGE pattern.

About 15 km south of the ISB (SOISB), up to several hundred meter-sized ultramafic enclaves of possible mantle origin are exposed (Friend et al., 2002; Nutman et al., 2007). Most of them escaped complete recrystallization at amphibolite facies conditions and especially the cores of such ultramafic bodies are sometimes extraordinarily well preserved. The SOISB peridotites were assembled with mafic rocks and ocean-floor sediments already by about 3.8 Ga, when the ca. 3.8 Ga IGC tonalites intruded (Nutman et al., 1996; Friend et al., 2002). For this region, major element, olivine, and spinel compositions as well as Re-Os isotope data of peridotites were used to argue in favour of the preservation of Eoarchean mantle tectonites (Bennett et al., 2002; Friend et al., 2002). Moreover, the olivines from SOISB peridotites and the adjacent Ujaragssuit layered body display mantle-like $\delta^{18}O$ values (Lowry et al., 2003; Hiess et al., 2009). Minimum ages of the SOISB peridotite localities are constrained by U-Pb zircon geochronology of the surrounding TTGs and mafic dykes that locally intrude the ultramafic bodies, yielding Eoarchean ages between ca. 3.79 and 3.81 Ga (e.g., Friend et al. 2002; Amelin et al. 2010). Moreover, in the >3.81 Ga Ujargssuit Nunât layered intrusion to the east of the studied SOISB locality, Pt-Os model ages even as old as 4.36 Ga were reported (Coggon et al., 2013), but it is ambiguous if these localities remained undisturbed and if they directly relate to the peridotites studied here.

The ultramafic body at Narssaq peninsula (the Narssaq ultramafic body, NUB), ~25 km southeast of Nuuk, comprises harzburgites and dunites, enclosed by trondhjemitic-tonalitic-granodioritic gneisses that are older than 3.8 Ga. Large parts of the Narssaq ultramafic body are highly deformed and altered, showing, e.g., interaction of younger pegmatites with the ultramafic rock assemblages. However, some parts, especially at the northern end of the body, are well preserved (Nutman et al. 2007a, b). Referring to unpublished data, Nutman et al. (2007a) stated that dunites from the north of the Narssaq ultramafic body have chemical characteristics of strongly depleted upper mantle peridotites.

Nutman et al. 2002 suggested that some of the peridotite lenses from islands south of Ameralik (e.g. Qilanngaarsuit and Akilia Island), might be remnants of Archaean upper

mantle rocks, and were trapped into the crust during its accretion and growth. The potential mantle peridotites exposed on Qilanngaarsuit underwent early Archaean granulite facies metamorphism and in situ migmatization (Nutman et al., 2002). Thus, their mantle origin is questionable. Akilia Island consists mainly of 3.64 to 3.63 and 3.85 to 3.60 Ga old Archaean gneisses (e.g., Nutman et al. 2002). Embedded in the gneisses are small enclaves of supracrustal rocks, comprising amphibolites and occasionally ultramafic rocks and chemical sediments. However, previous studies have documented a complex, polyphase, tectono-metamorphic history for the Akilia Island rocks. Early Archean granulite facies metamorphism at about 3.60 Ga was followed by probably multiple episodes of late Archaean amphibolite facies metamorphism from ~2.83 to 2.70 Ga (e.g., Griffin et al., 1980; Myers and Crowley, 2000; Nutman et al., 1996b, 2002; Whitehouse et al., 2009). Thus, age constraints on mafic and ultramafic rocks based on field relationships are difficult to obtain and are often controversial (e.g. McGregor and Mason, 1977; Myers and Crowley, 2000; Nutman et al., 1996b, 2000, 2002a; Whitehouse and Kamber, 2005).

The samples investigated in this study comprise mafic and ultramafic rocks from one area located around lake 682 in the Isukasia terrane (SOISB) and two localities located in the Færingehavn terrane (NUB and Akilia Island) (Fig. 1-4).

1-3 OUTLINE OF THIS STUDY

This thesis gives a detailed petrographic description and chemical characterization of mafic and ultramafic rocks from the IGC. The focus of this study is on the chemical and isotopic compositions of the peridotites in context with early Earth differentiation and the Eoarchean mantle evolution. **Chapter 2** introduces the sample locations and provides a detailed sample description. Based on their microstructures and compositions, the peridotites are further subdivided into four different types. **Chapter 3** outlines the sample preparation and chemical separation methods as well as the geochemical methodology that was used to obtain the data presented in this study. The analytical methods applied include electron microprobe, XRF, N-TIMS, ICP-MS and MC-ICP-MS analyses. **Chapter 4** focuses on the PGE and Re inventory of 11 selected peridotites from SOISB and NUB. The PGE and Os isotope compositions were analyzed to provide new constraints on the origin of the peridotites and the timing and mixing history of the late accreted material that supplied highly siderophile elements to the Earth's mantle after core segregation. The findings confirm that the sample set indeed includes Earth´s oldest mantle peridotites found so far. Moreover, major element and PGE concentrations obtained for these mantle peridotites can be shown to be indistinguishable from Phanerozoic upper mantle rocks. Hence, the peridotites show clear evidence for the

presence of the entire inventory of late accreted material by ca. 3.8 Ga. **Chapter 5** presents the trace element compositions of the peridotites and amphibolites from SOISB and NUB. Based on a simple evolution-model for the mantle rocks investigated, we suggest that Earth's oldest mantle peridotites may have originated in a supra-subduction zone setting. Furthermore, whole rock Lu-Hf age regression lines mainly yield Eoarchean ages (~3.9 - 3.8 Ga), in agreement with minimum ages of ≥ 3.8 Ga, as inferred from dated crosscutting tonalite sheets. For the ^{147}Sm-^{143}Nd isotope system, no accurate age constraint is possible, due to lack of sufficient spread or too large scatter on the regression lines. Hence, open system behaviour during the Archean tectono-thermal events has significantly affected the Sm-Nd inventory of some peridotites. **Chapter 6** focuses on the chemical compositions of olivines, orthopyroxenes, amphiboles and spinels in the peridotites. Major and minor element compositions provide important information to distinguish between a mantle-, magmatic- or metamorphic origin of the minerals. These major and minor element abundances combined with Hf-Nd-Sr isotope data for olivine, orthopyroxene and amphibole separates allow a profound assessment of the metamorphic overprint and subsequent trace element mobility. The findings support previous conclusions that the Lu-Hf isotope system was less disturbed than the Sm-Nd and Rb-Sr systems by Neoarchean to Paleoproterozoic tectonothermal metamorphic events. The Lu, Hf, Sm, Nd, Rb and Sr abundances in olivine, orthopyroxene and amphibole separates of four peridotites confirm that amphibole is the main host for those elements, except for Rb, in the investigated peridotites. **Chapter 7** discusses the chemical compositions of the four peridotites from Akilia Island and compares them to the chemical characteristics of the peridotites from SOISB and NUB. Two of the Akilia Island peridotites are metaperidotites and differ from the SOISB and NUB peridotites. Their mineralogy and chemical composition indicates extensive metamorphic and metasomatic overprint. The other two Akilia Island peridotites show similarities to some SOISB and NUB peridotites. Yet, their major and mineral compositions are inconsistent with a mantle origin.

Chapter 2

Sample locations and petrography

2-1 INTRODUCTION

The sample set comprises 26 peridotites from SOISB (n=15), NUB (n=7) and Akilia Island (n=4), and seven amphibolites from SOISB (n=6) and NUB (n=1). The samples were collected by Carsten Münker and Elis Hoffmann in the 2010 field campaign in collaboration with Prof. Minik Rosing (Natural History Museum of Denmark and Greenland, Copenhagen). The sample set include three sample-subsets (10-05, 10-12, 10-20, 10-29), comprising each two samples from the same outcrop that were taken about 2 to 15 m apart from each other.

In all three localities ultramafic bodies or lenses occur that were postulated to represent well preserved remanences of Eoarchean mantle (SOISB) or were regarded as potential remanences of Eoarchean mantle rocks (NUB and Akilia Island). Most of the peridotites from SOISB, NUB and Akilia Island originate from such previously described outcrops or from nearby outcrops. In addition, the sample set include samples from ultramafic enclaves that show macroscopic textual evidence for a crustal cumulate origin, such as cumulate texture at outcrop scale. The peridotites investigated in this study show variable extent of secondary alteration, such as serpentinisation.

The investigated ultramafic samples are all spinel-peridotites and comprise three dunites (>90% olivine), 22 hornblende-bearing peridotites and four meta-peridotites. Note that we use the term hornblende-bearing peridotites (hbl-bearing peridotites) for hornblende-bearing ultramafic rocks with harzburgitic or lherzolitic normative composition that contain between 40-90% olivine and ≥ 5% amphibole, in order to distinguish them from dunites and meta-peridotites. The primary harzburgitic and lherzolitic mineralogy of the hbl-bearing peridotites has been modified to variable extent by secondary alteration, resulting in amphibole replacing or overgrowing pyroxene and olivine. In general, the hbl-bearing peridotites are dominated by olivine with variable contents of orthopyroxene, amphibole, spinel and occasionally serpentine. Other minerals, such as chlorite, mica, sulphides and carbonate also occur in low amounts. Clinopyroxene is absent except in one sample (10-34).

Table 2-1: Mineralogy of the peridotites this study

Location	Sample	Rock	Type	Olivine	Amphibole	Spinel*	Pyroxene	Others**
SOISB1								
	10-22	dunit	1	x	x	x	opx	chl, srp
	10-23	dunit	1	x	x	x	opx	chl, srp
	10-20C	hbl-P*	1	x	x	x	opx	chl, srp
	10-20A	hbl-P*	1	x	x	x	opx	chl, srp, sulphides
SOISB2								
	10-34	hbl-P	1	x	x	x	opx, cpx	carbonate, mica
	10-36	hbl-P	1	x	x	x	opx	mica
	10-29A	hbl-P*	2	x	x	x	opx	chl
	10-29B	hbl-P	2	x	x	x	opx	chl, mica, sulphides
	10-30	hbl-P*	2	x	x	x	opx	chl, Ilmenite, mica
	10-32	hbl-P	2	x	x	x	opx	chl, mica
	10-31	hbl-P	2	x	x	x	opx	mica
	10-35	meta-P	4	x	x	x	opx	
SOISB3								
	10-27	hbl-P	3	x	x	x	opx	
	10-28	hbl-P	3	x	x	x	opx	
	10-16	hbl-P	2	x	x	x	opx	carbonate
NUB								
	10-11	dunit	1	x	x	x	opx	chl, srp
	10-09	hbl-P*	1	x	x	x	opx	chl, srp
	10-10	hbl-P*	1	x	x	x	opx	chl, srp, mica
	10-12B	hbl-P	1	x	x	x	opx	chl, srp
	10-14	hbl-P	1	x	x	x	opx	chl, srp
	10-13	hbl-P	2	x	x	x.		chl, srp
	10-12A	meta-P	4	x	x	x	opx	mica
Akilia Island								
	10-05	hbl-P	2	x	x	x	cpx	chl
	10-04	meta-P	4	x	x	x	opx	chl, mica
	10-06	meta-P	4	x	x	x		chl, mica

Opx: orthopyroxene; cpx: clinopyroxene, chl: chlorite; srp: serpentine; hbl-P: hornblende-bearing peridotite; hbl-P* hornblende-bearing harzburgite with ol >70%; ** between 1 and 5 vol.% or grains ≥ 0.5 mm.

Based on their microstructure and composition, the peridotites are further subdivided into four types. The type 1 peridotites (n=11) display coarse-grained microstructure and comprise three dunites and nine hbl-bearing peridotites. The type 2 peridotites (n=9) are hbl-bearing peridotites that have generally heterogeneous grain sizes, dominated by either a coarse-to-medium, or medium-to-fine-grained microstructure. These rocks show variable degrees of recrystallization. The type 3 peridotites (n=2) are characterized by large orthopyroxene-poikiloblasts in a fine- to medium-grained matrix composed mainly of olivine, orthopyroxene and amphibole. The lithology of the type 4 peridotites comprises different meta-peridotites: one strongly hydrated hbl-peridotite from NUB (10-12A), one completely recrystallized peridotite from SOISB (10-35), and two from Akilia Island (10-04, 10-05).

2-2 SOUTH OF THE ISUA SUPRACRUSTAL BELT (SOISB)

The SOISB peridotite samples (n=15) originate from several up to hundred meter-sized ultramafic enclaves (Fig. 2-1). Most of them escaped complete recrystallization at amphibolite facies metamorphic conditions and especially the cores of these ultramafic bodies are occasionally extraordinary well preserved. The peridotite exposures south and southeast of Lake 682 and also a number of representative samples from those ultramafic enclaves were described in detail by Friend et al. (2002) and Bennett et al. (2002). Minimum ages of the peridotite enclaves are constraint by U-Pb zircon geochronology of the surrounding TTGs and mafic dykes that locally intrude the ultramafic bodies, yielding Eoarchean ages between ca. 3.79 and 3.81 Ga (e.g., Friend et al., 2002; Amelin et al., 2010). The peridotite enclaves are often embedded in the ca. 3.8 Ga tonalitic gneisses, together with amphibolites and smaller outcrops of cherts that may represent chemical sediments (Fig. 2-1) (Friend et al. 2002).

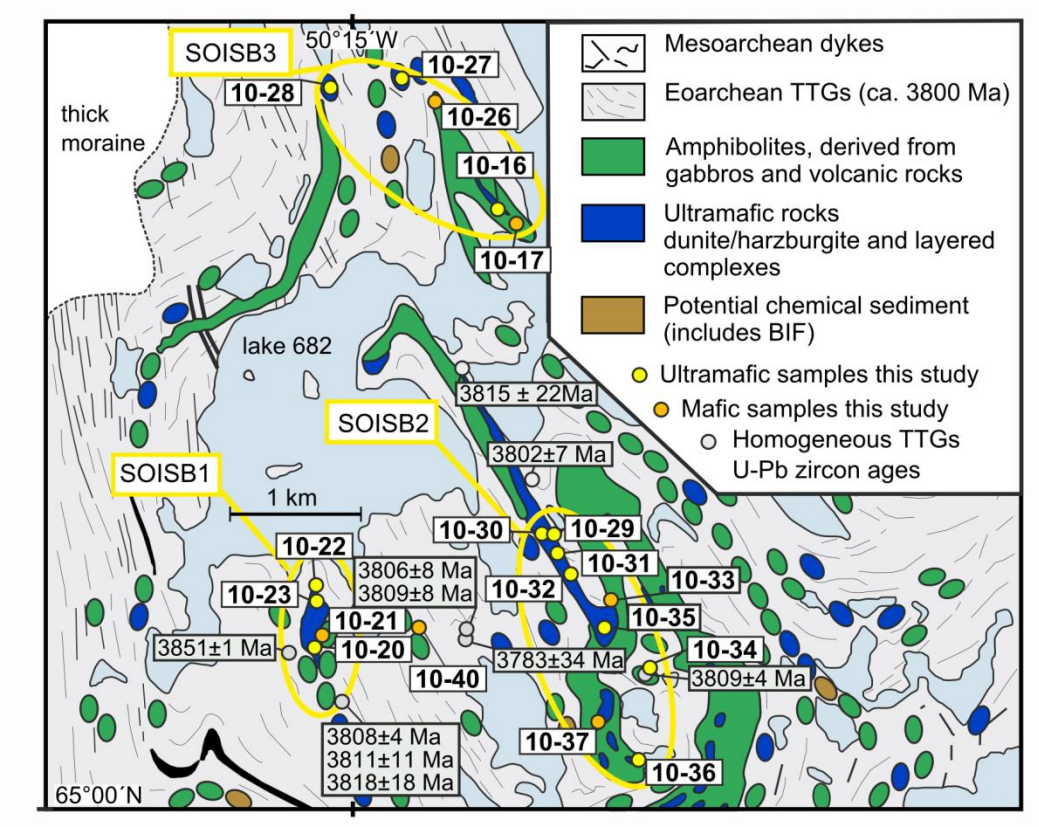

Figure 2-1: Simplified map of the region south of Isua Supracrustal Belt (SOISB) after Nutman et al. (2009). Age data are compiled from Nutman et al. (1996; 1999; 2007, 2009) and Amelin et al. (2010) and Sample numbers in the map refer to sample localities of this study.

Hence, the peridotites were already associated with mafic rocks and ocean floor sediments by ca. 3.8 Ga, when the IGC tonalites intruded at mid-crustal levels (Nutman et al. 1996; Friend et al. 2002). In this study, the SOISB locality is further subdivided in three geographic domains, namely SOISB1-3 (Fig. 2-1).

In addition to the peridotites, six amphibolites from SOISB were investigated in this study: one from locality SOISB1, two each from SOISB2 and SOISB3, and one intercalated in the TTGs between SOISB1 and SOISB2 (Fig. 2-1).

2-2.1 Peridotites from SOISB1

The four type 1 peridotites from SOISB1 comprise two massive dunites and two massive hbl-bearing harzburgites, which are from a single ultramafic enclave previously described by Friend et al. (2002). The peridotites are associated with metagabbros and layered ultramafic rocks, with an abrupt contact between the metagabbros and ultramafic units.

The coarse-grained dunites (10-22 and 10-23) (Fig. 2-2) are characterized by inclusion-rich olivine crystals up 5 mm in size, minor amphibole crystals up to 2 mm and abundant opaque phases. The latter occur either at grain boundaries or as inclusions in olivines and amphiboles. The amount of orthopyroxene and secondary phases like chlorite is less than 3 vol%. The two hbl-bearing harzburgites (10-20 and 10-20C) were collected about 15 meters apart from each other from the southern part of the ultramafic enclave. They are crosscut by fine veins of serpentine and occasionally chlorite. Amphibole occurs as single grains overgrowing olivine crystals or as large patches of irregular formed amphibole grains.

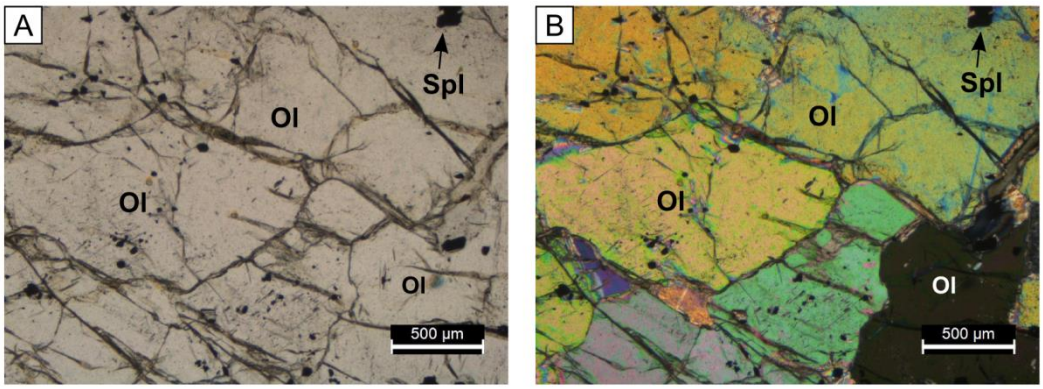

Figure 2-2: Microphotographs illustrating type 1 peridotite coarse-grained microstructure, dunite (10-23); (A) Microphotograph is in plane-polarised light and (B) cross polarised light. Ol: oivine; spl: Spinel.

2-2.2 Peridotites from SOISB2

The samples from SOISB2 comprise eight massive hbl-bearing peridotites, two type 1 peridotites (10-34 and 10-36), five type 2 peridotites (10-29A, 10-29B, 10-30, 10-31, 10-32), and one type 4 meta-peridotite (10-35). The type 2 peridotites and the type 4 peridotite are

from ultramafic pots embedded in a several km long mafic-ultramafic unit (Fig. 2-1). The two type 1 hbl-bearing peridotites are from two smaller isolated lenses that are located slightly southerly of this large mafic-ultramafic unit (Fig. 2-1). The two type 2 peridotites of the sample subset 10-29 were collected within a distance of ca. 5 m apart from each other. Ameralik dykes crosscut the ultramafic bodies near the outcrops 10-32 and 10-34 and one dyke penetrate the contact between Gneiss and the ultramafic body sampled by type 2 peridotite 10-30. Layering structures were observed in the outcrops 10-31, 10-32 and 10-35.

The two type 1 peridotites are characterised by a groundmass that is dominated by coarse-grained olivine minerals (grain sizes up to 5 mm), minor amounts of pyroxenes, amphiboles, and spinels and intermitted by mostly elongated patches of mainly amphibole. The samples contain a few percent of secondary phases like mica and chlorite, whereby chlorite occurs together with aggregates of spinel, especially in the amphibole-patches. Orthopyroxenes are more abounded in type 1 peridotite 10-36 than in the other type 1 and type 2 peridotites from SOISB. The type 1 peridotite 10-34 differs from other type 1 peridotites because it contains additionally small amounts of clinopyroxene and carbonate. Moreover, some olivine and pyroxene minerals are clearly altered and overgrown by mica and/or fibrous amphibole.

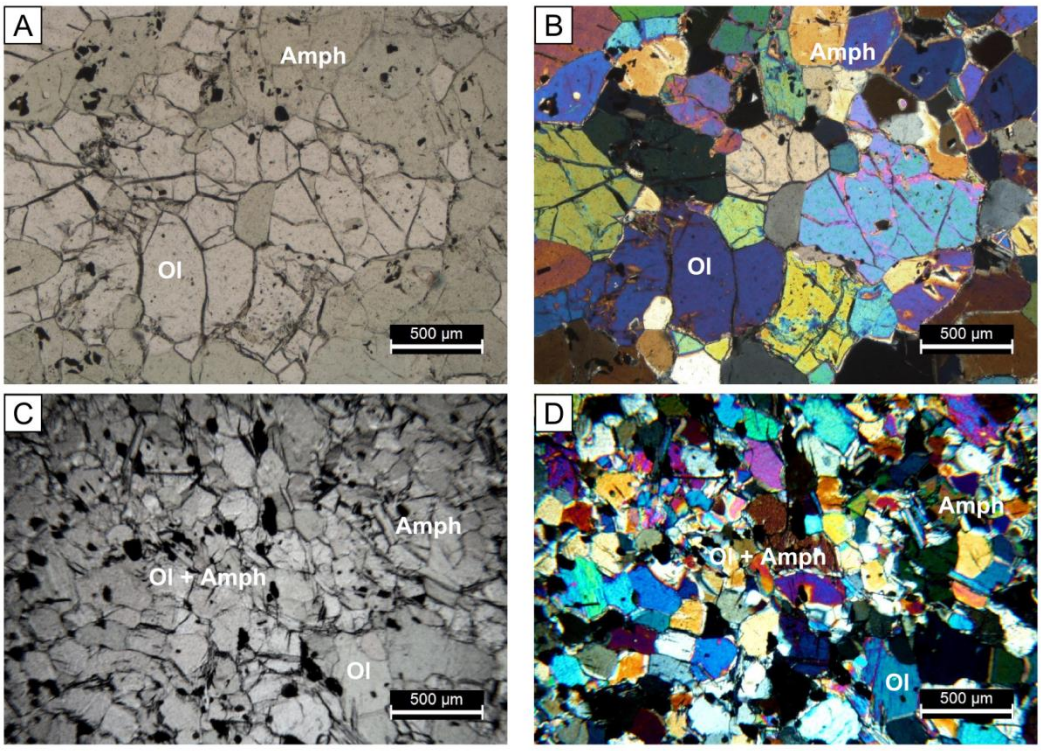

Figure 2-3: Microphotographs illustrate the different type 2 peridotite microstructures, (A-B) show an example for a partially re-crystallized type 2 peridotite (SOISB2 sample 10-29B) with a coarse-to-medium grained microstructure and (C-D) for a fine-grained type 2 peridotite (SOISB2 sample 10-31). Microphotographs are in plane-polarised light (A and CD) and in cross polarised light (B and D). Ol: olivine, Amp: amphibole

The type 2 peridotites 10-29A and 10-29B were collected within a distance of ca. 5m. These samples have heterogeneous grain-textures and grain sizes of olivine and amphibole minerals vary from <1mm up to several mm. The other three type 2 peridotites from SOISB2 display medium- to fine-grained microstructures.

Only the type 4 peridotite sample 10-35 has a granoblastic texture with abundant equilibrated 120° triple junctions between olivine grains and with equal orientations of elongated olivine and amphibole crystals.

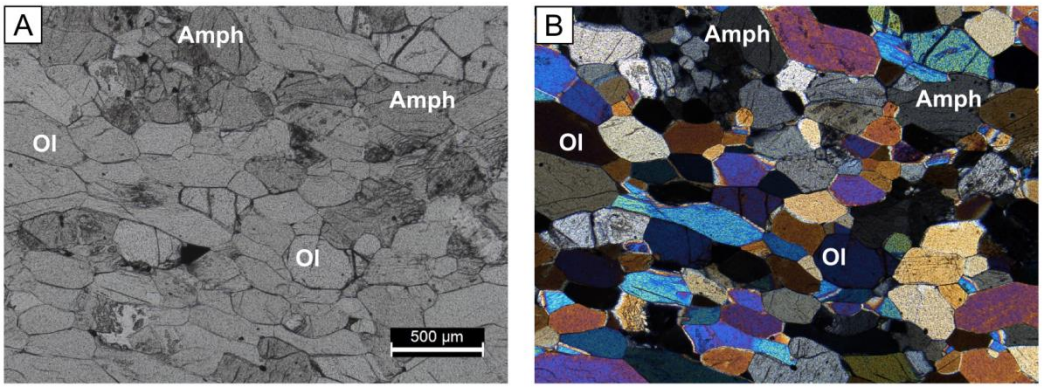

Figure 2-4: Microphotographs illustrate the microstructure of type 4 peridotites 10-35 with equal orientations of elongated olivine and amphibole crystals. Microphotographs are in plane-polarised light (A) and in cross polarised light (B). Ol: olivine, Amp: amphibole.

2-2.3 Peridotites from SOISB3

Location SOISB3 comprises the outcrops north of the lake 682 (Fig. 2a) and thus, one type 2 (10-16) and two type 3 hbl-bearing peridotites (10-27 and 10-28). The two type 3 peridotites are from small outcrops that display cumulated textures (Fig. 2-5). They are characterized by large orthopyroxene-poikiloblasts in a fine- to medium-grained matrix consisting of olivines, orthopyroxenes, amphiboles, oxides and few amounts of chlorite (Fig. 2-6). The orthopyroxene-poikiloblasts are rich in olivine, spinel, and amphibole inclusions. The SOISB3 type 2 peridotite is from a small ultramafic lens that is embedded in amphibolites (Fig. 2-1). The microstructure of this sample is similar to the fine-grained type 2 peridotites from SOISB2

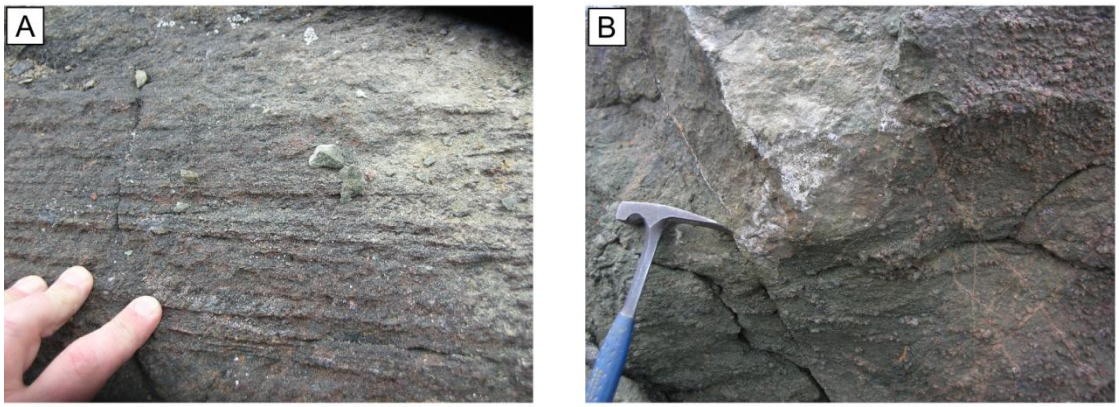

Figure 2-5: Field photographs illustrate macroscopic textures at SOISB3 sample locations, (A) 10-27 (B) 10-28.

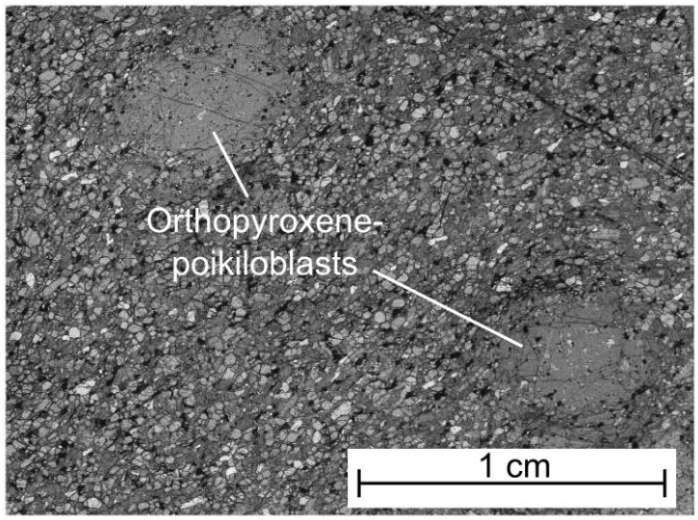

Figure 2-6: Thin section scan of type 3 peridotite 10-27 with orthopyroxene-poikiloblasts in a fine- to medium-grained matrix consisting of olivines, orthopyroxenes, amphiboles, oxides, and few amounts of chlorite.

2-2.4 Amphibolites from SOISB

Six amphibolites from SOISB were investigated in this study comprising one from locality SOISB1, two each from SOISB2 and SOISB3 and one intercalated in the TTGs between SOISB1 and SOISB2. The amphibolites contain mainly amphibole, plagioclase, minor quartz with variable amounts of mica and opaque phases. Generally, amphiboles grains are poor in inclusions, except for the large amphiboles in sample 10-17 (SOISB3). The sample 10-33 (SOISB2) contains additional garnet, which occurs as large poikoblastic grains as well as small grains of ≤ 50 µm in diameter.

2-3 NARSSAQ ULTRAMAFIC BODY (NUB)

Sven massive spinel-peridotites and one amphibolite investigated in this study originate from the NUB. The NUB is a ca. 1 km long body of ultramafic rocks associated with metagabbros, siliceous rocks, and amphibolites that are enclosed by polyphase TTGs (Fig. 2-7) and were previously described by Nutman et al. (2007b). Most of the ultramafic rocks are highly deformed and altered, and locally pervaded by discordant veins of coarse-grained phlogopite as well as fibrous amphibole. Those veins presumably formed by metasomatism in context with the emplacement of nearby granite bodies (Fig. 2-7), which are part of the ~2.56 Ga old Qôrqut Granitic complex (Nutman et al., 2007b). In addition, granitic dykes associated with the Qôrqut granite crosscut the NUB and the TTGs. Hence, late metasomatic overprint occurred throughout the NUB. However, small areas escaped the metasomatism and some core areas of the ultramafic body are well preserved. The surrounding TTGs contain tonalitic components with an age up to ca. 3.85 Ga and abundant ca. 3.6 Ga old neosomes (Nutman et al., 2007b). Yet, the relationship between the ≥ 3.8 Ga tonalites and the NUB is ambiguous due to superimposed deformation. Metamorphic zircons from the NUB provide an absolute minimum age of ca. 3.65 Ga (Nutman et al., 2007b; Fig. 2-7). Nonetheless, field observations suggest that the ultramafic rocks were likely tectonically juxtaposed with the mafic and sedimentary rocks prior to being engulfed in the ≥ 3.8 Ga tonalites, similarly to the scenario assumed for the SOISB peridotites (Nutman et al., 2007b).

From the NUB, five type 1 peridotites (10-09, 10-10, 10-11(dunite, Fig. 2-8A-B), 10-12B and 10-14), one type 2 (10-13) and one type 4 peridotite (10-12A) were sampled.

The peridotites generally show low to medium degrees of serpentinization. Except for sample 10-12B, olivine and orthopyroxene crystals in the NUB type 1 peridotites are crosscut by fine serpentine-veins. Those veins locally merge into thicker networks in some samples. The veinlets however tend to lose their vein-like structure and form diffuse reaction zones as soon as they are in contact with amphibole grains. This phenomenon is especially prominent in sample 10-14. Thus, serpentinization is in most NUB type 1 peridotites more pronounced than in the SOISB1 type 1 peridotites. Nonetheless, the NUB peridotites contain only a few percent of serpentine and chlorite.

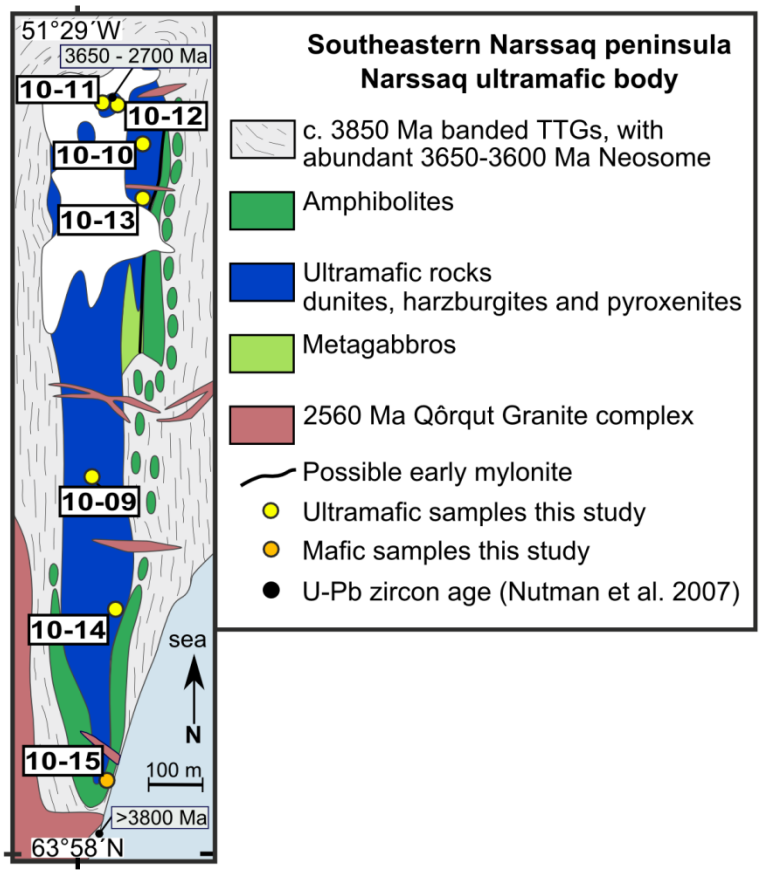

Figure 2-7: Simplified map of the Narssaq ultramafic body (NUB) after Nutman et al. (2007b). Age data are compiled from Nutman et al. (2007b). Sample numbers in the map refer to sample localities of this study.

Sample 10-12B lacks any serpentine-veins, yet, some larger amphibole grains clearly have overgrown other silicate minerals (Fig. 2-8 C-D). Small amphiboles in this sample have curvilinear grain boundaries or locally polygonal shapes similar to olivine and orthopyroxene minerals. This observation suggests two generations of amphiboles and a possible post-serpentinization recrystallization. Opaque phases occur in the NUB type 1 peridotites as inclusions and at grain boundaries either as single grains or as larger aggregates which are partly intergrown with amphiboles.

The type 4 peridotite 10-12A is characterized as a meta-peridotite and the mineralogy differ to all other peridotites. Veins consisting of coarse-grained and fibrous amphiboles, mica, minor amounts of chlorite and small grains of recrystallized olivine that intersect a groundmass of coarse-grained olivine, orthopyroxene and amphibole minerals. Those veins are irregular in thickness and vary from a few mm up to about 1 cm. Opaque phases are heterogeneously distributed and occur mainly associated with hydrous phases and less often as inclusions in olivine, orthopyroxene and amphibole.

One meta-gabbro associated with the NUB was sampled (Fig. 2-7). The amphibolite (10-15) mainly contains amphibole, plagioclase, minor quartz, mica, and opaque phases.

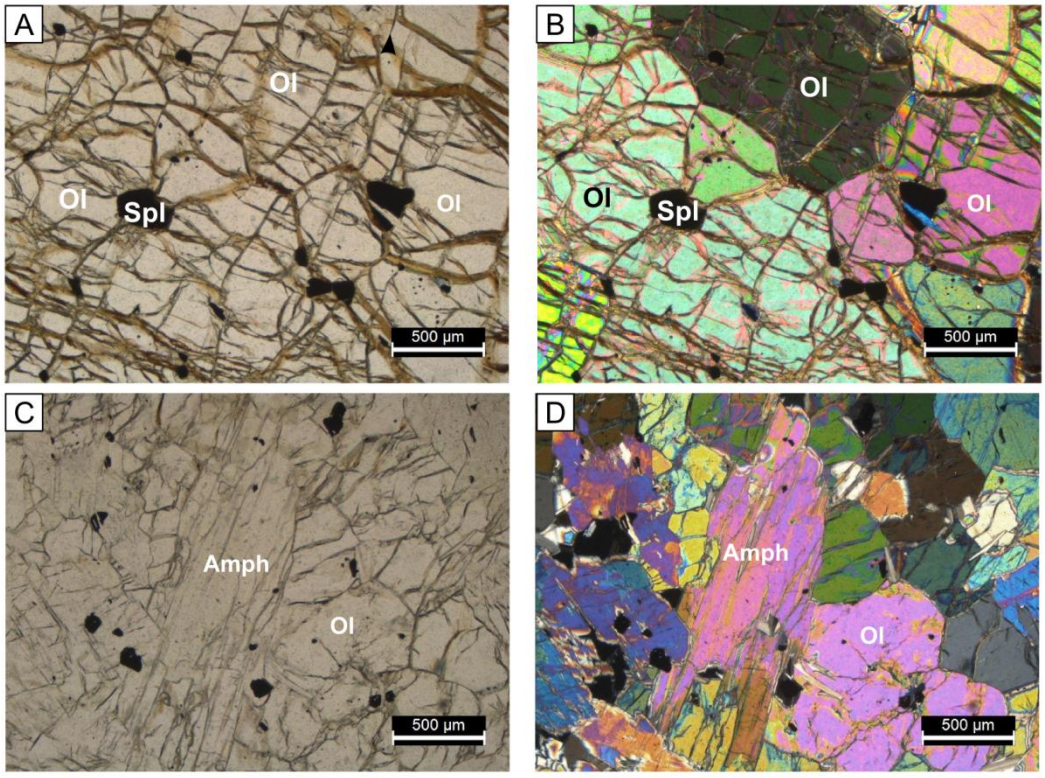

Figure 2-8: (A-B) Microphotographs illustrating type 1 peridotite coarse-grained microstructure, dunite (10-23). (C-D) Type 2 peridotite 10-12B lacks any serpentine-veins, yet some larger amphibole grains clearly have overgrown other silicate minerals. Microphotographs are in plane-polarised light (A, C) and cross polarised light (B, D). Ol: oivine; spl: spinel.

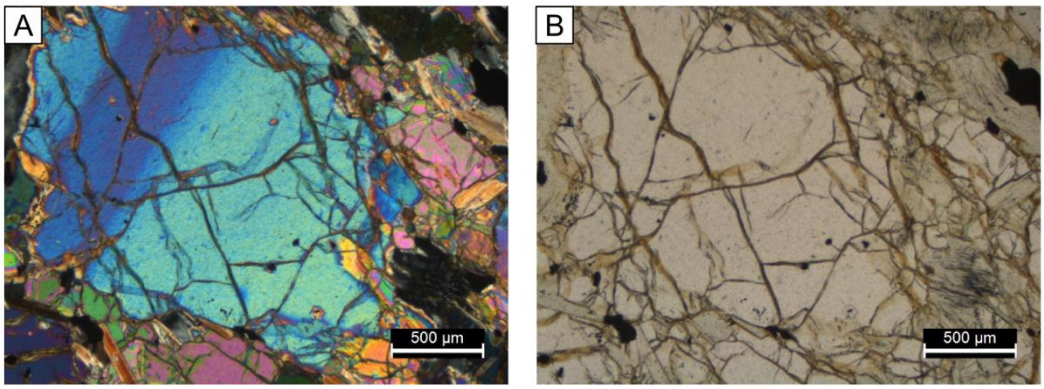

Figure 2-9: (A) Microphotographs illustrating undulose extinction in olivine, type 2 peridotite 10-13. Microphotographs are in plane-polarised light (A) and cross polarised light (B). Ol: oivine; spl: Spinel

2-4 AKILIA ISLAND

The four samples from Akilia Island originate from two locations in the SW part of Akilia Island (Fig. 2-10).

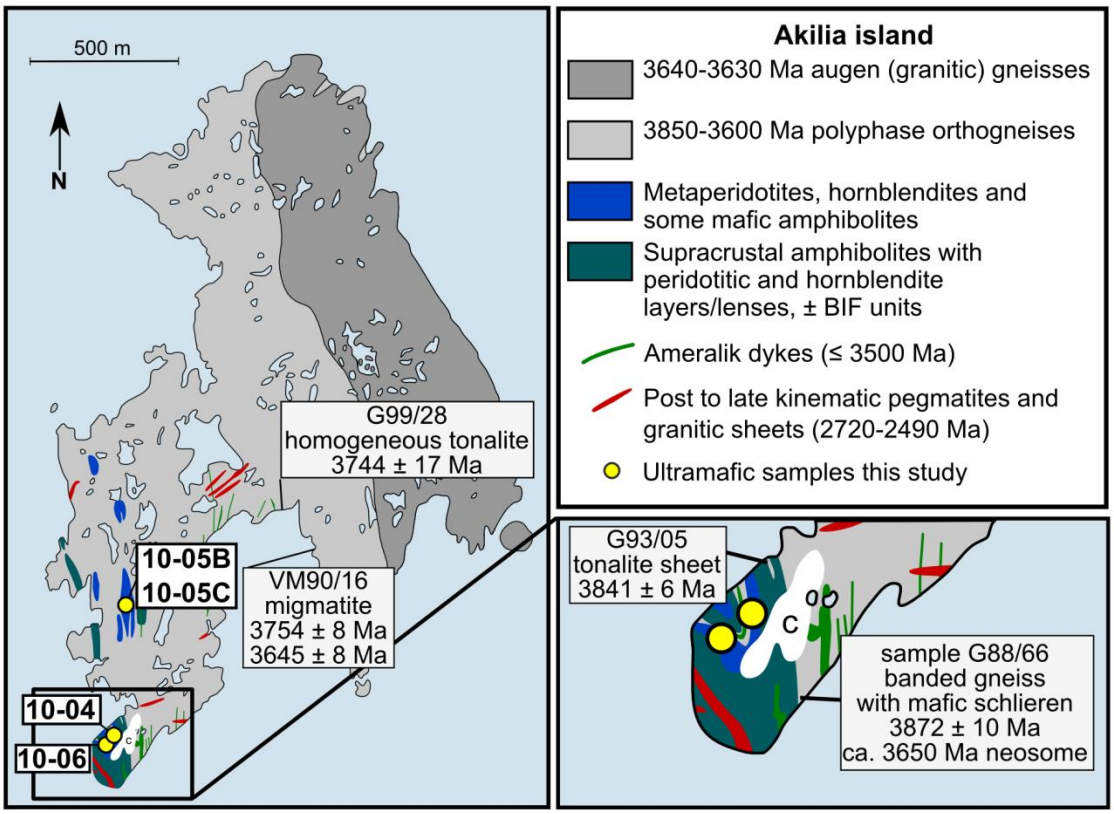

Figure 2-10: Simplified geological maps of the location Akilia Island indicated in Fig. 1-1 (A**)** Simplified map of Akilia Island after Nutman et al. (2002); (B**)** Simplified map of the "Akilia association" type locality after Nutman et al. (2002). Age data are compiled from (e.g., Nutman et al., 1996, 2002).

Tow type 4 peridotites (10-04 and 10-06) originate from a locality which is also known as the type locality of the "Akilia association" (McGregor, 1977), comprising amphibolites, ultramafic and siliceous rocks (Fig. 2-3 A and B). Macroscopic evidence for cumulate textures at outcrop scale was observed for both samples. The type locality of the "Akilia association" was studied in detail and the regarded subjects include e.g. evidence for Eoarchaean life or Earth's earliest water-lain sediments. The Archaean rocks of this location however record multiple events of deformation and high-grade metamorphism. Thus, age and field relationship of the putative metasediments as well as mafic and ultramafic rocks with the dated orthogneisses is still heavily debated (e.g., Nutman et al., 1996, 2000, 2002; Whitehouse et al., 1999, 2005, 2009; Myers and Crowley, 2000, Friend and Nutman, 2005; Manning et al., 2006).

Sample 10-04 is dominated by amphibole and olivine with minor amounts of orthopyroxene and only few percent of mica, chlorite and opaque phases. Occasionally, interstitial carbonates occur. Olivine and orthopyroxene grains occur as large poikiloblasts or as small irregular grains. Aggregates and trails of opaque phases are abundant in the samples. Sample 10-06 is dominated by inclusion-rich amphibole and olivine. Amphibole occurs as grains with irregular grain boundaries or fibroidal shape. Less abundant are pyroxene, mica, and spinel and other oxides.

The two type 2 peridotites from Akilia Island (sample-subset 10-05) originate from a mafic-ultramafic enclave ca. 400 m north of the "Akilia association type locality". The ultramafic enclave is embedded in the 3.60 to 3.85 Ga old Eoarchean polyphase orthogneiss-unit (Fig. 2-3). The two type 2 peridotites 10-05B and 10-05C were collected within a distance of only 2 m apart from each other, thereby sampling the same massive meta-peridotite body.

The type 2 peridotites 10-05B and 10-05C display microstructures similar to those of the medium to coarse-grained SOISB type 2 peridotites. The peridotites are characterised by predominant olivines and amphiboles with subordinate amounts of clinopyroxene, chlorite, spinel and ilmenite. Locally, clusters of hydrothermal veins occur with clear alteration zones of up to several mm, but generally less than 1 cm in width.

Chapter 3

Methods

3-1 INTRODUCTION

This chapter presents detailed descriptions of the applied methods. Prior to chemical analyses, the peridotites and amphibolites were investigated via polarization microscopy. For the peridotites additional polished thin sections were prepared for electron microprobe analyses in order to obtain major and minor element compositions for mineral phases such as olivine, pyroxene, spinel, and amphibole.

Conventional trace element bulk compositions were obtained for the amphibolites and peridotites by quadrupole ICP-MS measurements. Osmium, Ir, Ru, Pt, Pd, Re concentrations and Re-Os isotope data were obtained for eleven type 1 and type 2 peridotites from SOISB and NUB by isotope dilution with N-TIMS and ICP-MS measurements.

Combined Hf-Nd and Sm-Nd concentrations and isotope data as well as Nb-Ta-Zr-W (high-field-strength-element, HFSE) concentrations were determined by isotope dilution with MC-ICP-MS measurements for all peridotites. In addition, mineral separates were hand-picked for four peridotites and their Lu, Hf, Sm, Nd, Rb and Sr concentrations and isotope compositions were obtained by isotope dilution with MC-ICP-MS measurements. For those four peridotites the whole rock Rb-Sr concentrations and isotope compositions were obtained as well.

3-2 SAMPLE PREPARATION

One set of standard thin sections was prepared from all samples for microscopic investigations. A set of polished thin sections was prepared from the peridotites for electron microprobe analyses.

Starting materials for bulk rock chemical compositions of the peridotites and amphibolites were between ~2-4 kg of each sample. Any visible alteration domains were cut out using a diamond saw. The remaining sample materials were then first crushed to rock chips using a jaw crusher before 500-1000 g per sample were ground using an agate ball mill. In order to evaluate potential metal contamination regarding the platinum group elements due to the use of the stainless steel jaw crusher, aliquots of three samples (12B ~100g, 10-20C ~30g and 10-31 ~80g) and a piece of the stainless steel were processed in a different way. Rock pieces were sanded by corundum and crushed by hand in plastic bags avoiding any contact with metal tools. The samples were than powdered using an agate ball mill and/or agate mortar.

Prior to the preparation of the mineral separation, olivine, orthopyroxene and amphibole were identified via Rahman spectrometry and binocular microscope. The olivine, orthopyroxene and amphibole separates were obtained by hand-picking, comprising mineral separates for four peridotites, one sample from each locality, NUB, SOISB1, SOISB2 and SOISB3. Between 600 and 1000 mg olivine, 30 to 100 mg orthopyroxene and 40 to 45 mg amphibole were hand-picked (Table 3-1). In some cases small amount of mineral grains with small opaque inclusions were allowed, those mineral separates are marked with an asterisk in Table 3-1. Note that olivine in the 10-27 separate ($Ol_{10\text{-}27}$) is less transparent than in the other samples.

Table 3-1: Mineral separates

Sample	Location	ol [mg]	opx 1 [mg]	opx 2 [mg]	opx 3 [mg]	opx 4 [mg]	amph 1 [mg]	amph 2 [mg]
10-11	NUB	1041*	100*				39	48*
10-20C	SOISB1	1075*					40	46*
10-36	SOISB2	601	33	36	107*	116	41	
10-27	SOISB3	632*	33	109*	110		39	44

ol: olivine; opx: orthopyroxene; amph: amphibole; * small amount of opaque inclusions

3-3 SAMPLE DIGESTION AND CHEMICAL SEPARATION

3-3.1 Highly siderophile element

3-3.1.1 Sample digestion

For the Highly siderophile element (HSE) analyses about 2.5 g sample powder aliquots of 11 peridotites were mixed with ^{185}Re-^{190}Os and ^{191}Ir-^{99}Ru-^{194}Pt-^{105}Pd tracer solutions and with reverse aqua regia (2.5 ml 9 M HCl + 5 ml 14 M HNO_3) in a quartz vessel for digestion in a high-pressure asher (HPAS, Anton Parr^{TM}) (Fischer-Gödde et al., 2011). The HPAS vessels were heated to 320 ℃ for about 12 hours at 100 bars.

3-3.1.2 Osmium separation

The Os separation procedure followed the protocol outlined in Fischer-Gödde et al. (2011). The digested sample solutions were transferred into 50 ml centrifuge tubes, and mixed with 2-3 ml chloroform ($CHCl_3$). The mixture was first homogenized by shaking and then centrifuged for 5 minutes in order to extract Os into the $CHCl_3$. The Os-bearing $CHCl_3$ was transferred into 15 ml PFA beakers with 4 ml distilled HBr. This Os extraction procedure was repeated three times to yield high recovery. The extracted Os-bearing HBr-$CHCl_3$ mixture was heated in closed PFA beakers at 85℃ for 4 hours in order to back-extract Os into the HBr. The chloroform was removed and the Os-bearing HBr was evaporated to dryness. Osmium was further purified by micro-distillation using a H_2SO_4-dichromate solution and trapped into HBr (Cohen and Waters, 1996).

Following the extraction of Os, about 2-2.5 ml aliquots of the aqua regia digestion solution were centrifuged and transferred into 15 ml PFA beakers and evaporated to near dryness. The sample was then converted to chloride form by adding 2-3 ml 9 M HCl twice and 1 ml 1.25 M HCl and drying down. About half of the solution was loaded on platinum filaments and covered with $Ba(OH)_2$ as activator.

3-3.1.3 Separation of other highly siderophile elements

The chemical separation of Re, Ir, Ru, Pt, Rh and Pd from the matrix followed the procedure reported by Fischer-Gödde et al. (2011) using cation exchange chromatography. The samples were dissolved in 10 ml 0.5 M HCl + 40% acetone solution and loaded onto 10 ml cation exchange resin (Eichrom™ 50W-X8) and the elements of interest were collected into 14 ml HCl-acetone solution, after eluting the matrix.

The collected element cuts were separated into two equal aliquots, one for Re-Ir-Pt measurements, and the other for Ru-Pd-Ir-Pt.

The Ru-Pd-Ir-Pt aliquots were dried down and re-dissolved into 0.5 ml 0.2M HCl. Subsequently, a clean-up procedure for Pd was applied in order to remove Cd using 2 ml Eichrom 50W-X8 resin.

3-3.2 Trace elements

For conventional trace element analyses by quadrupole ICP-MS, 120 mg of the powder aliquots of all whole rock sample and standard materials (BIR-1, BHVO-2 and UB-N) were digested and measured together with the samples similar to the procedure described by Hoffmann et al. (2011).

The powder aliquots were mixed with a 1:1 mixture of HF and HNO_3 and digested for 24 h at 180°C in Savillex® beakers placed inside Parr® bombs. Prior to the evaporation 1ml of $HClO_4$ was added. The residues were treated three times with 3ml concentrated HNO_3 – trace HF (<0.05N), and subsequent evaporated (Method 1). This procedure failed to dissolve opaque phases completely in the case of six type 2 peridotite samples (10-27, 10-28, 10-30, 10-31, 10-32 and 10-35). Therefore, two modified versions of the described standard method were used to digest those samples. For once, only the digestion time in the Parr® bombs were increased up to four days (Method 2), whereby three (10-30, 10-31 and 10-32) of the six samples were dissolved completely. The remaining three samples (10-27, 10-28 and 10-35) were treated with 1.5 ml H_2SO_4 instead of the $HClO_4$ (Method 3). They were completely dissolved in HNO_3 and traces of HF.

3-3.3 Lutetium, Hf, Sm, Nd, Nb, Rb, Sr, Ta, Zr and W

3-3.3.1 Whole rocks

For MC-ICP-MS trace element analyses, 120 mg or 240 mg of the peridotites aliquots of the whole rock sample powder were used and processed following Method 1. From those sample aliquots further ca. 20% aliquots were taken for W concentration analyses. Note, that W-aliquots were not taken from all replicate sample aliquots reported in Table 3-1. In addition, 10 % aliquots were taken from four peridotites (10-11, 10-20C, 10-27 and 10-36) for Rb-Sr for isotope dilution measurements. In general, Lu, Hf, Sm, Nd, Nb and Ta concentrations are so low that 120 mg sample powder is not adequate for meaningful measurements. Thus, only accurate W and/or Zr concentrations were obtained from the 120 mg sample aliquots, with a few exceptions (e.g., 10-12A).

In order to obtain high precision Sm, Nd, Lu, Hf, Rb, Sr, Nb, Zr, W and Ta concentration and isotopic data for the peridotites, 120 - 240mg peridotite whole rock powder aliquots were spiked with mixed ^{149}Sm–^{150}Nd and ^{180}Ta–^{180}Hf–^{176}Lu–^{94}Zr–^{183}W tracers, prior to dissolution as described above. After drying down the HF-HNO_3-$HClO_4$ acid mixture, the samples were treated three times with concentrated HNO_3 and a trace of HF (<0.05N). Subsequently, the samples were equilibrated in 6N HCl–0.06 N HF and aliquots of 20% were taken for W separation. Both aliquots (Sm-Nd-Lu-Hf-Nb-Zr-Ta aliquot and W aliquot) were then dried down. The W fractions were separated using column chemistry, following the analytical protocol of Kleine et al. (2004) and the Sm, Nd, Lu, Hf, Nb, Zr and Ta eluded following the analytical protocols of the procedures described by Münker et al. (2001) and Pin and Zalduegui (1997).

The Sm-Nd-Lu-Hf-Nb-Zr-Ta-aliquots were dissolved in 3N HCl, followed by a three-step exchange column chemistry (Münker et al. 2001) in order to separate Lu, Hf, Nb, Zr and Ta from the matrix. Samarium and Nd were extracted from the residual matrix following the method of Pin and Zalduegui (1997).

For Rb-Sr isotope dilution data an aliquot of ca. 10% (Rb-Sr ID cut) was taken from some dissolved peridotite whole rock powder aliquots (10-11, 10-20C, 10-27 and 10-36) and spiked with ^{85}Rb-^{84}Sr tracers. The other aliquot, ca. 90% of the total solution, was used for Lu-Hf and Sm-Nd isotope dilution measurements (ID) and Rb-Sr isotope concentration measurements (Rb-Sr IC cut). The Rb-Sr ID cut was put on the hotplate for about 32 hours in closed vials to ensure full sample–spike equilibrium. Both cuts were afterwards dried down.

3-3.3.1 Mineral separates

The mineral separates were cleaned in an ultrasonic bath (5-10 minutes) with 0.1 N HNO_3 and deionized water. Near to dry samples were spiked with mixed ^{176}Lu-^{180}Hf and ^{149}Sm-^{150}Nd tracers and were dissolved and equilibrated via table-top digestion (e.g., Lagos et al., 2007). Because, table-top digestion selectively dissolves the olivine, orthopyroxene and amphibole fractions while leaving spinel and microscopic grains of Hf-bearing accessory phases like zircon and rutile largely intact. The separates were mixed with a 1:1 mixture of HF and HNO_3 and placed in closed Teflon vials on 120 °C hotplates for about 32 hours. After adding 1 ml $HClO_4$, the samples were dried down at 120°C and subsequently at 180°C. The residues were treated three times with 3 ml concentrated HNO_3, followed by subsequent evaporation. Then the separates were dissolved in a mixture of 6N HCl and 0.001N HF. This procedure failed to dissolve the olivine separates completely, hence, in case of the olivine separates the amount of acid was increased (20 -30 ml) and the acidity lowered to 3N HCl. Alternating heating of the samples in 3N HCl in closed vials and ultrasonic bath treatment (ca. 5 minutes) resulted in complete dissolution of the olivine separates.

For Rb-Sr isotope dilution data an aliquot of ca. 10% (Rb-Sr ID cut) was taken from the dissolved mineral separates and spiked with ^{85}Rb-^{84}Sr tracers. The other aliquot, ca. 90% of the total solution, was used for Lu-Hf and Sm-Nd isotope dilution measurements (ID) and Rb-Sr isotope concentration measurements (Rb-Sr IC). The Rb-Sr ID cut was put on the hotplate for about 32 hours in closed vials to ensure full sample–spike equilibrium. Both cuts were afterwards dried down.

3-4 DATA ACQUISITION

3-4.1 Mineral chemistry using electron microprobe

Electron microprobe analyses of polished thin sections were performed on a JEOL JXA-8900RL Superprobe at Cologne. Operating conditions were 20 kV accelerating voltage and 20 nA beam current, using a focussed electron beam. A counting time of 20s on peak and 10s on background was chosen for all elements. A set of natural silicate (for Si, Mg, Ca, Na, K, Mn, Fe) and oxide (for Al, Cr, Ti, Ni) standards was used for calibration and the ZAF-algorithm was used for correction.

3-4.2 Whole rock major and minor element concentrations

Major element contents were determined on $Li_2B_4O_7$-flux fusion discs by X-ray fluorescence (XRF) using a Philips PW 2400 X-ray spectrometer at Cologne. Analytical

uncertainty was estimated to ±1 wt% (2σ) for the major elements based on replicate measurements of in-house reference materials.

3-4.3 Highly siderophile element concentration and isotope composition measurements

Osmium isotope compositions were determined as oxide using a thermal ionization mass spectrometer in negative mode (N-TIMS, Thermal-Finnigan^{TM} Triton) at Freie Universität Berlin. Except of one sample (10-29A) that was measured using Faraday detectors, all other samples were measured using a secondary electron multiplier (SEM). Measured ratios were corrected for isobaric OsO_3- interferences, and mass fractionation was corrected for by using $^{192}Os/^{188}Os = 3.0827$. Measurements of the University of Maryland Os standard solution using SEM yielded for the first measurements (2015) $^{187}Os/^{188}Os= 0.1141 \pm 0.0002$ (2 SD, n=8), measurements (2017) $^{187}Os/^{188}Os= 0.1139 \pm 0.0002$ (2 SD, n=8), and using Faraday detectors $^{187}Os/^{188}Os= 0.11377 \pm 0.00003$ (n=1). Measured $^{187}Os/^{188}Os$ isotope compositions of the samples were corrected for the slight offset from the value of $^{187}Os/^{188}Os= 0.11379 \pm 0.00002$ (Shirey and Walker, 1998).

The collected element cuts were separated into two equal aliquots, one for Re-Ir-Pt measurement and the other for Ru-Pd-Ir-Pt. After evaporating the acetone, the Re-Ir-Pt aliquots were measured by sector-field inductively coupled plasma mass spectrometry (SF-ICPMS, ThermoElectron Element XR) at Freie Universität Berlin, using a Scott-type spray chamber following the methods outlined in Fischer-Gödde et al. (2011). The Ru-Pd-Ir-Pt aliquots were dried down and re-dissolved into 0.5 ml 0.2M HCl. Subsequently, a clean-up procedure for Pd was applied in order to remove Cd using 2 ml Eichrom 50W-X8 resin. The purified Ru-Pd aliquots were dried down and dissolved into 4 ml 0.28 M HNO_3 and then measured using an Aridus desolvator system (Aridus-I) with CeO^+/Ce^+ of < 0.002.

For the concentration calculation of Ir, Ru, Pt and Pd by isotope dilution, the following isotope ratios were used: $^{191}Ir/^{193}Ir$, $^{99}Ru/^{101}Ru$, $^{194}Pt/^{195}Pt$ and $^{105}Pd/^{106}Pd$. $^{111}Cd/^{106}Pd$ ratios were generally low (< 0.01), making an interference correction of Cd on ^{106}Pd negligible.

Duplicate analyses were conducted for two samples (10-11 and 10-22). The relative deviation of HSE concentrations were on average < 5% for Ir and Ru, and <10% for Pt, Os, Re and Pd (10-22 duplicate). Only Pd (10-11duplicate) displays a higher deviation of 18.4%. Ir and Pt were measured on different aliquots of the same digestion, using the Scott-type spray chamber and the Aridus desolvator system. The relative difference of Ir concentration obtained from both aliquots is 0.14% and 2.2%, and <0.7% for Pt concentration obtained from group 2 peridotites, whereas the relative difference of Pt concentrations obtained from the

group 1 peridotites is higher (0.95% – 8.71%) due to much lower Pt abundances and lower intensities during the measurements.

A reference material, harzburgite MUH-1 (Meisel and Horan, 2016) was digested and analyzed twice together with the peridotite samples. Duplicate analyses were in good agreement for Os, Ru, however, for Ir, Pt, Pd and Re large discrepancies of 34% for Ir, 86% for Pt, 20% for Pd and 36% for Re between the duplicate digestions were observed (see Appendix Table 4-1). The large discrepancy for most HSE contents, particularly Pt is probably due to sample heterogeneities (see the compiled data of Meisel and Horan, 2016). However, MUH-1 duplicates still yielded similar $^{187}Os/^{188}Os$.

Typical procedural blanks were between 0.1 and 6 pg for Os, between 1 and 7 pg for Re, between 0.5 and 20 pg for Ir, <7 pg for Ru, <58 pg for Pt and <83 pg for Pd.

3-4.4 ICP-MS whole rock trace element concentration measurements

Trace element analyses were performed on a quadrupole ICP-MS, using an Agilent 7500cs, at the Christian-Albrechts-Universität zu Kiel following the protocol of Gabe-Schönberg (1993). As reference materials BIR-1, BHVO-2 and UB-N were measured in the same analytical sessions. The analytical precisions (1σ) were determined by analyses of several rock sample- and reference material-replicates. Most samples yield RSD% far below ±6% except for some low abundance elements (< 3 times the limit of detection). Independent of the different digestion methods describe above (see 3-2), no significant differences in the measured element abundances were found, except for one type 2 peridotite (10-30: La and Ce > 6 RSD%). Thus, the obtained results of the alternative digestion methods were not included in Table 5-1. Trace element concentrations obtained for reference materials and sample replicates, including those obtained via different digestion methods are reported in the Appendix Table B-1.

3-4.5 MC-ICP-MS Lu, Hf, Sm, Nd, Nb, Ta, Zr, W concentration and isotope composition measurements

Measurements were conducted on a Thermo Scientific NeptuneTM MC-ICP-MS instrument (upgraded with a Plus interface) at facilities at the joint Cologne-Bonn MC-ICP-MS laboratory, Germany

The Sm, Nd, Lu, Hf, Rb, Sr, Nb, Zr, W and Ta inventory were obtained by isotope dilution via MC-ICP-MS at the Cologne/Bonn University facility, using the analytical protocol described in Münker et al. (2001), Nebel et al. (2005) and Weyer et al.(2002). Niobium concentrations were measured as Zr/Nb against a Zr/Nb standard (>99.9% pure Ames Laboratory metals) and calculated from the Zr/Nb ratio using the Zr concentration

obtained by isotope dilution (Weyer et al., 2002). Concentrations of Sm, Nd, Lu, Hf, Nb, and Ta in most peridotites are at the ppb level. The reproducibility of reference materials and replicate measurements of samples were better than ± 6% (2σ r.s.d.) for Sm, Nd, Lu, Hf, Nb, and W, and < 9% (2σ r.s.d.) for Zr and Ta, with only few exceptions due to very low concentrations or to sample heterogeneity (Tables B-2 and B-3). Total procedural blanks for Parr bomb digestions were mainly > 100pg for Sr, <90pg for Hf and Rb, <75pg for Lu, <60pg for Nd and Sm, <80pg for Ta and < 1ng for Zr.

Measured $^{176}Hf/^{177}Hf$ and $^{143}Nd/^{144}Nd$ were mass bias corrected to $^{179}Hf/^{177}Hf$ of 0.7325 and $^{146}Nd/^{144}Nd$ of 0.7219, respectively and using the exponential law. Münster AMES ($^{176}Hf/^{177}H$ =0.282160, indistinguishable from JMC-475) was used as reference for measured Hf values and La Jolla ($^{143}Nd/^{144}Nd$ = 0.511859) for measured Nd. External reproducibility were ±53 ppm for $^{176}Hf/^{177}Hf$ and ±30 ppm for $^{143}Nd/^{144}Nd$. Mass bias correction for Lu was applied using the measured $^{173}Yb/^{171}Yb$ of the Lu cuts (e.g., Blichert-Toft et al., 2002; Vervoort et al., 2004; Lagos et al., 2007).

Mass bias and isobaric interferences on Rb was corrected with the exponential law and using Zr Alfa-Aesar standard solution **(**$^{94}Zr/^{90}Zr$ = 0.3381**)** and NBS 984 $^{87}Rb/^{85}Rb$ value of 0.38554 (Nebel et al., 2005). Measured NBS 984 $^{87}Rb/^{85}Rb$ yielded an average of 0.387054.

The NBS 987 standard solution yielded an average $^{87}Sr/^{86}Sr$ of 0.710293 with an external reproducibility of ±50 ppm for Sr. All $^{87}Sr/^{86}Sr$ data are given relative to NBS 987 value of 0.710260.

Chapter 4

Earth's oldest mantle peridotites show entire record of late accretion

4-1 INTRODUCTION

Our knowledge about the composition of Earth's mantle relies on data on mantle xenoliths, mantle tectonites, diamond inclusions, and indirect evidence from mafic to ultramafic magmas, geophysics, and experiments. Because Earth is a dynamic planet, compositional information about Eoarchean mantle reservoirs is scarce and was mainly available from metamorphosed basalts, magmatic cumulates, and komatiites that represent partial melts of ancient mantle and related crystallization products (e.g., Blichert-Toft and Puchtel, 2010; Hoffmann et al., 2011; Frank et al., 2016; Rizo et al., 2016). Direct information from ancient mantle rocks would offer a much better window into the early evolution of the mantle-crust system, early magma ocean processes, and the late accretion of chondritic material after Earth's core formed. The latter hypothesis has been advocated to account for the highly siderophile element [HSE; the platinum-group elements (PGEs), Re and Au] concentration excess and their broadly chondritic ratios in Earth's mantle, which are inconsistent with core formation models (e.g., Chou, 1978).

Resolvable excesses in ^{182}W in 3.8–3.7 Ga rocks from Isua (Greenland) and 4.0–3.6 Ga rocks from Acasta (Canada) together with apparently lower HSE contents in Archean komatiites have been interpreted as evidence for HSE-poor mantle sources that might reflect sluggish mixing of late accreted material into the Hadean and Eoarchean mantle (Maier et al., 2009; Willbold et al., 2015). Willbold et al. (2015) suggested that a small proportion of metal was retained in the mantle after core formation, thereby generating $\mu^{182}W$ (μ is the deviation in ppm from terrestrial reference standards) excesses at HSE abundances close to modern mantle values. It was further argued that some patches of mantle unaffected by late accretion may have become isolated in the lower mantle and survived, at least until the onset of modern plate tectonic processes ca. 3.0 Ga (Willbold et al., 2015). Alternatively, the ^{182}W excess in some Eoarchean rocks results from silicate-differentiation processes during the first ~50 m.y. of solar system history (Touboul et al., 2012, 2014; Rizo et al., 2016). The inferred low HSE concentrations in mantle sources of Mesoarchean komatiites (Maier et al., 2009) are in contrast to HSE abundance data on ultramafic Eoarchean rocks from Isua and Nuvvuagittuq (Quebec, Canada) that appear to be similar, as in modern analogues (Szilas et al., 2015; Rizo

et al., 2016). Szilas et al. (2015), and Rizo et al. (2016) inferred modern mantle-like compositions for the mantle sources of these rocks.

In order to directly address the mixing history of late accreted material in Earth's mantle, we have collected a new set of suspected mantle peridotites from several localities in the Itsaq Gneiss Complex (IGC). Eight peridotites were selected from the region south of the Isua supracrustal belt (SOISB), some from outcrops described by Friend et al. (2002). Three samples are from the Narssaq ultramafic body farther south (Fig. 1-4). Bennett et al. (2002) reported Re-Os isotope data for SOISB obtained from peridotites investigated by Friend et al. (2002). One of those samples is from the same mafic-ultramafic body sampled by type 2 peridotites 10-29A and B, 10-30 and 10-31 (Fig. 2-1) and three samples of Bennett et al. (2002) were collected from smaller enclaves northeast of this locality.

Our data set now provides combined PGE and Os-Re isotope data for the northern and the southern part of the IGC, including data for more SOISB localities and for the first time for the Narssaq ultramafic body. Because the peridotites studied here originate from two separate terranes with different histories (e.g., Nutman et al., 2007; see chapter 1), we regard the measured PGE abundances as representative of a larger domain of Eoarchean upper mantle.

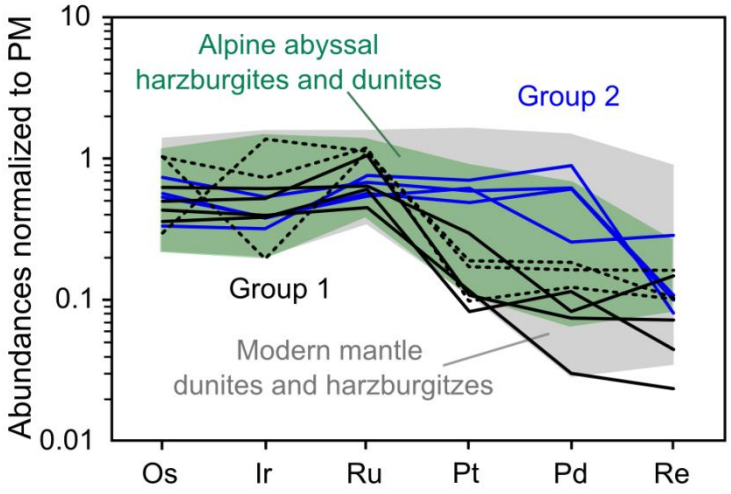

Figure 4-1: Primitive mantle (PM) normalized platinum group element patterns of Eoarchean dunites and harzburgites from southern west Greenland. Solid black lines are south of the Isua supracrustal belt group 1 peridotites, dashed black lines are Narssaq ultramafic body group 1 peridotites, blue lines represent group 2 peridotites; fields for modern mantle dunites and harzburgites (Rehkämper et al. (1997 and 1999), Pearson et al. (2004), Luguet et al. (2007), Fischer-Gödde et al. (2011) and Wang et al. (2013). All of these samples are discussed in context of their tectonic setting by Becker and Dale (2016).) and alpine abyssal peridotites (Italian Alps; Wang et al., 2013) are shown for comparison. PM values are from Becker et al. (2006).

4-2 PGES AND RE-OS ISOTOPES

Mantle peridotites and ultramafic crustal cumulates can be distinguished by their distinct PGE fractionation patterns, if these are combined with petrological data and major element compositions. The PGEs behave rather robustly during alteration and metamorphism (Barnes et al., 1985), and therefore likely preserve primary igneous features. Based on primitive mantle normalized PGE-Re patterns and petrography (see also Chapter 2), two groups of peridotites can be identified. The groups can be discriminated by their PPGE (Pt and Pd) and Re contents (Fig. 4-1).

Group 1 peridotites (n = 7) are harzburgites and dunites comprising all samples from Narssaq peninsula and four from SOISB. These samples all display a characteristic strong depletion of the PPGE relative to the IPGEs (Os, Ir, and Ru) and they exhibit minor fractionation between the IPGEs. Group 1 samples are similar to melt depleted harzburgites and dunites from modern abyssal peridotites or other mantle tectonites (Wang et al., 2013; Becker and Dale, 2016). Their PGE patterns are consistent with high degrees of mantle melting, where the IPGEs are compatible and the PPGEs and Re are incompatible (e.g., Mungall and Brenan, 2014; Becker and Dale, 2016). With one exception (sample 10-23), Re-depletion ages of group 1 peridotites are all Eoarchean. Except for two samples (10-20C, 10-34), all group 1 samples have Fo# > 89 (Fig. 4-2A). In Al/Si-Mg/Si space, group 1 samples overlap with modern depleted mantle peridotites (Fig. 4-2A). Group 2 peridotites (n = 4) are all amphibole-bearing harzburgites and were collected from a single locality SOISB (Fig. 2-1).

Group 2 harzburgites display IPGE abundances similar to group 1 peridotites, but they are characterized by higher PPGE concentrations and nearly flat PGE patterns with some variability in Pd and Re (Fig. 4-1). Except for one sample (10–31) that has a Paleoarchean Re-depletion age of 3.54 Ga, all other group 2 samples yield significantly younger Re-depletion ages (2.45–1.66 Ga), indicating later resetting. These young Re-depletion ages are broadly consistent with ages for widespread metamorphic overprint in the Isua region (e.g., Polat et al., 2015; Appendix B). Three group 2 samples have preserved mantle-like Fo# in olivine. However, re-enriched PPGE and higher Al/Si ratios than group 1 peridotites (Fig. 2-2A) provide combined evidence for metasomatic enrichment processes (Appendix B). Previously published PGE and Re-Os data for peridotites from SOISB (Bennett et al., 2002; Dale et al., 2017) overlap with our data. However, most previously reported PGE data for Isua peridotites showed PPGE enrichment, indicative of ultramafic cumulates or refertilization of depleted mantle peridotites (Szilas et al., 2015; Fig. 4-3).

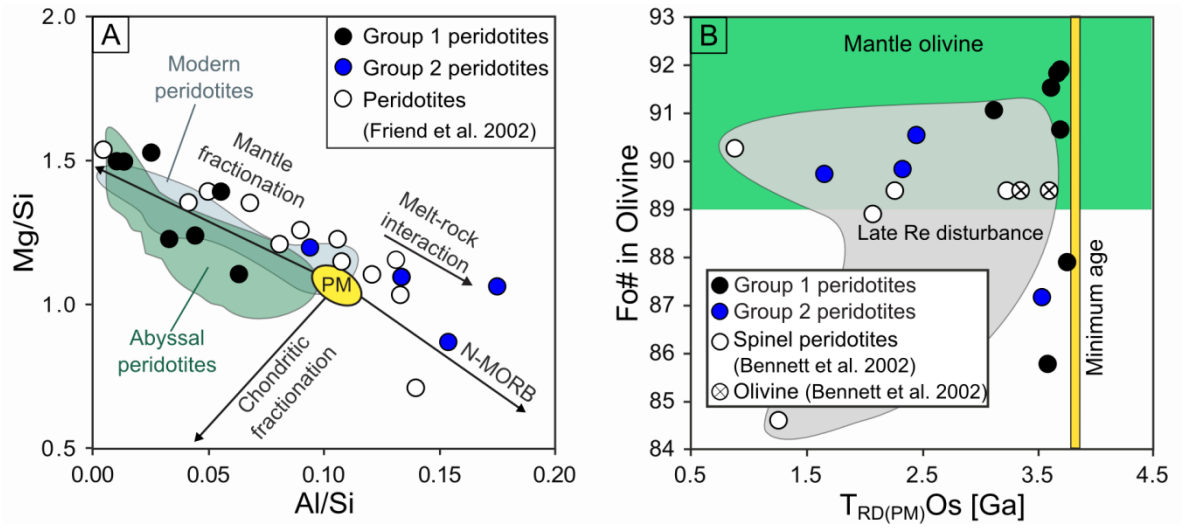

Figure 4-2: (A) Al/Si versus Mg/Si diagram (after Jagoutz et al., 1979). Fields for modern mantle (Palme and O'Neill, 2014) and abyssal peridotites (cf. Rollinson, 2007) are shown for comparison. Primitive mantle (PM) values from Palme and O'Neill (2014). N-MORB-normal mid-oceanic ridge basalt. (B) Fo# (forsterite) in olivine versus Re- depletion age (T_{RD}) highlighting the samples with mantlelike Fo# composition in olivine and Eoarchean minimum age for mantle depletion. Open symbols are literature data for peridotites from south of the Isua supracrustal belt (Bennett et al., 2002; Friend et al., 2002) for comparison.

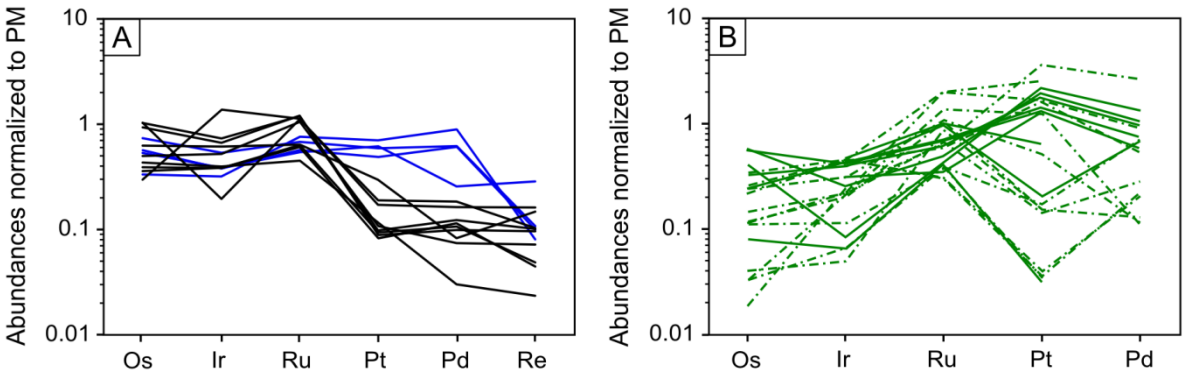

Figure 4-3: Primitive mantle-normalized platinum-group-element patterns of Eoarchean dunites and harzburgites from southern West Greenland examined in this study. (A), Black lines are group 1 peridotites, and blue lines represent group 2 peridotites; (B) solid green lines Isua Supracrustal Belt basalt cumulates (Szilas et al., 2015) and stippled green lines Isua boninitic cumulates (Szilas et al. 2015).

4-3 MIXING HISTORY OF LATE ACCRETED MATERIAL

The low Re abundances and $^{187}Os/^{188}Os$ in group 1 peridotites provide a unique window into the initial Os isotopic composition in the Eoarchean mantle. The low Re contents have only led to minor ingrowth of radiogenic ^{187}Os with time after melt extraction, in line with Eoarchean Re-depletion model ages. If recalculated to the minimum age of 3.81 Ga, the initial $^{187}Os/^{188}Os$ ratios are mostly subchondritic and it is important that they are negatively correlated with $^{187}Re/^{188}Os$ (Fig. 4-4). Both features indicate overcorrection for radiogenic

ingrowth due to a minor, relatively recent re-enrichment of Re by metasomatism, as suggested for group 2 peridotites.

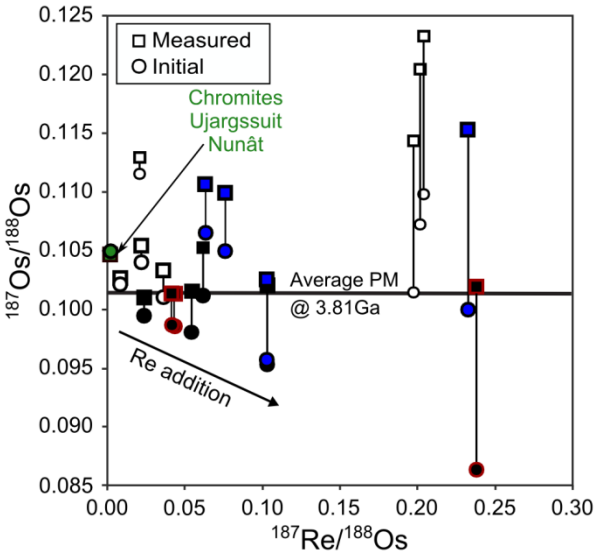

Figure 4-4: The $^{187}Os/^{188}Os$ versus $^{187}Re/^{188}Os$ isotope diagram showing measured and initial Os isotope compositions after Bennett et al. (2002). The measured $^{187}Os/^{188}Os$ obtained from group 1 peridotites overlap with those of PM (Meisel et al., 2001) recalculated to 3.81 Ga. The initial Os isotope compositions are unrealistically low and reveal over-correction of radiogenic ingrowth due to young addition of Re. Open symbols are literature data from Bennett et al. (2002), and grey symbols Frei and Jensen (2003, ultramafic rocks ISB with Re <200 ppt). The Ujargssuit Nunât layered intrusion data are taken from Bennett et al. (2002), Frei and Jensen (2003) and Coggon et al. (2013) green symbols. Black symbols represent SOISB group 1 peridotites, black symbols with red frame are NUB group 1 peridotites, and blue symbols group 2 peridotites.

The highly unradiogenic $^{187}Os/^{188}Os$ compositions in most group 1 peridotites (0.1010–0.1089; Table 4-1) overlap the average chondritic $^{187}Os/^{188}Os$ composition recalculated as 3.81 Ga. Thus, the predominantly Eoarchean Re-depletion ages provide a robust minimum estimate for melt extraction of mantle rocks with a chondritic $^{187}Os/^{188}Os$ ca. 3.81 Ga, in line with geological relationships and previous suggestions (Bennett et al., 2002). In addition to the direct evidence for Eoarchean melt depletion, the mantle rocks older than 3.8 Ga described here can provide important information on mixing time scales of late accreted material and its homogenization in the mantle. Notably, the absolute abundances of the IPGEs (Os, Ir, Ru) in harzburgites and dunites overlap those of modern mantle peridotites (Fig. 4-1), indicating that mantle abundances of HSEs by 3.8 Ga appear to be indistinguishable from HSE abundances in modern mantle rocks. In Phanerozoic mantle harzburgites and dunites, the absolute abundances of IPGEs are somewhat variable due to redistribution by melt infiltration and “nugget effects” by micrometer-sized PGE alloy and chromite grains (Becker and Dale,

2016; Lorand and Luguet, 2016). Taking into account this uncertainty, our data indicate that at least 60%, but likely a higher fraction, of late accreted material with a chondritic composition was efficiently mixed into the mantle represented by these peridotites, consistent with previous estimates based on PGE abundances in mafic crustal rocks from Isua (Rizo et al., 2016), Nuvvuagituq (Touboul et al., 2014), and Acasta (Li et al., 2014). The low ends of our data are still in agreement with estimates from Dale et al. (2017), but clearly in contrast to the estimate by Creech et al. (2017) based on stable Pt isotopes, implying admixing of ≤50% of late accreted material into the Isua mantle source. Comparing to previous studies and modern mantle rocks, our larger sample set of Eoarchean abyssal mantle rocks indicates that probably as much as 100% of late accretion component was mixed into the sampled mantle domains. Our results also are in marked contrast to the hypothesis developed to explain ^{182}W excesses in Isua rocks, that the chemical signature of late accreted material may be lacking in the Eoarchean Isua rock record (Willbold et al., 2015). With respect to ^{182}W, our data support models that invoke early silicate differentiation events, also consistent with ^{142}Nd variations in Archean rocks (Caro et al., 2003; Bennett et al., 2007; Rizo et al., 2016). To fully evaluate the significance of the ^{182}W excesses, future studies are now required that aim for better understanding of W elemental behavior and element mobility in Archean metamorphic rocks (e.g., Rizo et al., 2016).

4-4 CONCLUSIONS

Based on the first data set combining major element and HSE data with mineral chemistry, our study now provides conclusive evidence for the preservation of Eoarchean depleted upper mantle relics in two different Eoarchean terranes in the IGC. The peridotites from IGC show clear evidence for the presence of the entire inventory of late accreted material of broadly chondritic composition. This finding is based on combined PGE and Os isotope compositions that are indistinguishable from Phanerozoic upper mantle rocks. The Greenland peridotites can therefore provide an early anchor for studies concerned with the development of Earth's mantle reservoirs through geologic time and place an Eoarchean lower limit for mixing late accreted material into Earth's mantle.

Table 4-1: PGE, Re, Os, Re-Os isotopes and model ages of peridotites from south of ISB (SOISB) and Narssaq ultramafic body (NUB)

	Rock	PGE-group	Os ppb	Ir ppb	Ru ppb	Pt ppb	Pd ppb	Re ppb	$^{187}Re/^{188}Os$	$^{187}Os/^{188}Os$**	γ(Os)i (t=3.80 Ga)	$^{187}Os/^{188}Os(t)$ (t=3.80 Ga)	$T_{Ma(PM)}$ Os(Ga)	$T_{RD(PM)}$ Os(Ga)	$T_{Ma(ch)}$ Os (Ga)	$T_{RD(ch)}$ Os (Ga)
NUB																
10-09	H	1	3.95	0.679	7.76	1.43	1.31	0.036	0.044(2)	0.1013	-2.3	0.09845	4.1	3.70	4.2	3.79
10-11	D	1	4.00	2.53	8.27	0.73	0.87	0.035	0.042(2)	0.1013	-2.2	0.09857	4.1	3.70	4.2	3.79
10_11 (duplicate)	D	1	3.59	2.29	8.35	0.68	0.71	0.033	0.045(2)	0.1011	-2.5	0.09818	4.2	3.73	4.2	3.81
10-12B	H	1	1.14	4.73	7.75	1.29	1.16	0.056	0.238(6)	0.1019	-14.3	0.08631	8.8	3.62	8.0	3.71
10-12B II*	H	1		4.57	7.68	0.83	0.58	0.017								
SOISB											(t=3.81 Ga)	(t=3.81 Ga)				
10_20C	H	1	2.40	2.09	4.44	2.24	0.59	0.051	0.103(3)	0.1021	-5.3	0.09539	4.8	3.58	4.8	3.68
10_20C II*	H	1	1.92	1.76	2.20	1.67	1.11	0.075	0.189(1)	0.1086	-4.5	0.09625	4.9	2.83	5.0	2.68
10_22	D	1	1.39	1.33	4.27	0.62	0.82	0.016(1)	0.054(5)	0.1016	-2.7	0.09800	4.2	3.67	4.3	3.76
10_22 (duplicate)	D	1	1.51	1.34	4.41	0.70	0.75	0.017(1)	0.054(5)	0.1015	-2.7	0.09795	4.2	3.68	4.3	3.77
10_23	D	1	1.94	1.81	7.39	0.81	0.53(7)	0.025(1)	0.062(4)	0.1052	0.5	0.10117	3.7	3.14	3.8	3.28
10_34	H	1	1.68	1.33	3.13	0.87	0.21(7)	0.008(1)	0.023(4)	0.1010	-1.3	0.09942	4.0	3.75	4.0	3.84
10_29A	h	2	2.82	1.86	4.74	4.41	4.39	0.037	0.063(3)	0.1107	5.8	0.10652	2.8	2.34	3.0	2.56
10_29B	H	2	2.06	1.41	3.75	4.65	1.83	0.099	0.233(3)	0.1153	-0.7	0.10002	4.0	1.66	4.1	1.95
10_30	H	2	2.18	1.32	3.96	3.69	4.42	0.034	0.076(3)	0.1099	4.2	0.10495	3.0	2.45	3.2	2.66
10_31	H	2	1.30	1.10	5.29	5.32	6.36	0.028	0.103(5)	0.1024	-4.9	0.09570	4.8	3.54	4.7	3.64
10_31 II*	H	2	1.06	1.27	6.80	5.22	4.46	0.023	0.107(1)	0.1057	-1.9	0.09875	4.2	3.21	4.2	3.09
Reference material																
MUH-1			4.29	3.41	7.28	18.6	20.4	0.055	0.062(2)	0.1267						
MUH-1			5.01	5.22	8.51	9.99	17.0	0.086	0.083(1)	0.1275						
Jaw breaker			14.1	78.5	19.2	18.8	13.7	30.3	12.75	0.1142						

CI Chondrite values for $^{187}Os/^{188}Os = 0.1262$ and $^{187}Re/^{188}Os = 0.3915$ (Shirey and Walker (1998) and primitive mantle values for $^{187}Os/^{188}Os = 0.1296$ and $^{187}Re/^{188}Os = 0.434$ (Meisel et al., 2001) were used for the calculation of T_{Ma} and T_{RD} ages

H, harzburgite; D, dunite; * duplicate crushed per hand, without jaw breaker; * *2σ: precision of $^{187}Os/^{188}Os$, including blank contribution;

Typical uncertainties on HSE concentrations are 1-4 % RSD, including blank contribution. For some HSE data, the uncertainties are larger due to blank correction and are listed in brackets as for the last significant number

Chapter 5

Preservation of Eoarchean mantle processes from ~3.8 Ga peridotite enclaves in the Itsaq Gneiss Complex, southern West Greenland

5-1 INTRODUCTION

A major open question in Earth's geological history is how geodynamic processes operated during the Hadean and Archean, and when modern-like plate tectonic processes were established (e.g., Condie and Pease, 2008). A larger abundance of heat-producing radiogenic isotopes and a less differentiated mantle-crust system likely resulted in about 150-200 °C higher mantle potential temperature compared to the present value (e.g., Herzberg et al., 2010; Brown, 2014). These conditions may have triggered a geodynamic regime that was substantially different from present-day plate tectonics (e.g., Bédard, 2006; Kamber, 2015), possibly involving stagnant lid tectonics (e.g., O'Neill and Debaille, 2014). In such a regime, crustal recycling would either be driven by delamination (e.g., Johnson et al., 2014) or by episodic subduction events (Moyen and van Hunen, 2012). Many recent studies postulated the onset of plate tectonics by the Meso- to Neoarchean (3.2 - 2.5 Ga; e.g., Dhuime et al., 2011; Shirey and Richardson, 2011; Naeraa et al., 2012; Laurent et al., 2014). In contrast to this view, rocks from Eoarchean terranes of the Itsaq Gneiss Complex (IGC), southern West Greenland (e.g., Polat et al., 2003; Polat et al., 2002; Polat and Hofmann, 2003; Jenner et al., 2009; Hoffmann et al., 2011b; Polat et al., 2011) and Hadean/Eoarchean supracrustal enclaves of the Minto Block of the Superior Province, Canada (e.g., O'Neil et al., 2008; O'Neil et al., 2011; Turner et al., 2014; Caro et al., 2017) comprise mafic and ultramafic rocks, that may resemble analogues of modern subduction zone assemblages (boninites, picrites, tholeiites, high-K basalts). Within the Eoarchean IGC in SW Greenland, evidence for horizontal tectonics is also supported by field observations and geochronology (e.g., Nutman et al., 2007, 2013; Furnes et al., 2009). Trace element compositions of boninite-like and island-arc tholeiite- and picrite-like rocks from the Isua Supracrustal Belt (ISB) reveal, that these rocks derived from metasomatized mantle sources that were overprinted by melt- and fluid-like subduction components (Polat et al., 2002; Polat and Hofmann, 2003; Jenner et al., 2009; Hoffmann et al., 2011b), in support of early subduction processes. An alternative interpretation is, that Ca- and Mg-perovskite fractionation in a Hadean magma ocean may have imprinted a similar trace element signature on the mantle sources (Rizo et al., 2011;

Jackson et al., 2014), in line with decoupled Hf-Nd isotope compositions in rocks from ISB (e.g., Hoffmann et al., 2011b; Rizo et al., 2011).

Beyond the mafic rock record, direct chemical evidence for Eoarchean subduction processes was inferred from the finding of Ti-clinohumite-bearing dunite enclaves in the ISB (Friend and Nutman, 2011) and also from micro-structural observations in mantle-derived dunite samples (Kaczmarek et al., 2016). These ultramafic assemblages were interpreted as slivers of Eoarchean depleted mantle, thrusted into a package of Eoarchean mafic rocks with subduction-zone geochemical affinity (e.g., Nutman et al., 2009a). However, this interpretation has been challenged by Szilas et al. (2015), who interpreted these enclaves as magmatic cumulates of the local mafic volcanic sequences based on platinum group element (PGE) systematics. Other peridotite occurrences, comprising harzburgites and dunites have been reported from IGC, in the area south of the ISB (SOSIB) (e.g., Bennett et al., 2002; Friend et al., 2002) and on the Narssaq peninsula (Fig. 2-1) (Nutman et al., 2007; van de Löcht et al., 2018). Field observations and geochemical data indicate similarities with obducted sequences of Phanerozoic oceanic abyssal peridotites, making these ultramafic units the oldest preserved remnants of Earth's upper mantle yet found (e.g., Bennett et al., 2002; Friend et al., 2002; Chapter 4). In this chapter we report major and trace element compositions combined with Hf-Nd isotope data of >3.8 Ga peridotites and major and trace element compositions of associated amphibolites from two mantle localities, SOISB and NUB to place direct constrains on the chemical and isotopic composition of Eoarchean mantle and potential crustal recycling processes. Based on the dataset we evaluate their relationship to adjacent Eoarchean metabasalts and it is further discussed, as to whether subduction-like processes were already operating during the Eoarchean.

5-2 RESULTS

The abundances of major and trace elements obtained for the peridotites and amphibolites are given in Tables 5-1 and Table 5-2, and the Lu-Hf and Sm-Nd isotope data are given in Table 5-3 and Table 5-4 (replicates and reference materials see Appendix Tables B-1 to B-4).

5-2.1 Major elements

Type 1 peridotites from SOISB1 and NUB show similar major element compositions, with 39.1-47.9 wt.% MgO, 0.38-2.14 wt.% Al_2O_3, 0.40–2.37wt.% CaO, 2271-3499 ppm Ni, and Mg# 85–91 (Mg# = 100*molar Mg/(Mg+Fe)). Type 2 and SOIB2 type 1 major element concentrations overlap with SOISB1 and NUB type 1 peridotites, but exhibit often lower MgO (31.7-44.5 wt%), Ni (1574-2549 ppm), Mg# (83-88), highly variable CaO (0.61-6.19

wt%), and higher Al_2O_3 (2.35-6.42 wt%). Prominent differences between SOISB2 type 1 (10-34 and 10-36) and other type 1 peridotites are higher CaO (6.19 wt%; 10-34) and higher Al_2O_3 (6.21 wt%; 10-36). Compared to type 2 peridotites, type 3 peridotites and SOISB type 4 peridotite 10-35 have even lower contents of MgO (27.8 - 31.6 wt%), Ni (1056 -1546 wt%), lower Mg# (80-86), and higher or similar CaO (5.25 -7.24 wt%) and Al_2O_3 contents (5.30 and 6.15 wt%). NUB type 4 peridotite 10-12A exhibits relatively high Al_2O_3 (4.34 wt%) compared to the other NUB peridotites, whereas CaO (0.33 wt%), MgO (37.8 wt%), Ni (2101 ppm), Cr (6333 ppm) contents and an Mg# 90 are in the range of the other NUB peridotites.

Table 5-1: Major and trace element data for peridotites this study (selected measurements, for details and replicates see Appendix C, Tables B-1 to B-4). Analysis by (1) XRF; (2) ICP-MS at University Kiel; (3) MC-ICP-MS; Data from van de Löcht et al. (2018) marked in italics.

Location	**SOISB1**				**SOISB2**							
Name	10-20	10-20C	10-22	10-23	10-34	10-36	10-29A	10-29B	10-30*	10-31	10-32	10-35
Type	1	1	1	1	1	1	2	2	2	2	2	4
(1) XRF data												
wt%												
SiO_2	41.1	*41.3*	*40.9*	*39.9*	*42.6*	44.5	*44.2*	*41.6*	*42.5*	*47.0*	44.0	48.8
TiO_2	0.12	*0.081*	*0.030*	*0.040*	*0.077*	0.11	*0.12*	*0.13*	*0.087*	*0.14*	0.16	0.11
Al_2O_3	1.20	*1.25*	*0.38*	*0.47*	*2.38*	6.21	*3.67*	*6.42*	*5.01*	*6.38*	7.40	6.02
Fe_2O_3	14.3	*11.3*	*10.0*	*11.2*	*8.69*	8.82	*9.34*	*8.34*	*8.34*	*10.1*	9.47	7.77
MnO	0.18	*0.15*	*0.15*	*0.16*	*0.15*	0.12	*0.13*	*0.13*	*0.12*	*0.15*	0.15	0.11
MgO	39.1	*40.9*	*47.5*	*46.2*	*36.5*	38.3	*40.9*	*34.2*	*36.0*	*31.7*	33.0	27.8
CaO	2.37	*2.33*	*0.46*	*0.40*	*6.19*	0.61	*0.75*	*5.61*	*5.22*	*2.37*	4.30	7.24
K_2O	<LOQ	*<LOQ*	*<LOQ*	*<LOQ*	*<LOQ*	0.09	*0.07*	*0.13*	*0.09*	*0.21*	0.06	0.07
Na_2O	<LOQ	*<LOQ*	*<LOQ*	*<LOQ*	*<LOQ*	<LOQ	*<LOQ*	*0.84*	*<LOQ*	*<LOQ*	<LOQ	<LOQ
P_2O_5	<LOQ	*<LOQ*	*<LOQ*	*<LOQ*	*<LOQ*	<LOQ	*<LOQ*	*<LOQ*	*<LOQ*	*<LOQ*	<LOQ	<LOQ
ppm												
Cr	3499	*1834*	*1549*	*4432*	*1642*	4462	*2627*	*2344*	*3914*	*3973*	4412	2050
Ni	2271	*2410*	*2858*	*3140*	*1673*	1724	*2549*	*1647*	*1667*	*1574*	1875	1056
LOI	1.61	*3.23*	*0.79*	*0.88*	*3.48*	1.31	*1.61*	*2.34*	*0.82*	*1.58*	1.00	1.09
Total	100	*101*	*100*	*99.3*	*100*	100	*101*	*100*	*98.2*	*100*	100	99.0
Mg#	82.6	*86.2*	*89.1*	*87.7*	*87.9*	88.3	*88.3*	*87.6*	*88.2*	*84.4*	85.8	86.1
(2) ICP-MS data												
ppm												
Rb	0.972	0.280	<0.2	0.271	0.432	5.61	0.419	0.765	6.83	9.45	0.369	0.696
Sr	8.04	7.63	0.411	1.22	37.9	5.61	24.0	28.2	11.3	5.3	22.0	14.2
Y	2.18	1.83	0.766	0.348	6.79	3.62	2.89	4.34	1.86	4.09	4.42	3.97
La	0.443	0.413	0.0961	0.129	0.628	0.314	0.244	0.485	0.109	0.478	0.748	0.630
Ce	1.28	1.15	0.256	0.274	1.83	0.736	0.426	0.879	0.307	0.979	1.72	1.39
Pr	0.210	0.189	0.0463	0.0396	0.324	0.100	0.0565	0.106	0.0595	0.136	0.243	0.185
Eu	0.136	0.124	0.0352	<0.028	0.256	0.0374	0.0820	0.0755	0.0454	0.0836	0.126	0.251
Gd	0.460	0.402	0.142	<0.082	1.16	0.322	0.238	0.361	0.267	0.419	0.543	0.400
Tb	0.0773	0.0670	0.0261	<0.013	0.211	0.0726	0.0564	0.0846	0.0523	0.0894	0.107	0.0842
Ho	0.0963	0.0810	0.0348	0.0160	0.285	0.145	0.117	0.175	0.0791	0.163	0.178	0.158
Er	0.260	0.219	0.0981	0.0472	0.754	0.464	0.368	0.551	0.224	0.500	0.536	0.492
Tm	0.0387	0.0321	0.0158	<0.013	0.101	0.0777	0.0604	0.0893	0.0348	0.0797	0.0835	0.0789
Yb	0.253	0.210	0.102	<0.060	0.581	0.543	0.426	0.618	0.242	0.559	0.566	0.547
Pb	0.732	0.809	0.895	0.299	0.748	1.72	2.69	2.04	0.401	0.882	0.730	0.880
Th	0.0326	0.0467	<0.019	<0.019	0.0305	0.0369	<0.019	0.0792	0.0214	0.0457	0.0585	0.0437
U	0.0396	0.0406	0.0329	0.0221	0.0306	0.0546	0.0846	0.188	<0.019	0.105	0.0450	0.0609
(2) MC-ICP-MS data												
wt%												
Nd	0.901	0.922	0.211	0.15	1.58	0.429	0.224	0.355	0.304	0.552	1.17	0.687
Sm	0.321	0.304	0.0830	0.0441	0.649	0.155	0.0927	0.133	0.140	0.213	0.312	0.214
Lu	0.0328	0.0293	0.0139	0.00882	0.0688	0.0794	0.0625	0.0855	0.0377	0.0821	0.0808	0.0809
Hf	0.148	0.144	0.0245	0.0311	0.111	0.159	0.134	0.200	0.151	0.196	0.258	0.172
Zr	4.39	4.58	0.586	0.991	3.12	4.04	3.57	5.12	4.12	5.30	7.37	4.69
Nb	0.214	0.191	0.0603	0.0757	0.0967	0.127	0.120	0.185	0.176	0.114	0.234	0.175
Ta	0.0130	0.00886	0.00265	0.00395	0.00545	0.00763	0.00391	0.00640	0.00944	0.00692	0.0130	0.00634
W	0.265	0.279	0.414	0.387	5.33	0.500	1.41	0.214	0.297	0.214	0.139	0.128
Zr/Hf	29.66	31.81	23.92	36.22	28.11	25.41	26.64	25.60	27.28	27.04	28.57	27.27
Nb/Ta	16. 5	23.2	18.8	19.2	17.7	16.6	32.8	28.9	17.1	14.4	18.0	27.5
Zr/Nb	20.5	24.0	9.72	14.9	32.3	31.8	30.0	27.7	23.4	46.5	31.5	26.8
$(Sm/Yb)_{PM}$	1.396	1.589	0.8948		1.227	0.3143	1.396	0.2372	0.6347	0.4187	0.6458	0.4289
$(La/Yb)_{PM}$	1.224	1.372	0.6588		0.7562	0.4043	0.3995	0.5487	0.3136	0.5971	0.8993	0.8047

Mg# = 100*molar Mg/(Mg+Fe); PM: primitive mantle normalized, Primitive mantle values are from Palme and O´Neill (2014).

Table 5-1 continued

Location	**SOISB3**			**NUB**						
Name	10-16*	10-27	10-28	10-09	10-10	10-11	10-12B	10-14	10-13	10-12A*
Type	2	3	3	1	1	1	1	1	2	4
XRF data										
wt%										
SiO_2	44.6	45.6	44.9	39.5	40.3	38.8	43.5	39	41.5	43.7
TiO_2	0.32	0.18	0.19	0.088	0.088	0.043	0.064	0.084	0.12	0.054
Al_2O_3	2.35	5.30	6.15	1.92	2.14	0.87	1.70	1.83	2.85	4.34
Fe_2O_3	13.0	9.83	11.7	9.81	11.2	9.15	8.43	11.4	11.9	8.54
MnO	0.18	0.16	0.21	0.14	0.12	0.14	0.13	0.15	0.16	0.15
MgO	35.6	31.6	30.4	42.5	41.7	45.9	41.8	42.1	37.9	37.8
CaO	3.74	5.66	5.25	1.66	2.13	0.49	1.99	1.63	2.65	0.33
K_2O	<LOQ	0.06	0.08	<LOQ	<LOQ	<LOQ	0.007	<LOQ	0.59	1.17
Na_2O	<LOQ	<LOQ	<LOQ	<LOQ	<LOQ	<LOQ	<LOQ	<LOQ	<LOQ	<LOQ
P_2O_5	<LOQ	<LOQ	<LOQ	<LOQ	<LOQ	<LOQ	<LOQ	<LOQ	<LOQ	<LOQ
ppm										
Cr	1500	2728	3038	5996	5665	7720	5397	6940	2779	6333
Ni	2306	1510	1546	2116	2104	2755	2539	2107	1443	2101
LOI	0.67	1.46	1.52	3.73	2.24	2.85	1.39	2.8	2.41	2.49
Total	100	100	100	99.4	100	98.2	99.0	99.0	100	98.6
Mg#	82.6	84.7	81.7	88.2	86.6	89.6	89.5	86.5	84.6	88.4
ICP-MS data										
ppm										
Rb	<0.227	0.410	0.560	2.76	0.935	1.05	0.281	0.421	93.7	71.1
Sr	11.5	25.7	33.1	1.73	5.89	0.942	3.59	2.12	4.46	4.98
Y	5.48	4.88	4.40	1.72	2.12	0.652	2.33	1.64	2.53	1.29
La	1.00	0.419	0.409	0.222	0.374	0.0772	0.509	0.179	0.969	6.53
Ce	2.61	1.30	1.18	0.610	1.01	0.214	1.21	0.498	2.06	10.6
Pr	0.416	0.230	0.203	0.100	0.162	0.0352	0.179	0.0883	0.248	1.04
Eu	0.284	0.161	0.166	0.0773	0.0584	<0.028	0.0813	0.0502	0.211	0.0490
Gd	1.19	0.690	0.613	0.273	0.359	0.0887	0.360	0.259	0.409	0.454
Tb	0.204	0.129	0.116	0.0494	0.0640	0.0169	0.0654	0.0473	0.0744	0.0517
Ho	0.247	0.199	0.182	0.0723	0.0884	0.0253	0.0961	0.0686	0.109	0.0509
Er	0.648	0.583	0.531	0.206	0.250	0.0753	0.278	0.198	0.314	0.151
Tm	0.0907	0.0908	0.0823	0.0321	0.0377	<0.013	0.0435	0.0308	0.0480	0.0252
Yb	0.568	0.617	0.564	0.218	0.251	0.0847	0.291	0.208	0.321	0.190
Pb	0.797	1.844	1.45	0.446	0.404	0.185	0.311	0.409	1.19	1.49
Th	0.0849	0.0301	0.0393	0.0255	0.0585	0.0178	0.0729	0.0411	0.0449	3.83
U	0.0421	<0.019	0.0233	0.0182	0.0286	0.0374	0.0672	0.0237	0.0444	0.292
MC-ICP-MS data										
ppm										
Nd	1.90	1.06	0.938	0.444	0.695	0.1726	0.725	0.416	0.835	2.98
Sm	0.784	0.394	0.370	0.159	0.242	0.0603	0.227	0.162	0.239	0.442
Lu	0.0736	0.0886	0.0814	0.0307	0.0348	0.0127	0.0372	0.0298	0.0442	0.0310
Hf	0.474	0.259	0.266	0.120	0.121	0.0470	0.0896	0.0968	0.160	1.06
Zr	13.3	7.51	7.85	3.30	3.47	1.25	2.79	2.65	4.74	32.1
Nb	0.485	0.224	0.248	0.102	0.172	0.115	0.170	0.114	0.213	2.35
Ta	0.0291	0.0129	0.0153	0.00690	0.00913	0.00386	0.00753	0.00549	0.00993	0.245
W	0.126	0.0476	0.0524	0.0604	0.0875	0.0330	0.118	0.0465	0.170	0.389
Zr/Hf	27.98	28.97	27.98	27.56	28.63	26.69	31.17	27.33	29.57	30.38
Nb/Ta	16.7	17.3	16.2	14.8	18.8	29.8	22.6	20.8	21.5	9.60
Zr/Nb	27.3	33.5	31.6	32.4	20.2	10.9	16.4	23.1	22.2	13.6
$(Sm/Yb)_{PM}$	1.517	0.7016	1.396	0.8017	1.057	0.7819	0.8581	1.396		
$(La/Yb)_{PM}$	1.234	0.4747	0.4843	0.7091	1.041	0.6370	1.223	0.6018	2.108	23.98

Table 5-2: Major and trace element data for amphibolites (selected measurements, for details and replicates see Appendix B, Table B-1). Analysis by (1) XRF; (2) ICP-MS at University Kiel.

Location	NUB	SOISB1	SOISB2	SOISB2	SOISB3	SOISB3	SOISB
Name	10-15	10-21	10-33	10-37	10-17	10-26	10-40
(1) XRF data							
wt%							
SiO_2	50.4	52.0	51.8	51.6	50.4	49.3	48.7
TiO_2	0.79	0.76	0.63	0.69	0.79	0.95	1.12
Al_2O_3	13.1	14.2	16.1	9.24	14.0	14.4	13.9
Fe_2O_3	13.8	11.2	12.1	12.2	13.3	13.2	16.2
MnO	0.24	0.15	0.30	0.21	0.19	0.21	0.24
MgO	7.26	7.91	3.50	11.1	7.29	7.52	5.58
CaO	8.97	7.23	14.8	12.1	9.81	11.0	10.9
K_2O	1.23	1.58	0.08	0.44	0.31	0.31	0.54
Na_2O	2.20	2.71	0.69	1.47	2.21	2.04	1.61
P_2O_5	0.05	0.04	0.05	0.05	0.07	0.07	0.06
ppm							
Cr	102	133	209	871	287	226	246
Ni	70.9	64.0	94.7	235	95.6	103	101
LOI	0.43	0.59	0.08	1.34	0.58	0.40	0.58
Total	98.3	97.8	100	101	98.5	99.2	99.0
Mg#	47.5	54.9	33.3	61.2	48.6	49.5	37.2
(2) ICP-MS data							
ppm							
Rb	50.7	45.2	45.5	54.1	52.5	45.0	55.2
Sr	20.3	17.1	17.0	12.5	19.5	17.7	20.1
Y	93.4	47.3	1.85	3.67	2.48	4.39	13.5
La	69.5	107	70.5	106	124	92.9	142
Ce	27.0	18.3	17.1	17.1	20.8	23.4	25.6
Pr	5.19	4.20	0.0351	0.0204	0.0346	0.0346	0.566
Eu	208	122	11.5	15.1	24.4	36.2	79.8
Gd	1.61	1.84	3.50	4.94	3.82	3.51	4.50
Tb	5.21	5.03	8.26	11.3	9.63	10.2	11.6
Ho	0.914	0.866	1.21	1.65	1.46	1.62	1.91
Er	0.854	0.679	0.677	0.762	0.782	0.930	1.04
Tm	3.27	2.50	2.48	3.02	3.13	3.48	4.10
Yb	0.648	0.472	0.459	0.524	0.567	0.630	0.723
Pb	4.61	3.26	3.15	3.37	3.81	4.23	4.74
Th	1.01	0.701	0.680	0.683	0.797	0.896	0.990
U	2.93	2.00	1.95	1.86	2.24	2.55	2.76
Nd	5.12	4.89	5.99	8.14	7.44	8.36	10.08
Sm	2.15	1.80	1.86	2.48	2.37	2.70	3.27
Lu	0.471	0.317	0.308	0.263	0.327	0.394	0.417
Hf	1.19	1.15	0.884	1.30	1.48	1.35	1.48
Zr	37.8	40.0	25.0	48.6	53.4	48.9	47.7
Nb	3.01	1.37	1.66	2.33	2.14	2.79	2.62
Ta	0.191	0.0974	0.114	0.166	0.142	0.185	0.175
W	0.151	0.320	0.589	0.174	0.232	0.399	0.748
Zr/Hf	31.75	34.64	28.34	37.37	35.97	36.23	32.27
Nb/Ta	15.8	14.1	14.5	14.0	15.1	15.1	15.0
Zr/Nb	12.6	29.2	15.1	20.9	25.0	17.5	18.2
$(Sm/Yb)_{PM}$	0.4781	0.6516	1.194	1.270	1.027	0.8276	0.8756
$(La/Yb)_{PM}$	0.3716	0.6329	1.236	1.987	1.233	0.9609	1.162

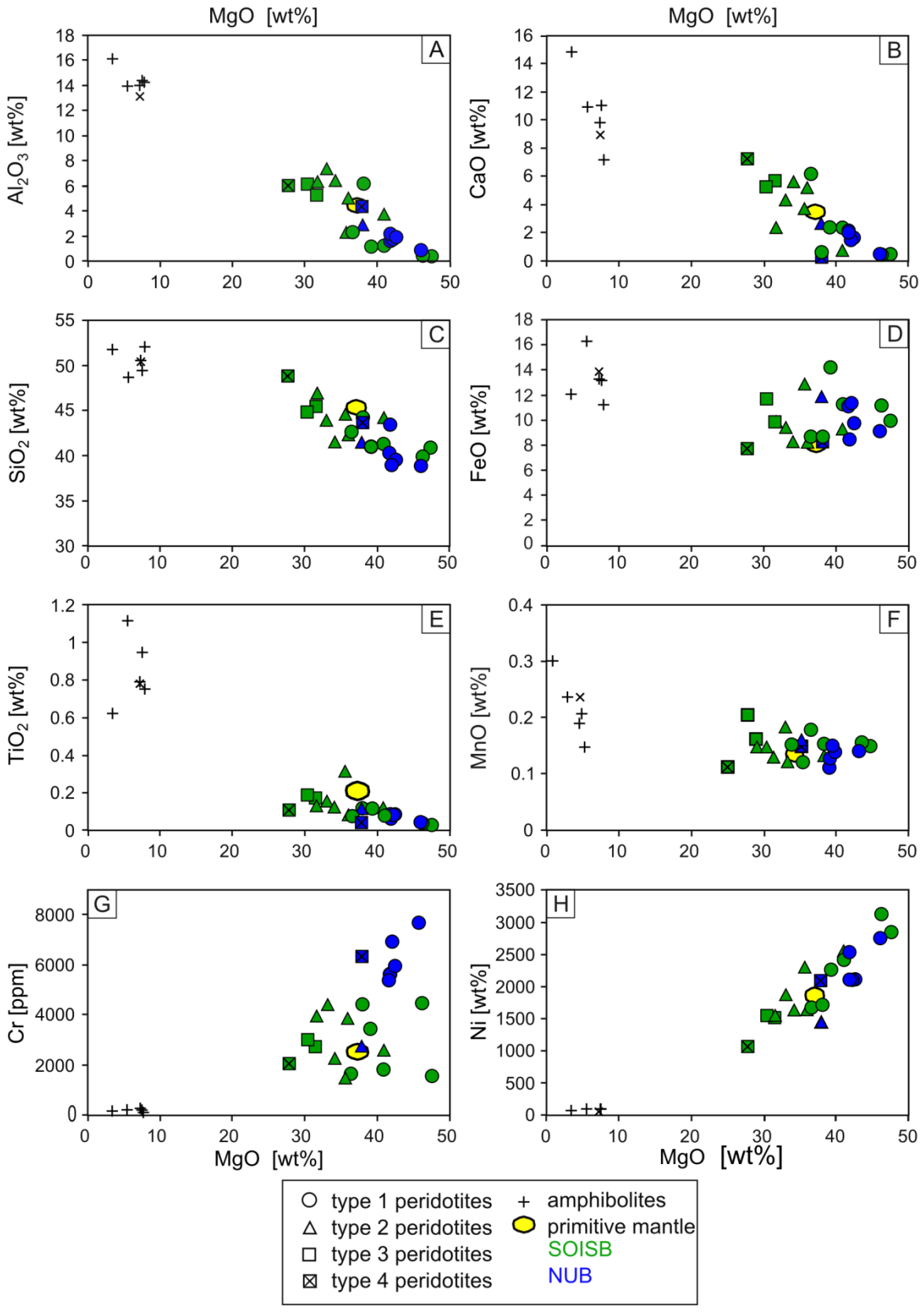

Figure 5-1: Variation diagrams for peridotites of this study showing Al_2O_3, CaO, SiO_2, Fe_2O_3, TiO_2, MnO, Cr and Ni versus MgO. Most type 1 peridotites and some type 2 peridotites plot on apparent mantle depletion trends such as CaO and Al_2O_3 versus MgO. Primitive mantle values are from McDonough and Sun (1995) and Palme and O´Neill (2014).

Generally, NUB peridotites have significant higher chromium contents (5397–7720 ppm) than all SOISB peridotites (1500–4462 ppm). Contents of Na_2O and K_2O are mostly very low in all investigated peridotites. The *loss of ignition* (LOI) from SOISB and NUB peridotites is generally low (0.67-3.73 wt.%) and is weakly correlated with the abundance of secondary hydrous phases, but not with Al_2O_3 or other major element concentrations. Generally, MgO is positively correlated to NiO and negatively correlated with Al_2O_3 and, with only few exceptions, with CaO, TiO_2 and SiO_2 (Fig. 5-1). Concentrations of TiO_2 and Al_2O_3 are positively correlated in most peridotites (Fig. 5-2A).

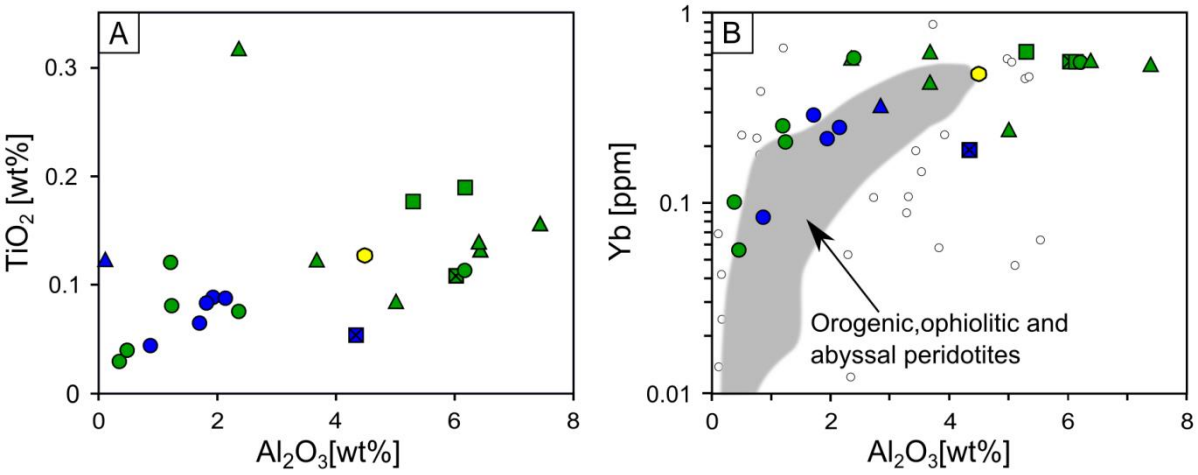

Figure 5-2: (A) TiO_2 versus Al_2O_3 variation diagram for peridotites of this study. Concentrations of TiO_2 and Al_2O_3 are positively correlated in most peridotites. (B) Yb versus Al_2O_3 variation diagram of SOISB and NUB for peridotites of this study in comparison to data compilation for orogenic, ophiolitic and abyssal peridotites from Bodinier and Godard (2014), illustrated by the open symbols and grey field (>95% compiled data). Most type 1 peridotites and some type 2 peridotites plot in the range of the orogenic, ophiolitic and abyssal peridotites. Symbols for peridotites of this study and primitive mantle are equivalent to those in Fig. 5-1.

The mafic amphibolites have SiO_2 contents ranging from 48.7 to 52.0 wt%, Al_2O_3 from 9.24 to 13.8 wt.% and high but variable contents of MgO (5. 58-11.1 wt%), CaO (7.23-14.8), and TiO_2 (0.63-1.12 wt%).

5-2.2 Trace elements

Primitive mantle-normalized trace element patterns are displayed in Fig. 5-3. Most type 1, 2 and 3 peridotites show relatively flat primitive mantle-normalized REE patterns, with 0.1 to 1.1 times primitive mantle abundances. All type 1 and most type 2 peridotites display insignificant Eu anomalies and only two samples (SOISB2 10-29A and NUB 10-13) display a clear positive Eu anomaly (Fig. 5-3B, D). The SOISB2 type 1 peridotites differ not only in their mineralogy and some major elements from other type 1 peridotites, but also in REE

abundances. They both show mainly higher HREE concentrations and 10-34 as well higher LREE compared to the other type 1 peridotites (Fig. 5-3A-B). Most SOISB type1 peridotites (except 10-36) are depleted in Zr and Hf relative to Nd and Sm. This feature is less distinct or absent in NUB type 1 peridotites, and type 2, 3 peridotites show no or even positive Zr-Hf anomalies relative to Sm and Nd (Fig. 5-3B, D, F).

The SOISB type 4 peridotite (10-35) shows similar primitive mantle normalised trace element pattern than the type 2 peridotites with no Zr-Hf anomaly, but with a distinct positive Eu anomaly. In contrast, the NUB type 4 peridotite (10-12A) shows a clearly discernable trace element pattern, with depleted HREE and increasing enrichment in MREE and LREE and a negative Eu anomaly (Fig. 5-3E-F).

All peridotites (except 10-11 and 10-30) show relative depletions in Nb and Ta compared to La and Ce (Nb/La = 0.15 to 0.65) (Fig. 5-3B, D, F). The Nb/Ta ratios obtained from the hbl-bearing peridotites and dunites are mainly sub-chondritic and range from 14.8 to 19.5. However, a few peridotites have superchondritic Nb/Ta ratios between 21.5 and 30.4 (Table 5-1). The NUB type 4 peridotite 10-12A shows distinctively elevated LREE, Nb and Ta concentrations, yet a comparably, low Nb/Ta ratio of 9.6 ± 0.3. All peridotites show sub-chondritic Zr/Hf ratios ranging from 25.3 to 32.8 (chondritic Zr/Hf = 34.2, Weyer et al., 2002).

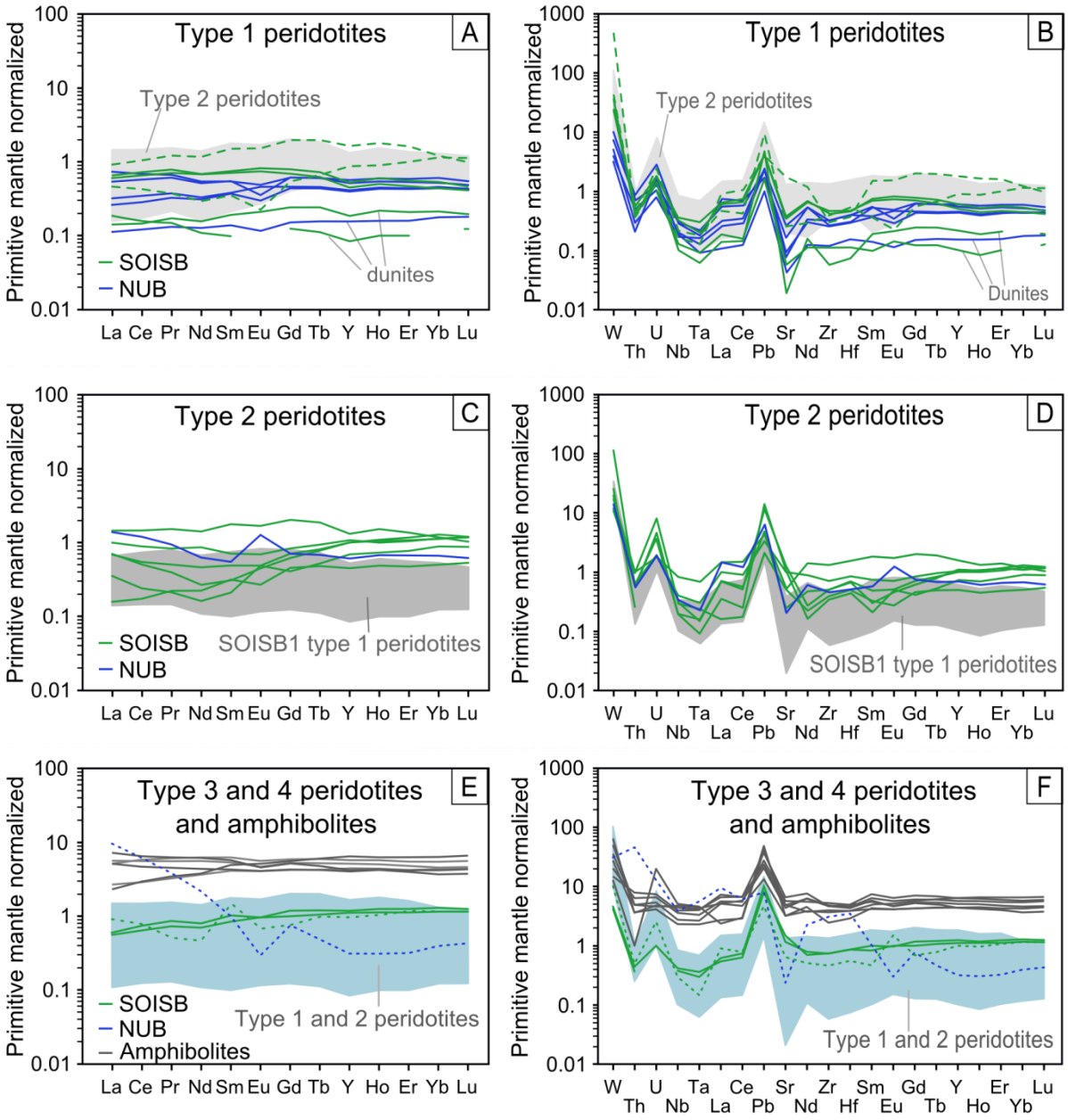

Figure 5-3: Primitive mantle normalized REE (A, C, D) and primitive mantle normalizes trace element patterns (E, F, G, H) of peridotites (A-E) and amphibolites (G-H). Most type 1, 2 and 3 peridotites show relatively flat primitive mantle-normalized REE patterns indicating LREE re-enrichment. Most peridotites show relative depletions in Nb and Ta and all peridotites show strong enrichments in Pb and W. The primitive mantle normalized trace element patterns obtained for the amphibolites are as well relatively flat with large positive anomalies for Pb and W, similar to those in the peridotite patterns. The green lines mark samples from SOISB and blue lines from NUB; (A-B) dashed lines are type 1 peridotites from SOISB2; (E-F) dashed lines are type 4 peridotites. Light grey fields in (A) and (B) indicate type 2 peridotites for comparison, light grey field in (C) and (D) indicate type 1 peridotites from location SOISB 1 for comparison, blue fields in (E) and (F) indicate type 1 and 2 peridotites for comparison. Primitive mantle values are from Palme and O´Neill (2014).

In all peridotites, W and Pb are strongly enriched and positive U anomalies relative to REEs concentrations are common. Peridotites from SOISB1 and NUB display selective depletions in Sr, whereas this is less distinct or absent in the peridotites from SOISB2 and SOISB3 (except for SOISB3 sample 10-16). Notably, SOISB2 type 1 peridotite 10-34 shows the highest W (5.33 ppm) and Sr (37.9 ppm) concentrations coupled with a high CaO (6.19 wt%) abundance. The peridotites (except type 4 peridotite 10-12A) show highly variable W/Th ratios (1.13 to 175.1) (Fig. 5-4) that are higher than in MORBs (0.090 to 0.24), OIBs (0.040 to 0.23) and primitive mantle (ca. 0.14) (König et al., 2011).

The primitive mantle normalized trace element patterns obtained for the amphibolites are relatively flat with large positive anomalies for Pb and W relative to similarly incompatible elements, similar to those in the peridotite patterns. Only the amphibolites from NUB (10-15) and SOISB1 (10-21) show slight depletions of LREE relative to MREE and HREE. Interestingly, the NUB amphibolite additionally shows a distinct selective enrichment in U and a relative depletion in Sr, mirroring the anomalies observed in the NUB peridotites (Fig. 5-3E, F). In the case of the amphibolites from SOISB, W concentrations and Th/W ratios are positively correlated. The W/Th ratios (0.27 to 2.47) overlap with those of MORB, OIB and arc lavas (0.04 to 1) (König et al. 2011). The amphibolite from NUB data does not plot on the W-W/Th correlation trend defined by the SOISB amphibolites, but shows W concentration and W/Th ratio in the range of NUB type 1 peridotites (Fig.5-4).

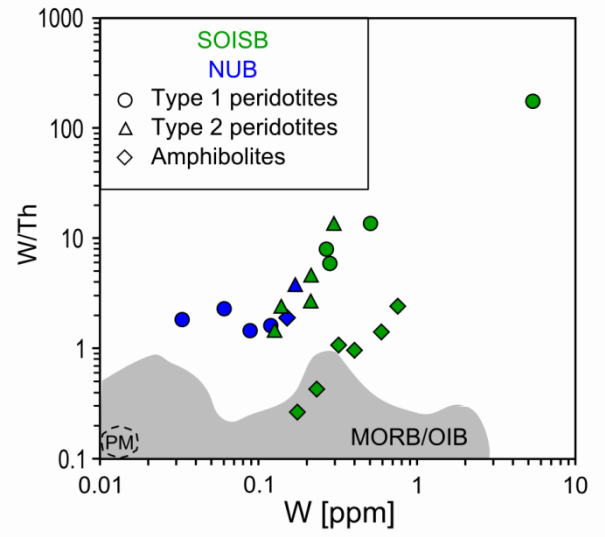

Figure 5-4: The W/Th vs. W diagram illustrates highly variable W concentrations and W/Th ratios obtained for the peridotites investigated in this study consistent with subsequent W mobility. The amphibolites from SOISB sow positive correlated W/Th and W values that overlap with the MORB-OIB field after König et al. (2011); primitive mantle PM (Palme and O´Neill, 2014).

5-2.3 Lu-Hf and Sm-Nd isotope compositions

Measured Lu-Hf and Sm-Nd isotope data and recalculated initial εHf and εNd values at 3.81 Ga are given in Table 5-2. Measured $^{176}Lu/^{177}Hf$ in type 1 peridotites (0.02901 to 0.08785) and in SOISB type 2 and type 3 peridotites ($^{176}Lu/^{177}Hf$=0.02412 to 0.06643) are highly variable and range up to depleted values. In comparison, the $^{176}Lu/^{177}Hf$ ratios obtained from NUB type 1 and 2 peridotites are less variable, ranging from 0.03440 to 0.04816. The SOISB type 4 peridotite (metaperidotite, 10-35) show $^{176}Lu/^{176}Hf$ (0.06671) whereas the NUB type 4 metaperidotite (10-12A) $^{176}Lu/^{176}Hf$ of 0.00408 deviates clearly from all other peridotites.

The measured $^{147}Sm/^{144}Nd$ (0.1731 to 0.2501) ratios obtained for type 1, 2 and 3 peridotites from NUB and SOISB overlap, independent of type and location. Similar to Lu-Hf systematics, Sample 10-12A differ from the other peridotites with a very low $^{147}Sm/^{144}Nd$ of 0.08417.

Excluding the significantly disturbed sample 10-12B ($\varepsilon Hf_{(3.81\ Ga)}$ = -8.0) and type 4 peridotites, NUB and SOISB peridotites are characterised by mainly positive initial $\varepsilon Hf_{(3.81)}$ (type 1 = -0.9 to +3.3; type 2 = +2.4 to +7.3, type 3 = +3.4 to +5.4). Likewise, mainly positive initial $\varepsilon Nd_{(3.81)}$ were obtained for type 1 peridotites (-0.2 to +5.1; except for sample 10-14 $\varepsilon Nd_{(3.81)}$= -1.6), and SOISB type 2 and type 3 peridotites (+1.5 to +5.2). In comparison, type 4 peridotites and NUB type 2 peridotite 10-13 display more radiogenic $\varepsilon Nd_{(3.81)}$ (+6.2 to +7.9).

Table 5-3: ^{176}Lu–^{176}Hf and ^{147}Sm–^{143}Nd isotope compositions of peridotites from NUB and SOISB. Initial εHf and εNd values were calculated using the CHUR values of Bouvier et al. (2008), the ^{176}Lu decay constant of 1.867 × 10−12 a-1 of Scherer et al. (2001) and Söderlund et al.(2004), and ^{146}Sm decay constant of 6.54 × 10-12 a-1 (Lugmaier and Marti, 1978). Initial εHf and εNd were calculated to 3.81 Ga, minimum ages obtained from field relationships.

Sample	Type	Lu	Hf	Lu/Hf	$^{176}Lu/^{177}Hf$	$^{176}Hf/^{177}Hf$	$\varepsilon Hf_{(t)}$	Sm	Nd	Sm/Nd	$^{147}Sm/^{144}Nd$	$^{143}Nd/^{144}Nd$	$\varepsilon Nd_{(t)}$
SOISB1		ppm	ppm				(3.81Ga)	ppm	ppm				(3.81Ga)
10-20A	1	0.0328	0.148	0.2221	0.03241 ±8	0.282751 ±6	+1.9 ±0.5	0.301	0.901	0.3566	0.2048 ±4	0.513059 ±7	+4.1 ±0.4
10-20C	1	0.0295	0.144	0.2040	0.02901 ±7	0.282462 ±6	+0.6 ±0.5	0.304	0.922	0.3300	0.1995 ±4	0.512840 ±8	+2.4 ±0.4
10-22	1	0.0139	0.0245	0.5683	0.08071 ±23	0.286294 ±23	+1.3 ±0.9	0.0830	0.211	0.3933	0.2378 ±4	0.513675 ±14	-0.2 ±0.4
10-23	1	0.00882	0.0344	0.2564	0.04020 ±13	0.283364 ±23	+3.3 ±0.8	0.0441	0.146	0.3023	0.1826 ±4	0.512466 ±22	+3.4 ±0.5
SOISB2							(3.81Ga)						(3.81Ga)
10-34	1	0.0688	0.111	0.6184	0.08789 ±18	0.286796 ±13	+0.4 ±0.6	0.649	1.580	0.4101	0.2483 ±5	0.513954 ±5	+0.1 ±0.5
10-36	1	0.0790	0.159	0.4961	0.07089 ±14	0.285507 ±9	-0.9 ±0.6	0.155	0.430	0.3620	0.2189 ±4	0.513468 ±11	+5.1 ±0.5
10-29A	2	0.0625	0.134	0.4678	0.06643 ±17	0.285390 ±12	+5.6 ±0.6	0.0927	0.220	0.4138	0.2501 ±5	0.514160 ±14	+3.2 ±0.5
10-29B	2	0.0855	0.200	0.4271	0.06067 ±15	0.284981 ±7	+7.2 ±0.5	0.133	0.360	0.3757	0.2271 ±5	0.513682 ±10	+5.2 ±0.5
10-30	2	0.0377	0.151	0.2497	0.03545 ±9	0.283033 ±8	+4.0 ±0.5	0.140	0.300	0.4594	0.2778 ±6	0.514769 ±15	+1.5 ±0.5
10-31	2	0.0821	0.196	0.4190	0.05957 ±15	0.284828 ±10	+4.3 ±0.5	0.213	0.550	0.3859	0.2234 ±4	0.513546 ±11	+4.4 ±0.5
10-32	2	0.0808	0.258	0.3135	0.04456 ±11	0.283698 ±8	+3.4 ±0.5	0.296	0.952	0.3283	0.1883 ±4	0.512660 ±9	+4.4 ±0.4
10-35	4	0.0809	0.172	0.4697	0.06671 ±17	0.285376 ±6	+5.4 ±0.6	0.214	0.687	0.3112	0.1814 ±11	0.512576 ±10	+6.2 ±0.7
SOISB3							(3.81Ga)						(3.81Ga)
10-16	2	0.0744	0.474	0.1554	0.02412 ±6	0.282149 ±7	+2.2 ±0.4	0.784	1.90	0.4119	0.2306 ±5	0.513733 ±9	+4.5 ±0.5
10-27	3	0.0886	0.259	0.3416	0.04944 ±12	0.284041 ±7	+4.1 ±0.5	0.394	1.06	0.3709	0.2243 ±4	0.513500 ±4	+3.1 ±0.5
10-28	3	0.0814	0.266	0.3059	0.04312 ±11	0.283586 ±6	+3.4 ±0.5	0.370	0.940	0.3948	0.2258 ±5	0.513607 ±10	+4.4 ±0.5
NUB							(3.81Ga)						(3.81Ga)
10-09	1	0.0307	0.120	0.2567	0.03440 ±9	0.282955 ±6	+3.9 ±0.5	0.166	0.440	0.3736	0.2168 ±4	0.513268 ±7	+2.2 ±0.5
10-10	1	0.0348	0.121	0.2876	0.04082 ±10	0.283448 ±8	+4.7 ±0.5	0.242	0.690	0.3477	0.1997 ±4	0.512849 ±8	+2.5 ±0.4
10-11	1	0.0130	0.0374	0.3473	0.04816 ±13	0.284009 ±46	+5.4 ±0.7	0.0603	0.170	0.3494	0.2111 ±4	0.513167 ±24	+1.1 ±0.5
10-12B	1	0.0386	0.0897	0.4299	0.04385 ±11	0.283316 ±9	-8.0 ±0.5	0.227	0.730	0.3134	0.1894 ±4	0.512588 ±8	+2.4 ±0.4
10-14	1	0.0295	0.0968	0.3044	0.04321 ±11	0.283585 ±6	+3.0 ±0.4	0.162	0.416	0.3879	0.2267 ±5	0.513322 ±10	-1.6 ±0.5
10-13	2	0.0446	0.160	0.2778	0.03944 ±10	0.283321 ±11	+3.8 ±0.5	0.239	0.835	0.2864	0.1731 ±3	0.512408 ±7	+7.0 ±0.4
10-12A	4	0.0306	1.06	0.02899	0.004080 ±1	0.280814 ±11	+7.3 ±0.4	0.442	2.981	0.1482	0.08416 ±17	0.510210 ±3	+7.9 ±0.4

5-3 DISCUSSION

5-3.1 Effect of metamorphic disturbance and post-emplacement element mobility on major and trace elements

The early Archean rocks of the IGC were affected by multiple tectono-metamorphic events (e.g., Nutman et al., 1996), modifying the primary magmatic chemical inventory. Hence, secondary overprint by metasomatic agents needs to be evaluated and needs to be carefully distinguished from potential metasomatic processes that may have modified the protoliths of the peridotites or the mantle sources of the amphibolites as a primary process.

The SOISB1 and most NUB peridotites are crosscut by fine serpentine veins, however, this is not reflected by overall low LOIs (0.8 – 3.7 wt.%). The silicate minerals are mainly unzoned and reaction zones are very limited or nearly absent. Thus, post emplacement serpentinization seems to have had only a minor effect on the bulk peridotite compositions. Only samples 10-12A, 10-12B and 10-13 show textural indications for potential post-serpentinisation recrystallization (Chapter 2). Generally, most type 1 peridotites therefore appear to have been exceptionally well preserved, as also evident from features like, e.g., low K, Ca, and Ba contents, low LOI, unzoned olivine and low abundances of secondary hydrous minerals.

The NUB type 1 peridotites and the dunites (± hbl-bearing -peridotites) from SOISB1 plot on typical major element melt depletion trends (e.g., Figs. 5-1 and 5-5) and their olivines show mantle-like compositions such as, e.g., Fo# >89 and low CaO contents (Chapter 4 and 6). Thus, these trends may reflect primary melt depletion trends, although re-fertilisation via melt-rock reaction of penetrating melts and refractory mantle can also produce such co-variations (e.g., Griffin et al., 2009; Tang et al., 2013; Bodinier and Godard, 2014). The main differences in major element abundances between type 1 peridotites from SOISB2 and those from SOISB1 and NUB are the higher CaO or Al_2O_3 concentrations (e.g., Figs. 5-1, 5-5).

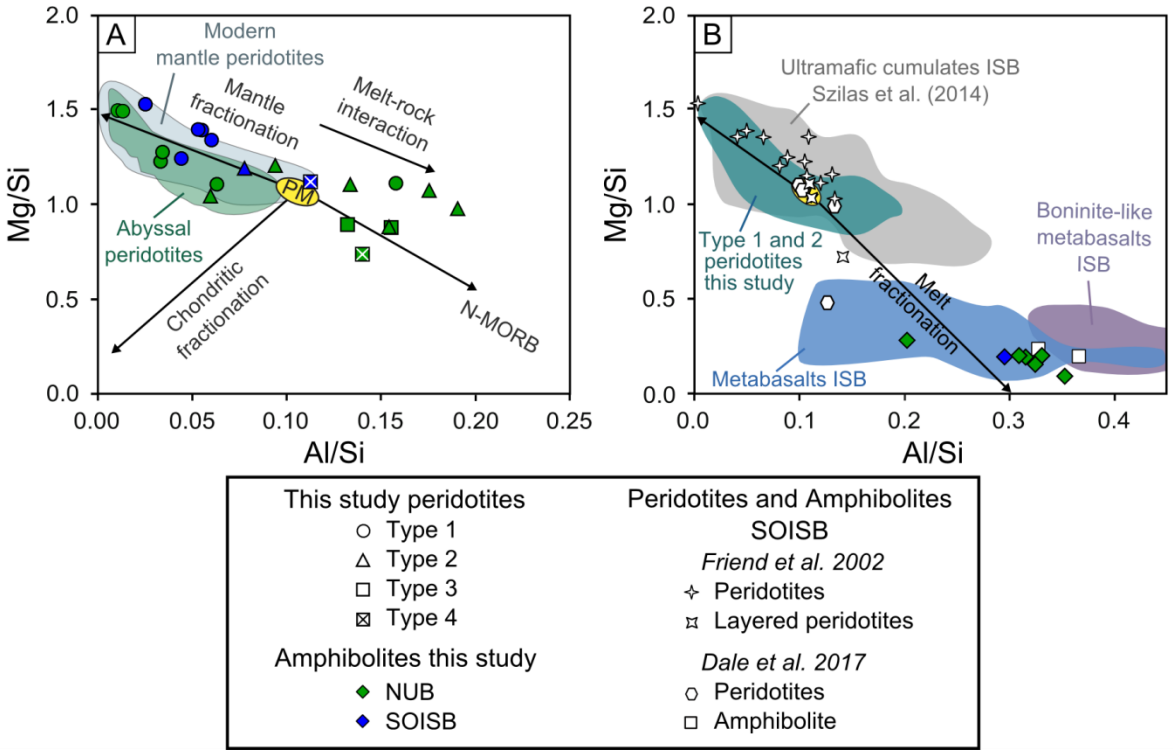

Figure 5-5: Mg/Si versus Al/Si diagram after Jagoutz (1979). Most type 1 peridotites plot along the Mg/Si vs. Al/Si mantle fractionation trend and most amphibolites investigated in this study plot in the field defined by metabasalts from ISB. (A) Greenland peridotites of this study in comparison to modern mantle peridotites (cf. Rollinson, 2007) and abyssal peridotites (Niu, 2004); Symbols indicate the peridotite types, green symbols indicate samples from SOISB and blue symbols samples from NUB. (B) Type 1 and type 2 peridotites and amphibolites of this study in comparison to literature data compiled for peridotites from SOISB (Friend et al., 2002, Szilas et al. 2015 and Dale et al., 2017) and amphibolites from SOISB and ISB (Polat et al., 2002; Polat and Hofmann, 2003; Jenner et al., 2009; Rizo et al., 2011, 2013; Dale et al., 2017).

These elevated CaO and Al_2O_3 concentrations can be explained by secondary Ca and Al gain. This is supported be the occurrence of interstitial carbonates in sample 10-34 and higher of orthopyroxene, spinel and biotite abundances in sample 10-36 compared to the other type 1 peridotites. Likewise, secondary mineral formation (e.g. spinel, mica, chlorite and interstitial carbonates) may account for higher aluminium and calcium contents at least in some type 2 peridotites (e.g. 10-29A, 10-29B and 10-30). Generally, type 2 peridotites virtually lack significant major and minor element correlations (e.g., Figs. 5-1 and 5-6). This can be explained by metamorphic and metasomatic overprint. Similar to most type 1 peridotites, phases indicative for low temperature alteration, like Mg-chlorite, are rare in type 3 peridotites and serpentine veins are absent. Moreover, potassium and sodium abundances are all low in type 1, 2 and 3 peridotites, which may be interpreted as lack of metasomatic overprint during later magmatic intrusions. Likewise, most type 1 and 2 peridotites lack clear correlation between LREE and indicators for secondary alteration or fluid mobile elements

(Fig. 5-7). Hence, extensive fluid induces alteration, e.g. seafloor alteration or fluid induced alteration in context with magmatic intrusions has not occurred, or a younger metamorphic event had obscured all traces. Trace element co-variations, such as between MgO and REE and HFSE would indicate melt depletion or re-fertilization of the peridotites by a melt-like component. However, in contrast to type 1 peridotites, type 2 peridotites show no or only weak correlations between HFSE, REE and MgO (Fig. 5-8) suggesting a metamorphic overprint.

Type 4 peridotites were completely recrystallized during amphibolite facies metamorphism (10-35) or strongly metasomatised in addition to metamorphic overprint (sample 10-12A). Collectively, based on the petrographic and geochemical observations, type 1 peridotites (except SOISB2) and type 3 peridotites can be characterised as being least affected by metasomatic and metamorphic overprint, type 2 peridotites as variably altered and type 4 peridotites as strongly altered. Consequently, type 4 peridotites were excluded from the following discussion about mantle processes and mantle-crust evolution and type 1 (mantle) peridotites from NUB and SOISB1 are discussed below as best candidates to investigate Eoarchean mantle processes.

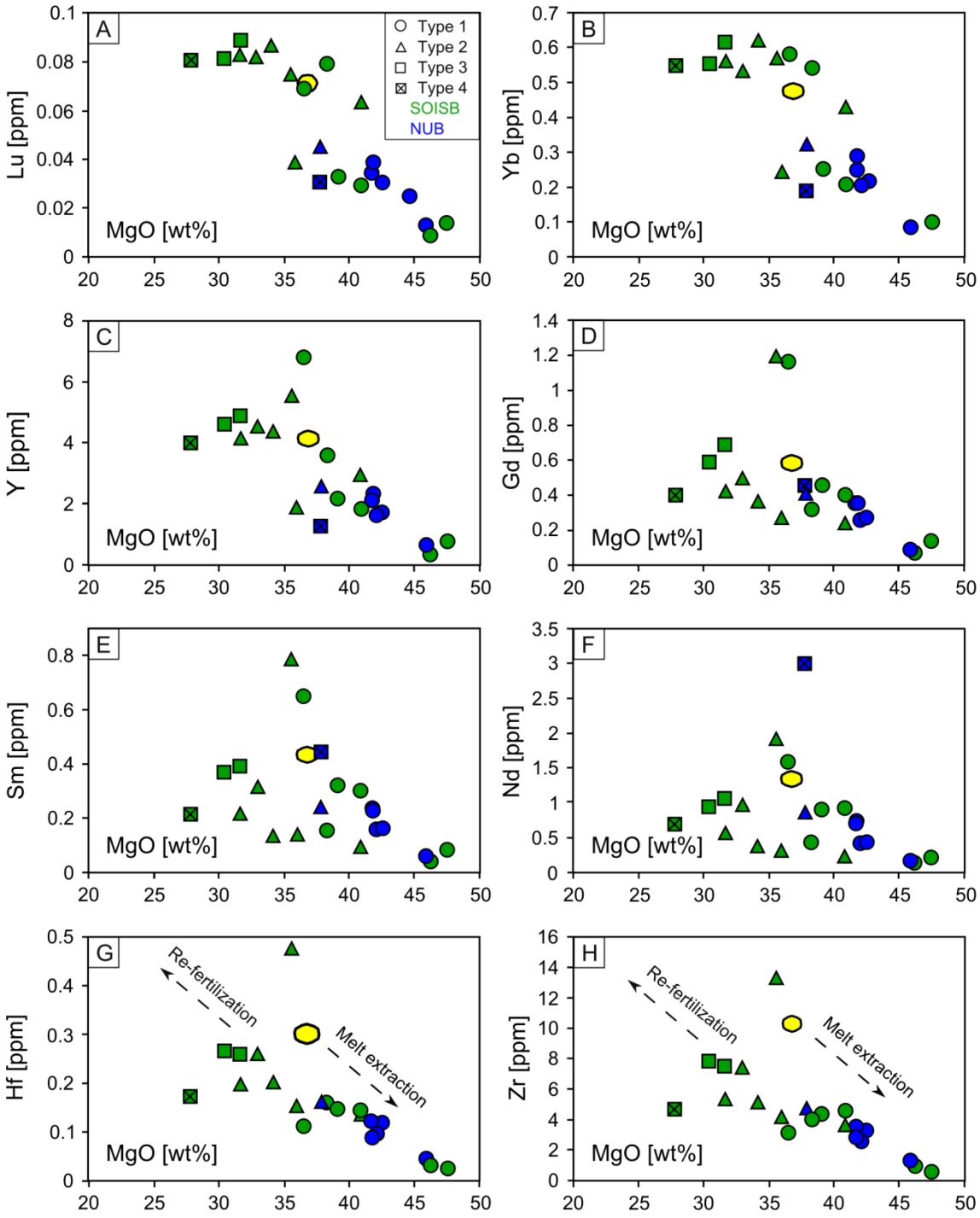

Figure 5-6: Variation diagrams for peridotites in this study, showing Lu, Yb, Y, Gd, Sm, Nd, Hf and Zr versus MgO contents. The element co-variations trends between MgO and most REE and HFSE obtained from the type 1 peridotites are in agreement with depletion and subsequent re-fertilization of the mantle rocks. In contrast to type 1 peridotites, type 2 peridotites show no or only weak correlations between REE, HFSE and MgO, suggesting a metamorphic overprint. The arrows in G and H indicate melt extraction and re-fertilization trends. Primitive mantle values from McDonough and Sun (1995) Palme, and O´Neill (2014). Note NUB type 4 sample 10-12A is not included in (G) and (H) (10-12A Hf=1.06 ppm, Zr= 32.1 ppm). Symbols are equivalent to those in Fig. 5-1 and 5-5.

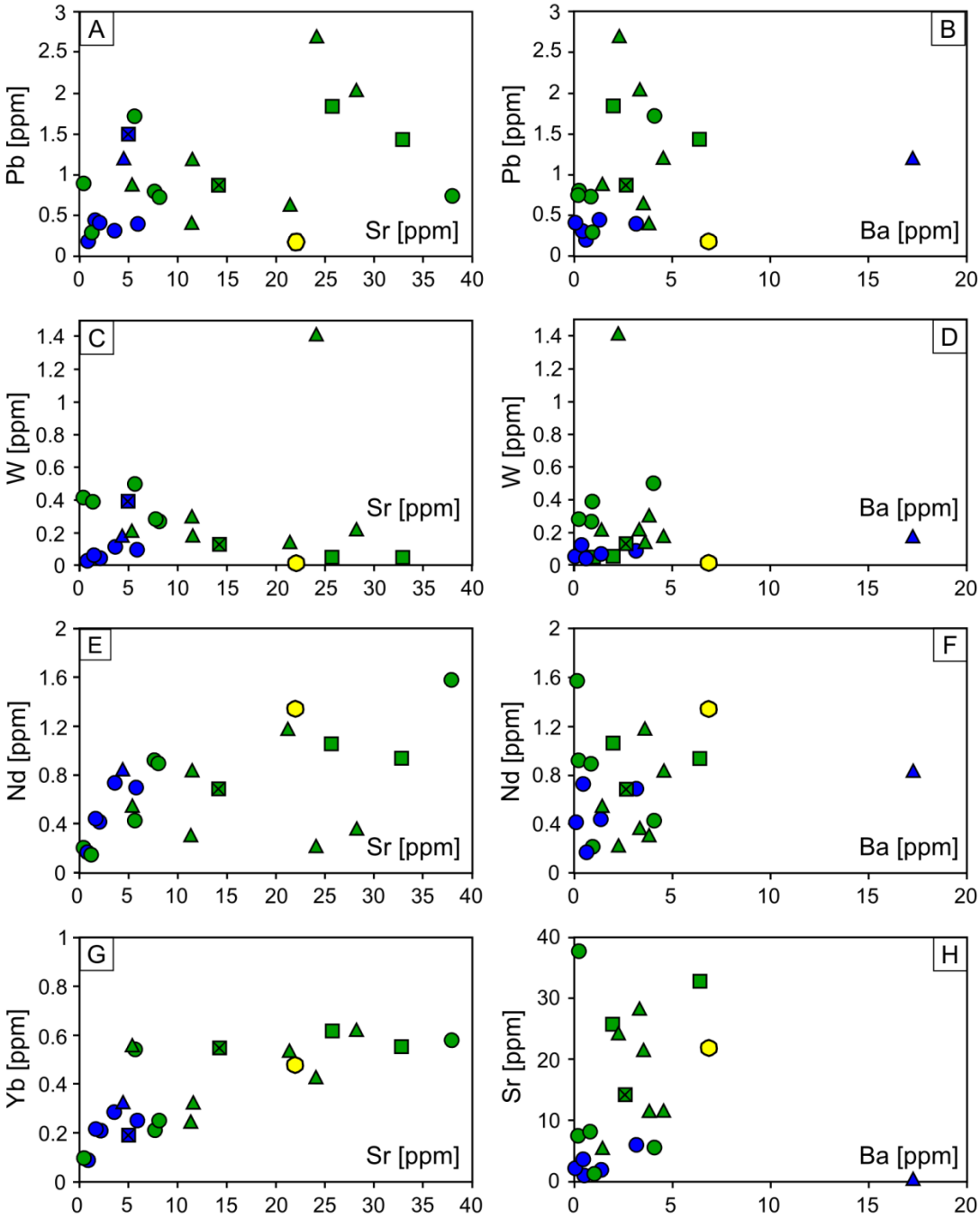

Figure 9-7: Variation diagrams for peridotites of this study showing (A, C, E, F) Pb, W, Nd, Yb versus Sr and (B, C, D, F, H) Pb, W, Nd, Sr versus Ba contents. All peridotites lack clear correlation between fluid mobile elements Sr and Ba with Pb, W, Nd and Yb. Thus, elevated Pb and W concentrations cannot clearly be linked to one distinct metasomatic event. Primitive mantle values are from McDonough and Sun (1995) and Palme and O´Neill (2014). Note that NUB type 4 sample 10-12A (10-12A Ba= 73 ppm) is not included in the diagrams (B, D, F,H). Symbols are equivalent to those in Fig. 5-1 and 5-5.

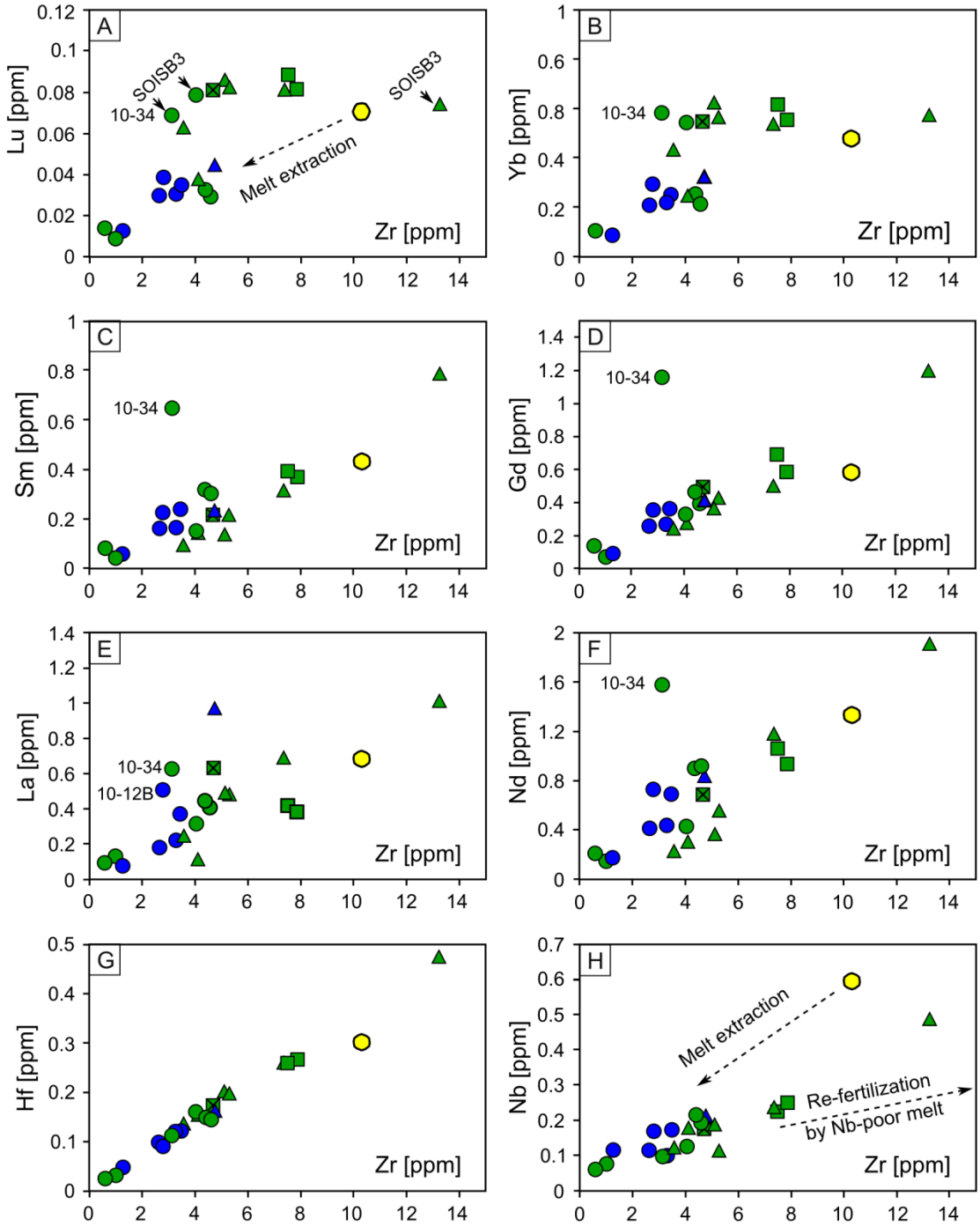

Figure 5-8: Variation diagrams for peridotites in this study showing Lu, Yb, Sm, Gd, La, Nd, Hf and Nb versus Zr contents. The element co-variations trends between Zr and most REE and HFSE obtained from the type 1 peridotites are in agreement with re-fertilization of depleted mantle rocks. The a*rrow in (A) indicates melt extraction trend and the arrows in (H) indicate melt extraction trend and a mixing trend with a Nb-poor melt.* Type 1 peridotite 10-34 from SOISB3 show mainly higher REE concentration than the other type 1 peridotites. Type 2 peridotite 10-12B show higher Zr concentration than all other type 2 peridotites, e.g. panel (A). For comparison primitive mantle (McDonough and Sun, 1995 and Palme and O´Neill, 2014). Note NUB type 4 sample 10-12A is not included in (H) (10-12A Zr= 32.1 ppm). Symbols are equivalent to those in Fig. 5-1 and 5-5

5-3.2 Trace element systematics and evidence for HFSE decoupling

Generally, the normative mineral compositions of the investigated peridotites vary between depleted lherzolite, harzburgite and dunite, in agreement with PGE systematics (Löcht et al., 2018). However, this petrological evidence contrasts with the observed mantle normalized REE patterns, which are overall relatively flat (except sample 10-12A, Fig. 5-3). This is inconsistent with models for high-degree melt extraction, which would trigger strong LREE depletions. Hence, post-melting refertilization of the mantle peridotites via melt/fluid-solid interaction must have occurred.

The absence of garnet as well as the low to moderate HREE concentrations in the type 1 mantle peridotites indicate, that the major melt extraction occurred in the spinel stability field. The nearly flat mantle-normalized REE patterns combined with trace element co-variations, such as between Zr or MgO and most REE and HFSE (Figs. 5-5 and 5-8*)* indicate refertilization of the peridotites by a melt-like, LREE-rich component (e.g., Niu, 2004; Paulick et al., 2006; Bodinier and Godard, 2014). All type 1 peridotites show negative Nb-Ta anomalies relative to LREE, whereas pure melt extraction would produce slightly positive Ta anomalies relative to Nb and La-Ce (e.g., Hoffmann and Wilson, 2017). In addition, slightly negative Zr-Hf anomalies relative to Sm-Nd are present in many samples (Fig. 5-3), arguing for a contaminant similar in composition to felsic melts such as tonalites (e.g., Hoffmann et al. 2011) that all exhibit marked Nb-Ta depletions. Diagnostic signatures for mantle overprint by a subduction-related re-enrichment agent are selective Nb-Ta depletion and enrichment of light-rare-earth-elements (LREE). Thus, the re-enriched LREE signature as well as the selective depletions in Nb-Ta in type 1 peridotites can be explained by replenishment of initially depleted peridotites by melt-like subduction components.

Notably, all peridotites show strong enrichments in Pb and W, but lack positive Sr anomalies. This signature is also characteristic for the investigated amphibolites and was previously observed in metabasalts from the ISB and from SOISB (e.g., Kamber et al., 2003; Hoffmann et al., 2011a; Rizo et al., 2013; Szilas et al., 2015; Dale et al., 2017) (Fig. 5-9). Proposed explanations for the high concentrations of W present in many Eoarchean mafic and ultramafic rocks invoked W addition during fluid-rock interaction in the mantle source region or metasomatic input via LREE-enriched fluid phases expelled from the surrounding tonalites (Touboul et al., 2014; Liu et al., 2016; Rizo et al., 2016).

Tungsten and Pb abundances show no correlations with MgO, Al_2O_3 or Zr contents, or with any fluid mobile element (Fig. 5-7). Hence, the enriched W concentrations in the

peridotites are consistent with mantle metasomatism, but cannot clearly be linked with a distinct metamorphic or metasomatic event.

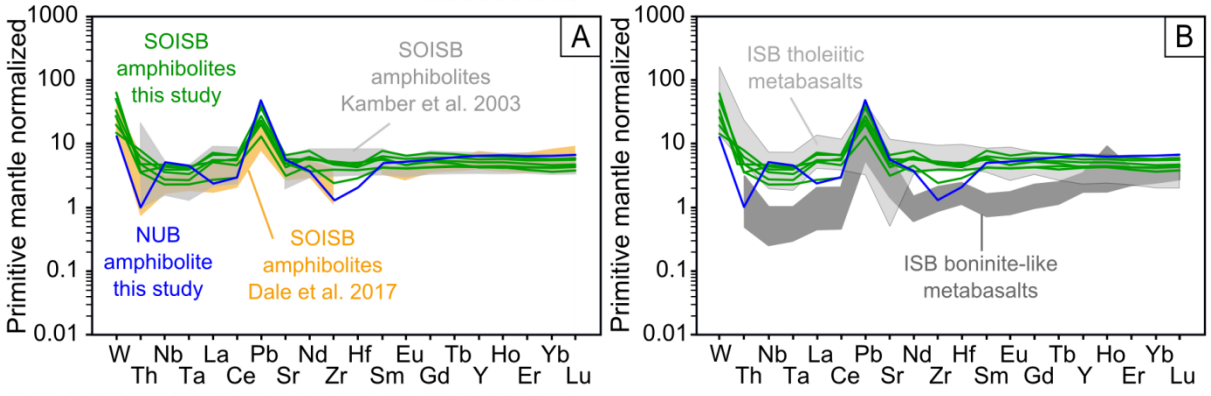

Figure 5-9: Primitive mantle normalized trace element patterns of amphibolites from SOISB and NUB compared to compiled literature data. The amphibolites show similar primitive mantle normalized trace element patterns than previously studied amphibolites from SOISB and tholeiitic metabasalts from ISB. (A) amphibolites from SOISB in comparison to literature data; the grey field indicates amphibolites from SOISB from Kamber et al., (2003) and yellow field amphibolites from SOISB from Dale et al., (2017). (B) Amphibolites from SOISB in comparison to tholeiitic metabasalts from the ISB and boninite-like metabasalts; the light grey field indicates tholeiitic metabasalts (Polat and Hofmann, 2003; Hoffmann et al., 2011a; Rizo et al., 2011; Rizo et al., 2016) and dark grey field ISB boninite-like metabasalts (Polat et al., 2002; Polat and Hofmann, 2003).Primitive mantle values are from Palme and O´Neill (2014).

5-3.3 Mantle versus crustal cumulate origin of the peridotites

Typical indicators to distinguish between crustal, ultramafic cumulates of magmatic origin and mantle residues are compositions of olivine and spinel (e.g. Fo#, Cr# vs. Fe#), whole rock major element chemistry (e.g. Al/Si vs. Mg/Si) as well as trace element ratios and inter-element co-variations (e.g., Yb vs. Al_2O_3, La_N vs Yb_N) (e.g., Haggerty, 1991; Arai, 1994; Bernstein et al., 2006; Rollinson, 2007; Hoog et al., 2010; Palme and O'Neill, 2014). Most of the type 1 and some of the type 2 peridotites show mantle-like chemical characteristics, and olivine with mantle-like forsterite contents (e.g., Figs. 5-1, 5-2, 5-5B, Chapter 4). Unfortunately, those criteria are indicative in their combination, but not always coherent, because metasomatic and metamorphic processes can partly obliterate the original chemical compositions. For example, the MgO content in olivine can be lowered by Mg-Fe diffusion during metamorphism, resulting in lower Fo#. Metasomatically induced growth of secondary phases would cause significant changes in the whole rock composition (e.g. CaO and Al_2O_3 contents), but inter-mineral element exchange might be limited. For instance, sample 10-36 contains olivine with mantle-like composition (e.g. Fo# = 90) but does not plot along the Mg/Si vs. Al/Si (Fig. 5-5A) mantle fractionation trend, due to its higher Al_2O_3 content. Yet, sample 10-20A plots along the trend but has Fo# < 89. For some parameters, ultramafic

crustal cumulates can overlap with mantle peridotites, for instance in some major element compositions (e.g., Fig. 5-5B and Szilas et al., 2015).

The overall flat REE patterns and the lack of LREE depletion in the peridotites cannot be used as an argument against a mantle origin. This is because, trace element patterns are often not a diagnostic feature to discriminate mantle rocks from crustal ultramafic cumulates, since mantle residues are often far more enriched in incompatible elements than can be produced by a melt extraction models alone (e.g., Bodinier and Godard, 2014). Hence, trace element abundances, and especially LREE inventories are often controlled by melt/fluid-rock interaction and not only by the degree of melt extraction. Such LREE enrichment can occur either as a primary process in the mantle source or alternatively, due to secondary element enrichment at crustal level, e.g., during tectono-thermal events.

Platinum group elements (PGE) behave rather robust during alteration and metamorphism (e.g., Barnes et al., 1985). Thus, PGE signatures can be key indicators to distinguish between crustal ultramafic cumulates and mantle residues. The peridotites that were investigated in terms of their PGE composition, comprising seven type 1 peridotites from SOISB1, SOISB2 and NUB (= PGE-group 1 Chapter 4) and four type 2 peridotites from SOISB2 (=PGE-group 2 Chapter 4). Based on primitive mantle normalised PGE pattern in combination with the petrological observations and the chemical compositions, type 1 peridotites were characterised as mantle peridotites (Chapter 4). Note that three of these type 1 peridotites (10-12B, 10-20C and 10-34) show preserved mantle-like PGE patterns, even though these peridotites differ in some aspects in their chemical composition from the other type 1 peridotites (e.g. Fo# <89, higher CaO or HREE concentrations). Correspondingly, based on the petrological and chemical similarities and spatial distribution, all type 1 peridotites are classified here as mantle peridotites. The four type 2 peridotites exhibit nearly flat primitive mantle normalised PGE patterns and are therefore neither diagnostic for mantle residues nor for ultramafic, crustal cumulates. Yet, these samples might represent mantle rocks, with altered PGE inventory due to melt–rock interaction (e.g., Büchl et al., 2002; Chapter 4). Several SOISB2 type 2 peridotites display some characteristics of mantle peridotites, like Fo#>89 and/or plot along mantle fractionation trends (e.g., Figs. 5-2, 5-5, 5-6). Friend et al. (2002) studied major and trace elements of ultramafic rocks from SOISB and proposed that they represent remnants of Eoarchean mantle. One of these peridotite (G93-42) that contains mantle-like spinel (Rollinson, 2007), is from the same ultramafic unit than sampled here by SOISB2 type 2 peridotites. Furthermore, Dale et al. (2017) investigated four peridotites from the same region in terms of highly siderophile elements (HSE including PGE). Except for one

sample, the Dale et al. 2017 samples are similar to the type 2 peridotites discussed here, with respect to most major and trace elements and Pt-Pd-enriched PGE patterns. Dale et al. (2017) concluded that these peridotites are likely of mantle origin. Altogether, these findings support the assumption, that some of the type 2 peridotites might be of mantle origin. However, in the case of our type 2 peridotites, primary signatures have clearly been obliterated by metamorphic or metasomatic processes, so that an unambiguous characterisation of their origin is not possible with the available data. In contrast, type 3 peridotites are well preserved and can be regarded as ultramafic, crustal cumulates, based on field observations (cumulate textures), microtexture, and their whole rock and olivine chemical compositions (e.g. Figs. 5-2, 5-5, 5-6 and abundant fresh olivine with Fo#< 89). Thus, type 3 peridotites do not provide direct evidence for mantle processes, and will therefore not be included in the following discussion on Eoarchean mantle evolution.

5-3.4 Lu-Hf and Sm-Nd isotope constraints on Eoarchean mantle evolution and timing of refertilization

Nine well preserved SOISB peridotites define a whole rock ^{176}Lu-^{176}Hf age regression line corresponding to an age of 3908 ± 50 Ma (MSWD = 4.3) (Fig. 5-10A). Generally, most Lu-Hf whole rock age regression lines obtained for the individual types of peridotites overlap this age within error, independent of location or origin (Fig. 5-10 and B-1). For example, ^{176}Lu-^{176}Hf whole rock errorchrons obtained from SOISB1 and NUB mantle peridotites (type 1) (except altered sample 10-12B) yield an age of 3908 ± 230 Ma (MSWD = 22, n = 8, initial εHf = +3.9) (Fig. B-1E) and pooled with potential mantle peridotites (type 2) from SOISB2, an age of 3967 ± 96 Ma (MSWD = 16, n=14) and an initial εHf of +2.7 (Fig. B-1F) is calculated. Considering the re-enriched trace element compositions of the peridotites, the Lu-Hf isotope signatures most likely represent a mixture between refractory mantle and the re-fertilization agent. Hence, we interpret the Lu-Hf ages as the time of replenishment of the mantle sources by re-fertilization agent, most likely slab melts with negative Nb-Ta anomalies.

In contrast to ^{176}Lu-^{176}Hf, the ^{147}Sm–^{143}Nd data generally yield younger mainly Eoarchean to Neoarchean errorchron ages with a smaller spread and larger scatter on the regression lines (Figs. 5-10C-D and B-2), suggesting metamorphic disturbance of Sm-Nd isotope systematics.

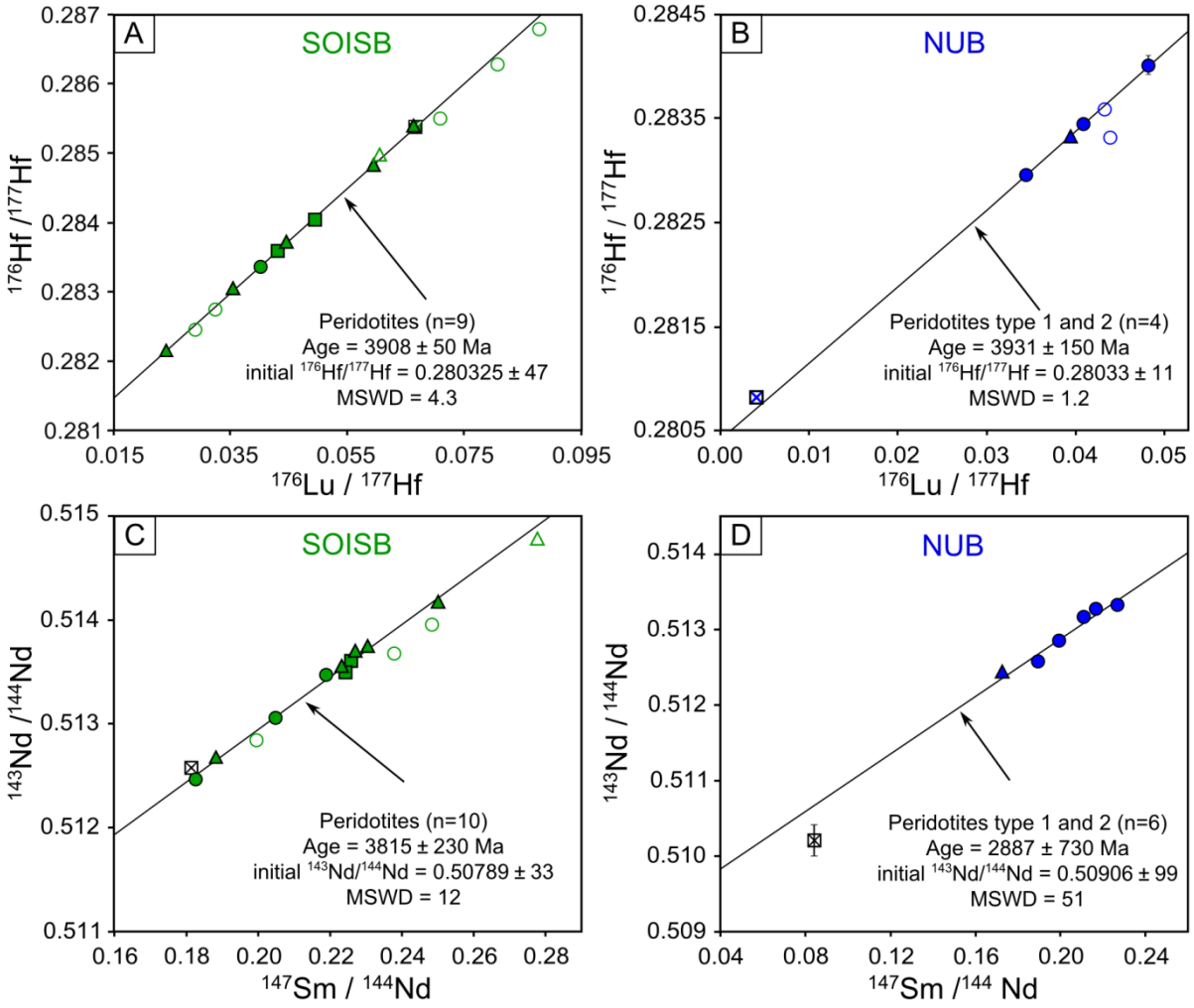

Figure 5-10: Measured (A-B) $^{176}Lu/^{177}Hf$ versus $^{176}Hf/^{177}Hf$ and (B-C) $^{147}Sm/^{144}Nd$ versus $^{143}Nd/^{144}Nd$ data obtained for the SOISB and NUB peridotites with age regression lines calculated using Isoplot (version 3.41d, Ludwig, 2006). The whole-rock Lu-Hf age regression lines obtained from the peridotites from SOISB and NUB, yield Eoarchean ages and are therefore consistent with estimated minimum ages > 3.81 Ga. The ^{147}Sm–^{143}Nd data yield Eoarchean to Neoarchean errorchron ages with a smaller spread and larger scatter on the regression lines, suggesting metamorphic disturbance of Sm-Nd isotope systematics. The panels show regression lines for all peridotites from the locations SOISB (A and C) and NUB (B and D). Symbols are equivalent to those in Fig. 5-1 and 5-5, open symbols indicate samples not being included in the regression line calculations.

A 10 point regression line in the Sm-Nd space obtained from SOISB type 1, 2 and 3 peridotites yield an age of 3815 ± 230 Ma (MSWD = 12) (Fig. 5-10C). Interestingly, as for the ^{176}Lu - ^{177}Hf data, ^{147}Sm-^{143}Nd data obtained from NUB mantle peridotites plot in the same range than SOISB type 1 and 2 peridotites, a regression line obtained for NUB and SOISB mantle (type 1) peridotites (except 10-14 and 10-36) yields an age of 3403 ± 260 Ma (MSWD = 16) (Fig. B-2B). Although no accurate age constraint is possible for the ^{147}Sm-^{143}Nd isotope system due to lack of sufficient spread or too large scatter on the regression

lines, the Lu-Hf errorchron ages are in good agreement with the postulated minimum ages of >3.81 Ga based on U-Pb dated crosscutting tonalite sheets (e.g. Friend and Nutman, 2005; A. P. Nutman et al., 2007).

Initial εHf and εNd values, calculated back to the minimum age of 3.81 Ga, show an appearing decoupling of the two isotope systems (Fig. 5-11). Such a decoupling was also found in TTGs and metabasalts from the IGC (e.g., Hoffmann et al., 2011b).

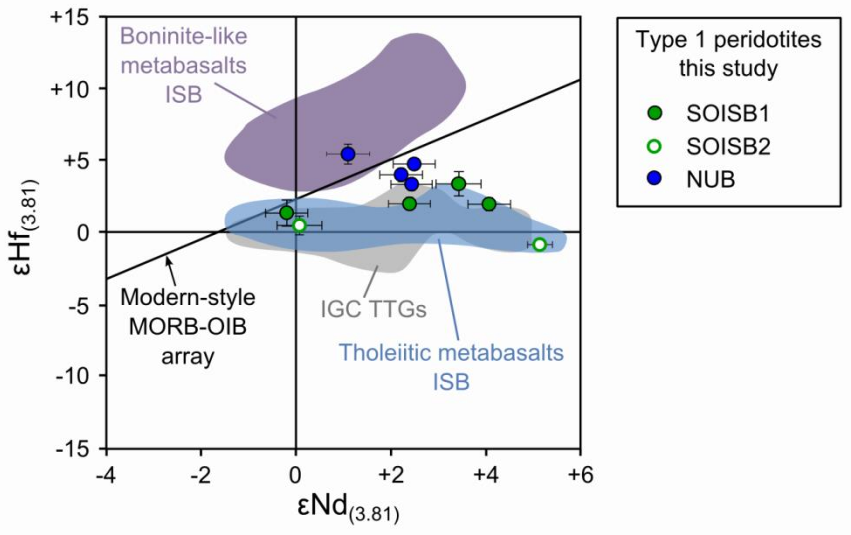

Figure 5-11: Initial $\varepsilon Hf_{(3.81)}$ vs. $\varepsilon Nd_{(3.81)}$ values of SOISB and NUB type 1 (except altered sample 10-12B) peridotites in comparison to tholeiitic and boninitic metabasalts from the ISB and TTGs from the IGC, and the modern style MORB-OIB array after Vervoort et al., (2011). The figure illustrates the apparent decoupling of the initial εHf and εNd values for the type 1 peridotites from SOISB and NUB, calculated back to the minimum age of 3.81 Ga. The blue field indicates tholeiitic metabasalts and the purple field indicates boninite-like metabasalts from the ISB. (Data sources: (Blichert-Toft et al., 1999; Boyet et al., 2003; Polat et al., 2003; Hoffmann et al., 2010a, 2011); the grey field indicate TTGs from the IGC (Bennett et al., 1993; Vervoort et al., 1996; Vervoort and Blichert-Toft, 1999; Bennett et al., 2007; Hiess et al., 2009; Hoffmann et al., 2011a, 2014). The datasets were calculated using the ^{176}Lu decay constant parameters of Scherer et al., 2001 and Söderlund et al., 2004) and CHUR parameters of Bouvier et al. (2008).

Generally, Lu-Hf and Sm-Nd isotope systems behave similar during mantle melting (e.g., Chauvel et al., 2008; Vervoort et al., 1996, 2011), and, thus, an additional process is needed to explain the apparent decoupling. One scenario to explain the observed decoupling of εHf and εNd in TTGs and metabasalts from the IGC is metasomatism of depleted mantle with a subduction-derived component (e.g., Jenner et al., 2009; Hoffmann et al., 2011b). Refertilization of the Greenland peridotites by an LREE-rich component would cause less prominent changes in the element inventory for Lu-Hf than for Sm-Nd. Yet, in the case of the investigated peridotites, the Nd-isotope inventory may to some extent reflect open system behavior during Archean tectono-thermal events, which are well documented for the regions.

Hence, the apparent εNd and εHf decoupling might partly be a source signature of the metasomatized mantle, but blurred due to isotopic disturbance superimposed by late post-emplacement metamorphic events. Consequently, it is not possible to provide an unambiguous interpretation of the initial $\varepsilon Nd_{(t)}$ and thus, no strong statement regarding the apparent εNd and εHf decoupling can be made here. The overlap with TTGs and mafic rocks, however, suggest that the observed Hf-Nd decoupling is indeed a primary feature of the peridotites investigated here.

5-3.5 Mantle melting and refertilization

Petrological observations combined with major and trace element compositions of the type 1 peridotites can be explained by melt depletion, mainly in the spinel stability field (~1-2 GPa), followed by subsequent refertilization by melt/fluid-rock interaction. In addition, the low Al, Ca and Na concentrations provide limitations for the volume of the metasomatic melt entrapped. The trace element signatures suggest that the infiltrating melt was rich in Th, HFSE and LREE, combined with selective depletions in Nb-Ta, and in some cases Zr-Hf, as well as elevated Nb/Ta.

Niobium and Ta concentrations and Nb/Ta ratios in melts can be used to discriminate between residual mineralogies that are present at different source depths such as (garnet)–amphibolite or rutile–bearing eclogite. Because residual phases like amphibole or rutile control the Nb–Ta budget. Residual low Mg-amphibole can result in lower Nb/Ta ratios in the coexisting melt whereas residual rutile would cause higher Nb/Ta ratios in the coexisting melt (e.g., Green, 1995; Foley et al., 2002; Klemme et al., 2002; Rapp et al., 2003; Münker et al., 2004; Klemme et al., 2005; Xiong, 2006; John et al., 2011; Li et al., 2017).Hence, partial melting of subducted oceanic crust in the stability field of rutile–eclogite can indeed produce melts that are rich in Th and LREE, combined with selective depletions in Nb-Ta and elevated Nb/Ta (e.g., Klemme et al., 2002; Münker et al., 2004; Hoffmann et al., 2010). Most modern and late Archean adakites and adakitic rocks as well as many Achean TTGs resemble such melt compositions and often overlap in their Zr/Hf and Nb/Ta ratios with the peridotites investigated here (e.g., Figs. B-4D and B-5).

Adakites (sensu stricto) are oceanic slab-melts (Defant and Drummond, 1990) and adakitic rocks are not necessarily slab-melt derived, but subduction zone related (e.g., Polat and Kerrich, 2000; Martin et al. 2005). TTG formation is commonly assumed to be either associated with a subduction-related setting (e.g., Martin, 1986; Drummond and Defant, 1990; Kamber et al., 2002) or with melting of thickened mafic crust (e.g., Smithies, 2000; Condie, 2005; Bédard, 2006; Hoffman et al. 2011A). The Eoarchean IGC TTGs presumably

originated from melting of a thickened mafic crust (e.g., Hoffmann et al., 2011a; Nagel et al., 2012; Hoffmann et al., 2014). Collectively, most modern and late Archean adakites and adakitic rocks, and many Achean TTGs are characterised by high LREE, low HREE, selective HFSE anomalies and highly variable Nb/Ta (Fig. B-4 and B-5). Therefore, the observed Th-HFSE-REE systematics in the peridotites can be reasonably well explained by variable degrees of hydrous melt extraction from a primitive mantle source in the spinel stability field and subsequent addition of a low quantity of a TTG-like or adakitic melt with selective HFSE depletion.

Interestingly, all investigated peridotites and amphibolites plot above and parallel to the MORB-OIB trend in the Nb/Yb - Th/Yb discrimination diagram of Pearce (2008) (Fig. 5-12A), consistent with contamination by slab melts (e.g., Polat et al., 2011). Such a scenario is also consistent with observations based on combined Zr/Hf - Nb/Ta and εNd - εHf systematics and of metabasalts from the ISB, where interaction and refertilization of IGC Archean mantles sources with subduction related components was postulated previously (e.g., Polat et al., 2002; Polat and Hofmann, 2003; Jenner et al., 2009; Hoffmann et al., 2011b; Polat et al., 2011; Hoffmann et al., 2012).

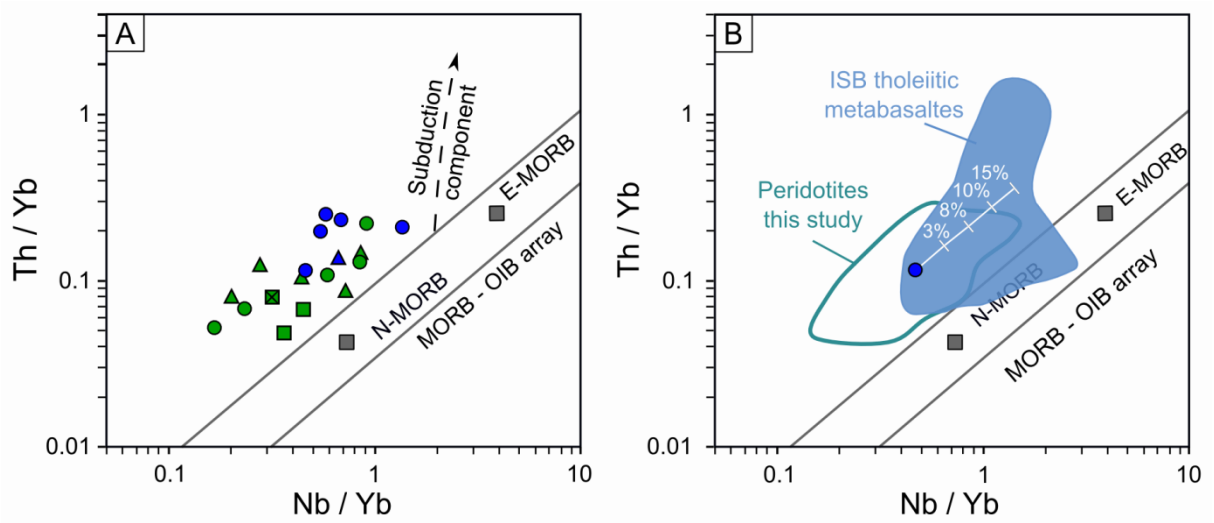

Figure 5-12: Th/Yb versus Nb/Yb diagram adopted from Pearce (2008), showing (A) compositions of SOISB and NUB peridotites and (B) fields for ISB tholeiitic metabasalts (Polat and Hoffmann, 2003 and Hoffman et al., 2011a) together with mantle peridotite 10-9, consistent with the formation model for the amphibolites discussed in paragraph 5-3.6. Symbols are equivalent to those in Fig. 5-1 and 5-5

To evaluate this model further, we modelled harzburgite formation by partial melting and subsequent refertilization by slab melts (Fig. 5-13). For clarity, only mantle peridotites from SOISB1 and NUB are considered in the model presented. The details of the model parameters are provided and discussed in the Appendix B. As starting mantle composition the primitive mantle composition from Palme and O'Neill (2014) was used and initial mineral modes were

assumed as 53% olivine, 29% orthopyroxene and 18% clinopyroxene, and spinel is considered to be inert (Salters and Stracke, 2004). In the case of the dunites, clinopyroxene exhaustion at > 25% melting was taken into account and a simplistic two stage melting-model was applied (Fig. 5-14). In the second step the residuum after 25% melt extraction (step 1) were further melted using a mineral mode of 71% olivine, 23% opx and 3% spinel (McDade et al., 2003a) (step 2). However, this simplistic model does not incorporate the full complexity

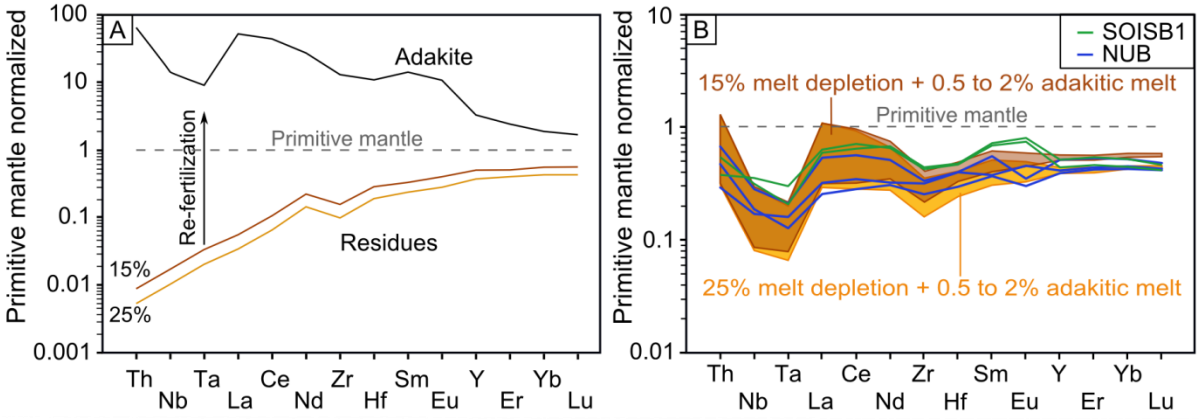

of dunite formation, e.g. does not account for olivine formation by (reactive) melt transport.

Figure 5-13: Melting-refertilization-model used in this study. (A) Primitive mantle normalized melt residues calculated assuming a primitive mantle source being depleted by 15% and 25% melting, respectively, shown together with Archean adakite MW96-6 (Polat et al., 2000) that was used as representative slab melt being added. (B) Primitive mantle normalized trace element patterns of NUB and SOISB1 harzburgitic mantle peridotites in comparison to the modelled re-fertilized mantle rocks. The brown field illustrates the modelled range of trace element abundances after 15% of partial melt extraction and addition of 0.5 to 2% of slab-derived adakitic melt. The orange field illustrates the modelled range of trace element abundances after 25% of partial melt extraction of a primitive mantle source and addition of 0.5 to 2% of slab-derived adakitic melt.

Mineral-melt partition coefficients for hydrous melting of primitive mantle at 1.3-1.5 GPa and 1245 – 1315°C are taken from McDade et al. (2003a and 2003b), assuming that the H_2O effect on the olivine-melt partition coefficients is negligible. Alternative, mineral-melt partition coefficients for 2GPa and 1080 – 1100°C from Adam and Green (2006) and Green et al. (2000) were applied (see Appendix B-1.1 and Fig. B-3). Both approaches indicate melt extraction mainly between 15 - 25% in the case of the NUB and SOISB1 hbl-bearing -peridotites, and >30% in the case of the dunites.

Certainly, the refertilization processes was likely complex involving multistage melt, fractional crystallisation and fluid overprint. Yet, in order to test if mantle refertilization by a slab derived melt is a plausible scenario for the investigated Eoarchean mantle peridotites, we employ a simplified mixing model, using a late Archean (~2.7Ga) high SiO_2 adakite composition (M96-6, Appendix B-2) as refertilization agent that was derived mainly from

slab melting (Polat and Kerrich, 2001; Polat and Münker, 2004). This adakite is a typical representative of late Archean and modern high SiO_2 adakitic rocks from arc-settings (Polat and Kerrich, 2000; Martin et al., 2005; Hidalgo et al., 2014).

For the mantle hbl-bearing peridotites from NUB and SOISB1, our trace element modelling approach yields about 15 to 25% melt depletion followed by about 0.5 to 2% addition of slab melt (Fig. 5-13B). For the dunites the melting-refertilization-model indicates between 30 and 40% melt depletion and less than 1.5% of slab melt addition (Fig. 5-14). Note that the primitive mantle normalized trace element patterns of the resulting refertilised peridotite are either entirely dominated by the melt signature (Th-Nb-Ta-La), represent a mixed signature (Nd-Zr-Hf-Sm-Eu) or record the signature of the melt depletion prior to the refertilization (HREE) (Fig. 5-13 and B-3B).

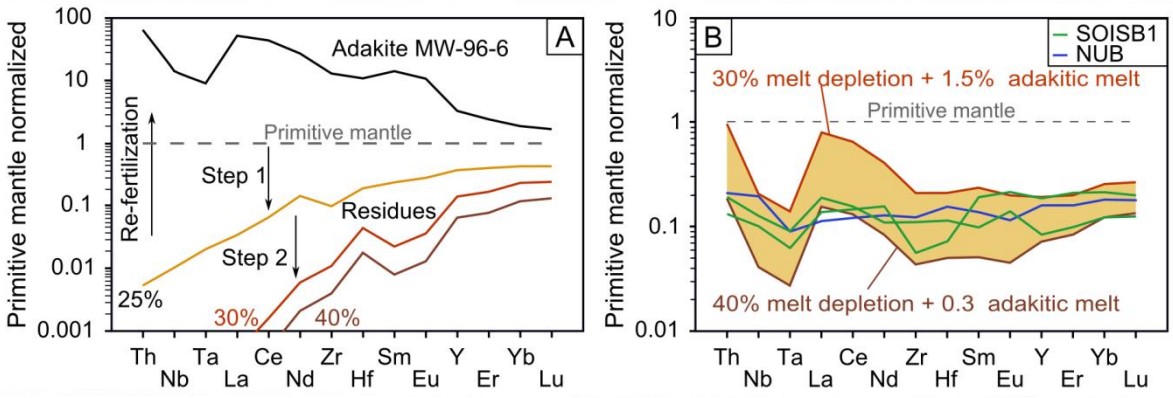

Figure 5-14: The dunite melting-re-fertilization-model: For the dunites, the melting-refertilization-model indicates between 30 and 40% melt depletion and less than 1.5% of slab melt addition. (A) A two-step melting-model was used for the dunites, to account for clinopyroxene exhaustion at >25%. The labels on the melting lines indicate amounts of total extracted melt after step 1 (30%) and step 2 (30-40%). (B) Primitive mantle normalized trace element patterns of NUB and SOISB1 dunites of this study in comparison to the modelled re-fertilized mantle rocks. The field indicate the modelled range of trace element abundances after 30-40 % of partial melting and 0.3–1.5% addition of adakitic melt.

As a alternative to the above model, a more complex, non-subduction related mantle-refertilization-model as presented by Bédard (2006) might produce similar trace element patterns. Such models would include crystal fractionation, melting of a delaminated, eclogitic mafic crust or tectonic incorporation of refractory mantle rocks in a thick mafic crust and melting of the underlying “eclogitic” crust.

However, the major purpose of the simplified modelling performed here was to test, whether refertilization of the mantle peridotites by a slab derived melt is plausible and in fact, this appears to be the case.

Importantly, the mantle peridotites from both Eoarchean terranes (SOISB1: Isukasia terrane and NUB: Færingehavn terrane), overlap in their trace element abundances and Lu-Hf and Sm-Nd isotope compositions. Hence, similar mantle depletion and replenishment scenarios can be inferred for the investigated mantle peridotites from both terranes. The differences between the mantle peridotite compositions most likely reflect variations in previous melt extraction, in the composition of the re-fertilizing agent and to a limited degree in additional metasomatic overprint (e.g., for LREE).

5-3.6 Implications on mantle-crust evolution

Recent studies argued in favour of a subduction-related setting of Eoarchean mafic rocks in the IGC that involve mantle source overprinted by melts and fluids derived from subducting crust (Polat et al., 2002, 2011; Polat and Hofmann, 2003; Jenner et al., 2009; Hoffmann et al., 2011b). The investigated amphibolites exhibit similar primitive mantle normalized trace element patterns than previously studied tholeiitic metabasalts from SOISB and ISB with arc-like signatures (Fig. 5-9) (Kamber et al., 2003; Jenner et al., 2009; Hoffmann et al., 2011a; Rizo et al., 2011; Rizo et al., 2013; Szilas et al., 2015; Dale et al., 2017). Less than 15% melting of least altered peridotites (e.g., sample 10-09) can produce melts with similar primitive mantle normalized trace element patterns to those obtained for metabasalts from SOISB and ISB (Fig. 5-15, and Appendix B-3), and also Th/Yb and Nb/Yb ratios (Fig. 5-12B). This strongly supports formation models for the ISB metabasalts that postulated melting of a depleted and subsequently refertilised mantle source (e.g., Polat et al., 2011; Polat and Hofmann, 2003; Jenner et al., 2009; Hoffmann et al., 2011b). Ratios of Zr/Hf in type 2 and 3 peridotites overlap those obtained from the type 1 mantle peridotites and also overlap with Zr/Hf ratios for ISB and SOISB metabasalts (Fig. C-5D). Together with partially overlapping positive initial $\varepsilon Hf_{(3.81)}$ this supports the scenarios where the mafic rocks in the ISB and SOISB might originate from a depleted mantle domain similar to that sampled by the peridotites investigated here.

If and how plate tectonics operated in the Eoarchean is a highly controversial issue. This is particularly because the use of present day subduction zone proxies (e.g. Nb/Yb-Th/Yb discrimination diagram) for Archean rocks has been challenged (e.g., Pearce et al. 2008). Metamorphic overprint may have obscured some of these signatures. However, increasing evidence for horizontal tectonics to have operated in the Greenlandic and North American part of the North Atlantic Craton was reported over the past years, also combining structural observations and geochemical data (e.g., Friend et al., 2002; Hanmer et al., 2002; Nutman et

al., 2007, 2009, 2013; Næraa et al., 2012; Dziggel et al., 2014, 2017; Komiya et al., 2015; Polat et al., 2015, Polat et al. 2015).

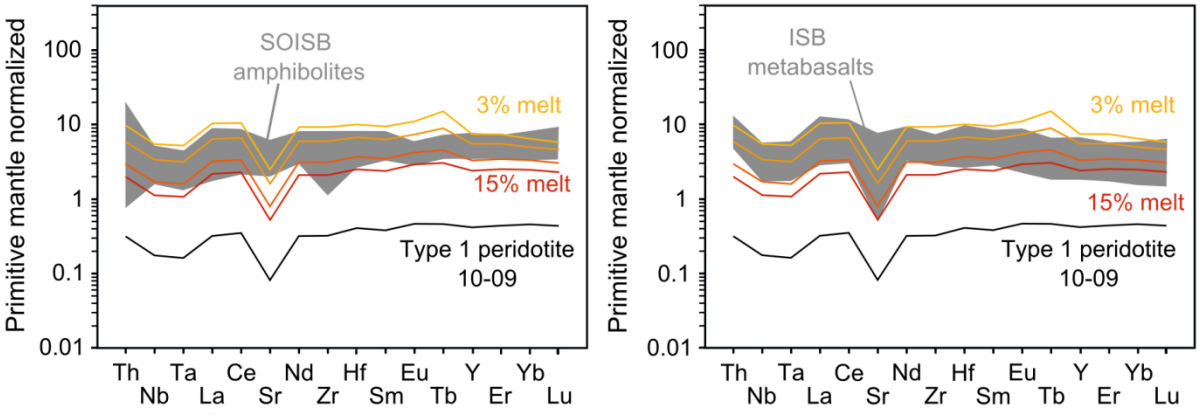

Figure 5-15: Primitive mantle-normalized trace element patterns of metabasalts from (A) SOISB and (B) ISB (same as in Figure 5-3) are in the range of trace element abundances for modelled melts generated by 3 to 15% of partial melting of the representative peridotite sample 10-09. The red to yellow lines indicate 15%, 10%, 5% and 3% melting. Thus, the ISB and SOISB metabasalts might originate from a depleted mantle domain similar to that sampled by the peridotites investigated here.

5-4 CONCLUSIONS

Peridotite enclaves from the IGC of southern West Greenland allow valuable insight into the history of the Eoarchean mantle. These enclaves occur in both the Isukasia and Faeringehavn terranes, but petrologic types and compositions overlap between the two terranes. Based on their optical properties and microstructure, the investigated spinel-peridotites can be subdivided into four different types. Type 1 peridotites are characterized as mantle peridotites, based on petrological observations, major element concentration, olivine composition, and PGE inventory. In contrast, type 3 peridotites are considered as magmatic crustal cumulates. Element remobilisation and recrystallization during metasomatism and amphibolite facies metamorphism can account for the petrography and chemical compositions of type 2 and type 4 peridotites. Hence, a clear characterisation of their protoliths as mantle peridotites or magmatic crustal cumulates remains ambiguous.

Whole-rock Lu-Hf age regression lines obtained from the peridotites from SOISB and NUB, predominantly yield Eoarchean ages and are therefore consistent with estimated minimum ages > 3.81 Ga, as inferred mainly from dated crosscutting tonalite sheets. Collectively, Lu-Hf isotope data together with contents of MgO and immobile trace elements such as Zr suggest that post-emplacement disturbance of the Lu-Hf isotope systematics was minor. The peridotites show apparent decoupling of initial εHf-εNd values, similar to

metabasalts from the ISB and IGC TTGs. Yet, open system behaviour during the Archean tectono-thermal events may have affected the Sm-Nd isotope patterns of some samples. Interestingly, chemical compositions and radiogenic isotope signatures of mantle peridotites from both Eoarchean IGC terranes overlap, and the differences in element concentrations between samples mainly reflect differences in the degree of melt-depletion, subsequent refertilization, and to minor extent alteration.

In the case of the SOISB1 and NUB mantle peridotites, their Th-REE and HFSE signature can be well explained by hydrous batch melting of primitive mantle in the spinel stability field and subsequent addition of low quantities of an adakitic melt, similar to modern melts derived from subducting slabs of oceanic crust. Higher potential mantle temperatures in the Eoarchean had likely facilitated partial melting of subducting oceanic crust, making slab melt overprint an important mechanisms to modify primary geochemical signatures in the Archean upper mantle. Melting of such metasomatized mantle peridotites can account for the near primitive mantle normalized trace element pattern obtained from mafic rocks in the ISB and SOISB, including the investigated amphibolites from SOISB. Thus, the investigated mantle peridotites likely provide direct evidence for the preservation and operation of Eoarchean subduction processes that were in fact very similar to those operating today. In addition, our findings broadly support the proposed formation of Eoarchean lavas in SW Greenland in a supra-subduction zone geodynamic setting.

Chapter6

Composition and radiogenic isotope systematics of mineral phases in Eoarchean peridotites from the Itsaq Gneiss Complex, southern West Greenland

6-1 INTRODUCTION

Major and minor element compositions and radiogenic isotope patterns of minerals from peridotites are helpful to differentiate between a mantle-, magmatic- or metamorphic origin and to evaluate the metamorphic overprint and subsequent element mobility. Hence, mineral chemical compositions are important for the detailed characterisation of rocks and for the reconstruction of their petrogenetic evolution. Therefore, major and minor element concentrations in olivine, pyroxene, amphibole, and spinel were determined for the peridotites from SOISB and NUB. In addition, selected major element compositions of chlorite and mica were obtained for some representative peridotites to place constraints on the metamorphic processes. It is shown in chapter 3 that olivines in most type 1 peridotites show mantle-like major element compositions and thus support the conclusion that those rocks are mantle peridotites (see also Chapters 4 and 5). In this chapter, olivine analyses are discussed in more detail, together with the other mineral data.

In order to evaluate the trace element distribution in the peridotites and to gain a better understanding of their isotope signatures and ages, Lu-Hf-Sm-Nd-Rb-Sr concentrations and isotope compositions were obtained via isotope dilution MC-ICP-MS measurements for mineral separates of four peridotites (one peridotite from each location (NUB, SOISB1, SOISB2 and SOISB3). This isotope dataset includes Olivine, orthopyroxene and amphibole separates for three type 1 peridotites from NUB (10-11), SOISB1 (10-20C) and SOISB2 (10-36) and one type 3 peridotite (10-27). Rubidium and Sr isotope compositions were obtained for those four peridotites from the same whole rock aliquots as used for Lu, Hf, Sm and Nd MC-ICP-MS measurements (Chapter 5).

Clinopyroxene and, if present, amphibole are the main phases in spinel peridotites that incorporate Lu, Hf, Sm and Nd. Yet, Clinopyroxene is absent in most of the investigated peridotites, except for sample 10-34. However, even sample 10-34 contains only trace amounts of clinopyroxene. Hence, amphibole is the main phase incorporating Lu, Hf, Sm and Nd in the peridotites of this study. Textural patterns for amphiboles in some samples clearly indicate a secondary origin, but this is less obvious for most samples. Moreover, textural observations suggest preservation of fresh olivine and orthopyroxene. Hence, mineral

compositions and an internal isochron approach are highly useful to evaluate the origin and potential alteration of the amphiboles, olivines and orthopyroxenes.

6-2 RESULTS

6-2.1 Major and minor element abundances in olivine, pyroxene, amphibole and spinel

Representative mineral analyses of olivine, orthopyroxene, amphibole and spinel are given in Table 6-1 and the full range of mineral analyses and those obtained for chlorite and mica are given in Appendix C Tables C-1 to C-4.

6-2.1.1 Olivine

Most type 1 peridotite olivine compositions are Mg-rich with Fo# (Fo# = 100*Mg/(Mg+Fe)) ranging from 90 to 92. Only three samples (10-20A, 10-20C and 10-34) yield lower Fo# between 86 and 88. Type 2 peridotite olivine compositions overlap with those obtained for the type 1 peridotites (Fo# 85-91). Olivines of type 3 peridotites have Fo# < 89 (83 and 87). In the type 3 peridotites, the compositions of olivine inclusions in poikiloblastic orthopyroxenes are indistinguishable from those in the matrix. NUB type 4 peridotite olivines are Mg-rich (Fo# 90), whereas SOISB type 4 peridotite olivines have comparably lower Mg contents (Fo# 88). In all SOISB and NUB olivines, the concentrations of CaO and Cr_2O_3 are very low, with contents of <0.03 wt% and <0.05 wt%, respectively (Table 6-1). The amount of NiO (0.20-0.53 wt%) exceeds that of MnO (0.12-0.28 wt%), expect for one sample (10-29B).

Table 6-1: Representative electron microprobe mineral analyses

Sample	Type	SiO_2 wt%	TiO_2 wt%	Al_2O_3 wt%	Cr_2O_3 wt%	FeO wt%	MnO wt%	MgO wt%	CaO wt%	Na_2O wt%	NiO wt%	Total	Fo#	Fo# median
Olivine														
NUB														
10-09	1	40.5	0.065	<0.01	<0.01	9.23	0.19	49.7	<0.01	<0.01	0.36	100	90.6	90.6 (n=57)
10-10	1	40.8	0.018	<0.01	<0.01	9.71	0.14	50.3	<0.01	<0.01	0.35	101	90.2	90.2 (n=48)
10-11	1	40.9	<0.01	<0.01	0.01	8.01	0.11	51.1	<0.01	<0.01	0.43	101	91.9	90.9 (n=61)
10-12B	1	41.1	<0.01	<0.01	<0.01	8.23	0.11	50.0	0.01	<0.01	0.49	100	91.6	91.6 (n=71)
10-14	1	40.7	<0.01	<0.01	<0.01	9.71	0.16	50.1	0.02	<0.01	0.34	101	90.2	90.2 (n=51)
10-13	2	40.3	0.032	<0.01	<0.01	11.0	0.25	48.1	0.01	0.01	0.26	100	88.6	88.6 (n=76)
10-12A	4	40.5	0.010	<0.01	0.01	9.62	0.15	49.2	0.01	<0.01	0.50	100	90.1	90.1 (n=68)
SOISB1														
10-20A	1	39.6	0.032	<0.01	<0.01	13.8	0.20	46.0	<0.01	<0.01	0.24	99.9	85.6	85.7 (n=39)
10-20C	1	40.5	<0.01	<0.01	0.01	12.1	0.22	47.7	<0.01	<0.01	0.31	101	87.6	87.6 (n=61)
10-22	1	41.3	<0.01	<0.01	0.03	8.07	0.15	50.7	<0.01	<0.01	0.39	101	91.8	91.8 (n=47)
10-23	1	41.0	<0.01	<0.01	<0.01	8.43	0.14	50.9	<0.01	<0.01	0.30	101	91.5	91.1 (n=52)
SOISB2														
10-34	1	40.4	<0.01	<0.01	<0.01	12.5	0.16	47.7	0.02	<0.01	0.31	101	87.2	87.7 (n=79)
10-36	1	40.5	<0.01	<0.01	<0.01	9.59	0.13	49.8	<0.01	<0.01	0.43	101	90.3	90.3 (n=60)
10-29A	2	41.0	<0.01	<0.01	<0.01	10.0	0.16	49.2	<0.01	<0.01	0.34	101	89.8	89.8 (n=48)
10-29B	2	41.0	<0.01	<0.01	<0.01	10.2	0.17	49.7	<0.01	<0.01	0.20	101	89.7	89.7 (n=52)
10-30	2	40.6	<0.01	<0.01	<0.01	9.35	0.13	49.7	<0.01	<0.01	0.54	100	90.5	90.5 (n=34)
10-31	2	40.6	<0.01	<0.01	<0.01	12.6	0.14	46.5	<0.01	<0.01	0.56	100	86.8	86.7 (n=75)
10-32	2	40.5	<0.01	<0.01	<0.01	11.1	0.17	49.0	<0.01	<0.01	0.41	101	88.7	88.7 (n=42)
10-35	4	40.2	<0.01	<0.01	<0.01	11.6	0.14	49.1	<0.01	<0.01	0.27	101	88.3	88.3 (n=40)
SOISB3														
10-16	2	39.7	0.015	<0.01	<0.01	14.9	0.24	45.3	<0.01	<0.01	0.47	101	84.5	84.5 (n=44)
10-27	3	39.8	<0.01	<0.01	<0.01	13.0	0.19	46.1	0.01	<0.01	0.36	99.6	86.3	84.5 (n=44)
10-28	3	39.6	<0.01	<0.01	0.01	16.0	0.29	43.4	<0.01	<0.01	0.42	99.8	82.8	82.8 (n=35)
Orthopyroxen													En	En median
NUB														
10-09	1	55.9	0.087	1.83	0.15	6.85	0.19	34.1	0.11	0.01	0.06	99.2	91.7	91.5 (n=6)
10-11	1	57.3	0.022	1.25	0.16	5.72	0.19	35.1	0.16	<0.01	0.08	100	91.8	91.8 (n=5)
10-12B	1	57.3	0.027	0.81	0.21	6.01	0.16	35.2	0.09	<0.01	0.07	99.9	92.4	92.3 (n=4)
10-12A	4	57.4	0.021	1.02	0.10	6.85	0.23	35.0	0.16	<0.01	0.05	101	91.3	90.8 (n=12)
SOISB2														
10-36	1	57.2	0.054	2.00	0.07	6.63	0.17	34.6	0.08	0.02	0.07	101	91.2	91.2 (n=11)
10-30	2	56.4	0.076	1.88	0.06	6.37	0.20	34.6	0.10	<0.01	0.08	99.8	91.8	91.8 (n=15)
10-31	2	56.7	0.056	2.18	0.10	8.70	0.23	32.9	0.11	0.01	0.06	101	87.6	87.3 (n=4)
10-32	2	56.8	0.049	2.07	0.07	7.79	0.23	33.0	0.08	<0.01	0.05	100	88.1	88.1 (n=15)
10-35	4	55.8	<0.01	2.12	0.11	8.10	0.19	33.4	0.18	<0.01	0.04	99.9	89.6	89.6 (n=5)
SOISB3														
10-16	2	55.5	0.072	1.65	0.08	9.80	0.22	32.3	0.11	0.01	0.07	99.8	87.6	87.1 (n=16)
10-27	3	57.0	0.10	1.44	0.13	8.73	0.33	33.3	0.16	<0.01	0.06	101	87.7	87.2 (n=13)
10-28	3	56.9	<0.01	1.05	0.28	10.5	0.06	31.5	0.13	<0.01	0.06	101	83.7	83.7 (n=7)
Clinopyroxene													En	En median
SOISB2														
10-34	1	54.2	0.15	0.76	0.06	1.60	0.05	17.4	24.9	<LOQ	0.03	99.1	48.2	48.5 (n=6)

Fo# = 100*Mg/(Mg+Fe); En= $Mg/(Mg+Fe^{2+}+Ca)*100$ (Nomenclature after Morimoto, 1988 (Fe^{3+} after Ryburn et al.)

Table 6-1 continued

Sample	Type	SiO_2 wt%	TiO_2 wt%	Al_2O_3 wt%	Cr_2O_3 wt%	FeO wt%	MnO wt%	MgO wt%	CaO wt%	Na_2O wt%	NiO wt%	Total
Calcic amphiboles												
NUB												
10-09	1	49.7	0.41	6.17	0.55	3.24	0.03	20.4	12.7	1.28	0.09	94.6
10-10	1	50.7	0.25	7.67	0.62	3.65	0.06	20.5	12.8	1.60	0.08	97.9
10-11	1	53.3	0.39	4.74	0.71	2.11	0.04	21.9	12.7	0.64	0.09	96.6
10-12B	1	53.0	0.15	4.09	0.56	2.25	0.07	22.6	12.5	1.14	0.11	96.5
10-14	1	49.6	0.34	7.45	0.62	3.51	0.06	20.3	12.6	1.31	0.09	95.9
10-13	2	53.0	0.13	2.90	0.21	2.55	0.08	22.1	12.6	0.76	0.06	94.4
10-12A	4	55.0	0.02	2.65	0.58	2.44	0.11	22.4	12.4	0.91	0.06	96.6
SOISB1												
10-20A	1	52.5	0.25	4.67	0.29	3.81	0.09	20.5	12.4	1.17	0.05	95.6
10-20C	1	52.5	0.27	5.70	0.48	3.28	0.10	21.5	12.5	1.18	0.09	97.6
10-22	1	55.6	0.18	2.97	0.05	2.24	0.08	22.8	12.6	0.73	0.12	97.3
10-23	1	53.6	0.23	4.47	0.36	3.02	0.02	21.8	12.4	1.34	0.11	97.3
SOISB2												
10-34	1	56.4	0.05	1.53	0.08	2.36	0.07	22.7	12.6	0.37	0.11	96.3
10-36	1	47.1	0.89	13.0	0.68	3.42	0.09	18.7	12.2	2.33	0.12	98.6
10-29A	2	48.7	0.23	9.69	0.54	3.66	0.04	19.9	12.7	1.71	0.09	97.3
10-29B	2	47.9	0.16	9.61	0.83	4.23	0.01	19.1	13.0	1.88	0.06	96.8
10-30	2	46.9	0.23	11.1	0.47	3.96	0.09	19.5	12.4	2.18	0.05	96.9
10-31	2	47.8	0.47	11.0	0.42	4.87	0.10	18.8	12.0	1.86	0.13	97.3
10-32	2	50.0	0.46	8.54	0.32	3.89	0.06	19.4	12.4	0.86	0.12	96.0
10-35	4	51.6	0.12	7.53	0.32	4.07	0.09	20.7	12.5	0.89	0.06	97.8
SOISB3												
10-16	2	51.4	0.34	6.69	0.34	4.22	0.09	20.6	12.2	1.13	0.09	97.1
10-27	3	52.4	0.44	7.28	0.32	3.77	0.10	20.2	12.8	0.67	0.11	98.1
10-28	3	47.7	0.40	9.01	0.31	4.79	0.11	17.8	12.4	0.97	0.11	93.6
Selected rim analyses from calcic amphiboles												
NUB												
10-12B	1	54.9	0.19	2.39	0.50	1.95	0.07	23.0	12.8	0.73	0.10	96.6
SOISB1												
10-20A	1	52.1	0.36	4.73	0.04	3.82	0.08	20.5	12.5	1.15	0.04	95.8
Selected Mg-Fe-amphibole analyses												
NUB												
10-12B	1	58.8	0.027	0.05	<0.01	7.66	0.36	29.7	0.48	<0.01	0.11	97.2
SOISB1												
10-20A	1	57.7	0.043	0.06	0.02	9.68	0.35	27.4	0.60	0.07	0.07	95.9
SOISB2												
10-32	2	53.6	0.055	2.21	0.08	7.92	0.20	32.0	0.12	<0.01	0.07	96.2

Cr#=100*Cr/(Cr+Al); Mg#Spl=100*Mg/(Mg+Fe2+); Fe3+#=100*(Fe3+/(Al+Fe3++Cr))

Table 6-1 continued

Sample	Type	SiO_2 wt%	TiO_2 wt%	Al_2O_3 wt%	Cr_2O_3 wt%	FeO wt%	MnO wt%	MgO wt%	CaO wt%	NiO wt%	Total	Cr#	$Mg\#_{spl}$	$Fe^{3+}\#$
Selected analyses of Chromite, ferrian chromite and Al-chromite														
NUB														
10-09	1	0.01	0.84	4.51	37.9	50.8	0.57	2.99	<0.01	<0.01	97.6	84.9	15.9	35.0
10-10	1	0.01	1.05	1.12	24.0	67.7	0.38	1.75	<0.01	<0.01	96.5	93.5	9.52	61.0
10-11	1	0.01	0.55	17.2	43.8	30.9	0.50	7.45	<0.01	<0.01	101	63.1	36.0	10.0
10-12B	1	0.04	1.16	4.07	50.1	36.9	0.59	3.73	0.11	<0.01	96.6	89.2	20.1	16.3
10-14	1	<0.01	0.70	5.09	27.4	59.7	0.45	3.06	<0.01	<0.01	96.4	78.3	16.4	49.1
10-12A	4	0.02	0.51	6.15	46.8	41.0	0.66	2.44	0.02	<0.01	97.6	84.6	11.7	19.1
SOISB														
10-20C	1	<0.01	1.54	0.85	41.0	52.8	0.54	1.63	<0.01	<0.01	98.3	97.0	8.73	35.9
10-29B (rim)	2	0.03	0.55	9.13	28.2	54.3	0.48	3.18	0.20	0.04	96.0	67.4	17.1	40.4
Selected analyses of Al-spinel														
SOISB2														
10-34	1	0.03	<0.01	57.8	6.30	17.0	0.11	16.3	<0.01	<0.01	97.5	6.81	65.3	1.82
10-36	1	<0.01	0.014	57.9	11.2	13.0	0.12	19.0	<0.01	<0.01	101	11.5	73.2	0.68
10-29A	2	0.04	0.011	38.7	24.8	25.3	0.26	11.1	<0.01	<0.01	100	30.0	48.5	5.16
10-29B	2	<0.01	<0.01	54.6	9.36	15.6	0.14	16.7	0.01	<0.01	96.4	10.3	68.2	1.97
10-30	2	<0.01	<0.01	60.7	7.84	11.9	0.13	19.6	<0.01	<0.01	100	7.95	75.3	0.39
10-31	2	<0.01	0.071	46.6	17.6	24.0	0.16	12.3	<0.01	0.01	101	20.2	51.3	3.79
10-32	2	0.02	0.029	58.9	7.35	16.3	0.13	17.7	<0.01	<0.01	100	7.72	68.8	2.12
10-35	4	0.02	<0.01	49.3	13.3	21.9	0.23	15.2	<0.01	<0.01	100	15.3	62.3	6.27
SOISB3														
10-16	2	0.05	0.056	40.0	20.1	27.2	0.25	9.50	<0.01	<0.01	97.2	25.2	42.7	5.46
10-27	3	0.01	0.010	55.4	9.72	19.2	0.14	15.9	<0.01	<0.01	100	10.5	63.2	2.97
10-28	3	<0.01	0.018	56.1	8.54	21.7	0.20	14.4	<0.01	<0.01	101	9.27	57.6	3.00
Selected analyses of magnetite, Cr-magnetite and ilmenite														
NUB														
10-14	1	0.02	1.40	2.98	18.1	71.8	0.28	1.87	<0.01	<0.01	96.5	80.3	9.92	66.1
10-13	2	0.01	2.76	0.45	7.88	81.4	0.21	1.37	0.02	<0.01	94.1	92.1	7.29	86.1
SOISB														
10-22	1	<0.01	0.15	0.06	11.3	80.9	0.27	1.11	<0.01	<0.01	93.8	99.3	6.34	82.7
10-23	1	<0.01	0.81	0.21	31.1	61.5	0.65	1.77	<0.01	<0.01	96.0	99.0	9.86	52.4
10-20A	1	0.03	1.83	0.53	28.0	62.0	0.44	1.34	<0.01	<0.01	94.2	97.3	7.36	53.9
10-29B (rim)	2	<0.01	0.76	2.69	20.4	70.7	0.40	1.14	0.10	<0.01	96.2	83.6	6.25	63.5
SOISB3														
10-28	3	<0.01	2.18	5.69	21.0	65.1	0.50	2.14	<0.01	<0.01	96.5	71.2	11.1	55.3

Cr#=100*Cr/(Cr+Al); $Mg\#_{Spl}$=100*Mg/(Mg+Fe^{2+}); $Fe^{3+}\#$=100*(Fe^{3+}/(Al+Fe^{3+}+Cr))

6-2.1.2 Pyroxene

All measured orthopyroxene mineral grains are of enstatitic composition. Note that SOISB1 peridotites contain no or only trace amounts of orthopyroxene and none were found in the thin sections prepared for electron microprobe analyses. CaO concentrations are low (≤ 0.20 wt.%) and Al_2O_3 concentrations range between 0.37 and 2.40 wt%. The amounts of En-component (En= Mg/(Mg+Fe2++Ca)*100; Fe^{3+} calculated after Edwards, 1976) in orthopyroxenes are positively correlated with Fo# of the co-existing olivines (Fig 6-1). Proportions of En in orthopyroxenes from sample 10-36 and NUB type 1 peridotites range from 90 to 92, overlapping with En values obtained for orthopyroxenes in type 2 peridotites (87 to 92). Orthopyroxenes in SOISB type 3 and 4 peridotite are characterised by mainly

lower En than type 1 peridotites (84 to 90). Only one sample 10-34 (SOISB2 type 1) contains small amounts of Cr- and Na-poor diopside, beside trace amounts of orthopyroxene.

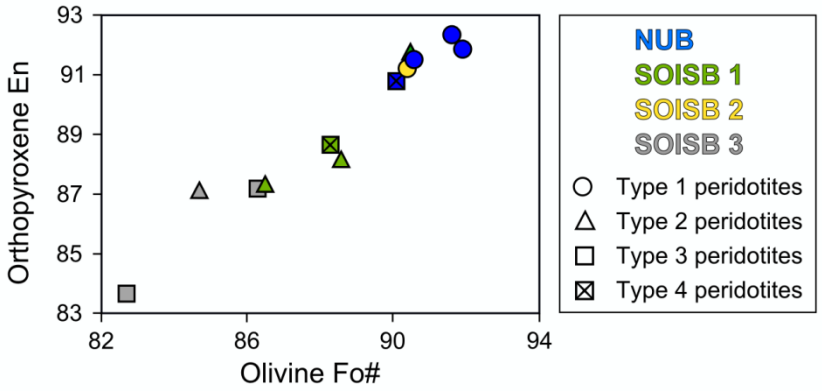

Figure 6-1: En in orthopyroxene versus Fo# in olivine obtained for the peridotites from SOISB and NUB. The amounts of En-component in orthopyroxenes are positively correlated with Fo# of the co-existing olivines.

6-2.1.3 Amphibole

All samples contain calcic amphiboles with about 12 wt% CaO content and variable contents of MgO (17. 2 to 23.9 wt.%), Al_2O_3 (0.90 to 13 wt.%), FeO (1.74 to 7.66 wt.%), Na_2O (ca. 0.02 to 2.33 wt.%) and TiO_2 (0.05 to 0.89 wt%). Thus, these calcic amphiboles, generally contain low proportions of pargasite ($NaCa_2(Mg_4Al)(Al_2Si_6)O_{22}(OH)_2$), hastingsite ($NaCa_2(Fe^{2+}{}_4Fe^{3+})(Si_6Al_2)O_{22}(OH)_2$) and kaersuite ($(NaCa_2(Mg_4Ti_2)(Si_6Al_2)(O+OH)_{24}$) components. In some calcic amphiboles, the rims have gradually decreasing contents of Na_2O and Al_2O_3 and increasing contents of SiO_2 (e.g. 10-09, 10-12A, 10-12B, 10-20A; Table 6-1, D-2). The amphibole core compositions, calculated using the spreadsheet of Locock (2014), mainly vary between tremolite, magnesio- and magnesio-ferri-hornblende. Only in samples 10-36 (SOISB1 type 1) and 10-30 (SOISB2 type 2) pargasite occurs, (following the IMA recommended calcic amphibole classification after Hawthorne et al., 2012; amphibole general formula: $A_{0\text{-}1}B_2C_5T_8O_{22}W_2$). Calcic amphibole compositions in NUB and SOISB type 1 peridotites overlap, except for amphiboles from SOISB2 type 1 peridotite 10-36 (e.g. higher Al_2O_3 and TiO_2, see also Fig. 6-2). Likewise, calcic amphibole compositions obtained for NUB type 2 and 4 peridotites show no clear difference to those of NUB type 1 peridotites. However, calcic amphiboles from SOISB type 2, 3 and 4 peridotites show some differences in their calculated A (A*=(Na+2Ca) and C (C*=(Al+Fe^{3+} 2Ti)) position cations, as is illustrated in Figure 6-2. Notably, like 10-27 olivines, Ca-amphibole embedded in the 10-27 orthopyroxene-poikiloblasts and in the matrix have indistinguishable compositions.

Three type 1 peridotite samples (10-12B, 10-20A and 10-20C) and one type 2 peridotite (10-32) additionally contain ferromagnesian amphiboles (FeO 7 to 11 wt.%, MgO 25 - 32

wt.% and CaO < 1 wt.%), with cummingtonite core compositions (calculated with the excel spreadsheet of Locock, 2014, Hawthorne et al., 2012) (Mg-Fe-Mn-amphiboles; nomenclature after Leak, 1978). Ferromagnesian amphiboles in the type 2 peridotite 10-32 display higher Al_2O_3 contents (1.79 to 2.30 wt.%) than aluminium poor type 1 ferromagnesian amphiboles (Al_2O_3 < 0.2 wt.%).

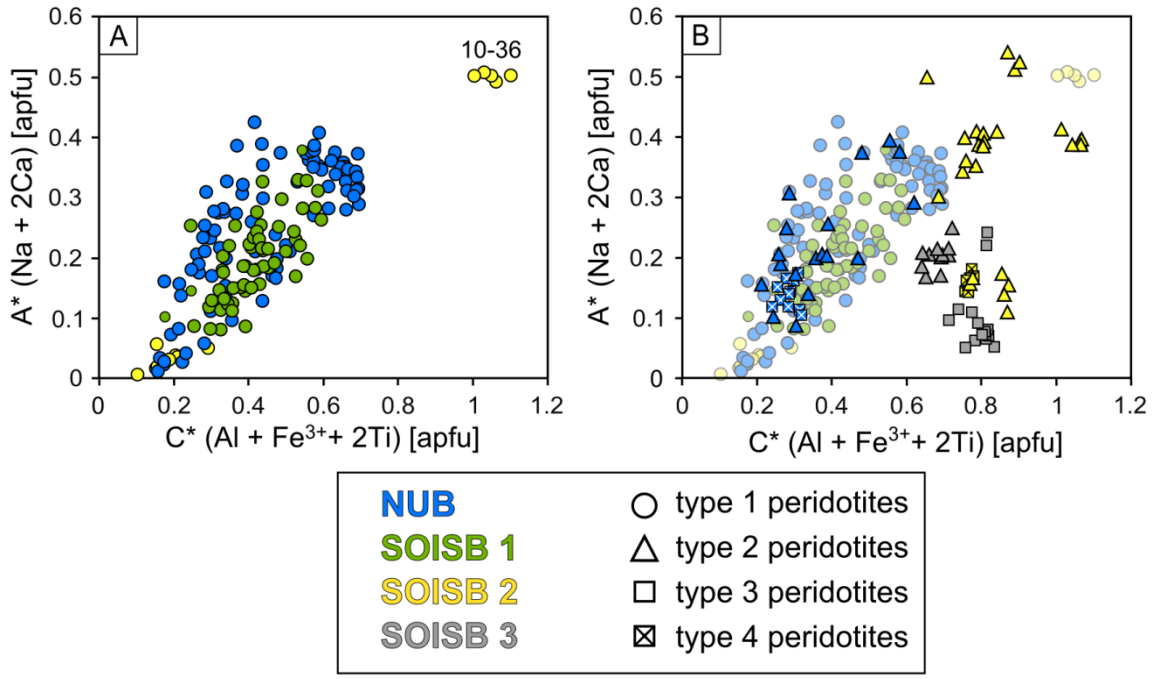

Figure 6-2: Calcic amphibole core compositions plotted in the A*(Na + 2Ca) versus C* (Al+Fe^{3+} 2Ti) diagrams (following IMA recommendation, Hawthorne et al., 2012). A+ and C* were calculated using the excel spreadsheet of Locock (2014). (A) The calcic amphibole compositions of the type 1 peridotites from all locations overlap. Only sample 10-36 contains amphiboles of a different composition (pargasite). (B) Type 2, 3 and 4 peridotites in comparison to type 1 peridotites (transparent). Calcic amphibole compositions of type 3 and 3 peridotites from NUB are within the range of the NUB type 1 peridotites. In contrast, calcic amphibole compositions of the SOISB type 2, 3 and 4 peridotites differ from those of the SOISB type 1 peridotites.

6-2.1.4 Spinel

Spinel is abundant in all peridotites, occurring as small inclusions within minerals or at grain boundaries. Spinel compositions (Table 6-1) are illustrated in Figure 6-3 as relative proportions of Cr, Al and Fe^{3+} and in Figure 6-4 with respect to their Cr# (Cr#=100*Cr/(Cr+Al)) and $Mg\#_{Spl}$ ($Mg\#_{Spl}$=100*Mg/(Mg+Fe^{2+})). In some peridotites, only magnetite and chromian-magnetite grains were found (10-10, 10-13, 10-22, and 10-23). The individual grains generally tend to be homogeneous, yet also zoned grains occur, with decreasing Cr contents from the cores to the rims.

Chromites in the NUB hbl-bearing peridotites contain low Al_2O_3 (Al_2O_3<10%) and variable iron contents. In the NUB dunite (10-11), Al-chromite also occurs. The Cr# values in

the NUB spinels range from 57 to 90, and roughly correlate with whole rock chromium contents. The $Mg\#_{Spl}$ in these rocks vary between 15 and 27.

SOISB1 type 1 peridotites contain mainly Al-poor chromian-magnetite and magnetite, and only occasional Cr-magnetites with cores of ferrian -chromite composition. The two SOISB1 hbl-bearing peridotites contain low amounts of single pure ferrian-chromite grains. Chromite is absent in the SOISB2 and SOISB3 peridotites. However, Al-spinels occur instead, in addition to Cr-magnetite and magnetite. The compositions of the Al-spinels range from herzynite to picotite. Some Al-spinels show rims with decreasing Al contents and with compositions that range from picotite or ferrian-chromite to Cr-magnetite or magnetite (e.g. 10-29B; Figure 6-2B). Generally, most chromite and Al-spinel grains are rimmed or are closely associated with magnetite. Note, magnetite and Cr-magnetite occur in all peridotites but were measured only in some representative samples, and the orange field in Figure 6-2B illustrates the range of common Cr-magnetite and magnetite compositions valid for all peridotites.

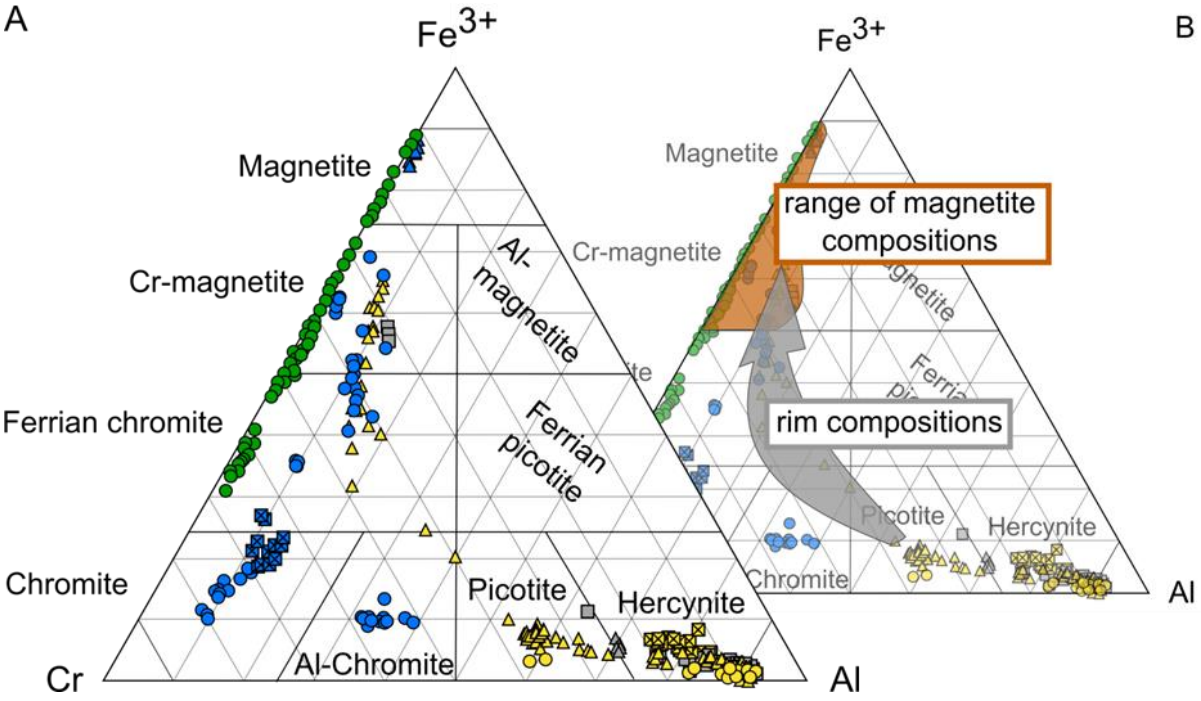

Figure 6-3: (A) Spinel compositions of peridotites of this study are plotted in the triangular Cr-Fe^{3+}-Al classification diagram after Ghiorso & Sack (1991) and Gargiulo et al. (2013), Cr=Cr/(Cr+Fe^{3+}+Al); Fe^{3+}=Fe^{3+}/(Cr+Fe^{3+}+Al); Al=Al/(Cr+ Fe^{3+} +Al). Al-spinels (picotite and hercynite) occur only in the peridotites from SOISB2 and SOISB3, whereas chromite occur only in the NUB peridotites. (B) The brown field indicates the range of magnetite compositions in the peridotites and the grey field indicates the range of typical rim compositions of altered Al-spinel, with decreasing Al and increasing Fe content towards the grain boundaries. Symbols and colours for the minerals are equivalent to those in Fig. 6-2.

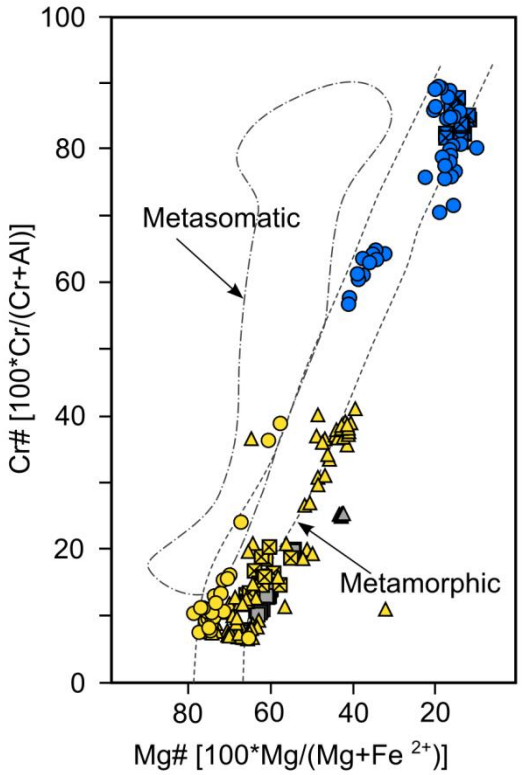

Figure 6-4: SOISB and NUB chromite and Al-spinel core compositions obtained for the peridotites are plotted in the Cr# vs Mg# diagram after Haggerty (1991). The spinel compositions are consistent with metamorphic origin or metamorphic re-equilibration. Symbols and colours for the minerals are equivalent to those in Fig. 6-2.

6-2.2 Lu, Hf, Sm, Nd, Rb and Sr abundances and isotope compositions in olivine, orthopyroxene and amphibole

The MC-ICP-MS data set comprises Lu-Hf-Sm-Nd-Rb-Sr-analyses from olivine, orthopyroxene and amphibole separates obtained for four samples, including three type 1 peridotites 10-11 (NUB), 10-20C (SOISB1), 10-36 (SOISB2), and one type 3 peridotite 10-27(SOISB3). The Lu, Hf, Sm, Nd, Rb and Sr concentrations and isotope data are summarized in Table 6-2, 6-3 and 6-4 and Figures 6-5, 6-6 and 6-7.

The concentrations in the amphibole separates ($Amph_{10\text{-}11}$, $Amph_{10\text{-}20C}$, $Amph_{10\text{-}36}$ and $Amph_{10\text{-}27}$) are generally higher as in the associated olivine ($Ol_{10\text{-}11}$, $Ol_{10\text{-}20C}$, $Ol_{10\text{-}36}$ and $Ol_{10\text{-}27}$) and orthopyroxene separates ($Opx_{10\text{-}11}$, $Opx_{10\text{-}20C}$, $Opx_{10\text{-}36}$ and $Opx_{10\text{-}27}$). Lutetium, Hf, Sm, Nd and Rb concentrations are especially low in the olivine separates (Lu, Hf, Sm and <14ppb, Rb <60ppb) and the Sr concentrations are low as well, but highly variable (57 - 881 ppb). Thus, the concentrations in amphibole separates are ca. 60-500 times higher for Lu and Hf, ca. 150-1700 times higher for Sm and Nd, and ca. 8-300 times higher for Rb and Sr than in the olivine separates. The difference between amphibole and orthopyroxene separates is similarly pronounced for Sm and Nd, being ca. 50-400 times higher in amphibole than in

orthopyroxene separates. The differences in Lu, Hf, Rb and Sr concentrations are less distinct, between ca. 1 and 80 times higher in amphibole than in associated orthopyroxene separates.

$Ol_{10\text{-}11}$ and $Ol_{10\text{-}20C}$ are characterised by high Lu/Hf ratios (ca. 1.8) and more radiogenic Hf isotope signatures ($^{176}Hf/^{177}Hf_{Ol}$ = 0.29386 and 0.29454) than those obtained for $Ol_{10\text{-}36}$ and $Ol_{10\text{-}27}$ ($^{176}Hf/^{177}Hf_{Ol}$ = 0.28541 and 0.28473), or obtained for any orthopyroxene separates ($^{176}Hf/^{177}Hf_{Opx}$ = 0.28470 to 0.28837), amphibole separates ($^{176}Hf/^{177}Hf_{Amph}$ = 0.28541 and 0.28764), or the bulk compositions ($^{176}Hf/^{177}Hf$ = 0.28246 and 0.28551) (Table 6-2).

$Ol_{10\text{-}11}$ and $Ol_{10\text{-}20C}$ are characterised by high Lu/Hf ratios (ca. 1.8) and more radiogenic Hf isotope signatures ($^{176}Hf/^{177}Hf_{Ol}$ = 0.29386 and 0.29454) than those obtained for $Ol_{10\text{-}36}$ and $Ol_{10\text{-}27}$ ($^{176}Hf/^{177}Hf_{Ol}$ = 0.28541 and 0.28473), or obtained for any orthopyroxene separates ($^{176}Hf/^{177}Hf_{Opx}$ = 0.28470 to 0.28837), amphibole separates ($^{176}Hf/^{177}Hf_{Amph}$ = 0.28541 and 0.28764), or the bulk compositions ($^{176}Hf/^{177}Hf$ = 0.28246 and 0.28551) (Table 6-2).

Generally, $^{176}Hf/^{177}Hf$ ratios obtained for each sample, comprising mineral separates and whole rocks, are at least roughly positive correlated with $^{176}Lu/^{177}Hf$ ratios (Fig. 6-5). Yet, $^{143}Nd/^{144}Nd$ virtually lack significant correlation with $^{147}Sm/^{144}Nd$ (Fig. 6-6). Nonetheless, the Sm-Nd isotope data show highly radiogenic signatures for the mineral separates, with measured $^{143}Nd/^{144}Nd$ between 0.5129 and 0.5135, and measured $^{147}Sm/^{144}Nd$ between 0.15654 and 0.22487.The type 1 peridotites 10-11, 10-20C and 10-36 mineral separates show generally highly variable measured $^{87}Sr/^{86}Sr$ ratios ($^{87}Sr/^{86}Sr_{10\text{-}11}$ = 0.72545 to 0.81292, $^{87}Sr/^{86}Sr_{10\text{-}20C}$ = 0.72432 to 0.75332 and $^{87}Sr/^{86}Sr_{10\text{-}36}$ = 0.73494 to 0.93823) (Fig. 6-7). In contrast, the type 3 peridotite 10-27 mineral separates show relative constant, lower $^{87}Sr/^{86}Sr$ ratios between 0.70330 and 0.70530. Measured $^{87}Sr/^{86}Sr$ and $^{87}Rb/^{86}Sr$ ratios for the whole rocks are within the range of the mineral separates in the case of the samples 10-20C, 10-36 and 10-27, except for sample 10-11 (Table 6-3 and Fig. 6-7). All samples lack internal correlations between the $^{87}Sr/^{86}Sr$ and the $^{87}Rb/^{86}Sr$ ratios (Fig. 6-7).

Table 6-2: Hafnium and Nd isotope composition and Lu, Hf, Sm and Nd concentration data for mineral separates.
*Data for whole rock composition are taken from Table 2-2 in Chapter 2.

	Sample [mg]	Lu (ppm)	Hf (ppm)	Lu/Hf	$^{176}Lu/^{177}Hf$	2σ	$^{176}Hf/^{177}Hf$	2σ	Sm (ppm)	Nd (ppm)	Sm/Nd	$^{147}Sm/^{144}Nd$	$^{143}Nd/^{144}Nd$
10-11 (NUB)													
Dunite*	240	0.0130	0.0470	0.2700	0.04816	± 10	0.284009	± 46	0.0603	0.170	0.3547	0.2111	±4 0.513167 ±2
Olivine	1000	0.00267	0.00152	1.759	0.2503	± 5	0.293861	± 80	0.000805	0.00247	0.3261	0.1978	±4 0.512859 ±7
Opx	100	0.0123	0.0192	0.6418	0.09116	± 18	0.286227	± 32	0.0175	0.0516	0.3385	0.1996	±4 0.513147 ±4
Amph 1	40	0.161	0.510	0.3191	0.04494	± 9	0.283515	± 15	1.51	4.30	0.3513	0.2124	±4 0.513130 ±2
Amph 2	45	0.151	0.460	0.3290	0.04670	± 9	0.283638	± 7	1.50	4.46	0.3376	0.1877	±4 0.512912 ±2
10-20C (SOISB1)													
Hbl-peridotite*	240	0.0293	0.144	0.2040	0.02901	± 9	0.282462	± 6	0.304	0.920	0.3307	0.1995	±4 0.512840 ±2
Olivine	1000	0.00334	0.00187	1.785	0.2539	± 5	0.294536	± 466	0.00396	0.0148	0.2677	0.1565	±3 0.512303 ±3
Amph 1	40	0.314	0.985	0.3165	0.04530	± 9	0.283704	± 12	1.56	4.62	0.3366	0.2035	±4 0.512913 ±1
Amph 2	45	0.336	1.06	0.3174	0.04506	± 9	0.283707	± 5	1.45	4.13	0.3522	0.1966	±4 0.513144 ±2
10-36 (SOISB2)													
Hbl-peridotite*	240	0.0790	0.159	0.4961	0.07087	± 14	0.285507	± 9	0.155	0.430	0.3615	0.2189	±4 0.513468 ±2
Olivine	600	0.00481	0.00876	0.5508	0.07821	± 16	0.285412	± 17	0.00211	0.00794	0.2659	0.1578	±3 0.512431 ±5
Opx 1*	30	0.0273	0.0288	0.9495					0.00625	0.0177	0.3538		
Opx 2	35	0.0271	0.0317	0.8560	0.1217	± 2	0.288368	± 99	0.00730	0.0208	0.3507	0.2097	±4 0.513319 ±9
Opx 3	100	0.0282	0.0262	1.074	0.1527	± 3	0.290265	± 25	0.0110	0.0319	0.3433	0.2055	±4 0.513269 ±9
Opx 4	100	0.0280	0.0364	0.7683	0.1092	± 2	0.287492	± 13	0.0122	0.0349	0.3507	0.2092	±4 0.513402 ±5
Amph 1	40	1.56	2.12	0.7321	0.1042	± 2	0.287638	± 11	3.16	8.61	0.3665	0.2216	±44 0.513510 ±2
10-27 (SOISB3)													
Hbl-peridotite*	240	0.0886	0.259	0.3416	0.04944	± 10	0.284041	± 7	0.394	1.06	0.3709	0.2243	±5 0.513500 ±2
Olivine	600	0.00190	0.00413	0.4609	0.06544	± 13	0.284728	± 120	0.00484	0.0140	0.3444	0.2038	±4 0.513220 ±4
Opx 1*	30	0.00902	0.0187	0.4821					0.0183	0.0492	0.3709	0.2225	±4 0.513480 ±10
Opx 2	100	0.00871	0.0182	0.4776	0.06782	± 14	0.285439	± 47	0.0186	0.0506	0.3719	0.2191	±4 0.513533 ±6
Opx 3	100	0.0118	0.0288	0.4106	0.05830	± 12	0.284700	± 16					
Amph 1	40	0.197	0.553	0.3561	0.05055	± 10	0.284154	± 21	0.902	2.43	0.3717	0.2247	±5 0.513482 ±7
Amph 2	40	0.197	0.560	0.3517	0.04993	± 10	0.284087	± 14	0.878	2.36	0.3719	0.2249	±5 0.513477 ±4

Opx: orthopyroxene; Amph: amphibole

Table 6-3: Sr isotope composition and Rb and Sr concentration data for mineral separates and corresponding whole rocks

	ppm Rb	ppm Sr	Rb/Sr	$^{87}Rb/^{86}Sr$	$^{87}Sr/^{86}Sr$	±2σ
10-11 (NUB)						
Dunite	0.757	0.467	1.622	4.758	0.868777	± 27
Olivine	0.0110	0.0573	0.1911	0.5550	0.758618	± 72
Opx	0.251	3.14	0.08012	0.2326	0.812917	± 210
Amph 1	1.97	17.4	0.1128	0.3279	0.753713	± 12
Amph 2	2.02	17.9	0.1126	0.3272	0.725445	± 9
10-20C (SOISB1)						
Hbl-peridotites	0.217	5.61	0.03860	0.1120	0.735785	± 10
Olivine	0.00760	0.227	0.03345	0.09695	0.725409	± 34
Amph 1	1.35	64.4	0.02103	0.06090	0.724312	± 14
Amph 2	1.39	28.0	0.04967	0.1440	0.753317	± 23
10-36 (SOISB3)						
Hbl-peridotites	4.56	4.67	0.9766	2.873	0.879429	± 13
Olivine	0.00501	0.231	0.02171	0.06321	0.852598	± 46
Opx 1	0.423	1.91	0.2212	0.6412	0.888739	± 199
Opx 2	0.630	1.73	0.3638	1.058	0.937424	± 117
Opx 3	0.571	0.750	0.7613	2.234	0.890405	± 50
Opx 4	1.01	0.790	1.280	3.780	0.938225	± 47
Amph	0.878	62.8	0.01398	0.04057	0.734943	± 14
10-27 (SOISB2)						
Hbl-peridotites	0.342	22.53	0.01520	0.04397	0.704077	± 9
Olivine	0.0532	0.881	0.06034	0.1746	0.708031	± 28
Opx 1	0.0854	2.49	0.03432	0.09925	0.705303	± 63
Opx 2	0.0538	1.39	0.03886	0.1124	0.704930	± 29
Opx 3	0.0698	2.72	0.02563	0.07413	0.704383	± 18
Amph 1	0.746	49.7	0.01501	0.04342	0.703299	± 13
Amph 2	1.329	49.7	0.02675	0.07736	0.703302	± 16

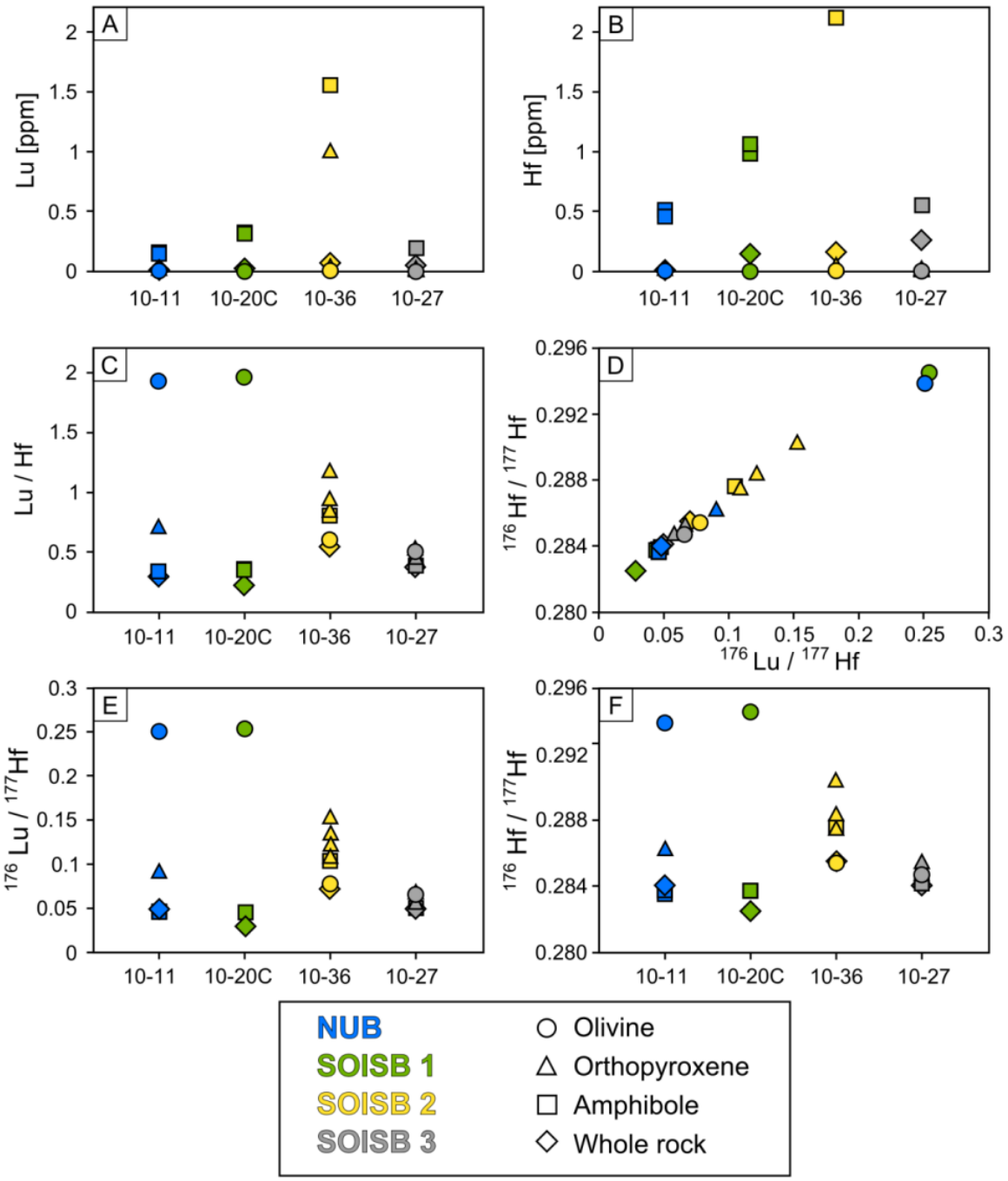

Figure 6-5: Lutetium-Hf concentrations (A-C) and isotope data (D-F) obtained for the four peridotites and their mineral separates. (A-F) The type 1 peridotites 10-11, 10-20C and 10-36 mineral separates display variable Lu, Hf concentrations and isotope compositions. In contrast the type 3 peridotite 10-27 mineral separates show relative small range in Lu, Hf concentrations and isotope compositions. (D) Generally, $^{176}Hf/^{177}Hf$ ratios are at least roughly positive correlated with $^{176}Lu/^{177}Hf$ ratios. (D, F) The olivine separates of the type 1 peridotites 10-11 and 10-20C [Ol10-11 and Ol10-20C] show significant more radiogenic Hf isotopic ratios, than the whole rocks and the other mineral separates. The colours indicate the sample locations and the symbols indicate the minerals separates and whole rock.

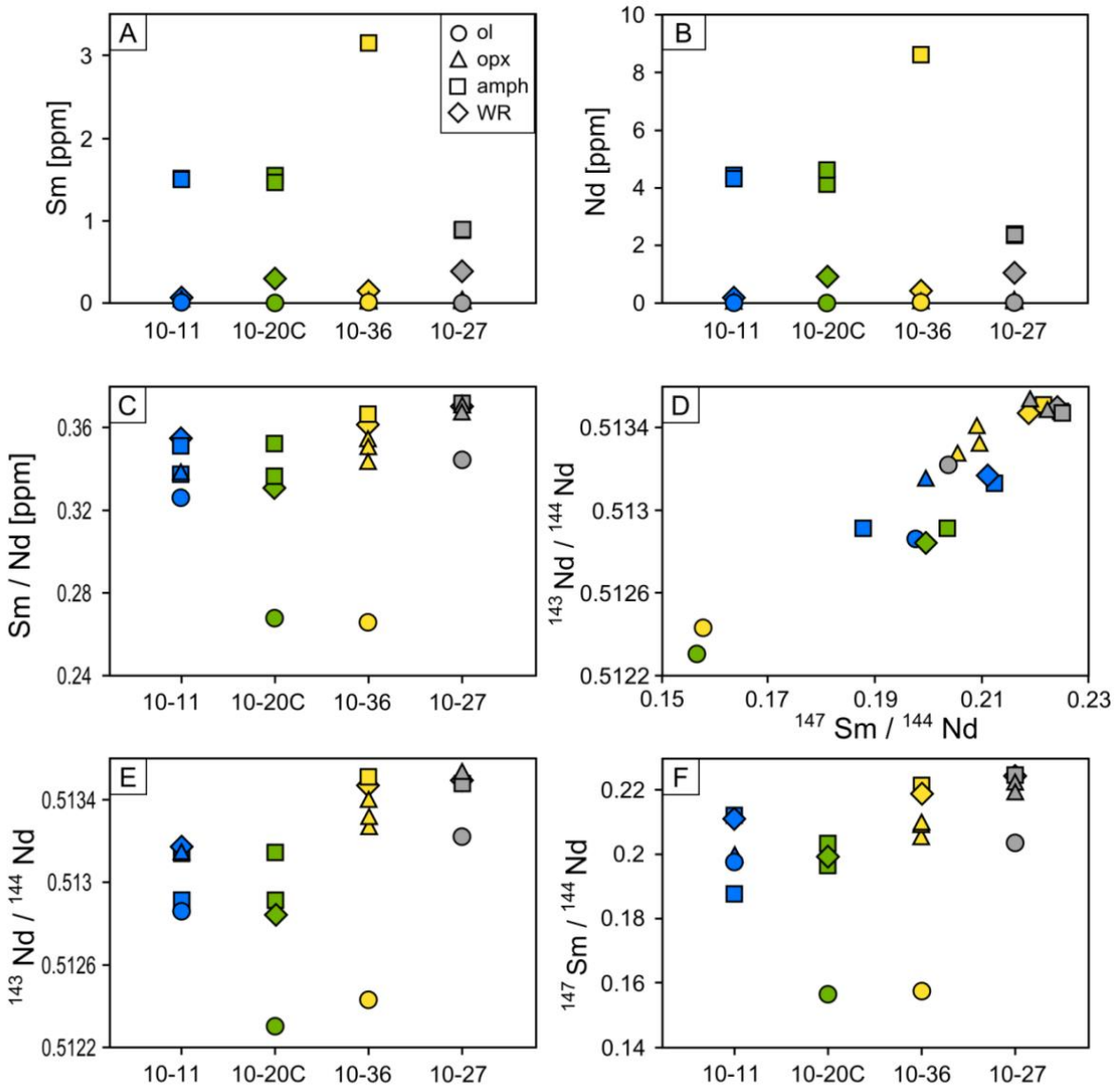

Figure 6-6: Samarium-Nd concentrations (A-C) and isotope data (D-F) obtained for the mineral separates and corresponding whole rocks. (A-F) The mineral separates display variable Lu, Hf concentrations and isotope compositions. (A-B) Notably, the amphibole separates have higher Sm and Nd concentrations than the orthopyrxene and olivine separates. (D) All samples virtually lack significant correlation between measured $^{143}Nd/^{144}Nd$ and $^{147}Sm/^{144}Nd$ ratios, suggesting significant metamorphic resetting of the ^{147}Sm–^{143}Nd isotope systematics. Symbols and colours are equivalent to those in Fig. 6-5.

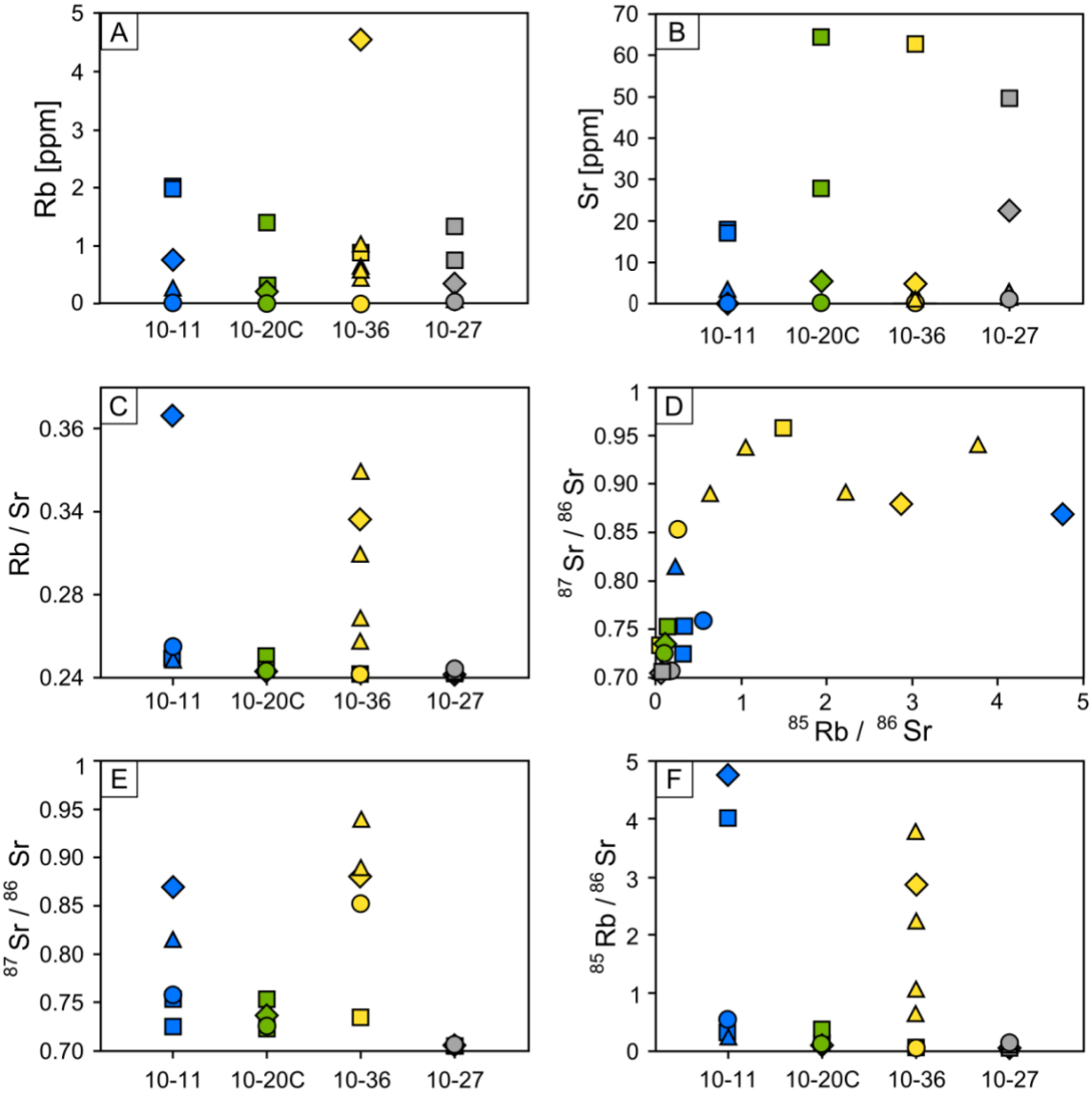

Figure 6-6: Rb-Sr concentrations (A-C) and isotope data (D-F) obtained for the mineral separates and corresponding whole rocks. (D) All samples lack internal correlations between the $^{87}Sr/^{86}Sr$ and the $^{87}Rb/^{86}Sr$ ratios. (D-E) The type 1 peridotites 10-11, 10-20C and 10-36 mineral separates show generally variable measured $^{87}Sr/^{86}Sr$ ratios, in contrast the type 3 peridotite 10-27 mineral separates show relative constant, lower $^{87}Sr/^{86}Sr$ ratios. Symbols and colours for are equivalent to those in Fig. 6-5.

6-3 DISCUSSION

6-3.1 Primary versus secondary mineral compositions

Based on the petrographic and geochemical observations, NUB and SOISB1 type 1 peridotites and type 3 peridotites can be characterised as being least affected by subsequent, metasomatic and metamorphic overprint, type 2 peridotites are variably altered and type 4 peridotites are strongly altered (see also discussion chapter 5).

The lack of major and minor element zonation in olivine (except occasionally the outer < 10 µm), orthopyroxene and most anhedral amphibole, as well as the lack of optically observable indications for considerable alteration, indicate that those mineral grains either preserved primary equilibrium compositions or were internally homogenized during secondary metamorphism.

Whole rock trace element compositions indicate re-fertilisation of the type 1 peridotites due to melt-rock interaction, possible in a suprasubduction setting (chapter 5). Silicate melt reaction with depleted mantle peridotites in a suprasubduction setting mainly results in the formation of secondary orthopyroxene ± spinel and amphibole at the expense of predominantly olivine, and clinopyroxene, orthopyroxene and spinel (e.g., Sen and Dunn, 1995; Rapp et al., 1999; Prouteau et al., 2001; Corgne et al., 2018). The simplified mantle re-enrichment-model, presented in chapter 5, predicts for the NUB and SOISB1 type 1 peridotites, approximately less than 2% melt addition, thus, primary olivine ± orthopyroxene would not completely be consumed during the melt-rock interaction. Hence, olivine and orthopyroxene in most type 1 peridotites, and some type 2 peridotites (10-29A, 10-29B and 10-30) may have preserved primary mantle signatures, at least regarding major and minor element compositions.

6-3.1.1 Effects of secondary metasomatism from major and minor element compositions of olivine, orthopyroxene, amphibole and spinel

6-3.1.1.1 Olivine

Formation of secondary olivine**,** grains or narrow rims is not always observed in high SiO_2 melt–peridotite reaction experiments and seems to be more common as a result of peridotite interaction with a low SiO_2 melt (e.g., Corgne et al., 2018). Importantly, the preservation of "primary" olivine (primary regarding major element composition, e.g. Fo#) was observed in hydrous, high SiO_2 melt-peridotite reaction experiments at conditions appropriate for a mantle wedge metasomatism above a partially melting slab (≤2.0 GPa and <1100°C) (e.g., Sen and Dunn, 1995; Corgne et al., 2018).

The olivine compositions of the type 1 peridotites are internally consistent, thus no sample contains clearly distinguishable olivine populations. Thus, the type 1 peridotite olivines with Fo# ≥ 89 may have preserved their primary major and minor element compositions. The lower Fo# (< 89) obtained for some type 1 peridotites (samples10-20A and 10-20C, 10-34 and 10-12B) can be explained by Mg-Fe subsolidus exchange between olivine and neighbouring mineral phases during subsequent metamorphism. Metamorphically induced Mg-Fe exchange likely affected all type 2 peridotites. Yet, three type 2 peridotites have olivine with Fo# ~90 (10-29A+B and 10-30) and those samples might be of mantle origin and the olivine compositions seem to be less affected by subsequent metamorphic overprint. Olivines in type 3 peridotites differ from the type 1 peridotite olivines mainly in their lower Fo# (83 and 87) and their compositions are consistent with a crustal cumulate origin. Importantly, olivines in the orthopyroxene poikiloblasts and in the matrix are indistinguishable from each other, providing additional evidence that they likely preserved primary major and minor compositions.

6-3.1.1.2 Pyroxene

Metasomatic orthopyroxene is the most common mineral that forms during mantle wedge metasomatism (e.g., Kelemen et al., 1998; Corgne et al., 2018). The metasomatic orthopyroxene compositions are highly variable in both natural metasomatised peridotites and obtained for high pressure and high temperature melt-peridotite interaction experiments. In general, compositions of metasomatic orthopyroxenes are highly dependent on the metasomatic agent composition (e.g., Sen and Dunn, 1995; Rapp et al., 1999; Prouteau et al., 2001; Corgne et al., 2018), and the discrimination between primary and secondary orthopyroxene is often difficult and in some cases impossible. Yet, metasomatic orthopyroxene formed due to reactions of mantle peridotite with a high SiO_2 melt tend to have more iron-enriched compositions (En primary orthopyroxene > En secondary orthopyroxene). Such a high SiO_2 melt was assumed as the re-fertilizing agent in the case of the type 1 peridotites (chapter 5).

Importantly, orthopyroxene compositions are consistent for each sample and thus, only one type of orthopyroxene could be identified for each sample. All measured type 1 peridotite orthopyroxenes are Mg-rich (En ≥ 90) and low in CaO (>0.2 wt.%) and, hence, have major element compositions within the range of mantle orthopyroxenes. Consequently, secondary metasomatic orthopyroxene is either missing or indistinguishable from mantle orthopyroxene. However, except for sample 10-36, orthopyroxene abundances are generally low in the peridotites and orthopyroxene were likely also consumed during primary and secondary amphibole formation.

Type 2 peridotite 10-30 orthopyroxene compositions (En =92) are within the range of mantle orthopyroxene compositions, supporting the assumption that sample 10-30 might be of mantle origin. In contrast, the orthopyroxenes in type 2 peridotites 10-31 and 10-32 show lower En of about 87, consistent with either crustal cumulate, secondary metasomatic or metamorphic origin. Likewise, the type 3 peridotite orthopyroxene compositions (e.g., En 84 and 87) are consistent with a crustal cumulate origin and might have preserved their primary major and minor element compositions.

In summary, from the major element perspective, some peridotites may contain pristine orthopyroxene, but for all samples, a metasomatic origin or subsequent metamorphic re-equilibration cannot be excluded.

SOISB2 type 1 peridotite 10-34 contain, in addition to trace amounts of orthopyroxene, small amounts of Cr- and Na-poor clinopyroxene. Corgne et al. (2018) reported Ti-rich, Cr- and Na-poor clinopyroxene compositions as a crystallization product of the adakitic component in their high P-T experiments, an analogue for mantle wedge adakitic metasomatism. Consequently, 10-34 clinopyroxene likely represents relicts of metasomatic clinopyroxene and primary clinopyroxenes in all other peridotites were likely consumed during partial melting or amphibole formation.

6-3.1.1.3 Amphibole

Stability of amphibole at high pressure and temperature conditions is highly dependent on the activity of H_2O and the alkali / H_2O ratio. The addition of Ti and Fe^{3+} can further increase the thermal stability of amphibole (e.g., Wallace and Green, 1991; Frost, 2006). Thus, pargasite and hastingite can be stable at temperatures above 1100°C and pressures above 2 GPa (e.g., Frost, 2006). Observed metasomatic amphiboles in peridotites from supra-subduction zone settings were predominantly pargasite and to a minor extant Mg-hastingsites, magnesio-hornblendes and other calcic amphiboles (Coltorti et al., 2007 and references therein). Those results are in line with results from high pressure and high temperature experiments that investigated mantle wedge metasomatism (e.g., Sen and Dunn, 1995; Rapp et al., 1999; Corgne et al., 2018).

Only one type 1 (10-36) and one type 2 (10-30) peridotite contain pargasite and sample 10-30 magnesio-hastingsite, beside magnesio-hornblende. Those calcic amphiboles might have formed during mantle metasomatism. All other calcic amphiboles (type 1, 2, 3 and 4) compositions range between tremolite and magnesio-hornblende and contain some amount of Al, Na, Fe^{2+}, Fe^{3+} and Ti, and thus a small amount of a pargasite, hastingsite and kaersuite component. Hence, their stability field expands to higher pressure and temperature conditions compared to pure tremolite (Frost et al., 2006), but still below typical temperatures in the

mantle wedge. Moreover, the surrounding felsic and mafic rocks record amphibole facies metamorphism and amphibole is prone to element diffusion at amphibole facies condition. Consequently, the calcic amphiboles (maybe except pargasite) in the studied peridotites likely have formed during amphibole facies metamorphism on the expense of clinopyroxene and/or metasomatic amphibole ± orthopyroxene ± trapped melt inclusion. The metamorphic amphibole formation was accompanied by the formation of spinel and in some cases mica. The water sources required were either metasomatic amphibole or aqueous fluids/melts released by felsic magmatic intrusions or breakdown of hydrous phases in the bedrocks during metamorphism.

Yet, only few samples (10-20A, 10-20C and 10-12B) contain Ca-amphiboles with pronounced retrograde zonation or amphibole crystals overgrowing other silicates (10-13, 10-20A, 10-20C, 10-34) indicating significant late metamorphic changes in these cases. However, amphibole dominated patches are a distinctive micro-textual feature in some peridotites (10-13, 10-12A, 10-16, 10-20A, 10-20C 10-29B and 10-34) and this might suggest recrystallization of metasomatized domains in the peridotites.

Cummingtonite (ferromagnesian amphibole), a typical metamorphic amphibole in ultramafic rocks, occurs in some type 1 and 2 peridotites and most likely replaced orthopyroxene in the context of the late tectono-thermal events. This can explain the very low amounts of orthopyroxene in the type 1 peridotites 10-20A and 10-20C.

Similar to olivine, the type 3 peridotite amphiboles in the orthopyroxene-poikiloblasts are indistinguishable from those in the matrix. Hence, subsequent element exchange and re-equilibration between orthopyroxene-poikiloblasts and enclosed amphiboles were insignificant. Measured type 3 peridotite amphiboles have slightly different core composition than the calcic amphiboles in the type 1 peridotites, such as higher Al_2O_3 and calculated A- and C- cations (Fig. 6-2). This difference might point to variable conditions during amphibole formation.

Yet, the measured major and minor element compositions in calcic amphibole cannot be used to clearly distinguish between mantle-, crustal cumulate- or metamorphic origin.

6-3.1.1.4 Spinel

A marked difference between NUB and SOISB type 1 peridotites is that chromite only occurs in NUB peridotites and Al-spinel in SOISB peridotites. This might be directly linked to the higher Cr content in NUB peridotites than in SOISB peridotites. However, in the case of peridotites from SOISB1, metamorphic spinels with ferrian chromite cores might represent recrystallized chromite. Moreover, the abundant Cr-magnetite and magnetite in all peridotites and the fact that most chromites and Al-spinels are rimmed or are closely associated with

and/or Cr-magnetite, indicates re-equilibration, alteration and secondary spinel formation for all peridotites during retrograde metamorphism (e.g., Gargiulo et al., 2013).

The spinel Fe^{3+}# (Fe^{3+}#=100*[Fe^{3+}/(Al+Fe^{3+}+Cr)]) is often used as a parameter to distinguish between highly altered Cr-rich spinel cores and less altered cores (Fe^{3+}#<10) that potentially retain their primary Cr# (e.g. Bernstein et al., 2013). Only in rare cases, the Al-spinels of some SOISB peridotites have core compositions of Fe^{3+}#<10 (e.g. 10-34 and 10-36, Table 6-1) and might represent pristine compositions, but this interpretation is arguable. Generally, the spinel compositions are consistent with a metamorphic origin or metamorphic re-equilibration (Fig. 6-4).

6-3.1.2 Changes in the mineralogy of type 1 peridotites over time

Overall, three major events affected the chemical compositions and mineralogy of type 1 peridotites: (1) partial mantle-melting and melt extraction, (2) mantle-re-fertilisation by metasomatic melt, and (3) subsequent metamorphism. Those events presumably changed the main mineral assemblage as followed:

(1) Mineralogy 1 (M1) - Primary mantle minerals (*p*):

$Ol_p + Opx_p \pm Cpx_p + Spl_p$

(2) Mineralogy 2 (M2) – Primary and secondary metasomatic mineral (*m*):

$Ol_p + Opx_m + [Cpx_m \text{ or Ca-Amph}_m] + Spl_m \pm Ol_m \pm Opx_p \pm Spl_p$

(3) Mineralogy 3 (M3) - Primary and metasomatic and metamorphic minerals (*x*):

$Ol_{p \text{ or } x} + Opx_{x \text{ or } m \text{ or } p} + \text{Ca-Amph}_x + Spl_x \pm \text{Mg-Fe-Amph}_x$

This nomenclature will be used below to discuss the timing of mineral growth as constrained by radiogenic isotopes.

6-3.2 Lu-Hf-Sm-Nd-Rb-Sr abundances in olivine, orthopyroxene and amphibole

Due to the low Lu, Hf, Sm, Nd, Rb and Sr concentrations in orthopyroxene and especially in olivine, the element budget is sensitive to impurities, like melt inclusions, mineral grain coatings or crack fillings (e.g., Eggins et al., 1998). In order to avoid these effects as much as possible, clear, inclusion-free minerals were preferentially picked (Chapter 3). Moreover, the mineral separates were digested via table-top-digestion, because this method selectively dissolves olivine, orthopyroxene and amphibole while leaving spinel and microscopic grains of Hf-bearing accessory phases like zircon and rutile largely intact. The later two phases however, are unlikely to occur in the peridotite samples investigated here. Orthopyroxene separates from samples 10-27 (three separates) and 10-36 (four separates) include one separate each with a small amount of opaque inclusions. Opaque phases remained behind after table-top digestion, yet, partial dissolution of the opaque phases or of invisible

microscopic phases in general, cannot be excluded completely. However, the "impure" orthopyroxene separates are within the compositional range of the "pure" ones and no systematic concentration differences can be clearly attributed to impurities, as can be predicted from the abundances of the elements analyzed in spinel which are generally low.

It should be mentioned here that EMP analyses show no major and minor element zonation in all investigated olivine and orthopyroxene grains, except occasionally the outer < 10 µm. Microscope observations indicate no preferential occurrence of inclusion in the core or rim, or optically visible zonations. Hence, even if trace element zonations would occur, it is unlikely that preferentially rims or cores were picked. Consequently, the Lu-Hf-Sm-Nd-Rb-Sr concentration variations in the 10-27 and 10-36 replicate orthopyroxene separates more likely indicate element concentration variations between orthopyroxene grains and not necessarily trace element zonation. Moreover, the Sm/Nd ratios are rather constant, whereas Lu/Hf and Rb/Sr ratios are slightly variable in the 10-27 and 10-36 orthopyroxene replicate separates. Lu and Hf are immobile during low-grade metamorphism and the observed variations in Lu/Hf ratios can be interpreted as indication for low primary heterogeneities or incomplete eradiation of primary heterogeneities. In contrast, Rb and Sr are more susceptible to metamorphic re-mobilisation, and thus the variations in Rb/Sr ratios are likely a result of open system disturbance superimposed by later metamorphic or metasomatic events.

Note that the concentrations in olivines were not measured on single grains and the overall concentrations are very low, thus, the concentration data must be interpreted with caution. Nevertheless, elemental relationship between LREE and HREE can be useful to evaluate subsequent alteration. In spite of large variations of available partition coefficients for REE in olivine and orthopyroxene, all published data regarding Lu, Hf, Sm and Nd partitioning behaviour in olivine and orthopyroxene indicate increasing partition coefficients for REE with decreasing cationic radius for olivine and orthopyroxene ($Lu_{PM} > Sm_{PM} > Nd_{PM}$, PM= mantle normalized) (e.g., Lee et al., 2007; Rampone et al., 2016; Scott et al., 2016). $Ol_{10\text{-}11}$ and $Ol_{10\text{-}27}$ show this trend, and $Ol_{10\text{-}20C}$ and $Ol_{10\text{-}36}$ show $Lu_{PM} > Nd_{PM}$ and Sm_{PM}, but $(Sm/Nd)_{PM} < 1$. Likewise, partition coefficient studies indicate that Lu is more compatible than Hf in olivine and orthopyroxene. In fact, all olivine and orthopyroxene separates show $(Lu/Hf)_{PM} > 1$, yet, $Ol_{10\text{-}36}$ and $Ol_{10\text{-}27}$ $(Lu/Hf)_{PM}$ ratios are considerably lower than $(Lu/Hf)_{PM}$ values obtained for $Ol_{10\text{-}11}$ and $Ol_{10\text{-}36}$. Unlike $Ol_{10\text{-}11}$, the primitive mantle-normalized Sm concentration in $Opx_{10\text{-}11}$ is above the Lu, Hf and Nd concentrations (Fig. 6-8). The deviation from the expected relationship of $Lu_{PM} > Sm_{PM} > Nd_{PM}$ might suggest that olivines or orthopyroxenes were affected by sub-solidus element exchange or selective enrichment of LREE.

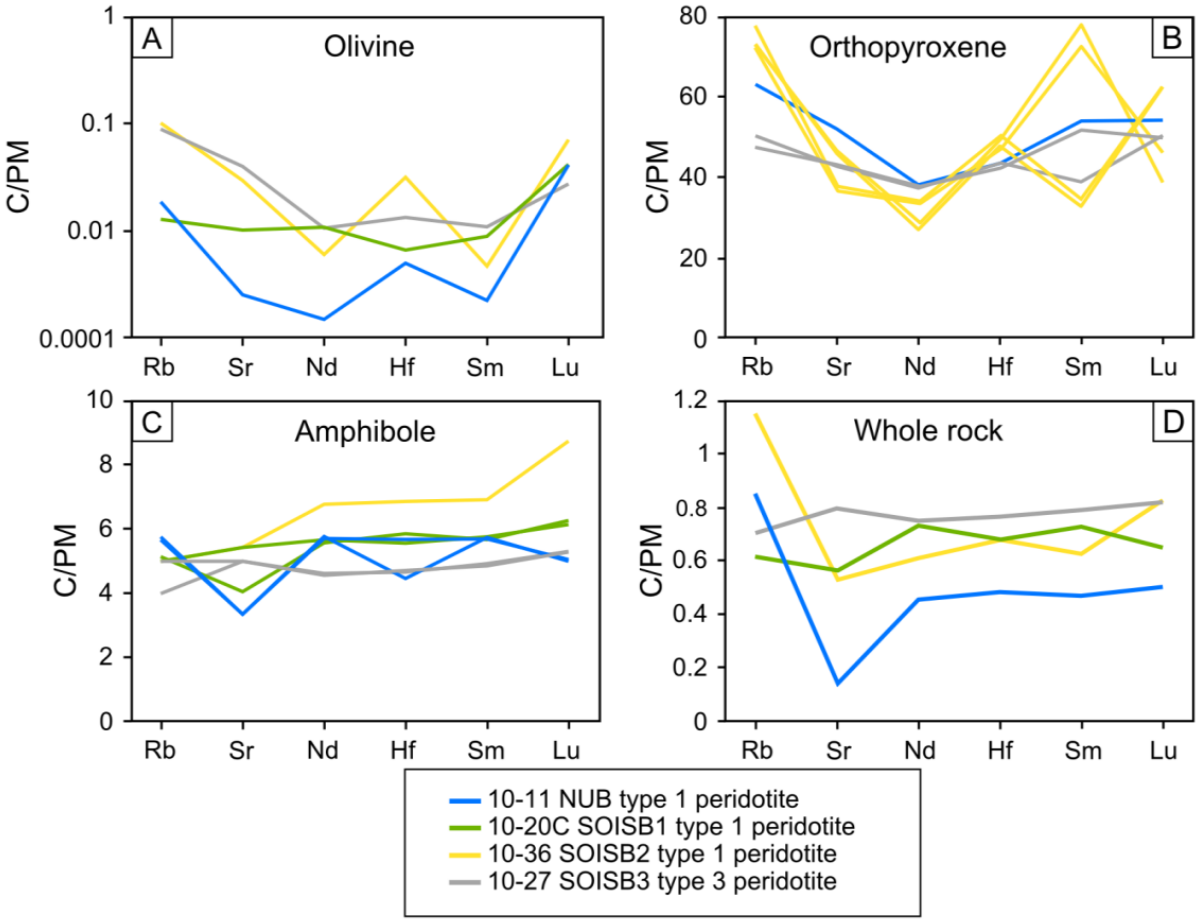

Figure 6-8: Primitive mantle-normalized Lu-Hf-Sm-Nd-Rb-Sr patterns (C/PM) obtained for (A) olivine separates, (B) orthopyroxene separates, (C) amphibole separates and (D) whole rocks. (A) $Ol_{10\text{-}11}$ and $Ol_{10\text{-}27}$ show the expected relationship of Lu_{PM} >Sm_{PM} >Nd_{PM}. (A-B) The deviation from the expected relationship of LuPM >SmPM >NdPM might suggest that $Ol_{10\text{-}20C}$ and $Ol_{10\text{-}36}$ or orthopyroxenes were affected by sub-solidus element exchange or selective enrichment of LREE. (C) $Amph_{10\text{-}36}$ show higher Lu, Hf, Sm and Nd concentration than the other amphibole separates, but no selective re-enrichment of Nd or Sm over Lu is evident from the primitive mantle-normalized patterns. Thus, the Lu-Hf-Sm- Nd-Rb-Sr concentrations in $Amph_{10\text{-}36}$ provide no clear evidence for a metasomatic origin. Primitive mantle values (PM) are from Palme and O´Neill (2014).

Notably, the amphibole separates represent a mixture of amphiboles of variable compositions. Because the amphiboles were not distinguishable under the binocular microscope. The amphiboles in type 3 peridotite 10-27 show smaller variations in their compositions, mainly magnesio-hornblende, in contrast to the amphiboles in the type 1 peridotites 10-11, 10-20C and 10-36. The compositions of calcic amphiboles in peridotite 10-36 mainly range from magnesio-hornblende to pargasite, and in peridotites 10-11 and 10-20C the calcic amphibole compositions vary between tremolite, magnesio- and magnesio-ferri-hornblende endmembers. Moreover, sample 10-20C contains Mg-Fe-amphibole (cummingtonite) beside calcic amphibole. Metamorphic element redistribution, as indicated by the major element concentrations, especially for sample 10-20C, has to be considered

when interpreting the trace element and isotope data. However, the variations of Lu, Hf, Sm and Nd concentration in the amphibole replicate separates are less than 10%, except for Nd and Rb in 10-20C amphibole separates, and Sr in the 10-27 amphibole separates. Therefore, the amphibole separates provide meaningful average concentrations of Lu, Hf and Sm for amphibole in the four peridotites and with the aforementioned exception as well for Nd, Rb and Sr.

In general, Lu, Hf, Sm, Nd, Rb and Sr are far more compatible in amphibole than in olivine and orthopyroxene (e.g., Sen and Dunn, 1994; Zack et al.. 1997; Adam and Green, 1994, 2006) and in the absence of clinopyroxene, amphibole is the major host phase for most incompatible trace elements. This is in line with the MC-ICP-MS analyses showing that Lu, Hf, Sm, Nd, Rb and Sr concentrations are in general several magnitudes higher in amphibole than in the associated olivines and orthopyroxenes.

Selective LREE enrichment in the primitive mantle-normalized patterns for metasomatic amphibole in mantle peridotites is a use full tool to trace mantle metasomatism by LREE-enriched melts or fluids. Yet, only one type 1 peridotite (10-36) contains pargasite that might have been formed during mantle metasomatism. Even though $Amph_{10\text{-}36}$ show higher Lu, Hf, Sm and Nd concentration than the other amphibole separates, no selective re-enrichment of Nd or Sm over Lu is evident from the primitive mantle-normalized patterns ($(Lu/Sm)_{PM}$ and $(Lu/Nd)_{PM}$ >1). Thus, the Lu-Hf-Sm- Nd-Rb-Sr concentrations in the amphibole separate from sample 10-36 provide no clear evidence for a metasomatic origin. Furthermore, the mantle-normalized Lu-Hf-Sm-Nd-Rb-Sr patterns for type 3 peridotite mineral separates are not clearly distinguishable from those obtained for the type 1 peridotites (Fig. 6-8).

6-3.3 Lu-Hf-Sm-Nd-Rb-Sr Mass balance calculations

Knowing the trace element distribution in the whole rocks can provide important information for interpreting whole rock trace element and isotope signatures. In order to evaluate the trace element distribution in the peridotites, the whole rock Lu-Hf-Sm-Nd-Rb-Sr compositions were reconstructed using estimated mineral proportions (modal and normative) and measured Lu-Hf-Sm-Nd-Rb-Sr concentrations in olivine, orthopyroxene and amphibole (Fig. 6-9).

Importantly, orthopyroxene contributes less than 10% to the Lu-Hf-Sm-Nd-Rb-Sr whole rock budgets, thus, the effect of the small variations in element concentration in orthopyroxene on the mass balance calculations is negligible. Moreover, it is not the aim of this study to provide precise numbers for trace element distribution in the peridotites, but rather to gain a better understanding of the formation and alteration history of the major

mineral phases and the possible implications on the trace element and isotope whole rock signatures.

The mass balance calculations infer that even small amounts of amphibole (e.g. < 4% amphibole in dunite 10-11) dominate the Lu, Sm, Nd and Sr whole rock budget (Figs. 6-4 to 6-6 and 6-9). Only in the case of the dunite 10-11, olivine contributes a significant amount of Lu (ca. 20%) to the whole the rock budget (Fig. 6-9). This is in line with previous studies (e.g., Witt-Eickschen and O'Neill, 2005; Scott et al., 2016).

Importantly, the comparison of the mass balance calculations with the measured data show considerable deficits in Rb and Hf calculated concentration for all three type 1 peridotites (10-11, 10-20C and 10-36) and a considerable deficit in Sm and Nd for type 1 peridotite 10-20C (Fig. 6-9 C-D). The Rb deficits amount between ca. 30% (10-20C) to more than 80% (10-11 and 10-36) of the whole rock budgets and for Hf between ca. 30% (10-20C and 10-36) and ca. 50% (10-11) of the Hf whole rock budgets. The mass balance calculations indicate a smaller deficit in calculated Hf concentration (ca. 15%) for type 3 peridotite 10-27 compared to type 1 peridotites. The hbl-peridotite 10-36 contains notable amounts of mica and thus, mica is likely the main Rb host phase in this sample. Other secondary phases such as mica presumably host significant amount of Rb in the case of the peridotites 10-11 and 10-20C. The dunite 10-11 show the highest Hf deficit together with a slight Lu deficit, however, due to the very low concentrations in the sample (47 ppb Hf and 13 ppb Lu), the addition of minute amounts of a Hf-rich phase would be sufficient to complement the whole rock budget.

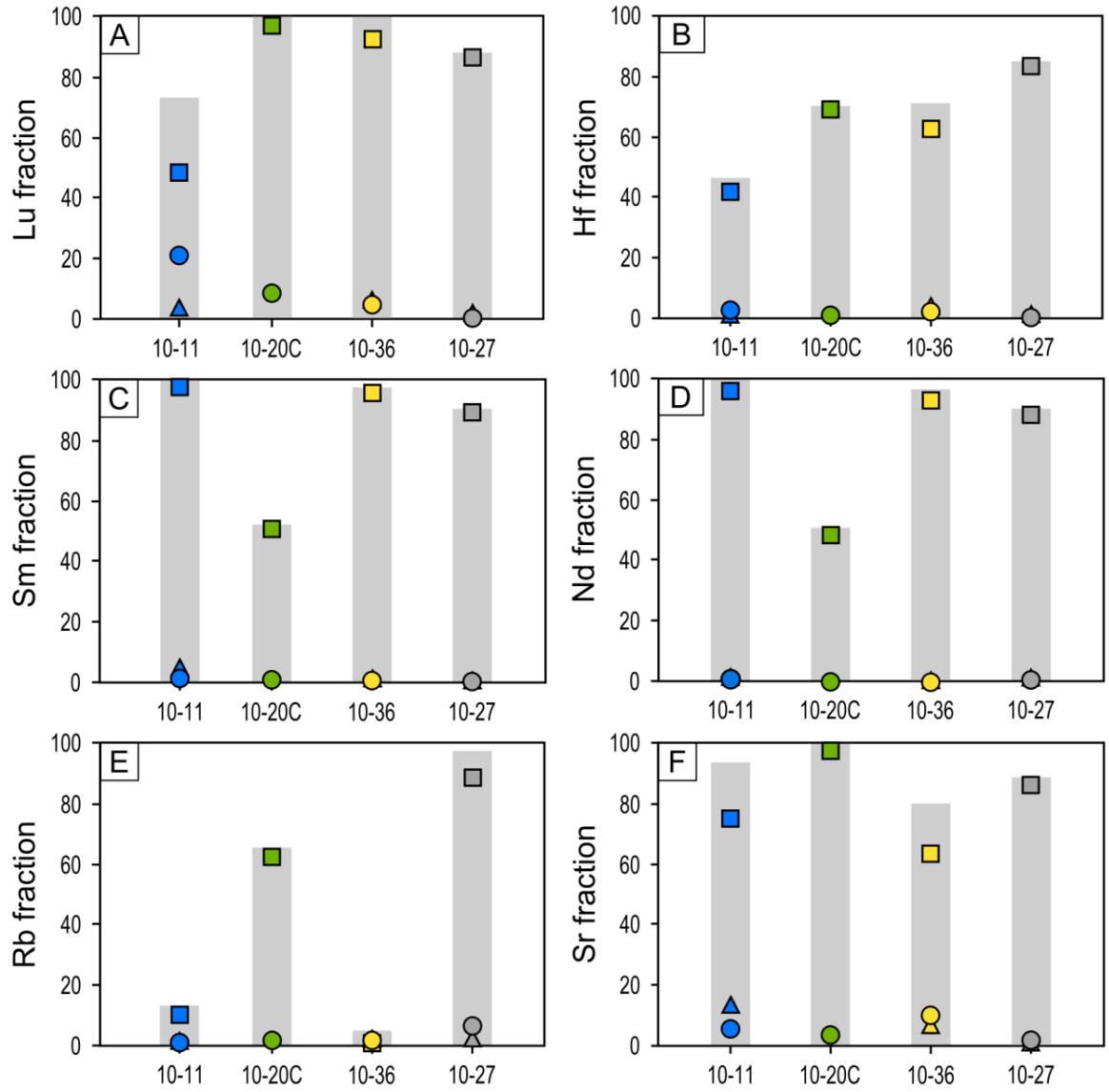

Figure 6-9: Calculated Lu, Hf, Sm, Nd, Rb and Sr fractions of the whole rock concentrations in olivine, orthopyroxene and amphibole. Grey columns indicate the total amount of the elements based on the mass balance calculations relative to the measured concentrations. The figure illustrates that amphibole generally dominates the Lu, Sm, Nd and Sr whole rock budget. Only in the case of the dunite 10-11, olivine contributes a significant amount of Lu (ca. 20%) to the whole the rock budget. The mass balance calculations (grey columns) indicate that additional phases are necessary to balance the whole rock concentrations of Hf in all four peridotites, Rb in the three type 1 and Sm and Nd in the case of the type 1 peridotite 10-20C. Symbols and colours for the peridotites and mineral separates are equivalent to those in Fig. 6-4.

Collectively, the comparison of the calculated value with the measured data show that additional phases are necessary to balance the bulk concentrations of Hf in all samples, of Rb in samples 10-11, 10-20C and 10-36, and of Sm and Nd in sample 10-20C. Those phases can have significant effects on the whole rock isotope signatures. For example, mica and grain boundary impurities, or thin films of glass and its breakdown products, can have significant effects on the whole rock trace element budged (e.g., Zindler and Emil, 1988; Eggins et al., 1998; Ionov et al., 2002).

6-3.4 Isotope signatures of olivine, orthopyroxene and amphibole

The internal isochron approach can help to determine disturbance of isotope systems, because minerals of the same age (growth or metamorphic age) would plot on a regression line. Major element compositions indicate that amphiboles in type 1 peridotites 10-11 and 10-20C formed during retrograde metamorphism and amphiboles in 10-36 might had been formed during mantle metasomatism. Thus, the type 1 peridotite olivine and orthopyroxene separates would only plot together with the amphibole separates on a regression line if they were completely reset during the amphibole formation event.

However, the scatter in the ^{176}Lu-^{176}Hf isotope space for all type 1 peridotites indicates incomplete resetting of the ^{176}Lu-^{176}Hf isotope during re-fertilization of the mantle peridotites or subsequent amphibole facies metamorphism (Fig. 6-10). Nonetheless, the Lu-Hf isotope signatures appear to be less affected by later alteration than the Sm-Nd and Rb-Sr isotope signatures. For example, $Ol_{10\text{-}11}$ and $Ol_{10\text{-}20C}$ display, as expected, significant more radiogenic Hf isotopic ratios than the whole rocks and the amphibole separates (see also e.g., Stracke et al., 2011) and are more radiogenic than the orthopyroxene separates (Fig. 6-4). Moreover, both olivine separates are not in isotopic equilibrium with the associated amphibole separates. Hence, $Ol_{10\text{-}11}$ and $Ol_{10\text{-}20C}$ were not rest during amphibole formation and might have preserved their primary ^{176}Lu-^{176}Hf isotope signatures.

The mass balance calculations presented above indicate that an additional Hf-rich phase is necessary to balance the Hf whole rock budget. Such an Hf-rich phased with very low Lu/Hf and low ^{176}Hf/^{177}Hf values is also necessary to explain the whole rock ^{176}Lu-^{176}Hf signatures obtained for the four peridotites. For example, the 10-20C whole rock measured ^{176}Hf/^{177}Hf and ^{176}Lu/^{177}Hf ratios are lower than all those obtained for the mineral separates (Fig. 6-10C).

The 10-11 orthopyroxene and amphibole separates define an age regression line yielding an age of 3040 ± 73 Ma (MSWD= 1.2, n=3) (Fig. 6-10A). The 10-20C whole rock and amphibole separates define an age regression line yielding an age of 3991 ± 55 Ma (MSWD= 2.8, n=3) (Fig. 6-10C). However, the geological relevance of the two three-point regression lines is ambiguous. Figure 6-10B illustrates a simplified four-stage isotopic evolution scenario for the minerals in sample 10-11, including mineral isotope compositions after (1) melt extraction, (2) mantle metasomatism, (3) amphibole facies metamorphism, and (4) present day isotope compositions after a significant time of closed system isotope evolution. The orthopyroxenes in sample 10-11 are either of metasomatic or metamorphic origin and thus, orthopyroxenes might not be in isotopic equilibrium with the amphiboles (see also 6-3.1.2 and Fig. 6-10B). Consequently, the age regression line defined by the 10-11 orthopyroxene and amphibole separates might not give a meaningful geological age information.

Nonetheless, the NUB sample 10-11 ^{176}Lu-^{176}Hf regression line age falls within the age range obtained for metamorphic zircons from the northern part of the NUB (3.65-2.70 Ga) and might indicate amphibole formations or significant metamorphic resetting during Paleoarchean to Neoarchean metamorphic events. Moreover, in the case of the SOISB1 sample 10-20C, the amphibole separates grouped with the two whole rocks from the sample subset 10-20 (10-20C and 10-20A) define a ^{176}Lu-^{176}Hf age regression line corresponding to an age of 3952 ±250 Ma (MSWD=5.8, n=4) (Fig. 6-10C). This age is in line with Eoarchean regression line ages defined by SOISB peridotites and the assumed minimum age of > 3.81 Ga. These findings can be interpreted as amphibole formation or significant metamorphic resetting of the amphiboles to have taken place in the Eoarchean, possible in context to the TTGs intrusions. Geochronological data in combination with detailed field studies indicates numerous magmatic and metamorphic events throughout the IGC between 3.85 Ga and 3.60 Ga (e.g., Baadsgaard 1973; Baadsgaard et al. 1984; Nutman et al. 1997, 2002a, b; Frei and Rosing 2001; Amelin et al. 2010; Horie et al. 2010; Hoffmann et al. 2011b; Polat et al. 2015).

In contrast to all other olivine separates, $Ol_{10\text{-}36}$ shows lower $^{176}Hf/^{177}Hf$ and $^{176}Lu/^{177}Hf$ ratios than the 10-36 amphibole and orthopyroxene separates, and the $^{176}Hf/^{177}Hf$ and $^{176}Lu/^{177}Hf$ ratios of $Ol_{10\text{-}36}$ are within ~10% of the whole rock values (Fig. 6-9D). In Lu-Hf isotope space, $Ol_{10\text{-}36}$ and the 10-36 orthopyroxene separates define an age regression line corresponding to an age of 3393 ± 84 Ma (MSWD = 1.2, n=4) (Fig. 6-10D), indicating intense metamorphic overprint and re-equilibration of olivine and orthopyroxene in the Neoarchean. Notably, the whole rock and the amphibole separate plot above the regression line and are not in isotopic equilibrium with olivine and orthopyroxene.

In the case of the type 3 peridotite 10-27, only the olivine separate deviates significantly from the $^{176}Lu/^{177}Hf$ regression line that is defined by the orthopyroxene and amphibole separates and the whole rock. This regression line corresponds to an age of 3864 ± 160 Ma (MSWD=0.75, n=5; Fig. 6-10E). This age is in good agreement with the assumed minimum age of 3.81 Ga for the SOISB3 peridotites. Based on petrographic and field observations, sample 10-27 is characterised as a preserved crustal cumulate and thus, we interpret the Lu-Hf age as an approximate age for the cumulate formation.

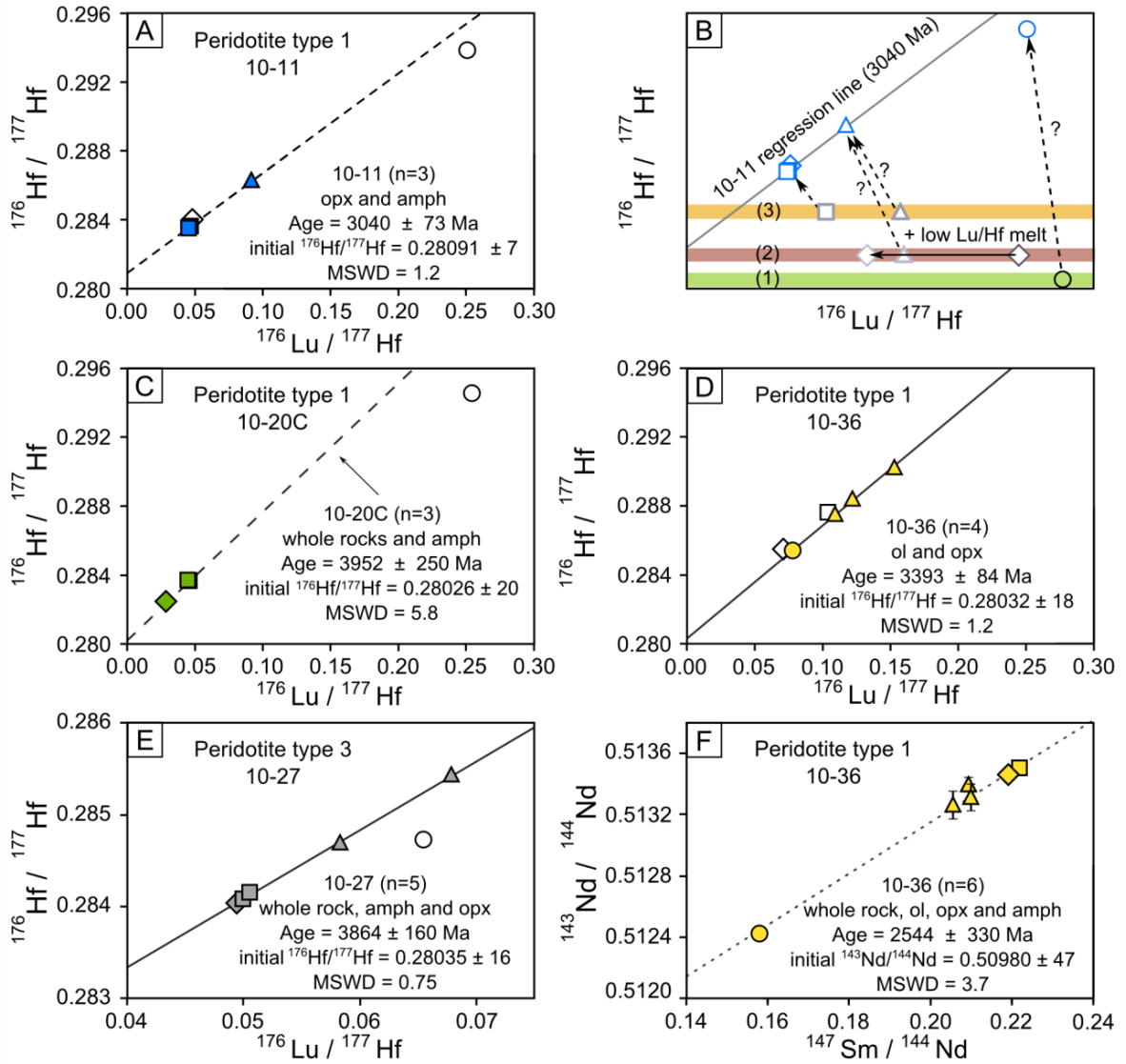

Figure 6-10: Measured (A-E) $^{176}Lu/^{177}Hf$ versus $^{176}Hf/^{177}Hf$ obtained for the mineral separates and whole rock of the four peridotites. The age regression lines were calculated using Isoplot (version 3.41d, Ludwig, 2006). Symbols and colours for the peridotites and mineral separates are equivalent to those in Fig. 6-4. The panel (B) illustrates a simplified four-stage isotopic evolution scenario for the minerals in sample 10-11. Stage (1) indicates the mineral isotope compositions after melt extraction and isotopic equilibrium of the primary (*p*) mantle minerals assemblage including primary olivine (open circle; M1 = olivine$_p$ + orthopyroxene$_p$ ± clinopyroxene$_p$ ± high-Hf-Phase$_p$). Stage (2) indicates mantle metasomatism and its effect on the whole rock isotope composition (grey-white diamonds) due to the addition of an LREE-rich melt with low Lu/Hf values. The metasomatism triggered the formation of metasomatic (*m*) orthopyroxene (grey-white triangles) and clinopyroxene or amphibole, but primary olivine and possibly orthopyroxene remained. Thus, the mineral assemblage changed (M2 = orthopyroxene$_m$ + [clinopyroxene/amphibole]$_m$ + olivine$_p$ + orthopyroxene$_p$ + high-Hf-Phase$_{p/m}$). Stage (3) indicates the isotope evolution over a significant time interval, followed by amphibole facies metamorphism (am) that triggered metamorphic amphibole formation or resetting of metasomatic amphibole (grey-white square), and possibly resetting of the Lu-Hf isotope signature in orthopyroxene (M3 = orthopyroxene$_{m\ or\ am}$ + amphibole$_{am}$ + olivine$_p$ + high-Hf-Phase$_{p\ or\ m}$). Stage (4) indicates the present day isotope compositions of olivine, orthopyroxene and amphibole (blue-white symbols) after a significant time of closed system isotope evolution (broken line arrows). We assume that

primary olivine had been preserved or that the isotopic re-equilibration induced during metamorphism was incomplete. Accordingly, the present day mineral phases controlling the Lu-Hf inventory (M4) are olivine$_{p}$ + amphibole$_{am}$ + orthopyroxene$_{m\ or\ am}$ + high-Hf-Phase$_{p/m}$. The grey line in panel (B) indicates the same amphibole-orthopyroxene age regression line as shown in panel (A). ol: olivine; opx orthopyroxene; amph: amphibole.

As for ^{147}Sm–^{143}Nd, only 10-36 mineral separates together with the whole rock define a meaningful age regression line corresponding to an age of 2544 ± 330 Ma (MSWD = 3.7, n=6; Fig. 6-11A). This result indicates a significant metamorphic resetting of the ^{147}Sm–^{143}Nd isotope systematics during the Neoarchean to Paleoproterozoic.

For the other three peridotites no precise meaningful age constraint is possible, with the ^{147}Sm–^{143}Nd or the ^{87}Rb-^{87}Sr isotope systems, due to lack of sufficient spread or too large scatter on the regression lines (Figs. 6-5, 6-6, 6-11 and D-1). Nonetheless, some of the ^{147}Sm–^{143}Nd and ^{87}Rb-^{87}Sr age regression lines can provide estimates of when the element mobility events might have taken place.

Figure 6-11 (B-C) show ^{147}Sm-^{143}Nd age regression lines that were calculated using the^{146}Sm decay constant of 6.54×10^{-12} a^{-1} (Lugmaier and Marti, 1978) and the whole rock or olivine isotope compositions. Most mineral separates plot on those regression lines yielding ages between 3.10 and 1.00 Ga. Those results suggest that the apparent Sm-Nd ages may correspond to Mesoarchean to Mesoproterozoic tectonothermal events recorded in the region south of the ISB and the southern part of the Færingehavn terrane (e.g., Pankhurst et al., 1973; Baadsgaard et al., 1984; Frei et al., 1999; Frei et al., 2002; Nutman et al., 2002; Polat et al., 2003; Nutman and Friend, 2007). For example, several deformation, greenschist to amphibolite facies metamorphic events have been reported for the IGC, mainly at about 3.20 to 2.6 Ga, 2.2-1.8Ga, and 1.60-1.80 Ga (e.g., Pankhurst et al., 1973; Baadsgaard et al., 1984; Frei et al., 1999; Frei et al., 2002; Nutman et al., 2002; Polat et al., 2003; Nutman and Friend, 2007).

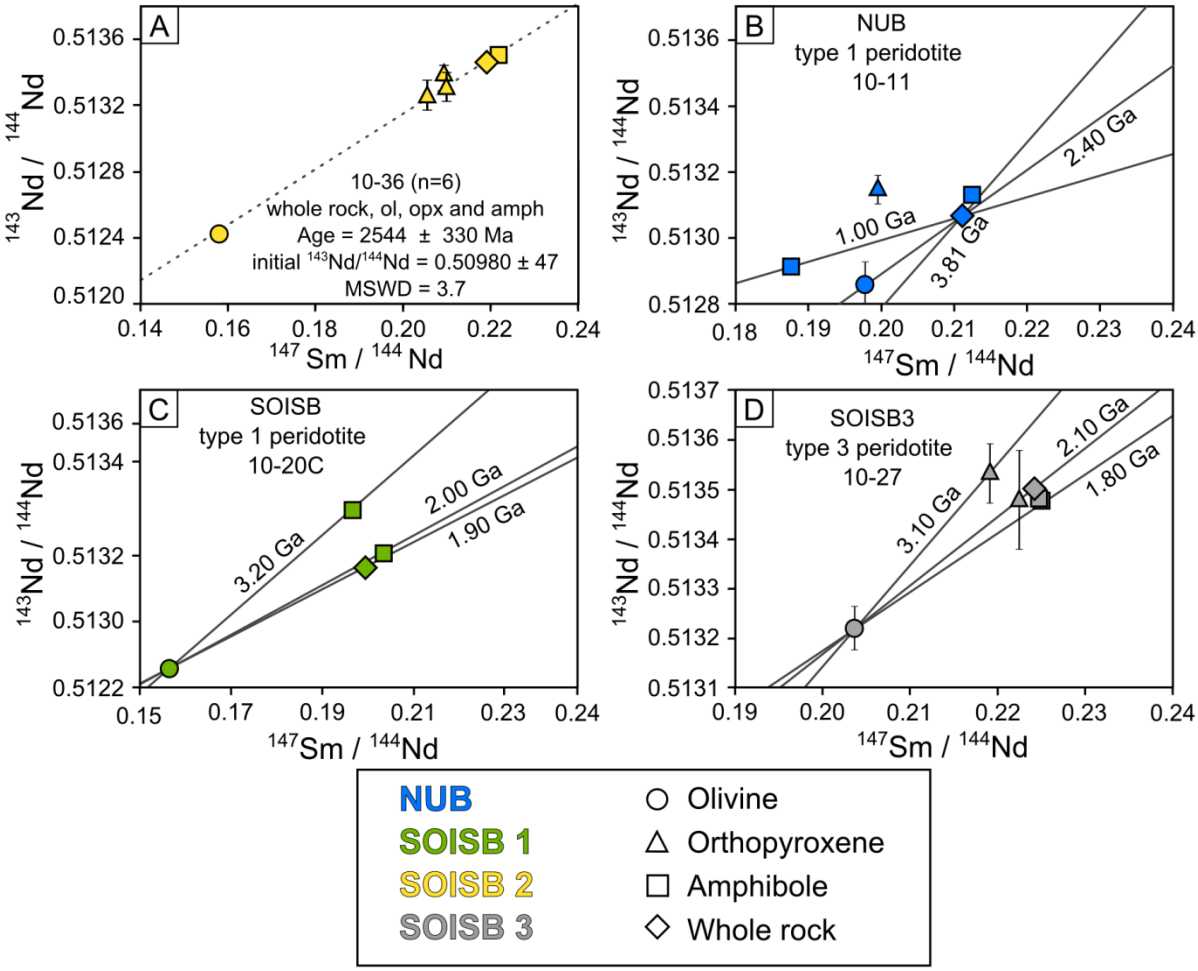

Figure 6-11: Measured $^{147}Sm/^{144}Nd$ versus $^{143}Nd/^{144}Nd$ data obtained for the mineral separates and whole rock of the four peridotites. The large scatter in the $^{147}Sm/^{144}Nd$ - $^{143}Nd/^{144}Nd$ space indicate extensive subsequent disturbance of the isotope systems. (A) The ^{147}Sm–^{143}Nd age regression line obtained for sample 10-36 corresponding to an age of 2544 ± 330 Ma (MSWD = 3.7) and overlaps within error with the timing of Neoarchean to mid-Proterozoic tectonothermal metamorphic event recorded in the Isua region. (B-C) The age regression lines were calculated using the whole rock or olivine isotope compositions and the ^{146}Sm decay constant of 6.54×10^{-12} a^{-1} (Lugmaier and Marti, 1978) Some apparent Sm-Nd ages (3.10 to 1.80 Ga) may correspond to late Archean to mid Proterozoic tectonothermal events recorded throughout the IGC (ca. 3.20 to 1.60 Ga).

The mass balance calculations indicate that additional phases are necessary to balance the Rb whole rock budget of type 1 peridotites, such as mica Thus, subsequent metamorphism certainly had a large effect on the ^{87}Rb-^{87}Sr isotope signatures. The high $^{87}Sr/^{86}Sr$ and $^{87}Rb/^{86}Sr$ ratios obtained for the type 1 peridotites are consistent with metamorphic resetting of the ^{87}Rb-^{87}Sr system reported for ISB rocks (e.g., Moorbath et al., 1998; Frei et al., 2002; Polat et al., 2003). The large scatter in the $^{87}Sr/^{86}Sr$-$^{87}Rb/^{86}Sr$ space indicate extensive subsequent disturbance of the ^{87}Rb-^{87}Sr isotope system. In contrast to the three type 1 peridotites, the calculated Rb deficit for the type 3 peridotite 10-27 is very small and amphibole is the main host for Rb.

The ^{87}Rb-^{87}Sr age regression lines (Fig. 6-12 A) that were calculated for the NUB peridotites 10-11, using the ^{87}Sr decay constant of 1.42 10^{-11} a^{-1} (Nebel et al., 2005).and the whole rock isotope compositions suggest resetting and significant disturbance of the ^{87}Rb-^{87}Sr system during the Mesoproterozoic to Neoprotrozoic (ca. 1.70 – 0.70 Ga) . The ^{87}Rb-^{87}Sr age regression lines calculated for the SOISB peridotites 10-27 and 10-36 (Fig. 6-12 C and D) suggest late Archean (< 3.30 Ga, e.g. sample 10-36) to Proterozoic (ca. 1.6 Ga, sample 10-27) resetting of the isotope system followed by open system

For the 10-20C peridotites no meaningful age constraint is possible, with the ^{87}Rb-^{87}Sr system (Fig. 12-B). Based on the age regression line defined by the olivine separate and one of the amphibole separates yielding and age of ca. 2.11 Ga, a similar scenario as suggested for the other SOISB peridotites seem to be plausible.

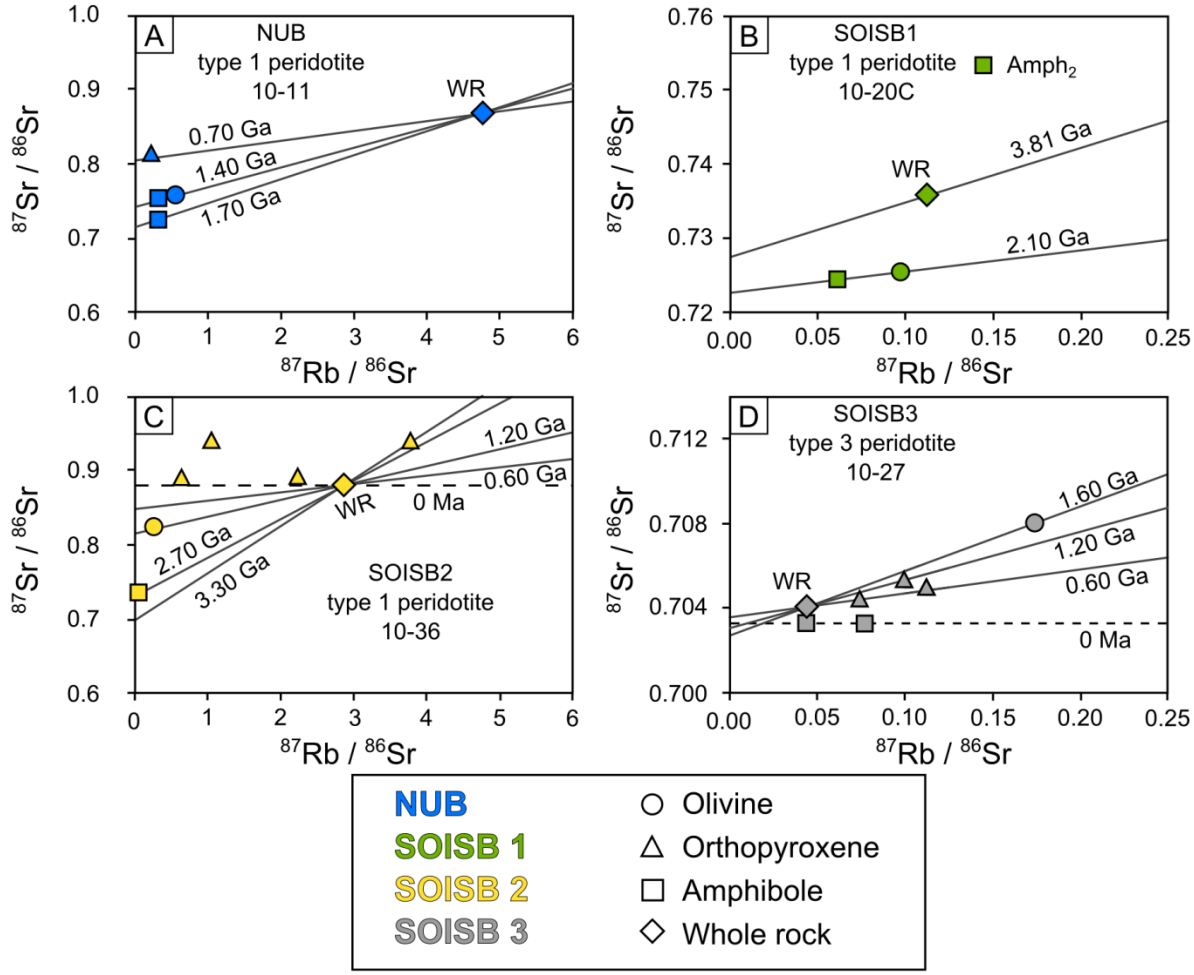

Figure 6-12: Measured ^{87}Rb-^{87}Sr versus $^{87}Sr/^{86}Sr$ data obtained for the mineral separates and whole rock of the four peridotites. The large scatter in the ^{87}Rb-^{87}Sr - $^{87}Sr/^{86}Sr$ space indicate extensive subsequent disturbance of the isotope systems. (A-C) The age regression lines were calculated using the whole rock isotope compositions and the ^{87}Sr decay constant of 1.42 10^{-11} a^{-1} (Nebel et al., 2005). The Rb-Sr isotope data suggest resetting during the late Archean and Proterozoic followed by subsequent disturbance by Proterozoic and Post-Precambrian metamorphic or metasomatic events.

6-4 CONCLUSIONS

From the major and minor element perspective, olivine and orthopyroxene in most type 1 peridotites and some type 2 peridotites might have preserved pristine mantle-like mineral compositions. In contrast, amphibole and spinel were formed or extensively re-equilibrated during subsequent metamorphism.

The Lu, Hf, Sm, Nd, Rb and Sr abundances in olivine, orthopyroxene and amphibole separates of four peridotites confirm that amphibole is the main host for Lu, Hf, Sm, Nd and Sr in the investigated peridotites. Yet, the mass balance calculations indicate that additional phases are necessary to balance the whole rock concentrations of Hf in all four peridotites, Rb in the three type 1 and Sm and Nd in the case of the type 1 peridotite 10-20C. Moreover, the addition of a (so far not identified) Hf-rich phase with very low Lu/Hf is also necessary to explain the whole rock ^{176}Lu-^{176}Hf isotope compositions. The isotope data obtained for the mineral separates indicate only partial attainment of ^{176}Lu-^{176}Hf isotope equilibrium during mantle metasomatism or metamorphism.

The low Lu, Hf, Sm and Nd concentrations in olivines and the more radiogenic Hf isotope ratios in olivine separates from 10-11 and 10-20C are consistent with a potentially preserved mantle signature. In contrast, isotope signatures of olivine from sample 10-36, and orthopyroxene separates from samples 10-11 and 10-36 indicate at least partial metamorphic resetting of the ^{176}Lu-^{176}Hf isotope system. A ^{176}Lu-^{176}Hf age regression line defined by olivine and orthopyroxene separates from sample 10-36 suggest metamorphic resetting of the ^{176}Lu-^{176}Hf system in olivines and amphiboles at about 3.3 Ga.

In the case of the type 3 peridotite 10-27 the major and trace element compositions in olivine, opx, amph are consistent with the a crustal cumulate origin. A five point mineral and Lu-Hf whole rock age regression line obtained for the type 3 peridotite 10-27 yields an age of 3864 ± 160 (MSWD = 0.75). This age is in good agreement with the postulated minimum ages of >3.81 Ga for the peridotite.

No accurate ^{147}Sm-^{143}Nd age can be obtained for the four peridotites, due to lack of sufficient spread in Sm/Nd or, due to large scatter on the regression lines. Nonetheless, a ^{147}Sm-^{143}Nd age regression line defined by whole rock and mineral separates from sample 10-36 yield an age of 2544 ± 330 Ma (MSWD=3.7, n=6) and suggests metamorphically induced extensive resetting of the ^{147}Sm-^{143}Nd system in the late Neoarchean to early Paleoproterozoic. The Sm-Nd errorchron age may correspond, within errors, to late Archean tectonothermal metamorphic events recorded in the region. Likewise, the ^{87}Rb – ^{87}Sr data obtained for all four samples indicate significant disturbance of this isotope system by tectonothermal metamorphic events. The apparent ^{147}Sm–^{143}Nd and the ^{87}Rb-^{87}Sr regression

line ages obtained for all four the samples suggest resetting of the isotope systems by the Neoarchean to Paleoproterozoic, followed by subsequent disturbance superimposed by late metamorphic or metasomatic events.

Notably, whole rock and mineral separates of the type 3 peridotite 10-27 show significant less radiogenic $^{87}Sr/^{86}Sr$ values than those obtained for the type 1 peridotites. Collectively, type 3 peridotites differ clearly from type 1 peridotites in their olivine and orthopyroxne major element compositions (e.g. lower Fo# and En), the ^{176}Lu-^{176}Hf inventory (higher Lu/Hf) and ^{87}Rb – ^{87}Sr isotope signatures (lower $^{87}Rb / ^{86}Sr$).

In summary, the petrological observations and geochemical data obtained for the type 1 peridotites can be explained by melt extraction in the spinel stability field, followed by mantle metasomatism and later metamorphism. Those events caused significant changes in the type 1 peridotite mineralogy and triggered partial resetting of the ^{176}Lu-^{176}Hf isotope signatures at a mineral scale, and extensive reset or disturbance of the ^{147}Sm-^{143}Nd and ^{87}Rb-^{87}Sr isotope signatures.

Chapter 7

Geochemistry and Petrology of Peridotites from Akilia Island

7-1 INTRODUCTION

Four peridotites from Akilia Island have been analysed during the course of this study. Akilia Island has received major attention due to a controversy about the origin of early life and the effect of metamorphism on early biosignatures (e.g., Mojzsis et al.,1996, 2003; Nutman et al., 1996b, 2002; Myers and Crowley, 2000; Whitehouse et al., 2005, 2009; Fedo et al., 2006; Manning et al., 2006) Deciphering the preservation state of ultramafic rocks that also occur on Akilia Island might help to contribute towards this question. The peridotites examined here originate from supracrustal enclaves from two locations on southwest part of Akilia Island (Fig. 2-3). The enclaves are embedded in a 3.60 to 3.85 Ga old polyphase orthogneiss-unit (Fig. 2-3). In general, the Archean rocks on Akilia Island were affected by multiple tectono-metamorphic events. Thus, the most ultramafic rocks on Akilia Island are highly deformed and strongly modified. Nutman et al. (2002) tentative suggested that some ultramafic rocks on Akilia island night resemble remnants of Eoarchean mantle, but their detailed petrogenetic history is so far poorly constrained.

The Akilia Island sample set investigated in this study comprises two type 2 peridotites (10-05B and 10-05C) from a new sample location and two type 4 peridotites (10-04 and 10-06) from the type locality of the "Akilia association" (McGregor and Mason, 1977). The type locality of the "Akilia association", which comprises amphibolites, ultramafic and siliceous rocks record multiple events of deformation and high-grade metamorphism. Thus, there is a lack of agreement concerning the ages as well as the field relationships of the dated orthogneisses to the sedimentary, mafic and ultramafic rocks (e.g. Nutman et al., 1996, 2000, 2002; Whitehouse et al., 1999, 2005, 2009; Myers and Crowley, 2000, Friend and Nutman, 2005; Manning et al., 2006).

Consequently, the minimum ages of the four Akilia Island peridotites are less well contained, than for the SOISB and NUB peridotites. Postulated minimum ages range from ≥3.85 to >3.60 Ga. An absolute minimum age of >3.6 Ga can be assumed (e.g., Bennett et al, 1993; Nutman et al., 1996, 2000, 2002, 2007; Whitehouse et al., 1999, 2005, 2009; Myers and Crowley, 2000, Friend and Nutman, 2005; Manning et al., 2006).

This study provides for the first time combined petrological observations, comprehensive major and trace element data as well as Lu-Hf and Sm-Nd isotope data for Eoarchean ultramafic rocks from Akilia Island. In addition, major and minor element compositions of

olivine, orthopyroxene, amphibole, and spinel were obtained for the samples 10-05C and 10-04. The focus of this chapter is on the detailed characterisation of the four Akilia Island peridotites in comparison to the SOISB and NUB peridotites.

7-2 RESULTS

7-2.1. Whole rock major and trace elements

The abundances of major and trace elements obtained for the Akilia Island peridotites are given in Table 7-1. The two type 2 peridotites from sample-subset 10-05 (10-05B and 10-05C) show similar abundances of MgO (41.2 and 39.5 wt.%), Ni (2760 and 2672 ppm), Al_2O_3 (2.07 and 1.86 wt.%), and nearly identical Mg# of ca. 84. The CaO concentration is higher in10-05C (1.64 wt%) than in 10-05B (1.15 wt.%). The major element compositions obtained for both type 2 peridotites are mainly within the same range than those of SOISB and NUB type 1 peridotites (Figs. 7-1, 7-2A) and also those of crustal cumulates from ISB (Fig. 7-2B).

The two type 4 Akilia Island peridotites (10-06 and 10-04) exhibit lower contents of MgO (22.7 and 26.9 wt.%), Ni (1117 and 843 ppm), and Mg# (ca. 76). Their CaO (5.24 and 7.67 wt.%) and Al_2O_3 (6.57 and 9.29 wt.%) concentrations are higher than in the Akilia Island type 2 peridotites. Moreover, K_2O concentrations of the Akilia island type 4 peridotites are above 0.1 wt.% (0.67 and 0.14 wt.%). These samples also show significant higher TiO_2 concentrations (0.34 and 0.35 wt.%) than the SOISB and NUB peridotites except for the SOISB3 type 2 peridotites (0.32 wt%; Fig. 7-1). The Loss of ignition (LOI) obtained for the four Akilia Island peridotites is generally low, ranging from 1.46 to 2.94 wt.%.

Table 7-1: Major and trace element data for peridotites from Akilia Island

Name	10-05B	10-05C	10-06	10-04
Type	2	2	4	4
XRF analyses at University of Cologne				
wt.%				
SiO_2	41.3	41.6	43.7	45.0
TiO_2	0.22	0.22	0.34	0.39
Al_2O_3	2.07	1.86	6.57	9.29
Fe_2O_3	12.7	13.0	14.4	12.3
MnO	0.20	0.20	0.21	0.16
MgO	41.2	39.5	26.9	22.7
CaO	1.15	1.64	5.24	7.67
K_2O	0.01	0.01	0.67	0.14
Na_2O	<0.01	<0.01	0.55	0.97
P_2O_5	0.02	0.01	0.03	0.02
ppm				
Cr	1381	1415	2771	3066
Ni	2760	2672	1117	843
LOI	1.72	2.94	1.46	2.33
Total	101	101	100	101
Mg#	84.9	84.0	76.2	76.1
ICP-MS analyses at University Kiel				
ppm				
Rb	0.425	0.755	50.1	1.90
Sr	4.92	6.41	17.7	23.0
Y	1.84	2.72	7.66	9.21
La	0.419	0.642	1.46	2.40
Ce	1.14	1.74	4.05	6.65
Pr	0.189	0.278	0.605	0.870
Eu	0.101	0.128	0.246	0.707
Gd	0.395	0.603	1.29	1.45
Tb	0.0651	0.101	0.232	0.263
Ho	0.0818	0.124	0.324	0.394
Er	0.228	0.331	0.908	1.13
Tm	0.0346	0.0484	0.140	0.171
Yb	0.229	0.318	0.889	1.16
Pb	0.398	1.61	2.45	1.81
Th	0.0648	0.0976	0.178	0.0967
U	0.0272	0.0304	0.107	0.0990

(Mg# = 100*molar Mg/(Mg+Fe))

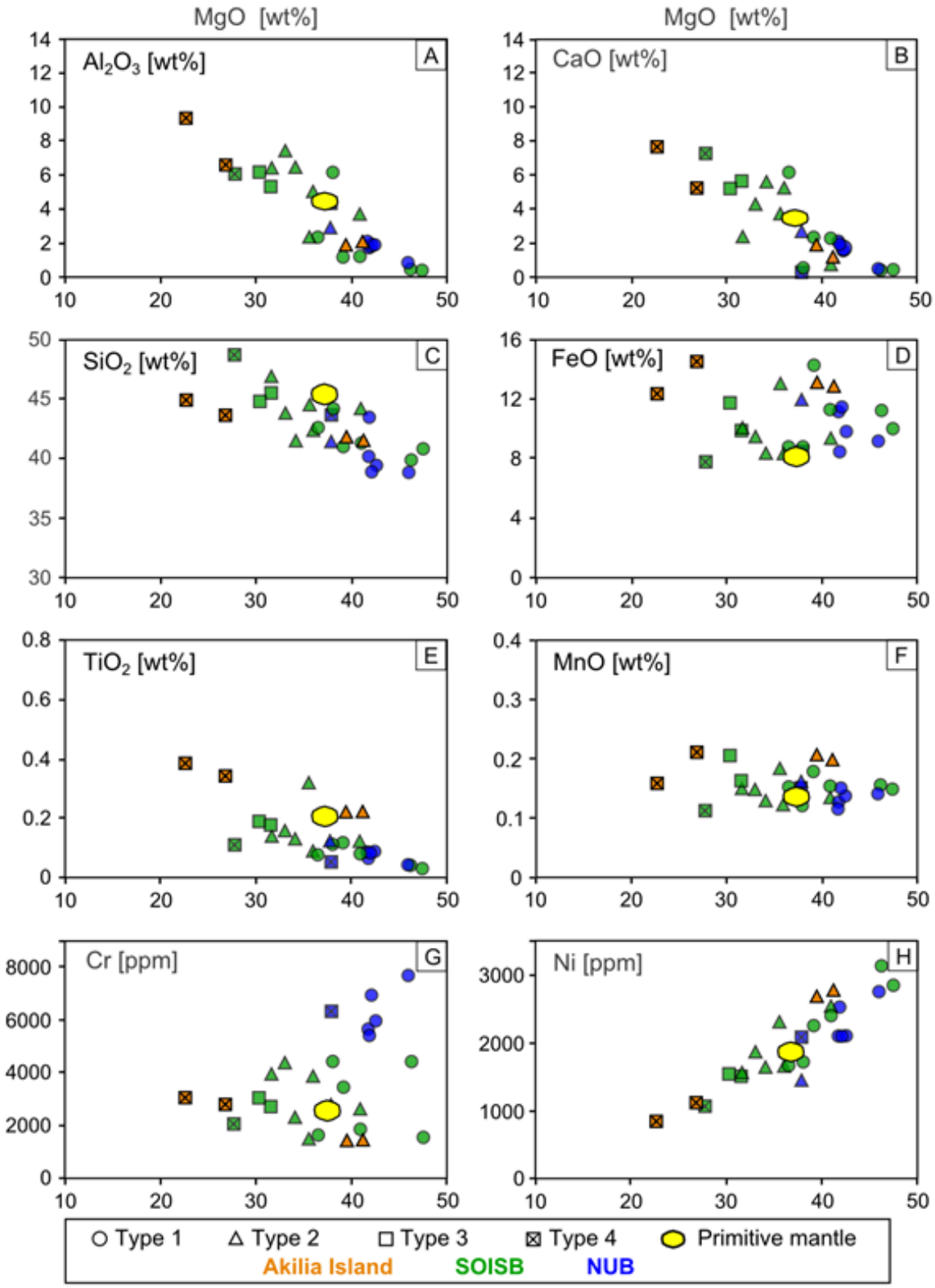

Figure 7-1: Whole rock abundances of Al_2O_3, CaO, SiO_2, FeO, Mn, TiO_2 and Ni plotted versus MgO from Alkali island peridotites in comparison to SOISB and NUB peridotites as well as primitive mantle composition. The major element compositions obtained for both type 2 peridotites are mainly within the same range than those of SOISB and NUB type 1 peridotites.. Primitive mantle values are from McDonough and Sun (1995) and Palme and O´Neil (2014).

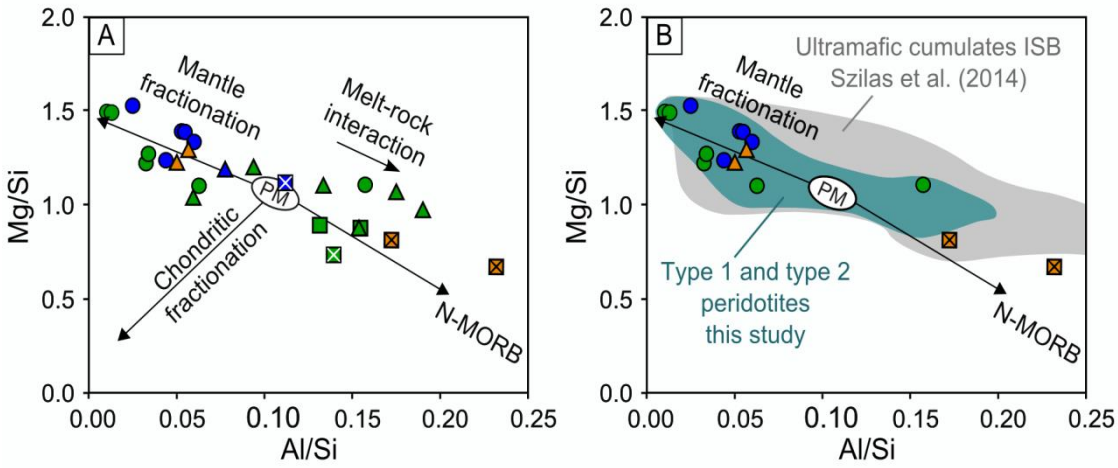

Figure 7-2: Mg/Si versus Al/Si diagrams after Jagoutz (1979). (A) Akilia Island peridotites in comparison to SOISB and NUB peridotites of this study; (B) Akilia Island peridotites in comparison to crustal cumulates from ISB (Szilas et al. 2015); the green field indicates type 1 and 2 peridotites of this study; the grey field indicates ISB ultramafic crustal cumulates (Szilas et al. 2015). Symbols are equivalent to those in Fig. 7-1., The Akilia Island type 2 peridotites lie in the fields of the SOISB and NUB type 1 peridotites (Fig. 7-2A) and of the crustal cumulates from ISB. Pprimitive mantle values (PM; yellow field) are from Palme and O´Neill (2014).

All four Akilia Island peridotites show relative flat mantle-normalized REE patterns (Fig. 7-3A). The incompatible trace element abundances of the two type 2 peridotites 10-05B and 10-05C are within the range of the SOISB type 2 peridotites. Note that sample 10-05C shows markedly higher REE, Hf and Zr abundances (up to 55%) than sample 10-05B. Likewise, the W concentration (0.65 ppm) of sample 10-05C is about 60% higher than that in sample 10-05B (0.16 ppm). Concentrations of Pb are enriched in both samples, yet to a greater degree in sample 10-05C (1.61 wt.%) than in sample 10-05B (0.398 wt.%) (Fig. 7-3B). However, all samples show similar primitive mantle-normalized REE patterns, except for Eu that shows anomalies (Fig. 7-3A).

The Akilia Island type 4 peridotites (10-04 and 10-06) exhibit general higher trace element concentrations than all SOISB peridotites (Fig. 7-3). Sample 10-06 has a small negative Eu anomaly while sample 10-04 has a distinct positive Eu anomaly. In contrast to most SOISB and NUB peridotites, the four Akilia Island peridotites lack negative Zr-Hf anomalies and mostly do not show selective Nb-Ta depletions, except for sample 10-06 (Fig. 7-3B). The Zr/Hf ratios in all four peridotites are sub-chondritic and range from 25.6 to 30.6. All four peridotites show sub-chondritic Nb/Ta ratios ranging from 12.4 to 17.6. Thus, their Zr/Hf and Nb/Ta are within the range displayed by the SOISB and NUB peridotites. The strong enrichment of W and Pb and the significant depletion of Sr relative to REEs concentrations in all Akilia Island peridotites resemble the anomalies observed in the SOISB and NUB peridotites.

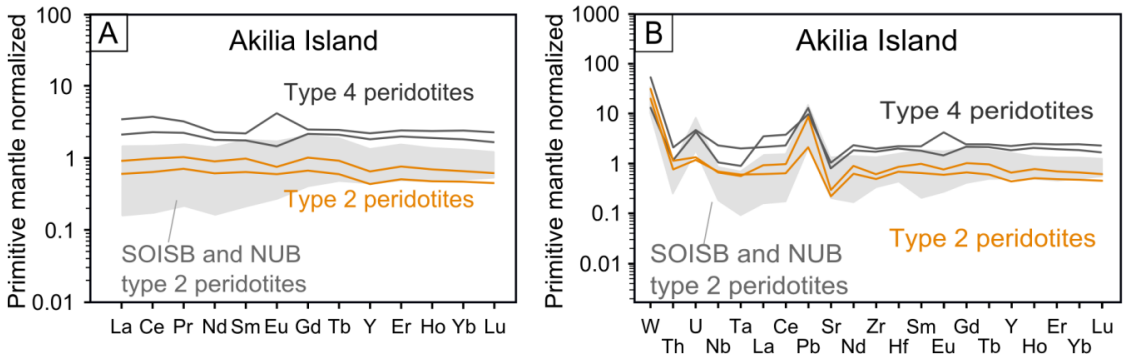

Figure 7-3: Primitive mantle normalized REE (A) and primitive mantle normalized trace element patterns (B) of Akilia Island peridotites. The light grey fields in (A) and (B) indicate SOISB and NUB type 2 peridotites for comparison. The Akilia Island peridotites show relatively flat primitive mantle-normalized REE patterns indicating LREE re-enrichment. The strong enrichment of W and Pb and the significant depletion of Sr relative to REEs concentrations in all Akilia Island peridotites resemble the anomalies observed in the SOISB and NUB peridotites. Primitive mantle values are from Palme and O´Neill (2014).

7-2.2 Whole rock Lu-Hf and Sm-Nd isotope compositions

Measured Lu-Hf and Sm-Nd isotope data and recalculated initial εHf and εNd values at 3.81 Ga are given in Table 7-2. Measured $^{176}Lu/^{177}Hf$ in type 2 peridotites (0.02299 and 0.02536) and in the type 4 peridotites (0.02796 and 0.03449) overlap with $^{176}Lu/^{177}Hf$ ratios obtained from the SOISB and NUB type 2 peridotites. Likewise, the measured $^{147}Sm/^{144}Nd$ ratios (0.1698 to 0.2002) obtained for the Akilia Island peridotites are within the range of the NUB and SOISB peridotites. The peridotites mainly show positive initial $\varepsilon Hf_{(3.81\ Ga)}$ between +2.2 and +2.6 and initial $\varepsilon Nd_{(3.81)}$ between -2.2 and +5.6.

Table 7-2: ^{176}Lu–^{176}Hf and ^{147}Sm–^{143}Nd isotope compositions of peridotites from Akilia Island. Initial εHf and εNd values were calculated using the CHUR values of Bouvier et al. (2008), a ^{176}Lu decay constant of 1.867×10^{-12} a^{-1} of Scherer et al. (2001) and Söderlund et al.(2004), and ^{146}Sm decay constant of 6.54×10^{-12} a^{-1} (Lugmaier and Marti, 1978). Initial εHf and εNd were calculated to 3.81 Ga, minimum ages obtained from field relationships.

	Sample [mg]	Lu [ppm]	Hf [ppm]	Lu/Hf	$^{176}Lu/^{177}Hf$	$^{176}Hf/^{177}Hf$	εHf (3.81 Ga)
10-05B	240	0.0323	0.199	0.1620	0.02299±6	0.282074 ±7	+2.5 ±0.5
10-05B-R	240	0.0314	0.210	0.1492			
10-05C	240	0.0442	0.247	0.1787	0.02536±6	0.282249 ±7	+2.5 ±0.5
10-05C-R	240	0.0443	0.261	0.1694	0.02404±6	0.282141 ±9	+2.2 ±0.5
10-06	240	0.119	0.605	0.1970	0.02796±7	0.282438 ±12	+2.5 ±0.5
10-06-R	120	0.121	0.619	0.1961			
10-04	240	0.164	0.674	0.2430	0.03449±10	0.282924 ±6	+2.6 ±0.5
	Sample [mg]	Sm [ppm]	Nd [ppm]	Sm/Nd	$^{147}Sm/^{144}Nd$	$^{143}Nd/^{144}Nd$	εNd (3.81 Ga)
10-05B	240	0.269	0.841	0.3199	0.1934±4	0.512815±10	+4.9 ±0.4
10-05B-R	240	0.265	0.828	0.3205	0.1938±4	0.512859±10	+5.6 ±0.4
10-05B-R	120	0.260	0.854	0.3046			
10-05C	240	0.398	1.20	0.3311	0.2002±4	0.512873±6	+2.7 ±0.4
10-05C-R	240	0.401	1.21	0.3313	0.1999±3	0.512619±8	-2.2 ±0.4
10-06	240	0.790	2.44	0.3237	0.1957±4	0.512515±8	-2.1 ±0.4
10-06-R	120	0.780	2.45	0.3180			
10-04	240	0.870	3.10	0.2809	0.1698±4	0.512239±8	+5.3 ±0.3

7-2.3. Major and minor element abundances in minerals

Selected representative mineral analyses are given in Table 7-3 and the full range of analyses are given in Appendix E, Table E-1.

The olivines from sample 10-05C have Fo# (86) within the range of SOISB type 2 peridotite olivines, at similar low CaO and Cr_2O_3 concentrations. Only the NiO concentrations in the 10-05C olivines are significant lower (<0.03 wt%) than in SOISB type 2 peridotites (>0.10 wt.%). Olivines in sample 10-04 have similarly low NiO, CaO and Cr_2O_3 concentrations than Akilia Island type 2 peridotites, but show lower Mg contents (Fo# ~77) than olivines of all other peridotites which were investigated in this study.

Sample 10-04 contains orthopyroxenes of enstatitic composition with slightly higher iron contents (En81) than orthopyroxenes in the SOISB and NUB peridotites. Yet, the CaO (<0.2 wt.%) and Al_2O_3 (~2.2 wt.%) concentrations are within the same range as SOISB and NUB orthopyroxenes. Sample 10-05C contains small amounts of Cr- and Na-poor diopside, that differ from the diopside in the SOISB peridotite 10-34 mainly in their lower FeO and TiO_2 concentrations.

Table 7-3: Representative electron microprobe mineral analyses for Akilia Island peridotites

Sample	10-05C	10-04	10-04	10-05C	10-04	10-05C	10-05C	10-05C	10-05C
Type	2	4	4	2	4	2	2	2	2
Mineral	Olivine	Olivine	Opx	Cpx	Ca-amph	Ca-amph1	Ca-amph2	Spinel	Ilmenite
[wt%]									
SiO_2	40.3	38.8	55.1	54.5	46.9	50.9	55.9	0.01	<0.01
TiO_2	<0.01	<0.01	0.054	<0.01	0.45	<0.01	<0.01	1.13	54.2
Al_2O_3	<0.01	<0.01	2.11	0.44	10.6	7.02	2.12	2.52	<0.01
Cr_2O_3	<0.01	<0.01	0.08	<0.01	0.31	<0.01	<0.01	42.1	0.12
FeO	13.3	20.6	12.5	0.61	6.87	4.03	2.89	47.5	40.3
MgO	46.8	40.3	29.8	17.4	17.6	20.2	22.7	1.37	3.81
CaO	0.02	0.02	0.16	25.5	11.9	12.0	12.2	0.06	0.06
Na_2O	40.3	38.8	0.025	0.00	2.04	<0.01	<0.01	<0.01	<0.01
NiO	0.01	<0.01	<0.01	<0.01	<0.01			<0.01	<0.01
Total	100	99.7	99.8	98.5	96.7	93.9	95.8	94.6	98.5
Fo#	86.3	77.7							
En			81.0						
Cr#								91.8	
$Mg\#_{spl}$								7.53	
Fe^{3+}#								28.8	

Opx: orthopyroxene; Cpx: clinopyroxene; Ca-amph: calcic amphiboles

Both Akilia Island peridotites contain calcic amphiboles with CaO concentrations of ca. 12 wt%, similar to SOISB and NUB calcic amphiboles. The calcic amphibole compositions of type 2 peridotite 10-50C are between tremolite, magnesio-hornblende and ferri-magnesio-hornblende endmembers. In contrast to the SOISB and NUB calcic amphiboles, their Na_2O, TiO_2 and Cr_2O_3 concentrations are below the detection limit. The type 4 peridotite 10-04 contains manly magnesio-hornblende within the compositional range of magnesio-hornblendes in the SOISB type 2 peridotites, except for slightly higher FeO concentrations. Sample 10-05C contains ilmenite, in addition to ferri-chromite and magnetite.

7-3 DISCUSSION

7-3.1 Major and trace element systematics of the Akilia Island peridotites

Clusters of thin, fine-grained veins, with clear alteration zones, pervade the Akilia Island type 2 peridotites. Yet, the effect of this late-stage alteration at the mineral scale seems to decrease rapidly within a radius of less than 1 cm away from the veins. Olivines and amphiboles are usually unzoned and secondary phases such as chlorite are rare.

In Fig. 7-2, Mg/Si and Al/Si compositions are plotted for the Akilia Island type 2 peridotites, which lie in the fields of the SOISB and NUB type 1 peridotites (Fig. 7-2A) and of the crustal cumulates from ISB (Fig. 7-2B). However, 10-05C olivine and orthopyroxene compositions are similar to SOISB type 3 peridotites, inconsistent with a mantle origin. In fact, these mineral compositions are more consistent with a crustal cumulate origin. Hence, the measured major and minor element compositions in olivines, pyroxenes and calcic amphibole cannot be used to clearly distinguish between crustal cumulate origin and metamorphic reequilibration or recrystallization. In some distance from the metasomatic

veins, the amphibole grains show no clear sign of any reaction, which suggests that the mineral assemblage had reached some equilibrium and was not affected by the late stage alteration event.

The type 2 peridotites (10-05B and 10-05C) were collected less than 2 meters apart from each other, but sample 10-05C show slightly higher CaO concentrations and significantly higher incompatible trace element abundances than sample 10-05B. Thus, the two type 2 peridotites record relatively constant major element concentrations for the 10-05 peridotite body, but clear variations in terms of CaO and trace element abundances. This can be explained by variable degrees of metasomatic overprint. Collectively, the petrological observations and the chemical compositions of the Akilia Island type 2 whole rocks and minerals are consistent with a crustal cumulate origin, followed by strong metamorphic and metasomatic overprint that even affected diagnostic trace elements such as the LREE.

Notably, the Akilia Island type 4 peridotites exhibit general higher REE concentrations than the type 2 peridotites from Akilia Island and all SOISB peridotites. The higher REE concentrations of the type 4 peridotites might be a secondary signature. The major element compositions of olivine and orthopyroxene in type 4 peridotite 10-04 indicate a crustal cumulate origin or, alternatively, resetting by metamorphic re-crystallization and re-equilibration. Thus, Mg-Fe exchange and reequilibration between olivine, orthopyroxene and spinel had most likely occurred and obliterated the primary mineral compositions. Moreover, interstitial carbonates, heterogeneously distributed fibrous amphibole and mica, the appearance of chlorite as well as the clusters or trails of iron oxides in the two type 4 peridotites indicate late metamorphic and metasomatic overprint.

Importantly, the Archaean rocks of this region record multiple events of deformation, magmatic intrusions, and high-grade metamorphism after the complex formation (ca. 3.85 - 3.66) (e.g., Nutman et al., 1996, 2000, 2002; Whitehouse et al., 1999, 2009; Myers and Crowley, 2000, Friend and Nutman, 2005; Whitehouse and Kamber, 2005; Manning et al., 2006).

Collectively, the data suggest that the Akilia Island peridotites investigated in this study are most likely crustal cumulates and not remnant of Eoarchean mantle. All four Akilia Island peridotites were affected by variable degrees of metamorphic and metasomatic overprint. Importantly, the four Akilia Island peridotites all show similarly strong W and Pb enrichments relative to REE concentrations, as were observed in the SOISB and NUB peridotites, and also reported for mafic and ultramafic rocks from the ISB and SOISB (e.g., Kamber et al., 2003; Hoffmann et al., 2011a; Rizo et al., 2013; Szilas et al., 2015; Dale et al., 2017). Hence,

positive W and Pb anomalies seem to be a common feature in Eoarchean ultramafic rocks all over the IGC.

7-3.2 Isotope systematics of the Akilia Island peridotites

The initial $\varepsilon Hf_{(3.81Ga)}$ values obtained for the two type 2 peridotites from sample-subset 10-05 are consistent within error (+2.2 and +2.6), but their initial $\varepsilon Nd_{(3.81\ Ga)}$ values strongly deviate from each other. This discrepancy can be explained by heterogeneous metamorphic disturbance of the Sm-Nd isotope system, without simultaneous disturbance of the Lu-Hf isotope system. This is also evident from the above observation that the LREE budget of the two samples appears to be disturbed.

All four Akilia Island peridotites define a Lu-Hf age regression line that yields an age of 3822 ±91 Ma (MSWD = 0.03) (Fig. 7-4). However, the four-point whole rock regression line might represent a mixing line without any geological significance. Nonetheless, the Akilia Island ^{176}Lu-^{176}Hf data are within the range of SOISB and NUB peridotites and also plot along Lu-Hf regression lines defined by SOISB and NUB peridotites that yield Eoarchean ages of about 3.8 Ga (Fig. 7-4).

This finding can be interpreted in favour of the preservation of the Lu-Hf isotope signatures since ~ 3.8 Ga. Yet, if the type 2 peridotites preserved a primary magmatic Lu-Hf signature remains ambiguous. The Lu-Hf isotope system may have been reset during granulite facies metamorphism in the early or late Eoarchean, shortly after their formation (e.g., McGregor and Mason, 1977; Baadsgaard et al., 1984; Nutman et al., 2002; Whitehouse and Kamber, 2005; Manning et al., 2006). In such a case, both events would not be resolvable in Lu-Hf space.

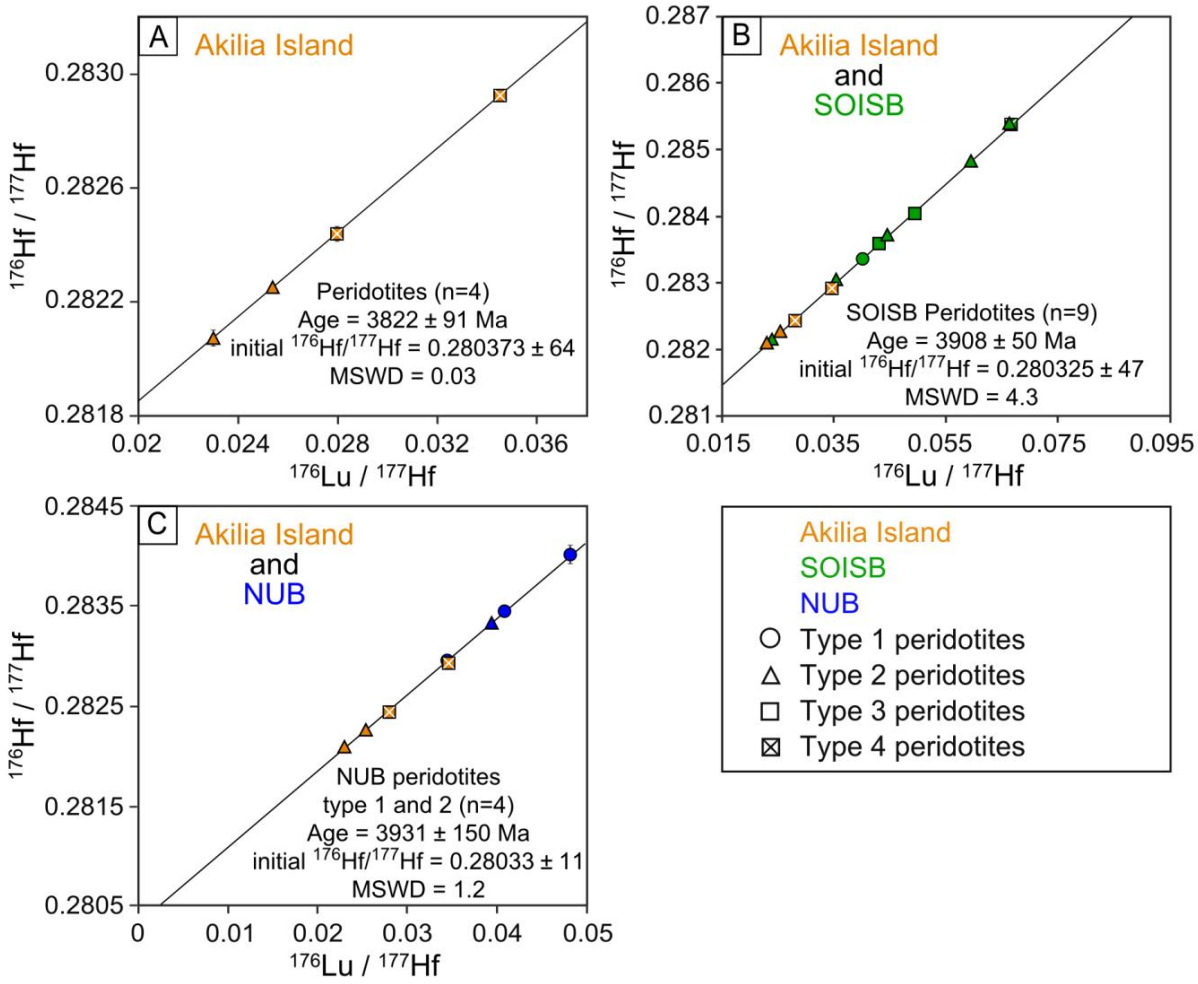

Figure 7-4: (A) Measured $^{176}Hf/^{177}Hf$ versus $^{176}Lu/^{177}Hf$ data obtained for the Akilia Island peridotites; (B-C) Measured $^{176}Hf/^{177}Hf$ versus $^{176}Lu/^{177}Hf$ data obtained for the Akilia Island peridotites in comparison to SOISB and NUB peridotites with age regression lines calculated using Isoplot (version 3.41d, Ludwig, 2006). The panels show regression lines for selected peridotites from the locations SOISB (B) and NUB (C). The Akilia Island ^{176}Lu-^{176}Hf data are within the range of SOISB and NUB peridotites and also plot along Lu- Hf regression lines defined by SOISB and NUB peridotites that yield Eoarchean ages of about 3.8 Ga.

For the Akilia Island peridotites no precise meaningful age constraint is possible, with the ^{147}Sm–^{143}Nd system, due to too large scatter in the ^{147}Sm–^{143}Nd space. Nonetheless, an isochron approach can provide estimates of when the element mobility events might have taken place. The ^{147}Sm-^{143}Nd age regression lines (Fig. 7-5 A) defined by samples 10-04 with 10-05B and 10-4 with 10-06 yield ages of 3689 ± 190 Ma and 1627± 170 Ma, respectively. The ^{147}Sm-^{143}Nd data of the Akilia Island peridotites are within the range of SOISB and NUB peridotites and scatter on regression lines defined by SOISB and NUB peridotites (Fig. 7-5 A-B), corresponding to ages of ca. 3.82 and 2.89 Ga. The ^{147}Sm-^{143}Nd data for Akilia Island peridotites scatter on an age regression line defined by amphibolites from Akilia Island and neighbouring Islands (Bennett et al., 1993) that yield an age of 3681 ± 36 Ma (MSWD = 0.81)

(Fig. 7-5). This age regression line likely indicates metamorphic resetting of the Sm-Nd isotope system (e.g., Moorbath et al., 1997). Those results suggest that the ^{147}Sm-^{143}Nd signature of the two Akilia Island type 2 peridotites and the type 4 0-04 peridotite were most likely disturbed between 3.80 and 1.6 Ga.

Structural and geochronological evidence from Akilia Island and the surrounding islands indicate upper amphibolite to granulite facies metamorphic events at ca. 3.65-3.66 Ga and ca. 3.55 - 3.59 Ga and multiple episodes of magmatic intrusions especially at ca. 3.64 – 3.64, ca. 3.51 – 3.26 Ga and 2.55 – 2.73 Ga. The late Archean terrane assembly of the IGC (ca. 2.82-2.73 Ga) triggered multiple tectonothermal events throughout the IGC. Additionally, superimposed metamorphic events (maximum upper amphibole facies) and intense ductile deformation occurred from 2.73 to 2.55 Ga (e.g., McGregor and Mason, 1977; Baadsgaard et al., 1984; Nutman et al., 2002b; Manning et al., 2006). The two type 4 peridotites (10-04 and 10-06) are from the type locality of the "Akilia association" (McGregor and Mason, 1977). The age constraints on mafic and ultramafic rocks of this location is controversial (e.g. McGregor and Mason, 1977; Myers and Crowley, 2000; Nutman et al., 1996b, 2000, 2002a; Whitehouse and Kamber, 2005). For example, the one amphibolite (90-525) from Akilia Island that is included in the data set of Bennett et al., (1993) (Fig. 7-5D) was sampled near the type 4 peridotite location and is hosted in a well-studied gneiss (98-462, Bennett et al., 1993; G88-66 Nutman et al., 1996, 1997; SM/GR/97/2 Whitehouse et al., 1999). The polyphase gneiss contains multiple generations of zircons with U-Pb zircon ages that ranging from 3.87 to 3.65 Ga (e.g., Bennett et al., 1993; Nutman et al., 1996, 2002; Whitehouse et al. 1999). There is a lack of agreement concerning the interpretation of the zircon ages and the field relationships to the adjacent rocks. Nonetheless, structural and geochronological evidence from Akilia Island and the surrounding islands indicate several amphibole to granulite facies metamorphic events between 3.65 and 2.70 Ga that triggered in situ partial melting, as well as growth of metamorphic zircon and recrystallization (e.g., Nutman et al. 2002). Thus, it is a plausible scenario that the Sm-Nd isotope signatures of the two type 2 peridotites and the type 4 peridotite 10-04 from Akilia Island were significantly disturbed during the late Eoarchean to Paleoarchean tectono-metamorphic events which is recorded by the calculated age of 3681 ± 36 Ma (Fig. 7-5D).

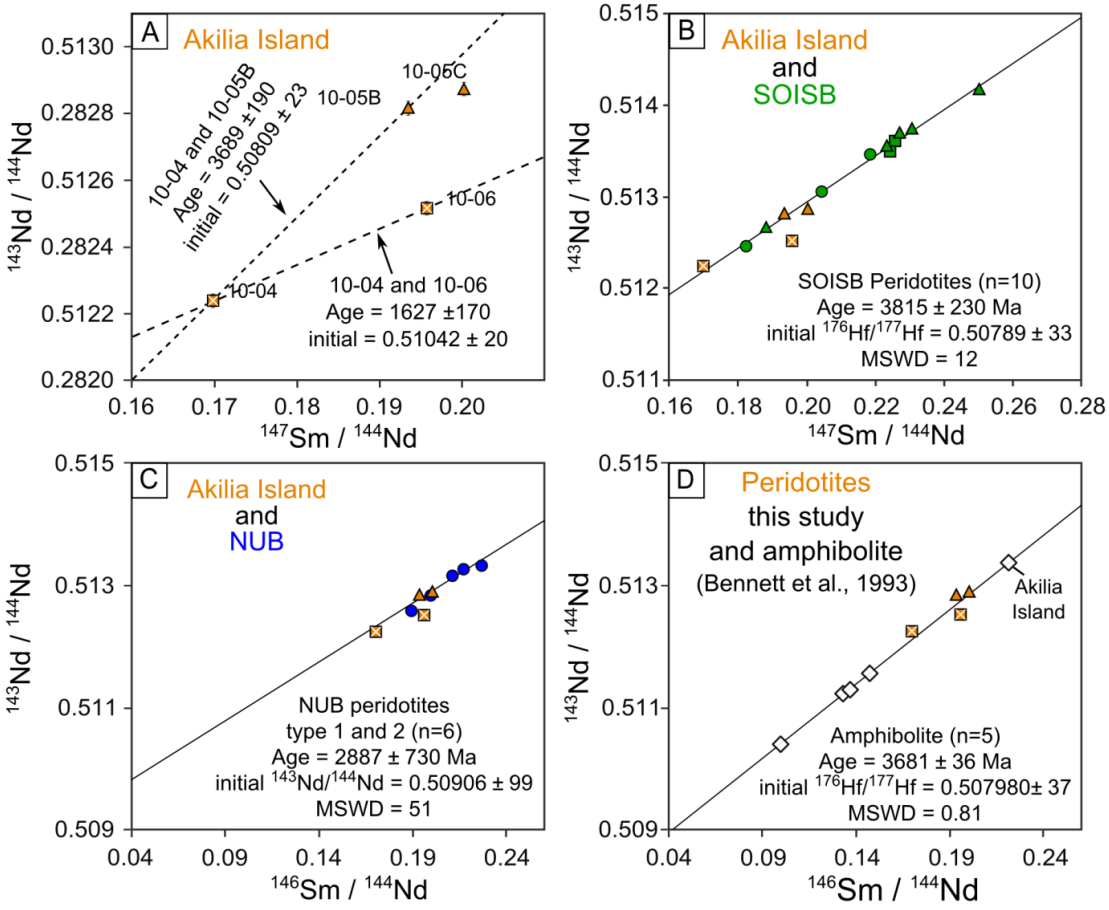

Figure 7-5: Measured $^{147}Sm/^{144}Nd$ versus $^{143}Nd/^{144}Nd$ data obtained for the four Akilia Island peridotites. The large scatter in the $^{147}Sm/^{144}Nd$ - $^{143}Nd/^{144}Nd$ space indicate extensive subsequent disturbance of the isotope systems. (B-D) Measured $^{143}Nd/^{144}Nd$ versus $^{147}Sm/^{144}Nd$ data obtained for the Akilia Island peridotites in comparison to (B) SOISB peridotites, (C) NUB peridotites, and (D) amphibolites from Akilia Island and neighbouring island (Bennett et al., 1993). The age regression lines were calculated using Isoplot (version 3.41d, Ludwig, 2006). Symbols for the peridotites of this study are equivalent to those in Fig. 7-4; open symbols indicate measured $^{143}Nd/^{144}Nd$ versus $^{147}Sm/^{144}Nd$ data for amphibolites from Akilia Island and neighbouring island (Bennett et al., 1993).

7-5 SUMMARY AND CONCLUSION

The Akilia Island type 2 peridotites microtexture and trace element abundances are within the range of those from the SOISB type 2 peridotites. Yet, olivines and orthopyroxenes show higher FeO concentrations, similar to olivines and orthopyroxenes of SOISB type 3 peridotites. In contrast, the two type 4 peridotites differ from the SOISB and NUB peridotites with respect to most major and trace element abundances. In particular their LREE budget appears to be overprinted by metasomatic processes. Their mineralogy and their chemical compositions can be explained by extensive metamorphic and metasomatic overprint. Hence, a clear characterisation of their protoliths remains ambiguous.

Importantly, in case of the four Akilia Island peridotites, there is no clear evidence for a possible mantle origin. Indeed, the chemical compositions of the type 2 peridotites are more consistent with a crustal cumulate origin.

Similar to the scenario postulated for the SOISB and NUB peridotites, the ^{147}Sm-^{143}Nd isotope signatures of the Akilia Island peridotites were significantly affected by LREE mobility during slightly younger tectono-metamorphic events. The disturbances of the ^{176}Lu-^{176}Hf signatures triggered by those events might have been minor. However, complete metamorphic resetting of the ^{176}Lu-^{176}Hf signatures during Eoarchean high granulite facies metamorphism cannot be completely ruled out for all four Akilia Island peridotites.

Consequently, care must be taken when interpreting the trace element and isotope signatures of the four Akilia Island peridotites, as extensively metasomatic and metamorphic alteration had effected these peridotites. In fact, the Akilia Island peridotites cannot contribute unambiguous information concerning Eoarchean mantle evolution or the mantle source of the Akilia Island peridotites.

8 References

Adam J, Green T (2006) Trace element partitioning between mica- and amphibole-bearing garnet lherzolite and hydrous basanitic melt: 1. Experimental results and the investigation of controls on partitioning behaviour. Contrib Mineral Petrol 152:1–17. doi: 10.1007/s00410-006-0085-4

Adam J, Green TH (1994) The effects of pressure and temperature on the partitioning of Ti, Sr and REE between amphibole, clinopyroxene and basanitic melts. Trace-Elem Partitioning Appl Magmat Process 117:219–233. doi: 10.1016/0009-2541(94)90129-5

Amelin Y, Kamo SL, Lee D-C (2010) Evolution of early crust in chondritic or non-chondritic Earth inferred from U–Pb and Lu–Hf data for chemically abraded zircon from the Itsaq Gneiss Complex, West GreenlandThis article is one of a series of papers published in this Special Issue on the theme of Geochronology in honour of Tom Krogh. Can J Earth Sci 48:141–160. doi: 10.1139/E10-091

Appel PW., Rollinson HR, Touret JL. (2001) Remnants of an Early Archaean (>3.75 Ga) sea-floor, hydrothermal system in the Isua Greenstone Belt. Precambrian Res 112:27–49. doi: 10.1016/S0301-9268(01)00169-3

Arai S (1994) Characterization of spinel peridotites by olivine-spinel compositional relationships: Review and interpretation. Chem Geol 113:191–204. doi: http://dx.doi.org/10.1016/0009-2541(94)90066-3

Aulbach S, Mungall JE, Pearson DG (2016) Distribution and Processing of Highly Siderophile Elements in Cratonic Mantle Lithosphere. Rev Mineral Geochem 81:239–304. doi: 10.2138/rmg.2016.81.5

Baadsgaard H (1973) U-Th-Pb dates on zircons from the early precambrian Amiˆtsoq Gneisses, Godthaab District, West Greenland. Earth Planet Sci Lett 19:22–28. doi: 10.1016/0012-821X(73)90174-X

Baadsgaard H, Nutman AP, Bridgwater D, et al (1984) The zircon geochronology of the Akilia association and Isua supracrustal belt, West Greenland. Earth Planet Sci Lett 68:221–228. doi: 10.1016/0012-821X(84)90154-7

Barnes S-J, Naldrett AJ, Gorton MP (1985) The origin of the fractionation of platinum-group elements in terrestrial magmas. Chem Geol 53:303–323. doi: 10.1016/0009-2541(85)90076-2

Becker H, Dale CW (2016) Re–Pt–Os Isotopic and Highly Siderophile Element Behavior in Oceanic and Continental Mantle Tectonites. Rev Mineral Geochem 81:369–440. doi: 10.2138/rmg.2016.81.7

Becker H, Horan MF, Walker RJ, et al (2006) Highly siderophile element composition of the Earth's primitive upper mantle: Constraints from new data on peridotite massifs and xenoliths. Geochim Cosmochim Acta 70:4528–4550. doi: http://dx.doi.org/10.1016/j.gca.2006.06.004

Bédard JH (2006) A catalytic delamination-driven model for coupled genesis of Archaean crust and sub-continental lithospheric mantle. Geochim Cosmochim Acta 70:1188–1214. doi: 10.1016/j.gca.2005.11.008

Bennett VC, Brandon AD, Nutman AP (2007) Coupled 142Nd-143Nd Isotopic Evidence for Hadean Mantle Dynamics. Science 318:1907–1910. doi: 10.1126/science.1145928

Bennett VC, Nutman AP, Esat TM (2002) Constraints on mantle evolution from 187Os/ 188Os isotopic compositions of Archean ultramafic rocks from southern West Greenland (3.8 Ga) and Western Australia (3.46 Ga). Geochim Cosmochim Acta 66:2615–2630

Bennett VC, Nutman AP, McCulloch MT (1993) Nd isotopic evidence for transient, highly depleted mantle reservoirs in the early history of the Earth. Earth Planet Sci Lett 119:299–317. doi: 10.1016/0012-821X(93)90140-5

Bernstein S, Hanghøj K, Kelemen P, Brooks CK (2006) Ultra-depleted, shallow cratonic mantle beneath West Greenland: dunitic xenoliths from Ubekendt Ejland. Contrib Mineral Petrol 152:335–347. doi: 10.1007/s00410-006-0109-0

Bernstein S, Szilas K, Kelemen PB (2013) Highly depleted cratonic mantle in West Greenland extending into diamond stability field in the Proterozoic. Lithos 168–169:160–172. doi: http://dx.doi.org/10.1016/j.lithos.2013.02.011

Bleeker W (2003) The late Archean record: a puzzle in ca. 35 pieces. Tale Two Cratons Slave-Kaapvaal Workshop 71:99–134. doi: 10.1016/j.lithos.2003.07.003

Blichert-Toft J (1999) Lu-Hf Isotope Systematics of Garnet Pyroxenites from Beni Bousera, Morocco: Implications for Basalt Origin. Science 283:1303–1306. doi: 10.1126/science.283.5406.1303

Blichert-Toft J, Boyet M, Télouk P, Albarède F (2002) 147Sm–143Nd and 176Lu–176Hf in eucrites and the differentiation of the HED parent body. Earth Planet Sci Lett 204:167–181. doi: 10.1016/S0012-821X(02)00976-7

Bodinier J-L, Godard M (2014) 3.4 - Orogenic, Ophiolitic, and Abyssal Peridotites A2 - Holland, Heinrich D. In: Turekian KK (ed) Treatise on Geochemistry (Second Edition). Elsevier, Oxford, pp 103–167

Bouvier A, Vervoort JD, Patchett PJ (2008) The Lu–Hf and Sm–Nd isotopic composition of CHUR: Constraints from unequilibrated chondrites and implications for the bulk composition of terrestrial planets. Earth Planet Sci Lett 273:48–57. doi: 10.1016/j.epsl.2008.06.010

Bowring S, Chacko T, Heaman LM, Reimink J (2015) Acasta Gneiss Complex. In: Jack Rink W, Thompson JW (eds) Encyclopedia of Scientific Dating Methods. Springer Netherlands, Dordrecht, pp 1–2

Bowring S, Housh T (1995) The Earth's early evolution. Science 269:1535. doi: 10.1126/science.7667634

Bowring SA, Williams IS (1999) Priscoan (4.00–4.03 Ga) orthogneisses from northwestern Canada. Contrib Mineral Petrol 134:3–16

Boyet M, Blichert-Toft J, Rosing M, et al (2003) 142Nd evidence for early Earth differentiation. Earth Planet Sci Lett 214:427–442. doi: 10.1016/S0012-821X(03)00423-0

Brown M (2014) The contribution of metamorphic petrology to understanding lithosphere evolution and geodynamics. Spec ISSUE Tecton Cent Asia – Tribute Alfred Kröner Guowei Zhang 5:553–569. doi: 10.1016/j.gsf.2014.02.005

Büchl A, Brügmann G, Batanova VG, et al (2002) Melt percolation monitored by Os isotopes and HSE abundances: a case study from the mantle section of the Troodos Ophiolite. Earth Planet Sci Lett 204:385–402. doi: 10.1016/S0012-821X(02)00977-9

Caro G, Bourdon B, Birck J-L, Moorbath S (2003) 146Sm-142Nd evidence from Isua metamorphosed sediments for early differentiation of the Earth's mantle. Nature 423:428–432. doi: 10.1038/nature01668

Caro G, Morino P, Mojzsis SJ, et al (2017) Sluggish Hadean geodynamics: Evidence from coupled 146,147Sm–142,143Nd systematics in Eoarchean supracrustal rocks of the Inukjuak domain (Québec). Earth Planet Sci Lett 457:23–37. doi: 10.1016/j.epsl.2016.09.051

Chauvel C, Lewin E, Carpentier M, et al (2007) Role of recycled oceanic basalt and sediment in generating the Hf–Nd mantle array. Nat Geosci 1:64

Chou C-L (1978) Fractionation of siderophile elements in the Earth's upper mantle: In: Proceedings of the 9th Lunar and Planetary Science Conference. pp 219–230

Coggon JA, Luguet A, Nowell GM, Appel PWU (2013) Hadean mantle melting recorded by southwest Greenland chromitite 186Os signatures. Nat Geosci 6:871–874

Cohen AS, Waters FG (1996) Separation of osmium from geological materials by solvent extraction for analysis by thermal ionisation mass spectrometry. Anal Chim Acta 332:269–275. doi: http://dx.doi.org/10.1016/0003-2670(96)00226-7

Collerson KD, Campbell LM, Weaver BL, Palacz ZA (1991) Evidence for extreme mantle fractionation in early Archaean ultramafic rocks from northern Labrador. Nature 349:209–214. doi: 10.1038/349209a0

Coltorti M, Bonadiman C, Faccini B, et al (2007) Amphiboles from suprasubduction and intraplate lithospheric mantle. Melt-Rock React Process Mantle Their Bear Mantle Petrol Chem 99:68–84. doi: 10.1016/j.lithos.2007.05.009

Compston W, Pidgeon RT (1986) Jack Hills, evidence of more very old detrital zircons in Western Australia. Nature 321:766

Condie KC (2005) TTGs and adakites: are they both slab melts? Granitic Syst 80:33–44. doi: 10.1016/j.lithos.2003.11.001

Condie KC, Pease V (2008) When did plate tectonics begin on planet Earth? Geological Society of America

Corgne A, Schilling ME, Grégoire M, Langlade J (2018) Experimental constraints on metasomatism of mantle wedge peridotites by hybridized adakitic melts. Lithos 308–309:213–226. doi: 10.1016/j.lithos.2018.03.006

Creech JB, Baker JA, Handler MR, et al (2017) Late accretion history of the terrestrial planets inferred from platinum stable isotopes. Geochem Perspect Lett 3:94–104. doi: 10.7185/geochemlet.1710

Dale CW, Kruijer TS, Burton KW (2017) Highly siderophile element and 182W evidence for a partial late veneer in the source of 3.8 Ga rocks from Isua, Greenland. Earth Planet Sci Lett 458:394–404. doi: 10.1016/j.epsl.2016.11.001

Dale CW, Luguet A, Macpherson CG, et al (2008) Extreme platinum-group element fractionation and variable Os isotope compositions in Philippine Sea Plate basalts: Tracing mantle source heterogeneity. Highly Siderophile Elem Geochem 248:213–238. doi: 10.1016/j.chemgeo.2007.11.007

David J, Godin L, Stevenson R, et al (2009) U-Pb ages (3.8–2.7 Ga) and Nd isotope data from the newly identified Eoarchean Nuvvuagittuq supracrustal belt, Superior Craton, Canada3.8 Ga Nuvvuagittuq supracrustal sequence. GSA Bull 121:150–163. doi: 10.1130/B26369.1

Defant MJ, Drummond MS (1990) Derivation of some modern arc magmas by melting of young subducted lithosphere. Nature 347:662

Dhuime B, Hawkesworth C, Cawood P (2011) When Continents Formed. Science 331:154. doi: 10.1126/science.1201245

Dymek RF, Brothers SC, Schiffries CM (1988) Petrogenesis of Ultramafic Metamorphic Rocks from the 3800 Ma Isua Supracrustal Belt, West Greenland. J Petrol 29:1353–1397. doi: 10.1093/petrology/29.6.1353

Dziggel A, Diener JFA, Kolb J, Kokfelt TF (2014) Metamorphic record of accretionary processes during the Neoarchaean: The Nuuk region, southern West Greenland. Precambrian Res 242:22–38. doi: 10.1016/j.precamres.2013.12.010

Dziggel A, Kokfelt TF, Kolb J, et al (2017) Tectonic switches and the exhumation of deep-crustal granulites during Neoarchean terrane accretion in the area around Grædefjord, SW Greenland. Precambrian Res 300:223–245. doi: 10.1016/j.precamres.2017.07.027

Eggins S., Rudnick R., McDonough W. (1998) The composition of peridotites and their minerals: a laser-ablation ICP–MS study. Earth Planet Sci Lett 154:53–71. doi: 10.1016/S0012-821X(97)00195-7

Fedo CM, Whitehouse MJ, Kamber BS (2006) Geological constraints on detecting the earliest life on Earth: a perspective from the Early Archaean (older than 3.7 Gyr) of southwest Greenland. Philos Trans R Soc B Biol Sci 361:851. doi: 10.1098/rstb.2006.1836

Fischer-Gödde M, Becker H, Wombacher F (2010) Rhodium, gold and other highly siderophile element abundances in chondritic meteorites. Geochim Cosmochim Acta 74:356–379. doi: 10.1016/j.gca.2009.09.024

Fischer-Gödde M, Becker H, Wombacher F (2011) Rhodium, gold and other highly siderophile elements in orogenic peridotites and peridotite xenoliths. Chem Geol 280:365–383. doi: 10.1016/j.chemgeo.2010.11.024

Foley S, Tiepolo M, Vannucci R (2002) Growth of early continental crust controlled by melting of amphibolite in subduction zones. Nature 417:837–840. doi: 10.1038/nature00799

Frei R, Polat A, Meibom A (2004) The Hadean upper mantle conundrum: evidence for source depletion and enrichment from Sm-Nd, Re-Os, and Pb isotopic compositions in 3.71 Gy boninite-like metabasalts from the Isua Supracrustal Belt, Greenland1. Geochim Cosmochim Acta 68:1645–1660. doi: 10.1016/j.gca.2003.10.009

Frei R, Rosing MT (2001) The least radiogenic terrestrial leads; implications for the early Archean crustal evolution and hydrothermal–metasomatic processes in the Isua Supracrustal Belt (West Greenland). Chem Geol 181:47–66. doi: 10.1016/S0009-2541(01)00263-7

Frei R, Rosing MT, Waight TE, Ulfbeck DG (2002) Hydrothermal-metasomatic and tectono-metamorphic processes in the Isua supracrustal belt (West Greenland): a multi-isotopic investigation of their effects on the earth's oldest oceanic crustal sequence. Geochim Cosmochim Acta 66:467–486. doi: 10.1016/S0016-7037(01)00781-5

Friend C, Bennett V, Nutman A (2002) Abyssal peridotites >3,800 Ma from southern West Greenland: field relationships, petrography, geochronology, whole-rock and mineral chemistry of dunite and harzburgite inclusions in the Itsaq Gneiss Complex. Contrib Mineral Petrol 143:71–92. doi: 10.1007/s00410-001-0332-7

Friend CR., Nutman A (2011) Dunites from Isua, Greenland: A ca. 3720 Ma window into subcrustal metasomatism of depleted mantle. Geology 39:663–666. doi: 10.1130/G31904.1

Friend CRL, Nutman AP (2005) New pieces to the Archaean terrane jigsaw puzzle in the Nuuk region, southern West Greenland: steps in transforming a simple insight into a complex regional tectonothermal model. J Geol Soc 162:147–162. doi: 10.1144/0016-764903-161

Friend CRL, Nutman AP (2010) Eoarchean ophiolites? New evidence for the debate on the Isua supracrustal belt, southern West Greenland. Am J Sci 310:826–861. doi: 10.2475/09.2010.04

Frost DJ (2006) The Stability of Hydrous Mantle Phases. Rev Mineral Geochem 62:243. doi: 10.2138/rmg.2006.62.11

Froude DO, Ireland TR, Kinny PD, et al (1983) Ion microprobe identification of 4,100–4,200 Myr-old terrestrial zircons. Nature 304:616

Furnes H, Rosing M, Dilek Y, de Wit M (2009a) Isua supracrustal belt (Greenland)—A vestige of a 3.8 Ga suprasubduction zone ophiolite, and the implications for Archean geology. Mantle Dyn Crust-Mantle Interact Collisional Orogens 113:115–132. doi: 10.1016/j.lithos.2009.03.043

Furnes H, Rosing M, Dilek Y, de Wit M (2009b) Isua supracrustal belt (Greenland)—A vestige of a 3.8 Ga suprasubduction zone ophiolite, and the implications for Archean geology. Mantle Dyn Crust-Mantle Interact Collisional Orogens 113:115–132. doi: 10.1016/j.lithos.2009.03.043

Gabe-Schönberg C-D (1993) SIMULTANEOUS DETERMINATION OF THIRTY-SEVEN TRACE ELEMENTS IN TWENTY-EIGHT INTERNATIONAL ROCK STANDARDS BY ICP-MS. Geostand Geoanalytical Res 17:81–97

Gargiulo MF, Bjerg EA, Mogessie A (2013) Spinel group minerals in metamorphosed ultramafic rocks from Río de Las Tunas belt, Central Andes, Argentina. Geol Acta 11:133–148

Ghiorso MS, Sack RO (1991) Thermochemistry of the oxide minerals. Rev Mineral Geochem 25:221–264

Green T., Blundy J., Adam J, Yaxley G. (2000) SIMS determination of trace element partition coefficients between garnet, clinopyroxene and hydrous basaltic liquids at 2–7.5 GPa and 1080–1200°C. Lithos 53:165–187. doi: 10.1016/S0024-4937(00)00023-2

Green TH (1995) Significance of Nb/Ta as an indicator of geochemical processes in the crust-mantle system. Chem Evol Mantle 120:347–359. doi: 10.1016/0009-2541(94)00145-X

Griffin WL, McGregor VR, Nutman A, et al (1980) Early Archaean granulite-facies metamorphism south of Ameralik, West Greenland. Earth Planet Sci Lett 50:59–74. doi: 10.1016/0012-821X(80)90119-3

Griffin WL, O'Reilly SY, Afonso JC, Begg GC (2009) The Composition and Evolution of Lithospheric Mantle: a Re-evaluation and its Tectonic Implications. J Petrol 50:1185–1204. doi: 10.1093/petrology/egn033

Haggerty SE (1991) Oxide mineralogy of the upper mantle. Rev Mineral Geochem 25:355–416

Hanmer S, Greene DC (2002) A modern structural regime in the Paleoarchean (~3.64 Ga); Isua Greenstone Belt, southern West Greenland. Tectonophysics 346:201–222. doi: 10.1016/S0040-1951(02)00029-X

Hanmer S, Hamilton MA, Crowley JL (2002) Geochronological constraints on Paleoarchean thrust-nappe and Neoarchean accretionary tectonics in southern West Greenland. Tectonophysics 350:255–271. doi: 10.1016/S0040-1951(02)00120-8

Harrison TM, Watson EB, Aikman AB (2007) Temperature spectra of zircon crystallization in plutonic rocks. Geology 35:635–638. doi: 10.1130/G23505A.1

Hawthorne FC, Oberti R, Harlow GE, et al (2012) Nomenclature of the amphibole supergroup. Am Mineral 97:2031–2048. doi: 10.2138/am.2012.4276

Herzberg C, Condie K, Korenaga J (2010) Thermal history of the Earth and its petrological expression. Earth Planet Sci Lett 292:79–88. doi: 10.1016/j.epsl.2010.01.022

Hidalgo PJ, Rooney TO (2014) Petrogenesis of a voluminous Quaternary adakitic volcano: the case of Baru volcano. Contrib Mineral Petrol 168:1011. doi: 10.1007/s00410-014-1011-9

Hiess J, Bennett VC, Nutman AP, Williams IS (2009) In situ U–Pb, O and Hf isotopic compositions of zircon and olivine from Eoarchaean rocks, West Greenland: New insights to making old crust. Geochim Cosmochim Acta 73:4489–4516. doi: http://dx.doi.org/10.1016/j.gca.2009.04.019

Hoffmann JE, Münker C, Næraa T, et al (2011a) Mechanisms of Archean crust formation inferred from high-precision {HFSE} systematics in {TTGs}. Geochim Cosmochim Acta 75:4157–4178. doi: http://dx.doi.org/10.1016/j.gca.2011.04.027

Hoffmann JE, Münker C, Polat A, et al (2011b) The origin of decoupled Hf–Nd isotope compositions in Eoarchean rocks from southern West Greenland. Geochim Cosmochim Acta 75:6610–6628. doi: 10.1016/j.gca.2011.08.018

Hoffmann JE, Münker C, Polat A, et al (2010) Highly depleted Hadean mantle reservoirs in the sources of early Archean arc-like rocks, Isua supracrustal belt, southern West Greenland. Geochim Cosmochim Acta 74:7236–7260. doi: 10.1016/j.gca.2010.09.027

Hoffmann JE, Nagel TJ, Münker C, et al (2014) Constraining the process of Eoarchean {TTG} formation in the Itsaq Gneiss Complex, southern West Greenland. Earth Planet Sci Lett 388:374–386. doi: http://dx.doi.org/10.1016/j.epsl.2013.11.050

Hoffmann JE, Svahnberg H, Piazolo S, et al (2012) The geodynamic evolution of Mesoarchean anorthosite complexes inferred from the Naajat Kuuat Complex, southern West Greenland. Precambrian Res 196–197:149–170. doi: 10.1016/j.precamres.2011.12.002

Hoffmann JE, Wilson AH (2017) The origin of highly radiogenic Hf isotope compositions in 3.33Ga Commondale komatiite lavas (South Africa). Role Intraplate Magmas Their Incl Earth's Mantle Evol 455:6–21. doi: 10.1016/j.chemgeo.2016.10.010

Hoog JCMD, Gall L, Cornell DH (2010) Trace-element geochemistry of mantle olivine and application to mantle petrogenesis and geothermobarometry. Chem Geol 270:196–215. doi: http://dx.doi.org/10.1016/j.chemgeo.2009.11.017

Horie K, Nutman AP, Friend CRL, Hidaka H (2010) The complex age of orthogneiss protoliths exemplified by the Eoarchaean Itsaq Gneiss Complex (Greenland): SHRIMP and old rocks. Impact SHRIMP Underst Precambrian 183:25–43. doi: 10.1016/j.precamres.2010.06.016

Iizuka T, Komiya T, Ueno Y, et al (2007) Geology and zircon geochronology of the Acasta Gneiss Complex, northwestern Canada: New constraints on its tectonothermal history. Precambrian Res 153:179–208. doi: 10.1016/j.precamres.2006.11.017

Ionov DA, Bodinier J-L, Mukasa SB, Zanetti A (2002) Mechanisms and Sources of Mantle Metasomatism: Major and Trace Element Compositions of Peridotite Xenoliths from Spitsbergen in the Context of Numerical Modelling. J Petrol 43:2219–2259. doi: 10.1093/petrology/43.12.2219

Ishikawa A, Suzuki K, Collerson KD, et al (2017) Rhenium-osmium isotopes and highly siderophile elements in ultramafic rocks from the Eoarchean Saglek Block, northern Labrador, Canada: implications for Archean mantle evolution. Geochim Cosmochim Acta. doi: 10.1016/j.gca.2017.07.023

Jackson CRM, Ziegler LB, Zhang H, et al (2014) A geochemical evaluation of potential magma ocean dynamics using a parameterized model for perovskite crystallization. Earth Planet Sci Lett 392:154–165. doi: 10.1016/j.epsl.2014.01.028

Jacobsen SB (1988) Isotopic and chemical constraints on mantle-crust evolution. Geochim Cosmochim Acta 52:1341–1350. doi: http://dx.doi.org/10.1016/0016-7037(88)90205-0

Jenner FE, Bennett VC, Nutman AP, et al (2009) Evidence for subduction at 3.8 Ga: Geochemistry of arc-like metabasalts from the southern edge of the Isua Supracrustal Belt. Appl Interpret Micro-Anal Data Geochronological Syst 261:83–98. doi: 10.1016/j.chemgeo.2008.09.016

John T, Klemd R, Klemme S, et al (2011) Nb–Ta fractionation by partial melting at the titanite–rutile transition. Contrib Mineral Petrol 161:35–45. doi: 10.1007/s00410-010-0520-4

Johnson TE, Brown M, Kaus BJP, VanTongeren JA (2014) Delamination and recycling of Archaean crust caused by gravitational instabilities. Nat Geosci 7:47–52

Kaczmarek M-A, Reddy SM, Nutman AP, et al (2016) Earth's oldest mantle fabrics indicate Eoarchaean subduction. Nat Commun 7:

Kamber B, Ewart A, Collerson K, et al (2002) Fluid-mobile trace element constraints on the role of slab melting and implications for Archaean crustal growth models. Contrib Mineral Petrol 144:38–56. doi: 10.1007/s00410-002-0374-5

Kamber BS (2015) The evolving nature of terrestrial crust from the Hadean, through the Archaean, into the Proterozoic. Precambrian Res 258:48–82. doi: 10.1016/j.precamres.2014.12.007

Kamber BS, Greig A, Schoenberg R, Collerson KD (2003) A refined solution to Earth's hidden niobium: implications for evolution of continental crust and mode of core formation. Precambrian Res 126:289–308. doi: http://dx.doi.org/10.1016/S0301-9268(03)00100-1

Kelemen PB, Hart SR, Bernstein S (1998) Silica enrichment in the continental upper mantle via melt/rock reaction. Earth Planet Sci Lett 164:387–406. doi: 10.1016/S0012-821X(98)00233-7

Kemp AIS, Wilde SA, Hawkesworth CJ, et al (2010) Hadean crustal evolution revisited: New constraints from Pb–Hf isotope systematics of the Jack Hills zircons. Earth Planet Sci Lett 296:45–56. doi: 10.1016/j.epsl.2010.04.043

Kleine T, Mezger K, Münker C, et al (2004) 182Hf-182W isotope systematics of chondrites, eucrites, and martian meteorites: Chronology of core formation and early mantle differentiation in Vesta and Mars1 1Associate editor: R. J. Walker. Geochim Cosmochim Acta 68:2935–2946. doi: 10.1016/j.gca.2004.01.009

Klemme S, Blundy J, Wood B (2002) Experimental constraints on major and trace element partitioning during partial melting of eclogite

Klemme S, Prowatke S, Hametner K, Günther D (2005) Partitioning of trace elements between rutile and silicate melts: Implications for subduction zones. Geochim Cosmochim Acta 69:2361–2371. doi: 10.1016/j.gca.2004.11.015

Komiya T, Yamamoto S, Aoki S, et al (2017) A prolonged granitoid formation in Saglek Block, Labrador: Zonal growth and crustal reworking of continental crust in the Eoarchean. Front Early Earth Hist Primordial Life- Part I 8:355–385. doi: 10.1016/j.gsf.2016.06.013

Komiya T, Yamamoto S, Aoki S, et al (2015) Geology of the Eoarchean, > 3.95 Ga, Nulliak supracrustal rocks in the Saglek Block, northern Labrador, Canada: The oldest geological evidence for plate tectonics. Tectonophysics 662:40–66. doi: 10.1016/j.tecto.2015.05.003

König S, Münker C, Hohl S, et al (2011) The Earth's tungsten budget during mantle melting and crust formation. Geochim Cosmochim Acta 75:2119–2136. doi: http://dx.doi.org/10.1016/j.gca.2011.01.031

Lagos M, Scherer E, TOMASCHEK F, et al (2007) High precision Lu–Hf geochronology of Eocene eclogite-facies rocks from Syros, Cyclades, Greece. Chem Geol 243:16–35. doi: 10.1016/j.chemgeo.2007.04.008

Laurent O, Martin H, Moyen JF, Doucelance R (2014) The diversity and evolution of late-Archean granitoids: Evidence for the onset of "modern-style" plate tectonics between 3.0 and 2.5Ga. Lithos 205:208–235. doi: 10.1016/j.lithos.2014.06.012

Leake BE, Woolley AR, Birch WD, et al (2003) NOMENCLATURE OF AMPHIBOLES: ADDITIONS AND REVISIONS TO THE INTERNATIONAL MINERALOGICAL ASSOCIATION'S 1997 RECOMMENDATIONS. Can Mineral 41:1355. doi: 10.2113/gscanmin.41.6.1355

Lee C-TA, Harbert A, Leeman WP (2007) Extension of lattice strain theory to mineral/mineral rare-earth element partitioning: An approach for assessing disequilibrium and developing internally consistent partition coefficients between olivine, orthopyroxene, clinopyroxene and basaltic melt. Geochim Cosmochim Acta 71:481–496. doi: 10.1016/j.gca.2006.09.014

Li L, Xiong XL, Liu XC (2017) Nb/Ta Fractionation by Amphibole in Hydrous Basaltic Systems: Implications for Arc Magma Evolution and Continental Crust Formation. J Petrol 58:3–28. doi: 10.1093/petrology/egw070

Liu J, Touboul M, Ishikawa A, et al (2016) Widespread tungsten isotope anomalies and W mobility in crustal and mantle rocks of the Eoarchean Saglek Block, northern Labrador, Canada:

Implications for early Earth processes and W recycling. Earth Planet Sci Lett 448:13–23. doi: 10.1016/j.epsl.2016.05.001

Locmelis M, Pearson NJ, Barnes SJ, Fiorentini ML (2011) Ruthenium in komatiitic chromite. Geochim Cosmochim Acta 75:3645–3661. doi: 10.1016/j.gca.2011.03.041

Locock AJ (2014) An Excel spreadsheet to classify chemical analyses of amphiboles following the IMA 2012 recommendations. Comput Geosci 62:1–11. doi: 10.1016/j.cageo.2013.09.011

Lorand J-P, Luguet A, Alard O (2013) Platinum-group element systematics and petrogenetic processing of the continental upper mantle: A review. Lithos 164–167:2–21. doi: http://dx.doi.org/10.1016/j.lithos.2012.08.017

Lowry D, Appel PWU, Rollinson HR (2003) Oxygen isotopes of an Early Archaean layered ultramafic body, southern West Greenland: implications for magma source and post-intrusion history. Precambrian Res 126:273–288. doi: 10.1016/S0301-9268(03)00099-8

Ludwig K. R. (2001) Users manual for Isoplot/Ex version 2.49. Berkeley Geochronology 1022 Center, Special Publication No. 1a. 2455 Ridge Road, Berkeley, CA. p. 48.

Lugmair G. W. and Marti K. (1978) Lunar initial 143Nd/144Nd: differential evolution of the lunar crust and mantle. Earth Planet. Sci. Lett. 39, 349–357.

Maier WD, Barnes SJ, Campbell IH, et al (2009) Progressive mixing of meteoritic veneer into the early Earth/'s deep mantle. Nature 460:620–623. doi: 10.1038/nature08205

Manning CE, Mojzsis SJ, Harrison TM (2006) Geology, Age and Origin of Supracrustal Rocks at Akilia, West Greenland. Am J Sci 306:303–366. doi: 10.2475/05.2006.02

Martin H (1986) Effect of steeper Archean geothermal gradient on geochemistry of subduction-zone magmas. Geology 14:753–756. doi: 10.1130/0091-7613(1986)14<753:EOSAGG>2.0.CO;2

Martin H, Smithies RH, Rapp R, et al (2005) An overview of adakite, tonalite–trondhjemite–granodiorite (TTG), and sanukitoid: relationships and some implications for crustal evolution. Lithos 79:1–24. doi: 10.1016/j.lithos.2004.04.048

McDade P, Blundy JD, Wood BJ (2003a) Trace element partitioning between mantle wedge peridotite and hydrous MgO-rich melt. Am Mineral 88:1825–1831. doi: 10.2138/am-2003-11-1225

McDade P, Blundy JD, Wood BJ (2003b) Trace element partitioning on the Tinaquillo Lherzolite solidus at 1.5GPa. Phys Earth Planet Inter 139:129–147. doi: 10.1016/S0031-9201(03)00149-3

McDonough WF, Sun S -s. (1995) The composition of the Earth. Chem Geol 120:223–253. doi: 10.1016/0009-2541(94)00140-4

McGregor VR, Mason B (1977) Petrogenesis and geochemistry of metabasaltic and metasedimentary enclaves in the Amitsoq gneisses, West Greenland. 62:887–904

Meisel T, Horan MF (2016) Analytical Methods for the Highly Siderophile Elements. Rev Mineral Geochem 81:89–106. doi: 10.2138/rmg.2016.81.02

Menneken M, Nemchin AA, Geisler T, et al (2007) Hadean diamonds in zircon from Jack Hills, Western Australia. Nature 448:917

Moorbath S, AllaarT JH, Bridgwater D, McGregor VR (1977) Rb–Sr ages of early Archaean supracrustal rocks and Amîtsoq gneisses at Isua. Nature 270:43

Moorbath S, O'Nions RK, Pankhurst RJ (1975) The evolution of early precambrian crustal rocks at Isua, West Greenland — Geochemical and isotopic evidence. Earth Planet Sci Lett 27:229–239. doi: 10.1016/0012-821X(75)90034-5

Moorbath S, Whitehouse MJ, Kamber B (1997) Extreme Nd-isotope heterogeneity in the early Archaean - fact or fiction?. Chem. Geol. 135, 213-231

Moyen J-F, van Hunen J (2012) Short-term episodicity of Archaean plate tectonics. Geology 40:451–454. doi: 10.1130/G322894.1

Mungall JE, Brenan JM (2014) Partitioning of platinum-group elements and Au between sulfide liquid and basalt and the origins of mantle-crust fractionation of the chalcophile elements. Geochim Cosmochim Acta 125:265–289. doi: http://dx.doi.org/10.1016/j.gca.2013.10.002

Münker C, Weyer S, Scherer E, Mezger K (2001) Separation of high field strength elements (Nb, Ta, Zr, Hf) and Lu from rock samples for MC-ICPMS measurements. Geochem Geophys Geosystems 1:. doi: 10.1029/2001GC000183

Münker C, Wörner G, Yogodzinski G, Churikova T (2004) Behaviour of high field strength elements in subduction zones: constraints from Kamchatka–Aleutian arc lavas. Earth Planet Sci Lett 224:275–293. doi: 10.1016/j.epsl.2004.05.030

Myers JS, Crowley JL (2000) Vestiges of life in the oldest Greenland rocks? A review of early Archean geology in the Godthåbsfjord region, and reappraisal of field evidence for >3850 Ma life on Akilia. Precambrian Res 103:101–124. doi: 10.1016/S0301-9268(00)00089-9

Naeraa T, Schersten A, Rosing MT, et al (2012) Hafnium isotope evidence for a transition in the dynamics of continental growth 3.2 Gyr ago. Nature 485:627–630. doi: 10.1038/nature11140

Nagel TJ, Hoffmann JE, Münker C (2012) Generation of Eoarchean tonalite-trondhjemite-granodiorite series from thickened mafic arc crust. Geology 40:375–378. doi: 10.1130/G32729.1

Nebel O, Mezger K, Scherer EE, Münker C (2005) High precision determinations of $^{87}Rb/^{85}Rb$ in geologic materials by MC-ICP-MS. Int J Mass Spectrom 246:10–18. doi: 10.1016/j.ijms.2005.08.003

Nebel-Jacobsen Y, Münker C, Nebel O, et al (2010) Reworking of Earth's first crust: Constraints from Hf isotopes in Archean zircons from Mt. Narryer, Australia. Precambrian Res 182:175–186. doi: 10.1016/j.precamres.2010.07.002

Nisbet EG (1987) The young Earth: An introduction to Archaean geology. Allen & Unwin, Boston

Niu Y (2004) Bulk-rock Major and Trace Element Compositions of Abyssal Peridotites: Implications for Mantle Melting, Melt Extraction and Post-melting Processes Beneath Mid-Ocean Ridges. J Petrol 45:2423–2458. doi: 10.1093/petrology/egh068

Nutman A, Bennett V, Friend CL, et al (2007a) ~3,850 Ma tonalites in the Nuuk region, Greenland: geochemistry and their reworking within an Eoarchaean gneiss complex. Contrib Mineral Petrol 154:385–408. doi: 10.1007/s00410-007-0199-3

Nutman AP, Allaart JH, Bridgwater D, et al (1984) Stratigraphic and geochemical evidence for the depositional environment of the early archaean isua supracrustal belt, southern west greenland. Precambrian Res 25:365–396. doi: 10.1016/0301-9268(84)90010-X

Nutman AP, Bennett VC, Friend CRL, et al (2013) The Itsaq Gneiss Complex of Greenland: Episodic 3900 to 3660 Ma juvenile crust formation and recycling in the 3660 to 3600 Ma Isukasian orogeny. Am J Sci 313:877–911. doi: 10.2475/09.2013.03

Nutman AP, Bennett VC, Friend CRL, et al (2009a) Eoarchaean crustal growth in West Greenland (Itsaq Gneiss Complex) and in northeastern China (Anshan area): review and synthesis. Geol Soc Lond Spec Publ 318:127–154. doi: 10.1144/SP318.5

Nutman AP, Bennett VC, Friend CRL, Mcgregor VR (2000) The early Archaean Itsaq Gneiss Complex of southern West Greenland: the importance of field observations in interpreting age and isotopic constraints for early terrestrial evolution. Geochim Cosmochim Acta 64:3035–3060. doi: http://dx.doi.org/10.1016/S0016-7037(99)00431-7

Nutman AP, Bennett VC, Friend CRL, Rosing MT (1997) ~ 3710 and ⩾ 3790 Ma volcanic sequences in the Isua (Greenland) supracrustal belt; structural and Nd isotope implications. Chem Geol 141:271–287. doi: http://dx.doi.org/10.1016/S0009-2541(97)00084-3

Nutman AP, Friend CR., Bennett VC (2002a) Evidence for 3650–3600 Ma assembly of the northern end of the Itsaq Gneiss Complex, Greenland: Implication for early Archaean tectonics. Tectonics 21:1944–9194. doi: 10.1029/2000TC001203

Nutman AP, Friend CRL (2007) Adjacent terranes with ca. 2715 and 2650 Ma high-pressure metamorphic assemblages in the Nuuk region of the North Atlantic Craton, southern West Greenland: Complexities of Neoarchaean collisional orogeny. Precambrian Res 155:159–203. doi: 10.1016/j.precamres.2006.12.009

Nutman AP, Friend CRL, Horie K, Hidaka H (2007b) Chapter 3.3 The Itsaq Gneiss Complex of Southern West Greenland and the Construction of Eoarchaean Crust at Convergent Plate Boundaries. In: Martin J. van Kranendonk RHS, Bennett VC (eds) Earth's Oldest Rocks. Elsevier, pp 187–218

Nutman AP, Friend CRL, Paxton S (2009b) Detrital zircon sedimentary provenance ages for the Eoarchaean Isua supracrustal belt southern West Greenland: Juxtaposition of an imbricated ca. 3700 Ma juvenile arc against an older complex with 3920–3760 Ma components. Precambrian Res 172:212–233. doi: http://dx.doi.org/10.1016/j.precamres.2009.03.019

Nutman AP, McGregor VR, Friend CRL, et al (1996) The Itsaq Gneiss Complex of southern West Greenland; the world's most extensive record of early crustal evolution (3900-3600 Ma). Precambrian Res 78:1–39. doi: http://dx.doi.org/10.1016/0301-9268(95)00066-6

Nutman AP, McGregor VR, Shiraishi K, et al (2002b) ⩾3850 Ma BIF and mafic inclusions in the early Archaean Itsaq Gneiss Complex around Akilia, southern West Greenland? The difficulties of precise dating of zircon-free protoliths in migmatites. Precambrian Res 117:185–224. doi: 10.1016/S0301-9268(02)00045-1

Nutman, Bennett CV, Friend LCR, Norman DM (1999) Meta-igneous (non-gneissic) tonalites and quartz-diorites from an extensive ca. 3800 Ma terrain south of the Isua supracrustal belt, southern West Greenland: constraints on early crust formation. Contrib Mineral Petrol 137:364–388. doi: 10.1007/s004100050556

O'Neil J, Carlson RW, Francis D, Stevenson RK (2008) Neodymium-142 Evidence for Hadean Mafic Crust. Science 321:1828. doi: 10.1126/science.1161925

O'Neil J, Carlson RW, Paquette J-L, Francis D (2012) Formation age and metamorphic history of the Nuvvuagittuq Greenstone Belt. Precambrian Res 220–221:23–44. doi: 10.1016/j.precamres.2012.07.009

O'Neil J, Francis D, Carlson RW (2011a) Implications of the Nuvvuagittuq Greenstone Belt for the Formation of Earth's Early Crust. J Petrol 52:985–1009. doi: 10.1093/petrology/egr014

O'Neil J, Francis D, Carlson RW (2011b) Implications of the Nuvvuagittuq Greenstone Belt for the Formation of Earth's Early Crust. J Petrol 52:985–1009. doi: 10.1093/petrology/egr014

O'Neill C, Debaille V (2014) The evolution of Hadean–Eoarchaean geodynamics. Earth Planet Sci Lett 406:49–58. doi: http://dx.doi.org/10.1016/j.epsl.2014.08.034

Palme H, O'Neill HSC (2014) 3.1 - Cosmochemical Estimates of Mantle Composition A2 - Holland, Heinrich D. In: Turekian KK (ed) Treatise on Geochemistry (Second Edition), 2nd edn. Elsevier, Oxford, pp 1–39

Pankhurst RJ, Moorbath S, Rex DC, Turner G (1973) Mineral age patterns in ca. 3700 my old rocks from West Greenland. Earth Planet Sci Lett 20:157–170. doi: 10.1016/0012-821X(73)90154-4

Patchett PJ (1983) Importance of the Lu-Hf isotopic system in studies of planetary chronology and chemical evolution. Geochim Cosmochim Acta 47:81–91

Patchett PJ, Tatsumoto M (1981) A routine high-precision method for Lu-Hf isotope geochemistry and chronology. Contrib Mineral Petrol 75:263–267. doi: 10.1007/BF01166766

Paulick H, Bach W, Godard M, et al (2006) Geochemistry of abyssal peridotites (Mid-Atlantic Ridge, 15°20′N, ODP Leg 209): Implications for fluid/rock interaction in slow spreading environments. Chem Geol 234:179–210. doi: 10.1016/j.chemgeo.2006.04.011

Pearce JA (2008) Geochemical fingerprinting of oceanic basalts with applications to ophiolite classification and the search for Archean oceanic crust. Links Ophiolites LIPs Earth Hist 100:14–48. doi: 10.1016/j.lithos.2007.06.016

Pin C, Zalduegui JS (1997) Sequential separation of light rare-earth elements, thorium and uranium by miniaturized extraction chromatography: Application to isotopic analyses of silicate rocks. Anal Chim Acta 339:79–89. doi: 10.1016/S0003-2670(96)00499-0

Polat A, Appel PWU, Fryer BJ (2011) An overview of the geochemistry of Eoarchean to Mesoarchean ultramafic to mafic volcanic rocks, {SW} Greenland: Implications for mantle depletion and petrogenetic processes at subduction zones in the early Earth. Gondwana Res 20:255–283. doi: http://dx.doi.org/10.1016/j.gr.2011.01.007

Polat A, Hofmann AW (2003) Alteration and geochemical patterns in the 3.7–3.8 Ga Isua greenstone belt, West Greenland. Precambrian Res 126:197–218. doi: 10.1016/S0301-9268(03)00095-0

Polat A, Hofmann AW, Münker C, et al (2003) Contrasting geochemical patterns in the 3.7–3.8 Ga pillow basalt cores and rims, Isua greenstone belt, Southwest Greenland: implications for postmagmatic alteration processes. Geochim Cosmochim Acta 67:441–457. doi: 10.1016/S0016-7037(02)01094-3

Polat A, Hofmann AW, Rosing MT (2002) Boninite-like volcanic rocks in the 3.7–3.8 Ga Isua greenstone belt, West Greenland: geochemical evidence for intra-oceanic subduction zone processes in the early Earth. Chem Geol 184:231–254. doi: 10.1016/S0009-2541(01)00363-1

Polat A, Kerrich R (2001) Magnesian andesites, Nb-enriched basalt-andesites, and adakites from late-Archean 2.7 Ga Wawa greenstone belts, Superior Province, Canada: implications for late Archean subduction zone petrogenetic processes. Contrib Mineral Petrol 141:36–52. doi: 10.1007/s004100000223

Polat A, Kerrich R (2000) Archean greenstone belt magmatism and the continental growth–mantle evolution connection: constraints from Th–U–Nb–LREE systematics of the 2.7 Ga Wawa subprovince, Superior Province, Canada. Earth Planet Sci Lett 175:41–54. doi: 10.1016/S0012-821X(99)00283-6

Polat A, Münker C (2004) Hf–Nd isotope evidence for contemporaneous subduction processes in the source of late Archean arc lavas from the Superior Province, Canada. Chem Geol 213:403–429. doi: 10.1016/j.chemgeo.2004.08.016

Polat A, Wang L, Appel PWU (2015) A review of structural patterns and melting processes in the Archean craton of West Greenland: Evidence for crustal growth at convergent plate margins as opposed to non-uniformitarian models. Tectonophysics 662:67–94. doi: http://dx.doi.org/10.1016/j.tecto.2015.04.006

Prouteau G, Scaillet B, Pichavant M, Maury R (2001) Evidence for mantle metasomatism by hydrous silicic melts derived from subducted oceanic crust. Nature 410:197

Puchtel IS, Blichert-Toft J, Touboul M, et al (2016) The coupled 182W-142Nd record of early terrestrial mantle differentiation. Geochem Geophys Geosystems 17:2168–2193. doi: 10.1002/2016GC006324

Rapp R., Shimizu N, Norman M., Applegate G. (1999) Reaction between slab-derived melts and peridotite in the mantle wedge: experimental constraints at 3.8 GPa. Chem Geol 160:335–356. doi: 10.1016/S0009-2541(99)00106-0

Rapp RP, Shimizu N, Norman MD (2003) Growth of early continental crust by partial melting of eclogite. Nature 425:605

Rizo H, Boyet M, Blichert-Toft J, Rosing M (2011) Combined Nd and Hf isotope evidence for deep-seated source of Isua lavas. Earth Planet Sci Lett 312:267–279. doi: 10.1016/j.epsl.2011.10.014

Rizo H, Boyet M, Blichert-Toft J, Rosing MT (2013) Early mantle dynamics inferred from 142Nd variations in Archean rocks from southwest Greenland. Earth Planet Sci Lett 377:324–335. doi: 10.1016/j.epsl.2013.07.012

Rizo H, Walker RJ, Carlson RW, et al (2016) Early Earth differentiation investigated through 142Nd, 182W, and highly siderophile element abundances in samples from Isua, Greenland. Geochim Cosmochim Acta 175:319–336. doi: 10.1016/j.gca.2015.12.007

Rollinson H (2007) Recognising early Archaean mantle: a reappraisal. Contrib Mineral Petrol 154:241–252. doi: 10.1007/s00410-007-0191-y

Rollinson HR, Appel PWU, Frei R (2002) A Metamorphosed, Early Archaean Chromitite from West Greenland: Implications for the Genesis of Archaean Anorthositic Chromitites. J Petrol 43:2143–2170. doi: 10.1093/petrology/43.11.2143

Rosing MT, Rose NM (1993) Fluid-rock Interaction in the Deeper Continental Lithosphere The role of ultramafic rocks in regulating the concentrations of volatile and non-volatile components during deep crustal metamorphism. Chem Geol 108:187–200. doi: 10.1016/0009-2541(93)90324-C

Salters VJM, Stracke A (2004) Composition of the depleted mantle. Geochem Geophys Geosystems 5. doi: 10.1029/2003GC000597

Scherer E (2001) Calibration of the Lutetium-Hafnium Clock. Science 293:683–687. doi: 10.1126/science.1061372

Scott JM, Liu J, Pearson DG, Waight TE (2016) Mantle depletion and metasomatism recorded in orthopyroxene in highly depleted peridotites. Chem Geol 441:280–291. doi: 10.1016/j.chemgeo.2016.08.024

Sen C, Dunn T (1995) Experimental modal metasomatism of a spinel lherzolite and the production of amphibole-bearing peridotite. Contrib Mineral Petrol 119:422–432. doi: 10.1007/BF00286939

Sen C, Dunn T (1994) Dehydration melting of a basaltic composition amphibolite at 1.5 and 2.0 GPa: implications for the origin of adakites. Contrib Mineral Petrol 117:394–409. doi: 10.1007/BF00307273

Shirey SB, Richardson SH (2011) Start of the Wilson Cycle at 3 Ga Shown by Diamonds from Subcontinental Mantle. Science 333:434–436. doi: 10.1126/science.1206275

Shirey SB, Walker RJ (1998) THE Re-Os ISOTOPE SYSTEM IN COSMOCHEMISTRY AND HIGH-TEMPERATURE GEOCHEMISTRY. Annu Rev Earth Planet Sci 26:423–500. doi: 10.1146/annurev.earth.26.1.423

Stern RA, Bleeker W (1998) Age of the World's Oldest Rocks Refined Using Canada's SHRIMP: The Acasta Gneiss Complex, Northwest Territories, Canada. Geosci Can 25:27–31

Stern RJ (2004) Subduction initiation: spontaneous and induced. Earth Planet Sci Lett 226:275–292. doi: 10.1016/j.epsl.2004.08.007

Stracke A, Snow JE, Hellebrand E, et al (2011) Abyssal peridotite Hf isotopes identify extreme mantle depletion. Earth Planet Sci Lett 308:359–368. doi: http://dx.doi.org/10.1016/j.epsl.2011.06.012

Szilas K, Kelemen PB, Rosing MT (2015) The petrogenesis of ultramafic rocks in the > 3.8 Ga Isua supracrustal belt, southern West Greenland: Geochemical evidence for two distinct magmatic cumulate trends. Gondwana Res 28:565–580. doi: http://dx.doi.org/10.1016/j.gr.2014.07.010

Tang Y-J, Zhang H-F, Ying J-F, Su B-X (2013) Widespread refertilization of cratonic and circum-cratonic lithospheric mantle. Earth-Sci Rev 118:45–68. doi: 10.1016/j.earscirev.2013.01.004

Touboul M, Liu J, O'Neil J, et al (2014) New insights into the Hadean mantle revealed by 182W and highly siderophile element abundances of supracrustal rocks from the Nuvvuagittuq Greenstone Belt, Quebec, Canada. Chem Geol 383:63–75. doi: http://dx.doi.org/10.1016/j.chemgeo.2014.05.030

Turner S, Rushmer T, Reagan M, Moyen J-F (2014) Heading down early on? Start of subduction on Earth. Geology 42:139–142. doi: 10.1130/G34886.1

Valley JW (2008) The Origin of Habitats. Geology 36:911–912. doi: 10.1130/focus112008.1

Valley JW, Cavosie AJ, Ushikubo T, et al (2014) Hadean age for a post-magma-ocean zircon confirmed by atom-probe tomography. Nat Geosci 7:219–223

van de Löcht J, Hoffmann JE, Li C, et al (2018) Earth's oldest mantle peridotites show entire record of late accretion. Geology 46:199–202. doi: 10.1130/G39709.1

Van Kranendonk M (2011) Onset of Plate Tectonics. Science 333:. doi: 10.1126/science.1208766

Vervoort JD, Blichert-Toft J (1999) Evolution of the depleted mantle: Hf isotope evidence from juvenile rocks through time. Geochim Cosmochim Acta 63:533–556. doi: 10.1016/S0016-7037(98)00274-9

Vervoort JD, Patchett PJ, Gehrels GE, Nutman AP (1996) Constraints on early Earth differentiation from hafnium and neodymium isotopes. Nature 379:624

Vervoort JD, Patchett PJ, Söderlund U, Baker M (2004) Isotopic composition of Yb and the determination of Lu concentrations and Lu/Hf ratios by isotope dilution using MC-ICPMS. Geochem Geophys Geosystems 5:n/a-n/a. doi: 10.1029/2004GC000721

Vervoort JD, Plank T, Prytulak J (2011) The Hf–Nd isotopic composition of marine sediments. Geochim Cosmochim Acta 75:5903–5926. doi: 10.1016/j.gca.2011.07.046

Walker RJ (2016) Siderophile Elements in Tracing Planetary Formation and Evolution. Geochem Perspect 5:1–2

Wallace M, Green DH (1991) The effect of bulk rock composition on the stability of amphibole in the upper mantle: Implications for solidus positions and mantle metasomatism. Mineral Petrol 44:1–19. doi: 10.1007/BF01167097

Weyer S, Münker C, Rehkämper M, Mezger K (2002) Determination of ultra-low Nb, Ta, Zr and Hf concentrations and the chondritic Zr/Hf and Nb/Ta ratios by isotope dilution analyses with multiple collector ICP-MS. Chem Geol 187:295–313. doi: 10.1016/S0009-2541(02)00129-8

Whitehouse MJ, Kamber BS (2005) Assigning Dates to Thin Gneissic Veins in High-Grade Metamorphic Terranes: A Cautionary Tale from Akilia, Southwest Greenland. J Petrol 46:291–318. doi: 10.1093/petrology/egh075

Whitehouse MJ, Kamber BS, Fedo CM, Lepland A (2005) Integrated Pb- and S-isotope investigation of sulphide minerals from the early Archaean of southwest Greenland. Chem Geol 222:112–131. doi: 10.1016/j.chemgeo.2005.06.004

Whitehouse MJ, Kamber BS, Moorbath S (1999) Age significance of U–Th–Pb zircon data from early Archaean rocks of west Greenland—a reassessment based on combined ion-microprobe and imaging studies. Chem Geol 160:201–224. doi: 10.1016/S0009-2541(99)00066-2

Whitehouse MJ, Myers JS, Fedo CM (2009) The Akilia Controversy: field, structural and geochronological evidence questions interpretations of >3.8 Ga life in SW Greenland. J Geol Soc 166:335–348. doi: 10.1144/0016-76492008-070

Wilde SA, Valley JW, Peck WH, Graham CM (2001) Evidence from detrital zircons for the existence of continental crust and oceans on the Earth 4.4 Gyr ago. Nature 409:175

Willbold M, Mojzsis SJ, Chen H-W, Elliott T (2015) Tungsten isotope composition of the Acasta Gneiss Complex. Earth Planet Sci Lett 419:168–177. doi: 10.1016/j.epsl.2015.02.040

Xiong X-L (2006) Trace element evidence for growth of early continental crust by melting of rutile-bearing hydrous eclogite. Geology 34:945–948. doi: 10.1130/G22711A.1

Zack T, Foley S, Jenner G (1997) A consistent partition coefficient set for clinopyroxéne, amphibole and garnet from laser ablation microprobe analysis of garnet pyroxenites from Kakanui, New Zealand

Zindler A, Emil J (1988) Mantle cryptology. Geochim Cosmochim Acta 52:319–333. doi: 10.1016/0016-7037(88)90087-7

9 Danksagung

Zu Beginn möchte ich mich bei meinem Doktorvater Carsten Münker bedanken; für das faszinierende Thema, die gute Betreuung und die Möglichkeit in einer so tollen Arbeitsgruppe zu promovieren. Danke Carsten!

Elis Hoffmann, der mich mitbetreut hat, gilt ebenfalls ein ganz großes Dankeschön. Vielen Dank für die unermüdliche Unterstützung, auch aus der Ferne, und die so oft im richtigen Moment ausgesprochenen Ermutigungen.

Vielen Dank auch an Reiner Kleinschrodt für die Betreuung an der Mikrosonde und für seine stete Hilfsbereitschaft.

Peter Sprung möchte ich danken dafür, wie er mir mit Rat und Tat bezüglich Labor und vor allem MS-ICP-MS Messungen geholfen hat. Auch für so machen Kaffee (zu) früh am Morgen an gemeinsamen Messtagen.

Harry Becker möchte ich danken für die Möglichkeit in Berlin in seinem Labor zu arbeiten und auch für die fachliche Unterstützung bezüglich meines „PGE Papers". An dieser Stelle auch ein ganz herzliches Dankeschön an die andern „Berliner", vor allem Yogita, Chunhui und Zaicong für: die gute Zeit in Berlin, die Einführung in die „Geheimnisse der HSE-Chemie", die Hilfe im Labor und beim Messen.

Ein sehr großes Dankeschön geht an die AG Münker inklusive Ehemaliger:

Ohne euch hätte ich die Zeit nie so gut überstanden und so viel Spaß dabei gehabt.

Liebe langfristige – oder auch nur temporäre Bürokollegen: Ninja, Christiane, Mario, Peter, Vicki und Jens - ich hätte mir keine bessern wünschen können.

Danke für die schöne Zeit!

Pia möchte ich ganz herzlich danken fürs Korrekturlesen und für die schöne gemeinsame Studien- und Promotionszeit Wer hätte gedacht dass wir solange gemeinsam an der Uni Köln bleiben würden…

Meinen Eltern, Ulrike und Hajo van de Löcht bin ich vor allem dankbar, weil sie mich mit viel Vertrauen meinen eigenen Weg gehen lassen und für die liebevolle Unterstützung dabei.

Meinem Bruder Jonas danke ich für sein Interesse an dem was sein Schwesterchen so „abgefahrenes" macht und für den unerschütterlichen Glauben daran, dass sie die Promotion schon schafft.

Ein – nein gleich mehrere - riesige und herzliche DANKE gehen an Florian Finke für seine Unterstützung und sein Verständnis vor allem in den stressigen Phasen der Promotion.

VIELEN DANK EUCH ALLEN!

Appendix A

A-1 PGE-RE ABUNDANCES

A-1.1 IPGE variations

Group 1 peridotites show minor fractionation between IPGEs, this is common in peridotites because these elements are mainly controlled by residual alloys ("nugget effect"), once high degrees of partial melting lead to full exhaustion of sulphur (Mungall and Brenan 2014). Therefore, the absolute abundances of IPGE are not only somewhat variable due to redistribution during melt infiltration processes, but can also have an influence on the reproducibility of IPGE. Since IPGEs alloys are occasionally heterogeneously distributed in the sample powders and IPGE abundances obtained from different powder fractions may vary and result in non-representative, minor variations in Os/Ir, Ir/Ru, Ru/Os ratios (Lorand et al. 2013; Aulbach et al. 2016). Alternatively, PGE patterns with positive Ru and negative Ir anomalies similar to group 1 samples could be ascribed to chromite accumulation as it is observed in layered intrusions or cumulates of komatiite flows (Puchtel et al. 2009; Coggon et al. 2015). However, field relationships and petrography clearly indicate that chromite cumulates are absent in these rocks and komatiite flows are also not found in western Greenland.

Coggon et al. (2015) reported PGE patterns of meta-peridotites and chromitites from the Ujaragssuit Nunât layered ultramafic body and nearby ultramafic enclaves, showing clear evidence for magmatic chromitite accumulation (Fig. A-1). All but one of these samples display negative Ir anomalies and positive Ru anomalies. Based on low magnitude positive anomalies in Os and Ru relative to Ir, Coggon et al. (2015) concluded that the IPGE budget was not only controlled by chromite and/or any chromite-hosted PGM, but at least one further phase that exerted a control on IPGE fractionation. Ujaragssuit Nunât meta-peridotites show distinct, negative Pt anomalies relative to Pd. This contrasts with the peridotites of this study, where this is far less distinct or absent (Fig. A-1). Our samples do not show a positive correlation of Os concentrations versus Os/Pt ratios as reported for the Ujaragssuit Nunât whole-rock samples. In addition, no correlation exists between PGEs and Al_2O_3, (e.g. Os/Ir versus Al_2O_3 (Fig. A-2 a), Ru and Cr (e.g., Locmelis et al. 2011; Fig. A-2 b), amount of Cr-Spinel with Pt/Os ratios (Coggon et al. 2015), and Os/Ir versus Os (Fig. A-2 c), supporting our conclusion that the IPGE contents in the investigated samples were not controlled by chromite accumulation.

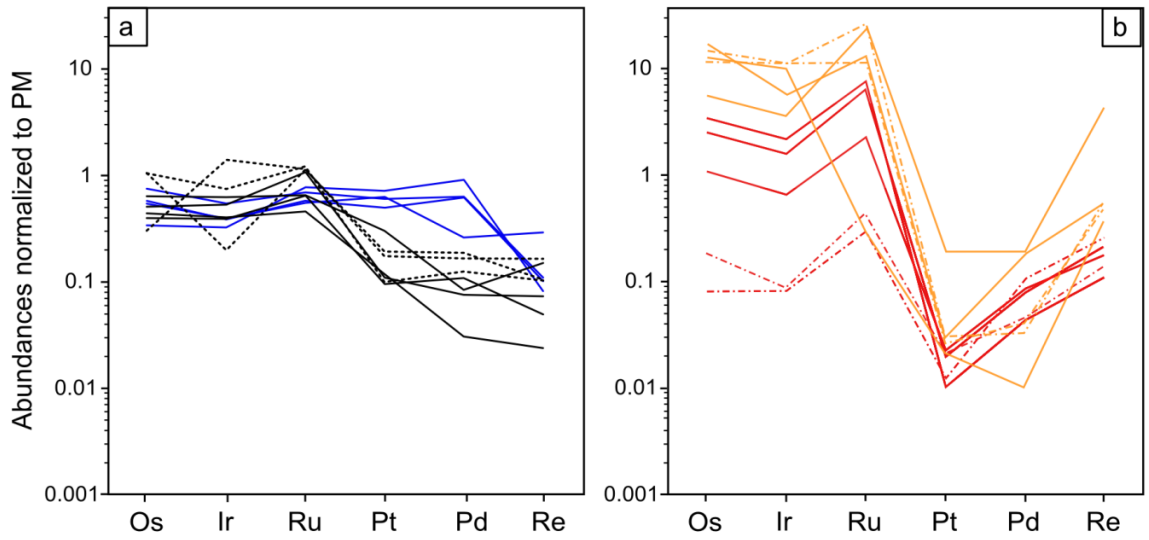

Figure A-1: Primitive mantle-normalized platinum-group-element patterns of Eoarchean dunites and harzburgites from southern west Greenland. **a)** solid black lines are SOISB group 1 peridotites, stippled black lines represent NUB group 1 peridotites, blue lines represent group 2 peridotites; **b**) red solid lines meta-peridotites from the Ujaragssuit Nunât layered ultramafic body (Coggon et al. 2015) and stippled red lines meta-peridotites from peridotite enclaves in the vicinity of the Ujaragssuit Nunât layered ultramafic body (Coggon et al. 2015), solid orange lines chromitites from the Ujaragssuit Nunât layered ultramafic body (Coggon e t al. 2015) and stippled orange from peridotite enclaves in the vicinity of the Ujaragssuit Nunât layered ultramafic body (Coggon et al. 2015).

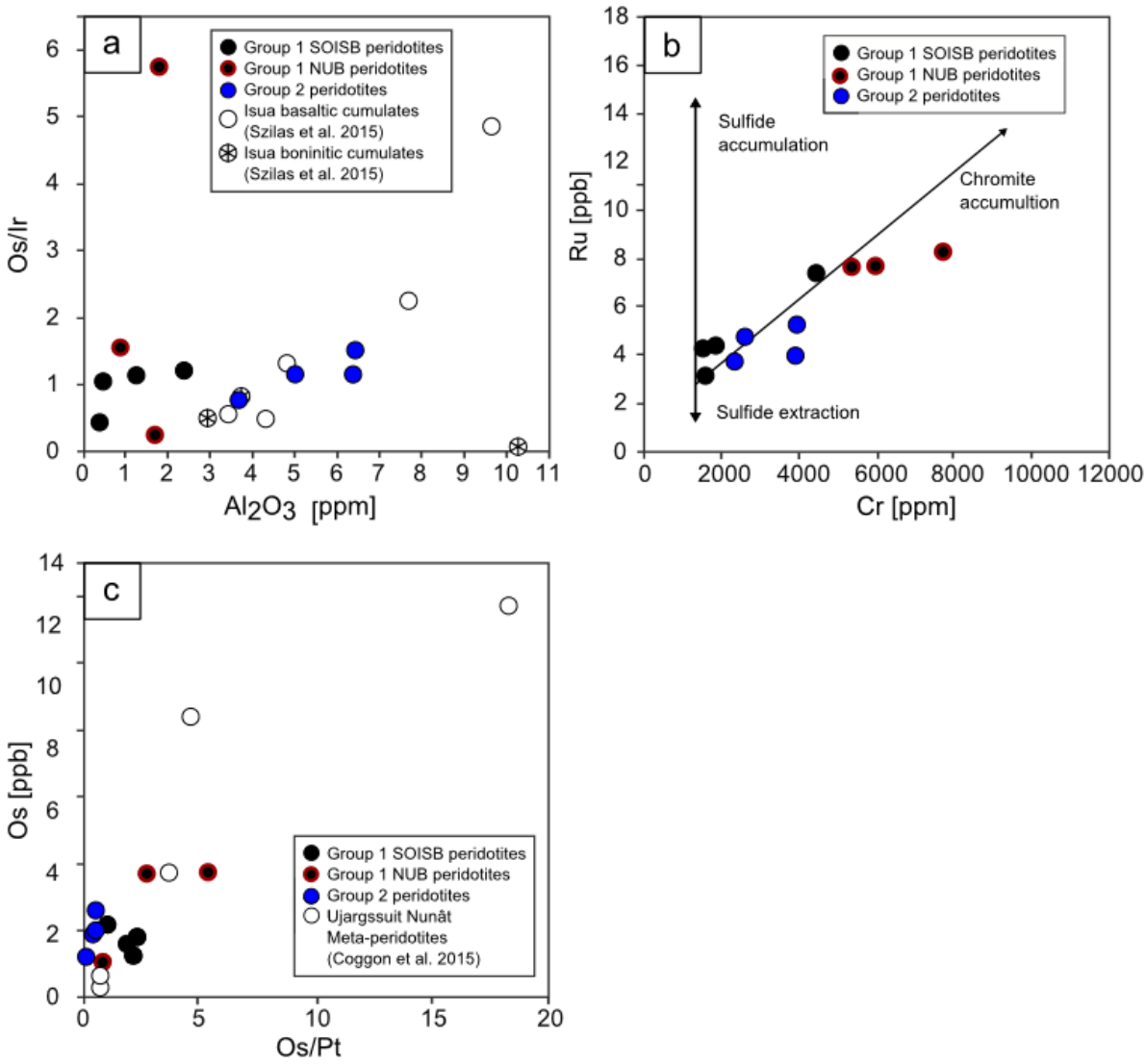

Figure A-2: a) Os/Ir versus Al_2O_3 concentration; open symbol mafic cumulates from the Isua Supracrustal Belt (Szilas et al. 2015); **b**) Ru concentration versus Cr, chromite accumulation and sulfide accumulation and extraction trend after Locmelis et al. (2011); **c)** Os versus Os/Pt; open symbols Ujaragssuit Nunât layered ultramafic body meta-peridotite and from peridotite enclaves in the vicinity (Coggon et al. 2015).

Szilas et al. (2015) reported PGE pattern obtained from ultramafic rocks from the Isua Supracrustal Belt, and characterized them as basaltic and boninitic cumulates. Samples of Szilas et al. (2015) yielding cumulate PGE signature are shown for comparison in figure 4-3. Moreover, group 1 peridotite IPGE abundances are in the range of the Balmuccia dunites and harzburgites (Fig.4-1, A-3a) and ophiolitic harzburgites and dunites (Becker and Dale 2016) e.g. Shetland Ophiolite (UK) (Fig. A-3b) (O'Driscoll et al. 2012).

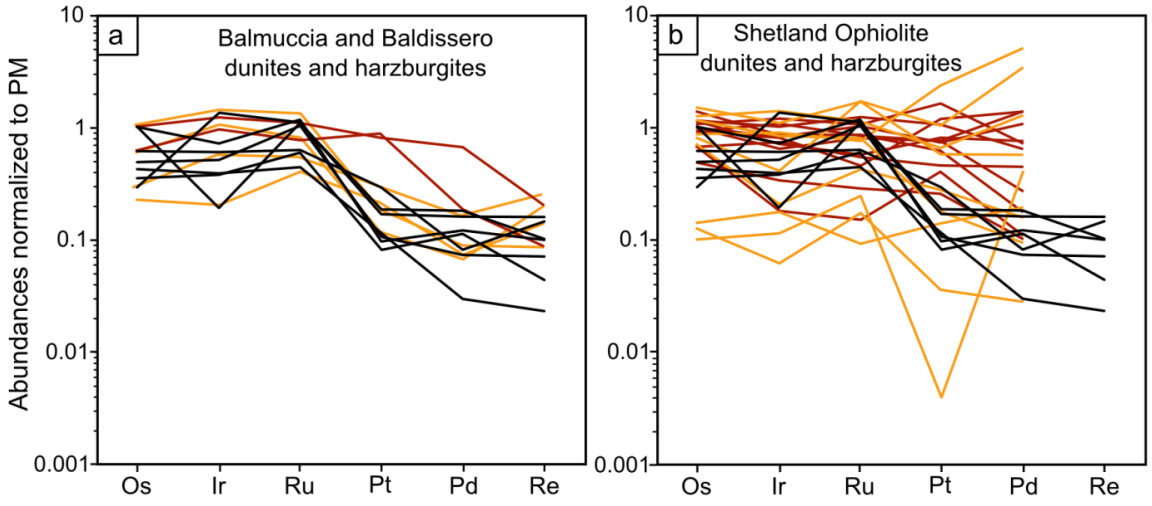

Figure A-3: Primitive mantle -normalized platinum-group-element (PGE) patterns of Eoarchean dunites and harzburgites from southern West Greenland examined in this study. Black lines are SOISB group 1 peridotites, red lines represent harzburgites and orange lines dunites from, **a**) Balmuccia (Wang et al. 2013); **b**) Shetland ophiolite (UK) (O´Driscoll et al., 2012).

A-1.2 PPGE refertilization and disturbance of Re-Os systematics

The different Re-depletion ages combined with re-enriched PPGE and higher Al/Si ratios of group 2 suggest a multistage evolution history for the peridotites, comprising melt depletion and interaction with infiltrating melt at upper mantle level and presumably also later alteration in the crust likely associated to metamorphic events. Co-precipitation of sulphides and Al-phases (e.g. pyroxene and spinel) during interaction of percolating melt and peridotite in the lherzolith stability field can account for the re-enriched PPGE and Al (e.g. Becker and Dale, 2016). Alternatively, fluid-rock interaction during amphibole facies metamorphism can cause enrichment of aluminium in ultramafic rocks up to wt% levels (Rosing and Rose 1993). Group 2 peridotites contain biotite indicative for metasomatic processes. Relative enrichment of PPGEs combined with low Re abundances and varying Re depletion ages (1.66-3.54 Ga) indicate a decoupling of PPGEs and Re during later metasomatic disturbance of the ^{187}Re-^{187}Os decay system, such ages are possibly related to terrane assembly. Alternatively, early Archean melt-rock interaction at upper mantle conditions involving melt from Re-depleted sources may also explain the observed re-enrichment of PPGEs of group 2 samples. Chondritic normalized Pd/Ir and Pt/Ir ratios of three group 2 samples are positive correlated with Al_2O_3 and Re/Os isotopic composition and negative with MgO, indicates that these PGE ratios might be modified by interaction with melts (Pearson et al. 2004).

In addition, Re can be mobilized easily during later disturbance and during recent weathering. Hence, the young Re-depletion ages may reflect artefacts and have therefore no geological relevance.

Bennett et al. (2002) reported Re-Os isotope data for four peridotites from SOISB. One peridotite of their suite of samples was collected from the same ultramafic unit as group 2 samples (10-29A and B, 10-30 and 10-31; Fig. 2-1). As discussed above, group 2 peridotites show indications for later metasomatic disturbance of the Re–Os isotopic system and nearly flat PGE patterns, with some variability in Pd and Re. Thus, care must be taken for the interpretation of Re-Os data obtained from group 2 peridotites.

Several initial Os isotope compositions obtained for group 1 peridotites are unrealistically low and reveal over-correction of radiogenic ingrowth due to young addition of Re (Fig. 4-4).

The isochron diagram (Fig. A-4) shows as well that some Re was added recently, however, not influencing significantly the Os isotope composition of these samples which remains near to primitive mantle at 3.81 Ga.

As mentioned above, three samples were processed differently, avoiding all contact with metal tools, and a piece of the jaw breaker were analysed in order to evaluate potential metal contamination. As listed in Table 4-1, the results are very similar and do not hint toward significant contamination by unrelated PGE during the first analytical session. The results are not consistently lower for these samples than for those analysed in the first analytical session, where the samples were crushed in a jaw breaker. Os and Ir concentrations were reproduced (discrepancies of < 4%) for sample 10-12B, Pt for sample 10-31 (discrepancies 1.9%) and some HSE were even clearly enrich in some "metal-free" aliquots. Pd and Re were significantly enriched in 10-20C-II and Ir and Ru in 10-31-II. Hence, sample heterogeneity has a major impact on slightly different PGE abundances. This is very common for these types of depleted peridotites. In addition, the reference material (harzburgite MUH-1) show similar concentration variations for Ir, Pt, Pd and Re, indicating likewise sample heterogeneity. Moreover, the amount rock pulverized is an imported factor. For the first set, powder between 500-1000g rocks were processed, the available rock material for the "metal-free" aliquots was limited (between 30 and 100g). Thus, higher effects of sample heterogeneity were expected and seen in the data obtained from the "metal-free" set, especially regarding elements with low concentrations, e.g. Pt and Pd.

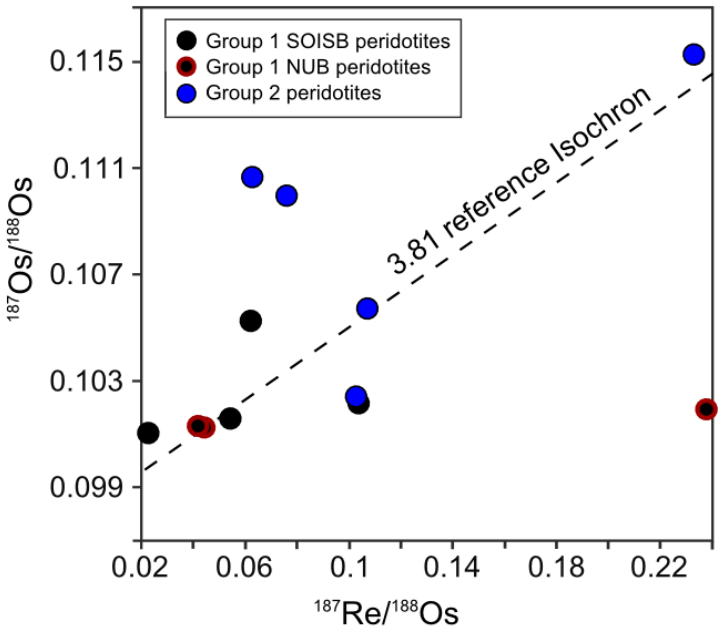

Figure A-4: Re-Os Isochron diagram for group 1 with reference 3.81 Isochron using ^{187}Re decay constant $\lambda = 1.666 \times 10^{-11}$ year^{-1} (Smoliar et al., 1996).

Recent Re addition, as indicated by the isochron diagram (Fig. A-4) may be likely, however, it is not clear if Re was introduced by the jaw crusher steel or by recent weathering and Re mobility, because the newly prepared samples were not in contact to steel and show also a re-enrichment of Re.

Even though, contamination by jaw-breaker-metal cannot be ruled out completely, the difference in primitive mantle normalized PGE pattern between Group 1 and 2 are still clear. The unradiogenic Os isotopic composition and reproduced $^{187}Re/^{188}Os$ and $^{187}Os/^{188}Os$ ratios (e.g. 10-30 II) support the assumption that the potential jaw-breaker-metal contamination was low.

A-2 TABLES

Table A-1: Measurements of the UMD Os Standard Solution

SEM	183/188 fc	185/188 fc	186/188 fc	187/188 fc	189/188 fc	190/188 fc	192/188
100 ppb Os STD SEM 1µl 1	0.00014	0.00003	0.1206	0.1140	1.2210	1.9870	3.0872
100 ppb Os STD SEM 1µl 2	0.00012	0.00002	0.1201	0.1141	1.2200	1.9852	3.0905
100 ppb Os STD SEM 1µl 3	0.00006	0.00001	0.1205	0.1141	1.2199	1.9847	3.0832
100 ppb Os STD SEM 1µl 4	0.00010	0.00000	0.1204	0.1142	1.2215	1.9853	3.0946
100 ppb Os STD SEM 1µl 5	0.00014	0.00003	0.1208	0.1141	1.2199	1.9857	3.0900
100 ppb Os STD SEM 1µl 6	0.00245	0.00005	0.1249	0.1139	1.2181	1.9818	3.0703
100 ppb Os STD SEM 1µl 7	0.00015	0.00005	0.1209	0.1141	1.2192	1.9836	3.1052
100 ppb Os STD SEM 1µl 8	0.00018	0.00005	0.1205	0.1141	1.2194	1.9836	3.0908
100 ppb Os STD SEM 1µl 9	0.00051	0.00007	0.1204	0.1140	1.2203	1.9872	3.0940
100 ppb Os STD SEM 1µl 10	0.00008	0.00001	0.1206	0.1141	1.2171	1.9763	3.0635
100 ppb Os STD SEM 1µl 11	0.00012	0.00004	0.1207	0.1140	1.2186	1.9831	3.0835
100 ppb Os STD SEM 1µl 12	0.00008	0.00002	0.1204	0.1142	1.2193	1.9826	3.0871
100 ppb Os STD SEM 1µl 13	0.00013	0.00002	0.1203	0.1142	1.2195	1.9832	3.0882
100 ppb Os STD SEM 1µl 14	0.00003	0.00001	0.1203	0.1141	1.2205	1.9850	3.0854
Mean	**0.0003**	**0.0000**	**0.1208**	**0.1141**	**1.2196**	**1.9839**	**3.0867**
2 x StdDev	0.0013	0.0000	0.0024	0.0002	0.0023	0.0054	0.0203
run no.	14	14	14	14	14	14	14
				2015 (n=8)			
			Mean	**0.1141**			
			2 x StdDev	**0.0002**			
Farraday cups							
35 ppm Os STD SEM 0.5µl			0.1192	0.1138	1.2192	1.9822	3.0778
2 x StdDev			0.0000	0.0000	0.0000	0.0001	0.0001
Shirey & Walker (1998) (*35*)			0.1198	0.1138	1.2197	1.9845	3.0827

Table A-2: Measurements of the UMD Os Standard Solution, "metal free" samples

SEM	183/188 fc	185/188 fc	186/188 fc	187/188 fc	189/188 fc	190/188 fc	192/188
100 ppb Os STD SEM 2µl 1	0.00000	0.00005	0.12001	0.11377	1.21966	1.98303	3.07853
100 ppb Os STD SEM 2µl 2	0.00000	0.00005	0.12005	0.11380	1.22037	1.98769	3.09191
100 ppb Os STD SEM 1µl 1	0.00113	0.00018	0.12155	0.11370	1.22209	1.99231	3.10731
100 ppb Os STD SEM 1µl 2	0.00107	0.00017	0.12189	0.11394	1.21753	1.98793	3.08151
100 ppb Os STD SEM 1µl 3	0.00132	0.00007	0.12143	0.11388	1.22041	1.98789	3.09083
100 ppb Os STD SEM 1µl 4	0.00000	0.00036	0.12244	0.11400	1.22065	1.99252	3.09327
100 ppb Os STD SEM 1µl 5	0.00000	0.00027	0.12394	0.11396	1.22002	1.98295	3.07088
100 ppb Os STD SEM 1µl 6	0.00000	0.00003	0.11994	0.11388	1.22105	1.98862	3.09314
100 ppb Os STD SEM 1µl 7	0.00075	0.00005	0.12048	0.11403	1.21900	1.98941	3.07569
100 ppb Os STD SEM 1µl 8	0.00107	0.00017	0.12189	0.11394	1.21753	1.98793	3.08151
Mean	**0.00053**	**0.00014**	**0.12136**	**0.11389**	**1.21983**	**1.98803**	**3.08646**
2 x StdDev	0.00116	0.00023	0.00256	0.00022	0.00293	0.00639	0.02155
run no.	10	10	10	10	10	10	10

	2017 (n=8)
Mean	**0.1139**
2 x StdDev	**0.0002**

A-3 REFERENCES APPENDIX A

Amelin, Y., Kamo, S.L., Lee, D.-C, 2010, Evolution of Early Crust in Chondritic or Non-Chondritic Earth Inferred from U–Pb and Lu–Hf Data for Chemically Abraded Zircon from the Itsaq Gneiss Complex, West Greenland: Canadian Journal of Earth Sciences, v. 48, p. 141–160

Aulbach S, Mungall JE, Pearson DG (2016) Distribution and Processing of Highly Siderophile Elements in Cratonic Mantle Lithosphere. Rev Mineral Geochem 81:239–304. doi: 10.2138/rmg.2016.81.5

Becker H, Dale CW (2016) Re–Pt–Os Isotopic and Highly Siderophile Element Behavior in Oceanic and Continental Mantle Tectonites. Rev Mineral Geochem 81:369–440. doi: 10.2138/rmg.2016.81.7

Bennett, V.C., Nutman, A.P. and Esat, T.M., 2002, Constraints on mantle evolution from 187Os/ 188Os isotopic compositions of Archean ultramafic rocks from southern West Greenland (3.8 Ga) and Western Australia (3.46 Ga): Geochimica et Cosmochimica Acta, v. 66, p. 2615–2630.

Coggon JA, Luguet A, Fonseca ROC, et al (2015) Understanding Re–Os systematics and model ages in metamorphosed Archean ultramafic rocks: A single mineral to whole-rock investigation. Geochim Cosmochim Acta 167:205–240. doi: 10.1016/j.gca.2015.07.025

Coggon, J. A., Luguet, A., Nowell, G. M. and Appel, P. W. U., 2013, Hadean Mantle Melting Recorded by Southwest Greenland Chromitite 186Os Signatures. Nature Geosci v. 6(10), p. 871–874.

Frei, R., and Jensen K.B., 2003, Re–Os, Sm–Nd Isotope- and REE Systematics on Ultramafic Rocks and Pillow Basalts from the Earth's Oldest Oceanic Crustal Fragments (Isua Supracrustal Belt and Ujaragssuit Nunât Area, W Greenland): Highly Siderophile Elements in the Earth and Meteorties: A Volume in Honor of John Morgan, v. 196, p. 163–191.

Locmelis M, Pearson NJ, Barnes SJ, Fiorentini ML (2011) Ruthenium in komatiitic chromite. Geochim Cosmochim Acta 75:3645–3661. doi: 10.1016/j.gca.2011.03.041

Lorand J-P, Luguet A, Alard O (2013) Platinum-group element systematics and petrogenetic processing of the continental upper mantle: A review. Lithos 164–167:2–21. doi: http://dx.doi.org/10.1016/j.lithos.2012.08.017

Meisel T, Walker RJ, Irving AJ, Lorand J-P (2001) Osmium isotopic compositions of mantle xenoliths: a global perspective. Geochim Cosmochim Acta 65:1311–1323. doi: http://dx.doi.org/10.1016/S0016-7037(00)00566-4

Mungall JE, Brenan JM (2014) Partitioning of platinum-group elements and Au between sulfide liquid and basalt and the origins of mantle-crust fractionation of the chalcophile elements. Geochim Cosmochim Acta 125:265–289. doi: http://dx.doi.org/10.1016/j.gca.2013.10.002

O'Driscoll B, Day JMD, Walker RJ, et al (2012) Chemical heterogeneity in the upper mantle recorded by peridotites and chromitites from the Shetland Ophiolite Complex, Scotland. Earth Planet Sci Lett 333–334:226–237. doi: 10.1016/j.epsl.2012.03.035

Pearson DG, Irvine GJ, Ionov DA, et al (2004) Re–Os isotope systematics and platinum group element fractionation during mantle melt extraction: a study of massif and xenolith peridotite suites. Chem Geol 208:29–59. doi: http://dx.doi.org/10.1016/j.chemgeo.2004.04.005

Puchtel IS, Walker RJ, Brandon AD, Nisbet EG (2009) Pt–Re–Os and Sm–Nd isotope and HSE and REE systematics of the 2.7 Ga Belingwe and Abitibi komatiites. Geochim Cosmochim Acta 73:6367–6389. doi: 10.1016/j.gca.2009.07.022

Rosing MT, Rose NM (1993) Fluid-rock Interaction in the Deeper Continental Lithosphere The role of ultramafic rocks in regulating the concentrations of volatile and non-volatile components during deep crustal metamorphism. Chem Geol 108:187–200. doi: 10.1016/0009-2541(93)90324-C

Shirey, S.B., and Walker R.J., 1998, The Re-Os isotope system in cosmochemistry and high-temperature geochemistry: Annual Review of Earth and Planetary Sciences, v. 26, p. 423–500.

Smoliar, M.I, Walker, R.J, Morgan, J.W., 1996, Re–Os ages of group IIA, IIIA, IVA, and IVB iron meteorites: Science, v. 271, p. 1099–1102

Szilas K, Kelemen PB, Rosing MT (2015) The petrogenesis of ultramafic rocks in the > 3.8 Ga Isua supracrustal belt, southern West Greenland: Geochemical evidence for two distinct magmatic cumulate trends. Gondwana Res 28:565–580. doi:http://dx.doi.org/10.1016/j.gr.2014.07.010

Wang Z, Becker H, Gawronski T (2013) Partial re-equilibration of highly siderophile elements and the chalcogens in the mantle: A case study on the Baldissero and Balmuccia peridotite massifs (Ivrea Zone, Italian Alps). Geochim Cosmochim Acta 108:21–44. doi: 10.1016/j.gca.2013.01.021

Appendix B

B-1 TABLES

Table B-1: Trace element abundances of peridotite and amphibolite samples from the IGC; ICP-MS-Lab, Institute of Geosciences, University of Kiel, Germany ; R: replicate analysis

Method*	1	1	1	1	1	1	1	1	1
Location	SOISB1	SOISB1	SOISB1	SOISB1	SOISB2	SOISB2	SOISB2	SOISB2	SOISB2
Sample	10-20A	10-20C	10-22	10-23	10-34	10-34-R	10-36	10-29A	10-29B
Peridotite type	1	1	1	1	1	1	1	2	2
Li	7.36	5.71	8.23	6.61	5.83	5.82	7.11	6.41	6.52
Sc	9.39	8.34	5.03	4.51	10.6	10.6	21.4	16.9	20.1
V	44.9	29.6	16.7	27.1	55.6	55.6	90.9	80.1	91.0
Cr	3044	1683	1433	4193	1478	1459	3970	3246	2228
Co	127	122	130	141	91.3	93.2	94.4	93.3	87.7
Ni	1852	2061	2774	2615	1501	1521	1737	1744	1387
Cu	67.0	21.5	1.07	5.11	34.1	36.6	4.98	6.96	12.7
Zn	65.1	55.1	47.6	67.0	55.1	56.3	68.1	52.9	64.8
Ga	1.83	1.67	0.621	1.04	3.05	3.05	4.41	4.17	5.24
Rb	0.972	0.280	<0.2	0.271	0.432	0.400	5.61	0.419	0.765
Sr	8.04	7.63	0.411	1.22	37.9	37.8	5.61	24.0	28.2
Y	2.18	1.83	0.766	0.348	6.79	6.72	3.62	2.89	4.34
Zr	4.06	5.96	0.611	1.14	3.51	2.92	4.58	3.63	5.46
Nb	0.239	0.195	0.0667	0.0903	0.102	0.102	0.142	0.111	0.175
Mo	0.334	0.411	0.310	0.322	0.215	0.270	0.227	0.379	0.290
Sn	0.371	0.274	<0.05	0.215	0.508	0.436	0.204	0.215	0.364
Cs	0.169	0.0575	<0.037	0.0586	0.0465	0.0508	0.905	<0.037	<0.037
Ba	0.828	0.234	<0.064	0.939	0.156	0.148	4.10	2.27	3.35
La	0.443	0.413	0.0961	0.129	0.628	0.624	0.314	0.244	0.485
Ce	1.28	1.15	0.256	0.274	1.83	1.81	0.736	0.426	0.879
Pr	0.210	0.189	0.0463	0.0396	0.324	0.320	0.100	0.0565	0.106
Nd	1.12	1.02	0.264	0.194	1.95	1.94	0.478	0.279	0.467
Sm	0.386	0.347	<0.091	<0.091	0.811	0.803	0.184	0.121	0.181
Eu	0.136	0.124	0.0352	<0.028	0.256	0.252	0.037	0.0820	0.0755
Gd	0.460	0.402	0.142	<0.082	1.16	1.15	0.322	0.238	0.361
Tb	0.0773	0.0670	0.0261	<0.013	0.211	0.209	0.0726	0.0564	0.0846
Dy	0.485	0.413	0.169	0.0753	1.40	1.38	0.589	0.467	0.705
Ho	0.0963	0.0810	0.0348	0.0160	0.285	0.284	0.145	0.117	0.175
Er	0.260	0.219	0.0981	0.0472	0.754	0.747	0.464	0.368	0.551
Tm	0.0387	0.0321	0.0158	<0.013	0.101	0.100	0.0777	0.0604	0.0893
Yb	0.253	0.210	0.102	<0.06	0.581	0.580	0.543	0.426	0.618
Lu	0.0389	0.0332	0.0170	<0.015	0.079	0.079	0.089	0.070	0.101
Hf	0.155	0.190	<0.048	<0.048	0.131	0.118	0.188	0.141	0.228
Ta	0.0138	<0.014	<0.014	<0.014	<0.014	<0.014	<0.014	<0.014	<0.014
W	0.309	0.312	0.435	0.424	5.23	<0.076	0.603	1.43	0.259
Pb	0.732	0.809	0.895	0.299	0.748	0.758	1.72	2.69	2.038
Th	0.0326	0.0467	<0.019	<0.019	0.0305	0.0301	0.0369	<0.019	0.0792
U	0.0396	0.0406	0.0329	0.0221	0.0306	0.0307	0.0546	0.0846	0.188

*Methods	ParrBomb step			table top step	dry down
	acid	**temperature**	time	acid	temperature
1	1:1 mixture of HF and HNO3	**180°C**	24 hours	+ 1ml HClO4	120-180°C
2	1:1 mixture of HF and HNO3	**180°C**	4 days	+ 1ml HClO4	120-200°C
3	1:1 mixture of HF and HNO3	**180°C**	24 hours	+ 1.5ml H_2SO_4	120-200°C

Table B-1 continued

Method	1	1	1	2	3	1	2	3
Location	SOISB2	SOISB2	SOISB2	SOISB2	SOISB2	SOISB2	SOISB2	SOISB2
Sample	10-29B-R	10-30	10-30-RI	10-30-RII	10-30-RIII	10-31	10-31-RI	10-31-RII
Peridotite type	2	2	2	2	2	2	2	2
Li	6.26	8.68	9.75	9.79	9.05	5.35	6.04	5.82
Sc	21.8	12.9	14.7	15.5	11.5	18.5	22.0	18.3
V	87.4	52.9	50.8	54.3	41.0	94.1	97.9	88.7
Cr	2198	2087	2175	2407	1836	3393	3706	3353
Co	90.1	109	115	119	90.8	92.2	102	88.6
Ni	1392	2164	2249	2285	1737	1248	1328	1202
Cu	12.9	4.84	5.45	5.56	4.05	1.06	1.49	0.936
Zn	67.2	51.2	52.7	59.6	49.8	59.2	70.4	63.5
Ga	5.35	2.99	3.04	3.54	2.66	5.69	6.21	5.63
Rb	0.694	6.83	6.65	6.71	5.61	9.45	9.38	9.04
Sr	27.6	11.3	11.4	11.6	10.0	5.30	5.61	5.19
Y	4.38	1.86	1.92	1.94	1.68	4.09	4.30	4.00
Zr	5.81	3.49	3.39	5.15	3.29	5.29	5.86	5.08
Nb	0.175	0.153	0.154	0.156	0.121	0.126	0.130	0.119
Mo	0.390	0.296	0.358	0.356	0.249	0.178	0.248	0.180
Sn	0.334	0.0695	0.0786	0.0765	0.0962	0.218	0.221	0.172
Cs	<0.037	1.05	1.07	1.07	1.17	0.769	0.798	0.757
Ba	3.60	3.85	3.99	3.98	3.49	1.46	1.72	1.43
La	0.432	0.109	0.0811	0.0799	0.0845	0.478	0.452	0.474
Ce	0.798	0.307	0.262	0.263	0.256	0.979	0.945	0.979
Pr	0.0958	0.0595	0.0538	0.0543	0.0545	0.136	0.131	0.138
Nd	0.415	0.373	0.358	0.355	0.360	0.673	0.647	0.688
Sm	0.159	0.174	0.166	0.165	0.172	0.252	0.238	0.259
Eu	0.0670	0.0454	0.0426	0.0421	0.0447	0.0836	0.0796	0.0856
Gd	0.321	0.267	0.254	0.252	0.263	0.419	0.404	0.433
Tb	0.0772	0.0523	0.0501	0.0500	0.0516	0.0894	0.0874	0.0935
Dy	0.645	0.367	0.356	0.356	0.363	0.694	0.677	0.720
Ho	0.159	0.0791	0.0772	0.0769	0.0781	0.163	0.160	0.170
Er	0.505	0.224	0.218	0.218	0.222	0.500	0.490	0.520
Tm	0.0814	0.0348	0.0338	0.0337	0.0343	0.0797	0.0789	0.0832
Yb	0.564	0.242	0.235	0.236	0.236	0.559	0.546	0.577
Lu	0.0923	0.0417	0.0412	0.0408	0.0408	0.0899	0.0885	0.0935
Hf	0.190	0.141	0.119	0.156	0.141	0.206	0.190	0.215
Ta	<0.014	<0.014	<0.014	0.0120	<0.014	<0.014	<0.014	<0.014
W	0.244	0.326	0.340	0.338	0.306	0.232	0.244	0.245
Pb	1.94	0.401	0.406	0.388	0.430	0.882	0.879	0.898
Th	0.0721	0.0214	0.0200	0.0204	0.0190	0.0457	0.0458	0.0443
U	0.182	<0.019	<0.019	<0.019	<0.019	0.105	0.0985	0.0947

R: replicate analysis

Table B-1 continued

Method	1	2	2	3	1	3	1	1
Location	SOISB2	SOISB2	SOISB2	SOISB2	SOISB2	SOISB2	SOISB3	SOISB3
Sample	10-32	10-32-RI	10-32-RII	10-32-RIII	10-35	10-35-R	10-16	10-27
Peridotite type	2	2	2	2	4	4	2	3
Li	10.7	10.6	10.9	10.7	10.3	11.8	7.94	7.25
Sc	19.9	21.6	22.8	18.3	16.6	15.4	14.9	18.4
V	89.5	96.9	101	87.8	87.4	78.7	79.8	90.7
Cr	2723	3884	3894	3574	1580	1600	1277	1669
Co	82.4	98.1	101	87.8	59.8	56.4	123	79.2
Ni	1461	1569	1606	1431	777	724	2118	1376
Cu	2.55	2.98	3.00	2.39	3.21	2.80	18.1	1.45
Zn	49.6	71.8	75.0	69.9	27.1	26.8	67.7	35.3
Ga	4.77	7.00	7.29	6.53	4.82	5.03	4.02	3.13
Rb	0.369	0.348	0.356	0.398	0.696	0.603	<0.2	0.410
Sr	22.0	21.4	22.2	21.5	14.2	13.7	11.5	25.7
Y	4.42	4.50	4.65	4.31	3.97	3.87	5.48	4.88
Zr	7.40	7.90	8.16	6.93	4.69	4.47	13.59	7.54
Nb	0.238	0.243	0.256	0.227	0.175	0.161	0.500	0.222
Mo	0.253	0.325	0.291	0.256	0.329	0.202	0.221	0.187
Sn	0.128	0.273	0.0793	0.0779	0.245	0.189	0.215	0.115
Cs	<0.037	<0.037	<0.037	<0.037	<0.037	<0.037	<0.037	<0.037
Ba	3.50	3.59	3.73	3.53	2.65	2.71	4.55	1.98
La	0.748	0.684	0.711	0.746	0.630	0.634	1.00	0.419
Ce	1.72	1.59	1.66	1.73	1.39	1.41	2.61	1.30
Pr	0.243	0.226	0.234	0.248	0.185	0.192	0.416	0.230
Nd	1.17	1.09	1.13	1.19	0.831	0.880	2.30	1.31
Sm	0.368	0.338	0.352	0.381	0.251	0.270	0.893	0.494
Eu	0.126	0.116	0.122	0.132	0.251	0.270	0.284	0.161
Gd	0.543	0.495	0.515	0.552	0.400	0.423	1.19	0.690
Tb	0.107	0.101	0.104	0.111	0.0842	0.0911	0.204	0.129
Dy	0.785	0.741	0.766	0.818	0.666	0.713	1.27	0.909
Ho	0.178	0.169	0.175	0.186	0.158	0.170	0.247	0.199
Er	0.536	0.503	0.524	0.558	0.492	0.530	0.648	0.583
Tm	0.0835	0.0783	0.0814	0.0863	0.0789	0.0851	0.0907	0.0908
Yb	0.566	0.531	0.553	0.586	0.547	0.590	0.568	0.617
Lu	0.0900	0.0838	0.0880	0.0930	0.0884	0.0954	0.0844	0.0978
Hf	0.272	0.240	0.248	0.279	0.179	0.194	0.460	0.270
Ta	0.0137	0.0157	0.0161	0.0138	<0.014	<0.014	0.0299	0.0136
W	0.173	0.168	0.165	0.320	0.154	0.162	0.174	<0.076
Pb	0.730	0.638	0.666	0.745	0.880	0.914	0.797	1.844
Th	0.0585	0.0568	0.0588	0.0593	0.0437	0.0443	0.0849	0.0301
U	0.0450	0.0433	0.0460	0.0458	0.0609	0.0628	0.0421	<0.019

R: replicate analysis

Table B-1 continued

Method	3	1	3	1	1	1	1	1
Location	SOISB3	SOISB3	SOISB3	NUB	NUB	NUB	NUB	NUB
Sample	10-27-R	10-28	10-28-R	10-09	10-10	10-11	10-11-R	10-12B
Peridotite type	3	3	3	1	1	1	1	1
Li	7.65	7.98	8.60	10.6	6.92	7.30	7.30	7.74
Sc	18.0	19.2	17.8	8.07	8.22	6.04	6.04	6.67
V	91.3	83.9	79.3	43.5	49.8	30.1	30.1	30.1
Cr	2300	1862	2424	5262	4941	7622	7622	4761
Co	84.0	89.4	89.8	115	110	119	119	99
Ni	1355	1274	1192	1897	1798	2411	2411	2268
Cu	1.34	2.38	1.89	0.40	0.51	0.41	0.41	1.27
Zn	54.2	42.3	63.8	54.5	48.3	81.3	81.3	66.4
Ga	4.41	3.86	5.14	2.31	2.60	1.33	1.33	1.85
Rb	0.530	0.560	0.571	2.76	0.935	1.05	1.05	0.281
Sr	24.5	33.1	31.5	1.73	5.89	0.942	0.942	3.59
Y	4.74	4.40	4.24	1.72	2.12	0.652	0.652	2.33
Zr	7.23	7.83	7.52	3.46	3.38	1.56	1.56	2.19
Nb	0.211	0.243	0.229	0.111	0.182	0.0896	0.0896	0.171
Mo	0.195	0.327	0.234	0.256	0.263	0.497	0.497	0.293
Sn	0.116	0.0939	0.0981	0.131	0.201	0.130	0.130	0.138
Cs	<0.037	<0.037	<0.037	0.307	<0.037	0.199	0.199	0.041
Ba	1.97	6.23	6.21	1.40	3.2	0.621	0.621	0.456
La	0.409	0.409	0.403	0.222	0.374	0.0772	0.0772	0.509
Ce	1.28	1.18	1.17	0.610	1.01	0.214	0.214	1.21
Pr	0.233	0.203	0.207	0.100	0.162	0.0352	0.0352	0.179
Nd	1.34	1.14	1.17	0.541	0.851	0.186	0.186	0.880
Sm	0.505	0.428	0.443	0.200	0.285	<0.091	0.0656	0.281
Eu	0.165	0.166	0.175	0.0773	0.0584	<0.028	0.0194	0.0813
Gd	0.704	0.613	0.630	0.273	0.359	0.0887	0.0887	0.360
Tb	0.134	0.116	0.122	0.0494	0.0640	0.0169	0.0169	0.0654
Dy	0.937	0.824	0.862	0.340	0.4201	0.1160	0.1160	0.4410
Ho	0.206	0.182	0.190	0.0723	0.0884	0.0253	0.0253	0.0961
Er	0.605	0.531	0.560	0.206	0.250	0.075	0.075	0.278
Tm	0.0936	0.0823	0.0871	0.0321	0.0377	<0.013	0.0122	0.0435
Yb	0.635	0.564	0.589	0.218	0.251	0.0847	0.0847	0.291
Lu	0.101	0.0891	0.0940	0.0346	0.0393	<0.015	0.0143	0.0433
Hf	0.279	0.281	0.296	0.133	0.125	<0.048	0.042	0.082
Ta	0.0140	0.0154	0.0161	0.00796	<0.014	<0.014	0.00618	<0.014
W	<0.076	<0.076	<0.076	0.0849	0.113	0.0620	0.0620	0.141
Pb	2.01	1.45	1.50	0.446	0.404	0.185	0.185	0.311
Th	0.0301	0.0393	0.0378	0.0255	0.0585	0.0178	0.0178	0.0729
U	0.0092	0.0233	0.0236	0.0182	0.0286	0.0374	0.0374	0.0672

R: replicate analysis

Table B-1 continued

Method	1	1	1	1	**1**	**1**	**1**	**1**
Location	NUB	NUB	NUB	NUB	SOISB1	SOISB2	SOISB2	SOISB2
Sample	10-14	10-13	10-12A	10-12A-R	10-21	10-33	10-33-2	10-37
Peridotite type	1	2	4	4	A	A	A	A
Li	9.09	29.8	65.7	44.0	152	12.1	12.0	14.2
Sc	7.75	12.64	6.54	6.99	57.9	41.5	41.6	48.6
V	58.5	62.8	35.1	31.1	278	195	191	219
Cr	6123	2617	6138	6041	103	133	121	628
Co	131	137	103	106	45.2	45.5	45.3	54.1
Ni	1826	1295	1949	1959	58.0	54.5	54.4	150.0
Cu	0.74	1.95	0.32	0.52	6.38	64.7	65.4	49.2
Zn	60.1	66.8	107	111	56.5	65.1	64.9	80.0
Ga	2.62	3.12	7.35	7.52	17.1	17.0	17.0	12.5
Rb	0.421	93.7	71.1	65.2	47.3	1.85	1.85	3.67
Sr	2.12	4.46	4.98	5.27	107	70.5	70.3	106
Y	1.64	2.53	1.29	1.33	18.3	17.1	17.0	17.1
Zr	2.53	4.72	33.5	37.5	40.0	25.0	19.4	48.6
Nb	0.123	0.209	2.34	2.31	1.37	1.66	1.64	2.33
Mo	0.257	0.256	0.282	0.327	0.134	0.401	0.401	0.170
Sn	0.282	1.461	0.236	0.244	0.347	0.451	0.402	0.599
Cs	<0.037	13.0	5.85	5.79	4.20	<0.037	<0.037	<0.037
Ba	0.117	17.3	73.0	68.2	122	11.5	11.5	15.1
La	0.179	0.969	6.53	6.55	1.84	3.50	3.53	4.94
Ce	0.498	2.06	10.6	10.6	5.03	8.26	8.26	11.34
Pr	0.0883	0.248	1.04	1.04	0.866	1.21	1.20	1.65
Nd	0.501	1.01	3.41	3.40	4.89	5.99	5.95	8.14
Sm	0.192	0.300	0.521	0.503	1.80	1.86	1.87	2.48
Eu	0.0502	0.211	0.0490	0.0441	0.679	0.677	0.673	0.762
Gd	0.259	0.409	0.454	0.388	2.50	2.48	2.49	3.02
Tb	0.0473	0.0744	0.0517	0.0488	0.472	0.459	0.460	0.524
Dy	0.321	0.506	0.264	0.251	3.26	3.15	3.17	3.37
Ho	0.0686	0.109	0.0509	0.0480	0.701	0.680	0.683	0.683
Er	0.198	0.314	0.151	0.142	2.00	1.95	1.97	1.86
Tm	0.0308	0.0480	0.0252	0.0232	0.305	0.295	0.297	0.270
Yb	0.208	0.321	0.190	0.178	2.04	1.98	1.99	1.74
Lu	0.0332	0.0502	0.0355	0.0337	0.317	0.308	0.309	0.263
Hf	0.096	0.174	1.119	1.085	1.15	0.884	0.756	1.30
Ta	<0.014	<0.014	0.219	0.260	0.097	0.114	0.113	0.166
W	<0.076	0.211	0.102	0.0899	0.320	0.589	0.585	0.174
Pb	0.409	1.19	1.49	1.51	7.22	2.41	2.40	4.25
Th	0.0411	0.0449	3.83	4.12	0.298	0.419	0.420	0.658
U	0.0237	0.0444	0.292	0.233	0.094	0.123	0.116	0.166

A: amphibolite

R: replicate analysis

Table B-1 continued

Method	1	1	1	1	**1**
Location	SOISB3	NUB	NUB	NUB	SOISB1
Sample	10-17	10-26	10-40	10-15	10-15-R
Peridotite type	A	A	A	A	A
Li	34.8	34.3	27.7	129	128
Sc	43.4	48.8	47.6	62.5	64.0
V	261	308	217	337	342
Cr	204	140	171	80.1	73.8
Co	52.5	45.0	55.2	50.7	51.4
Ni	69.5	86.3	64.3	62.2	63.0
Cu	99.8	12.4	14.7	11.2	11.5
Zn	94.8	86.8	117	124	125
Ga	19.5	17.7	20.1	20.3	20.5
Rb	2.48	4.39	13.5	93.4	94.0
Sr	124	92.9	142	69.5	70.1
Y	20.8	23.4	25.6	27.0	27.2
Zr	53.4	48.9	47.7	37.8	36.7
Nb	2.14	2.79	2.62	3.01	3.03
Mo	0.246	0.341	0.355	0.490	0.707
Sn	0.623	0.717	0.717	2.24	2.26
Cs	<0.037	<0.037	0.566	5.19	5.23
Ba	24.4	36.2	79.8	208	208
La	3.82	3.51	4.50	1.61	1.62
Ce	9.63	10.2	11.6	5.21	5.24
Pr	1.46	1.62	1.91	0.914	0.912
Nd	7.44	8.36	10.1	5.12	5.13
Sm	2.37	2.70	3.27	2.15	2.16
Eu	0.782	0.930	1.04	0.854	0.860
Gd	3.13	3.48	4.10	3.27	3.29
Tb	0.567	0.630	0.723	0.648	0.652
Dy	3.81	4.23	4.74	4.61	4.62
Ho	0.797	0.896	0.990	1.01	1.01
Er	2.24	2.55	2.76	2.93	2.94
Tm	0.332	0.383	0.411	0.450	0.450
Yb	2.16	2.55	2.71	3.03	3.02
Lu	0.327	0.394	0.417	0.471	0.470
Hf	1.48	1.35	1.48	1.19	1.17
Ta	0.142	0.185	0.175	0.191	0.191
W	0.232	0.399	0.748	0.151	0.179
Pb	4.95	3.74	6.65	8.67	8.62
Th	0.531	0.405	0.303	0.0788	0.0771
U	0.148	0.104	0.107	0.451	0.443

Table B-1 continued

Method	1	1	1	3	1	1	1	2
Name	UB-N	BVO-2	BIR-Köln	BIR-Köln Replicate	DTS-1	DTS-1 Replicate	DTS-2b	DTS-2b Replicate
Li	47.0	4.58	3.70	3.09	2.26	2.20	2.22	2.09
Sc	12.6	32.1	44.1	26.8	3.58	3.54	3.15	3.12
V	65.6	313	319	203	15.8	11.7	27.5	24.8
Cr	2254	269	435	318	4058	3852	15024	14777
Co	100	44.7	56.7	39.5	140	126	134	122
Ni	1845	116	197	137	2218	1979	3448	3052
Cu	27.5	127	130	94.8	4.97	6.70	2.62	2.60
Zn	73.1	102	71.0	54.1	50.0	49.7	49.0	50.2
Ga	2.54	22.0	15.7	13.1	0.435	0.403	1.03	1.02
Rb	3.30	9.45	0.255	0.232	0.0588	0.0572	< 0.23	0.0218
Sr	7.07	404	104	95.3	0.186	0.361	0.370	0.589
Y	2.58	25.3	15.9	14.6	< 0.07	0.0357	< 0.07	0.0375
Zr	3.67	173	14.9	13.2	< 0.2	0.160	< 0.2	0.171
Nb	0.0500	18.3	0.556	0.487	0.0232	0.0242	0.0347	0.046
Mo	0.472	3.83	<0.07	<0.07	0.247	0.319	0.321	0.466
Sn	0.364	1.77	0.290	0.247		0.513	0.598	0.599
Cs	10.1	0.113	<0.037	<0.037	0.007	0.00894	< 0.037	< 0.037
Ba	22.3	141	6.54	6.6832	0.096	0.506	11.6	13.0
La	0.341	16.1	0.667	0.6761	0.0356	0.0252	0.0248	0.0145
Ce	0.826	38.0	2.02	2.0509	0.0565	0.0519	0.0336	0.0281
Pr	0.125	5.60	0.396	0.4073	< 0.013	0.00675	< 0.013	0.00371
Nd	0.660	26.2	2.53	2.5958	< 0.08	0.0260	< 0.08	0.0167
Sm	0.247	6.48	1.17	1.2003	<0.091	<0.091	< 0.003	0.00573
Eu	0.0936	2.20	0.550	0.5682	<0.028	<0.028	< 0.001	0.00242
Gd	0.351	6.54	1.87	1.9288	< 0.082	0.00678	< 0.003	0.00579
Tb	0.0667	0.992	0.369	0.3854	<0.013	<0.013	<0.013	0.00096
Dy	0.468	5.62	2.67	2.77	<0.053	<0.053	<0.053	0.00643
Ho	0.103	1.03	0.589	0.6087	< 0.013	< 0.013	< 0.013	0.00168
Er	0.302	2.57	1.68	1.7556	<0.040	<0.040	<0.040	0.00608
Tm	0.0477	0.341	0.255	0.2627	<0.013	<0.013	<0.013	0.00138
Yb	0.322	2.08	1.70	1.75	0.01836	0.01185	0.0138	0.01230
Lu	0.0518	0.298	0.263	0.2709	<0.015	<0.015	<0.015	0.00275
Hf	0.138	4.21	0.605	0.6089	<0.048	<0.048	<0.048	0.00558
Ta	< 0.014	1.22	0.0365	0.0341	<0.014	<0.014	<0.014	0.00373
W	0.0539	0.255	<0.059	<0.059	<0.059	<0.059	<0.059	0.0174
Pb	12.4	1.65	0.581	0.6158	8.54	7.96	3.74	3.89
Th	0.0564	1.25	0.0502	0.0472	<0.019	<0.019	<0.019	0.00391
U	0.0483	0.426	< 0.076	< 0.076	< 0.076	< 0.076	< 0.076	<0.015

Table B-2 Lu-Hf MC-ICP-MS replicate (R) measurements of peridotites from SOISB and NUB. Initial εHf values were calculated using the CHUR values of Bouvier et al. (2008), the ^{176}Lu decay constant of 1.867 × 10−12 a^{-1} of Scherer et al. (2001) and Söderlund et al. (2004). Initial εHf were calculated to 3.81 Ga (minimum ages obtained from field relationships).

Sample	Type	Lu [ppm]	Hf [ppm]	Lu/Hf	^{176}Lu/^{177}Hf	^{176}Hf/^{177}Hf	$\varepsilon Hf_{(t)}$
SOISB1							(3.81Ga)
10-20C-RI	1	0.0291	0.154	0.1885	0.02675 ±7	0.282362 ±7	+0.3 ±0.5
10-23-RI	1	0.00852	0.0275	0.3101	0.04473 ±15	0.283787 ±34	+6.5 ±1.2
SOISB2							
10-34-RI	1	0.0684	0.106	0.6471	0.09190 ±23	0.287088 ±7	-1.5 ±0.5
10-36-RI	1	0.0791	0.159	0.4965	0.07055 ±18	0.285484 ±6	-0.9 ±0.6
10-29A-RI	2	0.0624	0.134	0.4668	0.06629 ±17	0.285363 ±7	+6.0 ±0.6
10-29B-RI	2	0.0840	0.195	0.4308	0.06117 ±15	0.284966 ±5	+7.2 ±0.5
10-35-RI	4	0.0814	0.173	0.4709	0.06671 ±17	0.285390 ±13	+5.0 ±0.6
10-35-RII	4	0.0809	0.172	0.4697	0.06713 ±17	0.285385 ±9	+4.6 ±0.6
SOISB3							
10-16-RI	2	0.0747	0.474	0.1577	0.02411 ±6	0.282149 ±8	+2.0 ±0.4
10-27-RI	3	0.0886	0.254	0.3482	0.04944 ±12	0.284041 ±6	+3.1 ±0.5
10-27-RII	3	0.0884	0.259	0.3416	0.04847 ±12	0.283984 ±5	+3.3 ±0.5
NUB							
10-09-RI	1	0.0307	0.120	0.2567	0.03643 ±9	0.283082 ±8	+3.2 ±0.5
10-11-RI	1	0.0130	0.0474	0.2765	0.04429 ±13	0.283569 ±46	-0.1 ±1.7
10-12B-RI	1	0.0386	0.0866	0.4453	0.06323 ±16	0.284746 ±9	-8.0 ±0.5
10-13-RI	2	0.0442	0.154	0.2876	0.04078 ±10	0.283375 ±9	+1.9 ±0.5
10-12A-RI	4	0.0307	1.06	0.02901	0.004116 ±1	0.280811 ±7	+7.1 ±0.4
10-12A-RII	4	0.0310	0.980	0.03167	0.004492 ±1	0.280828 ±11	+7.6 ±0.4

Table B-3 Sm-Nd MC-ICP-MS replicate (R) analyses of peridotites from NUB and SOISB. Initial εNd values were calculated using the CHUR values of Bouvier et al. (2008), ^{146}Sm decay constant of 6.54 × 10-12 a-1 (Lugmaier and Marti, 1978). Initial εNd were calculated to 3.81 Ga (minimum ages obtained from field relationships)

Sample	Type	Sm [ppm]	Nd [ppm]	Sm/Nd	$^{147}Sm/^{144}Nd$	$^{143}Nd/^{144}Nd$	$\varepsilon Nd_{(t)}$ (3.81Ga)
SOISB1							
10-20C-R1	1	0.276	0.836	0.3300	0.1995 ±4	0.512900 ±12	+3.6 ±0.4
10-20C-R2	1	0.275	0.833	0.3302	0.1996 ±4	0.512857 ±7	+2.7 ±0.4
10-22-R1	1	0.0806	0.204	0.3955	0.2392 ±5	0.513723 ±7	+0.1 ±0.5
10-23-R1	1	0.0421	0.137	0.3082	0.1863 ±4	0.512637 ±22	+5.0 ±0.5
SOISB2							
10-34-R1	1	0.650	1.582	0.4111	0.2486 ±5	0.513961 ±7	+0.1 ±0.5
10-36-R1	1	0.138	0.382	0.3620	0.2189 ±4	0.513461 ±11	+5.0 ±0.5
10-36-R2	1	0.139	0.386	0.3611	0.2184 ±4	0.513521 ±8	+6.4 ±0.4
10-29A-R1	2	0.0927	0.224	0.4145	0.2507 ±5	0.514156 ±13	+2.9 ±0.5
10-29A-R2	2	0.0898	0.219	0.4103	0.2482 ±5	0.514185 ±23	+4.7 ±0.5
10-29B-R1	2	0.133	0.357	0.3724	0.2252 ±5	0.513655 ±8	+5.7 ±0.5
10-35-R1	4	0.389	0.686	0.5679	0.1813 ±4	0.512574 ±12	+6.2 ±0.4
SOISB3							
10-27-R1	3	0.402	1.081	0.3717	0.2248 ±4	0.513568 ±9	+4.2 ±0.5
10-27-R2	3	0.399	1.07	0.3720	0.2250 ±4	0.513476 ±7	+2.3 ±0.5
10-27-R3	3	0.449	1.21	0.3718	0.2248 ±4	0.513479 ±8	+2.4 ±0.5
NUB							
10-09-R1	1	0.159	0.445	0.3585	0.2168 ±4	0.513415 ±12	+5.1 ±0.4
10-12B-R1	1	0.226	0.722	0.3132	0.1893 ±4	0.512685 ±9	+4.4 ±0.4
10-12B-R2	1	n.a.	0.697		±4	0.512592 ±9	+1.6 ±0.4
10-13-R1	2	0.238	0.829	0.2866	0.1733 ±3	0.512411 ±8	+7.0 ±0.4
10-13-R2	2	0.238	0.836	0.2847	0.1721 ±3	0.512348 ±7	+6.3 ±0.4
10-12A-R1	4	0.435	2.96	0.1468	0.08868 ±4	0.510311 ±8	+7.7 ±0.4
10-12A-R2	4	0.442	2.98	0.1482	0.08952 ±2	0.510316 ±7	+7.3 ±0.4

Table B-4: Zr-Nb-Ta-W MC-ICP-MS replicate (R) measurements of peridotites from NUB and SOISB

	Sample [mg]	Type	Zr [ppm]	Nb [ppm]	Ta [ppm]	W [ppm]
SOISB1						
10-20C-R1	240	1	4.19*		0.00829	0.278*
10-20C-R2	240	1	4.58*	0.249*****	0.00805	n.a.
10-20C-R3	120	1	4.94*			n.a.
10-22-R1	240	1	0.663*****	0.0578	0.00265	n.a.
10-22-R2	120	1				0.402
10-23-R1	240	1	0.889*	0.0774	0.00377	0.395
SOISB2						
10-34-R1	240	1	2.96*	0.103*	0.00518	n.a.
10-34-R2	120	1	3.29*			5.52
10-34-R3	120	1	2.89*			n.a.
10-36-R1	240	1	4.01*	0.161*	0.00734	n.a.
10-36-R2	240	1	4.65*	0.128*	0.00759	0.497
10-36-R3	240	1			0.00750	0.502
10-36-R4	120	1	4.40*			0.500
10-29A-1	240	2	3.52	0.120	0.00363	n.a.
10-29A-2	120	2	3.62			n.a.
10-29A-3	120	2	3.51			1.45
10-29B-1	240	2	5.11	0.207*	0.00626	n.a.
10-29B-2	120	2	5.19			0.265
10-29B-3	120	2	5.24			n.a.
10-30-R1	120	2	3.55			0.298
10-31-R1*	120	2	5.21			n.a.
10-32-R1	120	2	7.12			n.a.
10-35-R1	240	4	4.67	0.175	0.00636	0.128
10-35-R2	120	4	4.71			
SOISB3						
10-16-R1	240	2	13.9	0.431	0.0313	0.125
10-27-R1	240	3	7.37		0.0132	n.a.
10-27-R2	240	3	7.59	0.244	0.0132	n.a.
10-27-R3	120	3	7.37	0.202		n.a.
10-28-R1	240	3	7.73	0.237	0.0161	0.0481
NUB						
10-09-R1	240	1	3.21	0.100		n.a.
10-11-R1	240	1	0.960		0.00398	n.a.
10-12B-R1	240	1	2.84	0.162	0.00740	0.116
10-12B-R2	240	1	2.79	0.269	0.00718	n.a.
10-14-R1	240	1	2.55*	0.112	0.00558	0.0465
10-13-R1	240	2	4.46*	0.234*	0.00993	n.a.
10-13-R2	120	2	5.88*	0.186*	0.0104	n.a.
10-12A-R1	240	4	30.2	2.40*****	0.243	n.a.
10-12A-R2	120	4	31.9	2.12*	0.225	n.a.

* The reproducibility of replicate measurements of samples were above ± 6%, due to very low concentrations or to sample heterogeneity. n.a. = no W- aliquot

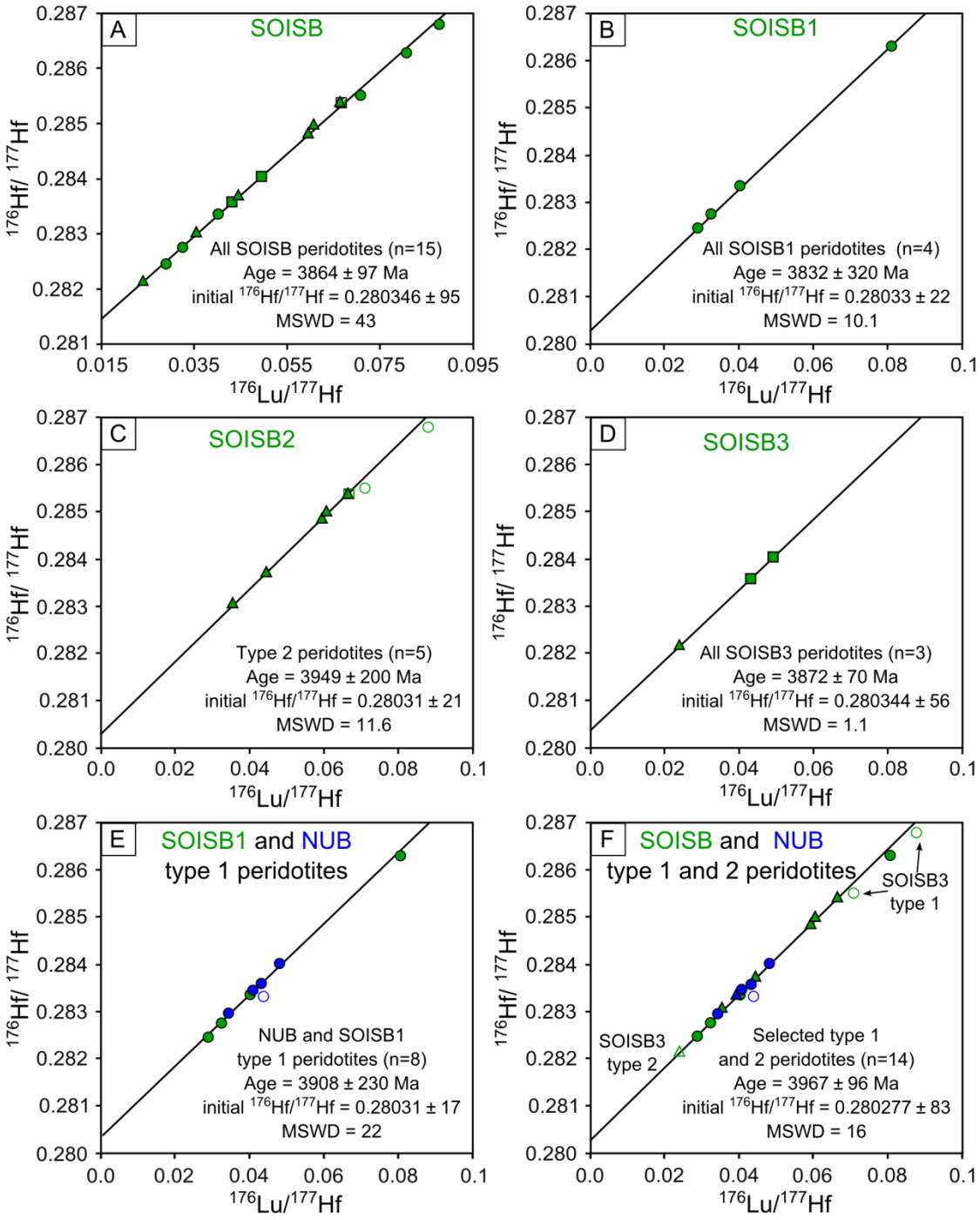

Figure B-1: Measured $^{176}Lu/^{177}Hf$ versus $^{176}Hf/^{177}Hf$ data obtained for peridotites of this study and age regression lines calculated using Isoplot (version 3.41d, Ludwig, 2006). The Lu-Hf whole rock age regression lines obtained for the peridotites overlap in the corresponding ages within error, independent of location or origin. The Panels show the isotope data and regression lines grouped according to location or type; (A) all type 1, 2 and 4 peridotites from SOISB; (B) all peridotites from SOISB1; (C) all type 2 peridotites from SOISB2; (D) all peridotites from SOISB3; (E) type 1 peridotites from NUB and SOISB1, except altered sample 10-12B (open symbol); (F) pooled type 1 and 2 peridotites from SOISB1, SOISB2 and NUB. Symbols are equivalent to those in Fig. S2, open symbols indicate those samples not being included in the regression line calculations.

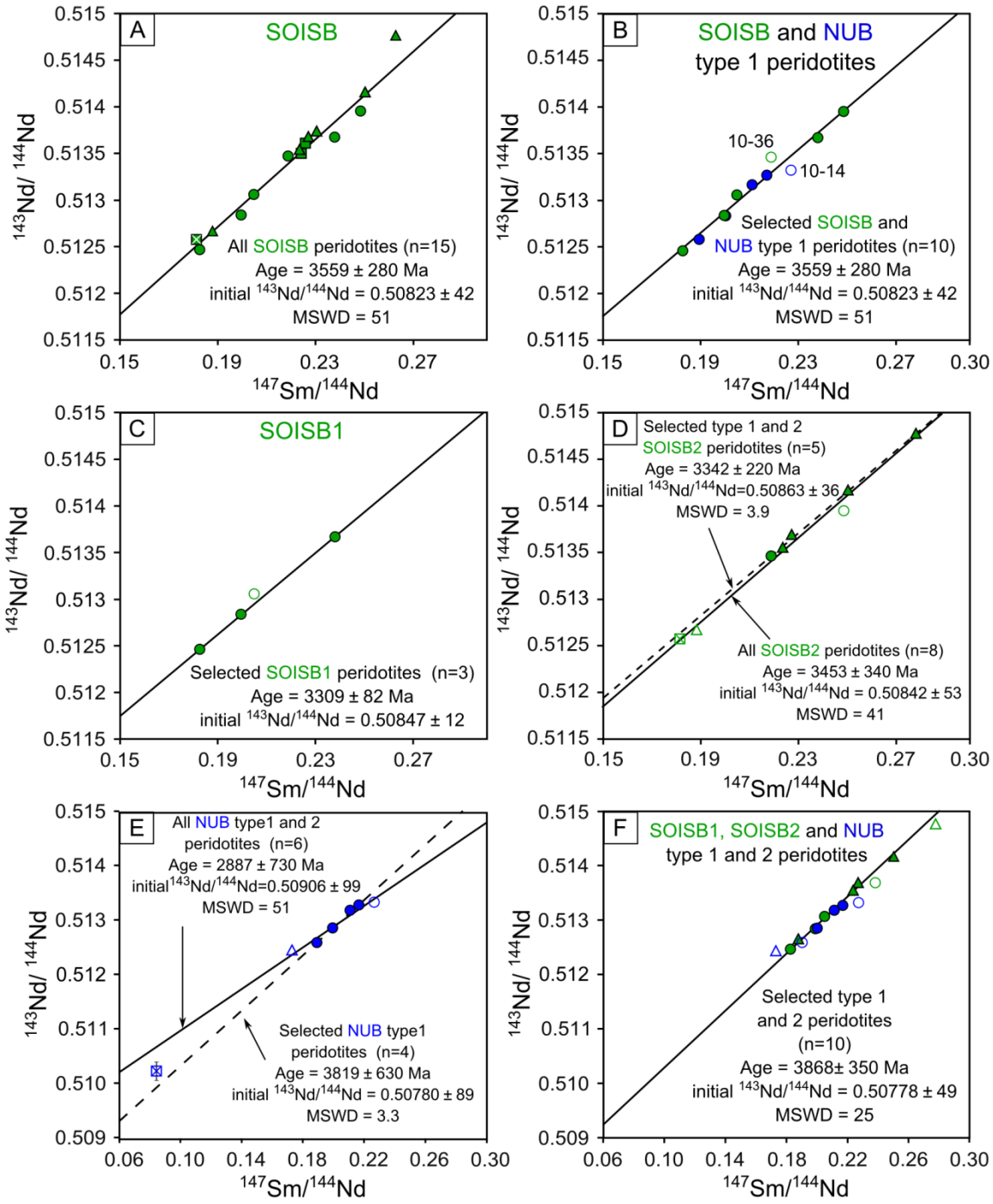

Figure B-2: Measured $^{143}Nd/^{144}Nd$ versus $^{147}Sm/^{144}Nd$ obtained from peridotites with age regression lines calculated using Isoplot (version 3.41d, Ludwig, 2006). The ^{147}Sm–^{143}Nd data generally show a smaller spread and larger scatter on the regression lines than the ^{176}Lu-^{176}Hf data. The Panels show Sm-Nd regression lines for peridotites, (A) all type 1, 2 and 4 peridotites from SOISB; (B) NUB and SOISB type 1 peridotites, except 10-14 and 10-36 (open symbols); (C) all SOISB1 peridotites; (D) all SOISB2 peridotites and selected type 1 and 2 peridotites (dashed line); (E) all NUB type 1 and 2 peridotites and NUB type 1 peridotites, except sample 10-14 (open symbol) and type 1 peridotites, except 10-14 (dashed line); (F) subset (n=10) of type 1 and type 2 peridotites that define the Lu-Hf age regression line Fig. S7F (n=14).

B-2 MANTLE MELTING AND RE-FERTILIZATION MODELS

B-2.1 Partition coefficients

The available trace element mineral/melt partition coefficients data sets are internally inconsistent for a single set of olivine-orthopyroxene-clinopyroxene±spinel for hydrous melting in the spinel stability field at a single pressure and a single temperature. Furthermore, the data sets strongly vary in the included list of trace elements (e.g., compilation by Scott et al., 2016).

Two combined mineral/melt partition coefficients data sets seem to be the most appropriate ones for our model; mineral/melt partition coefficients (set A) from McDade et al. (2003a and 2003b) and (set B) Green (2000) and Adam and Green (2006) (Table C-5).

Table B-5: Melt/rock partition coefficient compilation and mineral modes used for mantle melting-models.

	A			B		
	McDade et al., 2003a	McDade et al., 2003a	McDade et al., 2003b	Adam & Green (2006)	Green et al. (2000)	Adam & Green (2006)
T [°C]	1245	1245	1315	1100	1080	1080
P [GPa]	1.3 hydrous	1.3 hydrous	1.5 anhydrous	2 hydrous	2 hydrous	2 hydrous
	D_{cpx}	D_{opx}	$D_{olivine}$	D_{cpx}	D_{opx}	$D_{olivine}$
Th	0.021*	0.0032*	0.000112	0.007	0.027	0.00017
Nb	0.008	0.0028	0.0001	0.004	0.02	0.0007
Ta	0.022	0.0041		0.011	0.053	0.0002
La	0.043	0.003	0.0000082	0.047	0.089	0.0001
Ce	0.089	0.005	0.000039	0.083	0.16	0.0001
Sr	0.077	0.0044		0.102	0.062	0.00002
Nd	0.211	0.009	0.00021	0.19	0.36	0.0005
Zr	0.103	0.027	0.000107	0.11	0.27	0.001
Hf	0.206	0.062	0.013	0.25	0.55	0.0008
Sm	0.363	0.021	0.00059	0.35	0.67	0.001
Eu	0.449	0.031	0.00036		0.38	
Ti	0.296	0.141	0.017	0.28		0.011
Y	0.561	0.101	0.008	0.53	1.27	0.003
Er	0.578	0.121	0.00965		1.44	
Yb	0.543	0.164	0.0228	0.39	1.43	0.05
Lu	0.52	0.186	0.02495	0.49	1.48	0.024

* McDade et al. 2003b, melt/rock partition coefficients

Mineral mode

	clinopyroxene	orthopyroxene	olivine
hbl-P	18	29	53
Dunites		23	71

Set (A) is the preferred one. It was used for the peridotite melting--models (Figs. 5-13, 5-14 and B-3) and for the amphibolite meltig-model (Fig. 5-15). The advantage of set (A) is, that it provides consistent mineral/melt partition coefficients at the same pressure (1.3GPa) and temperature (1245°C) at hydrous conditions for orthopyroxene (opx) and clinopyroxene (cpx) (McDade et al., 2003a) and for olivine (McDade et al. 2003b) at a similar pressure and temperature (1.5GPa and 1315°C). The olivine partition coefficients were obtained for

anhydrous melting, yet water appears to have a negligible effect on olivine-melt partition coefficients (e.g., McDade et al., 2003a). Moreover, set A includes cpx- and opx/melt partition coefficients for Er and Eu for opx, cpx and olivine in contrast to set (B).

Figure B-3A illustrates that the differences in the trace element patterns are small (< 10%), if both sets of partition coefficients are used for the melting-models, except for Th, Nb and Ta. Note that the mineral/melt partition coefficient data set from McDade et al. (2003a) for hydrous melting does not include cpx- and opx/melt partition coefficients for Th. Thus, those for anhydrous melting from McDade et al. (2003b) were used. In general, all trace elements, as well as Th, are more incompatible in clinopyroxene and orthopyroxene during hydrous melting than during anhydrous melting (e.g., McDade et al. 2003a; Adam and Green, 2006; Scott et al. 2016). Hence, the Th content was overestimated in the residue using mineral/melt partition coefficient set A (Fig. B-3B). However, Th concentrations are extremely low in mantle residues after > 15% melt extraction and thus, the Th concentrations in the re-fertilized peridotites depend on the concentration in the re-fertilizing agent. This fact is illustrated in Fig. S10A. Likewise, Nb and Ta concentrations in the re-fertilized peridotites are dominated by the concentrations in the re-fertilizing agent (Fig. B-3A). Hence, the use of mineral/melt partition coefficient set B instead of A does not change the conclusions drawn from the melting-re-fertilization-models. The amount of extracted melt is calculated based on the HREE contents and using mineral/melt partition coefficient sets A or B result in similar estimates for the SOISB1 and NUB type 1 peridotites.

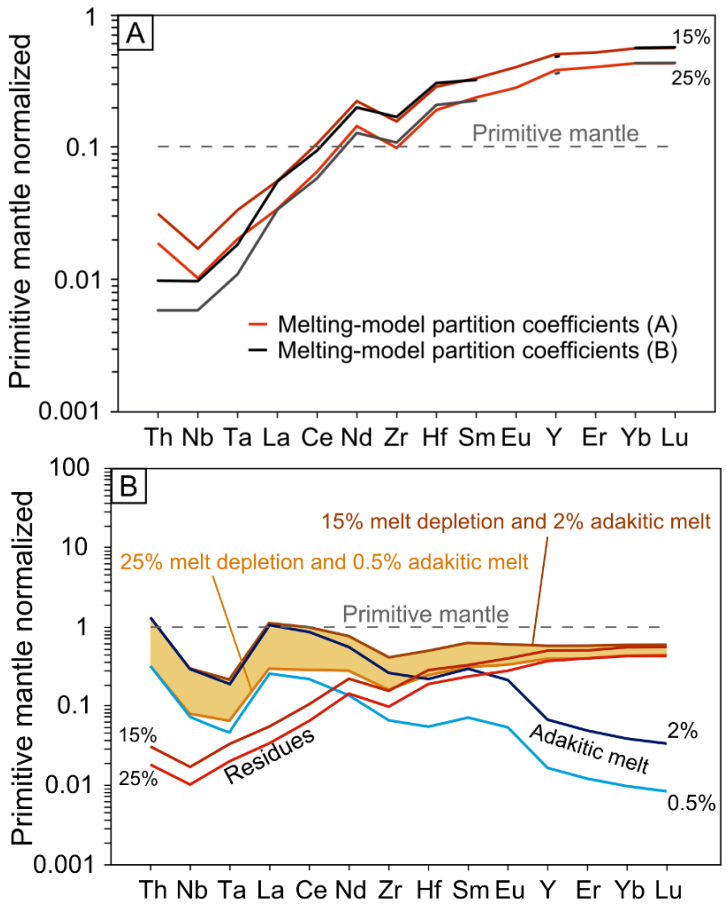

Figure B-3: (A) Primitive mantle normalized melt residues calculated assuming a primitive mantle source and using partition coefficient sets A and B. (B) In order to illustrate the effect 1) melt extraction and 2) subsequent re-fertilization by adakitic melts on the primitive mantle-normalized trace element patterns or the modelled re-fertilized mantle peridotites (Fig. 9). Red and black lines indicate residues after 15% and 25% melt extraction, using partition coefficient set A and B, respectively; blue lines indicate amounts of adakitic melt; the orange field illustrates the modelled range of trace element abundances after 25% of partial melt extraction and addition of 0.5 to 2% of slab-derived adakitic melt (Fig. 9).

B-2 Re-fertilization agent

As re-fertilization agent we used a late Archean (~2.7Ga) high SiO_2 adakite (M96-6), from Wawa subprovince, Superior Province, Canada (Polat and Kerrich 2000), that was interpreted to be derived mainly from slab-melting (Polat and Kerrich 2001; Polat and Münker 2004). This adakite has a similar primitive mantle-normalized pattern than other late Archean and modern high SiO_2, adakitic rocks from late Archean and modern arc-settings, including slab derived adakites (*adakite sensu stricto: pure oceanic slab-melts; Defant and Drummond, 1990; Polat and Kerrich, 2000; Martin et al. 2005) and not necessarily slab-melt derived, but subduction zone related Quaternary adakites (Hidalgo and Rooney, 2014) (Fig. B-4 A-C).

Alternatively, TTGs are potential candidates for the re-fertilisation agent. Figure B-4 D show adakite M96-6 in comparison to TTGs from the IGC (Hoffmann et al., 2014).

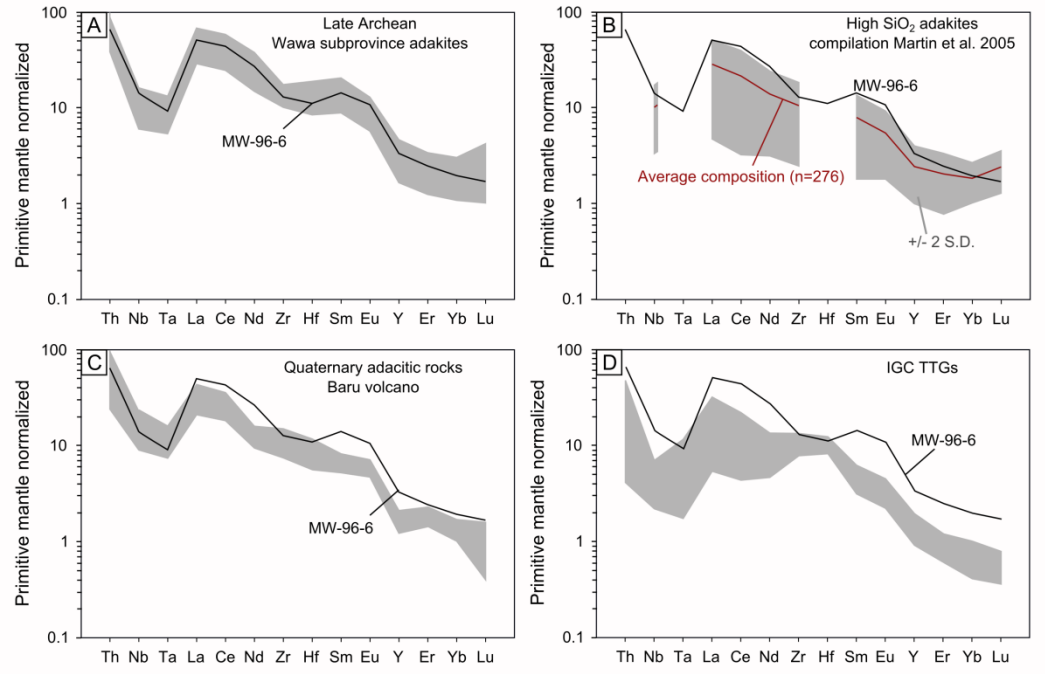

Figure B-4: The ~2.7 Ga Wawa subprovince adakite M96-6, Superior Province, Canada (black line; Polat and Kerrich 2000) in comparison to other adakitic rocks that are characterised by high SiO2, low Cr and Ni, Nb/Ta >1 (A - C) and to Eoarchean IGC TTGs (D). (A) The grey field indicate ~2.7 Ga Wawa subprovince adakites (Polat and Kerrich 2000); (B) The grey field indicate Quaternary adakitic rocks form the Baru volcano, Panama (Hidalgo and Rooney, 2014); In (C) the red line indicate the average composition of the compiled data for high SiO2 adakites and the grey field indicate the ±2 S.D. range (Martin et al., 2005); (D) The grey field indicate Eoarchean TTGs from the IGC (Hoffmann et al., 2014).

In the case of the dunites, a two-step melting-model was applied in order to address clinopyroxene exhaustion at > 25 % partial melting. This two-step melting-model is illustrated in Fig 5-14A. Figure 5-14 show the modelled range of trace element abundances after 30% and 40% of partial melt extraction and addition of 0.3 to 1.5% of slab-derived adakitic melt. Note that the simplified dunite-melting-re-fertilization model fails to reproduce the near flat primitive mantle-normalized trace element patterns, because this simplistic model does not incorporate the full complexity of dunite formation. However, the model can provide rough estimates for the amount of melt extracted (>30%) from the source as well as added re-fertilization agent, which is approximately less than 1.5%.

B-3 Amphibolite formation model

Recent studies proposes formation models for the ISB metabasalts that postulate melting of a depleted and subsequently refertilised mantle source (e.g., Polat et al., 2011; Polat and Hofmann, 2003; Jenner et al., 2009; Hoffmann et al., 2011b). The investigated amphibolites exhibit primitive mantle normalized trace element patterns than tholeiitic meta-basalts from ISB and SOISB with arc-like signatures (Fig. 5-9) (Kamber et al. 2003; Jenner et al. 2009; Hoffmann et al. 2011a; Rizo et al. 2011, 2013; Szilas et al. 2015; Dale et al. 2017). Therefore, the trace element signatures of the amphibolites investigated in this study may reflect a similar enrichment of their mantle source. In order to test if such a re-fertilized mantle source might have had a similar composition than the mantle peridotites investigated in this study we modelled amphibole formation using a well preserve mantle peridotite (10-09). We assume hydrous melting of primitive mantle at the spinel stability field and thus, the mineral/melt partition coefficients set A (Table B5) were used. The model indicates that between 3 to 15% melting of sample 10-09 can produce melts with similar primitive mantle normalized trace element patterns to those obtained for meta-basalts from ISB and SOISB, including the amphibolites investigated in this study (Fig. 5-15). Additionally, the Th/Yb and Nb/Yb ratios for those modelled melts are in the rage of Th/Yb and Nb/Yb ratios reported for ISB tholeiitic meta-basalts (Fig. 5-12B).

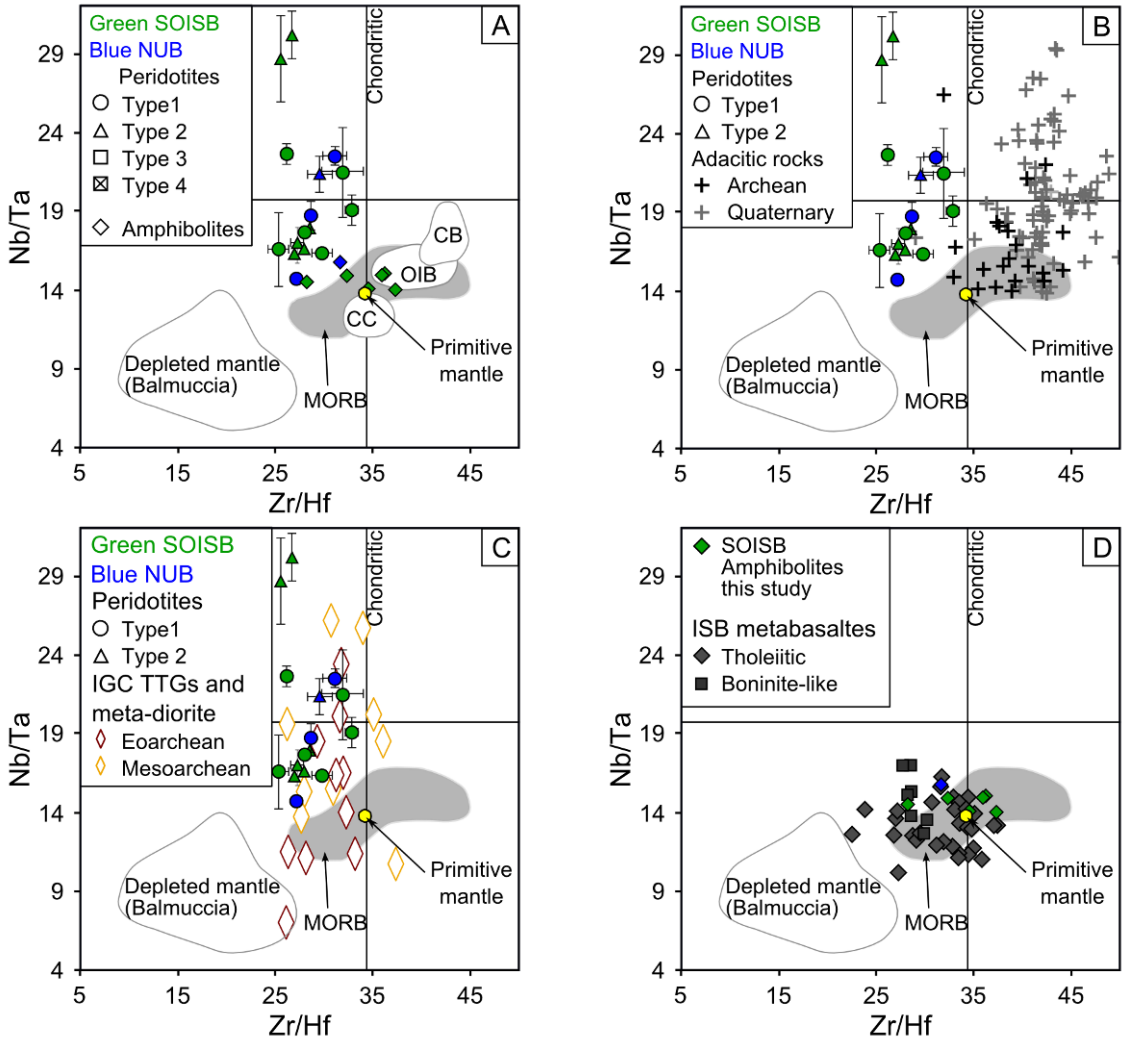

Figure B-5: Nb/Ta versus Zr/Hf diagrams for peridotites and amphibolites of this study in comparison to compiled literature data. (A) Peridotites and amphibolites in comparison to mid-ocean ridge basalts (MORB), continental basalts (CB), continental crust (CC), ocean island basalts (OIB) (Arai, 1994; Bernstein et al., 2006; Haggerty, 1991; Hoog et al., 2010; (Münker et al., 2003), Rollinson, 2007), primitive mantle (Palme and O´Neill, 2014). (B) Type 1 and type 2 peridotites of this study in comparison to Archean adakites (Polat and Kerrich, 2000) and Quaternary adakitic rocks (Hidalgo et al. 2011 and 2014), and (C) to Archean TTGs from Greenland (Hoffmann et al. 2011a, 2014). (D) SOISB amphibolites this study in comparison to tholeiitic and boninite-like metabasalts from the ISB (Polat et al., 2002; Polat and Hofmann, 2003).

Appendix C

Table C-1: Electron microprobe mineral analyses of NUB peridotites [wt.%]

10-09 Nr.	Mineral	Na_2O	FeO	SiO_2	CaO	MgO	MnO	Al_2O_3	NiO	TiO_2	Cr_2O_3	Total
47	Ol	0.06	8.86	40.7	0.01	49.2	0.18	<0.01	0.36	<0.001	0.02	99.4
48	Ol	<0.01	9.14	40.5	<0.01	49.9	0.17	0.01	0.37	<0.001	0.01	100
49	Ol	<0.01	9.19	40.7	0.01	49.1	0.13	<0.01	0.36	<0.001	0.01	99.6
50	Ol	<0.01	9.37	40.7	0.01	49.3	0.17	<0.01	0.34	0.011	0.01	99.9
51	Ol	0.03	8.99	40.4	0.02	49.3	0.20	<0.01	0.37	0.054	<0.01	99.3
52	Ol	0.04	9.06	41.0	<0.01	49.3	0.14	0.03	0.38	0.022	<0.01	100
53	Ol	0.04	9.10	40.3	0.02	48.7	0.18	<0.01	0.34	<0.001	0.01	98.7
54	Ol	0.01	9.22	40.7	0.01	48.4	0.16	<0.01	0.37	<0.001	0.01	99.0
55	Ol	<0.01	9.24	40.6	<0.01	49.4	0.15	<0.01	0.33	0.011	0.01	99.8
56	Ol	<0.01	9.26	40.5	0.01	49.1	0.19	<0.01	0.37	0.049	<0.01	99.5
57	Ol	<0.01	9.26	40.3	<0.01	49.4	0.16	<0.01	0.35	<0.001	<0.01	99.5
58	Ol	<0.01	9.26	39.9	0.02	48.9	0.13	<0.01	0.35	0.043	0.01	98.6
59	Ol	0.06	9.00	40.4	0.03	48.7	0.16	0.03	0.33	0.065	<0.01	98.7
60	Ol	<0.01	9.28	40.6	0.02	49.7	0.19	0.01	0.35	<0.001	0.01	100
63	Ol	<0.01	9.19	40.3	0.01	49.0	0.17	0.02	0.33	0.011	0.01	99.1
64	Ol	<0.01	9.20	40.4	<0.01	49.0	0.19	<0.01	0.36	0.016	<0.01	99.1
65	Ol	<0.01	9.21	40.7	<0.01	49.6	0.14	0.01	0.36	0.022	0.02	100
66	Ol	<0.01	9.10	40.5	<0.01	49.2	0.15	<0.01	0.33	<0.001	0.02	99.4
67	Ol	<0.01	8.83	40.6	<0.01	49.4	0.17	0.02	0.33	<0.001	0.01	99.3
68	Ol	0.02	8.90	40.3	0.01	49.5	0.18	<0.01	0.31	0.016	<0.01	99.2
69	Ol	<0.01	9.11	40.7	0.01	49.6	0.20	0.02	0.35	0.005	<0.01	100
70	Ol	0.07	8.91	40.4	0.01	49.2	0.12	<0.01	0.33	0.027	0.01	99.1
72	Ol	0.02	9.04	42.4	0.01	51.1	0.19	<0.01	0.33	<0.001	0.02	103
74	Ol	<0.01	9.21	40.2	0.01	49.4	0.15	<0.01	0.36	0.038	0.02	99.4
75	Ol	0.02	9.25	40.5	0.01	49.4	0.18	<0.01	0.35	<0.001	0.01	99.7
76	Ol	<0.01	9.36	40.3	0.01	49.2	0.16	<0.01	0.32	0.011	0.01	99.4
77	Ol	0.02	9.08	40.6	0.02	49.3	0.20	<0.01	0.33	0.022	<0.01	99.6
78	Ol	0.03	8.93	40.3	<0.01	49.6	0.12	0.01	0.35	<0.001	0.01	99.3
79	Ol	<0.01	9.31	40.5	0.01	49.9	0.15	<0.01	0.35	0.033	0.01	100
80	Ol	0.01	9.07	40.2	0.02	49.5	0.13	0.02	0.32	<0.001	<0.01	99.3
81	Ol	0.05	8.88	40.3	<0.01	49.6	0.17	<0.01	0.35	<0.001	<0.01	99.3
82	Ol	<0.01	9.34	39.5	<0.01	49.9	0.15	<0.01	0.33	<0.001	<0.01	99.2
83	Ol	<0.01	9.21	39.9	<0.01	49.7	0.13	0.01	0.34	0.033	0.01	99.3
84	Ol	<0.01	9.34	40.3	0.01	49.9	0.14	<0.01	0.34	0.027	<0.01	100
85	Ol	<0.01	9.20	40.1	0.01	49.2	0.14	<0.01	0.32	<0.001	<0.01	99.0
86	Ol	0.03	9.13	40.1	<0.01	48.9	0.14	<0.01	0.34	0.049	0.01	98.7
87	Ol	<0.01	9.26	40.2	0.01	49.1	0.15	<0.01	0.32	<0.001	0.01	99.0
88	Ol	<0.01	9.05	40.3	<0.01	48.7	0.09	<0.01	0.36	<0.001	<0.01	98.5
89	Ol	0.02	9.09	40.3	0.01	49.2	0.13	<0.01	0.38	0.065	0.01	99.2
90	Ol	<0.01	9.16	40.4	<0.01	49.2	0.13	<0.01	0.32	0.005	<0.01	99.1
91	Ol	<0.01	9.08	40.3	<0.01	49.8	0.17	<0.01	0.33	0.027	<0.01	99.7
92	Ol	<0.01	8.83	40.4	0.01	49.4	0.16	0.01	0.37	0.016	<0.01	99.2
97	Ol	0.01	9.08	40.3	<0.01	49.7	0.15	<0.01	0.32	0.027	0.02	99.6
98	Ol	0.02	9.05	40.3	0.02	49.9	0.17	<0.01	0.31	0.005	0.01	99.7
99	Ol	<0.01	8.87	40.1	0.01	49.5	0.21	<0.01	0.34	<0.001	<0.01	99.1
100	Ol	0.01	9.03	40.3	0.01	49.9	0.18	<0.01	0.33	<0.001	<0.01	99.7
101	Ol	<0.01	9.23	40.5	<0.01	49.7	0.19	<0.01	0.36	0.065	<0.01	100
102	Ol	<0.01	8.98	40.5	0.02	49.7	0.19	0.01	0.34	<0.001	<0.01	99.7
103	Ol	<0.01	9.07	40.5	<0.01	50.0	0.10	<0.01	0.34	<0.001	0.02	100
104	Ol	<0.01	8.86	40.7	0.01	49.5	0.16	<0.01	0.30	<0.001	0.01	99.5
105	Ol	<0.01	8.89	40.6	<0.01	49.0	0.12	0.01	0.35	<0.001	<0.01	98.9
106	Ol	<0.01	8.95	40.7	0.01	49.5	0.20	<0.01	0.35	0.033	0.01	99.7
107	Ol	<0.01	8.87	40.0	0.01	49.5	0.15	0.02	0.32	0.038	<0.01	99.0
108	Ol	0.01	8.66	40.0	0.02	49.6	0.15	<0.01	0.33	0.065	0.02	98.9
109	Ol	0.01	8.95	39.9	<0.01	49.2	0.20	0.03	0.34	0.016	0.01	98.7
110	Ol	0.01	8.56	40.1	<0.01	49.1	0.12	<0.01	0.32	<0.001	<0.01	98.2
111	Ol	<0.01	9.13	40.3	0.02	49.6	0.17	<0.01	0.31	<0.001	<0.01	99.5
1	Opx	0.02	6.84	56.1	0.12	34.5	0.22	1.29	0.07	0.027	0.15	99.4
2	Opx	<0.01	6.56	55.9	0.13	33.9	0.14	1.60	0.07	0.066	0.16	98.6
3	Opx	0.01	6.85	55.9	0.11	34.1	0.19	1.83	0.06	0.087	0.15	99.2
4	Opx	0.02	6.71	55.7	0.09	34.2	0.16	1.67	0.07	0.066	0.14	98.8
5	Opx	0.01	6.63	56.5	0.11	34.3	0.22	0.91	0.04	<0.001	0.13	98.8
6	Opx	0.02	6.70	56.6	0.10	34.3	0.18	1.10	0.06	<0.001	0.15	99.3
7	Amph 1	0.38	2.12	56.4	12.8	23.2	0.08	1.31	0.08	0.10	0.08	96.5
8	Amph 1	0.36	1.97	56.6	12.8	22.8	0.05	1.32	0.07	0.11	0.07	96.1
9	Amph 1	0.28	2.07	56.4	12.8	22.7	0.10	1.19	0.11	0.085	0.10	95.9
10	Amph 1	0.26	2.09	56.3	12.9	22.8	0.07	1.09	0.11	0.023	0.06	95.8
11	Amph 1	0.34	2.07	56.4	12.8	22.7	0.04	1.21	0.11	0.034	0.07	95.7
12	Amph 1	0.36	2.17	55.9	12.7	22.9	0.11	1.52	0.08	0.15	0.08	96.0
13	Amph 1	0.44	2.37	55.5	12.8	22.5	0.06	2.12	0.11	0.15	0.07	96.1
14	Amph 1	0.77	2.65	54.0	12.6	22.0	0.07	3.20	0.09	0.20	0.32	96.0

C-1 continued

10-09

Nr.	Mineral	Na_2O	FeO	SiO_2	CaO	MgO	MnO	Al_2O_3	NiO	TiO_2	Cr_2O_3	Total
15	Amph 1	0.90	2.74	52.9	12.9	21.6	0.06	3.90	0.09	0.24	0.37	95.6
16	Amph 1	1.12	2.78	51.9	12.8	21.2	0.08	4.78	0.07	0.34	0.44	95.5
17	Amph 1	1.14	2.99	51.2	12.6	20.5	0.11	5.28	0.07	0.34	0.52	94.7
18	Amph 1	1.48	3.18	50.8	12.5	20.7	0.09	5.88	0.06	0.42	0.52	95.5
19	Amph 1	1.35	3.38	50.3	12.5	20.7	0.07	6.21	0.08	0.33	0.54	95.5
20	Amph 1	1.36	3.28	50.2	12.7	20.4	0.07	6.35	0.07	0.36	0.52	95.3
21	Amph 1	1.60	3.38	50.4	12.6	20.2	0.05	6.42	0.10	0.34	0.48	95.6
22	Amph 1	1.37	3.37	50.2	12.4	20.6	0.07	6.56	0.10	0.39	0.48	95.6
23	Amph 1	1.51	3.39	49.9	12.6	20.3	0.06	6.46	0.09	0.38	0.47	95.2
24	Amph 1	1.41	3.32	49.6	12.9	20.6	0.10	6.38	0.07	0.39	0.47	95.2
25	Amph 1	1.60	3.14	49.6	12.7	20.6	0.09	6.60	0.08	0.34	0.52	95.3
26	Amph 1	1.57	3.42	49.4	12.8	20.2	0.11	6.87	0.07	0.41	0.50	95.3
27	Amph 1	1.54	3.37	49.6	12.6	20.4	0.05	6.79	0.09	0.34	0.55	95.3
28	Amph 1	1.45	3.35	49.6	12.5	20.0	0.04	6.77	0.08	0.39	0.49	94.8
29	Amph 1	1.42	3.46	49.6	12.6	20.5	0.07	6.76	0.09	0.38	0.49	95.3
30	Amph 1	1.44	3.49	49.8	12.8	20.0	0.05	6.76	0.09	0.41	0.52	95.4
31	Amph 1	1.42	3.50	50.1	12.8	20.5	0.11	6.71	0.07	0.28	0.58	96.1
32	Amph 1	1.45	3.37	50.2	12.9	20.7	0.08	6.48	0.09	0.41	0.55	96.2
33	Amph 1	1.28	3.24	49.7	12.7	20.4	0.03	6.17	0.10	0.41	0.55	94.6
34	Amph 1	1.36	3.28	50.1	12.7	20.4	0.03	6.29	0.09	0.37	0.51	95.1
35	Amph 1	1.41	3.14	50.3	12.7	20.7	0.06	6.10	0.08	0.30	0.51	95.4
36	Amph 1	1.32	3.16	50.3	12.8	21.0	0.05	6.15	0.10	0.36	0.56	95.7
37	Amph 1	1.35	3.18	50.4	12.7	20.9	0.03	6.11	0.07	0.40	0.52	95.7
38	Amph 1	1.22	3.22	50.6	12.6	20.5	0.04	6.18	0.06	0.32	0.55	95.3
39	Amph 1	1.43	3.24	50.1	12.6	20.3	0.04	6.32	0.09	0.42	0.53	95.0
40	Amph 1	1.42	3.35	49.8	12.6	20.3	0.05	6.64	0.08	0.24	0.52	94.9
41	Amph 1	1.45	3.35	50.0	12.6	20.2	0.10	6.67	0.09	0.37	0.51	95.3
42	Amph 1	1.46	3.37	49.9	12.7	20.4	0.11	6.82	0.10	0.34	0.51	95.7
43	Amph 1	1.48	3.53	49.8	12.7	20.0	0.01	6.88	0.09	0.44	0.51	95.4
44	Amph 1	1.53	3.46	49.8	12.6	20.7	0.09	6.94	0.09	0.36	0.48	96.0
45	Amph 1	1.46	3.36	49.9	12.7	20.4	0.04	7.00	0.09	0.43	0.50	95.9
46	Amph 1	1.48	3.52	49.8	12.6	20.5	0.03	7.00	0.07	0.52	0.51	96.1
61	Amph	1.45	3.25	50.1	12.6	20.1	0.04	6.15	0.09	0.41	0.56	94.7
62	Amph	1.36	3.34	49.9	12.7	20.4	0.073	5.87	0.11	0.39	0.56	94.7
93	Amph	1.49	3.35	50.7	12.9	20.7	0.08	5.50	0.07	0.39	0.54	95.7
94	Amph	1.54	3.51	49.1	12.6	20.0	0.08	6.79	0.09	0.32	0.54	94.5
95	Amph	1.42	3.33	49.7	12.7	20.0	0.13	6.31	0.08	0.33	0.52	94.5
96	Amph	1.38	3.32	49.8	12.5	19.9	0.03	6.39	0.07	0.41	0.56	94.4
113	Spl	<0.01	50.9	<0.01	<0.01	2.66	0.56	4.13	0.30	0.74	37.0	96.2
115	Spl	<0.01	50.8	0.01	<0.01	2.99	0.57	4.51	0.31	0.84	37.9	97.9
116	Spl	<0.01	49.8	<0.01	0.02	3.11	0.60	4.50	0.28	0.86	37.2	96.4
117	Spl	<0.01	50.8	0.01	<0.01	3.03	0.61	4.40	0.33	0.85	37.1	97.2
112	Spl	<0.01	71.6	0.01	<0.01	1.74	0.37	1.41	0.56	0.92	18.1	94.7
114	Spl	<0.01	35.4	0.06	0.02	7.65	0.86	0.016	0.13	53.6	0.60	98.3

10-10

No.	Mineral	Na_2O	FeO	SiO_2	CaO	MgO	MnO	Al_2O_3	NiO	TiO_2	Cr_2O_3	Total
116	Ol	0.01	9.60	41.5	0.01	50.0	0.13	0.02	0.32	<0.001	0.01	102
117	Ol	<0.01	9.74	41.4	<0.01	49.8	0.13	0.02	0.33	<0.001	<0.01	101
118	Ol	0.03	9.62	41.1	<0.01	49.8	0.13	<0.01	0.37	<0.001	<0.01	101
120	Ol	0.02	9.60	41.7	<0.01	49.9	0.11	<0.01	0.31	<0.001	<0.01	102
121	Ol	<0.01	9.59	41.3	<0.01	50.6	0.13	<0.01	0.34	<0.001	0.01	102
122	Ol	<0.01	9.53	40.9	<0.01	50.3	0.13	<0.01	0.34	<0.001	0.03	101
125	Ol	<0.01	9.51	41.1	<0.01	49.3	0.12	<0.01	0.35	<0.001	<0.01	100
126	Ol	<0.01	10.1	41.4	<0.01	49.8	0.13	0.03	0.37	<0.001	<0.01	102
128	Ol	0.02	9.58	41.4	<0.01	50.1	0.08	0.02	0.36	<0.001	0.02	102
129	Ol	0.01	10.0	41.6	<0.01	50.1	0.12	<0.01	0.32	<0.001	<0.01	102
130	Ol	<0.01	9.59	41.6	<0.01	50.2	0.16	0.01	0.34	<0.001	<0.01	102
133	Ol	<0.01	9.34	41.4	<0.01	50.3	0.12	<0.01	0.34	<0.001	0.02	101
135	Ol	<0.01	9.68	41.2	<0.01	49.7	0.16	<0.01	0.34	<0.001	<0.01	101
136	Ol	<0.01	9.63	41.2	<0.01	49.7	0.15	<0.01	0.34	<0.001	0.01	101
137	Ol	0.01	9.66	41.2	<0.01	50.2	0.13	0.01	0.33	<0.001	0.01	102
138	Ol	0.01	9.82	41.5	<0.01	50.5	0.12	<0.01	0.37	0.003	<0.01	102
143	Ol	0.04	9.65	41.4	<0.01	50.5	0.11	0.01	0.38	<0.001	0.01	102
144	Ol	<0.01	9.68	41.0	<0.01	50.2	0.16	0.03	0.33	<0.001	<0.01	101
147	Ol	0.01	9.81	41.3	<0.01	50.3	0.15	0.02	0.32	<0.001	0.01	102
148	Ol	<0.01	9.70	41.0	<0.01	49.9	0.13	0.01	0.34	0.001	0.02	101
149	Ol	0.02	9.94	41.0	0.02	50.4	0.11	0.02	0.34	<0.001	<0.01	102
150	Ol	<0.01	9.71	40.8	<0.01	50.3	0.14	<0.01	0.35	0.018	<0.01	101
151	Ol	0.01	9.47	40.2	<0.01	49.7	0.16	<0.01	0.35	<0.001	<0.01	99.9
152	Ol	<0.01	9.61	40.1	<0.01	49.6	0.15	<0.01	0.35	0.025	<0.01	99.8
155	Ol	0.03	9.63	41.3	<0.01	49.9	0.16	<0.01	0.32	<0.001	<0.01	101
156	Ol	<0.01	9.83	41.3	<0.01	50.2	0.11	<0.01	0.31	<0.001	<0.01	102
157	Ol	0.03	9.50	41.2	<0.01	50.1	0.10	<0.01	0.33	<0.001	<0.01	101
158	Ol	<0.01	9.68	41.0	<0.01	49.8	0.19	<0.01	0.35	<0.001	<0.01	101
159	Ol	<0.01	9.39	40.5	<0.01	50.5	0.15	0.01	0.34	0.026	0.01	101

C-1 continued

10-10

Nr.	Mineral	Na_2O	FeO	SiO_2	CaO	MgO	MnO	Al_2O_3	NiO	TiO_2	Cr_2O_3	Total
160	Ol	<0.01	9.66	40.9	<0.01	50.1	0.16	<0.01	0.33	<0.001	<0.01	101
161	Ol	<0.01	9.69	40.3	<0.01	49.6	0.15	<0.01	0.35	<0.001	<0.01	100
162	Ol	0.02	9.54	40.1	<0.01	49.0	0.11	0.02	0.33	<0.001	0.01	99.1
163	Ol	<0.01	9.63	41.1	<0.01	49.5	0.12	<0.01	0.31	<0.001	<0.01	101
164	Ol	<0.01	9.80	41.4	<0.01	50.2	0.10	<0.01	0.35	<0.001	<0.01	102
165	Ol	0.03	9.49	41.0	<0.01	49.7	0.16	<0.01	0.32	<0.001	0.01	101
166	Ol	0.01	9.65	40.9	<0.01	49.9	0.12	<0.01	0.32	<0.001	0.009	101
167	Ol	<0.01	9.61	40.5	<0.01	49.0	0.11	<0.01	0.36	<0.001	<0.01	99.6
171	Ol	<0.01	9.61	41.4	<0.01	49.8	0.07	0.01	0.34	0.001	0.01	101
172	Ol	<0.01	9.67	40.9	0.01	50.1	0.13	0.002	0.34	0.014	<0.01	101
173	Ol	0.04	9.53	40.5	<0.01	48.9	0.12	<0.01	0.34	<0.001	0.01	100
177	Ol	0.06	9.52	41.4	<0.01	49.4	0.14	0.01	0.38	<0.001	<0.01	101
178	Ol	<0.01	9.31	41.2	<0.01	49.3	0.15	0.02	0.36	0.011	0.01	100
183	Ol	0.01	9.63	41.1	<0.01	50.0	0.12	<0.01	0.37	<0.001	0.01	101
184	Ol	<0.01	9.49	41.3	<0.01	49.8	0.11	<0.01	0.36	<0.001	0.01	101
185	Ol	<0.01	9.61	40.3	<0.01	49.2	0.18	<0.01	0.35	<0.001	0.01	99.6
186	Ol	<0.01	9.66	41.6	<0.01	49.7	0.11	0.01	0.35	<0.001	0.01	101
187	Ol	0.02	9.75	41.2	<0.01	49.7	0.16	<0.01	0.35	<0.001	<0.01	101
192	Ol	<0.01	9.62	41.6	<0.01	50.3	0.12	<0.01	0.33	<0.001	0.01	102
193	Ol	<0.01	9.57	41.5	<0.01	50.3	0.09	<0.01	0.34	<0.001	0.01	102
194	Ol	0.01	9.84	41.6	<0.01	50.3	0.16	<0.01	0.35	<0.001	<0.01	102
195	Ol	<0.01	9.68	41.3	<0.01	49.7	0.09	0.02	0.32	<0.001	<0.01	101
200	Ol	<0.01	9.64	41.2	<0.01	50.3	0.10	<0.01	0.33	<0.001	0.01	102
201	Ol	<0.01	9.93	41.2	<0.01	50.4	0.17	0.03	0.35	0.001	<0.01	102
203	Ol	<0.01	9.89	41.0	<0.01	50.5	0.13	<0.01	0.35	0.007	<0.01	102
123	Amph	1.61	3.51	49.4	12.8	20.2	0.04	7.70	0.07	0.30	0.56	96.1
124	Amph	1.47	3.49	49.4	12.7	20.4	0.06	7.64	0.09	0.29	0.54	96.1
127	Amph	1.25	3.09	53.3	12.9	21.4	0.04	5.59	0.07	0.21	0.39	98.1
131	Amph	0.73	2.32	54.3	12.6	22.5	0.04	3.55	0.07	0.13	0.24	96.5
132	Amph	0.42	1.97	54.4	12.3	23.6	0.02	3.04	0.10	0.10	0.16	96.1
139	Amph	1.52	3.66	50.3	12.8	20.6	0.01	7.61	0.08	0.31	0.60	97.5
140	Amph	1.48	3.77	50.6	12.7	20.6	0.06	7.56	0.10	0.25	0.57	97.8
141	Amph	1.48	3.57	50.4	12.9	20.5	0.05	7.35	0.08	0.30	0.54	97.1
142	Amph	1.44	3.48	49.9	12.8	20.5	0.07	7.67	0.09	0.30	0.60	96.8
145	Amph	1.26	3.30	51.6	12.8	20.9	0.05	6.57	0.10	0.24	0.53	97.3
146	Amph	1.56	3.66	49.9	12.9	20.5	0.06	7.43	0.07	0.28	0.53	96.8
153	Amph	1.45	3.59	48.5	12.6	20.2	0.07	7.72	0.05	0.26	0.51	94.9
154	Amph	1.52	3.65	49.8	12.9	20.0	0.04	7.83	0.09	0.29	0.58	96.7
170	Amph	1.55	3.56	51.0	12.8	20.6	0.03	7.32	0.08	0.30	0.47	97.8
175	Amph	1.59	3.70	50.8	12.7	20.3	0.01	7.59	0.10	0.31	0.54	97.6
176	Amph	1.17	3.13	52.7	12.8	21.1	0.04	5.45	0.08	0.19	0.58	97.2
179	Amph	1.42	3.58	50.3	12.9	20.1	0.01	7.66	0.09	0.27	0.55	96.9
180	Amph	1.53	3.52	49.8	12.7	20.0	<0.01	7.65	0.07	0.28	0.57	96.1
181	Amph	1.49	3.62	50.5	12.9	20.8	0.02	7.86	0.09	0.27	0.56	98.1
182	Amph	1.54	3.47	51.3	12.9	20.6	0.01	7.07	0.07	0.29	0.52	97.7
188	Amph	1.05	3.96	45.3	11.3	20.2	0.09	5.45	0.10	0.24	0.53	88.3
189	Amph	1.19	3.33	48.5	12.3	20.2	0.06	7.21	0.10	0.32	0.49	93.7
190	Amph	1.47	3.47	50.4	12.7	20.4	0.08	7.85	0.08	0.23	0.61	97.2
191	Amph	1.42	3.69	50.1	12.8	20.1	0.02	8.01	0.07	0.25	0.60	97.0
196	Amph	1.45	3.61	50.3	12.7	20.1	<0.01	7.81	0.08	0.26	0.57	96.9
197	Amph	1.60	3.65	50.7	12.8	20.5	0.06	7.67	0.08	0.25	0.62	97.9
198	Amph	1.46	3.38	50.4	12.9	20.5	0.02	7.53	0.07	0.30	0.59	97.1
199	Amph	1.36	3.62	49.7	12.7	20.2	0.02	7.99	0.09	0.25	0.62	96.6
211	Spl	<0.01	66.5	0.03	<0.01	1.82	0.39	1.30	0.49	1.22	24.2	96.0
212	Spl	0.02	66.9	<0.01	<0.01	1.83	0.46	1.28	0.51	1.23	24.3	96.5
213	Spl	<0.01	67.7	0.01	<0.01	1.75	0.38	1.12	0.55	1.05	24.0	96.5
214	Spl	0.07	67.9	0.04	<0.01	1.42	0.37	1.06	0.50	0.98	23.1	95.5
215	Spl	0.02	68.8	<0.01	<0.01	1.53	0.35	0.99	0.52	1.12	23.1	96.4

10-11

Nr.	Mineral	Na_2O	FeO	SiO_2	CaO	MgO	MnO	Al_2O_3	NiO	TiO_2	Cr_2O_3	Total
217	Ol	0.05	7.99	41.1	<0.01	50.2	0.11	0.03	0.40	0.016	<0.01	99.9
219	Ol	0.04	7.79	40.2	<0.01	50.8	0.16	<0.01	0.41	0.001	<0.01	99.4
220	Ol	<0.01	7.70	40.7	<0.01	50.7	0.13	<0.01	0.42	<0.001	0.01	99.6
221	Ol	<0.01	7.66	41.3	<0.01	50.9	0.21	<0.01	0.37	<0.001	<0.01	101
222	Ol	0.03	8.09	41.3	<0.01	51.5	0.17	<0.01	0.41	<0.001	0.02	102
223	Ol	0.02	7.85	41.1	<0.01	50.6	0.14	<0.01	0.38	<0.001	0.02	100
224	Ol	<0.01	8.18	41.2	0.02	50.6	0.12	<0.01	0.42	<0.001	<0.01	101
225	Ol	0.02	7.74	41.1	<0.01	51.1	0.17	0.01	0.43	<0.001	<0.01	101
226	Ol	0.05	7.89	41.2	0.01	51.2	0.16	<0.01	0.41	0.009	0.01	101
227	Ol	<0.01	7.97	41.1	<0.01	51.5	0.15	<0.01	0.39	<0.001	<0.01	101
228	Ol	<0.01	7.81	41.2	0.01	51.6	0.15	0.01	0.38	<0.001	<0.01	101
229	Ol	<0.01	7.98	41.5	<0.01	51.3	0.13	<0.01	0.40	<0.001	<0.01	101
230	Ol	0.02	8.00	41.2	<0.01	51.5	0.14	<0.01	0.44	<0.001	<0.01	101
231	Ol	<0.01	8.08	41.3	<0.01	51.6	0.16	<0.01	0.41	<0.001	<0.01	102

C-1 continued

10-11

Nr.	Mineral	Na_2O	FeO	SiO_2	CaO	MgO	MnO	Al_2O_3	NiO	TiO_2	Cr_2O_3	Total
232	Ol	<0.01	7.94	41.1	<0.01	51.1	0.16	<0.01	0.42	<0.001	<0.01	101
233	Ol	<0.01	7.81	41.2	<0.01	51.2	0.16	<0.01	0.40	<0.001	<0.01	101
234	Ol	0.01	8.02	41.2	<0.01	51.3	0.16	0.02	0.43	<0.001	<0.01	101
235	Ol	0.03	7.81	41.0	0.02	51.1	0.12	<0.01	0.39	0.003	<0.01	101
236	Ol	<0.01	7.78	40.8	<0.01	50.6	0.16	0.02	0.40	<0.001	<0.01	99.8
237	Ol	<0.01	7.95	41.1	<0.01	50.8	50.8	0.14	<0.01	<0.001	<0.01	100
238	Ol	<0.01	8.04	41.0	<0.01	50.5	0.14	<0.01	0.41	<0.001	<0.01	100
239	Ol	<0.01	7.88	41.3	<0.01	50.8	0.18	<0.01	0.42	0.015	0.02	101
240	Ol	<0.01	8.15	40.6	<0.01	50.2	0.13	<0.01	0.41	<0.001	<0.01	99.5
241	Ol	<0.01	8.17	41.1	<0.01	50.5	0.14	0.02	0.38	<0.001	<0.01	100
242	Ol	<0.01	7.96	41.2	<0.01	50.2	0.18	<0.01	0.41	<0.001	<0.01	99.9
243	Ol	<0.01	8.06	40.9	<0.01	50.8	0.16	<0.01	0.40	0.011	0.01	100
244	Ol	0.01	7.80	40.4	<0.01	50.3	0.08	0.03	0.42	<0.001	<0.01	99.1
245	Ol	<0.01	8.25	40.4	<0.01	51.0	0.13	<0.01	0.43	<0.001	<0.01	100
246	Ol	0.03	7.78	41.1	0.01	51.0	0.15	0.01	0.41	0.026	0.03	101
247	Ol	<0.01	8.07	41.0	<0.01	51.4	0.09	0.02	0.43	0.003	<0.01	101
248	Ol	<0.01	8.21	41.3	<0.01	51.6	0.15	0.02	0.40	<0.001	<0.01	102
251	Ol	<0.01	8.16	41.0	0.02	50.9	0.08	0.00	0.41	<0.001	<0.01	101
252	Ol	0.05	8.02	40.9	<0.01	50.6	0.14	<0.01	0.40	<0.001	<0.01	100
253	Ol	<0.01	7.91	41.4	<0.01	51.5	0.16	0.01	0.39	0.006	0.01	101
254	Ol	<0.01	8.24	41.2	<0.01	51.6	0.11	<0.01	0.40	<0.001	<0.01	102
255	Ol	0.05	8.32	41.2	<0.01	51.9	0.12	<0.01	0.41	<0.001	<0.01	102
256	Ol	<0.01	8.07	41.3	<0.01	51.0	0.15	<0.01	0.40	<0.001	<0.01	101
257	Ol	0.02	8.04	41.5	<0.01	50.8	0.17	0.02	0.44	0.005	0.01	101
261	Ol	0.01	7.93	41.2	<0.01	51.1	0.11	<0.01	0.42	<0.001	<0.01	101
262	Ol	0.04	7.98	41.4	<0.01	50.9	0.13	<0.01	0.38	0.003	<0.01	101
268	Ol	0.01	8.24	41.2	<0.01	50.6	0.16	0.02	0.40	<0.001	<0.01	101
269	Ol	<0.01	7.97	41.5	0.01	50.2	0.12	<0.01	0.41	0.004	<0.01	100
270	Ol	<0.01	8.07	43.0	0.02	50.9	0.18	<0.01	0.44	<0.001	<0.01	103
271	Ol	0.01	7.90	40.9	<0.01	51.0	0.11	<0.01	0.42	<0.001	<0.01	100
274	Ol	<0.01	7.80	42.9	0.02	49.6	0.11	0.03	0.39	<0.001	<0.01	101
275	Ol	<0.01	7.78	41.3	<0.01	51.4	0.13	<0.01	0.40	<0.001	<0.01	101
276	Ol	<0.01	7.46	42.5	<0.01	51.8	0.18	<0.01	0.45	<0.001	<0.01	102
283	Ol	<0.01	7.71	40.6	<0.01	50.7	0.08	<0.01	0.38	<0.001	<0.01	99.6
284	Ol	<0.01	7.89	41.1	<0.01	51.4	0.16	0.02	0.41	<0.001	<0.00	101
285	Ol	<0.01	7.95	41.0	<0.01	51.4	0.11	0.01	0.40	0.001	<0.01	101
286	Ol	<0.01	7.78	40.5	<0.01	51.0	0.20	0.02	0.43	<0.001	<0.01	99.8
287	Ol	<0.01	7.93	40.4	<0.01	50.6	0.17	<0.01	0.37	<0.001	<0.01	99.5
288	Ol	<0.01	7.84	41.0	<0.01	50.9	0.13	<0.01	0.40	<0.001	<0.01	100
289	Ol	0.02	7.62	40.8	<0.01	50.8	0.11	<0.01	0.40	<0.001	<0.01	99.8
290	Ol	<0.01	8.01	41.4	<0.01	50.3	0.11	<0.01	0.42	<0.001	<0.01	100
291	Ol	<0.01	7.90	40.9	<0.01	50.7	0.20	<0.01	0.40	0.001	<0.01	100
292	Ol	<0.01	8.05	41.0	<0.01	50.6	0.15	0.01	0.42	<0.001	<0.01	100
293	Ol	<0.01	8.09	40.8	<0.01	50.9	0.18	0.01	0.41	<0.001	<0.01	100
296	Ol	<0.01	8.01	40.9	<0.01	51.1	0.15	<0.01	0.42	<0.001	<0.01	101
297	Ol	<0.01	8.18	41.1	0.01	50.9	0.11	<0.01	0.43	0.012	0.01	101
263	Opx	<0.01	5.86	57.5	0.19	35.1	0.22	1.28	0.06	0.039	0.17	100
264	Opx	<0.01	5.79	57.1	0.19	35.1	0.16	1.32	0.08	0.035	0.13	99.9
265	Opx	<0.01	5.72	57.3	0.16	35.1	0.19	1.25	0.08	0.022	0.16	100
266	Opx	<0.01	5.69	57.0	0.17	34.6	0.14	1.17	0.06	0.039	0.16	99.1
267	Opx	<0.01	5.74	55.6	0.19	34.5	0.16	1.31	0.07	0.036	0.17	97.7
249	Amp	0.82	2.37	52.5	12.6	21.7	0.05	5.22	0.10	0.37	0.57	96.3
250	Amp	0.68	2.36	47.3	12.0	19.2	0.02	4.60	0.10	0.35	0.56	87.2
258	Amp	0.23	1.74	58.0	13.0	23.4	0.06	1.53	0.11	0.056	0.15	98.2
259	Amp	0.23	1.82	56.8	12.9	23.2	0.05	1.59	0.13	0.087	0.17	96.9
260	Amp	0.27	1.75	56.3	13.0	22.9	0.07	1.76	0.10	0.076	0.16	96.4
294	Amp	0.64	2.11	53.3	12.7	21.9	0.04	4.74	0.09	0.39	0.71	96.6
295	Amp	0.75	2.35	52.5	12.5	21.9	0.06	5.12	0.08	0.37	0.70	96.3
272	Spl	0.02	30.9	0.01	<0.01	7.45	0.50	17.2	0.16	0.55	43.8	101
273	Spl	<0.01	31.2	0.07	<0.01	7.28	0.50	16.3	0.12	0.59	44.2	100
277	Spl	<0.01	29.5	<0.01	<0.01	8.65	0.41	19.9	0.15	0.44	41.0	100
278	Spl	<0.01	29.4	<0.01	<0.01	8.76	0.47	20.6	0.15	0.52	40.6	101
279	Spl	<0.01	30.5	0.03	<0.01	8.23	0.41	18.0	0.14	0.55	42.9	101
280	Spl	<0.01	30.8	0.03	<0.01	7.80	0.51	16.8	0.12	0.49	44.0	101
281	Spl	<0.01	30.1	0.01	<0.01	8.12	0.36	18.5	0.15	0.56	42.4	100
282	Spl	<0.01	30.3	0.01	<0.01	0.12	0.41	18.2	0.11	0.56	43.5	101
299	Spl	<0.01	31.9	0.02	<0.01	6.61	0.46	16.1	0.11	0.56	43.5	99.3
300	Spl	<0.01	31.5	<0.01	<0.01	7.10	0.52	16.0	0.14	0.56	44.3	100
301	Spl	<0.01	29.9	0.02	<0.01	7.84	0.43	17.7	0.12	0.54	42.7	99.2
302	Spl	<0.01	29.6	0.12	<0.01	9.41	0.49	16.9	0.13	0.47	40.8	98.0
303	Spl	<0.01	29.7	0.14	<0.01	6.69	0.43	14.1	0.14	0.48	42.6	94.3
304	Spl	<0.01	31.1	0.03	<0.01	7.00	0.50	15.9	0.12	0.46	44.2	99.2

C-1 continued

10-11

Nr.	Mineral	Na_2O	FeO	SiO_2	CaO	MgO	MnO	Al_2O_3	NiO	TiO_2	Cr_2O_3	Total
305	Spl	<0.01	31.3	0.02	<0.01	7.28	0.56	16.8	0.14	0.58	43.5	100
306	Spl	<0.01	31.4	<0.01	<0.01	7.26	0.46	16.7	0.13	0.59	43.6	100
307	Spl	<0.01	30.4	0.02	<0.01	7.30	0.58	16.6	0.12	0.57	43.7	99.2
308	Spl	<0.01	31.1	<0.01	<0.01	7.30	0.47	16.9	0.13	0.54	43.5	100
309	Spl	<0.01	30.6	0.05	<0.01	7.09	0.54	17.1	0.12	0.46	44.6	101
310	Spl	<0.01	30.5	0.01	<0.01	7.09	0.57	16.9	0.11	0.56	43.5	99.2

10-12A

Nr.	Mineral	Na_2O	FeO	SiO_2	CaO	MgO	MnO	Al_2O_3	NiO	TiO_2	Cr_2O_3	Total
151	Ol	0.01	9.61	40.7	<0.01	49.9	0.19	<0.01	0.49	0.036	<0.01	101
152	Ol	0.01	9.58	40.6	<0.01	49.7	0.16	0.01	0.49	<0.001	<0.01	101
153	Ol	<0.01	9.67	40.4	<0.01	49.8	0.20	0.01	0.48	<0.001	<0.01	101
154	Ol	<0.01	9.42	40.8	<0.01	49.4	0.11	<0.01	0.47	0.031	<0.01	100
155	Ol	0.01	10.0	40.8	0.01	50.1	0.24	<0.01	0.49	<0.001	0.01	102
156	Ol	<0.01	9.91	40.8	0.01	50.4	0.18	<0.01	0.50	0.046	<0.01	102
157	Ol	0.01	9.93	40.7	<0.01	50.1	0.17	<0.01	0.47	0.041	<0.01	101
158	Ol	<0.01	9.86	40.6	0.01	49.5	0.19	<0.01	0.48	0.005	<0.01	101
159	Ol	0.02	9.98	40.7	<0.01	50.1	0.22	<0.01	0.49	0.036	<0.01	102
160	Ol	0.01	10.0	40.9	0.03	49.8	0.19	<0.01	0.46	<0.001	<0.01	101
177	Ol	0.02	9.70	40.4	0.02	49.7	0.20	<0.01	0.47	<0.001	<0.01	100
179	Ol	<0.01	9.52	40.3	0.02	49.6	0.16	0.01	0.48	0.005	0.01	100
180	Ol	<0.01	9.89	40.7	<0.01	49.1	0.17	<0.01	0.48	0.031	<0.01	100
182	Ol	<0.01	9.52	40.8	0.02	49.7	0.24	<0.01	0.46	0.036	0.01	101
183	Ol	<0.01	9.64	40.6	<0.01	49.3	0.14	<0.01	0.47	<0.001	<0.01	100
184	Ol	<0.01	9.68	40.8	<0.01	49.5	0.12	0.02	0.42	<0.001	0.02	101
185	Ol	<0.01	9.64	40.5	<0.01	49.4	0.20	0.01	0.45	0.005	0.02	100
186	Ol	<0.01	9.86	40.8	0.02	49.6	0.20	<0.01	0.48	<0.001	<0.01	101
187	Ol	0.02	9.13	40.5	<0.01	49.7	0.14	0.02	0.46	0.01	<0.01	100
188	Ol	<0.01	9.50	40.9	<0.01	50.2	0.22	<0.01	0.46	<0.001	<0.01	101
189	Ol	0.02	9.52	40.7	<0.01	50.1	0.18	<0.01	0.50	<0.001	0.01	101
190	Ol	<0.01	9.46	40.9	0.01	50.6	0.21	0.01	0.46	0.046	<0.01	102
191	Ol	0.00	9.53	41.1	<0.01	49.7	0.20	0.01	0.45	<0.001	<0.01	101
192	Ol	0.01	9.88	41.1	<0.01	49.7	0.17	0.02	0.47	<0.001	0.02	101
193	Ol	0.00	9.80	40.9	<0.01	49.9	0.19	0.01	0.44	<0.001	<0.01	101
194	Ol	<0.01	9.64	40.8	<0.01	50.2	0.27	<0.01	0.45	<0.001	<0.01	101
195	Ol	<0.01	9.56	40.9	<0.01	50.1	0.16	<0.01	0.44	0.005	0.01	101
196	Ol	<0.01	9.82	40.5	0.01	49.7	0.19	0.01	0.48	0.041	<0.01	101
197	Ol	<0.01	9.97	40.5	0.01	50.0	0.20	<0.01	0.45	0.015	0.01	101
198	Ol	0.02	10.3	40.6	<0.01	49.9	0.23	<0.01	0.48	<0.001	<0.01	102
199	Ol	<0.01	9.67	40.7	<0.01	50.2	0.13	<0.01	0.46	<0.001	0.01	101
200	Ol	<0.01	9.91	40.8	0.01	50.2	0.20	<0.01	0.45	<0.001	0.01	102
201	Ol	<0.01	9.55	40.6	0.01	50.0	0.21	<0.01	0.46	<0.001	<0.01	101
202	Ol	<0.01	10.0	40.4	0.02	49.4	0.20	<0.01	0.46	<0.001	<0.01	101
203	Ol	0.02	10.3	40.0	<0.01	49.4	0.19	0.02	0.45	<0.001	0.01	100
204	Ol	0.01	9.69	40.6	<0.01	49.6	0.22	<0.01	0.49	0.077	0.01	101
205	Ol	<0.01	9.64	40.5	0.01	49.9	0.18	0.01	0.48	0.010	0.02	101
206	Ol	<0.01	9.46	40.7	<0.01	49.7	0.21	<0.01	0.50	<0.001	<0.01	101
207	Ol	0.01	10.0	40.6	<0.01	50.2	0.19	0.02	0.46	<0.001	<0.01	101
208	Ol	0.01	10.2	40.7	<0.01	50.2	0.23	<0.01	0.48	<0.001	<0.01	102
209	Ol	<0.01	10.2	40.8	<0.01	50.3	0.22	<0.01	0.48	0.036	<0.01	102
210	Ol	0.03	9.91	40.1	<0.01	49.3	0.17	<0.01	0.48	<0.001	0.01	100
211	Ol	<0.01	10.0	40.5	0.01	49.9	0.16	<0.01	0.48	0.041	<0.01	101
212	Ol	0.01	9.78	40.4	<0.01	49.6	0.24	<0.01	0.45	<0.001	<0.01	100
213	Ol	0.03	9.80	41.0	0.01	49.2	0.19	<0.01	0.48	0.046	<0.01	101
214	Ol	0.02	9.66	40.6	<0.01	49.6	0.18	<0.01	0.49	0.005	<0.01	101
215	Ol	0.01	9.79	40.5	0.02	49.5	0.19	<0.01	0.45	<0.001	<0.01	100
216	Ol	<0.01	9.72	40.3	<0.01	49.3	0.20	<0.01	0.46	<0.001	<0.01	100
217	Ol	0.01	9.84	40.3	<0.01	49.4	0.25	<0.01	0.45	0.036	<0.01	100
218	Ol	<0.01	9.64	40.5	<0.01	49.8	0.23	<0.01	0.47	0.051	0.01	101
219	Ol	<0.01	9.96	40.4	0.02	47.9	0.19	<0.01	0.50	0.026	0.00	98.9
220	Ol	<0.01	9.59	40.4	0.01	49.6	0.22	<0.01	0.49	0.036	0.01	100
221	Ol	<0.01	9.37	40.8	0.02	49.4	0.21	<0.01	0.52	0.010	<0.01	100
222	Ol	<0.01	9.62	40.5	0.01	49.2	0.15	<0.01	0.50	0.010	0.01	100
223	Ol	0.04	9.81	40.7	<0.01	49.4	0.16	<0.01	0.44	<0.001	<0.01	101
224	Ol	0.00	9.57	40.3	0.02	49.5	0.13	<0.01	0.47	0.010	0.03	100
225	Ol	<0.01	9.33	40.1	<0.01	49.5	0.24	<0.01	0.46	<0.001	0.02	99.7
226	Ol	0.02	9.63	40.6	0.01	49.3	0.20	<0.01	0.49	0.026	0.01	100
227	Ol	<0.01	9.43	39.8	<0.01	48.2	0.22	<0.01	0.45	<0.001	<0.01	98.1
228	Ol	<0.01	9.78	40.3	<0.01	48.9	0.25	<0.01	0.45	0.021	0.01	99.6
229	Ol	0.01	9.73	39.7	0.02	48.5	0.21	<0.01	<0.01	<0.001	0.46	98.7
230	Ol	<0.01	9.60	39.7	<0.01	48.8	0.14	<0.01	<0.01	<0.001	0.46	98.7
231	Ol	<0.01	9.54	40.0	0.02	49.1	0.14	<0.01	<0.01	<0.001	0.50	99.3
232	Ol	<0.01	9.42	42.2	0.02	47.2	0.21	<0.01	<0.01	0.010	0.42	99.5
233	Ol	<0.01	9.47	40.5	0.01	49.8	0.15	<0.01	<0.01	0.026	0.50	100
234	Ol	0.01	9.68	40.5	0.02	49.6	0.25	<0.01	<0.01	0.021	0.45	101
235	Ol	<0.01	9.60	40.5	0.02	49.6	0.23	<0.01	<0.01	<0.001	0.45	100

C-1 continued

10-12A

Nr.	Mineral	Na_2O	FeO	SiO_2	CaO	MgO	MnO	Al_2O_3	NiO	TiO_2	Cr_2O_3	Total
1	Amph	1.27	4.02	50.3	12.2	19.9	0.12	7.41	0.13	0.37	0.40	96.2
2	Amph	1.15	4.07	51.1	12.4	20.2	0.08	7.06	0.12	0.40	0.32	96.9
117	Amph	1.11	4.00	51.1	12.4	20.1	0.06	7.08	0.11	0.38	0.35	96.7
118	Amph	1.08	4.09	51.7	12.4	20.6	0.15	6.66	0.13	0.38	0.26	97.4
119	Amph	0.97	4.03	52.0	12.4	20.5	0.12	5.98	0.13	0.35	0.18	96.7
120	Amph	1.13	4.22	51.4	12.2	20.6	0.09	6.69	0.09	0.34	0.34	97.1
121	Amph	0.97	4.07	51.9	12.4	20.8	0.10	5.95	0.13	0.35	0.21	97.0
122	Amph	1.12	3.96	51.8	12.4	20.5	0.08	6.45	0.12	0.37	0.24	97.0
124	Amph	1.00	4.30	51.5	12.3	20.3	0.09	6.29	0.09	0.37	0.22	96.4
125	Amph	1.06	4.06	51.1	12.5	20.3	0.07	6.12	0.13	0.32	0.24	95.9
138	Opx	<0.01	7.02	57.2	0.16	34.7	0.23	1.15	0.06	<0.001	0.10	101
139	Opx	<0.01	6.85	57.4	0.16	35.0	0.23	1.02	0.05	0.021	0.10	101
140	Opx	0.002	6.53	57.6	0.18	35.2	0.27	1.07	0.05	<0.001	0.14	101
141	Opx	0.007	6.85	57.6	0.14	35.2	0.26	0.93	0.10	0.010	0.07	101
142	Opx	0.020	6.56	57.7	0.14	34.7	0.22	0.99	0.08	0.041	0.02	100
143	Opx	0.014	7.08	56.6	0.17	34.0	0.22	1.22	0.07	0.010	0.13	100
144	Opx	<0.01	6.86	56.9	0.14	34.6	0.23	0.95	0.05	0.031	0.18	100
145	Opx	<0.01	6.91	57.1	0.20	34.7	0.21	1.20	0.05	0.015	0.16	101
146	Opx	<0.01	7.38	57.6	0.12	35.1	0.17	0.85	0.09	<0.001	0.16	101
147	Opx	0.002	6.76	57.2	0.13	34.7	0.23	0.86	0.09	<0.001	0.14	100
149	Opx	0.009	7.01	57.7	0.07	34.8	0.25	0.37	0.09	0.021	0.11	100
150	Opx	0.005	6.91	57.3	0.15	34.5	0.21	1.08	0.05	0.093	0.13	100
161	Spl	0.09	41.6	<0.01	0.03	2.33	0.67	6.42	0.15	0.67	45.2	97.1
162	Spl	<0.01	40.8	0.03	<0.01	2.27	0.66	6.57	0.15	0.51	45.6	96.7
163	Spl	<0.01	41.2	0.01	0.01	2.41	0.67	6.24	0.15	0.45	47.1	98.3
164	Spl	<0.01	41.4	0.01	<0.01	2.44	0.70	6.17	0.16	0.56	47.0	98.4
165	Spl	<0.01	40.3	0.02	<0.01	2.41	0.75	6.04	0.14	0.38	46.8	96.8
166	Spl	<0.01	41.0	0.02	0.02	2.44	0.66	6.15	0.16	0.51	46.8	97.8
167	Spl	<0.01	41.0	0.02	<0.01	2.13	0.75	5.72	0.14	0.45	46.9	97.2
168	Spl	0.05	40.6	0.03	0.02	2.15	0.74	5.66	0.14	0.51	47.2	97.0
169	Spl	0.08	43.0	0.03	<0.01	2.46	0.74	6.64	0.17	0.37	44.4	97.8
170	Spl	<0.01	42.9	<0.01	0.02	2.57	0.69	6.80	0.20	0.63	43.9	97.7
171	Spl	0.01	40.7	0.03	0.01	2.88	0.75	4.81	0.16	0.38	46.3	96.0
172	Spl	0.02	42.2	<0.01	<0.01	2.80	0.74	4.86	0.20	0.48	45.6	96.9
173	Spl	<0.01	44.7	<0.01	0.01	2.53	0.69	4.13	0.17	0.31	43.6	96.2
174	Spl	0.01	44.3	<0.01	0.01	2.61	0.76	4.52	0.17	0.41	43.3	96.0
175	Spl	<0.01	42.6	0.07	0.02	3.23	0.71	6.45	0.15	0.45	45.2	98.9
176	Spl	<0.01	42.8	<0.01	<0.01	3.22	0.63	6.57	0.14	0.55	43.8	97.7

10-12B

Nr.	Mineral	Na_2O	FeO	SiO_2	CaO	MgO	MnO	Al_2O_3	NiO	TiO_2	Cr_2O_3	Total
267	Ol	0.03	8.07	40.3	<0.01	49.9	0.15	<0.01	0.47	<0.001	0.01	99.0
268	Ol	<0.01	8.15	40.2	0.03	50.3	0.14	<0.01	0.47	0.021	0.03	99.3
269	Ol	<0.01	7.93	40.1	<0.01	50.3	0.14	<0.01	0.43	<0.001	<0.01	98.9
270	Ol	<0.01	8.04	40.5	0.01	50.0	0.15	<0.01	0.44	<0.001	0.01	99.2
272	Ol	0.04	8.25	40.2	0.01	50.1	0.15	<0.01	0.49	<0.001	<0.01	99.3
273	Ol	0.06	8.05	40.7	<0.01	50.4	0.14	0.01	0.47	0.027	0.01	99.9
274	Ol	<0.01	8.30	40.5	0.02	49.8	0.14	0.01	0.49	<0.001	0.01	99.3
275	Ol	0.01	8.32	40.6	0.01	50.3	0.15	<0.01	0.46	0.011	<0.01	99.9
277	Ol	<0.01	8.35	40.3	0.01	50.3	0.12	0.01	0.44	<0.001	0.01	99.6
278	Ol	0.08	8.30	40.5	0.03	50.1	0.11	<0.01	0.45	<0.001	<0.01	99.6
279	Ol	<0.01	8.08	40.4	<0.01	50.1	0.11	<0.01	0.47	0.091	0.01	99.3
280	Ol	0.07	8.13	40.5	0.01	50.6	0.19	0.02	0.51	0.048	0.01	100
281	Ol	0.03	8.15	40.4	0.01	50.5	0.14	<0.01	0.50	0.027	0.01	99.7
282	Ol	<0.01	8.29	40.5	0.01	50.9	0.15	0.01	0.47	<0.001	0.01	100.3
283	Ol	0.01	8.23	40.1	0.02	50.2	0.15	<0.01	0.47	0.005	0.01	99.3
284	Ol	0.04	7.95	40.4	0.01	50.1	0.15	0.01	0.50	<0.001	<0.01	99.1
285	Ol	<0.01	8.04	40.4	0.03	50.4	0.16	<0.01	0.43	0.005	<0.01	99.4
286	Ol	0.02	8.21	40.4	<0.01	49.9	0.09	0.01	0.47	<0.001	0.01	99.1
287	Ol	<0.01	8.21	40.8	0.03	50.6	0.09	<0.01	0.46	<0.001	0.02	100
288	Ol	<0.01	8.40	40.2	0.03	51.1	0.17	<0.01	0.48	<0.001	<0.01	100
289	Ol	0.01	8.42	39.9	<0.01	50.7	0.15	<0.01	0.40	0.022	<0.01	99.6
290	Ol	<0.01	8.55	39.7	0.01	50.1	0.12	<0.01	0.47	0.032	<0.01	99.0
291	Ol	<0.01	8.29	40.9	0.01	50.4	0.14	<0.01	0.49	<0.001	0.01	100
292	Ol	0.04	8.10	40.6	0.03	50.3	0.07	<0.01	0.47	0.011	<0.01	99.7
293	Ol	0.03	8.16	41.0	0.02	50.2	0.14	<0.01	0.46	<0.001	0.01	100
294	Ol	0.01	8.22	40.8	0.01	50.9	0.15	0.02	0.48	<0.001	0.01	101
297	Ol	<0.01	8.27	40.7	<0.01	50.9	0.15	0.02	0.46	<0.001	0.02	101
298	Ol	0.02	8.24	41.4	0.01	50.3	0.07	0.01	0.51	<0.001	0.01	101
299	Ol	0.04	8.54	41.1	0.01	50.3	0.11	0.01	0.46	<0.001	<0.01	101
300	Ol	0.01	8.30	40.4	0.01	49.4	0.13	0.01	0.50	<0.001	0.01	98.8
301	Ol	<0.01	8.17	40.1	<0.01	49.2	0.11	<0.01	0.52	0.059	0.01	98.1
302	Ol	<0.01	8.28	41.3	0.01	50.5	0.16	<0.01	0.47	0.021	<0.01	101
303	Ol	<0.01	8.07	41.4	<0.01	50.7	0.13	<0.01	0.47	<0.001	<0.01	101
304	Ol	<0.01	8.15	41.6	0.02	50.0	0.12	0.02	0.46	<0.001	<0.01	100
305	Ol	0.02	8.23	41.1	0.01	50.0	0.16	0.01	0.49	<0.001	0.01	100
306	Ol	<0.01	8.23	41.1	0.01	50.0	0.11	<0.01	0.49	<0.001	<0.01	100
307	Ol	<0.01	8.35	41.0	0.01	49.9	0.13	0.01	0.44	<0.001	<0.01	99.8

C-1 continued

10-12B

Nr.	Mineral	Na_2O	FeO	SiO_2	CaO	MgO	MnO	Al_2O_3	NiO	TiO_2	Cr_2O_3	Total
308	Ol	<0.01	8.10	41.2	0.01	50.0	0.13	<0.01	0.50	0.011	<0.01	100
309	Ol	<0.01	8.57	41.0	<0.01	50.3	0.16	0.03	0.45	0.027	0.01	101
310	Ol	<0.01	8.35	41.0	<0.01	50.0	0.17	<0.01	0.47	<0.001	<0.01	99.9
311	Ol	<0.01	8.09	40.8	0.05	50.0	0.15	<0.01	0.44	0.048	0.02	99.6
312	Ol	0.01	8.18	41.1	0.01	49.8	0.05	<0.01	0.44	0.011	<0.01	99.6
313	Ol	<0.01	7.97	40.9	<0.01	50.7	0.11	<0.01	0.51	0.043	0.05	100
314	Ol	0.02	8.05	40.9	0.01	50.8	0.12	<0.01	0.48	0.043	0.02	100
316	Ol	<0.01	7.85	40.7	0.02	50.2	0.09	0.01	0.44	<0.001	<0.01	99.3
318	Ol	<0.01	8.40	40.8	<0.01	51.0	0.08	<0.01	0.52	0.032	0.01	101
319	Ol	<0.01	8.17	40.4	0.02	49.9	0.12	0.02	0.46	0.011	<0.01	99.1
320	Ol	<0.01	8.24	40.3	0.02	49.7	0.13	<0.01	0.45	0.032	<0.01	98.9
321	Ol	0.05	8.23	40.7	0.02	50.1	0.16	0.01	0.44	<0.001	0.02	99.7
322	Ol	0.02	8.54	40.5	<0.01	50.3	0.08	0.01	0.49	0.027	<0.01	99.9
323	Ol	0.00	8.09	39.9	0.01	50.3	0.16	0.00	0.47	<0.001	0.01	98.9
326	Ol	0.03	8.07	41.1	0.03	50.6	0.13	<0.01	0.45	<0.001	<0.01	100
327	Ol	0.05	8.41	41.3	0.02	51.6	0.12	<0.01	0.46	0.022	<0.01	102
328	Ol	0.03	8.43	40.1	0.01	50.9	0.20	0.01	0.48	0.016	0.00	100
324	Ol	0.06	7.98	40.1	0.01	50.2	0.13	<0.01	0.49	<0.001	0.01	99.0
325	Ol	0.01	8.36	40.6	0.01	50.5	0.17	<0.01	0.49	<0.001	0.01	100
329	Ol	0.05	8.17	39.5	0.01	50.2	0.10	<0.01	0.47	0.044	<0.01	98.5
330	Ol	0.01	8.16	40.7	0.02	50.0	0.08	0.01	0.49	<0.001	<0.01	99.5
331	Ol	<0.01	8.41	41.1	<0.01	50.6	0.14	<0.01	0.49	0.022	<0.01	101
332	Ol	<0.01	8.41	40.8	<0.01	50.6	0.13	0.02	0.50	<0.001	0.02	101
333	Ol	0.02	8.40	41.0	<0.01	50.6	0.12	<0.01	0.51	0.043	<0.01	101
334	Ol	0.01	8.51	41.1	0.01	51.2	0.12	0.01	0.49	<0.001	0.01	101
335	Ol	0.03	8.72	41.4	<0.01	51.3	0.12	<0.01	0.50	<0.001	<0.01	102
336	Ol	<0.01	8.55	40.6	<0.01	50.1	0.14	0.01	0.48	<0.001	<0.01	99.9
337	Ol	0.01	8.40	40.7	<0.01	49.9	0.14	<0.01	0.50	0.016	<0.01	99.7
338	Ol	0.07	8.74	42.3	0.04	52.1	0.14	0.01	0.49	0.060	0.01	104
339	Ol	<0.01	8.50	41.1	0.01	50.5	0.15	<0.01	0.46	<0.001	0.03	101
340	Ol	0.01	8.61	41.5	<0.01	50.6	0.18	<0.01	0.50	<0.001	0.01	101
241	Opx	0.02	6.01	57.1	0.11	35.4	0.18	1.15	0.08	0.059	0.16	100
242	Opx	<0.01	5.92	57.4	0.06	34.8	0.13	0.29	0.07	0.032	0.13	98.9
243	Opx	<0.01	6.01	57.3	0.09	35.2	0.16	0.81	0.07	0.027	0.21	99.9
244	Opx	0.03	5.83	57.3	0.05	35.1	0.21	0.77	0.07	0.043	0.19	99.6
245	Opx	<0.01	5.96	56.6	0.10	34.8	0.21	1.11	0.08	0.059	0.22	99.1
241	Opx	0.02	6.01	57.1	0.11	35.4	0.18	1.15	0.08	0.059	0.16	100
242	Opx	<0.01	5.92	57.4	0.06	34.8	0.13	0.29	0.07	0.032	0.13	98.9
241	Opx	0.02	6.01	57.1	0.11	35.4	0.18	1.15	0.08	0.027	0.16	100
242	Opx	<0.01	5.92	57.4	0.06	34.8	0.13	0.29	0.07	0.043	0.13	98.9
243	Opx	<0.01	6.01	57.3	0.09	35.2	0.16	0.81	0.07	0.059	0.21	99.9
346	Amph	1.07	2.30	53.0	12.3	21.7	0.05	3.96	0.12	0.21	0.88	95.5
347	Amph	1.25	2.31	52.6	12.3	21.9	0.07	4.40	0.12	0.16	0.93	96.1
348	Amph	0.73	1.95	54.9	12.8	23.0	0.07	2.39	0.10	0.19	0.50	96.6
349	Amph	0.85	2.16	54.0	12.5	22.4	0.06	3.34	0.12	0.25	0.59	96.3
350	Amph	0.93	2.13	54.9	12.5	22.2	0.11	3.22	0.12	0.24	0.47	96.8
351	Amph	0.53	2.07	50.5	12.5	20.2	0.03	1.77	0.12	0.18	0.27	88.2
354	Amph	<0.01	7.65	59.3	0.46	29.2	0.29	0.05	0.13	0.044	0.01	97.2
355	Amph	0.45	1.98	56.3	13.0	23.4	0.13	1.69	0.11	0.10	0.44	97.5
353	Amph	0.08	6.27	53.4	3.79	27.2	0.22	1.03	0.14	0.040	0.18	92.4
362	Amph	0.59	1.90	57.0	12.6	23.6	0.09	1.95	0.11	0.12	0.48	98.4
365	Amph	0.46	1.87	56.0	12.5	23.3	0.07	1.71	0.11	0.090	0.33	96.4
366	Amph	0.59	1.98	55.6	12.5	22.8	0.03	1.78	0.12	0.079	0.34	95.8
356	Mg-Fe-Amph	0.03	7.17	58.7	0.60	29.8	0.27	0.14	0.12	<0.001	0.05	96.8
357	Mg-Fe-Amph	<0.01	7.08	59.0	0.48	29.5	0.28	0.06	0.15	<0.001	0.02	96.6
358	Mg-Fe-Amph	<0.01	7.66	58.8	0.48	29.7	0.36	0.05	0.11	0.022	<0.01	97.2
359	Mg-Fe-Amph	0.01	7.23	59.2	0.51	30.4	0.28	0.07	0.14	0.027	0.04	97.9
360	Mg-Fe-Amph	0.02	7.26	58.6	0.42	29.4	0.34	0.02	0.12	<0.001	<0.01	96.2
363	Mg-Fe-Amph	0.06	7.49	58.4	1.00	29.6	0.33	0.47	0.11	0.038	0.09	97.5
364	Mg-Fe-Amph	0.06	7.55	59.0	0.71	29.7	0.26	0.05	0.13	<0.001	0.02	97.6
369	Spl	0.04	37.0	0.04	0.02	3.11	0.67	4.37	0.12	0.79	53.3	99.5
370	Spl	0.07	37.2	<0.01	0.01	3.09	0.55	4.39	0.15	0.79	52.7	98.9
371	Spl	<0.01	36.5	0.26	0.01	3.10	0.56	4.29	0.15	0.79	52.4	98.0
372	Spl	0.04	38.1	0.09	0.01	3.28	0.58	4.84	0.18	0.99	52.4	101
373	Spl	<0.01	36.3	0.11	0.05	3.72	0.53	4.04	0.13	0.84	52.7	98.4
374	Spl	0.05	36.4	0.03	0.11	3.53	0.54	4.17	0.13	0.94	51.6	97.5
375	Spl	0.04	36.0	0.03	0.04	3.62	0.55	4.02	0.11	0.93	51.9	97.3
376	Spl	<0.01	36.4	0.10	0.08	3.67	0.55	4.00	0.15	1.00	51.6	97.5
377	Spl	<0.01	36.9	0.04	0.11	3.73	0.59	4.07	0.14	1.16	50.1	96.8
380	Spl	<0.01	39.2	0.01	0.01	3.84	0.60	5.28	0.15	1.15	48.4	98.7
381	Spl	<0.01	38.8	0.05	0.03	3.94	0.69	5.29	0.24	1.29	48.5	98.8

C-1 continued

10-13

Nr.	Mineral	Na_2O	FeO	SiO_2	CaO	MgO	MnO	Al_2O_3	NiO	TiO_2	Cr_2O_3	Total
132	Ol	0.01	11.1	40.5	0.01	47.6	0.23	<0.01	0.25	0.011	0.01	99.7
133	Ol	0.02	11.0	40.3	<0.01	47.9	0.19	<0.01	0.25	0.053	<0.01	99.7
135	Ol	0.01	11.1	40.3	<0.01	48.0	0.24	<0.01	0.24	0.005	<0.01	99.9
136	Ol	0.02	11.0	40.3	0.02	47.9	0.25	<0.01	0.23	0.016	<0.01	99.7
140	Ol	<0.01	11.3	40.5	<0.01	48.0	0.21	<0.01	0.23	<0.001	0.02	100
142	Ol	0.01	11.0	40.6	0.03	47.8	0.16	<0.01	0.25	<0.001	0.01	99.9
143	Ol	<0.01	11.2	40.8	0.01	48.1	0.23	<0.01	0.24	0.048	<0.01	101
144	Ol	0.049	10.8	40.6	0.01	48.2	0.23	<0.01	0.23	0.016	0.01	100
145	Ol	<0.01	11.0	40.5	0.01	48.2	0.24	<0.01	0.25	<0.001	<0.01	100
146	Ol	<0.01	11.2	40.3	<0.01	48.3	0.14	<0.01	0.24	<0.001	0.01	100
147	Ol	<0.01	11.2	40.4	0.01	48.0	0.23	<0.01	0.24	<0.001	0.02	100
149	Ol	<0.01	10.5	40.2	<0.01	47.8	0.16	0.03	0.22	0.011	<0.01	99.0
150	Ol	<0.01	10.9	40.3	<0.01	47.8	0.26	0.01	0.23	0.016	0.00	99.5
151	Ol	<0.01	11.2	40.5	0.01	47.8	0.21	0.01	0.22	<0.001	0.01	100
152	Ol	<0.01	11.2	40.2	<0.01	47.4	0.19	0.01	0.22	<0.001	0.00	99.3
154	Ol	0.03	11.0	40.3	0.02	48.1	0.22	0.02	0.23	<0.001	0.01	99.9
155	Ol	<0.01	11.3	40.5	0.02	47.9	0.25	<0.01	0.26	0.016	<0.01	100
156	Ol	<0.01	11.0	40.4	<0.01	47.8	0.21	<0.01	0.24	0.021	<0.01	99.7
157	Ol	<0.01	10.8	40.5	<0.01	47.9	0.24	0.01	0.27	<0.001	<0.01	99.7
158	Ol	0.01	11.0	40.0	0.01	47.6	0.24	0.01	0.21	<0.001	<0.01	99.2
159	Ol	0.01	11.3	40.2	<0.01	47.7	0.22	0.01	0.24	0.005	<0.01	99.7
160	Ol	<0.01	11.1	40.3	0.02	48.0	0.27	<0.01	0.24	<0.001	<0.01	99.9
161	Ol	0.01	11.3	40.4	0.02	47.9	0.19	0.01	0.27	<0.001	0.01	100
162	Ol	<0.01	11.1	40.2	<0.01	48.0	0.23	<0.01	0.20	<0.001	<0.01	99.7
163	Ol	<0.01	10.6	40.3	0.01	47.9	0.17	<0.01	0.24	0.005	<0.01	99.2
164	Ol	0.04	10.6	40.4	0.01	48.3	0.19	<0.01	0.25	0.043	<0.01	99.8
165	Ol	0.02	11.3	40.5	<0.01	47.4	0.21	<0.01	0.24	<0.001	<0.01	99.7
166	Ol	0.01	10.9	40.2	0.01	47.4	0.23	<0.01	0.26	<0.001	0.02	99.0
167	Ol	0.02	11.4	40.6	0.01	47.9	0.19	0.02	0.26	0.011	<0.01	100
168	Ol	0.01	11.3	40.3	<0.01	48.6	0.19	0.02	0.27	<0.001	<0.01	101
169	Ol	0.01	11.2	40.1	<0.01	48.1	0.22	<0.01	0.26	<0.001	0.01	99.8
170	Ol	<0.01	11.1	40.5	<0.01	48.6	0.25	0.03	0.24	<0.001	<0.01	101
171	Ol	<0.01	10.7	40.5	<0.01	48.9	0.26	0.01	0.24	0.069	<0.01	101
172	Ol	<0.01	10.5	40.2	0.02	48.6	0.22	<0.01	0.23	0.059	<0.01	99.8
173	Ol	0.02	11.0	40.7	0.02	48.3	0.24	<0.01	0.21	0.032	<0.01	101
174	Ol	<0.01	11.1	40.5	<0.01	48.4	0.16	<0.01	0.23	<0.001	0.02	100
175	Ol	<0.01	10.8	40.4	<0.01	48.5	0.24	<0.01	0.25	0.021	0.01	100
176	Ol	0.02	10.9	40.4	<0.01	48.2	0.25	<0.01	0.23	0.027	0.02	100
177	Ol	<0.01	11.4	40.4	<0.01	48.3	0.19	<0.01	0.23	<0.001	<0.01	101
178	Ol	0.05	11.3	40.2	<0.01	47.8	0.24	0.01	0.24	0.021	0.01	100
179	Ol	<0.01	10.9	40.4	<0.01	48.0	0.25	0.01	0.26	0.048	<0.01	99.9
180	Ol	0.00	10.8	40.5	0.02	47.7	0.18	<0.01	0.24	0.016	0.01	99.5
181	Ol	<0.01	11.0	40.3	0.01	48.0	0.20	<0.01	0.26	0.032	<0.01	99.8
182	Ol	<0.01	10.8	40.5	0.01	48.0	0.27	0.02	0.26	0.005	<0.01	99.8
183	Ol	<0.01	10.8	40.2	<0.01	48.2	0.19	<0.01	0.26	0.032	0.01	99.7
184	Ol	0.01	11.2	40.2	<0.01	48.3	0.20	<0.01	0.26	<0.001	<0.01	100
185	Ol	0.08	10.9	40.5	0.04	48.1	0.28	0.01	0.25	0.032	<0.01	100
186	Ol	0.01	10.9	40.0	0.01	48.3	0.27	<0.01	0.22	0.053	0.01	99.9
188	Ol	0.04	10.9	39.7	0.04	47.8	0.19	0.10	0.23	<0.001	<0.01	98.9
189	Ol	<0.01	10.8	40.1	0.00	48.6	0.23	<0.01	0.24	<0.001	0.01	99.9
190	Ol	0.01	11.1	39.9	0.02	48.1	0.23	<0.01	0.26	<0.001	0.00	99.6
191	Ol	<0.01	10.9	40.1	0.01	47.6	0.27	<0.01	0.22	<0.001	<0.01	99.2
192	Ol	<0.01	10.9	40.2	0.01	47.7	0.23	<0.01	0.26	<0.001	<0.01	99.2
193	Ol	0.07	10.6	39.9	<0.01	47.9	0.29	0.01	0.24	<0.001	<0.01	99.0
194	Ol	0.01	11.2	39.8	<0.01	47.3	0.18	0.01	0.26	<0.001	<0.01	98.7
195	Ol	<0.01	11.1	40.2	0.01	47.6	0.21	0.01	0.26	<0.001	0.01	99.4
196	Ol	0.01	11.2	40.0	0.01	47.8	0.25	0.01	0.23	<0.001	<0.01	99.5
197	Ol	<0.01	11.0	40.2	<0.01	48.2	0.16	<0.01	0.24	0.016	0.01	99.8
198	Ol	<0.01	10.6	40.5	0.02	47.7	0.19	<0.01	0.21	<0.001	<0.01	99.3
199	Ol	0.01	11.0	40.3	0.01	48.1	0.25	<0.01	0.26	0.032	<0.01	100
200	Ol	0.05	10.6	40.5	0.02	48.8	0.24	0.03	0.22	0.021	0.03	101
201	Ol	<0.01	11.0	40.5	<0.01	48.4	0.24	<0.01	0.24	0.053	0.01	100
202	Ol	0.03	10.6	40.7	<0.01	48.6	0.22	0.01	0.25	<0.001	0.02	101
203	Ol	<0.01	10.9	40.9	0.01	49.0	0.23	<0.01	0.22	<0.001	<0.01	101
204	Ol	<0.01	10.7	40.5	0.02	48.2	0.24	0.02	0.25	0.021	0.01	99.9
205	Ol	<0.01	10.9	39.8	0.03	50.7	0.28	<0.01	0.25	0.011	<0.01	102
207	Ol	<0.01	10.5	40.4	<0.01	48.4	0.15	<0.01	0.22	0.027	<0.01	99.7
208	Ol	0.02	10.8	40.3	<0.01	49.0	0.15	0.01	0.26	<0.001	<0.01	101
209	Ol	0.01	10.9	40.9	<0.01	48.8	0.19	0.01	0.24	0.016	<0.01	101
210	Ol	<0.01	10.9	40.5	0.01	47.9	0.16	0.01	0.23	<0.001	0.01	99.7
211	Ol	<0.01	10.8	40.5	<0.01	47.8	0.22	<0.01	0.25	<0.001	0.01	99.6
212	Ol	<0.01	11.1	40.4	<0.01	48.0	0.24	0.01	0.25	<0.001	0.00	100
213	Ol	0.07	11.4	40.7	0.01	48.4	0.19	0.02	0.22	0.043	<0.01	101
214	Ol	<0.01	11.5	40.4	0.02	48.3	0.23	<0.01	0.28	<0.001	0.01	101

C-1 continued

10-13

Nr.	Mineral	Na_2O	FeO	SiO_2	CaO	MgO	MnO	Al_2O_3	NiO	TiO_2	Cr_2O_3	Total
148	Amph	0.71	3.01	55.0	12.6	22.2	0.08	2.89	0.07	0.25	0.14	97.0
215	Amph	1.72	4.15	48.6	12.4	19.5	<0.01	7.36	0.06	0.35	0.29	94.5
216	Amph	2.01	4.39	48.2	12.7	19.7	0.09	8.33	0.06	0.34	0.28	96.0
217	Amph	1.09	3.35	52.0	12.6	21.6	0.11	4.39	0.05	0.19	0.22	95.7
218	Amph	1.12	3.41	52.0	12.7	21.2	0.11	4.54	0.07	0.21	0.13	95.5
219	Amph	0.55	2.78	54.6	12.7	22.1	0.07	2.38	0.07	0.13	0.09	95.6
220	Amph	0.76	2.55	53.0	12.6	22.1	0.08	2.90	0.06	0.13	0.21	94.4
221	Amph	0.92	3.36	52.9	12.7	21.8	0.08	3.48	0.06	0.21	0.17	95.7
222	Amph	1.72	3.79	50.5	12.0	20.9	0.10	6.62	0.06	0.31	0.29	96.3
223	Amph	1.58	3.83	50.9	12.6	20.8	0.12	5.90	0.05	0.34	0.25	96.3
224	Amph	0.99	3.45	53.1	12.5	21.7	0.07	4.46	0.05	0.21	0.07	96.6
225	Amph	0.94	3.06	53.0	12.6	21.9	0.08	3.61	0.05	0.16	0.13	95.6
226	Amph	0.58	2.42	54.9	12.6	22.6	0.08	2.06	0.06	0.080	0.25	95.7
227	Amph	0.50	2.91	50.2	10.1	24.4	0.07	5.59	0.07	0.24	0.23	94.3
228	Amph	1.16	3.10	52.6	12.7	21.7	0.09	4.15	0.08	0.18	0.27	96.0
229	Amph	0.41	2.38	40.0	16.6	22.5	0.13	2.27	0.03	0.26	0.17	84.8
226	Amph	0.58	2.42	54.9	12.6	22.6	0.08	2.06	0.06	0.08	0.25	95.7
227	Amph	0.50	2.91	50.2	10.1	24.4	0.07	5.59	0.07	0.24	0.23	94.3
228	Amph	1.16	3.10	52.6	12.7	21.7	0.09	4.15	0.08	0.18	0.27	96.0
229	Amph	0.41	2.38	40.0	16.6	22.5	0.13	2.27	0.03	0.26	0.17	84.8
111	Spl	<0.01	81.9	0.04	<0.01	0.97	0.16	0.51	0.39	0.18	9.05	93.2
112	Spl	<0.01	82.0	<0.01	<0.01	0.92	0.18	0.63	0.35	0.12	8.81	93.0
113	Spl	<0.01	82.1	0.02	<0.01	0.89	0.18	0.50	0.39	0.25	8.90	93.3
114	Spl	0.02	81.3	0.04	<0.01	0.90	0.21	0.48	0.38	0.20	9.29	92.8
115	Spl	0.06	81.8	0.02	0.03	0.83	0.11	0.41	0.35	0.27	8.82	92.7
116	Spl	0.07	80.6	0.03	<0.01	0.77	0.20	0.55	0.37	0.36	9.20	92.1
119	Spl	<0.01	84.7	0.08	<0.01	0.72	0.14	0.35	0.37	0.13	7.74	94.2
121	Spl	0.02	80.9	0.04	0.01	0.81	0.16	0.44	0.36	0.28	7.81	90.9
122	Spl	<0.01	81.7	0.01	0.01	0.80	0.18	0.54	0.37	0.37	8.32	92.3
123	Spl	<0.01	78.5	0.05	<0.01	0.98	0.16	0.54	0.37	0.33	8.49	89.4
124	Spl	<0.01	83.0	0.02	0.00	0.70	0.15	0.31	0.36	0.12	7.43	92.1
125	Spl	<0.01	81.3	<0.01	0.01	0.80	0.10	0.43	0.35	0.26	7.88	91.1
126	Spl	0.02	80.2	0.08	0.02	1.01	0.11	0.42	0.38	0.18	7.89	90.3
127	Spl	0.09	79.1	0.06	0.04	1.09	0.16	0.63	0.36	0.23	8.64	90.4
128	Spl	<0.01	81.5	0.02	<0.01	0.98	0.18	0.69	0.33	0.44	9.43	93.5
129	Spl	<0.01	81.9	<0.01	<0.01	0.97	0.17	0.52	0.35	0.31	8.62	92.9
130	Spl	0.03	81.3	0.01	<0.01	0.76	0.11	0.44	0.36	0.27	8.03	91.3
131	Spl	0.03	83.0	0.04	<0.01	0.84	0.16	0.29	0.37	0.17	7.57	92.4
141	Chlorit	0.07	11.4	36.0	<0.01	41.3	0.20	<0.01	0.28	0.021	0.02	89.2
187	Chlorit	0.02	10.7	33.6	0.04	38.7	0.20	0.06	0.25	<0.001	<0.01	83.5

10-14

Nr.	Mineral	Na_2O	FeO	SiO_2	CaO	MgO	MnO	Al_2O_3	NiO	TiO_2	Cr_2O_3	Total
311	Ol	0.02	9.2	40.5	<0.01	0.25	48.9	0.15	0.01	<0.001	0.01	99.01
312	Ol	0.01	9.45	41.0	<0.01	0.30	49.9	0.17	0.03	<0.001	0.01	101
313	Ol	0.03	9.61	40.6	<0.01	0.29	49.9	0.16	<0.01	<0.001	<0.01	101
316	Ol	<0.01	9.28	41.0	<0.01	0.22	50.8	0.14	<0.01	<0.001	<0.01	101
317	Ol	<0.01	9.12	41.0	0.01	0.21	50.5	0.18	0.01	<0.001	0.00	101
320	Ol	<0.01	9.49	40.6	<0.01	0.29	49.8	0.16	0.03	<0.001	0.00	100
321	Ol	<0.01	9.73	40.5	<0.01	0.32	50.0	0.16	0.00	<0.001	0.02	101
323	Ol	<0.01	9.43	40.5	<0.01	0.31	50.0	0.16	<0.01	0.021	<0.01	100
324	Ol	<0.01	9.51	40.5	<0.01	0.24	50.1	0.23	<0.01	<0.001	<0.01	101
325	Ol	0.01	9.52	40.3	<0.01	0.32	49.4	0.19	<0.01	<0.001	<0.01	99.8
328	Ol	<0.01	9.74	40.3	<0.01	0.29	49.2	0.23	<0.01	<0.001	<0.01	99.7
335	Ol	0.02	9.54	40.6	<0.01	0.32	49.8	0.13	0.02	0.017	<0.01	100
336	Ol	<0.01	9.28	40.8	<0.01	0.33	48.8	0.16	0.01	<0.001	0.01	99.4
339	Ol	0.01	9.77	41.0	<0.01	0.32	49.3	0.12	<0.01	<0.001	<0.01	100
340	Ol	0.06	9.62	41.0	<0.01	0.30	50.1	0.19	<0.01	<0.001	<0.01	101
341	Ol	<0.01	9.75	40.6	<0.01	0.30	49.6	0.17	<0.01	0.001	<0.01	100
342	Ol	<0.01	9.71	40.7	0.02	0.34	50.1	0.16	<0.01	<0.001	<0.01	101
343	Ol	<0.01	9.74	40.5	<0.01	0.32	49.3	0.20	<0.01	<0.001	<0.01	100
344	Ol	<0.01	9.80	40.8	<0.01	0.31	49.3	0.13	<0.01	0.001	0.01	100
345	Ol	0.01	9.60	40.7	<0.01	0.33	49.4	0.15	0.01	<0.001	<0.01	100
346	Ol	0.06	9.59	40.6	0.01	0.30	49.7	0.15	0.01	<0.001	0.01	100
347	Ol	0.02	9.80	40.6	<0.01	0.30	49.8	0.15	0.03	<0.001	<0.01	101
348	Ol	<0.01	9.32	40.8	<0.01	0.30	49.6	0.13	0.00	<0.001	<0.01	100
349	Ol	<0.01	9.82	40.0	<0.01	0.32	49.3	0.16	<0.01	<0.001	0.02	99.6
350	Ol	<0.01	9.92	40.8	0.00	0.31	50.0	0.17	0.03	<0.001	<0.01	101
351	Ol	0.01	9.52	40.6	<0.01	0.31	48.9	0.11	0.00	<0.001	<0.01	99.5
352	Ol	0.01	9.88	40.8	0.01	0.35	49.5	0.15	<0.01	<0.001	<0.01	101
354	Ol	<0.01	9.78	40.4	<0.01	0.34	49.2	0.20	0.01	<0.001	<0.01	99.9
355	Ol	<0.01	9.78	40.7	<0.01	0.29	49.9	0.13	0.01	<0.001	0.00	101
356	Ol	<0.01	9.64	40.5	<0.01	0.33	49.5	0.20	0.02	<0.001	<0.01	100
357	Ol	0.02	9.91	40.7	<0.01	0.29	49.8	0.20	<0.01	<0.001	0.00	101

C-1 continued

10-14

Nr.	Mineral	Na_2O	FeO	SiO_2	CaO	MgO	MnO	Al_2O_3	NiO	TiO_2	Cr_2O_3	Total
373	Ol	0.02	9.53	40.4	<0.01	0.29	49.0	0.18	<0.01	<0.001	0.01	99.4
374	Ol	0.01	9.49	40.7	<0.01	0.34	49.3	0.17	0.03	<0.001	<0.01	100
377	Ol	0.02	9.76	40.5	<0.01	0.37	49.0	0.12	<0.01	<0.001	<0.01	99.8
378	Ol	<0.01	10.1	40.4	0.01	0.31	49.0	0.17	<0.01	<0.001	<0.01	100
379	Ol	<0.01	9.92	40.7	<0.01	0.35	49.0	0.16	<0.01	<0.001	<0.01	100
380	Ol	0.02	9.70	40.4	<0.01	0.32	48.9	0.16	0.02	<0.001	<0.01	99.5
381	Ol	0.04	9.88	40.3	<0.01	0.34	49.8	0.16	<0.01	<0.001	0.01	101
382	Ol	<0.01	9.63	40.4	0.02	0.34	49.4	0.22	0.02	<0.001	<0.01	100
383	Ol	<0.01	9.73	40.5	<0.01	0.34	49.5	0.17	<0.01	<0.001	<0.01	100
384	Ol	0.02	9.75	40.3	0.00	0.31	49.5	0.14	0.01	<0.001	<0.01	100
387	Ol	<0.01	9.64	40.4	<0.01	0.32	49.7	0.21	0.01	<0.001	<0.01	100
388	Ol	<0.01	9.72	40.0	0.01	0.31	48.8	0.11	0.02	<0.001	0.01	99.0
389	Ol	<0.01	9.47	40.5	<0.01	0.30	49.6	0.19	<0.01	0.002	<0.01	100
390	Ol	0.01	9.33	40.6	<0.01	0.29	50.1	0.12	<0.01	<0.001	<0.01	100
393	Ol	0.03	9.45	40.5	<0.01	0.26	50.6	0.13	0.01	<0.001	<0.01	101
394	Ol	0.03	9.15	40.4	0.01	0.24	49.9	0.19	0.02	<0.001	0.02	99.9
318	Amp	1.27	3.48	50.7	12.6	0.07	20.7	0.07	7.05	0.27	0.67	96.9
319	Amp	1.36	3.43	50.7	12.8	0.08	20.5	0.05	6.86	0.29	0.64	96.7
329	Amp	1.52	3.78	49.8	12.5	0.06	20.3	0.02	7.80	0.29	0.62	96.6
330	Amp	1.36	3.83	49.8	12.6	0.06	20.3	0.07	7.73	0.25	0.58	96.5
331	Amp	1.37	3.69	49.5	12.5	0.07	20.0	0.09	7.64	0.30	0.57	95.7
332	Amp	1.31	3.51	49.6	12.6	0.09	20.3	0.06	7.45	0.34	0.62	95.9
333	Amp	1.40	3.71	49.2	12.4	0.07	20.4	0.05	7.77	0.32	0.59	95.9
334	Amp	1.05	3.13	52.1	12.6	0.08	21.1	0.09	5.39	0.16	0.42	96.1
337	Amp	1.15	3.32	50.1	12.6	0.09	20.1	0.10	6.85	0.23	0.56	95.1
338	Amp	1.09	3.27	48.9	12.5	0.09	20.3	0.02	7.04	0.29	0.64	94.1
358	Amp	1.33	3.74	49.7	12.5	0.09	20.2	0.09	7.51	0.29	0.59	96.0
359	Amp	0.99	3.32	48.7	11.7	0.07	21.4	0.08	5.79	0.23	0.54	92.8
360	Amp	1.18	3.77	49.1	12.7	0.07	20.0	0.02	7.50	0.29	0.63	95.2
361	Amp	0.92	2.87	52.5	12.8	0.09	21.0	0.05	5.11	0.19	0.25	95.8
362	Amp	1.06	3.30	51.9	12.6	0.07	20.8	0.04	5.61	0.19	0.30	95.9
365	Amp	1.22	3.66	50.2	12.7	0.09	20.3	0.06	7.26	0.29	0.62	96.4
366	Amp	0.80	2.99	52.9	12.9	0.07	21.4	0.06	4.82	0.14	0.33	96.4
375	Amp	1.40	3.45	49.1	12.5	0.10	20.2	0.05	7.67	0.21	0.45	95.1
376	Amp	1.53	3.72	48.6	12.6	0.09	20.0	0.06	8.02	0.25	0.58	95.4
385	Amp	0.92	3.05	51.7	12.7	0.08	21.2	0.04	5.37	0.21	0.50	95.7
386	Amp	0.85	2.81	51.9	12.8	0.08	21.3	<0.01	5.06	0.19	0.48	95.5
401	Amp	1.37	3.69	49.2	12.7	0.07	20.1	0.06	7.91	0.26	0.68	96.2
402	Amp	1.47	3.62	49.6	12.7	0.05	20.1	0.04	7.75	0.33	0.63	96.3
314	Spl	<0.01	61.4	<0.01	<0.01	0.13	2.98	0.59	4.21	1.00	26.1	96.4
315	Spl	<0.01	65.0	<0.01	<0.01	0.16	2.62	0.44	3.69	0.939	23.4	96.2
363	Spl	<0.01	58.6	<0.01	<0.01	0.27	3.33	0.40	5.97	0.809	28.1	97.4
364	Spl	0.04	71.8	0.02	<0.01	0.43	1.87	0.28	2.98	1.40	18.1	97.0
367	Spl	<0.01	64.1	<0.01	<0.01	0.49	2.95	0.39	6.02	0.754	22.7	97.4
368	Spl	<0.01	56.4	0.01	<0.01	0.40	3.64	0.48	7.85	0.911	28.3	98.0
369	Spl	0.03	58.9	<0.01	<0.01	0.37	2.91	0.50	5.53	0.893	27.6	96.7
370	Spl	<0.01	58.7	<0.01	<0.01	0.46	2.89	0.50	5.62	0.880	27.9	96.9
371	Spl	<0.01	57.7	0.01	<0.01	0.43	3.03	0.58	6.03	0.892	28.5	97.1
372	Spl	<0.01	56.9	<0.01	<0.01	0.39	3.38	0.46	6.33	0.682	29.5	97.7
395	Spl	<0.01	59.0	<0.01	<0.01	0.22	3.32	0.51	5.46	0.685	28.1	97.2
396	Spl	<0.01	59.7	<0.01	<0.01	0.26	3.06	0.45	5.09	0.698	27.4	96.7
397	Spl	<0.01	61.8	0.03	<0.01	0.09	3.06	0.51	4.37	0.703	26.3	96.9
398	Spl	<0.01	60.9	<0.01	<0.01	0.11	3.06	0.42	4.60	0.695	26.6	96.4
399	Spl	<0.01	60.0	<0.01	<0.01	0.12	3.43	0.56	4.88	0.789	27.6	97.3
400	Spl	<0.01	59.9	0.03	<0.01	0.26	3.05	0.50	4.85	0.792	27.5	96.8
403	Spl	0.09	58.5	0.03	<0.01	0.14	3.06	0.52	4.80	0.719	28.8	96.7
404	Spl	<0.01	59.5	0.07	<0.01	0.13	3.15	0.53	4.81	0.740	27.2	96.2
405	Spl	<0.01	53.8	<0.01	<0.01	0.11	4.29	0.52	6.74	0.658	31.7	97.8
406	Spl	0.06	61.2	<0.01	<0.01	0.14	3.02	0.45	4.56	0.603	25.9	96.0

Table C-2: Electron microprobe mineral analyses of SOISB1 peridotites [wt.%]

10-20A

Nr.	Mineral	Na_2O	FeO	SiO_2	CaO	MgO	MnO	Al_2O_3	NiO	TiO_2	Cr_2O_3	Total
7	Ol	0.01	13.6	39.6	<0.00	46.3	0.27	<0.00	0.22	0.016	0.01	100
9	Ol	<0.01	14.1	39.5	0.01	45.4	0.21	<0.01	0.24	0.011	0.01	99.5
10	Ol	0.03	13.9	39.4	0.01	45.3	0.18	<0.01	0.23	<0.001	<0.01	99.0
11	Ol	<0.01	13.9	39.4	<0.01	45.5	0.19	<0.01	0.18	<0.001	0.02	99.1
12	Ol	<0.01	13.9	39.3	0.01	45.1	0.20	0.01	0.20	0.032	<0.01	98.8
15	Ol	0.02	13.6	39.7	0.01	45.8	0.16	<0.01	0.21	0.047	0.01	99.6
16	Ol	<0.01	13.5	39.5	<0.01	45.6	0.16	0.01	0.23	<0.001	<0.00	98.9
17	Ol	0.00	13.4	39.5	<0.01	45.7	0.16	<0.01	0.20	0.032	0.01	99.0
18	Ol	0.05	13.3	39.8	0.02	45.9	0.20	<0.01	0.18	<0.001	<0.00	99.5
19	Ol	<0.01	13.0	39.7	<0.01	46.1	0.18	<0.01	0.21	<0.001	<0.01	99.2
20	Ol	<0.01	13.0	39.6	<0.01	46.2	0.19	0.01	0.17	0.005	0.01	99.2
21	Ol	0.04	13.1	39.3	0.01	46.0	0.18	<0.01	0.21	<0.001	<0.01	98.8
22	Ol	<0.01	13.3	39.6	0.02	45.9	0.17	<0.01	0.19	0.021	0.01	99.1
23	Ol	0.02	13.7	39.6	0.01	46.0	0.18	0.01	0.23	<0.001	<0.01	99.7
24	Ol	0.02	13.4	39.7	0.01	46.3	0.21	<0.01	0.22	0.016	0.03	99.8
25	Ol	<0.01	13.5	39.4	0.01	45.6	0.22	<0.01	0.21	0.016	<0.01	99.0
26	Ol	<0.01	13.6	39.6	<0.01	45.5	0.22	<0.01	0.18	<0.001	0.01	99.2
27	Ol	0.03	13.7	39.4	0.01	45.5	0.20	0.01	0.19	<0.001	<0.01	99.1
28	Ol	<0.01	13.8	39.6	<0.01	46.0	0.20	<0.01	0.24	0.032	<0.01	99.9
29	Ol	<0.01	13.8	39.6	<0.01	45.3	0.17	0.01	0.26	<0.001	0.03	99.1
32	Ol	<0.01	13.6	39.5	<0.01	45.6	0.21	<0.01	0.24	0.037	0.01	99.1
33	Ol	<0.01	13.4	39.2	<0.01	45.7	0.21	<0.01	0.22	0.021	<0.01	98.7
34	Ol	<0.01	13.8	39.9	0.01	46.3	0.22	0.01	0.22	0.021	0.02	100
35	Ol	<0.01	13.1	39.5	<0.01	46.4	0.18	0.02	0.21	0.037	<0.01	99.4
36	Ol	0.02	13.0	39.7	0.01	45.8	0.25	<0.01	0.22	<0.001	<0.01	98.9
51	Ol	0.03	13.7	39.4	0.01	45.4	0.22	<0.01	0.23	0.032	<0.01	98.9
52	Ol	0.04	13.7	39.4	<0.01	45.7	0.20	<0.01	0.25	<0.001	0.03	99.3
54	Ol	<0.01	13.8	39.6	<0.01	45.3	0.16	<0.01	0.24	0.027	<0.01	99.2
55	Ol	<0.01	13.8	39.5	0.02	45.5	0.22	0.01	0.22	<0.001	0.02	99.3
56	Ol	<0.01	13.6	39.6	<0.01	45.7	0.18	0.01	0.20	<0.001	0.01	99.3
57	Ol	<0.01	13.7	39.4	<0.01	45.5	0.19	<0.01	0.22	<0.001	<0.01	99.0
58	Ol	<0.01	13.8	39.4	<0.01	45.5	0.17	<0.01	0.21	<0.001	0.01	99.2
59	Ol	<0.01	13.9	39.8	<0.01	45.7	0.14	<0.01	0.21	0.111	0.01	99.8
60	Ol	<0.01	14.1	39.5	0.01	45.7	0.18	0.01	0.19	0.053	<0.01	99.7
61	Ol	<0.01	13.6	39.5	0.02	46.4	0.21	<0.01	0.23	<0.001	<0.01	100
62	Ol	<0.01	13.8	39.5	0.01	45.6	0.16	<0.01	0.20	<0.001	<0.01	99.3
63	Ol	<0.01	13.9	39.3	0.01	45.7	0.18	<0.01	0.21	0.026	0.01	99.3
64	Ol	0.06	14.3	39.4	0.01	45.3	0.23	<0.01	0.21	<0.001	<0.01	99.5
65	Ol	<0.01	13.6	39.1	0.01	45.1	0.18	<0.01	0.21	<0.001	<0.01	98.2
66	Ol	0.06	13.8	39.4	<0.01	44.9	0.20	0.01	0.21	0.032	<0.01	98.6
67	Ol	<0.01	13.8	39.7	<0.01	45.6	0.24	<0.01	0.24	<0.001	<0.01	99.5
68	Ol	<0.01	13.5	39.9	0.01	46.2	0.19	<0.01	0.20	<0.001	0.01	100
69	Ol	0.01	13.2	39.9	0.01	45.7	0.21	0.01	0.21	0.026	<0.01	99.3
70	Ol	0.05	13.2	39.7	<0.01	45.6	0.21	<0.01	0.21	0.026	0.02	99.1
71	Ol	<0.01	13.8	40.0	<0.01	45.3	0.24	<0.01	0.21	<0.001	<0.01	99.6
72	Ol	<0.01	13.6	39.8	<0.01	46.5	0.24	<0.01	0.23	0.047	<0.01	100
73	Ol	<0.01	13.8	39.9	0.01	45.7	0.16	0.02	0.20	0.011	<0.01	99.8
74	Ol	<0.01	13.8	39.5	<0.01	45.3	0.20	<0.01	0.22	<0.001	<0.01	99.0
75	Ol	<0.01	13.6	39.4	<0.01	45.9	0.18	<0.01	0.22	<0.001	0.01	99.4
76	Ol	<0.01	13.6	39.3	0.02	45.6	0.22	<0.01	0.21	<0.001	0.02	99.0
77	Ol	0.07	13.7	39.3	0.01	43.9	0.19	0.04	0.19	0.011	<0.01	97.4
78	Ol	<0.01	13.5	39.9	<0.01	45.5	0.17	<0.01	0.24	<0.001	<0.01	99.2
79	Ol	0.01	13.3	39.9	<0.01	45.8	0.13	<0.01	0.22	0.048	<0.01	99.4
80	Ol	0.07	13.7	39.9	<0.01	45.1	0.23	<0.01	0.20	<0.001	0.01	99.2
39	Amph	0.90	3.36	53.1	12.5	21.5	0.08	3.50	0.07	0.22	0.33	95.6
40	Amph	0.38	2.93	55.1	12.5	22.1	0.10	1.63	0.03	0.03	0.31	95.1
41	Amph	1.57	4.16	50.1	12.5	20.1	0.12	6.20	0.06	0.41	0.64	95.8
42	Amph	1.40	3.93	49.8	12.3	19.8	0.13	5.80	0.05	0.41	0.58	94.2
101	Amph	1.17	3.81	52.5	12.4	20.5	0.09	4.67	0.05	0.25	0.29	95.6
103	Amph	1.14	3.50	52.7	12.7	21.2	0.11	4.79	0.05	0.21	0.39	96.8
104	Amph	1.01	3.68	52.2	12.5	20.6	0.04	4.24	0.05	0.30	0.44	95.1
105	Amph	1.15	3.82	52.1	12.5	20.5	0.08	4.73	0.04	0.36	0.44	95.8
106	Amph	1.03	3.60	52.7	12.5	20.7	0.05	4.49	0.06	0.30	0.32	95.7
107	Amph	0.71	3.05	55.2	12.5	21.5	0.11	2.93	0.04	0.21	0.42	96.6
108	Amph	1.01	3.78	52.4	12.6	20.9	0.10	4.89	0.05	0.27	0.32	96.3
110	Amph	0.91	3.21	53.8	12.6	21.1	0.11	3.24	0.06	0.25	0.41	95.7
37	Fe-Mg-Amph	0.05	9.75	57.6	0.70	27.7	0.33	0.05	0.05	0.019	0.02	96.2
38	Fe-Mg-Amph	0.05	9.85	57.7	0.60	27.3	0.36	0.06	0.04	<0.001	0.03	96.0
45	Fe-Mg-Amph	0.05	9.73	57.7	0.70	27.7	0.43	0.06	0.06	<0.001	0.02	96.3
46	Fe-Mg-Amph	0.07	9.68	57.7	0.60	27.4	0.35	0.06	0.07	0.043	0.02	95.9

C-2 continued

10-20A

Nr.	Mineral	Na_2O	FeO	SiO_2	CaO	MgO	MnO	Al_2O_3	NiO	TiO_2	Cr_2O_3	Total
47	Fe-Mg-Amph	0.03	10.5	56.5	0.60	25.9	0.38	0.01	0.08	0.016	<0.01	94.0
48	Fe-Mg-Amph	0.04	9.64	57.6	0.60	27.6	0.30	0.10	0.07	<0.001	0.02	96.0
49	Fe-Mg-Amph	<0.01	9.28	57.4	0.60	27.5	0.30	0.04	0.06	0.048	<0.01	95.2
50	Fe-Mg-Amph	<0.01	9.71	57.6	0.70	27.5	0.38	0.08	0.06	0.032	0.04	96.0
109	Fe-Mg-Amph	0.03	9.70	57.7	0.60	26.8	0.35	0.07	0.06	0.016	0.02	95.4
1	Spl	<0.01	60.9	0.03	0.01	1.25	0.47	0.80	0.10	2.28	29.9	95.7
2	Spl	<0.01	60.9	0.04	<0.01	1.19	0.43	0.82	0.09	2.33	29.4	95.2
81	Spl	<0.01	64.0	<0.01	<0.01	1.29	0.43	0.49	0.14	2.03	27.8	96.2
82	Spl	<0.01	60.4	0.03	<0.01	1.30	0.46	0.63	0.11	2.12	30.3	95.3
83	Spl	0.04	61.3	0.01	<0.01	1.41	0.51	0.57	0.11	1.86	30.3	96.1
84	Spl	0.03	60.3	0.02	0.02	1.38	0.48	0.54	0.07	1.98	31.2	96.0
85	Spl	<0.01	60.3	0.00	0.02	1.36	0.53	0.59	0.12	1.83	30.8	95.6
86	Spl	<0.01	62.5	0.03	<0.01	1.31	0.45	0.47	0.11	1.82	28.7	95.4
87	Spl	0.06	62.5	0.04	<0.01	1.29	0.42	0.60	0.12	1.80	28.4	95.2
90	Spl	<0.01	59.7	0.01	<0.01	1.19	0.51	0.63	0.13	1.74	31.4	95.4
91	Spl	<0.01	60.2	0.08	<0.01	1.21	0.50	0.62	0.12	1.76	30.5	94.9
92	Spl	<0.01	60.4	<0.01	<0.01	1.13	0.53	0.51	0.13	1.62	29.8	94.1
93	Spl	<0.01	63.9	0.03	0.01	1.28	0.41	0.57	0.17	1.97	27.4	95.7
94	Spl	0.04	4.03	31.4	0.05	31.7	0.01	14.9	0.10	0.050	1.31	83.6
43	Chlorite	0.01	4.03	31.4	0.03	30.9	0.02	14.7	0.11	0.13	1.34	82.7
44	Chlorite	<0.01	5.41	31.3	0.05	30.1	0.31	14.1	0.09	0.01	1.42	82.8
102	Chlorite	<0.01	64.0	<0.01	<0.01	1.29	0.43	0.49	0.14	2.03	27.8	96.2

10-20C

Nr.	Mineral	Na_2O	FeO	SiO_2	CaO	MgO	MnO	Al_2O_3	NiO	TiO_2	Cr_2O_3	Total
109	Ol 1	<0.01	12.0	40.4	<0.01	48.0	0.14	<0.01	0.34	<0.001	<0.01	101
110	Ol 1	0.01	12.0	40.8	<0.01	48.0	0.09	0.01	0.31	<0.001	<0.01	101
111	Ol 1	0.01	12.2	40.5	0.01	48.0	0.17	<0.01	0.34	<0.001	<0.01	101
112	Ol 1	<0.01	12.0	40.5	<0.01	48.2	0.20	<0.01	0.32	<0.001	0.01	101
157	Ol 2	<0.01	12.2	40.6	<0.01	47.9	0.18	0.02	0.31	0.005	<0.01	101
162	Ol 2	<0.01	11.8	40.8	<0.01	48.4	0.18	0.01	0.32	<0.001	0.01	102
104	Ol	0.03	11.9	40.2	0.01	47.8	0.10	<0.01	0.31	<0.001	<0.01	100
106	Ol	<0.01	12.2	40.7	<0.01	47.5	0.21	0.01	0.33	<0.001	<0.01	101
108	Ol	<0.01	12.4	40.4	0.01	48.0	0.22	<0.01	0.31	<0.001	0.01	101
117	Ol	<0.01	12.0	39.9	<0.01	47.9	0.20	<0.01	0.33	<0.001	<0.01	100
118	Ol	<0.01	12.2	40.0	0.02	47.8	0.20	0.01	0.32	<0.001	0.01	101
119	Ol	<0.01	11.8	40.7	<0.01	48.1	0.16	<0.01	0.31	<0.001	<0.01	101
120	Ol	<0.01	12.1	40.3	<0.01	47.6	0.20	<0.01	0.31	<0.001	0.02	100
121	Ol	<0.01	11.8	40.8	<0.01	48.0	0.19	<0.01	0.31	0.016	<0.01	101
122	Ol	<0.01	11.9	40.4	<0.01	48.2	0.20	<0.01	0.35	<0.001	<0.01	101
123	Ol	<0.01	12.0	40.8	<0.01	47.9	0.15	0.02	0.31	<0.001	<0.01	101
124	Ol	<0.01	12.1	40.7	<0.01	48.7	0.19	0.01	0.35	<0.001	<0.01	102
130	Ol	<0.01	12.2	40.4	<0.01	48.4	0.13	0.02	0.31	<0.001	0.02	102
131	Ol	<0.01	12.1	40.8	<0.01	48.2	0.21	0.01	0.33	<0.001	<0.01	102
132	Ol	0.01	12.4	40.9	<0.01	48.0	0.19	<0.01	0.30	<0.001	<0.01	102
134	Ol	<0.01	12.3	40.5	<0.01	47.3	0.20	0.01	0.33	<0.001	<0.01	101
138	Ol	0.01	12.5	40.5	<0.01	47.8	0.16	<0.01	0.33	<0.001	<0.01	101
139	Ol	0.02	12.3	40.6	<0.01	47.4	0.17	<0.01	0.35	<0.001	0.01	101
140	Ol	0.01	12.1	40.6	<0.01	47.9	0.17	0.01	0.32	<0.001	<0.01	101
141	Ol	0.01	12.2	40.3	<0.01	47.3	0.20	<0.01	0.32	<0.001	<0.01	100
142	Ol	<0.01	12.3	40.5	<0.01	47.6	0.16	<0.01	0.33	0.019	<0.01	101
145	Ol	<0.01	12.7	40.8	<0.01	47.5	0.15	0.01	0.31	<0.001	0.01	102
146	Ol	<0.01	12.0	40.7	0.01	47.7	0.20	<0.01	0.32	<0.001	0.02	101
147	Ol	0.04	12.1	40.2	<0.01	47.6	0.20	<0.01	0.31	<0.001	<0.01	100
148	Ol	0.01	12.3	41.0	<0.01	48.3	0.18	0.01	0.32	<0.001	<0.01	102
149	Ol	0.02	12.2	40.6	<0.01	48.2	0.12	<0.01	0.31	<0.001	<0.01	101
150	Ol	<0.01	12.1	40.8	<0.01	48.7	0.17	0.01	0.33	<0.001	0.01	102
163	Ol	<0.01	11.7	40.6	<0.01	48.2	0.18	<0.01	0.36	<0.001	0.01	101
170	Ol	<0.01	12.1	40.4	<0.01	47.7	0.15	<0.01	0.33	0.015	0.02	101
171	Ol	0.02	12.1	40.5	<0.01	47.7	0.22	<0.01	0.31	<0.001	0.01	101
173	Ol	0.04	12.1	40.3	<0.01	47.4	0.20	0.02	0.34	0.007	<0.01	101
179	Ol	0.03	12.2	40.7	<0.01	47.1	0.20	<0.01	0.34	0.001	0.02	101
183	Ol	<0.01	11.7	40.2	<0.01	48.5	0.16	0.01	0.33	<0.001	<0.01	101
184	Ol	<0.01	12.1	40.1	<0.01	47.9	0.10	<0.01	0.35	0.029	<0.01	101
185	Ol	<0.01	11.8	40.4	<0.01	47.8	0.20	0.02	0.31	<0.001	0.03	101
186	Ol	<0.01	12.1	40.4	<0.01	48.6	0.21	<0.01	0.34	<0.001	0.01	102
187	Ol	0.02	12.0	40.8	<0.01	48.8	0.23	<0.01	0.32	<0.001	<0.01	102
193	Ol	<0.01	11.9	40.5	<0.01	48.7	0.12	0.01	0.31	<0.001	<0.01	102
195	Ol	<0.01	11.9	40.2	<0.01	48.0	0.20	<0.01	0.32	<0.001	0.03	101
196	Ol	<0.01	11.7	40.8	<0.01	48.4	0.16	<0.01	0.30	<0.001	0.01	101
197	Ol	<0.01	11.7	40.7	<0.01	48.1	0.17	<0.01	0.35	<0.001	0.01	101

C-2 continued

10-20C

Nr.	Mineral	Na_2O	FeO	SiO_2	CaO	MgO	MnO	Al_2O_3	NiO	TiO_2	Cr_2O_3	Total
125	Amp	1.39	3.49	51.8	12.6	20.9	0.07	6.02	0.09	0.40	0.57	97.2
127	Amp	1.27	3.53	51.5	12.4	20.9	0.09	6.46	0.09	0.36	0.57	97.1
159	Amp	0.04	2.03	58.5	12.9	23.6	0.09	0.07	0.05	0.010	0.02	97.2
160	Amp	0.02	2.17	58.8	12.7	23.9	0.07	0.07	0.04	0.010	0.02	97.7
161	Amp	0.03	2.11	58.8	12.8	23.5	0.12	0.07	0.02	<0.01	0.03	97.4
164	Amp	1.24	3.32	52.5	12.2	21.1	0.08	5.55	0.08	0.34	0.58	97.0
165	Amp	1.37	3.53	49.6	12.3	20.1	0.08	6.46	0.07	0.39	0.65	94.6
166	Amp	1.21	3.34	52.7	12.3	21.0	0.08	5.55	0.10	0.33	0.49	97.1
168	Amp	1.24	3.40	51.2	12.2	20.1	0.10	5.40	0.09	0.33	0.55	94.6
169	Amp	1.37	3.44	51.1	12.4	20.6	0.08	6.49	0.07	0.34	0.60	96.4
188	Amp	1.49	3.42	50.9	12.2	21.0	0.09	6.35	0.10	0.41	0.61	96.6
189	Amp	0.84	2.93	54.3	12.4	22.2	0.07	3.58	0.07	0.17	0.31	96.9
190	Amp	1.13	3.40	52.6	12.3	21.7	0.06	5.43	0.08	0.30	0.25	97.2
191	Amp	0.98	3.01	53.0	12.4	21.6	0.05	4.78	0.09	0.27	0.30	96.4
192	Amp	1.18	3.28	52.5	12.5	21.5	0.10	5.70	0.09	0.27	0.48	97.6
194	Amp	1.19	3.44	50.8	12.1	22.1	0.09	6.49	0.08	0.40	0.62	97.3
194	Amp	1.19	3.44	50.8	12.1	22.1	0.09	6.49	0.08	0.40	0.62	97.3
199	Amp	1.12	3.31	52.8	12.3	21.3	0.07	5.40	0.06	0.19	0.61	97.2
200	Spl	<0.01	51.7	<0.01	<0.01	1.55	0.73	0.57	0.10	1.10	43.1	98.8
201	Spl	<0.01	65.7	0.89	<0.01	2.78	0.48	0.76	0.13	0.33	28.9	99.9
202	Spl	0.02	56.3	<0.01	<0.01	1.23	0.59	0.45	0.10	1.15	37.9	97.7
203	Spl	<0.01	54.2	0.01	<0.01	1.65	0.76	0.62	0.20	1.44	39.2	98.0
204	Spl	<0.01	51.8	<0.01	<0.01	1.50	0.58	0.85	0.13	1.42	41.0	97.3
205	Spl	<0.01	50.6	0.02	<0.01	1.73	0.59	0.78	0.16	1.43	42.5	97.8
206	Spl	<0.01	48.9	0.02	<0.01	1.88	0.68	0.80	0.13	1.15	44.5	98.1
209	Spl	<0.01	52.8	<0.01	<0.01	1.63	0.54	0.85	0.21	1.54	41.0	98.5
210	Spl	<0.01	52.4	0.01	<0.01	1.52	0.64	0.73	0.15	1.57	41.2	98.3
211	Spl	<0.01	60.8	0.02	<0.01	1.23	0.56	0.36	0.30	1.46	32.5	97.3
212	Spl	<0.01	53.4	0.01	<0.01	1.39	0.46	0.73	0.13	1.50	39.9	97.5
213	Spl	<0.01	52.7	<0.01	<0.01	1.58	0.69	0.74	0.16	1.66	39.6	97.2
214	Spl	<0.01	53.6	0.03	<0.01	1.67	0.59	0.66	0.19	1.66	38.9	97.3
215	Spl	<0.01	53.1	0.03	<0.01	1.61	0.65	0.72	0.16	1.67	39.4	97.3
216	Spl	<0.01	51.0	0.02	<0.01	1.50	0.67	0.50	0.16	1.10	42.3	97.2
217	Spl	0.04	51.3	0.01	<0.01	1.52	0.68	0.51	0.13	1.11	42.7	98.0
218	Spl	0.11	51.2	0.01	<0.01	1.52	0.57	0.91	0.15	1.37	41.4	97.3
219	Spl	<0.01	52.8	0.00	<0.01	1.54	0.64	0.86	0.13	1.43	39.8	97.2
220	Spl	<0.01	51.7	0.01	<0.01	1.55	0.71	0.80	0.10	1.54	41.7	98.1
221	Spl	<0.01	52.4	<0.01	<0.01	1.53	0.60	0.75	0.11	1.50	41.7	98.6
222	Spl	<0.01	51.3	0.02	<0.01	1.58	0.63	0.80	0.13	1.42	42.3	98.1
223	Spl	<0.01	52.8	<0.01	<0.01	1.52	0.63	0.70	0.16	1.57	39.1	96.5
227	Spl	<0.01	54.3	<0.01	<0.01	1.81	0.53	1.04	0.17	2.42	37.9	98.1
228	Spl	0.03	52.4	0.02	<0.01	1.58	0.60	0.90	0.15	1.74	40.9	98.3
229	Spl	<0.01	51.9	<0.01	<0.01	1.58	0.62	0.88	0.15	1.78	41.0	97.9
230	Spl	<0.01	53.1	0.06	<0.01	1.60	0.56	0.87	0.16	1.44	40.5	98.3

10-22

Nr.	Mineral	Na_2O	FeO	SiO_2	CaO	NiO	MgO	MnO	Al_2O_3	TiO_2	Cr_2O_3	Total
1	Ol	0.03	8.16	41.7	<0.01	51.4	0.12	0.01	0.42	<0.001	<0.01	102
2	Ol	<0.01	8.53	41.4	<0.01	50.7	0.16	0.01	0.41	0.014	<0.01	101
3	Ol	<0.01	8.35	41.6	<0.01	50.8	0.13	0.02	0.42	<0.001	<0.01	101
4	Ol	<0.01	8.77	41.3	0.01	50.2	0.15	<0.01	0.44	0.008	<0.01	101
5	Ol	0.01	7.37	41.3	<0.01	51.4	0.16	<0.01	0.41	<0.001	<0.01	101
6	Ol	<0.01	7.74	41.4	<0.01	51.8	0.16	<0.01	0.41	0.012	0.01	102
7	Ol	<0.01	8.27	41.3	<0.01	51.6	0.16	<0.01	0.40	<0.001	<0.01	102
8	Ol	<0.01	7.84	41.4	<0.01	51.5	0.18	<0.01	0.44	0.037	<0.01	101
9	Ol	<0.01	7.52	41.7	<0.01	51.5	0.18	<0.01	0.44	<0.001	<0.01	101
10	Ol	0.02	7.77	41.3	<0.01	51.6	0.19	<0.01	0.44	<0.001	<0.01	101
14	Ol	<0.01	7.49	41.5	<0.01	51.9	0.21	<0.01	0.35	<0.001	<0.01	102
15	Ol	0.01	7.55	41.3	<0.01	52.0	0.18	<0.01	0.40	0.012	<0.01	102
16	Ol	0.02	7.79	41.7	<0.01	51.7	0.20	<0.01	0.35	0.013	0.02	102
17	Ol	<0.01	7.96	41.4	0.00	50.9	0.13	<0.01	0.39	0.015	<0.01	101
18	Ol	<0.01	7.97	41.8	<0.01	51.2	0.12	0.02	0.39	<0.001	0.01	102
19	Ol	<0.01	7.30	41.3	0.01	51.0	0.21	<0.01	0.38	<0.001	<0.01	100
23	Ol	0.01	8.10	41.3	<0.01	51.8	0.14	<0.01	0.39	<0.001	<0.01	102
24	Ol	0.05	8.07	41.7	<0.01	51.6	0.17	<0.01	0.39	<0.001	0.01	102
25	Ol	<0.01	8.53	41.3	<0.01	51.1	0.13	<0.01	0.40	<0.001	<0.01	102
26	Ol	<0.01	8.65	41.5	<0.01	51.1	0.18	<0.01	0.40	0.001	<0.01	102
27	Ol	<0.01	8.90	41.3	<0.01	50.5	0.12	<0.01	0.38	<0.001	<0.01	101
28	Ol	0.01	7.75	41.2	<0.01	51.4	0.16	0.01	0.40	<0.001	<0.01	101
29	Ol	<0.01	8.63	41.2	<0.01	50.8	0.14	<0.01	0.38	0.006	<0.01	101
30	Ol	0.20	7.99	41.7	0.01	51.1	0.08	<0.01	0.35	<0.001	<0.01	101
31	Ol	<0.01	8.26	41.6	<0.01	51.4	0.17	<0.01	0.36	0.042	<0.01	102
32	Ol	<0.01	7.38	41.5	<0.01	52.3	0.15	<0.01	0.38	0.019	<0.01	102
33	Ol	0.01	8.55	41.3	<0.01	51.0	0.14	0.02	0.38	0.005	0.01	101
34	Ol	0.01	8.57	41.5	0.01	52.0	0.15	<0.01	0.42	<0.001	<0.01	103

C-2 continued

10-22

Nr.	Mineral	Na_2O	FeO	SiO_2	CaO	MgO	MnO	Al_2O_3	NiO	TiO_2	Cr_2O_3	Total
35	Ol	<0.01	8.76	41.2	<0.01	51.5	0.21	<0.01	0.40	<0.001	0.01	102
36	Ol	0.01	8.15	41.7	<0.01	51.8	0.19	<0.01	0.33	<0.001	<0.01	102
37	Ol	<0.01	8.08	41.8	<0.01	51.0	0.18	<0.01	0.37	0.011	0.01	101
38	Ol	<0.01	8.77	41.2	<0.01	50.2	0.12	<0.01	0.42	<0.001	0.01	101
39	Ol	<0.01	8.42	41.3	<0.01	50.8	0.16	<0.01	0.42	<0.001	0.00	101
40	Ol	<0.01	8.89	41.3	<0.01	51.1	0.14	<0.01	0.43	<0.001	<0.01	102
41	Ol	<0.01	8.46	41.0	<0.01	50.6	0.13	0.01	0.35	<0.001	0.01	101
42	Ol	0.15	7.75	41.5	<0.01	51.1	0.13	<0.01	0.42	0.016	<0.01	101
43	Ol	<0.01	8.09	41.2	<0.01	51.4	0.11	0.01	0.42	0.027	0.03	101
44	Ol	<0.01	8.77	41.1	<0.01	50.8	0.20	<0.01	0.44	<0.001	<0.01	101
45	Ol	<0.01	8.61	40.5	<0.01	50.8	0.20	<0.01	0.44	<0.001	<0.01	101
46	Ol	<0.01	8.78	41.7	<0.01	51.1	0.21	<0.01	0.41	<0.001	<0.01	102
47	Ol	0.09	8.62	41.3	<0.01	50.6	0.18	0.01	0.40	<0.001	<0.01	101
48	Ol	<0.01	7.48	41.9	<0.01	51.2	0.16	<0.01	0.34	<0.001	<0.01	101
49	Ol	<0.01	8.07	41.3	<0.01	50.7	0.15	<0.01	0.39	<0.001	0.03	101
51	Ol	<0.01	8.12	41.2	<0.01	50.9	0.17	<0.01	0.41	0.005	<0.01	101
52	Ol	<0.01	7.98	41.2	<0.01	51.0	0.12	<0.01	0.38	<0.001	<0.01	101
53	Ol	<0.01	8.16	41.7	0.00	51.0	0.20	<0.01	0.43	<0.001	0.01	102
55	Ol	0.01	7.81	42.1	<0.01	51.9	0.18	0.01	0.33	<0.001	0.01	102
511	Amp	0.59	1.84	55.6	12.5	23.1	0.04	1.62	0.07	0.12	0.36	95.8
510	Amp	0.85	2.10	55.1	12.4	22.8	0.01	2.40	0.11	0.15	0.30	96.2
518	Amp	0.73	2.24	55.6	12.6	22.8	0.08	2.97	0.12	0.18	0.05	97.3
508	Amp	1.05	2.67	54.3	12.6	22.1	0.04	4.00	0.11	0.28	0.41	97.5
506	Amp	1.02	2.47	55.0	12.5	22.3	0.09	3.34	0.06	0.28	0.48	97.5
519	Amp	0.97	2.39	55.0	12.6	22.4	0.08	3.67	0.10	0.27	0.11	97.6
509	Amp	1.05	2.62	54.4	12.5	21.9	0.05	4.22	0.11	0.28	0.47	97.6
504	Amp	0.77	2.53	55.0	12.5	22.5	0.08	3.41	0.09	0.29	0.51	97.7
515	Amp	0.81	2.12	56.0	12.5	23.0	0.09	2.74	0.10	0.17	0.28	97.8
512	Amp	0.75	2.24	56.3	12.5	22.8	0.09	2.58	0.10	0.20	0.20	97.8
514	Amp	0.87	2.14	55.9	12.6	22.8	0.06	2.83	0.07	0.20	0.30	97.8
505	Amp	1.25	2.62	54.9	12.4	22.0	0.04	3.88	0.11	0.29	0.31	97.8
513	Amp	0.70	2.04	56.3	12.7	22.8	0.13	2.55	0.12	0.16	0.33	97.9
507	Amp	1.10	2.65	54.4	12.6	22.1	0.08	4.50	0.08	0.33	0.37	98.2
517	Amp	0.66	2.23	56.8	12.7	23.3	0.08	2.26	0.04	0.15	0.50	98.7
516	Amp	0.91	2.44	56.6	12.7	23.0	0.04	3.06	0.14	0.20	0.22	99.3
511	Amp	0.59	1.84	55.6	12.5	23.1	0.04	1.62	0.07	0.12	0.36	95.8
54	Spl	<0.01	82.9	<0.01	<0.01	0.99	0.16	0.04	0.46	0.04	9.11	93.7
56	Spl	<0.01	77.4	0.06	<0.01	1.18	0.41	0.06	0.44	0.17	15.2	94.9
57	Spl	<0.01	76.9	<0.01	<0.01	1.26	0.37	0.09	0.43	0.17	15.9	95.1
58	Spl	<0.01	80.9	<0.01	<0.01	1.11	0.27	0.06	0.46	0.15	11.3	94.3
59	Spl	<0.01	83.5	0.01	<0.01	1.03	0.10	0.06	0.51	0.08	8.01	93.3
60	Spl	0.01	84.7	0.00	<0.01	1.03	0.15	0.03	0.48	0.10	7.21	93.7

10-23

Nr.	Mineral	Na_2O	FeO	SiO_2	CaO	MgO	MnO	Al_2O_3	NiO	TiO_2	Cr_2O_3	Total
323	Ol	<0.01	8.92	41.2	0.00	50.5	0.20	0.01	0.40	0.026	0.02	101
324	Ol	<0.01	8.86	41.1	<0.01	51.3	0.16	<0.01	0.33	0.010	<0.01	102
325	Ol	<0.01	8.82	41.3	<0.01	50.9	0.13	<0.01	0.34	<0.001	<0.01	102
326	Ol	0.01	8.76	40.9	<0.01	50.7	0.15	<0.01	0.38	0.010	0.02	101
327	Ol	0.03	8.47	41.1	<0.01	51.4	0.22	<0.01	0.33	<0.001	0.02	102
328	Ol	<0.01	8.67	41.2	0.01	51.0	0.14	<0.01	0.33	<0.001	0.02	101
329	Ol	<0.01	8.43	41.0	<0.01	50.9	0.14	<0.01	0.30	<0.001	<0.01	101
330	Ol	0.02	8.85	40.9	<0.01	50.7	0.09	0.02	0.35	<0.001	0.04	101
331	Ol	<0.01	8.95	40.8	<0.01	50.5	0.21	<0.01	0.40	<0.001	<0.01	101
332	Ol	0.01	8.46	40.8	0.02	50.7	0.15	<0.01	0.27	0.031	0.08	101
333	Ol	<0.01	8.74	41.3	<0.01	51.3	0.17	<0.01	0.34	0.026	<0.01	102
334	Ol	0.00	8.48	40.9	<0.01	50.9	0.20	<0.01	0.30	<0.001	0.02	101
335	Ol	0.01	8.78	40.9	0.02	51.0	0.20	<0.01	0.39	0.015	0.01	101
336	Ol	<0.01	8.56	41.0	0.01	51.0	0.17	<0.01	0.32	<0.001	0.01	101
337	Ol	<0.01	8.53	41.1	<0.01	51.0	0.19	<0.01	0.39	0.031	<0.01	101
338	Ol	0.04	8.75	41.3	<0.01	50.8	0.18	<0.01	0.37	<0.001	<0.01	102
339	Ol	<0.01	8.42	41.3	<0.01	51.6	0.20	<0.01	0.35	0.005	<0.01	102
340	Ol	<0.01	8.37	40.9	0.02	0.02	50.7	0.19	0.32	0.021	0.01	101
341	Ol	<0.01	8.61	41.1	<0.01	0.03	51.3	0.18	0.39	0.005	<0.01	102
342	Ol	<0.01	8.98	40.9	<0.01	<0.01	50.4	0.17	0.39	<0.001	<0.01	101
343	Ol	<0.01	8.37	41.1	0.00	<0.01	50.9	0.19	0.33	0.026	<0.01	101
344	Ol	0.01	9.44	40.7	0.02	<0.01	50.1	0.18	0.43	<0.001	0.01	101
345	Ol	0.03	9.61	41.1	<0.01	0.01	50.3	0.15	0.44	0.010	0.01	102
346	Ol	<0.01	8.81	41.2	<0.01	<0.01	50.9	0.18	0.43	<0.001	<0.01	102
347	Ol	<0.01	9.17	40.9	<0.01	0.00	50.0	0.17	0.38	<0.001	<0.01	101
348	Ol	0.01	6.89	45.9	0.01	0.01	46.7	0.10	0.36	<0.001	0.01	100
349	Ol	0.01	8.97	41.1	<0.01	0.01	50.2	0.17	0.41	0.056	<0.01	101
350	Ol	0.01	9.21	40.9	<0.01	<0.01	49.9	0.19	0.41	0.010	<0.01	101
351	Ol	<0.01	8.89	41.1	<0.01	<0.01	50.1	0.18	0.36	0.005	<0.01	101
352	Ol	<0.01	8.53	41.0	<0.01	<0.01	50.8	0.17	0.34	0.056	0.02	101
353	Ol	<0.01	8.99	41.0	<0.01	<0.01	50.6	0.20	0.43	<0.001	0.02	101

C-2 continued

10-23

Nr.	Mineral	Na_2O	FeO	SiO_2	CaO	MgO	MnO	Al_2O_3	NiO	TiO_2	Cr_2O_3	Total
354	Ol	0.01	9.02	40.6	<0.01	<0.01	50.6	0.17	0.38	0.02	0.01	101
355	Ol	<0.01	9.40	40.2	<0.01	<0.01	49.5	0.18	0.40	0.06	0.02	99.8
356	Ol	<0.01	9.31	41.0	<0.01	0.01	49.9	0.20	0.39	<0.01	<0.01	101
357	Ol	<0.01	9.50	40.3	<0.01	0.01	49.5	0.13	0.42	0.02	0.02	99.9
358	Ol	<0.01	9.65	39.7	<0.01	0.01	50.1	0.14	0.41	<0.01	<0.01	100
359	Ol	<0.01	9.33	40.9	<0.01	<0.01	50.1	0.17	0.40	<0.01	0.01	101
360	Ol	<0.01	9.68	39.3	<0.01	0.01	49.4	0.18	0.41	0.03	<0.01	99.0
361	Ol	0.03	9.07	40.8	<0.01	<0.01	50.3	0.22	0.43	0.01	<0.01	101
362	Ol	<0.01	8.59	41.0	<0.01	0.01	49.8	0.17	0.35	<0.01	<0.01	100
363	Ol	<0.01	8.47	41.0	<0.01	<0.01	50.5	0.18	0.25	<0.01	0.03	100
364	Ol	0.01	8.77	40.8	0.01	0.01	50.1	0.17	0.38	<0.01	<0.01	100
365	Ol	<0.01	9.24	40.9	0.01	0.02	49.8	0.11	0.43	<0.01	<0.01	101
366	Ol	<0.01	9.18	40.5	0.01	<0.01	49.5	0.16	0.42	0.03	<0.01	99.8
367	Ol	<0.01	9.26	41.1	<0.01	0.01	50.2	0.20	0.41	<0.01	<0.01	101
368	Ol	<0.01	9.00	41.4	<0.01	<0.01	50.2	0.17	0.40	0.03	<0.01	101
369	Ol	<0.01	8.36	40.6	<0.01	<0.01	50.3	0.13	0.34	0.02	<0.01	99.7
370	Ol	0.02	8.41	40.9	<0.01	<0.01	50.5	0.16	0.37	0.01	<0.01	100
371	Ol	<0.01	8.42	40.6	0.02	<0.01	50.9	0.18	0.26	0.01	<0.01	100
372	Ol	<0.01	8.33	40.9	<0.01	<0.01	50.5	0.18	0.36	<0.01	0.02	100
373	Ol	<0.01	8.54	41.1	<0.01	<0.01	50.5	0.17	0.35	<0.01	<0.01	101
374	Ol	0.01	8.99	40.4	<0.01	0.01	49.8	0.22	0.42	<0.01	<0.01	99.8
375	Ol	<0.01	8.63	40.4	0.01	0.01	50.3	0.12	0.43	0.01	<0.01	99.9
376	Ol	<0.01	9.41	40.3	0.01	<0.01	50.3	0.14	0.41	<0.01	<0.01	101
377	Ol	0.01	8.98	41.0	<0.01	50.5	0.17	<0.01	0.39	0.031	<0.01	101
378	Ol	0.01	8.93	41.0	0.01	50.6	0.14	<0.01	0.39	0.005	<0.01	101
379	Ol	0.02	8.64	41.2	<0.01	50.7	0.10	<0.01	0.34	<0.00	<0.01	101
380	Ol	0.01	8.59	41.4	0.02	51.4	0.12	<0.01	0.30	0.021	0.01	102
381	Ol	<0.01	8.89	40.2	<0.01	49.8	0.16	0.01	0.43	<0.00	0.01	99.6
382	Ol	0.01	9.13	41.2	0.01	50.4	0.12	<0.01	0.40	0.021	<0.01	101
383	Ol	<0.01	8.86	41.0	0.02	51.0	0.12	<0.01	0.44	0.077	<0.01	102
384	Ol	0.06	9.08	41.0	0.02	50.5	0.19	0.01	0.40	<0.00	<0.01	101
385	Ol	<0.01	9.20	41.1	<0.01	50.7	0.15	<0.01	0.39	<0.00	<0.01	102
386	Ol	0.01	8.65	40.9	0.02	51.0	0.18	0.02	0.26	0.062	<0.01	101
387	Ol	0.02	8.58	41.1	<0.01	50.9	0.17	0.01	0.36	<0.00	<0.01	101
388	Ol	0.01	8.57	40.9	0.01	50.8	0.16	<0.01	0.42	0.010	<0.01	101
389	Ol	<0.01	9.61	40.9	<0.01	50.4	0.14	<0.01	0.40	0.051	<0.01	101
391	Ol	<0.01	8.66	40.9	0.02	51.0	0.20	0.01	0.37	<0.00	<0.01	101
392	Ol	0.05	8.72	41.2	0.02	50.9	0.16	0.02	0.43	<0.00	<0.01	102
393	Ol	<0.01	8.71	40.9	<0.01	50.6	0.19	<0.01	0.43	0.005	<0.01	101
394	Ol	<0.01	8.93	41.2	<0.01	50.4	0.17	0.01	0.41	0.010	<0.01	101
395	Ol	0.04	9.25	41.1	0.02	50.8	0.16	0.02	0.42	0.015	<0.01	102
396	Ol	<0.01	9.48	41.2	<0.01	50.5	0.15	<0.01	0.43	0.031	<0.01	102
397	Ol	<0.01	8.66	41.5	<0.01	50.8	0.21	0.02	0.33	0.046	<0.01	102
398	Ol	<0.01	9.35	40.7	0.02	50.1	0.11	<0.01	0.43	0.010	0.01	101
399	Ol	<0.01	8.94	40.8	0.02	50.1	0.15	<0.01	0.42	<0.00	<0.01	100
400	Ol	0.01	8.73	41.3	<0.01	51.1	0.17	0.02	0.44	0.010	<0.01	102
471	Amp	1.26	2.94	53.5	12.3	21.7	0.06	4.64	0.10	0.29	0.49	97.3
472	Amp	1.34	2.75	54.4	12.3	22.1	0.05	4.20	0.12	0.25	0.48	98.0
473	Amp	1.22	2.71	53.6	12.5	22.2	0.07	4.32	0.09	0.21	0.47	97.4
474	Amp	0.77	2.53	54.9	12.4	22.5	0.06	2.83	0.12	0.14	0.22	96.4
475	Amp	0.84	2.56	55.5	12.4	22.5	0.11	3.16	0.08	0.19	0.33	97.7
476	Amp	1.56	3.21	52.7	12.3	21.5	0.11	5.60	0.11	0.33	0.67	98.1
477	Amp	0.61	2.39	56.9	12.4	23.2	0.08	1.88	0.12	0.11	0.26	98.0
478	Amp	0.96	2.53	55.5	12.5	22.6	0.09	2.94	0.11	0.16	0.26	97.6
479	Amp	1.64	2.97	52.6	12.5	21.5	0.11	5.23	0.006	0.34	0.67	97.6
480	Amp	0.03	1.15	59.1	13.3	23.9	0.11	0.05	0.06	0.006	0.02	97.6
481	Amp	1.34	2.83	52.5	12.5	21.5	0.11	4.91	0.09	0.271	0.55	96.6
482	Amp	0.65	2.53	55.1	12.7	22.5	0.04	2.72	0.12	0.19	0.38	97.0
483	Amp	0.90	2.77	54.6	12.5	22.7	0.08	3.43	0.08	0.18	0.48	97.8
484	Amp	0.30	2.00	52.7	10.3	24.9	0.03	3.70	0.06	0.078	0.53	94.6
485	Amp	0.39	2.16	57.1	12.0	23.5	0.05	1.28	0.13	0.072	0.03	96.7
486	Amp	1.06	2.60	54.1	12.4	22.1	0.08	4.02	0.09	0.23	0.50	97.2
487	Amp	1.34	3.02	53.6	12.4	21.8	0.02	4.47	0.11	0.23	0.36	97.3
488	Amp	1.24	3.09	53.5	12.3	21.9	0.13	4.31	0.12	0.246	0.33	97.1
489	Amp	0.30	2.14	57.6	12.5	23.5	0.09	0.99	0.11	0.065	0.17	97.4
490	Amp	0.21	2.15	58.5	12.2	24.2	0.12	0.40	0.08	0.032	0.08	98.0
491	Amp	0.95	2.54	53.9	12.2	22.3	0.05	3.49	0.08	0.18	0.46	96.1
492	Amp	1.02	2.71	54.2	12.7	22.3	0.11	3.46	0.09	0.22	0.34	97.1
495	Amp	1.00	2.71	54.0	12.4	21.6	0.04	3.73	0.08	0.18	0.61	96.3
496	Amp	1.02	2.66	52.9	12.3	20.9	0.09	3.79	0.10	0.23	0.64	94.6
497	Amp	0.37	2.05	57.2	12.4	23.2	0.10	1.19	0.05	0.08	0.22	96.8
498	Amp	1.48	3.13	53.2	12.1	21.5	0.09	4.85	0.10	0.29	0.30	97.1
499	Amp	1.62	3.19	51.4	12.4	20.8	0.04	6.50	0.10	0.26	0.75	97.1

C-2 continued

10-23

Nr.	Mineral	Na_2O	FeO	SiO_2	CaO	MgO	MnO	Al_2O_3	NiO	TiO_2	Cr_2O_3	Total
500	Amp	1.02	2.78	54.2	12.3	21.8	0.03	3.89	0.11	0.24	0.54	96.9
501	Amp	0.45	2.23	56.8	12.8	23.4	0.09	1.41	0.08	0.067	0.26	97.5
268	Spl	<0.01	60.0	0.03	<0.01	2.04	0.66	0.26	0.21	0.95	31.7	95.8
269	Spl	0.07	58.4	0.02	0.01	1.88	0.63	0.25	0.22	0.99	32.5	95.0
270	Spl	<0.01	59.1	<0.01	<0.01	2.02	0.66	0.26	0.23	0.88	32.6	95.7
271	Spl	<0.01	59.5	0.01	<0.01	2.13	0.65	0.20	0.21	1.01	32.8	96.6
272	Spl	0.02	67.5	<0.01	<0.01	1.62	0.56	0.13	0.30	0.86	24.4	95.3
273	Spl	<0.01	61.5	0.01	0.02	1.97	0.63	0.24	30.7	0.93	0.20	96.2
274	Spl	0.01	66.1	<0.01	<0.01	1.68	0.47	0.18	25.0	0.74	0.28	94.4
275	Spl	<0.01	67.1	0.02	<0.01	1.57	0.48	0.19	24.7	0.62	0.29	94.9
276	Spl	<0.01	65.8	0.03	0.01	1.67	0.50	0.19	24.1	0.66	0.29	93.3
277	Spl	0.02	62.8	<0.01	<0.01	1.81	0.56	0.24	29.8	1.04	0.26	96.5
278	Spl	<0.01	67.7	0.01	<0.01	1.50	0.42	0.16	22.8	0.89	0.29	93.8
279	Spl	0.06	64.2	0.01	<0.01	1.58	0.56	0.17	26.7	0.95	0.28	94.5
280	Spl	0.01	61.9	<0.01	0.01	1.76	0.63	0.24	27.4	0.87	0.23	93.0
281	Spl	<0.01	63.6	0.04	<0.01	1.72	0.57	0.23	27.6	0.84	0.25	94.8
282	Spl	0.01	62.6	0.02	0.01	1.63	0.61	0.22	27.8	0.84	0.25	93.9
283	Spl	<0.01	64.9	0.04	<0.01	1.60	0.60	0.20	25.6	0.73	0.24	93.9
286	Spl	<0.01	69.9	0.03	0.01	1.31	0.43	0.13	21.9	0.59	0.28	94.6
287	Spl	0.05	65.2	<0.01	<0.01	1.52	0.56	0.17	26.5	0.69	0.24	94.9
288	Spl	<0.01	63.6	0.02	<0.01	1.77	0.58	0.21	28.4	0.69	0.24	95.5
289	Spl	<0.01	60.7	<0.01	0.01	2.01	0.72	0.26	32.3	0.83	0.19	97.0
290	Spl	<0.01	58.3	<0.01	<0.01	1.98	0.68	0.26	31.8	0.89	0.21	94.2
291	Spl	<0.01	62.1	<0.01	<0.01	1.71	0.57	0.19	29.8	0.79	0.22	95.4
292	Spl	0.08	67.6	<0.01	0.01	1.52	0.61	0.18	25.9	0.65	0.26	96.8
293	Spl	0.03	72.0	<0.01	<0.01	1.39	0.40	0.15	20.8	0.57	0.26	95.6
297	Spl	0.14	69.1	<0.01	<0.01	1.43	0.49	0.17	22.8	0.80	0.29	95.2
298	Spl	0.04	62.9	<0.01	0.03	1.67	0.51	0.25	29.2	0.84	0.24	95.7
299	Spl	0.06	60.8	0.07	0.01	1.98	0.65	0.27	32.5	1.11	0.26	97.7
300	Spl	0.03	60.9	<0.01	<0.01	1.84	0.75	0.22	32.5	1.03	0.23	97.5
301	Spl	<0.01	59.6	<0.01	0.02	2.03	0.64	0.29	33.0	0.97	0.22	96.8
302	Spl	<0.01	60.1	0.01	<0.01	1.92	0.66	0.28	31.2	0.94	0.21	95.4
303	Spl	<0.01	68.0	<0.01	<0.01	1.63	0.49	0.22	24.6	0.74	0.28	96.0
304	Spl	<0.01	71.1	0.02	0.01	1.49	0.42	0.12	20.6	0.62	0.32	94.8
305	Spl	0.01	73.4	0.02	0.01	1.43	0.40	0.12	20.0	0.58	0.32	96.3
306	Spl	<0.01	60.6	0.03	0.01	1.79	0.65	0.21	30.4	0.76	0.23	94.6
307	Spl	<0.01	57.7	0.02	<0.01	2.01	0.63	0.28	33.6	0.86	0.19	95.3
308	Spl	<0.01	59.6	<0.01	<0.01	1.88	0.62	0.23	33.5	1.01	0.22	97.1
309	Spl	0.06	60.1	<0.01	<0.01	1.95	0.71	0.28	32.8	0.90	0.23	97.1
310	Spl	0.01	61.5	<0.01	<0.01	1.77	0.65	0.21	31.1	0.81	0.21	96.2
311	Spl	0.01	58.9	0.01	<0.01	1.97	0.73	0.28	35.0	0.88	0.20	98.0
312	Spl	<0.01	59.3	0.01	0.01	1.87	0.74	0.25	34.4	0.99	0.20	97.7
313	Spl	<0.01	63.1	0.08	<0.01	1.76	0.62	0.23	29.2	0.84	0.25	96.0
314	Spl	<0.01	70.1	0.02	0.01	1.56	0.50	0.15	23.3	0.71	0.27	96.6
317	Spl	<0.01	60.8	<0.01	0.02	1.78	0.63	0.25	32.3	0.98	0.23	96.9
318	Spl	<0.01	59.3	<0.01	0.01	1.92	0.69	0.29	33.4	0.93	0.20	96.7
319	Spl	<0.01	58.3	<0.01	0.01	1.92	0.66	0.29	34.7	0.94	0.23	97.1
320	Spl	0.02	58.0	<0.01	0.01	1.95	0.65	0.26	34.8	0.82	0.21	96.7
321	Spl	<0.01	57.7	0.01	<0.01	2.03	0.69	0.30	34.9	0.83	0.17	96.7
322	Spl	0.02	61.0	0.06	0.01	1.97	0.61	0.26	32.5	0.98	0.22	97.6

Table C-3: Electron microprobe mineral analyses of SOISB2 peridotites [wt.%]

10-29A

Nr.	Mineral	Na_2O	FeO	SiO_2	CaO	MgO	MnO	Al_2O_3	NiO	TiO_2	Cr_2O_3	Total
61	Ol	0.01	10.4	41.1	<0.01	49.5	0.20	<0.01	0.34	<0.001	0.01	102
62	Ol	<0.01	9.80	41.0	0.01	49.7	0.18	<0.01	0.39	<0.001	0.01	101
63	Ol	0.01	9.90	41.1	0.01	49.9	0.22	0.03	0.34	0.007	<0.01	102
64	Ol	<0.01	9.90	41.3	<0.01	49.6	0.20	0.02	0.37	0.008	<0.01	101
65	Ol	0.01	10.2	41.2	<0.01	49.5	0.18	<0.01	0.33	<0.001	<0.01	101
66	Ol	<0.01	9.80	41.1	<0.01	48.9	0.26	<0.01	0.34	<0.001	<0.01	101
67	Ol	<0.01	9.80	41.5	<0.01	49.6	0.14	0.04	0.35	0.001	<0.01	102
68	Ol	<0.01	10.0	41.2	<0.01	49.5	0.17	0.01	0.35	<0.001	<0.01	101
70	Ol	<0.01	9.90	41.3	<0.01	50.0	0.18	<0.01	0.33	<0.001	<0.01	102
71	Ol	0.02	9.90	41.2	<0.01	49.4	0.21	<0.01	0.34	<0.001	<0.01	101
72	Ol	<0.01	10.2	41.0	<0.01	49.7	0.15	<0.01	0.33	0.024	0.01	101
73	Ol	<0.01	10.0	41.1	<0.01	49.0	0.22	<0.01	0.34	<0.001	<0.01	101
74	Ol	<0.01	10.0	41.1	<0.01	49.2	0.17	<0.01	0.37	0.006	0.01	101
75	Ol	<0.01	10.1	41.1	<0.01	50.4	0.15	0.02	0.39	<0.001	<0.01	102
76	Ol	<0.01	10.1	41.3	<0.01	49.8	0.16	<0.01	0.34	0.003	0.01	102
77	Ol	0.02	9.90	41.1	<0.01	49.5	0.15	<0.01	0.32	<0.001	0.01	101
78	Ol	<0.01	9.74	40.1	<0.01	49.0	0.15	0.03	0.36	<0.001	<0.01	99.4
79	Ol	<0.01	9.78	41.7	<0.01	49.5	0.18	<0.01	0.34	<0.001	<0.01	102
80	Ol	<0.01	10.3	41.7	<0.01	49.8	0.14	<0.01	0.35	<0.001	0.03	102
81	Ol	<0.01	9.91	41.2	<0.01	49.3	0.17	<0.01	0.37	0.004	<0.01	101
82	Ol	<0.01	10.4	41.0	0.01	49.6	0.19	<0.01	0.37	<0.001	0.01	102
83	Ol	<0.01	9.91	41.3	<0.01	50.0	0.14	<0.01	0.34	0.003	0.01	102
84	Ol	<0.01	9.90	41.1	<0.01	49.6	0.23	<0.01	0.35	<0.001	<0.01	101
85	Ol	<0.01	9.78	41.0	<0.01	49.5	0.15	0.02	0.34	<0.001	<0.01	101
86	Ol	0.02	10.3	41.5	<0.01	49.8	0.19	0.03	0.34	<0.001	0.01	102
87	Ol	<0.01	9.56	40.5	<0.01	49.2	0.06	<0.01	0.35	0.019	<0.01	99.7
88	Ol	<0.01	10.2	41.1	<0.01	48.9	0.17	<0.01	0.36	0.003	0.01	101
89	Ol	0.01	10.2	41.2	<0.01	49.4	0.16	<0.01	0.33	0.012	0.01	101
90	Ol	0.02	10.0	41.2	<0.01	49.6	0.22	<0.01	0.37	<0.001	0.01	101
91	Ol	<0.01	9.90	41.5	<0.01	49.8	0.18	<0.01	0.33	0.001	<0.01	102
92	Ol	<0.01	10.1	41.0	<0.01	49.8	0.20	<0.01	0.35	<0.001	<0.01	102
93	Ol	<0.01	9.94	41.0	<0.01	49.8	0.17	<0.01	0.31	<0.001	0.02	101
94	Ol	0.02	9.81	41.1	<0.01	49.3	0.19	<0.01	0.36	<0.001	<0.01	101
95	Ol	<0.01	10.3	41.2	<0.01	49.5	0.19	0.01	0.37	<0.001	0.01	102
96	Ol	0.02	9.91	41.2	<0.01	49.1	0.21	<0.01	0.31	<0.001	<0.01	101
98	Ol	0.03	10.1	40.9	<0.01	49.3	0.22	<0.01	0.33	<0.001	0.20	101
99	Ol	<0.01	10.0	40.7	0.01	49.2	0.21	0.02	0.40	<0.001	0.01	101
100	Ol	0.03	9.92	41.0	<0.01	49.7	0.22	<0.01	0.37	<0.001	<0.01	101
101	Ol	<0.01	10.4	40.8	<0.01	49.7	0.20	<0.01	0.35	0.001	0.01	101
102	Ol	<0.01	9.86	40.0	0.01	48.6	0.14	<0.01	0.35	<0.001	0.15	99.1
106	Ol	<0.01	9.80	41.2	<0.01	49.8	0.21	0.02	0.34	<0.001	0.02	101
108	Ol	<0.01	10.3	40.7	<0.01	49.8	0.21	<0.01	0.38	<0.001	0.04	101
109	Ol	0.01	10.2	41.1	<0.01	49.6	0.19	0.02	0.36	<0.001	<0.01	102
110	Ol	0.02	10.1	41.0	<0.01	49.8	0.20	<0.01	0.36	0.004	<0.01	102
111	Ol	0.03	10.1	41.2	<0.01	49.7	0.14	<0.01	0.31	<0.001	<0.01	102
112	Ol	<0.01	10.1	41.2	<0.01	50.1	0.13	0.02	0.37	<0.001	0.01	102
113	Ol	0.01	10.1	40.9	<0.01	49.5	0.17	<0.01	0.35	<0.001	<0.01	101
114	Ol	<0.01	10.0	41.0	0.01	50.2	0.17	<0.01	0.36	<0.001	<0.01	102
115	Ol	0.01	10.1	40.0	<0.01	49.3	0.22	<0.01	0.34	0.003	0.01	99.9
116	Ol	0.01	9.90	40.9	<0.01	49.4	0.18	0.01	0.40	<0.001	<0.01	101
117	Ol	<0.01	10.0	41.3	<0.01	49.5	0.12	<0.01	0.36	0.015	<0.01	101
119	Ol	<0.01	10.0	41.2	<0.01	49.7	0.22	0.01	0.35	0.011	<0.01	102
120	Ol	0.01	10.1	40.2	<0.01	48.5	0.18	<0.01	0.38	<0.001	0.02	99
121	Ol	<0.01	10.1	40.3	<0.01	49.2	0.20	<0.01	0.36	<0.001	0.02	100
3	Ol	<0.01	10.1	40.9	<0.01	49.6	0.19	0.02	0.33	<0.001	0.01	101
4	Ol	<0.01	10.2	40.8	<0.01	50.1	0.17	0.02	0.35	<0.001	0.01	102
5	Ol	<0.01	9.85	41.1	0.02	49.3	0.21	<0.01	0.35	<0.001	<0.01	101
9	Ol	<0.01	10.3	41.0	0.01	49.6	0.18	<0.01	0.36	0.002	0.01	102
10	Ol	0.01	10.0	40.9	0.02	49.1	0.16	<0.01	0.36	<0.001	<0.01	101
11	Ol	0.03	10.0	41.2	<0.01	50.3	0.20	<0.01	0.32	0.012	0.02	102
12	Ol	0.02	10.3	41.1	0.01	50.1	0.17	<0.01	0.37	<0.001	<0.01	102
13	Ol	0.03	10.1	39.5	<0.01	49.2	0.11	0.02	0.98	0.014	0.03	100
14	Ol	0.04	10.2	40.4	0.01	49.4	0.17	0.01	0.37	<0.001	<0.01	101
15	Ol	0.01	9.87	40.0	0.02	49.1	0.15	<0.01	0.36	<0.001	<0.01	100
16	Ol	0.01	10.1	40.3	<0.01	50.2	0.17	0.01	0.34	<0.001	<0.01	101
17	Ol	<0.01	10.0	39.9	<0.01	49.7	0.17	<0.01	0.33	<0.001	<0.01	100
18	Ol	<0.01	9.82	41.4	<0.01	50.0	0.18	<0.01	0.34	0.019	<0.01	102
19	Ol	<0.01	10.1	41.3	0.03	49.8	0.24	0.01	0.34	0.029	0.01	102
20	Ol	<0.01	10.1	41.4	<0.01	49.6	0.16	<0.01	0.34	<0.001	0.01	102
23	Ol	<0.01	9.67	41.1	0.01	49.2	0.13	0.03	0.34	<0.001	0.02	101
24	Ol	<0.01	9.95	41.3	<0.01	50.3	0.19	0.01	0.34	<0.001	0.03	102
25	Ol	<0.01	9.79	40.9	<0.01	50.0	0.22	<0.01	0.37	<0.001	0.01	101
26	Ol	<0.01	9.77	40.8	<0.01	49.7	0.17	<0.01	0.35	<0.001	<0.01	101
27	Ol	<0.01	10.3	41.1	0.03	49.4	0.17	0.02	0.37	<0.001	<0.01	101
28	Ol	0.05	10.0	41.2	<0.01	49.7	0.23	0.03	0.32	<0.001	<0.01	102
29	Ol	<0.01	10.0	41.0	<0.01	49.2	0.16	<0.01	0.34	<0.001	<0.01	101
30	Ol	<0.01	10.0	41.0	<0.01	49.3	0.13	0.01	0.36	<0.001	<0.01	101
31	Ol	<0.01	10.2	40.9	<0.01	48.9	0.19	0.02	0.37	0.003	<0.01	101
32	Ol	<0.01	9.82	40.7	<0.01	49.0	0.21	0.01	0.35	<0.001	0.01	100

C-3 continued

10-29A

Nr.	Mineral	Na_2O	FeO	SiO2	CaO	MgO	MnO	Al_2O_3	NiO	TiO_2	Cr_2O_3	Total
69	Amph	1.75	3.65	48.7	12.5	19.6	0.07	9.41	0.09	0.21	0.75	96.7
97	Amph	1.41	3.51	48.5	12.6	19.7	0.10	8.71	0.07	0.18	0.56	95.3
103	Amph	1.56	3.73	47.8	12.6	19.5	0.05	9.67	0.07	0.19	0.74	95.9
104	Amph	1.51	3.68	48.8	12.4	19.8	0.09	9.44	0.10	0.21	0.78	96.9
105	Amph	1.50	3.51	42.9	11.8	18.5	0.04	10.0	0.08	0.16	0.69	89.3
107	Amph	1.66	3.77	48.3	12.6	19.5	0.08	9.86	0.09	0.20	0.76	96.9
6	Amph	1.61	3.58	49.5	12.6	19.9	0.04	9.26	0.07	0.17	0.53	97.2
7	Amph	1.71	3.66	48.7	12.7	19.9	0.04	9.69	0.09	0.23	0.54	97.3
8	Amph	1.31	3.36	50.5	12.7	20.6	0.04	8.05	0.08	0.16	0.40	97.1
21	Amph	1.76	3.76	48.8	12.7	19.6	0.08	10.1	0.09	0.23	0.78	97.8
22	Amph	1.73	3.89	47.8	12.6	19.3	0.04	10.3	0.10	0.19	0.79	96.7
33	Spl	0.07	28.5	0.04	0.10	9.01	0.40	32.9	0.11	0.054	29.1	100
34	Spl	0.04	27.9	1.90	0.44	9.79	0.35	31.7	0.08	0.057	28.0	100
35	Spl	<0.01	26.1	0.11	<0.01	10.6	0.33	37.4	0.14	0.054	25.3	100
36	Spl	0.02	24.7	0.04	<0.01	11.2	0.31	38.9	0.12	0.036	24.4	99.6
37	Spl	0.01	21.8	0.04	<0.01	13.5	0.20	46.6	0.23	<0.001	18.4	101
38	Spl	<0.01	21.6	0.04	<0.01	13.6	0.21	46.6	0.17	0.032	18.1	100
39	Spl	<0.01	23.9	0.03	<0.01	11.9	0.26	41.0	0.17	0.037	22.6	99.9
40	Spl	0.02	24.3	0.04	<0.01	11.6	0.30	40.6	0.15	0.054	22.7	99.7
41	Spl	<0.01	27.1	0.02	0.03	10.2	0.38	35.7	0.12	0.050	26.9	101
42	Spl	0.02	25.3	0.04	<0.01	11.1	0.26	38.7	0.13	0.011	24.8	100
43	Spl	0.07	27.1	0.06	0.15	10.2	0.38	34.7	0.15	0.039	27.1	99.9
44	Spl	<0.01	28.5	0.03	<0.01	9.23	0.41	32.9	0.11	0.015	28.7	99.9
46	Spl	<0.01	28.6	0.01	0.09	9.44	0.33	33.2	0.14	0.032	29.4	101
47	Spl	0.03	22.0	0.04	<0.01	14.0	0.25	49.0	0.33	0.028	13.8	99.5
48	Spl	<0.01	28.6	0.03	<0.01	9.26	0.33	33.3	0.13	0.035	29.1	101
49	Spl	0.04	28.7	0.05	0.07	9.18	0.37	33.0	0.14	0.061	29.1	101
50	Spl	0.06	28.0	0.12	0.05	9.00	0.39	33.3	0.08	0.072	27.8	98.9
51	Spl	0.08	26.7	0.04	0.11	10.80	0.29	37.2	0.15	0.041	25.1	101

10-29B

Nr.	Mineral	Na_2O	FeO	SiO_2	CaO	MgO	MnO	Al_2O_3	Cr_2O_3	TiO_2	NiO	Total
101	Ol	0.02	10.1	40.6	0.01	48.8	0.19	<0.01	0.20	0.026	<0.01	99.9
104	Ol	<0.01	10.0	40.7	0.03	48.7	0.21	<0.01	0.19	0.010	0.00	99.8
105	Ol	0.02	10.0	41.1	0.01	49.7	0.21	<0.01	0.19	0.005	0.01	101
106	Ol	<0.01	10.3	40.9	0.02	49.7	0.18	<0.01	0.22	0.071	<0.01	101
107	Ol	0.01	10.2	40.8	<0.01	49.7	0.22	<0.01	0.20	0.031	0.01	101
108	Ol	0.04	10.1	40.9	0.03	49.4	0.20	0.01	0.20	<0.001	0.01	101
109	Ol	0.02	10.2	40.7	0.01	49.1	0.15	<0.01	0.19	<0.001	0.01	101
110	Ol	0.01	10.1	41.1	0.01	49.4	0.26	<0.01	0.18	0.020	0.00	101
111	Ol	<0.01	10.2	40.9	0.01	49.4	0.22	0.01	0.21	0.056	<0.01	101
112	Ol	<0.01	10.7	41.0	0.01	49.2	0.15	<0.01	0.20	<0.001	<0.01	101
113	Ol	0.03	9.84	41.0	<0.01	49.2	0.13	<0.01	0.21	0.025	0.01	101
114	Ol	0.01	10.2	40.9	0.01	49.8	0.19	<0.01	0.22	0.025	0.01	101
115	Ol	<0.01	10.4	41.1	0.00	49.2	0.17	0.02	0.19	<0.001	<0.01	101
116	Ol	0.00	10.1	41.0	0.01	49.8	0.21	0.02	0.20	<0.001	<0.01	101
117	Ol	<0.01	9.84	41.0	0.02	49.7	0.17	<0.01	0.20	<0.001	0.01	101
118	Ol	0.04	10.1	40.9	0.01	49.6	0.22	<0.01	0.20	<0.001	<0.01	101
119	Ol	<0.01	9.92	41.1	0.01	49.4	0.17	0.01	0.17	<0.001	<0.01	101
120	Ol	<0.01	9.92	40.6	<0.01	48.8	0.13	<0.01	0.19	0.031	<0.01	99.6
121	Ol	0.02	9.90	41.1	0.01	49.6	0.22	<0.01	0.17	0.020	0.01	101
122	Ol	0.01	10.0	41.0	0.01	49.6	0.19	<0.01	0.22	0.061	<0.01	101
123	Ol	<0.01	9.87	40.8	<0.01	49.3	0.22	<0.01	0.19	<0.001	<0.01	101
124	Ol	0.01	9.92	41.0	<0.01	49.8	0.26	<0.01	0.21	0.005	0.01	101
125	Ol	<0.01	10.2	41.0	<0.01	49.3	0.20	0.02	0.19	0.015	<0.01	101
126	Ol	<0.01	10.1	41.0	0.02	49.6	0.18	<0.01	0.19	<0.001	<0.01	101
131	Ol	<0.01	10.3	40.7	0.01	49.4	0.20	<0.01	0.23	0.005	<0.01	101
132	Ol	<0.01	9.84	40.9	<0.01	49.7	0.19	<0.01	0.20	<0.001	<0.01	101
133	Ol	<0.01	10.0	40.9	0.01	49.7	0.19	0.01	0.21	<0.001	<0.01	101
134	Ol	<0.01	10.1	40.6	0.03	49.6	0.19	<0.01	0.19	0.005	<0.01	101
135	Ol	<0.01	10.3	40.9	<0.01	49.4	0.24	0.01	0.20	<0.001	0.01	101
136	Ol	0.01	10.0	40.9	<0.01	49.5	0.20	<0.01	0.19	0.041	<0.01	101
137	Ol	<0.01	10.0	40.5	0.01	48.6	0.23	<0.01	0.18	0.005	<0.01	100
138	Ol	0.01	9.89	40.7	<0.01	49.2	0.19	<0.01	0.20	<0.001	<0.01	100
139	Ol	<0.01	10.1	40.8	<0.01	49.2	0.23	0.01	0.19	<0.001	<0.01	101
140	Ol	0.01	9.90	40.6	<0.01	49.5	0.23	0.01	0.19	<0.001	<0.01	100
141	Ol	0.01	10.2	40.7	0.02	48.3	0.28	<0.01	0.18	0.015	<0.01	99.8
142	Ol	0.02	10.1	40.9	0.01	49.0	0.21	<0.01	0.21	0.010	0.03	101
143	Ol	0.01	9.79	41.1	0.02	49.5	0.20	<0.01	0.21	0.031	0.01	101
144	Ol	0.01	10.0	40.7	0.01	48.7	0.19	<0.01	0.18	0.021	0.02	99.8
145	Ol	0.01	10.3	41.0	0.02	49.4	0.19	<0.01	0.22	0.026	<0.01	101
146	Ol	<0.01	10.1	40.6	<0.01	49.7	0.21	<0.01	0.18	0.005	<0.01	101
147	Ol	0.01	10.3	41.1	<0.01	49.9	0.17	<0.01	0.20	0.046	<0.01	102
148	Ol	0.02	10.2	40.9	<0.01	49.2	0.18	0.02	0.21	0.031	0.01	101
149	Ol	0.02	10.0	40.9	<0.01	49.3	0.11	0.01	0.17	0.036	<0.01	101
150	Ol	<0.01	10.0	40.8	<0.01	49.4	0.21	<0.01	0.18	0.087	<0.01	101
151	Ol	<0.01	10.2	41.0	<0.01	49.6	0.21	<0.01	0.18	<0.001	<0.01	101
152	Ol	0.03	9.87	40.6	0.01	49.0	0.23	0.01	0.18	<0.001	0.01	100
153	Ol	<0.01	10.2	41.0	<0.01	49.5	0.19	<0.01	0.22	0.072	0.01	101
154	Ol	<0.01	10.2	41.1	0.01	49.7	0.17	0.01	0.20	<0.01	<0.01	101

C-3 continued

10-29B

Nr.	Mineral	Na_2O	FeO	SiO_2	CaO	MgO	MnO	Al_2O_3	NiO	TiO_2	Cr_2O_3	Total
155	Ol	<0.01	10.1	40.7	0.02	49.9	0.18	<0.01	0.19	0.051	<0.01	101
156	Ol	0.01	10.3	40.9	<0.01	49.9	0.17	<0.01	0.19	0.005	0.01	101
157	Ol	<0.01	10.2	41.1	0.02	49.5	0.21	<0.01	0.20	0.015	<0.01	101
158	Ol	<0.01	10.1	41.1	0.03	49.7	0.22	<0.01	0.19	0.005	0.01	158
159	Ol	0.02	10.2	41.0	0.03	49.8	0.18	<0.01	0.22	0.072	0.02	102
160	Ol	0.01	10.0	41.0	0.02	49.5	0.18	<0.01	0.20	<0.001	<0.01	101
161	Ol	<0.01	10.2	41.2	<0.01	49.6	0.21	<0.01	0.20	<0.001	0.01	101
162	Ol	<0.01	9.89	41.1	0.03	56.0	0.20	<0.01	0.21	0.051	<0.01	108
163	Ol	<0.01	10.0	40.6	0.01	49.2	0.19	<0.01	0.20	<0.001	0.01	100
164	Ol	<0.01	10.5	41.1	0.02	49.0	0.24	0.03	0.16	0.046	0.01	101
165	Ol	0.02	10.0	40.9	<0.01	49.3	0.17	<0.01	0.22	0.031	<0.01	101
166	Ol	<0.01	10.0	41.2	<0.01	49.0	0.14	<0.01	0.22	<0.001	<0.01	101
167	Ol	<0.01	10.0	40.7	0.007	49.3	0.17	<0.01	0.21	0.015	<0.01	101
168	Ol	0.02	10.1	40.8	0.013	49.3	0.21	<0.01	0.20	<0.001	0.01	101
169	Ol	0.04	10.2	41.1	0.01	49.3	0.20	<0.01	0.23	<0.001	0.01	101
170	Ol	<0.01	10.2	40.7	0.01	49.2	0.18	<0.01	0.19	0.046	0.01	101
171	Ol	<0.01	10.1	41.1	<0.01	49.6	0.19	<0.01	0.21	<0.001	<0.01	101
172	Ol	<0.01	10.3	41.0	0.01	49.5	0.16	<0.01	0.21	0.036	<0.01	101
173	Ol	<0.01	10.0	40.9	<0.01	49.3	0.18	0.01	0.23	<0.001	<0.01	101
174	Ol	<0.01	10.2	41.0	<0.01	49.5	0.19	<0.01	0.20	<0.001	0.01	101
175	Ol	0.01	10.1	40.7	0.03	49.5	0.23	0.01	0.20	0.020	<0.01	101
176	Ol	<0.01	10.4	40.8	0.02	49.9	0.19	<0.01	0.20	<0.001	<0.01	102
177	Ol	<0.01	10.0	41.0	0.02	49.7	0.21	<0.01	0.22	<0.001	0.02	101
178	Ol	0.01	10.0	40.4	0.02	48.6	0.18	0.01	0.20	<0.001	0.01	99.4
179	Ol	<0.01	9.82	40.9	<0.01	49.5	0.18	0.01	0.19	<0.001	0.02	101
180	Ol	0.01	9.66	40.9	0.01	50.0	0.20	<0.01	0.21	0.005	0.01	101
181	Ol	<0.01	10.4	41.0	0.02	49.8	0.21	<0.01	0.20	0.025	<0.01	102
182	Ol	0.01	10.0	41.0	<0.01	49.6	0.23	0.03	0.21	0.056	0.01	101
183	Ol	0.01	10.1	40.7	0.01	49.2	0.21	0.01	0.20	<0.001	0.01	101
184	Ol	<0.01	10.1	40.9	<0.01	49.6	0.21	0.02	0.21	<0.001	<0.01	101
185	Ol	0.01	10.3	40.8	0.01	49.4	0.20	<0.01	0.20	<0.001	0.02	101
186	Ol	0.01	10.2	41.2	0.01	49.9	0.18	0.01	0.19	<0.001	0.01	102
187	Ol	0.01	10.0	40.7	0.02	53.3	0.23	<0.01	0.19	<0.001	0.01	105
188	Ol	0.02	10.0	41.1	0.02	49.6	0.18	<0.01	0.16	<0.001	<0.01	101
189	Ol	<0.01	9.82	40.9	0.02	49.6	0.19	<0.01	0.21	0.056	0.01	101
190	Ol	0.01	10.1	41.0	<0.01	49.2	0.23	<0.01	0.18	<0.001	<0.01	101
191	Ol	0.02	9.94	41.2	0.01	49.5	0.13	0.01	0.21	<0.001	0.01	101
192	Ol	<0.01	10.3	41.0	<0.01	49.1	0.22	<0.01	0.22	<0.001	<0.01	101
193	Ol	<0.01	10.2	41.3	0.02	49.8	0.18	<0.01	0.23	0.015	0.00	102
194	Ol	0.01	10.0	41.2	0.01	49.6	0.16	0.01	0.20	<0.001	0.01	101
196	Ol	0.02	10.3	41.0	<0.01	49.5	0.16	<0.01	0.20	0.010	<0.01	101
197	Ol	0.01	10.2	41.0	<0.01	49.7	0.17	<0.01	0.20	<0.001	0.01	101
198	Ol	<0.01	10.4	41.1	<0.01	49.6	0.25	<0.01	0.22	<0.001	<0.01	102
199	Ol	0.01	10.3	41.2	0.01	49.5	0.21	0.02	0.21	<0.001	<0.01	102
200	Ol	0.04	10.1	41.1	0.02	49.3	0.17	<0.01	0.19	0.015	<0.01	101
102	Amph	1.88	4.20	47.9	13.0	19.1	0.01	9.60	0.06	0.18	0.83	96.8
211	Amph	2.13	5.50	42.2	12.4	18.6	0.08	9.50	0.04	0.17	2.20	92.8
127	Spl	0.03	16.3	0.01	<0.01	16.9	0.11	55.7	0.20	0.044	8.46	97.7
128	Spl	<0.01	15.6	0.02	0.01	17.1	0.17	55.5	0.19	<0.001	8.38	97.0
129	Spl	0.01	15.6	<0.01	0.01	16.7	0.14	54.6	0.15	<0.001	9.36	96.6
130	Spl	0.05	16.1	<0.01	<0.01	16.9	0.14	55.0	0.18	0.005	8.94	97.4
201	Spl	<0.01	19.5	<0.01	<0.01	15.5	0.20	51.7	0.18	0.039	11.6	98.6
202	Spl	0.05	18.2	0.08	0.02	15.6	0.23	51.7	0.15	<0.001	11.4	97.3
203	Spl	0.03	17.1	0.33	0.03	5.40	0.16	38.1	0.18	0.019	10.1	71.6
204	Spl	0.06	17.2	0.04	0.01	16.4	0.17	54.0	0.17	0.039	10.0	98.1
205	Spl	0.07	17.8	0.01	0.01	15.9	0.14	52.2	0.15	<0.001	11.5	97.8
206	Spl	0.05	18.9	0.03	<0.01	15.7	0.15	52.3	0.17	0.015	10.6	98.0
207	Spl	0.05	26.9	0.03	0.20	10.6	0.33	32.3	0.06	0.041	28.0	98.6
208	Spl	<0.01	27.1	0.02	0.15	10.2	0.35	32.0	0.08	0.055	28.4	98.4
209	Spl	0.02	26.5	0.41	0.27	10.4	0.34	32.2	0.09	0.023	27.8	97.9
210	Spl	0.03	26.7	0.06	0.20	10.5	0.35	32.6	0.09	0.088	27.6	98.3
212	Spl	<0.01	64.6	0.04	0.16	1.55	0.57	3.58	0.17	0.859	23.5	95.1
213	Spl	<0.01	70.7	<0.01	0.10	1.14	0.40	2.69	0.16	0.759	20.4	96.4
214	Spl	0.05	30.0	0.02	0.09	8.52	0.55	29.1	0.04	0.055	29.3	97.7
215	Spl	0.03	28.1	0.04	0.09	8.60	0.40	30.8	0.03	0.069	29.4	97.6
216	Spl	0.05	28.2	0.01	0.12	8.82	0.43	30.7	0.03	0.069	29.5	98.0
217	Spl	0.04	27.2	0.04	0.11	9.34	0.40	31.7	0.03	<0.001	28.8	97.7
218	Spl	0.03	61.5	0.06	0.23	2.52	0.52	6.47	0.14	0.58	24.3	96.3
219	Spl	0.02	74.0	0.09	0.26	1.32	0.33	2.58	0.19	0.51	15.0	94.4
220	Spl	<0.01	54.3	0.03	0.29	2.45	0.63	6.43	0.13	0.86	29.5	94.6
221	Spl	0.04	56.3	0.02	0.24	2.44	0.54	5.90	0.13	0.81	28.3	94.7
222	Spl	<0.01	67.2	0.04	0.21	1.47	0.44	3.98	0.19	0.65	20.3	94.5
223	Spl	0.04	54.3	0.03	0.20	3.18	0.48	9.13	0.13	0.55	28.2	96.2
224	Spl	<0.01	38.0	0.03	0.19	6.38	0.44	20.0	0.06	0.35	29.4	94.9
225	Spl	0.02	27.3	0.07	0.15	8.81	0.41	30.3	0.04	0.041	28.4	95.5
226	Spl	0.05	27.3	0.02	0.15	9.35	0.45	31.8	0.06	0.050	28.4	97.6
227	Spl	<0.01	27.5	0.02	0.08	9.31	0.43	32.0	0.03	0.023	28.8	98.3
228	Spl	0.00	26.9	0.02	0.12	9.28	0.40	31.5	0.02	0.096	28.9	97.2

C-3 continued

10-29B

Nr.	Mineral	Na_2O	FeO	SiO_2	CaO	MgO	MnO	Al_2O_3	NiO	TiO_2	Cr_2O_3	Total
230	Spl	0.05	27.4	0.06	0.09	8.99	0.44	31.7	0.05	0.036	28.8	97.6
231	Spl	0.08	27.6	0.05	0.11	9.38	0.48	31.5	0.02	0.077	29.0	98.4
232	Spl	<0.01	27.3	0.07	0.10	8.96	0.42	30.9	0.01	0.050	28.9	96.7
233	Spl	<0.01	28.0	0.01	0.09	9.00	0.45	31.4	0.04	<0.001	28.9	97.9
234	Spl	0.06	28.0	0.05	0.11	9.03	0.43	30.9	0.05	0.036	29.1	97.8
235	Spl	0.05	27.3	0.04	0.06	8.89	0.37	30.8	0.05	0.032	29.0	96.6
236	Spl	0.05	27.8	0.01	0.09	8.87	0.47	31.1	0.05	0.050	29.3	97.8
237	Spl	0.02	27.6	0.02	0.11	8.82	0.46	31.1	0.04	0.041	29.2	97.4
238	Spl	<0.01	27.7	0.07	0.05	8.81	0.43	31.5	0.05	0.045	29.1	97.8
239	Spl	0.09	27.4	0.06	0.10	8.84	0.42	31.0	0.02	0.045	29.4	97.4
240	Spl	0.05	27.8	0.01	0.07	8.82	0.41	30.8	0.01	0.054	29.2	97.2
241	Spl	<0.01	27.4	0.02	0.09	8.80	0.49	30.9	0.04	0.027	29.5	97.3
242	Spl	0.08	28.1	0.05	0.08	9.08	0.38	30.8	0.05	0.014	29.3	97.9
243	Spl	0.05	28.0	0.02	0.08	8.84	0.44	30.4	0.02	0.073	29.3	97.2
244	Spl	0.00	29.7	0.03	0.08	8.10	0.45	27.7	0.05	0.12	29.1	95.3
245	Spl	<0.01	41.9	0.04	0.09	4.42	0.58	15.8	0.06	0.39	29.2	92.5
246	Spl	<0.01	55.2	0.00	0.09	2.42	0.52	7.74	0.12	0.61	28.1	94.8
247	Spl	0.02	57.5	0.02	0.13	2.32	0.49	6.56	0.13	0.83	28.0	96.0
248	Spl	<0.01	57.3	0.01	0.11	2.41	0.62	6.38	0.13	0.84	28.6	96.5
249	Spl	<0.01	65.8	0.06	0.12	1.74	0.43	4.48	0.17	0.74	22.2	95.8
250	Spl	0.03	68.3	0.04	0.10	1.40	0.40	3.60	0.20	0.52	20.8	95.4
251	Spl	<0.01	70.2	0.01	0.11	1.58	0.42	3.60	0.16	0.65	19.9	96.7
252	Spl	<0.01	65.9	0.05	0.12	1.75	0.42	4.16	0.18	0.78	22.6	95.9
253	Spl	0.02	66.2	0.02	0.13	1.71	0.44	4.35	0.13	0.71	22.0	95.7
254	Spl	0.06	62.7	0.00	0.16	2.14	0.45	5.26	0.12	0.87	25.0	96.7
255	Spl	0.02	60.3	0.05	0.13	2.38	0.56	5.88	0.17	0.90	26.8	97.2
256	Spl	<0.01	53.0	0.01	0.13	2.83	0.65	7.55	0.13	0.94	31.2	96.4
257	Spl	<0.01	57.7	0.05	0.15	2.17	0.56	6.00	0.14	0.87	28.0	95.7
258	Spl	<0.01	71.1	0.04	0.18	1.44	0.32	3.17	0.17	0.65	18.4	95.5
259	Spl	<0.01	64.5	0.04	0.17	1.92	0.47	4.37	0.16	0.75	22.9	95.3
260	Spl	0.04	67.2	0.06	0.21	1.39	0.45	3.39	0.17	0.70	20.8	94.4
261	Spl	0.10	70.3	0.24	0.27	1.69	0.37	3.55	0.18	0.62	18.9	96.2
262	Spl	0.50	46.0	6.27	1.61	6.33	0.59	7.82	0.09	0.81	29.0	99.1

10-30

Nr.	Mineral	Na_2O	FeO	SiO_2	CaO	MgO	MnO	Al_2O_3	NiO	TiO_2	Cr_2O_3	Total
55	Ol	0.04	9.33	40.8	<0.01	50.0	0.12	<0.01	0.55	<0.001	<0.01	101
56	Ol	<0.01	9.38	41.1	<0.01	49.8	0.10	<0.01	0.53	<0.001	0.01	101
57	Ol	<0.01	9.39	40.7	<0.01	50.3	0.14	0.01	0.51	<0.001	<0.01	101
58	Ol	<0.01	9.31	41.0	<0.01	49.9	0.09	<0.01	0.50	0.024	0.02	101
61	Ol	<0.01	9.33	40.3	<0.01	49.8	0.10	<0.01	0.54	<0.001	0.02	100
62	Ol	<0.01	9.36	40.5	<0.01	50.1	0.13	<0.01	0.50	<0.001	<0.01	101
63	Ol	0.03	9.46	41.0	<0.01	50.5	0.16	<0.01	0.53	0.003	<0.01	102
64	Ol	0.01	9.49	41.2	<0.01	50.5	0.14	<0.01	0.53	<0.001	0.02	102
67	Ol	0.03	9.04	40.8	<0.01	49.4	0.15	<0.01	0.53	<0.001	<0.01	100
72	Ol	<0.01	9.43	41.2	0.01	50.3	0.16	<0.01	0.52	<0.001	0.02	102
73	Ol	<0.01	9.49	41.3	<0.01	50.4	0.17	<0.01	0.55	<0.001	0.01	102
76	Ol	<0.01	9.25	41.1	<0.01	50.0	0.15	<0.01	0.52	<0.001	0.02	101
77	Ol	<0.01	9.31	40.9	<0.01	50.2	0.18	<0.01	0.52	0.014	<0.01	101
80	Ol	<0.01	9.11	41.1	<0.01	50.8	0.08	<0.01	0.51	<0.001	0.02	102
81	Ol	<0.01	9.30	41.0	<0.01	50.6	0.05	<0.01	0.51	<0.001	0.02	102
82	Ol	<0.01	9.23	41.6	<0.01	50.8	0.12	0.04	0.55	<0.001	0.05	102
83	Ol	<0.01	9.27	40.4	<0.01	50.5	0.13	<0.01	0.55	<0.001	0.03	101
84	Ol	<0.01	9.18	40.8	<0.01	50.0	0.09	0.01	0.54	<0.001	0.04	101
85	Ol	0.01	9.40	40.5	<0.01	49.9	0.10	<0.01	0.53	<0.001	<0.01	101
86	Ol	<0.01	9.45	40.8	<0.01	49.9	0.14	<0.01	0.52	<0.001	0.01	101
87	Ol	<0.01	9.16	40.4	<0.01	49.3	0.13	0.01	0.53	<0.001	<0.01	100
88	Ol	0.02	9.22	40.6	<0.01	49.8	0.10	<0.01	0.54	0.016	<0.01	100
89	Ol	0.03	9.46	41.4	<0.01	49.9	0.19	0.01	0.53	<0.001	<0.01	102
90	Ol	<0.01	9.28	41.1	<0.01	50.3	0.12	<0.01	0.56	<0.001	0.02	101
91	Ol	<0.01	9.23	40.4	0.01	49.5	0.12	0.04	0.52	0.007	<0.01	99.8
92	Ol	<0.01	9.35	40.6	<0.01	49.7	0.13	<0.01	0.54	<0.001	<0.01	100
93	Ol	0.01	9.32	40.8	<0.01	50.5	0.14	<0.01	0.54	0.005	0.03	101
94	Ol	<0.01	9.33	40.4	<0.01	50.1	0.12	<0.01	0.50	<0.001	0.02	101
95	Ol	<0.01	9.34	41.0	<0.01	50.2	0.15	<0.01	0.53	<0.001	0.00	101
96	Ol	0.02	9.19	40.7	<0.01	49.6	0.11	0.01	0.51	<0.001	0.01	100
97	Ol	<0.01	9.34	40.4	<0.01	49.9	0.14	0.01	0.52	0.012	0.01	100
98	Ol	<0.01	9.33	41.2	<0.01	49.7	0.16	0.02	0.54	<0.001	0.01	101
99	Ol	0.01	9.35	40.7	0.01	49.0	0.12	<0.01	0.52	<0.001	<0.01	99.7
177	Ol	0.03	9.48	40.9	<0.01	48.2	0.13	0.01	0.55	0.002	<0.01	99.4
178	Ol	<0.01	9.37	40.7	<0.01	48.2	0.22	0.02	0.57	<0.001	<0.01	99.1
179	Ol	0.06	9.68	40.9	<0.01	48.4	0.11	0.02	0.54	<0.001	0.03	99.7
180	Ol	0.01	9.54	41.2	<0.01	48.7	0.14	<0.01	0.51	<0.001	0.02	100
193	Ol	0.03	9.42	40.7	<0.01	48.6	0.10	<0.01	0.55	<0.001	<0.01	99.4
194	Ol	0.03	9.59	40.4	<0.01	48.3	0.12	0.00	0.49	<0.001	0.01	99
195	Ol	<0.01	9.62	41.1	<0.01	48.8	0.15	0.01	0.53	<0.001	0.00	100
198	Ol	<0.01	9.73	40.7	0.01	48.4	0.14	0.00	0.51	<0.001	0.01	99.4
199	Ol	<0.01	9.63	40.7	<0.01	47.9	0.16	<0.01	0.55	<0.001	<0.01	98.9
200	Ol	<0.01	9.83	41.2	<0.01	48.5	0.15	<0.01	0.57	<0.001	0.00	100
201	Ol	<0.01	9.56	40.9	<0.01	48.2	0.15	0.01	0.54	<0.001	0.01	99.4

C-3 continued

10-30

Nr.	Mineral	Na_2O	FeO	SiO_2	CaO	MgO	MnO	Al_2O_3	NiO	TiO_2	Cr_2O_3	Total
205	Ol	<0.01	9.77	40.8	<0.01	48.8	0.14	0.02	0.53	0.008	0.01	100
206	Ol	0.01	9.61	40.7	<0.01	48.5	0.12	0.01	0.54	0.003	<0.01	99.5
207	Ol	<0.01	9.61	40.8	<0.01	49.6	0.15	<0.01	0.52	0.013	0.01	101
208	Ol	<0.01	9.52	40.7	<0.01	47.7	0.16	<0.01	0.53	<0.001	<0.01	98.7
217	Ol	<0.01	9.50	40.9	<0.01	48.2	0.12	<0.01	0.54	<0.001	0.00	99.3
247	Ol	0.03	9.35	40.5	<0.01	48.4	0.12	0.01	0.58	<0.001	0.00	99
248	Ol	0.00	9.39	40.4	<0.01	48.3	0.11	0.02	0.57	<0.001	0.02	98.8
249	Ol	<0.01	9.46	40.3	<0.01	48.4	0.13	0.01	0.54	0.002	0.01	98.9
250	Ol	0.02	9.80	40.3	<0.01	49.2	0.14	<0.01	0.56	<0.001	<0.01	100
59	Opx	0.05	6.55	57.1	0.12	35.1	0.13	1.88	0.10	0.087	0.08	101
60	Opx	<0.01	6.78	56.1	0.10	34.9	0.14	1.80	0.10	0.091	0.10	100
65	Opx	0.03	6.43	56.4	0.11	34.1	0.12	1.86	0.08	0.066	0.06	99.3
66	Opx	<0.01	6.43	56.2	0.12	34.5	0.17	1.74	0.09	0.034	0.07	99.3
183	Opx	<0.01	6.55	57.0	0.08	33.8	0.20	1.70	0.07	0.068	0.14	99.7
184	Opx	0.01	6.91	56.5	0.09	33.5	0.17	1.91	0.09	0.054	0.22	99.5
53	OPx	0.02	6.45	55.7	0.11	34.2	0.20	1.83	0.08	0.031	0.05	98.7
54	OPx	0.20	6.62	56.5	0.12	34.6	0.18	1.88	0.07	0.073	0.05	100
70	Opx	<0.01	6.19	57.3	0.16	35.2	0.16	1.09	0.08	0.091	0.06	100
71	Opx	<0.01	6.37	56.4	0.10	34.6	0.20	1.88	0.08	0.076	0.06	99.8
74	Opx	0.01	6.47	58.1	0.13	35.2	0.22	1.55	0.08	0.054	0.06	102
75	Opx	0.01	6.53	57.5	0.09	34.7	0.18	1.63	0.08	<0.001	0.05	101
78	Opx	<0.01	6.42	57.4	0.12	35.0	0.18	1.75	0.09	0.061	0.05	101
79	Opx	0.03	6.61	57.3	0.11	35.2	0.16	1.96	0.09	0.063	0.09	102
100	Opx	0.03	6.58	55.8	0.11	34.2	0.18	2.02	0.07	0.077	0.09	99.1
111	Amp	2.18	3.96	46.9	12.4	19.5	0.09	11.1	0.05	0.23	0.47	96.9
112	Amp	1.91	4.17	44.9	12.4	18.9	0.08	11.6	0.03	0.18	0.75	94.9
113	Amp	2.22	4.34	47.5	12.4	19.1	0.09	11.3	0.06	0.22	0.65	97.9
114	Amp	1.83	4.19	47.8	12.6	19.5	0.06	11.0	0.07	0.20	0.51	97.7
115	Amp	2.10	4.01	47.9	12.6	19.4	0.06	11.1	0.05	0.17	0.76	98.2
169	Spl	0.02	15.7	0.03	<0.01	16.2	0.11	50.1	0.25	0.022	18.5	101
170	Spl	<0.01	15.8	0.01	<0.01	15.8	0.12	49.3	0.22	0.025	19.6	101
171	Spl	0.02	11.8	0.02	<0.01	18.8	0.09	60.3	0.49	<0.001	7.19	98.7
173	Spl	<0.01	11.6	0.01	<0.01	19.2	0.10	61.1	0.51	<0.001	7.25	99.8
174	Spl	<0.01	11.5	0.04	<0.01	19.3	0.07	61.4	0.49	<0.001	7.37	100
175	Spl	<0.01	11.9	0.04	<0.01	18.9	0.05	60.3	0.45	<0.001	8.64	100
176	Spl	<0.01	11.8	0.06	<0.01	19.3	0.10	60.1	0.44	<0.001	8.67	100
185	Spl	<0.01	12.2	0.01	<0.01	19.1	0.13	59.7	0.43	<0.001	9.00	101
186	Spl	0.01	11.9	<0.01	<0.01	19.6	0.11	60.7	0.46	0.005	7.82	101
187	Spl	<0.01	11.6	<0.01	<0.01	19.0	0.12	60.4	0.49	0.010	8.02	99.5
188	Spl	<0.01	11.4	<0.01	<0.01	19.2	0.10	60.4	0.49	0.019	7.95	99.4
189	Spl	0.01	12.8	0.03	<0.01	18.0	0.11	58.3	0.40	<0.001	10.5	100
190	Spl	0.02	11.9	0.02	<0.01	18.8	0.12	59.9	0.45	<0.001	8.24	99.5
191	Spl	0.02	11.6	0.04	<0.01	19.5	0.07	61.0	0.50	0.016	7.68	100
192	Spl	<0.01	12.0	0.05	<0.01	19.1	0.11	60.0	0.45	0.005	8.88	101
231	Spl	0.02	11.7	0.04	<0.01	18.9	0.09	59.2	0.54	0.006	8.29	98.8
232	Spl	<0.01	12.3	0.04	<0.01	18.7	0.09	59.0	0.43	0.031	8.59	99.1
101	Spl	<0.01	12.8	0.03	<0.01	18.0	0.14	57.5	0.37	0.028	11.4	100
102	Spl	0.02	12.1	0.01	<0.01	19.1	0.14	60.9	0.44	<0.001	8.52	101
104	Spl	<0.01	11.8	0.02	<0.01	19.4	0.07	61.2	0.50	0.003	8.16	101
105	Spl	<0.01	11.6	0.04	<0.01	19.1	0.09	60.1	0.43	0.013	8.74	100
106	Spl	<0.01	12.0	0.01	<0.01	19.3	0.10	61.0	0.46	0.017	8.22	101
107	Spl	<0.01	11.8	0.01	<0.01	19.1	0.09	60.8	0.43	<0.001	8.09	100
108	Spl	<0.01	12.1	0.02	<0.01	19.1	0.11	61.2	0.45	<0.001	7.91	101
109	Spl	0.04	12.5	0.01	<0.01	18.6	0.14	58.8	0.36	0.011	11.6	102
110	Spl	0.02	11.5	<0.01	<0.01	19.5	0.08	61.8	0.47	0.041	8.37	102
68	mica	0.97	2.50	41.5	<0.01	24.0	<0.01	17.2	0.28	0.87	0.39	87.8
69	mica	1.06	2.41	41.5	<0.01	24.0	<0.01	17.5	0.28	0.81	0.42	87.9

10-31

Nr.	Mineral	Na_2O	FeO	SiO_2	CaO	MgO	MnO	Al_2O_3	NiO	TiO_2	Cr_2O_3	Total
525	Ol	<0.01	13.2	40.4	<0.01	47.1	0.17	<0.01	0.50	<0.001	<0.01	102
526	Ol	0.02	12.6	40.7	<0.01	47.4	0.17	<0.01	0.55	<0.001	0.01	101
527	Ol	0.02	12.8	40.8	<0.01	47.4	0.14	0.00	0.53	<0.001	0.02	102
528	Ol	<0.01	13.2	40.3	<0.01	46.7	0.21	<0.01	0.55	<0.001	<0.01	101
529	Ol	<0.01	12.9	40.7	<0.01	46.8	0.21	<0.01	0.52	<0.001	<0.01	101
530	Ol	<0.01	13.1	40.8	0.01	47.4	0.21	<0.01	0.49	<0.001	0.01	102
531	Ol	0.02	12.9	40.7	<0.01	47.2	0.19	0.03	0.54	<0.001	0.01	102
532	Ol	<0.01	12.9	40.7	<0.01	47.0	0.18	<0.01	0.50	<0.001	0.01	101
533	Ol	<0.01	12.2	40.8	0.01	47.0	0.23	0.01	0.55	<0.001	0.01	101
534	Ol	<0.01	13.1	40.5	<0.01	46.5	0.14	<0.01	0.54	<0.001	<0.01	101
535	Ol	<0.01	12.6	40.6	<0.01	46.5	0.14	<0.01	0.56	<0.001	<0.01	100
537	Ol	<0.01	12.8	40.6	<0.01	46.4	0.16	<0.01	0.55	<0.001	<0.01	100
538	Ol	<0.01	12.9	40.7	0.03	47.1	0.17	0.02	0.47	<0.001	<0.01	101
540	Ol	0.05	13.1	41.0	<0.01	46.9	0.10	<0.01	0.47	0.011	<0.01	102
541	Ol	<0.01	13.0	40.5	<0.01	46.9	0.20	<0.01	0.50	0.009	<0.01	101
542	Ol	<0.01	13.0	40.7	<0.01	46.4	0.22	0.03	0.52	<0.001	<0.01	101
544	Ol	<0.01	13.3	40.7	<0.01	46.8	0.18	<0.01	0.50	0.001	<0.01	102
545	Ol	<0.01	13.1	41.1	<0.01	47.2	0.14	<0.01	0.48	<0.001	<0.01	102
546	Ol	<0.01	13.1	40.8	<0.01	47.4	0.14	0.01	0.50	0.028	0.02	102

C-3 continued

10-31

Nr.	Mineral	Na_2O	FeO	SiO_2	CaO	MgO	MnO	Al_2O_3	NiO	TiO_2	Cr_2O_3	Total
547	Ol	0.01	13.2	40.7	<0.01	47.1	0.07	0.02	0.51	<0.001	<0.01	102
548	Ol	<0.01	13.2	41.0	<0.01	46.8	0.14	<0.01	0.51	<0.001	0.01	102
549	Ol	<0.01	13.1	40.7	0.01	47.0	0.16	<0.01	0.50	0.012	<0.01	102
550	Ol	0.01	13.2	40.8	<0.01	47.2	0.23	<0.01	0.53	0.003	<0.01	102
551	Ol	0.02	12.9	40.5	<0.01	47.2	0.16	<0.01	0.57	<0.001	<0.01	101
552	Ol	0.04	13.3	40.8	<0.01	47.1	0.23	<0.01	0.49	<0.001	<0.01	102
553	Ol	0.01	13.2	40.6	<0.01	47.8	0.13	0.02	0.53	<0.001	0.01	102
554	Ol	<0.01	13.0	40.9	<0.01	47.6	0.18	<0.01	0.53	<0.001	0.02	102
556	Ol	0.04	13.0	40.9	<0.01	47.5	0.20	<0.01	0.55	<0.001	0.01	102
557	Ol	0.01	12.9	40.8	<0.01	47.6	0.17	0.01	0.48	<0.001	0.03	102
558	Ol	<0.01	13.1	40.8	<0.01	47.3	0.10	<0.01	0.50	<0.001	0.01	102
559	Ol	0.02	13.1	41.0	<0.01	47.4	0.16	<0.01	0.49	<0.001	0.02	102
560	Ol	<0.01	13.1	40.9	<0.01	47.2	0.19	0.01	0.53	<0.001	0.01	102
561	Ol	0.03	13.1	40.7	<0.01	47.3	0.18	0.02	0.53	<0.001	<0.01	102
562	Ol	0.03	12.9	40.7	<0.01	47.0	0.12	<0.01	0.51	<0.001	0.01	101
564	Ol	<0.01	13.0	41.0	<0.01	47.2	0.20	0.01	0.49	<0.001	<0.01	102
565	Ol	0.02	13.2	40.6	<0.01	46.8	0.16	0.00	0.48	<0.001	<0.01	101
587	Ol	0.01	11.9	40.2	<0.01	47.8	0.19	<0.01	0.54	<0.001	0.01	101
589	Ol	<0.01	12.2	40.7	<0.01	47.8	0.19	<0.01	0.51	<0.001	<0.01	101
590	Ol	<0.01	11.8	40.4	<0.01	47.3	0.13	<0.01	0.53	0.004	0.01	100
591	Ol	<0.01	11.8	40.0	<0.01	47.6	0.17	0.04	0.52	<0.001	<0.01	100
593	Ol	<0.01	11.6	40.3	<0.01	48.0	0.11	0.01	0.55	<0.001	<0.01	101
594	Ol	<0.01	12.2	40.7	<0.01	48.6	0.15	<0.01	0.58	0.004	0.02	102
595	Ol	0.01	12.4	39.5	<0.01	47.5	0.12	0.01	0.50	<0.001	<0.01	100
596	Ol	<0.01	12.1	40.0	<0.01	47.4	0.16	<0.01	0.49	<0.001	<0.01	100
597	Ol	<0.01	11.9	40.9	<0.01	47.8	0.16	0.02	0.54	<0.001	0.01	101
598	Ol	0.03	12.0	41.0	<0.01	48.1	0.15	<0.01	0.54	<0.001	0.02	102
599	Ol	<0.01	12.0	40.0	<0.01	47.1	0.16	<0.01	0.51	<0.001	<0.01	99.7
600	Ol	<0.01	11.8	39.9	<0.01	47.1	0.14	<0.01	0.50	<0.001	0.02	99.4
601	Ol	<0.01	11.8	40.0	<0.01	46.8	0.17	0.03	0.53	<0.001	<0.01	99.3
602	Ol	0.01	11.7	40.1	<0.01	47.0	0.14	<0.01	0.52	<0.001	0.03	99.6
603	Ol	<0.01	12.1	40.1	<0.01	47.3	0.18	<0.01	0.52	<0.001	0.03	100
604	Ol	<0.01	11.8	40.7	<0.01	47.9	0.22	<0.01	0.58	0.012	<0.01	101
605	Ol	<0.01	11.8	39.7	<0.01	47.6	0.16	<0.01	0.55	0.003	<0.01	99.8
606	Ol	0.02	11.6	40.1	<0.01	47.2	0.17	0.02	0.59	<0.001	0.02	99.7
607	Ol	<0.01	12.2	40.9	<0.01	47.6	0.10	<0.01	0.56	<0.001	<0.01	101
608	Ol	<0.01	12.1	40.8	<0.01	48.0	0.19	0.01	0.52	<0.001	0.01	102
609	Ol	<0.01	12.1	40.9	<0.01	47.6	0.15	<0.01	0.54	<0.001	0.01	101
611	Ol	0.01	12.0	40.6	<0.01	48.0	0.17	0.01	0.51	<0.001	<0.01	101
612	Ol	<0.01	11.7	40.6	<0.01	47.5	0.13	0.01	0.51	<0.001	<0.01	100
613	Ol	0.03	12.0	40.6	<0.01	47.2	0.12	<0.01	0.54	<0.001	<0.01	101
615	Ol	0.01	12.0	41.0	<0.01	47.7	0.18	0.02	0.51	<0.001	0.04	102
616	Ol	0.01	12.4	40.9	<0.01	47.9	0.12	0.03	0.52	<0.001	0.01	102
617	Ol	0.04	12.5	40.7	<0.01	47.8	0.16	<0.01	0.51	<0.001	0.01	102
618	Ol	<0.01	12.4	40.6	<0.01	47.4	0.13	<0.01	0.50	<0.001	<0.01	101
619	Ol	<0.01	12.1	40.9	<0.01	47.3	0.17	<0.01	0.46	<0.001	<0.01	101
521	Opx	0.01	8.70	56.7	0.11	32.9	0.23	2.18	0.06	0.056	0.10	101
522	Opx	0.02	8.78	57.2	0.10	33.0	0.12	2.16	0.08	0.059	0.10	102
523	Opx	0.01	8.74	55.8	0.08	32.6	0.21	2.17	0.08	0.040	0.11	99.9
524	Opx	<0.01	8.89	56.9	0.11	32.8	0.20	2.20	0.09	0.03	0.08	101
539	Amp	1.88	4.95	47.8	12.1	18.8	0.09	11.4	0.16	0.46	0.44	98.1
566	Amp	1.86	4.87	47.8	12.0	18.8	0.10	11.0	0.13	0.47	0.42	97.3
567	Amp	1.89	4.87	47.8	12.0	18.7	0.11	11.3	0.15	0.45	0.47	97.8
620	Amp	1.85	4.69	47.5	12.0	18.5	0.06	11.6	0.14	0.50	0.40	97.2
568	Spl	<0.01	24.4	0.03	<0.01	12.2	0.19	46.2	0.39	0.068	17.7	101
569	Spl	0.01	24.0	<0.01	<0.01	12.3	0.16	46.6	0.33	0.071	17.6	101
570	Spl	<0.01	25.7	0.04	<0.01	11.9	0.26	46.6	0.32	0.036	17.0	102
536	Spl	<0.01	22.8	0.01	0.01	12.5	0.17	47.4	0.38	0.02	16.5	99.7
571	Spl	<0.01	21.9	0.01	<0.01	14.1	0.16	53.9	0.49	0.025	10.6	101
584	Spl	<0.01	17.5	0.04	<0.01	16.2	0.10	58.5	0.56	0.014	9.04	102
578	Spl	0.02	17.5	<0.01	<0.01	16.3	0.09	58.7	0.57	0.038	8.37	102
581	Spl	<0.01	16.9	0.03	<0.01	16.3	0.14	58.8	0.55	0.008	8.30	101
580	Spl	0.05	16.0	0.01	<0.01	16.6	0.09	59.1	0.56	<0.001	8.72	101
583	Spl	<0.01	16.4	0.03	<0.01	16.5	0.14	59.2	0.53	0.001	8.61	101
585	Spl	<0.01	15.7	0.02	<0.01	16.8	0.12	59.4	0.59	<0.001	8.24	101
574	Spl	<0.01	16.8	0.02	<0.01	16.7	0.13	59.5	0.58	0.015	8.55	102
577	Spl	0.01	17.1	0.01	<0.01	16.7	0.17	59.8	0.57	<0.001	8.18	103
582	Spl	0.06	16.4	0.03	<0.01	16.6	0.12	59.9	0.56	0.034	8.14	102
575	Spl	<0.01	15.9	0.04	<0.01	17.5	0.11	60.0	0.58	0.045	7.39	102

10-32

Nr.	Mineral	Na_2O	FeO	SiO_2	CaO	MgO	MnO	Al_2O_3	NiO	TiO_2	Cr_2O_3	Total
427	Ol	0.02	10.8	40.4	<0.01	48.4	0.16	<0.01	0.47	<0.001	0.01	100
428	Ol	<0.01	10.7	40.9	<0.01	48.6	0.13	0.01	0.42	0.003	0.03	101
429	Ol	0.01	10.9	40.5	<0.01	48.5	0.14	<0.01	0.45	0.003	<0.01	100
430	Ol	0.01	11.0	40.7	<0.01	48.4	0.09	<0.01	0.40	<0.001	0.01	101
431	Ol	0.02	11.1	42.2	<0.01	50.0	0.19	<0.01	0.44	<0.001	0.02	104

C-3 continued

10-32

Nr.	Mineral	Na_2O	FeO	SiO_2	CaO	MgO	MnO	Al_2O_3	NiO	TiO_2	Cr_2O_3	Total
432	Ol	<0.01	10.5	40.3	0.01	48.6	0.14	<0.01	0.41	<0.00	0.01	100
433	Ol	<0.01	10.7	40.9	<0.01	49.3	0.22	0.02	0.40	<0.00	<0.01	102
434	Ol	<0.01	10.7	41.0	<0.01	49.5	0.18	<0.01	0.46	0.011	<0.01	102
435	Ol	0.03	10.9	40.6	<0.01	49.3	0.15	0.01	0.41	<0.00	0.01	101
436	Ol	<0.01	11.1	40.5	<0.01	49.0	0.17	<0.01	0.41	<0.00	<0.01	101
437	Ol	<0.01	10.8	40.4	<0.01	48.8	0.14	<0.01	0.49	<0.00	<0.01	101
438	Ol	<0.01	10.8	40.4	<0.01	48.1	0.19	<0.01	0.44	<0.00	<0.01	99.9
439	Ol	0.02	10.7	40.9	<0.01	48.4	0.16	0.03	0.45	<0.00	0.01	101
440	Ol	<0.01	10.8	41.0	<0.01	47.9	0.18	0.01	0.40	<0.00	0.02	100
441	Ol	<0.01	11.0	40.6	<0.01	48.2	0.12	<0.01	0.44	<0.00	<0.01	100
442	Ol	0.01	11.1	40.2	<0.01	48.2	0.20	0.02	0.39	0.003	0.00	100
443	Ol	0.01	11.3	40.3	<0.01	48.2	0.20	0.01	0.42	<0.00	0.02	100
444	Ol	<0.01	11.1	40.9	<0.01	48.7	0.20	<0.01	0.41	0.003	0.02	101
445	Ol	<0.01	11.1	41.0	<0.01	48.6	0.19	<0.01	0.42	0.004	0.03	101
446	Ol	0.01	11.2	41.2	<0.01	48.6	0.17	<0.01	0.45	<0.00	0.00	102
447	Ol	0.02	11.1	40.8	<0.01	48.8	0.18	<0.01	0.42	<0.00	0.02	101
448	Ol	<0.01	10.9	40.8	<0.01	48.2	0.20	<0.01	0.41	<0.00	0.01	101
449	Ol	0.01	11.2	40.7	<0.01	49.2	0.22	0.01	0.40	<0.00	0.09	102
450	Ol	<0.01	11.0	41.1	<0.01	48.3	0.21	0.05	0.44	<0.00	<0.01	101
451	Ol	0.01	11.1	41.0	<0.01	48.6	0.19	<0.01	0.41	0.010	0.01	101
452	Ol	<0.01	11.3	40.8	<0.01	49.3	0.17	<0.01	0.41	<0.00	<0.01	102
454	Ol	0.01	11.2	41.1	0.01	49.1	0.19	<0.01	0.44	0.016	<0.01	102
455	Ol	<0.01	11.4	41.2	<0.01	48.8	0.19	<0.01	0.40	<0.00	<0.01	102
456	Ol	0.02	10.9	41.0	<0.01	48.7	0.17	0.01	0.42	<0.00	<0.01	101
457	Ol	0.01	10.8	41.3	<0.01	48.4	0.21	<0.01	0.43	<0.00	0.04	101
458	Ol	<0.01	11.1	41.3	<0.01	48.5	0.16	<0.01	0.42	0.004	<0.01	101
459	Ol	<0.01	11.2	41.1	<0.01	48.5	0.24	<0.01	0.39	<0.00	<0.01	101
460	Ol	0.03	10.9	41.1	<0.01	48.1	0.17	<0.01	0.45	<0.00	<0.01	101
461	Ol	<0.01	10.9	40.6	<0.01	48.5	0.14	<0.01	0.39	<0.00	0.01	101
462	Ol	<0.01	10.8	40.7	<0.01	48.2	0.09	<0.01	0.41	<0.00	0.02	100
463	Ol	<0.01	11.2	41.3	<0.01	49.8	0.25	<0.01	0.40	<0.00	0.01	103
464	Ol	<0.01	11.0	41.3	<0.01	48.1	0.17	0.01	0.39	<0.00	0.01	101
466	Ol	<0.01	11.2	41.1	<0.01	48.2	0.18	<0.01	0.45	<0.00	<0.01	101
467	Ol	0.02	11.1	41.0	<0.01	48.7	0.12	<0.01	0.39	<0.00	0.04	102
468	Ol	<0.01	11.4	40.9	<0.01	48.8	0.17	<0.01	0.40	<0.00	<0.01	102
469	Ol	<0.01	11.3	41.0	<0.01	48.2	0.13	<0.01	0.43	<0.00	<0.01	101
470	Ol	<0.01	11.4	40.9	0.01	48.2	0.17	0.02	0.43	<0.00	<0.01	101
1	Opx	0.02	8.01	56.1	0.13	32.6	0.19	1.99	0.07	0.001	0.06	99.1
2	Opx	0.04	8.10	56.6	0.13	33.2	0.21	2.00	0.07	0.019	0.13	101
37	Opx	<0.01	8.02	56.1	0.11	32.3	0.22	1.89	0.05	0.016	0.09	98.8
38	Opx	<0.01	8.08	55.8	0.14	31.9	0.20	2.00	0.08	0.030	0.09	98.3
39	Opx	<0.01	7.79	56.8	0.08	33.0	0.23	2.07	0.05	0.006	0.07	100
8	Opx	<0.01	7.59	56.8	0.12	33.6	0.18	1.41	0.04	0.061	0.07	99.8
9	Opx	0.03	7.64	57.0	0.11	33.4	0.22	1.39	0.08	0.062	0.11	100
12	Opx	<0.01	7.90	55.2	0.11	33.0	0.21	2.04	0.08	0.031	0.08	98.6
13	Opx	0.02	8.04	55.4	0.13	32.6	0.22	1.88	0.06	0.049	0.06	98.4
16	Amp	0.71	3.89	50.6	12.3	19.6	0.07	8.34	0.10	0.44	0.31	96.4
18	Amp	0.80	3.82	50.2	12.4	19.3	0.11	7.98	0.11	0.44	0.31	95.5
17	Amp	0.68	3.86	50.3	12.4	19.5	0.09	8.18	0.09	0.46	0.31	95.8
22	Amp	0.78	3.83	49.5	12.4	19.0	0.06	8.32	0.12	0.43	0.33	94.7
40	Amp	0.86	3.89	50.0	12.4	19.4	0.06	8.54	0.12	0.46	0.32	96
40	Amp	0.86	3.89	50.0	12.4	19.4	0.06	8.54	0.12	0.46	0.32	96
67	Amp	0.82	3.72	49.4	12.5	19.0	0.08	8.55	0.11	0.42	0.28	94.9
68	Amp	0.84	3.84	49.2	12.6	19.2	0.08	8.47	0.12	0.42	0.42	95.2
66	Amp	0.80	3.72	49.2	12.7	19.1	0.07	8.02	0.10	0.44	0.36	94.5
23	Amp	0.75	3.85	49.9	12.7	19.2	0.09	8.29	0.10	0.43	0.33	95.7
10	Amp	0.01	7.79	53.2	0.12	31.4	0.22	1.97	0.08	0.063	0.06	94.9
11	Amp	<0.01	7.92	53.6	0.11	32.0	0.20	2.21	0.07	0.055	0.08	96.2
14	Amp	0.01	7.70	53.9	0.10	31.6	0.18	1.90	0.09	0.069	0.10	95.6
15	Amp	0.01	7.45	53.9	0.12	33.5	0.26	1.30	0.06	0.076	0.07	96.7
15	Amp	0.01	7.45	53.9	0.12	33.5	0.26	1.30	0.06	0.067	0.07	96.7
19	Amp	<0.01	8.02	53.4	0.12	31.8	0.19	2.19	0.05	0.087	0.10	95.9
20	Amp	<0.01	7.65	52.5	0.11	30.7	0.21	1.79	0.08	0.054	0.08	93.1
21	Amp	<0.01	7.85	54.4	0.16	31.3	0.23	1.94	0.07	0.064	0.09	96.1
25	Amp	0.01	7.96	54.6	0.10	32.7	0.24	1.76	0.06	0.052	0.09	97.5
26	Amp	<0.01	7.91	54.8	0.09	32.2	0.24	2.00	0.06	0.083	0.06	97.3
47	Amp	0.01	7.95	53.4	0.11	31.3	0.17	2.19	0.07	0.067	0.09	95.3
48	Amp	<0.01	7.70	53.8	0.12	31.6	0.17	2.30	0.05	0.063	0.09	95.8
3	Spl	<0.01	16.4	0.02	<0.01	17.6	0.13	58.2	0.45	0.022	7.49	100
4	Spl	0.01	17.1	<0.01	<0.01	17.7	0.17	57.6	0.42	0.350	7.61	101
27	Spl	<0.01	15.8	<0.01	<0.01	17.8	0.12	58.7	0.48	0.016	7.39	100
28	Spl	<0.01	16.2	0.01	<0.01	17.8	0.11	59.3	0.49	<0.00	7.11	101
117	Spl	<0.01	16.1	0.01	<0.01	17.8	0.08	58.5	0.48	<0.00	6.82	99.8
118	Spl	<0.01	16.3	0.02	<0.01	17.9	0.20	59.7	0.46	0.008	6.70	101
119	Spl	<0.01	16.3	0.02	<0.01	17.7	0.13	58.9	0.42	0.029	7.35	101
120	Spl	0.01	16.2	<0.01	<0.01	17.9	0.13	59.3	0.46	0.013	7.30	101
121	Spl	<0.01	16.2	0.02	<0.01	18.0	0.15	59.5	0.45	<0.00	6.97	101
122	Spl	<0.01	16.3	0.02	<0.01	18.1	0.13	60.5	0.50	0.019	7.01	103
123	Spl	<0.01	16.3	0.01	<0.01	18.2	0.14	59.4	0.48	0.005	6.72	101

C-3 continued

10-32

Nr.	Mineral	Na_2O	FeO	SiO_2	CaO	MgO	MnO	Al_2O	NiO	TiO_2	Cr_2O_3	Total
125	Spl	<0.01	14.8	0.04	0.04	17.6	0.16	58.7	0.43	0.008	7.10	98.9
126	Spl	<0.01	15.9	0.03	<0.01	17.8	0.14	59.3	0.46	<0.001	6.97	101
127	Spl	<0.01	16.3	0.00	<0.01	18.0	0.11	59.6	0.44	0.001	7.07	102
128	Spl	0.01	16.4	0.01	<0.01	18.2	0.16	59.9	0.45	<0.001	7.34	102
129	Spl	<0.01	16.6	0.05	<0.01	17.9	0.10	58.8	0.41	0.007	7.19	101
130	Spl	<0.01	16.6	<0.01	<0.01	17.2	0.12	58.5	0.46	0.032	7.16	100
131	Spl	0.01	16.8	0.04	<0.01	17.1	0.15	58.4	0.41	<0.001	7.06	100
132	Spl	0.03	17.3	0.01	<0.01	16.7	0.16	58.6	0.47	0.42	6.69	100
133	Spl	<0.01	16.5	0.02	<0.01	17.2	0.12	57.8	0.44	0.020	7.02	99.1
134	Spl	0.03	16.0	<0.01	<0.01	17.3	0.18	59.2	0.46	<0.001	6.63	99.9
135	Spl	0.03	16.0	0.03	<0.01	17.5	0.12	58.4	0.46	0.038	6.63	99.1
136	Spl	<0.01	16.1	0.02	<0.01	17.5	0.07	58.9	0.43	<0.001	6.60	99.7
137	Spl	0.00	16.0	0.02	<0.01	17.5	0.18	58.4	0.46	0.016	6.92	99.6
138	Spl	<0.01	16.6	0.01	<0.01	17.3	0.12	58.4	0.43	0.020	7.00	99.9
139	Spl	<0.01	15.9	0.01	<0.01	17.3	0.12	58.9	0.53	0.023	6.59	99.3
140	Spl	<0.01	16.4	0.04	<0.01	17.2	0.15	58.3	0.54	<0.001	6.91	99.6
142	Spl	<0.01	16.1	0.04	<0.01	17.3	0.14	59.1	0.53	<0.001	7.04	100
143	Spl	<0.01	16.3	<0.01	0.01	17.4	0.18	59.1	0.48	0.006	6.97	100
144	Spl	0.01	16.4	0.01	0.01	17.5	0.14	59.3	0.56	<0.001	6.81	101
145	Spl	<0.01	16.5	0.01	<0.01	17.6	0.11	58.6	0.54	<0.001	6.93	100
146	Spl	0.03	16.2	0.02	<0.01	17.6	0.17	59.5	0.49	0.013	6.90	101
147	Spl	0.01	16.3	0.00	<0.01	18.0	0.12	59.4	0.53	0.013	6.73	101
148	Spl	0.02	16.5	0.04	<0.01	17.7	0.15	58.9	0.49	0.014	7.10	101
149	Spl	<0.01	16.8	0.04	<0.01	18.0	0.15	58.7	0.50	0.006	7.19	101
150	Spl	<0.01	16.1	0.05	<0.01	18.4	0.18	59.3	0.52	0.034	7.08	102
151	Spl	<0.01	16.0	<0.01	<0.01	17.7	0.18	58.3	0.47	0.037	7.21	100
152	Spl	0.02	15.4	0.02	<0.01	17.3	0.16	58.4	0.53	0.190	7.09	98.9
153	Spl	<0.01	15.9	0.02	<0.01	17.9	0.08	59.1	0.50	0.012	6.78	100
154	Spl	0.02	16.1	<0.01	<0.01	17.8	0.19	59.3	0.45	0.011	6.93	101
155	Spl	0.04	15.6	0.01	<0.01	17.9	0.10	59.2	0.51	0.033	7.13	101
156	Spl	<0.01	15.7	<0.01	<0.01	17.9	0.10	58.6	0.46	<0.001	6.96	99.8
157	Spl	<0.01	16.0	<0.01	<0.01	17.6	0.19	58.4	0.49	0.029	7.41	100
158	Spl	<0.01	16.3	<0.01	<0.01	17.9	0.14	58.8	0.47	<0.001	7.34	101
159	Spl	<0.01	16.6	0.01	<0.01	17.1	0.15	58.0	0.46	0.015	7.57	99.9
160	Spl	<0.01	16.6	<0.01	<0.01	18.2	0.21	60.2	0.51	0.046	7.49	103
161	Spl	<0.01	15.9	0.01	<0.01	17.5	0.10	58.6	0.48	<0.001	7.67	100
162	Spl	<0.01	15.7	0.01	<0.01	17.5	0.11	58.4	0.44	<0.001	7.66	99.8
163	Spl	<0.01	16.3	<0.01	<0.01	17.4	0.11	58.2	0.45	<0.001	8.13	101
164	Spl	<0.01	16.0	<0.01	0.01	18.4	0.14	59.7	0.45	0.011	7.57	102
165	Spl	<0.01	15.7	0.01	<0.01	17.3	0.11	57.2	0.44	0.011	7.85	98.6
166	Spl	0.01	16.1	<0.01	<0.01	17.5	0.13	58.9	0.47	<0.001	7.44	101
167	Spl	<0.01	16.3	0.01	<0.01	17.0	0.16	57.9	0.47	<0.001	7.43	99.3
168	Spl	<0.01	16.2	<0.01	0.01	17.2	0.16	59.2	0.49	0.006	7.08	100

10-34

Nr.	Mineral	Na_2O	FeO	SiO_2	CaO	MgO	MnO	Al_2O_3	NiO	TiO_2	Cr_2O_3	Total
1	Ol	<0.01	11.5	40.2	0.01	48.3	0.18	<0.01	0.37	<0.001	<0.01	101
2	Ol	<0.01	11.9	40.8	0.02	48.5	0.24	<0.01	0.31	0.071	0.01	102
8	Ol	<0.01	12.2	40.5	0.01	48.3	0.19	<0.01	0.30	<0.001	<0.01	102
9	Ol	0.03	12.5	39.6	0.02	47.3	0.25	<0.01	0.34	<0.001	0.01	100
10	Ol	<0.01	12.3	40.1	0.03	47.7	0.21	0.02	0.32	0.010	0.01	101
11	Ol	<0.01	12.2	40.1	<0.01	47.7	0.20	<0.01	0.34	0.051	<0.01	101
12	Ol	<0.01	11.9	40.1	0.02	47.8	0.21	<0.01	0.30	0.071	<0.01	100
13	Ol	<0.01	12.1	39.8	0.01	47.3	0.22	0.01	0.32	<0.001	0.02	100
14	Ol	<0.01	12.0	40.2	<0.01	47.6	0.18	0.00	0.34	0.015	0.01	100
15	Ol	0.04	12.4	39.7	0.02	47.8	0.14	<0.01	0.37	0.076	<0.01	101
16	Ol	0.01	12.3	39.8	0.02	47.6	0.21	<0.01	0.31	0.010	<0.01	100
17	Ol	<0.01	12.2	41.1	0.01	47.7	0.20	<0.01	0.32	0.031	0.00	102
18	Ol	0.01	12.6	41.2	0.01	48.6	0.19	<0.01	0.33	<0.001	0.02	103
19	Ol	<0.01	12.4	41.0	0.02	48.2	0.17	<0.01	0.30	0.031	0.02	102
20	Ol	0.04	12.5	40.9	<0.01	47.7	0.20	<0.01	0.30	0.015	0.01	102
21	Ol	<0.01	12.3	40.8	0.01	48.3	0.20	<0.01	0.30	<0.001	<0.01	102
22	Ol	0.03	12.3	41.0	0.01	48.0	0.16	<0.01	0.36	<0.001	0.02	102
23	Ol	0.01	12.6	41.1	0.04	48.1	0.21	<0.01	0.30	<0.001	<0.01	102
24	Ol	<0.01	12.2	40.7	0.02	47.8	0.22	<0.01	0.34	<0.001	<0.01	101
25	Ol	<0.01	12.6	41.0	0.02	47.6	0.22	<0.01	0.30	<0.001	<0.01	102
26	Ol	<0.01	12.5	40.8	0.01	48.1	0.10	0.03	0.35	<0.001	<0.01	102
27	Ol	0.01	12.6	40.9	0.02	48.0	0.20	<0.01	0.35	0.010	<0.01	102
28	Ol	0.04	12.7	41.2	<0.01	48.3	0.24	<0.01	0.34	0.015	0.02	103
29	Ol1	<0.01	12.7	41.0	<0.01	48.4	0.18	0.02	0.33	<0.001	<0.01	103
30	Ol1	<0.01	12.1	40.6	0.02	48.1	0.22	0.01	0.32	0.025	0.01	101
31	Ol1	0.03	12.0	40.8	0.02	48.5	0.16	<0.01	0.31	0.005	0.02	102
32	Ol1	0.04	12.0	40.4	<0.01	48.3	0.18	<0.01	0.31	<0.001	0.01	101
33	Ol1	0.01	12.2	40.7	<0.01	48.8	0.19	<0.01	0.31	<0.001	<0.01	102
34	Ol1	<0.01	12.2	40.5	<0.01	48.5	0.22	0.01	0.34	<0.001	0.02	102
35	Ol1	<0.01	11.9	40.8	0.01	48.1	0.17	<0.01	0.32	<0.001	<0.01	101
36	Ol1	0.02	11.8	40.7	0.01	48.1	0.17	0.01	0.28	<0.001	<0.01	101
37	Ol1	<0.01	12.2	40.2	<0.01	48.4	0.19	0.02	0.28	<0.001	0.01	101
38	Ol1	<0.01	12.2	40.3	0.01	48.3	0.25	0.01	0.30	<0.001	0.01	101
39	Ol1	<0.01	11.9	40.3	<0.01	48.3	0.19	<0.01	0.28	<0.01	<0.01	101

C-3 continued

10-34

Nr.	Mineral	Na_2O	FeO	SiO_2	CaO	MgO	MnO	Al_2O_3	NiO	TiO_2	Cr_2O_3	Total
40	Ol1	<0.01	11.8	40.0	0.01	48.0	0.14	0.01	0.32	<0.001	<0.01	100
42	Ol	0.03	12.4	41.0	<0.01	48.7	0.17	<0.01	0.30	<0.001	<0.01	103
43	Ol	<0.01	12.5	40.8	<0.01	48.4	0.20	<0.01	0.31	<0.001	<0.01	102
44	Ol	<0.01	12.2	40.6	0.01	48.1	0.18	<0.01	0.32	<0.001	<0.01	101
45	Ol	<0.01	12.4	40.6	0.02	47.9	0.21	<0.01	0.30	0.036	0.01	102
46	Ol	<0.01	12.1	40.9	0.01	47.5	0.18	<0.01	0.33	<0.001	<0.01	101
47	Ol	<0.01	11.8	40.5	<0.01	48.1	0.18	<0.01	0.32	0.005	<0.01	101
48	Ol	<0.01	12.5	40.5	<0.01	48.4	0.20	0.01	0.32	<0.001	<0.01	102
49	Ol	0.03	12.5	40.4	0.02	47.7	0.16	<0.01	0.31	0.015	<0.01	101
50	Ol	<0.01	12.5	40.9	0.02	47.8	0.14	<0.01	0.32	<0.001	0.01	102
51	Ol	<0.01	12.6	40.7	0.05	48.1	0.15	0.01	0.33	0.005	<0.01	102
52	Ol	<0.01	12.4	41.0	<0.01	48.4	0.23	<0.01	0.31	<0.001	<0.01	102
53	Ol	<0.01	12.1	41.0	<0.01	48.2	0.18	0.01	0.31	<0.001	<0.01	102
54	Ol	0.01	12.3	41.0	0.02	47.9	0.21	0.01	0.31	<0.001	<0.01	102
55	Ol	0.02	12.0	40.9	<0.01	48.1	0.15	<0.01	0.29	0.015	<0.01	102
56	Ol	0.01	12.0	40.7	0.01	48.1	0.29	<0.01	0.34	<0.001	<0.01	101
57	Ol	0.01	12.1	40.7	<0.01	48.4	0.23	0.01	0.32	<0.001	<0.01	102
59	Ol	0.01	12.6	40.5	0.02	47.7	0.18	<0.01	0.28	0.041	<0.01	101
60	Ol	0.02	12.7	40.7	0.01	48.4	0.16	<0.01	0.32	<0.001	0.01	102
61	Ol	<0.01	12.5	40.6	<0.01	47.9	0.17	<0.01	0.32	<0.001	<0.01	102
62	Ol	0.02	12.3	40.6	<0.01	48.1	0.14	<0.01	0.31	<0.001	<0.01	102
63	Ol	0.01	12.4	40.6	0.02	48.1	0.17	<0.01	0.29	<0.001	<0.01	102
65	Ol	0.03	12.0	40.8	0.01	48.7	0.20	<0.01	0.32	<0.001	<0.01	102
67	Ol	<0.01	11.8	41.4	<0.01	48.6	0.20	<0.01	0.33	<0.001	0.01	102
68	Ol	0.06	11.5	41.0	<0.01	48.1	0.19	0.02	0.30	0.031	<0.01	101
69	Ol	0.04	11.5	41.4	0.00	49.0	0.18	0.02	0.34	0.020	<0.01	102
70	Ol	0.05	11.3	41.0	0.01	48.4	0.21	<0.01	0.32	0.010	<0.01	101
71	Ol	<0.01	11.5	41.1	<0.01	48.8	0.16	0.02	0.34	<0.001	<0.01	102
72	Ol	<0.01	11.1	40.9	0.02	48.8	0.26	0.03	0.36	0.005	<0.01	102
73	Ol	<0.01	11.4	41.2	0.01	48.5	0.22	<0.01	0.35	0.020	<0.01	102
74	Ol	0.01	11.4	41.1	0.03	48.9	0.15	<0.01	0.34	<0.001	0.02	102
75	Ol	<0.01	11.6	40.7	<0.01	48.7	0.23	<0.01	0.37	<0.001	0.01	102
76	Ol	0.01	11.2	41.1	0.01	48.8	0.21	<0.01	0.38	0.056	<0.01	102
77	Ol	<0.01	11.5	41.3	0.04	49.1	0.25	<0.01	0.34	<0.001	0.01	103
78	Ol	0.03	11.4	40.8	<0.01	48.6	0.19	<0.01	0.32	0.031	<0.01	101
79	Ol	0.01	11.3	41.2	0.01	48.5	0.19	<0.01	0.33	0.020	<0.01	102
80	Ol	0.03	11.2	41.2	0.01	48.5	0.22	0.02	0.36	0.041	0.01	102
81	Ol	0.02	11.2	41.1	0.01	48.5	0.24	<0.01	0.39	<0.001	<0.01	102
82	Ol	<0.01	11.7	41.0	0.02	49.1	0.24	<0.01	0.32	<0.001	0.01	102
83	Ol	0.01	11.6	41.1	<0.01	48.4	0.21	<0.01	0.36	<0.001	<0.01	102
84	Ol	<0.01	11.5	41.1	0.01	48.5	0.14	<0.01	0.37	0.010	0.02	102
85	Ol	0.01	11.2	40.6	<0.01	48.2	0.18	<0.01	0.37	<0.001	<0.01	101
86	Ol	0.01	11.0	40.5	0.02	48.0	0.19	0.02	0.33	<0.001	0.01	100
87	Ol	0.01	11.2	40.3	<0.01	48.1	0.22	<0.01	0.31	<0.001	<0.01	100
88	Ol	<0.01	11.1	40.2	0.02	47.8	0.14	<0.01	0.34	<0.001	<0.01	99.6
89	Ol	0.04	11.3	40.3	<0.01	47.7	0.18	<0.01	0.36	<0.001	<0.01	99.9
90	Ol	<0.01	11.3	40.1	<0.01	47.2	0.17	0.01	0.33	<0.001	<0.01	99.2
93	Ol	<0.01	11.5	41.1	<0.01	48.7	0.15	<0.01	0.34	<0.001	<0.01	102
94	Ol	0.02	11.5	40.8	<0.01	48.7	0.19	<0.01	0.34	<0.001	<0.01	102
95	Ol	<0.01	11.8	41.0	0.01	49.0	0.20	<0.01	0.36	0.077	<0.01	102
96	Ol	0.01	11.9	40.9	0.01	49.1	0.17	<0.01	0.34	0.037	0.01	102
97	Ol	<0.01	11.5	40.7	0.02	48.8	0.25	<0.01	0.36	0.082	<0.01	102
98	Ol	<0.01	11.3	40.6	0.02	48.2	0.21	<0.01	0.36	<0.001	0.00	101
99	Ol	0.01	11.5	41.0	<0.01	48.9	0.23	0.02	0.35	<0.001	<0.01	102
100	Ol	<0.01	11.4	40.8	0.01	48.7	0.19	0.01	0.32	<0.001	<0.01	102
420	Cpx	0.01	1.54	54.0	25.2	17.1	0.1	0.8	0.04	<0.001	0.09	98.9
421	Cpx	<0.01	1.60	54.2	24.9	17.4	0.0	0.8	0.03	0.036	0.06	99.1
423	Cpx	0.01	1.57	54.1	25.3	17.6	0.0	0.6	0.04	<0.001	0.04	99.4
407	Amp	0.26	2.38	55.8	12.4	22.9	0.06	1.50	0.08	0.11	0.10	95.6
408	Amp	0.23	2.89	54.4	11.4	23.7	0.10	1.70	0.07	0.084	0.05	94.6
409	Amp	0.13	2.37	57.0	12.8	23.0	0.08	1.34	0.08	0.069	0.08	96.9
412	Amp	0.37	2.36	56.4	12.6	22.7	0.07	1.53	0.07	0.048	0.08	96.2
413	Amp	0.28	2.39	55.8	12.9	22.5	0.07	1.58	0.07	0.14	0.05	95.7
414	Amp	0.15	2.30	56.9	12.9	22.6	0.06	0.90	0.07	0.047	0.02	96.0
415	Amp	0.03	1.47	52.9	24.5	17.4	0.05	0.55	0.03	0.090	0.05	97.0
416	Amp	0.05	1.48	54.1	24.9	17.6	0.07	0.35	0.04	0.048	0.05	98.7
417	Amp	0.21	1.95	56.5	13.0	22.7	0.09	1.27	0.08	0.084	0.07	96.0
424	Amp	0.26	1.87	56.3	13.3	22.9	0.06	1.43	0.07	0.069	0.08	96.4
419	Spl	0.04	17.0	0.02	<0.01	16.2	0.148	58.2	0.363	<0.001	6.23	98.2
411	Chl	0.03	9.50	37.6	1.80	27.0	0.15	0.07	0.50	<0.001	0.01	76.7

10-35

Nr.	Mineral	Na_2O	FeO	SiO_2	CaO	MgO	MnO	Al_2O_3	NiO	TiO_2	Cr_2O_3	Total
383	Ol 1	<0.01	11.4	40.9	<0.01	49.4	0.16	<0.01	0.27	<0.001	<0.01	102
384	Ol 1	<0.01	11.7	40.7	<0.01	48.7	0.16	<0.01	0.25	<0.001	<0.01	102
385	Ol 1	0.03	11.5	40.7	<0.01	48.5	0.21	<0.01	0.24	<0.001	0.02	101
359	Ol	0.01	11.6	40.8	<0.01	48.6	0.15	<0.01	0.26	<0.001	0.00	101
360	Ol	<0.01	11.8	40.8	<0.01	49.3	0.15	0.00	0.26	0.002	0.01	102
361	Ol	<0.01	11.7	40.6	<0.01	48.6	0.16	0.02	0.26	<0.001	<0.01	101
362	Ol	0.01	11.7	40.4	<0.01	49.0	0.12	<0.01	0.25	<0.001	0.02	101

C-3 continued

10-35

Nr.	Mineral	Na_2O	FeO	SiO_2	CaO	MgO	MnO	Al_2O_3	NiO	TiO_2	Cr_2O_3	Total
363	Ol	<0.01	11.5	40.5	<0.01	49.3	0.21	0.01	0.26	<0.001	0.01	102
365	Ol	<0.01	11.3	40.3	<0.01	48.9	0.18	<0.01	0.28	<0.001	0.01	101
367	Ol	<0.01	11.4	40.6	<0.01	49.0	0.18	<0.01	0.26	<0.001	0.02	102
368	Ol	0.01	11.2	40.8	<0.01	49.1	0.17	<0.01	0.26	<0.001	<0.01	102
371	Ol	0.03	11.3	39.5	<0.01	48.4	0.20	<0.01	0.25	<0.001	0.01	99.7
372	Ol	0.01	11.5	39.3	<0.01	48.1	0.16	0.01	0.27	<0.001	<0.01	99.3
374	Ol	<0.01	11.6	40.2	<0.01	49.1	0.14	<0.01	0.27	<0.001	<0.01	101
375	Ol	0.01	11.5	40.2	<0.01	49.1	0.17	<0.01	0.31	<0.001	0.03	101
376	Ol	<0.01	11.5	40.3	<0.01	49.0	0.15	0.01	0.29	0.007	0.02	101
377	Ol	0.01	11.5	40.6	<0.01	49.0	0.12	<0.01	0.29	<0.001	<0.01	102
378	Ol	<0.01	11.9	40.7	<0.01	48.7	0.21	<0.01	0.24	<0.001	0.02	102
379	Ol	0.01	11.6	40.4	<0.01	49.0	0.14	0.02	0.26	<0.001	<0.01	102
380	Ol	<0.01	11.5	40.7	<0.01	49.3	0.13	0.01	0.26	<0.001	<0.01	102
381	Ol	<0.01	11.7	39.9	<0.01	48.9	0.13	<0.01	0.25	<0.001	<0.01	101
386	Ol	<0.01	11.3	40.3	0.01	48.4	0.14	<0.01	0.26	<0.001	<0.01	100
387	Ol	<0.01	11.9	40.8	<0.01	49.2	0.20	<0.01	0.26	<0.001	<0.01	102
388	Ol	<0.01	11.5	40.9	<0.01	48.7	0.13	<0.01	0.27	<0.001	0.02	102
389	Ol	0.03	11.7	39.9	<0.01	48.2	0.12	<0.01	0.30	<0.001	<0.01	100
390	Ol	<0.01	11.8	39.5	<0.01	47.8	0.16	0.01	0.27	<0.001	<0.01	100
391	Ol	<0.01	11.3	40.4	<0.01	49.1	0.12	0.01	0.25	0.010	<0.01	101
392	Ol	<0.01	11.3	40.5	<0.01	49.6	0.19	<0.01	0.26	<0.001	0.01	102
393	Ol	0.01	11.4	40.8	0.01	49.6	0.18	0.01	0.22	0.032	<0.01	102
394	Ol	0.01	11.7	41.2	<0.01	49.7	0.14	0.01	0.24	<0.001	<0.01	103
395	Ol	<0.01	11.7	40.9	<0.01	49.4	0.20	0.01	0.24	<0.001	<0.01	103
396	Ol	0.01	11.5	41.3	<0.01	48.8	0.14	0.01	0.28	0.011	<0.01	102
397	Ol	<0.01	11.6	40.2	<0.01	48.2	0.15	<0.01	0.29	<0.001	<0.01	101
398	Ol	<0.01	11.5	40.1	<0.01	48.0	0.15	<0.01	0.24	<0.001	<0.01	100
399	Ol	<0.01	11.3	40.0	<0.01	48.1	0.16	<0.01	0.26	<0.001	0.01	100
400	Ol	0.026	11.9	40.7	<0.01	0.275	49.1	0.179	<0.01	<0.001	0.013	102
401	Ol	0.03	11.9	40.7	<0.01	49.1	0.18	<0.01	0.28	<0.001	0.01	102
402	Ol	0.03	11.8	40.7	<0.01	49.2	0.13	<0.01	0.24	<0.001	<0.01	102
403	Ol	<0.01	11.6	40.4	<0.01	49.0	0.15	<0.01	0.24	<0.001	<0.01	101
404	Ol	0.01	11.6	40.7	<0.01	49.5	0.17	<0.01	0.26	<0.001	0.03	102
406	Ol	0.04	11.4	40.5	0.02	49.4	0.17	0.02	0.26	<0.001	0.01	102
407	Ol	<0.01	11.6	40.6	<0.01	48.8	0.23	<0.01	0.25	<0.001	0.02	102
408	Ol	<0.01	11.8	40.7	<0.01	49.4	0.16	0.02	0.27	0.007	<0.01	102
409	Ol	0.01	11.5	40.5	<0.01	48.9	0.12	<0.01	0.26	<0.001	0.01	101
414	Ol	<0.01	11.7	41.1	<0.01	49.6	0.14	<0.01	0.26	<0.001	0.01	103
415	Ol	<0.01	11.6	40.1	<0.01	48.7	0.09	<0.01	0.27	<0.001	0.01	101
416	Ol	0.01	11.3	40.1	<0.01	47.9	0.12	<0.01	0.24	<0.001	<0.01	99.7
417	Ol	0.01	11.3	39.8	<0.01	47.7	0.17	<0.01	0.26	<0.001	0.01	99.3
2	Opx	<0.01	8.18	55.5	0.15	31.9	0.24	2.06	0.05	0.020	0.09	98.2
356	Opx	<0.01	8.25	56.0	0.11	32.7	0.17	2.00	0.01	0.002	0.09	99.3
357	Opx	<0.01	8.10	55.8	0.18	33.4	0.19	2.12	0.04	0.026	0.11	99.9
364	Opx	<0.01	10.1	46.8	0.02	41.2	0.18	0.64	0.13	0.027	0.02	99.1
355	Amp	0.71	3.90	50.8	12.3	19.5	0.04	7.02	0.08	0.16	0.35	94.8
369	Amp	0.84	4.02	51.0	12.5	20.3	0.06	7.38	0.08	0.11	0.35	96.6
370	Amp	0.77	3.95	51.6	12.2	20.6	0.11	7.15	0.10	0.13	0.42	97.0
405	Amp	0.78	3.86	51.6	12.3	20.6	0.08	7.12	0.07	0.12	0.39	96.9
410	Amp	0.89	4.07	51.6	12.5	20.7	0.09	7.53	0.06	0.15	0.32	97.8
411	Amp	0.87	4.00	51.8	12.4	20.6	0.04	7.41	0.04	0.11	0.36	97.7
412	Amp	0.79	3.94	51.4	12.4	20.7	0.05	7.23	0.09	0.11	0.39	97.1
413	Amp	0.78	3.98	51.8	12.4	20.9	0.11	6.90	0.07	0.10	0.23	97.4
418	Spl	0.83	3.88	51.6	12.3	20.9	0.08	6.91	0.06	<0.001	0.31	96.9
419	Spl	<0.01	21.8	0.02	0.02	14.9	0.14	48.5	0.24	0.009	13.9	99.5
420	Spl	<0.01	22.2	<0.01	<0.01	15.1	0.25	49.2	0.23	<0.001	13.6	101
422	Spl	0.05	22.0	0.07	0.08	15.0	0.19	54.7	0.24	<0.001	14.2	106
423	Spl	0.01	21.7	0.05	<0.01	14.8	0.25	48.7	0.24	0.010	14.4	100
426	Spl	<0.01	20.9	0.05	0.01	15.0	0.20	49.0	0.23	0.025	14.3	99.7
427	Spl	<0.01	22.2	0.06	<0.01	15.1	0.13	48.8	0.26	<0.001	13.6	100
428	Spl	0.01	21.9	0.02	<0.01	15.2	0.23	49.3	0.25	0.011	13.3	100
429	Spl	0.01	21.1	0.05	0.08	15.5	0.18	48.3	0.26	<0.001	14.6	100
430	Spl	<0.01	23.0	0.07	0.10	16.7	0.10	51.6	0.22	0.027	10.8	103
431	Spl	<0.01	22.5	0.04	<0.01	14.4	0.22	44.9	0.20	<0.001	17.0	99.2
432	Spl	<0.01	21.4	0.05	<0.01	15.4	0.15	49.9	0.25	<0.001	13.1	100
433	Spl	<0.01	23.1	0.03	<0.01	14.3	0.23	47.2	0.25	0.018	14.0	99.2
434	Spl	0.01	24.3	0.02	<0.01	13.3	0.17	46.5	0.23	0.013	16.1	101
435	Spl	<0.01	19.0	0.03	<0.01	16.4	0.20	52.6	0.31	<0.001	10.6	99.1
436	Spl	<0.01	19.0	0.03	<0.01	16.0	0.16	51.4	0.23	<0.001	11.9	98.8
437	Spl	0.03	19.1	0.03	<0.01	16.1	0.13	51.4	0.26	<0.001	11.8	98.9

C-3 continued

10-36

Nr.	Mineral	Na_2O	FeO	SiO_2	CaO	MgO	MnO	Al_2O_3	NiO	TiO_2	Cr_2O_3	Total
233	Ol	0.01	9.49	42.1	<0.01	47.8	0.10	0.01	0.44	<0.001	0.01	100
234	Ol	<0.01	9.70	41.4	<0.01	50.4	0.14	0.03	0.45	0.014	<0.01	102
237	Ol	<0.01	9.55	41.7	<0.01	50.7	0.12	<0.01	0.44	0.024	0.01	103
239	Ol	0.01	9.75	41.3	<0.01	51.2	0.07	<0.01	0.43	<0.001	<0.01	103
240	Ol	0.01	9.40	40.9	<0.01	50.2	0.17	0.02	0.43	<0.001	0.01	101
241	Ol	<0.01	9.31	41.6	<0.01	50.4	0.11	<0.01	0.46	<0.001	0.01	102
242	Ol	0.01	9.40	41.7	0.01	50.9	0.18	0.03	0.48	<0.001	<0.01	103
244	Ol	0.02	9.58	40.7	<0.01	50.1	0.11	0.01	0.43	<0.001	0.01	101
245	Ol	<0.01	9.36	40.6	<0.01	50.5	0.09	0.02	0.47	0.025	0.01	101
246	Ol	<0.01	9.62	40.8	<0.01	50.1	0.08	<0.01	0.45	<0.001	<0.01	101
247	Ol	0.01	9.46	41.3	<0.01	49.9	0.14	<0.01	0.43	<0.001	0.02	101
248	Ol	0.03	9.33	41.2	<0.01	50.7	0.11	<0.01	0.41	<0.001	<0.01	102
249	Ol	0.01	9.35	41.5	<0.01	50.6	0.11	<0.01	0.42	<0.001	<0.01	102
250	Ol	0.01	9.53	41.5	<0.01	50.5	0.13	<0.01	0.43	<0.001	0.01	102
251	Ol	0.01	9.52	42.0	<0.01	50.5	0.16	0.01	0.44	0.001	0.01	103
252	Ol	<0.01	9.38	41.0	<0.01	50.2	0.13	<0.01	0.43	<0.001	0.02	101
253	Ol	0.03	9.57	40.6	<0.01	49.5	0.11	<0.01	0.43	0.021	0.01	100
257	Ol	<0.01	9.48	41.7	<0.01	50.6	0.07	<0.01	0.41	<0.001	<0.01	102
258	Ol	0.02	9.43	41.3	<0.01	50.3	0.10	<0.01	0.43	<0.001	0.01	102
259	Ol	0.01	9.53	41.0	0.01	50.6	0.13	<0.01	0.43	0.013	<0.01	102
260	Ol	<0.01	9.54	41.2	0.01	50.6	0.14	0.01	0.44	0.014	<0.01	102
261	Ol	<0.01	9.54	41.4	<0.01	51.0	0.09	0.01	0.44	<0.001	0.01	102
262	Ol	<0.01	9.51	41.0	<0.01	50.8	0.12	<0.01	0.44	<0.001	0.01	102
263	Ol	0.02	9.58	41.3	<0.01	51.0	0.11	<0.01	0.44	<0.001	0.01	102
264	Ol	0.04	9.6	41.2	<0.01	50.8	0.12	<0.01	0.44	<0.001	0.01	102
265	Ol	<0.01	9.33	41.3	<0.01	50.3	0.12	<0.01	0.43	<0.001	<0.01	101
266	Ol	<0.01	9.55	41.1	<0.01	50.4	0.11	<0.01	0.43	<0.001	0.02	102
267	Ol	<0.01	9.59	40.8	<0.01	49.4	0.10	<0.01	0.46	<0.001	<0.01	100
268	Ol	<0.01	9.65	40.7	<0.01	49.6	0.13	0.01	0.44	<0.001	0.00	101
269	Ol	<0.01	9.14	41.1	<0.01	50.2	0.10	<0.01	0.41	<0.001	<0.01	101
270	Ol	<0.01	9.28	41.7	<0.01	51.0	0.10	<0.01	0.46	<0.001	0.01	103
271	Ol	0.01	9.28	41.3	<0.01	50.6	0.15	<0.01	0.40	<0.001	0.00	102
272	Ol	0.02	9.44	40.5	0.03	49.4	0.09	0.02	0.40	0.013	<0.01	99.9
273	Ol	<0.01	9.17	38.7	0.00	49.6	0.16	<0.01	0.47	<0.001	0.02	98.1
281	Ol	0.01	9.51	40.6	<0.01	50.4	0.13	<0.01	0.41	<0.001	<0.01	101
282	Ol	0.01	9.57	40.7	0.01	50.1	0.17	<0.01	0.45	<0.001	<0.01	101
283	Ol	<0.01	9.48	40.8	<0.01	50.0	0.11	<0.01	0.44	<0.001	0.01	101
284	Ol	<0.01	9.74	40.6	<0.01	50.4	0.16	<0.01	0.44	<0.001	0.01	101
285	Ol	<0.01	9.47	41.2	0.01	50.3	0.08	<0.01	0.45	<0.001	<0.01	102
288	Ol	<0.01	9.59	40.4	<0.01	49.6	0.14	0.01	0.45	<0.001	0.01	100
289	Ol	<0.01	9.59	40.5	<0.01	49.8	0.13	<0.01	0.43	<0.001	<0.01	101
290	Ol	<0.01	9.32	41.3	<0.01	50.3	0.10	<0.01	0.45	<0.001	<0.01	101
291	Ol	<0.01	9.58	41.2	<0.01	50.9	0.11	<0.01	0.47	0.003	<0.01	102
292	Ol	0.03	9.21	41.2	<0.01	50.8	0.10	0.01	0.44	<0.001	<0.01	102
293	Ol	0.02	9.42	41.1	0.01	50.7	0.15	<0.01	0.44	<0.001	0.02	102
294	Ol	0.02	9.62	40.8	<0.01	50.2	0.16	<0.01	0.42	<0.001	0.01	101
295	Ol	<0.01	9.39	41.1	<0.01	50.1	0.13	0.01	0.42	0.006	0.01	101
296	Ol	<0.01	9.46	41.1	0.01	50.3	0.14	<0.01	0.47	0.010	0.01	102
297	Ol	0.01	9.47	41.1	<0.01	49.9	0.14	0.01	0.48	<0.001	<0.01	101
298	Ol	<0.01	9.69	40.8	<0.01	49.8	0.18	0.01	0.45	0.011	<0.01	101
299	Ol	<0.01	9.25	41.2	<0.01	50.3	0.12	<0.01	0.44	<0.001	0.01	101
300	Ol	<0.01	9.36	40.5	<0.01	49.6	0.10	<0.01	0.47	0.003	<0.01	100
301	Ol	0.01	9.26	40.9	<0.01	50.4	0.14	<0.01	0.42	<0.001	<0.01	101
302	Ol	<0.01	9.58	41.0	<0.01	50.3	0.15	<0.01	0.45	<0.001	0.01	102
303	Ol	<0.01	9.59	42.3	<0.01	50.5	0.12	<0.01	0.43	<0.001	<0.01	103
304	Ol	<0.01	9.62	40.3	<0.01	49.4	0.14	<0.01	0.43	0.013	<0.01	100
305	Ol	0.02	9.56	41.1	<0.01	49.4	0.16	<0.01	0.42	<0.001	0.02	101
306	Ol	0.06	9.58	41.0	<0.01	50.1	0.11	<0.01	0.43	<0.001	0.01	101
307	Ol	<0.01	9.74	40.8	<0.01	49.8	0.12	<0.01	0.48	<0.001	0.02	101
309	Ol	<0.01	9.52	40.6	<0.01	49.2	0.13	<0.01	0.45	0.016	<0.01	99.9
310	Ol	0.01	9.45	40.5	<0.01	49.1	0.08	<0.01	0.46	<0.001	0.02	99.6
312	Ol	<0.01	9.57	40.6	<0.01	49.6	0.13	<0.01	0.46	<0.001	0.00	100
313	Ol	<0.01	9.47	41.0	<0.01	49.8	0.15	<0.01	0.44	<0.001	<0.01	101
314	Ol	<0.01	9.31	41.0	<0.01	49.5	0.11	<0.01	0.45	<0.001	0.03	100
316	Ol	0.01	9.55	41.0	<0.01	49.9	0.14	<0.01	0.44	<0.001	<0.01	101
317	Ol	<0.01	9.73	41.0	<0.01	50.1	0.17	<0.01	0.43	<0.001	<0.01	102

C-3 continued

10-36

Nr.	Mineral	Na_2O	FeO	SiO_2	CaO	MgO	MnO	Al_2O_3	NiO	TiO_2	Cr_2O_3	Total
235	Opx	0.03	6.87	58.3	0.06	35.3	0.16	1.94	0.06	0.05	0.12	103
236	Opx	0.02	6.73	57.9	0.06	35.2	0.12	1.75	0.07	0.09	0.11	102
275	Opx	0.01	6.53	56.5	0.08	34.6	0.13	1.85	0.04	0.06	0.08	99.9
276	Opx	<0.01	6.55	56.2	0.07	34.2	0.15	1.33	0.07	0.07	0.08	98.7
278	Opx	0.02	6.63	57.2	0.08	34.6	0.17	2.00	0.07	0.05	0.07	101
279	Opx	<0.01	6.49	57.6	0.11	34.7	0.14	1.84	0.09	0.07	0.06	101
286	Opx	<0.01	6.74	56.9	0.09	34.6	0.13	1.56	0.07	0.07	0.06	100
287	Opx	0.01	6.67	57.4	0.08	35.0	0.18	1.64	0.07	0.04	0.07	101
308	Opx	0.01	6.61	56.3	0.08	34.2	0.18	2.00	0.06	0.05	0.09	99.6
318	Opx	<0.01	7.15	57.8	0.06	35.3	0.16	1.38	0.10	0.02	0.03	102
319	Opx	0.01	7.03	57.7	0.06	35.0	0.10	1.68	0.07	0.04	0.14	102
320	Opx	0.02	6.91	57.4	0.03	35.2	0.13	1.61	0.07	0.02	0.09	102
254	Amp	2.33	3.42	47.1	12.2	18.7	0.09	13.0	0.12	0.89	0.68	98.6
255	Amp	2.19	3.48	47.7	12.2	19.3	0.09	13.0	0.12	0.86	0.44	99.4
256	Amp	2.21	3.35	47.3	12.2	19.2	0.05	12.2	0.12	0.84	0.43	97.8
277	Amp	2.18	3.45	46.6	12.1	18.8	0.06	12.4	0.10	0.79	0.47	96.9
321	Spl	<0.01	14.7	0.02	<0.01	17.9	0.15	52.9	0.32	0.03	14.8	101
322	Spl	0.01	14.8	<0.01	<0.01	18.2	0.13	53.6	0.27	0.02	14.8	102
323	Spl	0.02	13.0	0.06	<0.01	20.5	0.13	57.2	0.37	<0.01	10.1	101
324	Spl	<0.01	13.0	<0.01	<0.01	19.0	0.10	56.9	0.35	0.00	10.9	100
325	Spl	0.02	12.0	0.03	<0.01	19.7	0.07	60.7	0.38	0.03	8.34	101
326	Spl	<0.01	12.2	<0.01	<0.01	19.6	0.09	59.4	0.43	0.03	7.93	99.7
327	Spl	0.01	11.7	<0.01	<0.01	19.7	0.15	60.2	0.44	<0.01	7.74	99.9
331	Spl	<0.01	13.0	<0.01	<0.01	19.0	0.12	57.9	0.35	0.01	11.2	102
332	Spl	<0.01	14.7	<0.01	<0.01	17.6	0.10	52.4	0.34	0.01	15.4	101
333	Spl	<0.01	13.7	0.03	<0.01	18.4	0.14	55.0	0.35	0.01	12.9	101
334	Spl	<0.01	13.6	0.03	<0.01	18.5	0.13	57.7	0.36	0.02	10.5	101
335	Spl	<0.01	13.6	0.01	<0.01	18.7	0.12	55.3	0.34	0.02	12.6	101
336	Spl	<0.01	13.3	0.06	<0.01	18.9	0.14	56.3	0.36	0.03	11.6	101
337	Spl	<0.01	13.7	0.03	<0.01	18.9	0.12	56.6	0.33	0.03	11.5	101
338	Spl	<0.01	13.6	<0.01	<0.01	19.8	0.14	59.0	0.34	<0.01	11.7	105
339	Spl	<0.01	12.8	<0.01	<0.01	20.0	0.04	58.6	0.37	<0.01	9.66	101
340	Spl	<0.01	16.0	0.03	<0.01	16.4	0.12	45.5	0.21	0.07	21.7	100
341	Spl	<0.01	12.1	0.02	<0.01	20.2	0.10	60.1	0.43	0.02	7.49	100
342	Spl	<0.01	11.9	<0.01	<0.01	20.1	0.06	59.7	0.42	0.01	7.45	99.7
343	Spl	<0.01	12.8	0.03	<0.01	19.3	0.07	58.7	0.40	<0.01	9.71	101
344	Spl	<0.01	12.3	0.02	<0.01	19.5	0.11	59.8	0.43	0.02	8.13	100
345	Spl	0.04	12.6	<0.01	<0.01	19.4	0.12	59.4	0.44	<0.01	7.91	99.9
346	Spl	0.02	12.3	<0.01	<0.01	19.6	0.08	60.5	0.40	0.01	7.89	101
347	Spl	<0.01	12.9	0.05	<0.01	19.5	0.12	58.5	0.35	0.01	10.5	102
348	Spl	<0.01	12.6	0.02	<0.01	18.9	0.12	57.1	0.38	<0.01	10.5	99.7
350	Spl	0.02	12.6	<0.01	<0.01	19.4	0.07	58.5	0.37	<0.01	9.71	101
351	Spl	<0.01	13.6	0.03	<0.01	18.7	0.12	57.3	0.37	0.01	11.3	101
352	Spl	<0.01	13.4	<0.01	<0.01	18.7	0.10	57.8	0.35	0.02	10.5	101
353	Spl	<0.01	12.9	<0.01	<0.01	19.4	0.08	58.8	0.38	<0.01	9.52	101
329	Spl B	0.01	19.6	0.02	<0.01	14.1	0.21	36.0	0.13	0.085	30.8	101
328	Spl B	0.03	20.4	0.08	<0.01	13.4	0.22	34.7	0.16	0.12	33.2	102
238	Mica	1.34	2.53	41.0	0.015	24.3	<0.01	17.4	0.27	0.79	0.31	88.0

Table C-4: Electron microprobe mineral analyses of SOISB3 peridotites [wt.%]

10-16

Nr	Mineral	Na_2O	FeO	SiO_2	CaO	MgO	MnO	Al_2O_3	NiO	TiO_2	Cr_2O_3	Total
25	Ol 1	<0.01	14.6	39.5	<0.01	45.6	0.25	0.02	0.47	<0.001	<0.01	101
26	Ol 1	<0.01	15.2	39.9	0.02	46.1	0.24	0.02	0.44	<0.001	0.02	102
27	Ol 1	<0.01	14.8	39.8	<0.01	46.1	0.21	<0.01	0.44	0.015	0.02	101
28	Ol 1	0.01	14.8	39.7	0.01	45.6	0.22	<0.01	0.42	0.020	0.01	101
29	Ol 2	<0.01	13.8	40.0	0.01	45.8	0.22	<0.01	0.44	<0.001	0.02	100
30	Ol 3	<0.01	14.7	39.6	0.01	46.1	0.20	<0.01	0.43	<0.001	0.06	101
31	Ol 3	0.02	14.2	39.8	<0.01	45.8	0.21	<0.01	0.45	0.036	0.08	101
33	Ol 4	<0.01	14.5	40.0	0.01	46.0	0.19	0.01	0.44	0.046	0.04	101
34	Ol 4	<0.01	14.8	40.1	<0.01	46.1	0.15	0.02	0.43	<0.001	0.04	102
35	Ol 4	0.02	14.2	39.8	0.01	46.0	0.19	0.01	0.44	<0.001	0.10	101
36	Ol 4	<0.01	14.3	39.8	<0.01	46.2	0.16	0.03	0.45	<0.001	0.15	101
37	Ol 4	<0.01	14.6	35.9	0.01	43.9	0.20	3.50	0.43	<0.001	2.00	101
38	Ol 4	<0.01	14.3	39.8	<0.01	46.2	0.16	0.03	0.45	0.056	0.15	101
51	Ol 5	0.01	14.6	40.1	<0.01	45.3	0.24	0.01	0.40	0.071	0.01	101
52	Oi 5	0.01	14.9	39.8	0.02	45.4	0.21	<0.01	0.43	0.010	<0.01	101
53	Ol 5	0.01	15.1	39.9	<0.01	46.1	0.20	<0.01	0.41	<0.001	0.01	102
54	Ol 5	0.01	14.7	39.8	<0.01	45.7	0.24	<0.01	0.41	0.015	0.01	101
55	Ol 5	<0.01	14.9	39.6	0.01	45.7	0.18	0.02	0.48	0.025	<0.01	101
56	Ol 5	<0.01	14.8	40.0	<0.01	45.7	0.21	<0.01	0.47	0.010	<0.01	101
57	Ol 6	0.02	14.4	39.4	<0.01	45.3	0.22	0.01	0.44	<0.001	<0.01	100
58	Ol 6	<0.01	14.5	39.9	<0.01	46.2	0.23	<0.01	0.41	<0.001	<0.01	101
60	Ol	<0.01	15.4	39.6	<0.01	45.0	0.22	<0.01	0.44	0.025	<0.01	101
61	Ol	<0.01	14.9	39.3	<0.01	45.4	0.20	<0.01	0.47	<0.001	0.01	100
62	Ol	0.01	15.4	38.9	0.01	45.1	0.21	0.01	0.46	0.03	0.01	100
64	Ol	<0.01	15.7	38.6	0.02	44.8	0.24	<0.01	0.42	<0.001	<0.01	99.8
65	Ol	<0.01	15.8	38.4	0.01	44.8	0.21	<0.01	0.43	<0.001	0.01	99.7
66	Ol	0.04	15.8	38.8	0.02	45.1	0.26	<0.01	0.47	0.005	<0.01	100
67	Ol	0.03	15.5	38.3	<0.01	44.6	0.22	<0.01	0.39	0.076	0.01	99.0
68	Ol	0.03	15.5	38.6	<0.01	44.8	0.17	0.02	0.45	<0.001	0.01	99.6
69	Ol	<0.01	15.8	37.9	0.01	44.5	0.17	<0.01	0.44	<0.001	0.01	98.8
70	Ol	0.02	15.1	39.8	<0.01	45.0	0.26	<0.01	0.43	<0.001	0.02	101
71	Ol	<0.01	15.5	39.5	<0.01	45.3	0.24	<0.01	0.42	<0.001	<0.01	101
72	Ol	0.01	14.8	39.8	<0.01	45.5	0.25	<0.01	0.47	<0.001	0.01	101
73	Ol	0.01	14.9	39.7	<0.01	44.7	0.24	<0.01	0.48	0.015	0.01	100
74	Ol	0.01	14.8	39.7	<0.01	45.3	0.20	<0.01	0.46	0.02	0.02	101
75	Ol	<0.01	14.9	39.7	0.02	45.1	0.27	0.01	0.46	<0.001	<0.01	100
76	Ol	0.01	14.8	40.0	<0.01	45.3	0.20	<0.01	0.50	<0.001	<0.01	101
77	Ol	0.04	15.3	39.7	0.01	44.9	0.18	0.02	0.44	0.005	0.01	101
78	Ol	0.02	15.3	39.9	<0.01	45.2	0.23	<0.01	0.43	0.046	<0.01	101
79	Ol	0.05	14.9	39.7	0.02	45.0	0.28	0.01	0.45	<0.001	0.01	101
80	Ol	<0.01	15.2	40.0	0.02	45.6	0.24	0.03	0.46	<0.001	0.01	102
81	Ol	0.02	14.8	39.7	0.01	45.3	0.18	<0.01	0.41	0.041	0.01	101
82	Ol	<0.01	15.4	39.9	0.01	45.8	0.20	<0.01	0.46	0.015	0.01	102
83	Ol	0.01	15.1	39.9	<0.01	45.2	0.22	<0.01	0.44	0.076	0.03	101
84	Ol	<0.01	14.8	39.9	<0.01	45.2	0.24	0.02	0.45	<0.001	0.01	101
85	Ol	<0.01	14.5	41.0	0.03	44.9	0.20	0.01	0.42	0.005	0.01	101
86	Ol	0.01	14.8	39.6	<0.01	45.1	0.25	<0.01	0.45	<0.001	0.02	100
87	Ol	<0.01	15.3	39.8	0.01	45.7	0.20	<0.01	0.45	0.015	<0.01	102
88	Ol	<0.01	15.4	39.8	<0.01	45.9	0.23	<0.01	0.42	0.015	0.01	102
89	Ol	<0.01	14.9	39.7	<0.01	45.3	0.24	<0.01	0.47	0.071	<0.01	101
97	Ol	0.01	14.7	39.7	0.02	46.2	0.23	<0.01	0.46	0.015	0.01	101
98	Ol	0.04	14.6	39.7	<0.01	45.6	0.20	<0.01	0.46	0.015	<0.01	101
99	Ol	<0.01	15.2	39.8	<0.01	45.7	0.21	<0.01	0.45	0.046	0.01	101
100	Ol	<0.01	15.4	38.8	0.00	45.4	0.16	<0.01	0.43	0.015	0.02	100
105	Ol	<0.01	14.9	39.7	0.01	46.0	0.21	<0.01	0.46	0.025	0.02	101
106	Ol	<0.01	14.7	39.9	0.01	45.9	0.22	<0.01	0.46	<0.001	<0.01	101
107	Ol	<0.01	14.3	39.8	<0.01	45.6	0.23	<0.01	0.44	0.031	0.01	100
108	Ol	<0.01	15.0	40.2	0.01	45.7	0.21	<0.01	0.48	<0.001	0.01	102
109	Ol	<0.01	13.9	39.5	0.02	45.4	0.22	0.01	0.46	0.056	<0.01	99.4
110	Ol	<0.01	14.0	39.2	<0.01	44.4	0.20	<0.01	0.45	<0.001	<0.01	98.3
111	Ol	<0.01	14.5	39.3	0.01	45.5	0.18	<0.01	0.42	<0.001	0.01	100
112	Ol	<0.01	14.2	39.0	0.01	44.4	0.26	0.01	0.46	<0.001	<0.01	98.3
113	Ol	<0.01	13.8	38.7	0.02	44.6	0.24	0.01	0.44	0.015	<0.01	97.7
114	Ol	<0.01	14.0	38.3	0.01	44.6	0.24	<0.01	0.45	0.020	<0.01	97.7
115	Ol	<0.01	15.4	39.4	0.01	45.1	0.25	<0.01	0.46	<0.001	<0.01	101
8	Opx	<0.01	9.75	55.1	0.14	32.3	0.28	1.25	0.09	<0.001	0.05	98.9
9	Opx	<0.01	9.71	55.5	0.14	32.2	0.25	1.15	0.06	0.041	0.05	99.1
10	Opx	0.02	9.57	55.3	0.12	32.1	0.29	1.48	0.06	0.026	0.05	99.0
11	Opx	0.01	9.80	55.5	0.11	32.3	0.22	1.65	0.07	0.072	0.08	99.8
12	Opx	<0.01	10.0	55.9	0.11	32.3	0.27	1.42	0.07	0.021	0.06	100
15	Opx	<0.01	9.55	55.3	0.15	32.3	0.31	1.54	0.06	0.015	0.09	99.3
16	Opx	<0.01	9.95	55.8	0.15	32.3	0.27	1.56	0.07	0.021	0.07	100
17	Opx	<0.01	9.63	55.4	0.11	32.2	0.26	1.59	0.06	0.077	0.07	99.4
18	Opx	<0.01	9.76	56.0	0.13	32.3	0.26	1.42	0.08	0.041	0.02	100
1	Amph	1.27	4.02	50.3	12.2	19.9	0.12	7.41	0.13	0.37	0.40	96.2
2	Amph	1.15	4.07	51.1	12.4	20.2	0.08	7.06	0.12	0.40	0.32	96.9
116	Amph	0.87	6.32	47.4	10.3	20.7	0.15	6.57	0.16	0.39	0.37	93.3
117	Amph	1.11	4.00	51.1	12.4	20.1	0.06	7.08	0.11	0.38	0.35	96.7
118	Amph	1.08	4.09	51.7	12.4	20.6	0.15	6.66	0.13	0.38	0.26	97.4
119	Amph	0.97	4.03	52.0	12.4	20.5	0.12	5.98	0.13	0.35	0.18	96.7

C-4 continued

10-16

Nr	Mineral	Na_2O	FeO	SiO_2	CaO	MgO	MnO	Al_2O_3	NiO	TiO_2	Cr_2O_3	Total
120	Amph	1.13	4.22	51.4	12.2	20.6	0.09	6.69	0.09	0.34	0.34	97.1
121	Amph	0.97	4.07	51.9	12.4	20.8	0.10	5.95	0.13	0.35	0.21	97.0
122	Amph	1.12	3.96	51.8	12.4	20.5	0.08	6.45	0.12	0.37	0.24	97.0
124	Amph	1.00	4.30	51.5	12.3	20.3	0.09	6.29	0.09	0.37	0.22	96.4
125	Amph	1.06	4.06	51.1	12.5	20.3	0.07	6.12	0.13	0.32	0.24	95.9
39	Spl	<0.01	14.6	35.9	0.01	43.9	0.20	3.50	0.43	0.065	2.00	101
40	Spl	0.06	28.0	0.05	0.01	9.62	0.24	39.8	0.21	0.093	20.3	98.4
41	Spl	0.02	27.6	0.02	<0.01	9.57	0.28	40.2	0.24	0.056	20.1	98.1
42	Spl	<0.01	27.2	0.05	<0.01	9.54	0.25	40.0	0.20	0.070	20.1	97.4
43	Spl	<0.01	27.9	0.02	0.01	9.56	0.31	40.0	0.24	0.005	19.8	97.9
44	Spl	<0.01	27.7	0.06	<0.01	9.48	0.29	40.1	0.20	0.047	19.8	97.6
45	Spl	<0.01	28.3	0.04	0.01	9.48	0.35	39.7	0.24	0.060	20.1	98.3
46	Spl	<0.01	28.1	0.00	<0.01	9.34	0.33	39.7	0.24	0.074	19.9	97.7
47	Spl	<0.01	28.5	<0.01	0.01	9.47	0.28	39.4	0.23	0.074	20.1	98.1

10-27

Nr	Mineral	Na_2O	FeO	SiO_2	CaO	MgO	MnO	Al_2O_3	NiO	TiO_2	Cr_2O_3	Total
381	Ol	<0.01	12.9	39.9	0.01	45.9	0.21	0.02	0.38	0.020	<0.01	99.3
382	Ol	<0.01	13.3	40.2	<0.01	46.6	0.21	<0.01	0.38	0.010	0.02	101
383	Ol	<0.01	13.0	39.8	0.01	46.1	0.19	<0.01	0.36	0.005	<0.01	99.6
384	Ol	<0.01	13.0	39.9	0.02	46.2	0.20	<0.01	0.34	<0.001	<0.01	99.7
385	Ol	<0.01	12.7	39.6	0.00	46.0	0.20	0.01	0.42	<0.001	0.03	99.0
386	Ol	0.05	13.4	39.7	<0.01	45.9	0.28	0.00	0.37	0.051	<0.01	99.7
387	Ol	<0.01	13.2	40.0	0.02	45.8	0.22	0.01	0.38	<0.001	<0.01	99.6
388	Ol	<0.01	13.5	40.4	<0.01	46.8	0.27	0.00	0.36	<0.001	<0.01	101
389	Ol	<0.01	13.2	40.4	0.02	45.9	0.25	<0.01	0.36	0.041	<0.01	100
390	Ol	<0.01	13.5	40.1	0.01	46.2	0.21	<0.01	0.39	0.026	0.02	101
392	Ol	<0.01	13.0	40.2	0.03	46.6	0.17	<0.01	0.36	<0.001	0.00	100
393	Ol	<0.01	13.0	40.1	0.02	46.4	0.21	<0.01	0.37	0.056	<0.01	100
394	Ol	0.02	13.4	40.1	0.01	46.7	0.27	0.04	0.35	<0.001	<0.01	101
395	Ol	0.01	13.3	40.3	<0.01	46.7	0.23	0.02	0.37	<0.001	<0.01	101
396	Ol	<0.01	13.0	40.3	0.01	46.5	0.21	<0.01	0.34	<0.001	<0.01	100
397	Ol	<0.01	13.2	40.4	0.01	47.0	0.26	0.02	0.37	0.010	0.02	101
398	Ol	<0.01	13.1	40.3	<0.01	47.0	0.26	<0.01	0.35	<0.001	0.02	101
421	Ol	<0.01	13.4	40.2	0.01	47.2	0.24	<0.01	0.36	0.025	<0.01	102
422	Ol	<0.01	13.4	40.4	0.02	46.9	0.20	<0.01	0.38	0.020	0.02	101
449	Ol	0.01	13.1	40.2	<0.01	46.9	0.24	<0.01	0.37	0.036	<0.01	101
450	Ol	0.01	13.1	40.1	<0.01	47.0	0.24	0.01	0.35	0.051	0.02	101
451	Ol	0.03	13.9	40.4	<0.01	47.5	0.24	0.01	0.36	<0.001	0.02	102
452	Ol	0.01	13.5	40.3	<0.01	47.3	0.25	0.03	0.36	<0.001	<0.01	102
453	Ol	<0.01	13.3	40.4	<0.01	47.1	0.24	0.01	0.34	<0.001	<0.01	101
454	Ol	0.02	13.6	40.4	0.01	46.9	0.20	<0.01	0.37	0.010	0.02	102
455	Ol	<0.01	13.6	40.5	<0.01	47.3	0.21	<0.01	0.39	0.010	<0.01	102
456	Ol	<0.01	14.1	40.5	0.02	47.2	0.26	0.01	0.35	<0.001	0.01	102
457	Ol	0.05	13.2	40.1	<0.01	46.3	0.25	0.01	0.37	0.010	0.01	100
458	Ol	0.01	13.3	40.1	<0.01	46.5	0.24	<0.01	0.38	<0.001	<0.01	101
459	Ol	<0.01	13.4	40.3	<0.01	46.7	0.25	0.00	0.36	<0.001	<0.01	101
460	Ol	<0.01	13.3	40.1	0.03	46.2	0.20	0.01	0.37	<0.001	0.07	100
462	Ol	<0.01	13.4	40.5	<0.01	47.2	0.19	0.01	0.38	<0.001	<0.01	102
463	Ol	<0.01	13.6	40.4	0.05	47.0	0.22	0.00	0.36	<0.001	0.02	102
464	Ol	0.02	13.7	40.5	<0.01	47.2	0.26	<0.01	0.36	<0.001	<0.01	102
465	Ol	0.01	13.3	40.4	0.01	47.3	0.25	<0.01	0.37	<0.001	0.00	102
466	Ol	<0.01	13.4	40.1	<0.01	46.9	0.24	<0.01	0.37	0.005	0.00	101
467	Ol	<0.01	13.4	40.4	0.02	47.0	0.22	0.02	0.39	<0.001	<0.01	102
468	Ol	<0.01	13.6	40.5	<0.01	47.3	0.21	<0.01	0.39	<0.001	<0.01	102
469	Ol	<0.01	13.9	40.4	<0.01	47.4	0.24	0.01	0.38	<0.001	0.02	102
470	Ol	<0.01	13.4	40.3	0.02	47.2	0.23	<0.01	0.40	0.020	<0.01	102
471	Ol	0.07	13.4	40.5	0.02	46.8	0.26	<0.01	0.37	<0.001	0.01	101
472	Ol	<0.01	13.4	40.2	<0.01	46.9	0.21	<0.01	0.36	<0.001	0.01	101
473	Ol	0.03	13.1	40.5	0.01	46.7	0.25	<0.01	0.36	<0.001	<0.01	101
474	Ol	0.02	13.3	40.1	0.03	46.7	0.24	<0.01	0.36	<0.001	0.00	101
475	Ol	0.01	13.1	40.5	0.01	46.8	0.20	0.01	0.38	<0.001	0.00	101
476	Ol	0.02	13.6	40.5	0.01	47.1	0.22	<0.01	0.34	<0.001	<0.01	102
477	Ol	<0.01	13.5	40.4	<0.01	47.5	0.31	<0.01	0.38	0.020	0.01	102
478	Ol	0.01	13.5	40.6	0.01	47.2	0.23	<0.01	0.37	<0.001	0.03	102
479	Ol	<0.01	13.2	40.4	<0.01	47.5	0.31	<0.01	0.37	<0.001	0.01	102
480	Ol	0.03	13.4	40.7	0.03	47.2	0.21	0.03	0.36	0.015	0.00	102
481	Ol	<0.01	13.5	40.5	0.02	47.2	0.21	0.02	0.34	<0.001	<0.01	102
482	Ol	<0.01	13.3	40.9	<0.01	47.2	0.25	0.01	0.35	<0.001	<0.01	102
483	Ol	<0.01	13.5	40.7	0.01	46.7	0.25	0.00	0.35	<0.001	<0.01	102
484	Ol	<0.01	13.6	40.6	<0.01	47.2	0.22	0.02	0.35	<0.001	<0.01	102
485	Ol	<0.01	12.8	40.4	0.01	47.0	0.24	0.03	0.37	0.051	0.02	101
486	Ol	<0.01	13.2	40.4	<0.01	46.4	0.21	<0.01	0.35	<0.001	<0.01	101
487	Ol	0.02	12.8	40.0	<0.01	46.6	0.17	<0.01	0.34	<0.001	0.01	100
488	Ol	0.01	13.3	40.4	<0.01	47.2	0.23	0.00	0.37	0.046	0.02	102
489	Ol	<0.01	13.4	40.7	<0.01	46.9	0.23	0.01	0.35	0.031	0.01	102
490	Ol	<0.01	13.4	40.9	<0.01	47.3	0.22	<0.01	0.34	0.026	0.02	102
491	Ol	<0.01	13.7	40.9	0.01	46.9	0.21	0.00	0.38	<0.001	0.02	102
492	Ol	<0.01	13.7	40.8	<0.01	47.2	0.22	<0.01	0.37	<0.001	0.00	102
493	Ol	<0.01	13.4	40.9	<0.01	47.3	0.25	0.00	0.36	0.03	<0.01	102

C-4 continued

10-27

Nr	Mineral	Na_2O	FeO	SiO_2	CaO	MgO	MnO	Al_2O_3	NiO	TiO_2	Cr_2O_3	Total
494	Ol	0.01	13.8	40.7	<0.01	47.6	0.20	<0.01	0.38	<0.001	<0.01	103
495	Ol	<0.01	13.4	40.3	0.02	47.1	0.21	0.02	0.38	0.031	<0.01	101
496	Ol	0.03	13.7	39.8	0.02	47.0	0.21	<0.01	0.36	<0.001	<0.01	101
497	Ol	<0.01	13.5	40.7	0.01	47.0	0.26	0.02	0.36	0.010	<0.01	102
498	Ol	<0.01	13.3	40.9	<0.01	47.2	0.26	<0.01	0.36	0.010	0.03	102
499	Ol	<0.01	13.3	40.7	<0.01	47.2	0.29	0.01	0.36	<0.001	<0.01	102
500	Ol	0.03	12.9	40.0	<0.01	46.1	0.21	<0.01	0.38	<0.001	<0.01	99.6
501	Ol	<0.01	13.3	40.2	0.01	46.7	0.21	<0.01	0.38	<0.001	<0.01	101
502	Ol	0.01	13.2	40.3	0.03	46.3	0.20	<0.01	0.36	0.041	0.01	101
503	Ol	<0.01	13.0	40.1	<0.01	46.9	0.27	<0.01	0.36	<0.001	<0.01	101
504	Ol	<0.01	13.3	40.3	0.01	46.7	0.25	0.01	0.36	0.015	<0.01	101
505	Ol	<0.01	13.6	40.2	<0.01	47.1	0.21	0.01	0.37	<0.001	<0.01	102
399	Opx	<0.01	8.73	57.0	0.16	33.6	0.33	1.44	0.06	0.098	0.13	102
400	Opx	0.01	8.94	57.0	0.12	33.2	0.25	1.48	0.08	0.021	0.10	101
401	Opx	<0.01	9.00	57.2	0.18	33.6	0.25	1.38	0.08	0.041	0.12	102
402	Opx	<0.01	9.06	56.8	0.14	33.3	0.26	1.53	0.06	0.14	0.11	101
403	Opx	0.02	8.80	57.3	0.16	33.5	0.22	1.29	0.04	0.041	0.10	102
404	Opx	<0.01	9.05	57.3	0.16	33.3	0.18	1.16	0.05	0.041	0.10	101
405	Opx	0.01	8.81	57.6	0.15	33.2	0.22	0.97	0.06	0.005	0.10	101
406	Opx	<0.01	9.25	57.1	0.16	33.2	0.23	1.23	0.07	0.12	0.12	102
407	Opx	0.01	9.32	56.5	0.15	33.2	0.27	1.41	0.03	0.073	0.09	101
408	Opx	<0.01	9.31	55.9	0.15	32.6	0.22	1.79	0.05	0.073	0.13	100
409	Opx	<0.01	8.90	56.5	0.20	32.8	0.33	2.07	0.06	0.031	0.11	101
410	Opx	<0.01	9.39	55.7	0.16	32.2	0.25	2.22	0.06	0.010	0.07	100
411	Amph	0.59	3.73	52.1	12.6	20.0	0.01	7.21	0.07	0.41	0.27	97.0
412	Amph	0.56	3.63	52.6	12.5	20.2	0.08	7.48	0.09	0.44	0.36	98.0
413	Amph	0.66	3.83	52.3	12.4	20.3	0.12	7.40	0.09	0.36	0.33	97.8
414	Amph	0.64	3.76	52.2	12.6	20.1	0.07	7.19	0.11	0.41	0.33	97.4
415	Amph	0.60	3.94	52.7	12.5	20.5	0.06	7.22	0.12	0.50	0.29	98.4
416	Amph	0.56	3.75	52.1	12.8	20.1	0.06	7.29	0.09	0.30	0.39	97.5
417	Amph	0.57	3.71	52.4	12.8	20.4	0.09	7.21	0.14	0.47	0.29	98.0
418	Amph	0.59	3.65	53.0	12.9	20.3	0.11	7.11	0.12	0.39	0.36	98.5
419	Amph	0.48	3.50	52.7	12.7	20.5	0.07	6.80	0.07	0.35	0.15	97.2
420	Amph	0.67	3.77	52.4	12.8	20.2	0.10	7.28	0.11	0.44	0.32	98.1
423	Amph	0.64	3.91	52.2	12.8	20.1	0.07	7.56	0.08	0.43	0.33	98.1
424	Amph	0.58	3.77	52.3	12.4	20.4	0.05	7.31	0.12	0.37	0.31	97.7
425	Amph	0.57	3.75	52.7	12.6	20.4	0.07	6.96	0.13	0.40	0.26	97.8
426	Amph	0.61	3.74	52.0	12.6	20.3	0.07	7.22	0.12	0.28	0.33	97.2
427	Spl	<0.01	19.6	0.04	0.06	15.2	0.22	50.5	0.28	0.014	14.4	100
428	Spl	0.03	19.7	1.97	0.03	15.6	0.19	49.0	0.27	<0.001	14.1	101
432	Spl	<0.01	22.8	0.00	<0.01	12.9	0.24	46.4	0.23	0.019	17.4	100
433	Spl	<0.01	22.5	<0.01	<0.01	13.0	0.26	46.7	0.22	0.024	17.3	100
434	Spl	<0.01	20.0	0.01	<0.01	14.9	0.17	51.9	0.32	0.068	12.8	100
435	Spl	0.05	20.1	<0.01	<0.01	15.2	0.22	52.4	0.32	0.015	12.2	100
436	Spl	<0.01	19.9	0.01	0.02	15.2	0.25	53.1	0.31	0.126	12.2	101
437	Spl	0.02	19.6	0.02	<0.01	15.2	0.17	52.9	0.34	0.010	12.0	100
440	Spl	<0.01	19.2	0.01	<0.01	15.9	0.14	55.4	0.35	0.030	9.72	101
441	Spl	0.03	17.3	0.01	<0.01	17.4	0.18	58.4	0.43	0.069	7.02	101
442	Spl	0.01	16.8	<0.01	0.02	16.8	0.11	58.7	0.40	<0.001	6.68	99.6
443	Spl	0.03	16.9	<0.01	0.01	16.8	0.12	59.0	0.41	0.005	6.59	99.9
444	Spl	0.04	17.3	<0.01	<0.01	16.8	0.16	57.7	0.42	0.079	7.51	99.9
446	Spl	<0.01	17.1	0.02	0.01	17.0	0.14	58.1	0.42	0.010	7.30	100
447	Spl	<0.01	17.2	<0.01	0.03	16.7	0.17	58.2	0.42	0.030	7.25	100
448	Spl	<0.01	16.9	0.02	0.03	16.9	0.13	59.5	0.39	0.035	6.72	101
506	Spl	<0.01	17.2	<0.01	<0.01	17.4	0.15	59.2	0.42	0.035	6.73	101
507	Spl	<0.01	17.0	0.01	0.03	16.9	0.18	58.3	0.44	0.040	7.39	100
508	Spl	<0.01	16.7	0.03	0.04	17.0	0.17	58.3	0.42	0.020	6.58	99.3
509	Spl	0.02	17.2	<0.01	0.01	17.0	0.15	58.6	0.42	<0.001	6.76	100
510	Spl	<0.01	17.4	0.01	0.02	17.2	0.20	59.0	0.41	0.010	6.43	101
511	Spl	0.03	16.2	0.09	0.11	16.7	0.16	59.3	0.41	0.064	6.38	99
512	Spl	<0.01	17.2	0.01	<0.01	17.0	0.14	59.2	0.42	0.039	6.81	101
513	Spl	<0.01	17.7	<0.01	0.01	17.1	0.12	59.1	0.41	0.030	6.86	101
514	Spl	<0.01	17.4	<0.01	0.04	17.0	0.13	58.7	0.40	0.044	6.51	100
515	Spl	0.01	17.3	<0.01	<0.01	16.9	0.18	59.1	0.41	0.054	6.73	101
516	Spl	0.01	17.2	0.02	<0.01	17.1	0.17	59.5	0.42	0.014	6.64	101
391	Chl	0.02	3.38	40.3	0.01	38.8	0.01	0.50	0.30	0.030	0.01	83.3

10-28

Nr	Mineral	Na_2O	FeO	SiO_2	CaO	MgO	MnO	Al_2O_3	NiO	TiO_2	Cr_2O_3	Total
5	Ol	<0.01	15.9	39.5	<0.01	0.35	42.8	0.32	<0.01	<0.001	0.01	98.9
6	Ol	0.02	16.1	39.1	<0.01	0.39	42.9	0.31	<0.01	<0.001	<0.01	98.9
7	Ol	<0.01	16.1	39.1	<0.01	0.39	42.7	0.32	<0.01	0.002	<0.01	98.6
9	Ol	<0.01	16.1	39.7	<0.01	0.32	42.8	0.30	<0.01	<0.01	<0.01	99.2
10	Ol	0.02	16.1	39.7	<0.01	0.36	43.0	0.30	<0.01	0.01	<0.01	99.5
11	Ol	0.31	16.2	39.6	0.01	0.36	43.7	0.26	<0.01	0.022	0.02	101
12	Ol	0.01	16.1	39.8	<0.01	0.36	44.1	0.23	<0.01	<0.001	<0.01	101
13	Ol	0.03	16.2	39.1	<0.01	0.38	43.6	0.29	<0.01	<0.001	<0.01	99.7
14	Ol	<0.01	16.1	39.5	<0.01	0.37	44.0	0.28	<0.01	<0.001	<0.01	100
16	Ol	<0.01	16.2	39.4	<0.01	0.32	43.5	0.23	<0.01	0.013	0.01	99.6
17	Ol	<0.01	16.2	39.6	<0.01	0.39	43.6	0.28	0.02	<0.001	<0.01	100

C-4 continued

10-28

Nr	Mineral	Na2O	FeO	SiO_2	CaO	NiO	MgO	MnO	Al_2O_3	TiO_2	Cr_2O_3	Total
18	Ol	0.01	15.8	40.1	<0.01	0.36	43.7	0.27	0.02	<0.001	<0.01	100
19	Ol	0.02	16.2	40.3	<0.01	0.39	43.7	0.23	<0.01	<0.001	<0.01	101
20	Ol	0.00	16.0	40.2	<0.01	0.40	43.9	0.29	<0.01	0.003	<0.01	101
21	Ol	<0.01	16.6	40.2	<0.01	0.40	44.7	0.27	<0.01	0.003	<0.01	102
22	Ol	<0.01	16.1	39.2	<0.01	0.39	43.9	0.31	<0.01	<0.001	<0.01	99.9
23	Ol	<0.01	16.3	40.3	<0.01	0.39	44.8	0.26	<0.01	0.009	0.01	102
24	Ol	<0.01	16.4	40.1	<0.01	0.39	43.8	0.26	0.01	0.020	0.02	101
25	Ol	0.04	16.0	39.9	<0.01	0.37	43.0	0.26	0.01	<0.001	<0.01	99.5
26	Ol	<0.01	16.2	39.5	<0.01	0.39	44.3	0.31	<0.01	<0.001	<0.01	101
27	Ol	<0.01	16.1	39.6	<0.01	0.39	43.3	0.30	<0.01	<0.001	<0.01	99.7
28	Ol	<0.01	16.2	40.2	<0.01	0.38	43.7	0.31	0.02	0.009	0.01	101
29	Ol	<0.01	16.0	39.6	<0.01	0.42	43.4	0.29	<0.01	0.006	0.01	99.8
30	Ol	<0.01	15.8	39.4	<0.01	0.37	42.7	0.26	0.04	0.005	0.01	98.6
31	Ol	<0.01	16.1	39.5	<0.01	0.34	43.6	0.35	<0.01	0.018	0.02	99.9
32	Ol	<0.01	16.3	39.9	<0.01	0.34	44.0	0.26	<0.01	<0.001	<0.01	101
33	Ol	<0.01	16.0	39.2	<0.01	0.35	43.1	0.25	<0.01	0.013	0.01	98.8
34	Ol 1	<0.01	16.4	39.6	<0.01	0.41	43.0	0.29	<0.01	0.008	<0.01	99.7
35	Ol 1	0.01	16.6	39.9	<0.01	0.36	44.0	0.36	<0.01	<0.001	0.01	101
37	Ol 1	<0.01	16.4	39.8	<0.01	0.38	43.5	0.26	<0.01	0.009	0.03	100
38	Ol 1	<0.01	16.0	39.5	<0.01	0.36	43.1	0.26	<0.01	<0.001	<0.01	99.2
42	Ol	<0.01	15.8	39.7	<0.01	0.34	43.3	0.30	<0.01		0.01	99.4
43	Ol	<0.01	15.9	39.5	<0.01	0.35	43.1	0.27	<0.01	<0.01	<0.01	99.1
44	Ol	<0.01	16.0	39.4	<0.01	0.36	42.6	0.27	<0.01	<0.01	<0.01	98.7
51	Ol	<0.01	15.7	39.0	<0.01	0.40	42.6	0.26	0.01	<0.01	0.01	97.9
52	Ol	<0.01	15.8	38.6	<0.01	0.38	42.7	0.30	0.01	<0.01	<0.01	97.9
53	Ol	<0.01	15.9	39.4	<0.01	0.37	43.6	0.26	<0.01	<0.01	<0.01	99.5
73	Ol	<0.01	16.1	39.8	<0.01	0.40	43.1	0.27	<0.01	<0.01	0.01	99.8
74	Ol	<0.01	16.3	40.7	<0.01	0.38	43.0	0.32	<0.01	<0.01	<0.01	101
75	Ol	0.01	16.4	40.5	<0.01	0.41	43.8	0.30	<0.01	<0.01	<0.01	101
76	Ol	<0.01	16.3	39.1	<0.01	0.40	41.7	0.30	<0.01	<0.01	<0.01	97.9
80	Ol	0.02	16.2	39.8	<0.01	0.42	42.6	0.31	<0.01	0.02	0.01	99.3
82	Ol	0.01	16.6	39.4	<0.01	0.40	42.2	0.25	<0.01	<0.01	<0.01	98.9
46	Opx	<0.01	10.5	53.6	0.13	0.07	29.6	0.29	2.25	0.040	0.10	96.7
47	Opx	<0.01	10.7	55.0	0.17	0.05	30.6	0.30	2.25	0.011	0.10	99.2
48	Opx	<0.01	10.3	56.3	0.11	0.06	31.5	0.30	1.32	0.021	0.09	99.9
49	Opx	<0.01	10.5	56.9	0.13	0.06	31.5	0.28	1.05	0.039	0.09	101
54	Opx	0.01	10.3	56.4	0.10	0.07	31.9	0.33	1.36	0.078	0.36	101
92	Opx	0.02	10.9	55.4	0.14	0.07	30.8	0.36	1.03	0.040	0.12	99
93	Opx	<0.01	10.9	55.3	0.13	0.06	31.1	0.33	1.66	0.040	0.10	99.6
40	Amp	0.97	4.79	47.7	12.4	0.11	17.8	0.11	9.01	0.40	0.31	93.6
41	Amp	0.92	4.93	47.8	12.1	0.11	18.0	0.10	9.25	0.33	0.30	93.8
85	Amp	0.78	3.97	48.3	12.6	0.10	18.5	0.11	7.06	0.33	0.25	91.9
86	Amp	0.87	4.95	45.6	12.1	0.11	17.2	0.08	9.01	0.38	0.30	90.6
56	Spl	0.02	21.3	<0.01	<0.01	0.43	13.9	0.23	53.2	0.037	10.2	99.3
57	Spl	<0.01	21.3	<0.01	<0.01	0.43	14.0	0.24	53.1	0.005	10.2	99.4
61	Spl	<0.01	21.2	0.05	<0.01	0.44	14.2	0.15	55.1	<0.001	8.79	99.9
62	Spl	0.01	21.2	0.02	<0.01	0.44	14.2	0.21	55.4	0.054	8.85	100
63	Spl	<0.01	21.7	<0.01	<0.01	0.38	14.4	0.20	56.1	0.018	8.54	101
64	Spl	0.01	22.1	<0.01	<0.01	0.46	14.5	0.19	55.8	0.008	8.68	102
65	Spl	<0.01	21.0	<0.01	<0.01	0.40	14.6	0.18	56.7	<0.001	8.42	101
66	Spl	<0.01	21.3	0.02	<0.01	0.42	14.5	0.22	56.2	<0.001	8.50	101
67	Spl	<0.01	21.3	<0.01	<0.01	0.43	14.7	0.20	56.9	0.023	7.93	102
68	Spl	0.04	21.7	0.02	<0.01	0.43	14.7	0.18	56.9	0.038	7.97	102
69	Spl	<0.01	20.8	0.01	<0.01	0.45	14.5	0.22	57.1	0.021	7.85	101
70	Spl	0.01	21.4	0.02	<0.01	0.46	14.8	0.16	57.4	0.011	7.91	102
71	Spl	<0.01	21.5	0.02	0.01	0.41	14.6	0.20	57.1	0.005	7.61	101
72	Spl	<0.01	21.4	0.05	<0.01	0.45	14.5	0.17	57.0	0.023	7.72	101
98	Spl	0.05	23.0	0.03	<0.01	0.43	13.5	0.19	52.0	0.001	10.9	100
99	Spl	<0.01	23.1	<0.01	<0.01	0.35	13.8	0.22	52.9	0.002	11.2	102

Appendix D

Table D-1: Electron microprobe mineral analyses of Akilia Island peridotites [wt.%]

10-04											
Nr	Mineral	Na_2O	FeO	SiO_2	CaO	MgO	Al_2O_3	NiO	TiO_2	Cr_2O_3	Total
103	Ol	<0.01	20.2	38.9	0.03	40.5	<0.01	0.01	<0.001	0.01	99.6
104	Ol	0.05	20.3	39.2	0.01	40.9	<0.01	0.02	<0.001	<0.01	100
105	Ol	0.02	20.6	38.8	0.02	40.3	<0.01	<0.01	<0.001	<0.01	99.7
106	Ol	0.01	20.3	39.0	0.02	39.9	<0.01	0.01	<0.001	0.02	99.2
108	Ol	0.01	20.5	37.9	0.02	39.4	0.01	<0.01	0.003	<0.01	97.9
109	Ol	0.03	20.8	38.3	0.02	40.5	<0.01	<0.01	0.008	<0.01	99.7
110	Ol	<0.01	20.5	38.0	0.02	40.0	<0.01	0.01	<0.001	<0.01	98.5
111	Ol	<0.01	20.1	37.9	0.02	39.2	<0.01	<0.01	0.006	<0.01	97.2
112	Ol	0.01	20.2	37.8	0.01	40.0	<0.01	<0.01	0.006	<0.01	98.1
116	Ol	0.03	20.9	38.5	0.02	39.7	<0.01	<0.01	<0.001	<0.01	99.1
117	Ol	<0.01	20.8	38.2	0.02	39.9	<0.01	<0.01	<0.001	<0.01	98.9
118	Ol	<0.01	20.8	38.3	0.03	39.9	<0.01	<0.01	0.008	0.02	99.1
119	Ol	0.04	20.2	38.6	0.02	40.2	0.02	<0.01	0.007	<0.01	99.0
120	Ol	0.01	20.5	38.5	0.01	40.7	<0.01	<0.01	<0.001	<0.01	99.8
121	Ol	0.05	19.8	38.8	0.02	41.0	0.01	<0.01	0.020	0.03	99.8
122	Ol	0.02	19.9	39.1	0.02	41.3	0.02	<0.01	<0.001	<0.01	100
123	Opx	0.01	12.6	54.7	0.20	29.4	2.23	<0.01	0.05	0.06	99.2
124	Opx	0.02	12.7	54.4	0.17	29.5	2.25	<0.01	0.06	0.05	99.1
125	Opx	0.04	12.7	54.7	0.18	29.7	2.20	<0.01	0.06	0.06	99.5
113	Amph	2.04	7.01	46.6	11.9	17.4	10.6	<0.01	0.42	0.39	96.4
114	Amph	2.04	6.87	46.9	11.9	17.6	10.6	<0.01	0.45	0.31	96.7
101	Mica	0.07	22.8	0.03	0.01	11.1	53.6	<0.01	<0.001	7.70	95.3
102	Mica	0.05	22.7	0.01	0.02	10.9	53.4	<0.01	0.014	8.07	95.1
115	Chl	<0.01	5.58	29.3	0.01	28.9	20.0	<0.01	0.047	0.42	84.3
10-05C											
Nr	Mineral	Na_2O	FeO	SiO_2	CaO	MgO	Al_2O_3	NiO	TiO_2	Cr_2O_3	Total
1	Ol1	<0.01	13.3	40.3	0.01	47.0	<0.01	0.06	<0.001	<0.01	101
2	Ol1	<0.01	13.0	40.4	0.02	46.9	<0.01	<0.01	<0.001	<0.01	100
3	Ol1	<0.01	13.2	40.5	0.02	47.0	<0.01	<0.01	<0.001	<0.01	101
4	Ol1	<0.01	13.4	40.5	0.02	47.1	<0.01	<0.01	<0.001	<0.01	101
5	Ol1	<0.01	13.0	40.2	0.02	46.8	<0.01	0.03	<0.001	<0.01	100
6	Ol1	<0.01	13.4	40.3	0.02	46.9	<0.01	<0.01	<0.001	<0.01	101
7	Ol1	<0.01	13.1	40.1	0.01	46.6	<0.01	<0.01	<0.001	<0.01	99.8
8	Ol1	<0.01	13.2	40.3	0.02	46.8	<0.01	<0.01	<0.001	<0.01	100
9	Ol1	<0.01	13.6	40.3	0.02	47.0	<0.01	0.03	<0.001	<0.01	101
10	Ol1	<0.01	13.6	40.1	0.02	46.2	<0.01	0.02	<0.001	<0.01	99.9
11	Ol2	<0.01	13.2	40.1	0.01	47.1	<0.01	<0.01	<0.001	<0.01	101
12	Ol2	<0.01	13.4	39.6	0.02	47.1	<0.01	0.03	<0.001	<0.01	100
13	Ol2	<0.01	13.3	40.1	0.02	46.8	<0.01	<0.01	<0.001	<0.01	100
14	Ol2	<0.01	13.3	40.4	0.01	47.0	<0.01	<0.01	<0.001	<0.01	101
15	Ol2	<0.01	13.2	40.2	0.01	46.7	0.01	<0.01	<0.001	<0.01	100
24	Ol3	<0.01	13.3	40.2	0.01	46.4	<0.01	<0.01	<0.001	<0.01	99.9
25	Ol3	<0.01	13.7	40.5	0.03	46.3	<0.01	<0.01	<0.001	<0.01	101
26	Ol3	<0.01	13.6	40.0	0.05	46.3	0.01	<0.01	<0.001	<0.01	100
27	Ol4	<0.01	13.8	40.1	0.02	46.4	<0.01	<0.01	<0.001	<0.01	100
28	Ol4	<0.01	13.4	40.1	0.02	47.2	<0.01	<0.01	<0.001	<0.01	101
29	Ol4	<0.01	13.2	40.2	0.02	46.6	0.01	0.02	<0.001	<0.01	100
30	Ol4	<0.01	13.0	40.1	0.02	47.0	<0.01	<0.01	<0.001	<0.01	100
31	Ol4	<0.01	13.1	40.4	0.02	47.0	0.01	<0.01	<0.001	<0.01	101
32	Ol4	<0.01	13.1	41.5	0.03	46.7	0.02	<0.01	<0.001	<0.01	101
33	Ol4	<0.01	13.7	40.1	0.02	46.5	<0.01	0.01	<0.001	<0.01	100
34	Ol5	<0.01	13.4	40.0	0.01	46.5	0.01	0.02	<0.001	<0.01	99.9
35	Ol5	<0.01	13.3	40.2	0.02	46.5	0.01	0.02	<0.001	<0.01	100
36	Ol5	<0.01	13.3	40.1	0.02	46.8	0.01	0.01	<0.001	<0.01	100
37	Ol5	<0.01	13.3	40.1	0.02	47.1	0.01	<0.01	<0.001	<0.01	101
38	Ol5	<0.01	12.9	40.2	0.01	46.4	<0.01	<0.01	<0.001	<0.01	99.5
39	Ol5	<0.01	13.0	40.5	0.01	46.7	<0.01	<0.01	<0.001	<0.01	100
40	Ol5	<0.01	13.4	40.0	0.03	47.1	<0.01	<0.01	<0.001	<0.01	101
41	Ol5	<0.01	13.2	40.0	0.03	47.0	0.01	<0.01	<0.001	<0.01	100
42	Ol5	<0.01	13.4	40.3	0.02	46.7	<0.01	<0.01	<0.001	<0.01	100
43	Ol5	<0.01	13.5	40.2	0.01	46.6	<0.01	<0.01	<0.001	<0.01	100
44	Ol5	<0.01	13.6	39.9	0.01	46.2	0.01	0.01	<0.001	<0.01	99.7
45	Ol5	<0.01	13.8	40.2	0.04	46.4	<0.01	<0.01	<0.001	<0.01	101
46	Ol5	<0.01	13.9	39.9	0.03	46.1	<0.01	<0.01	<0.001	<0.01	100
70	Ol6	0.04	13.4	40.0	0.00	46.2	<0.01	<0.01	0.005	0.01	99.6
71	Ol7	0.01	14.1	39.9	0.03	45.4	<0.01	<0.01	<0.001	<0.01	99.4
79	Ol	0.01	13.5	40.3	0.02	46.3	0.01	<0.01	<0.001	<0.01	100
80	Ol	0.02	13.8	39.9	0.02	46.2	0.02	<0.01	<0.001	<0.01	100
81	Ol	0.01	14.1	40.0	0.02	46.0	<0.01	<0.01	0.003	<0.01	100
82	Ol	0.03	14.5	39.9	0.01	45.1	0.00	<0.01	<0.001	<0.01	99.5
83	Ol	<0.01	13.9	40.0	0.02	45.3	<0.01	0.03	0.004	<0.01	99.2
84	Ol	<0.01	14.7	39.9	0.01	45.5	0.03	<0.01	0.003	<0.01	100
85	Ol	0.02	13.4	40.1	0.01	46.1	0.02	<0.01	<0.001	0.02	99.7
86	Ol	<0.01	13.3	40.2	0.01	46.5	0.01	<0.01	0.015	<0.01	100
87	Ol	<0.01	14.4	39.9	0.01	45.8	<0.01	0.01	<0.001	<0.01	100

D-1 continued

10-05C

Nr	Mineral	Na_2O	FeO	SiO_2	CaO	MgO	Al_2O_3	NiO	TiO_2	Cr_2O_3	Total
88	Ol	0.01	13.2	40.1	0.02	46.7	0.01	<0.01	<0.001	<0.01	100
89	Ol	0.01	13.5	40.4	0.02	46.5	0.03	<0.01	<0.001	<0.01	100
90	Ol	0.01	13.1	40.2	0.02	46.5	<0.01	<0.01	<0.001	<0.01	99.9
91	Ol	<0.01	13.3	40.2	0.02	46.5	0.01	<0.01	<0.001	<0.01	100
92	Ol	0.01	13.1	40.2	0.01	46.2	0.02	<0.01	0.003	<0.01	99.5
93	Ol	<0.01	13.9	40.2	0.02	45.7	<0.01	<0.01	<0.001	<0.01	99.8
94	Ol	0.02	13.4	39.9	0.02	46.1	<0.01	0.01	<0.001	0.01	99.5
66	Cpx	<0.01	0.61	54.5	25.5	17.4	0.44	<0.01	<0.001	<0.01	98.5
60	Amph	<0.01	3.85	50.1	11.9	19.9	7.01	<0.01	<0.001	<0.01	92.8
61	Amph	<0.01	3.81	50.3	11.9	20.2	6.91	<0.01	<0.001	<0.01	93.1
57	Amph	<0.01	3.93	50.3	12.0	20.0	7.00	<0.01	<0.001	<0.01	93.3
58	Amph	<0.01	3.70	51.0	12.1	20.5	6.04	<0.01	<0.001	<0.01	93.3
53	Amph	<0.01	3.87	50.3	12.1	20.0	7.01	<0.01	<0.001	<0.01	93.3
56	Amph	<0.01	3.86	50.4	12.0	20.3	6.80	<0.01	<0.001	<0.01	93.4
63	Amph	<0.01	4.13	50.2	11.9	20.1	7.13	<0.01	<0.001	<0.01	93.4
62	Amph	<0.01	3.77	50.4	11.9	20.5	6.92	<0.01	<0.001	<0.01	93.5
52	Amph	<0.01	3.79	50.5	12.1	20.3	6.82	<0.01	<0.001	<0.01	93.5
65	Amph	<0.01	3.91	50.7	12.0	20.3	6.62	<0.01	<0.001	<0.01	93.5
51	Amph	<0.01	3.81	50.5	12.0	20.3	7.07	<0.01	<0.001	<0.01	93.7
49	Amph	<0.01	3.90	50.5	12.0	20.3	6.95	<0.01	<0.001	<0.01	93.7
48	Amph	<0.01	3.97	50.4	12.0	20.5	6.99	<0.01	<0.001	<0.01	93.8
50	Amph	<0.01	4.03	50.6	12.0	20.2	7.02	<0.01	<0.001	<0.01	93.9
64	Amph	<0.01	3.76	51.3	12.0	20.6	6.32	<0.01	<0.001	<0.01	93.9
59	Amph	<0.01	3.74	51.0	12.1	20.6	6.58	<0.01	<0.001	<0.01	94.0
54	Amph	<0.01	2.94	55.5	12.1	22.8	2.47	<0.01	<0.001	<0.01	95.8
55	Amph	<0.01	2.89	55.9	12.2	22.7	2.12	<0.01	<0.001	<0.01	95.9
68	Spl	<0.01	47.5	0.01	0.06	1.37	2.52	<0.01	0.12	54.2	98.5
67	Ilmenit	0.01	40.3	<0.01	0.06	3.81	<0.01	<0.01	42.1	1.13	94.6

ERKLÄRUNG

Ich versichere, dass ich die von mir vorgelegte Dissertation selbständig angefertigt, die benutzten Quellen und Hilfsmittel vollständig angegeben und die Stellen der Arbeit − einschließlich Tabellen, Karten und Abbildungen −, die anderen Werken im Wortlaut oder dem Sinn nach entnommen sind, in jedem Einzelfall als Entlehnung kenntlich gemacht habe; dass diese Dissertation noch keiner anderen Fakultät oder Universität zur Prüfung vorgelegen hat; dass sie − abgesehen von unten angegebenen Teilpublikationen − noch nicht veröffentlicht worden ist, sowie, dass ich eine solche Veröffentlichung vor Abschluss des Promotionsverfahrens nicht vornehmen werde. Die Bestimmungen der Promotionsordnung sind mir bekannt. Die von mir vorgelegte Dissertation ist von Prof. Dr. Carsten Münker betreut worden.

Nachfolgend genannte Teilpublikationen liegen vor:

van de Löcht J, Hoffmann JE, Li C, et al. (2018), Earth's oldest mantle peridotites show entire record of late accretion. Geology 46:199–202. doi: 10.1130/G39709.1

Paragraph 3-3.1 and 3-4.3

Chapter 4

Appendix A

Datum Unterschrift